investigating integrin $\alpha_v\beta_6$ activation status in breast cancer

September 2017

This thesis is submitted in partial fulfilment of the requirements of Queen Mary University of London for the academic award of PhD

Caroline Sproat

Centre for Tumour Biology
Barts Cancer Institute
School of Medicine and Dentistry
Queen Mary University of London

Dedicated to Nandad

John “Jack” Anthony Robertson

statement of originality

I confirm that the research included within this thesis is my own work or, that where it has been carried out in collaboration with, or supported by others, that this is duly acknowledged and cited. The main body of work presented in this thesis was undertaken at the Centre for Tumour Biology, Barts Cancer Institute, Barts and the London School of Medicine and Dentistry, University of London.

Where indicated, a body of external collaborative research was kindly hosted by the Receptor Dynamics in Cancer Laboratory and experiments therein performed at the School of Cellular and Molecular Physiology, Institute of Translational Medicine, University of Liverpool.

The research presented here was fully funded by Cancer Research UK.

I attest that I have exercised reasonable care to ensure that the work is original, and does not to the best of my knowledge break any UK law, infringe any third party's copyright or other Intellectual Property Right, or contain any confidential material.

I confirm that this thesis has not been previously submitted for the award of a degree by this, or any other university.

Caroline Sproat

29th September 2017

abstract

background

The extracellular matrix receptor integrin $\alpha_v\beta_6$ is known to potentiate breast cancer (BrCa) cell invasion, metastasis and tumour-trophic growth factor receptor crosstalk during tumourigenesis. Monoclonal antibody blockade of $\alpha_v\beta_6$ diminishes invasion *in vitro* and arrests BrCa tumour growth and metastasis *in vivo*. Aberrant integrin activation status has been implicated in progression to metastatic disease in BrCa; with differential internalisation and endocytic trafficking kinetics reported for active versus inactive integrin species in malignant disease. Despite its emerging potential for targeted therapy, little is known regarding regulation of integrin $\alpha_v\beta_6$–mediated activation and signalling during progression to an invasive, metastatic state. It is hypothesised that the aetiopathological significance of integrin $\alpha_v\beta_6$ during neoplastic transformation and malignant progression in BrCa is dependent specifically upon its activation status and associated conformation, since this active state will permit establishment of known integrin–mediated oncogenic signalling underpinning acquisition of a malignant phenotype, including activation of invasion and metastasis.

results

Canonical integrin activation studies using divalent cations and cognate ligand stimulation indicated antibodies 6.2E5 and 6.2G2 recognise activation-associated epitopes, which are also ligand-induced binding sites (LIBS) in live-labelled cells by FCM and IMF. However, their utility to discriminate the active fraction distinct from the total or inactive fractions of $\alpha_v\beta_6$ by IHC in primary BrCa samples could not be robustly established. Evaluation of the 6.2E5 and 6.2G2 epitopes in the MCF10 isogenic model revealed that relative surface abundance of these active epitopes determined by FCM was not significantly altered; but their subcellular redistribution upon neoplastic transformation and malignant progression was observed by IMF, implicating derailed internalisation and trafficking of active $\alpha_v\beta_6$ during breast tumourigenesis and metastatic disease progression. Proteomic interrogation and network analysis of the 2D-enriched adhesion assays identified 7 novel putative molecular regulators of a ligand-engaged, activated $\alpha_v\beta_6$–mediated adhesion environment (DMBT-1, MARCKS, MXRA5, SEPT6, SEPT9, MYH9, MYH10) in the BT-20 TNBC cell line. Functional validation of these candidate mediators of the "β_6 adhesome" by siRNA strategies was not achieved due to inconsistent stable knockdown. Phosphoproteomic definition of LAP ligand-engaged, active $\alpha_v\beta_6$–mediated signalling ("β_6 kinome") during receptor-ligand internalisation revealed EGFR-dependency for downstream ERK1/2 signal

activation in BT-20 and SUM159, but not MDA-MB-468 TNBC cells. Kinase substrate enrichment analysis (KSEA) identified 5 novel putative mediators of downstream $\alpha_v\beta_6$ signalling (COT, MAPKAPK2, PDPK1, Nuak1, TBK1) and implicated Akt1 isoform-specific activation downstream of $\alpha_v\beta_6$–LAP internalisation. Following LAP-induced $\alpha_v\beta_6$ activation and internalisation, EGFR underwent phosphorylation at multiple known activation sites, including a residue (Thr693) critical for EGFR receptor internalisation; suggesting integrin $\alpha_v\beta_6$–EGFR reciprocity during respective receptor activation and internalisation.

conclusion

The active conformer of integrin $\alpha_v\beta_6$ may be studied using antibodies 6.2E5 and 6.2G2 in live-labelled cells by FCM and IMF. Subcellular redistribution of activation-associated epitopes during BrCa progression implicates derailed internalisation and intracellular trafficking kinetics of active $\alpha_v\beta_6$ during tumourigenesis, while protein expression studies identified 7 putative molecular regulators of ligand-engaged, active $\alpha_v\beta_6$–mediated adhesion. Integrin $\alpha_v\beta_6$-mediated signalling during internalisation revealed an $\alpha_v\beta_6$–EGFR-Akt1 signalling axis during breast tumourigenesis and disease progression, while further understanding of integrin biology and growth factor receptor crosstalk may provide additional rationale for potential combination therapies in breast cancer.

c collaborations

Appreciative thanks and acknowledgements are extended to the following laboratories for their time and expertise invested in the following collaborative studies presented in this thesis:

Chapter V: Results part III

proteomic definition of a ligand-engaged integrin $\alpha_v\beta_6$-dependent adhesion environment using a 2D-enrichment approach: defining the β_6-adhesome

Dr Mark R Morgan

Principal Investigator
Receptor Dynamics in Cancer Laboratory
School of Cellular and Molecular Physiology
Institute for Translational Medicine
University of Liverpool

Chapter VI: Results part IV

phosphoproteomic dissection of early signalling events inducted upon integrin $\alpha_v\beta_6$ engagement with its cognate ligand LAP, ensuing activation and subsequent internalisation: defining the β_6-kinome

Dr Pedro R Cutillas

Principal Investigator
Cell Signalling and Proteomics Laboratory
Centre for Haemato-Oncology
Barts Cancer Institute
Queen Mary University of London

Dr Edmund Wilkes

Postdoctoral Research Scientist
Cell Signalling and Proteomics Laboratory
(as above)

acknowledgements

Beyond the customary expression of gratitude toward a PhD supervisor, I would like to extend my heartfelt thanks to Professor John F Marshall for affording me the opportunity of undertaking my doctoral studies within the Integrin β6 Biology Group. For his guidance, empathy and tolerance with this most trying of students, I shall be eternally grateful. Having (inadvertently) tested his patience on numerous occasions, I can confirm that I have not found the limit to the Prof's patience….yet!

I would also like to thank all of the illustrious past, present (and honorary) members of the Integrin β6 Biology Group with whom I have enjoyed the pleasure and privilege of working with during my tenure in Tumour Biology. Notably I would like to thank the β6-Fam: Ami, Banu, Claire, Ketan and Zareen for sharing the highs and lows of life in the lab ….and beyond! The bonds of these friendships forged in the fiery furnace and white heat of the PhD process shall never be broken.

For supervision of the β6-adhesome experiments and hosting a sojourn in the wilds of Liverpool, many thanks are extended to Dr Mark R Morgan, the Receptor Dynamics in Cancer Laboratory (University of Liverpool) and The infamous Manchester Superstores. Particular thanks are given to Dr Katia Wolanska and Dr Boleg Winiarski for keeping me fed, watered and sane at 34 Ellerman Road. It turns out it's not THAT grim up North after all. I will finish….because I chose to!

For kind assistance with the β6-kinome project arm, I would like to thank Dr Pedro Cutillas and especially Dr Edmund Wilkes for his expert assistance with all things phosphoproteomic and programming. Thanks are extended to Mr Philip Adeniran for spending the tenure of his MSc project performing validation work on the phosphoproteomic dataset and for his kind permission to incorporate some of his data herein.

To everybody in Tumour Biology with whom I have enjoyed the great privilege of working alongside (and who are too many to name in full here), thank you for your collective pool of knowledge and wisdom that helped guide me through the PhD process. I would like to thank Debbie, our long-suffering Lab Manager, for always

coming to the rescue with such good grace and aplomb. For their critical scientific appraisal and technical insight I would like to thank Dr Mike Allen, Dr Delphine M Lees and Dr Ed Carter.

Amongst the many wonderful friends I have made at Barts Cancer Institute I would like to thank Abbie, Bakouche, Beta, Fevzi, Rachel and Sara for their life-affirming presence, edifying conversation and uplifting humour. And to all my friends who remember that now pre-historic time before I started the PhD, I wish to express my thanks and love for their unyielding support and patience: HongHa, Jas, Ruth and Sophie. To my Northern Soul Contingent for keeping me in Talc and good times along the way: Steve, Ian, Fran, Jess and Mark – thank you!

And last, but definitely by no means least, a VERY long overdue thank you to my family for their support and encouragement. To Nandad, for teaching me the value and importance of education; to my parents, Kathryn and Christopher, for instilling in me a sense of wonder and ceaseless curiosity; to my sister, Joanne, my nephew Liam and niece Jessica also; and to my darling Tim, for your wise words and inspiration throughout.

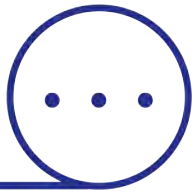

abbreviations

2D	2-dimensional
2D-E	2D-enrichment
3D	3-dimensional
ACN	acetonitrile
ACS	American Cancer Society
ADAM23	a disintegrin & metalloproteinase domain-containing protein 23
ADMIDAS	adjacent to MIDAS
AEBSF-HCl	4-(2-aminoethyl)benzenesulphonyl fluoride hydrochloride
AGC	protein kinase A, G & C families (PKA, PKG & PKC)
Akt	v-Akt murine thymoma viral oncogene homolue 1 (PKB)
AML	acute myeloid leukaemia
AMPK	5' adenosine monophosphate-activated protein kinase
ANOVA	analysis of variance
ARK5	AMPK-related kinase-5 (NUAK1)
α-SMA	alpha smooth muscle actin
ASPA	Animals (Scientific Procedures) Act 1986
ATCC	American Type Culture Collection®
ATM	ataxia telangiectasia mutated
AU	arbitrary units
BRAF	V-Raf Murine Sarcoma Viral Oncogene Homolog B
BrCa	breast cancer
BRCA1	breast cancer 1, early onset
BRCA2	breast cancer 2, early onset
BRIP1	BRCA1 interacting protein C-terminal helicase
BSA	bovine serum albumin
Ca^{2+}	calcium ion(s)
$CaCl_2$	calcium chloride
CDKN2A	cyclin-dependent kinase inhibitor 2A
cDNA	complementary DNA
CHEK2	checkpoint kinase 2
CHO	Chinese hamster ovary
CID	collision-induced dissociation
CK	cytokeratin(s)

CO_2	carbon dioxide
co-IP	co-immunoprecipitation
Col I	collagen type I
COSHH	Control of Substances Hazardous to Health
COT	Cancer Osaka thyroid (MAP3K8 / Tpl2)
CRT	Cancer Research Technology®
CR-UK	Cancer Research UK
CT	cholera toxin
CTCF	corrected total cell fluorescence
Da	dalton
DAPI	4',6-diamidino-2-phenylindole
DCIS	ductal carcinoma *in situ*
DMEM	Dulbecco's Modified Eagle Medium
DMEM/0.1/0.1	DMEM supplemented with 0.1% (w/v) BSA & 0.1% (v/v) NaN_3
DMEM5	DMEM supplemented with 25 mM HEPES
DMBT-1	deleted in malignant brain tumours 1
DNA	deoxyribonucleic acid
DRFS	distant recurrence-free survival
DTBP	dimethyl 3,3'dithiobispropionimidate·2HCl
ECL	enhanced chemiluminescence
ECM	extracellular matrix
EDTA	ethylenediaminetetraacetic acid
EE	early endosome
EGCG	epigallocatechin gallate
EGF	epidermal growth factor
EGFR	epidermal growth factor receptor (HER1)
EGTA	ethylene-bis(oxyethylenenitrilo)tetraacetic acid
ELISA	enzyme-linked immunosorbent assay
EpCAM	epithelial cell adhesion molecule
ER	oestrogen receptor
ERK	extracellular signal-related kinase
FA	formic acid
FAK	focal adhesion kinase
FB	functional blockade
FBS	foetal bovine serum
FCM	flow cytometry
FISH	fluorescence in situ hybridisation
FITC	fluorescein isothiocyanate
FMDV	foot and mouth disease virus
Fn	fibronectin

FWHM	full width at half maximum
G6PD	glucose-6-phosphate dehydrogenase
geoMFI	geometric mean fluorescence intensity
GFR	growth factor receptor
GSKA/B	glycogen synthase kinase (α/β isoform)
GST	glutathione S-transferase
GTP	guanosine triphosphate
hr	hour
H_2SO_4	sulphuric acid
HAX-1	HS1-associated protein X-1
HC	hydrocortisone
HEPES	4-(2-hydroxyethyl)piperazine-1-ethanesulphonic acid
HER1	human epidermal growth factor receptor 1 (EGFR / ErbB1)
HER2	human epidermal growth factor receptor 2 (ErbB2)
HGF	hepatocyte growth factor
HRP	horseradish peroxidase
HS	horse serum
HSc-70	heat shock cognate protein 70
HTA	Human Tissue Act (2004)
IAA	iodoacetamide
IDC	invasive ductal carcinoma
IHC	immunohistochemistry
ILK	integrin-linked kinase
IMF	immunofluorescence
IP	immunoprecipitation
IPI	international protein index
IPP	ILK/PINCH/parvin complex
IR	infrared
KCl	potassium chloride
KGM	keratinocyte growth medium
KLH	keyhole limpet haemocyanin
KRAS	Kirsten Rat Sarcoma Viral Oncogene Homolog
KSEA	kinase substrate enrichment analysis
LAP	latency associated peptide of TGF-β1
LAP-Fc	LAP tagged with human IgG (Fc') fragment
LC	liquid chromatography
LC-MS/MS	liquid chromatography coupled to tandem mass spectrometry
LCIS	lobular carcinoma *in situ*
LFA-1	lymphocyte function-associated antigen-1 ($\alpha_L\beta_2$)
LIBS	ligand-induced binding site

LIMBS	ligand-associated metal-binding site (aka LIMBS)
M	molar
mA	milliamp(s)
MAPK	mitogen-activated protein kinase
MAP3K8	mitogen-activated protein kinase kinase kinase 8 (COT / Tpl2)
MAPKAPK2	mitogen-activated protein kinase-activated protein kinase 2 (MAPK2 / MK2)
MARCKS	myristolated alanine-rich C kinase substrate
MBC	metastatic breast cancer
MIDAS	metal-ion dependent adhesion site
MCF	Michigan Cancer Foundation
MDT	multidisciplinary team
MEK	MAPK/ERK kinase
MES	2-(N-Morpholino)ethanesulphonic acid
MesNa	sodium 2-mercaptoethanesulphonate
MFI	mean fluorescence intensity
Mg^{2+}	magnesium ion(s)
$MgCl_2$	magnesium chloride
min	minute(s)
MIDAS	metal ion-dependent adhesion site
MLH1	MutL Homologue 1
mM	millimolar
MM	malignant melanoma
MMP	matrix metalloproteinase
Mn^{2+}	manganese ion(s)
MOAC	metal oxide affinity chromatography
MS	mass spectrometry
MS/MS	tandem mass spectrometry
MSI	microsatellite instability
MXRA5	matrix-remodelling-associated protein 5
MYH9	myosin, heavy chain-9
MYH10	myosin, heavy chain-10
N	Normal
NH_4HCO_3	ammonium bicarbonate
NH_4OH	ammonium hydroxide
Na_2CO_3	sodium carbonate
NaF	sodium fluoride
NaN_3	sodium azide
$NaVO_4$	sodium orthovanadate
NCOR1	nuclear receptor co-repressor-1
ng	nanogram

NICE	National Institute for Health and Care Excellence
NpxY	Asn-Pro-Xaa-Tyr amino acid motif
NSCLC	non-small cell lung carcinoma
Nuak1	NUAK family SNF-like kinase-1 (ARK5)
OD	optical density
OSCC	oral squamous cell carcinoma
PAGE	polyacrylamide gel electrophoresis
PALB2	partner and localiser of BRCA2
PARP	poly (ADP-ribose) polymerase
PBS-	phosphate-buffered saline without $CaCl_2$ and $MgCl_2$
PBS+	phosphate-buffered saline with $CaCl_2$ and $MgCl_2$
PCR	polymerase chain reaction
PDK1	3-phosphoinositide-dependent protein kinase-1 (PDPK1)
PFA	paraformaldehyde
pg	picogram
PIK3CA	phosphatidylinositol-4,5-bisphosphate 3-kinase, catalytic subunit alpha
PINCH	particularly interesting Cys-His-rich protein
PIP2	phosphatidylinositol 4,5-bisphosphate
PIPKIγ	phosphatidylinositol (4) phosphate 5 kinase type I gamma
PKB	protein kinase B (Akt)
PKCδ	protein kinase C delta isoform
PNRC	perinuclear recycling complex
PPE	personal protective equipment
PPI	protein-protein interaction
PR	progesterone receptor
PTB	phosphotyrosine-binding domain
PtdIns(3,4,5)P3	phosphatidylinositol (3,4,5)-triphosphate
PTEN	phosphatase and tensin homologue
PTM	post-translational modification
qPCR	quantitative (real-time) PCR
RB1	retinoblastoma protein
RCP	Rab-coupling protein
RGD	Arg-Gly-Asp tripeptide motif
RIPA	radioimmunoprecipitation assay
RNA	ribonucleic acid
RT	room temperature *(ambient laboratory temperature)*
RTK	receptor tyrosine kinase
SCBT	Santa Cruz® Biotechnology, Inc
SCID	severe combined immunodeficiency
s.d	standard deviation

SDS	sodium dodecyl sulphate
s.e.m	standard error of the mean
SEPT6	septin-6
SEPT9	septin-9
SILAC	stable isotope labelling with amino acids in cell culture
SMAD4	Mothers against decapentaplegic homolog 4
SMI	small molecule inhibitor
SNF	sucrose non-fermenting
SPE	solid-phase extraction
STAT3	signal transducer and activator of transcription-3
STR	short tandem repeat
SyMBS	synergistic metal ion binding site (aka LIMBS)
TANK	TRAF Family Member-Associated NFκB Activator
TBK1	TANK-binding kinase-1
TBS	Tris-buffered saline
Tf	transferrin
Tf-Fc	transferrin tagged with human IgG (Fc') fragment
TfRC	transferrin receptor complex
TFA	trifluoracetic acid
TGFαR	transforming growth factor alpha (α) receptor
TGF-β	transforming growth factor beta (β)
TMB	3,3'-5,5' tetramethylbenzidine
TNBC	triple negative breast cancer
TNM	tumour-node-metastases (tumour staging system)
TP53	tumour protein P53
TPCK	$_{L}$-(tosylamido-2-phenyl) ethyl chloromethyl ketone
Tpl-2	Tumour Progression Locus-2
TTP	time-to-tumour progression
Tris-HCl	Tris(hydroxymethyl)methylamine-hydrochloride
TRITC	tetramethylrhodamine
UPLC	ultra performance liquid chromatography
V	Volt(s)
VEGF	vascular endothelial growth factor
VEGFR2	vascular endothelial growth factor receptor 2
VHL	von Hippel-Lindau
Vn	vitronectin
WB	Western blot(ting) *(immunoblotting)*
WHO	World Health Organisation
WT	wild type

table of contents

index of figures

fig.	title	page

chapter IV: results part II

evaluating the role of integrin $\alpha_v\beta_6$ activation status during breast cancer progression using the isogenic MCF-10 model of breast tumourigenesis

chapter V: results part III

proteomic definition of a ligand-engaged integrin $\alpha_v\beta_6$-dependent adhesion environment using a 2D-enrichment approach

index of tables

chapter 1

introduction

I

investigating the role of integrin $\alpha_v\beta_6$ activation during breast cancer progression

1. introduction

breast cancer and the integrin $\alpha_v\beta_6$: an overview

Breast cancer (BrCa) is the most prevalent of all female cancers worldwide, accounting for 1.7 million new cancer diagnoses and constituting 12% of all cancers diagnosed globally in 2012 (CDC 2016). It is the most common of all cancers in the United Kingdom (UK) with 53 252 women and 344 men diagnosed with invasive BrCa, collectively accounting for 15% of all cancer cases, in the UK in 2013 (CR-UK 2016).

Although female BrCa incidence remains highest in the Western world where the lifetime risk is estimated to be 1 in 8, epidemiological studies highlight the increasing incidence of female BrCa in both the developing and developed worlds (Jemal *et al* 2011, WHO 2014, CDC 2016). Given the existing and projected global healthcare burden attributable to BrCa, the need to refine BrCa prevention and control strategies, including therapeutics, remains paramount.

Metastatic disease remains the most significant cause of BrCa-associated morbidity and mortality, remaining incurable, but treatable (Duffy *et al* 2008, Veiseh *et al* 2011, Dawson *et al* 2013). Worldwide, approximately 90% of BrCa-associated deaths are attributed to metastatic disease dissemination (Cummings *et al* 2014, WHO 2014), highlighting the pressing need to combat this all too frequently fatal complication.

Activation of tumour cell invasion and metastasis is a cardinal cancer hallmark, signifying disease progression from a potentially curable, localised benign lesion to malignant, potentially fatal cancer (Van't Veer and Weigelt 2003, Hanahan and Weinberg 2011). Malignant transformation is underpinned by the derailment of cell adhesion repertoires to facilitate tumour cell invasion and metastatic dissemination. Thus, inhibiting acquisition of a pro-invasive, or restitution of a non-invasive cell adhesion repertoire, are emerging strategies for the clinical management of disseminated disease (Desgrosellier and Cheresh 2010, Bendas and Borsig 2012, Zhong and Rescorla 2012).

Previous research has established the role of the integrin superfamily of cell-surface adhesion receptors during cell migration and invasion under both physiological and pathological conditions (Hood and Cheresh 2002, Wehrle-Haller and Imhof 2003, Sahai 2005, Harburger and Calderwood 2009, Desgrosellier and Cheresh 2010, Buchheit *et al* 2012). Notably, the poor-prognostic and tumour-trophic effects of integrin $\alpha_v\beta_6$ observed in multiple cancers, including BrCa, have been demonstrated both *in vitro* and *in vivo* (Thomas *et al* 2001b, Thomas *et al* 2006, Ramsay *et al* 2007, Yang *et al* 2012, Allen *et al* 2014, Moore *et al* 2014).

Recent investigations have demonstrated integrin $\alpha_v\beta_6$ expression is associated with risk of progression to invasive disease in ductal carcinoma *in situ* (DCIS) (Allen *et al* 2014). Furthermore, therapeutic blockade of integrin $\alpha_v\beta_6$ has been shown to reduce breast 4T-1 tumour cell growth and metastasis *in vivo* (Eberlein *et al* 2013) and potentiate trastuzumab efficacy in human epidermal growth factor-2 (HER2)-driven BrCa (Moore *et al* 2014). Given its established potential as a therapeutic target, the mechanisms by which integrin $\alpha_v\beta_6$ regulates invasive cellular processes and mediates cross-talk with other growth factor receptors (GFRs) to drive BrCa progression warrants further investigation to expedite its use to augment existing, or to develop novel, BrCa treatment modalities.

1.1 breast cancer

1.1.1 an overview

The term breast cancer (BrCa) collectively describes neoplasms arising from epithelial cells lining the mammary ducts and lobules, termed ductal carcinoma or lobular carcinoma respectively (Figure 1.1). BrCa is a markedly heterogeneous disease in terms of its histopathological features, clinical outcomes and therapeutic response. Since it cannot be defined as a single, discrete clinicopathological entity, BrCa has been classified into several more homogeneous morphological and molecular subtypes facilitating patient stratification to inform appropriate therapeutic management of disease (Crum *et al* 2003, Lakhani *et al* 2012, Bateman and Shaw 2013, Cummings *et al* 2014, Lakhtakia and Chinoy 2014, Vuong *et al* 2014, Makki 2015).

Currently, 25 histological breast pathologies are recognised by the World Health Organisation (WHO) which encompass not only malignant, invasive cancers of the breast, but also: pre-cursor lesions, benign lesions and neoplasms of fibroepithelial, myoepithelial and mesenchymal origin arising in the breast (Lakhani *et al* 2012, Sinn and Kreipe 2013).

Approximately 95% of BrCa are classified as adenocarcinomas upon diagnosis (Makki 2015). Advances in molecular medicine have permitted genetic interrogation of BrCa subtypes (Perou *et al* 2000), facilitating refinement of traditional histological classification to include molecular subtyping (Vuong *et al* 2014). These molecular approaches to BrCa more accurately reflect its complexity and marked histological and genetic heterogeneity, facilitating selection of the most suitable treatment regimen (Crum *et al* 2003, Stevens and Lowe 2005, Hsiao *et al* 2010, NICE 2011, Lakhani *et al* 2012, Viale 2012, Bateman and Shaw 2013, Cummings *et al* 2014).

However, in accordance with National Institute for Health and Care Excellence guidelines (NICE 2009a, NICE 2009b, NICE 2011), the current approach to molecular diagnostics informing treatment regimens for BrCa patients in the UK remains rooted in the evaluation of tumour oestrogen (ER), progesterone (PR) and human epidermal growth factor-2 (HER-2) receptor status.

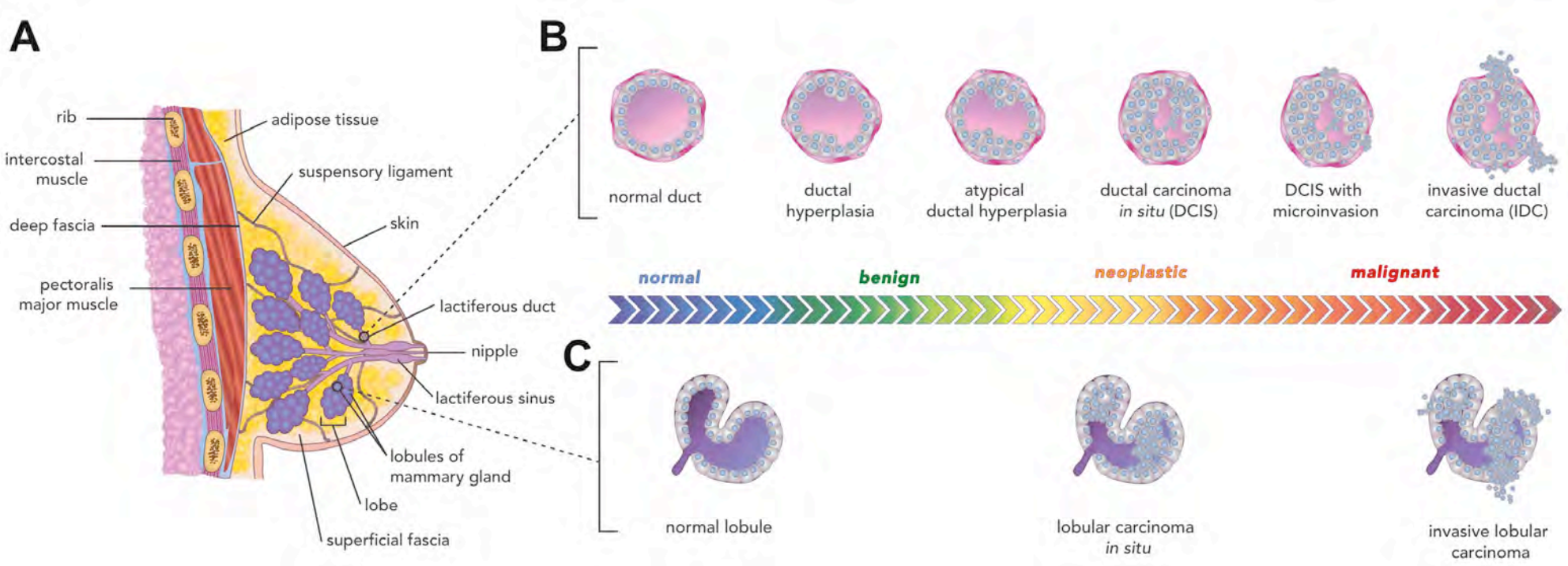

Figure 1.1
Basic breast anatomy (A) and multi-step model of the origins of: (B) ductal (DCIS) and (C) lobular carcinoma in situ (LCIS)

*(1.1A) The adult female breast parenchyma comprises 12 – 20 distinct lobes each feeding into a system of tributary lactiferous ducts opening into the nipple. Clusters of blind-ended terminal ductules and a drainage duct system form the mammary lobule. Both mammary ducts and lobules are encompassed by adipose (fatty) tissue containing supportive fibrocollagenous septa attached to the fascia covering the pectoralis muscle. Columnar or cuboidal epithelium lines each duct (luminal epithelial cells). Myoepithelial cells form a discontinuous circumferential cuff around the luminal epithelial cells. Epithelia of the ducts (intra- and extralobular) and terminal ductules may undergo neoplastic change. Cancers arising from the ducts are ductal carcinomas **(1.1B)**, whilst those originating in the terminal ductules are lobular carcinomas **(C)** (Crum et al 2003, Gudjonsson et al 2005, Stevens and Lowe 2005).*

1.1.2 BrCa risk factors

1.1.2.1 environment and lifestyle

Around 75% of BrCa risk is associated with environmental and lifestyle factors, with age showing the strongest association with BrCa incidence (Jemal *et al* 2011, CR-UK 2014, WHO 2014). On average, 80% of BrCa diagnoses in the UK between 2009 and 2011 were amongst women aged over 50, and as such, age is recognised as a key BrCa risk factor (CR-UK 2014).

Lifestyle is also known to influence BrCa risk. Approximately 27% of BrCa cases in the UK are linked to lifestyle choices that are believed to affect sex-hormone exposure. These include reproductive factors such as young age of first menarche, low or nil parity, older age of first parity and older age of menopause. Hormone-based interventions including oral contraceptives and hormone-replacement therapy also confer a risk of developing BrCa. Due to limited evidence, tobacco smoking is thought to be a probable cause of BrCa, possibly via increasing sex hormone levels, with which BrCa is associated. Alcohol intake is also recognised as a BrCa risk factor, with 6% of BrCa cases in the UK linked to alcohol consumption. However, alcohol is not deemed a BrCa risk factor in BRCA1/2 mutation carriers (CR-UK 2014, CR-UK 2016).

Curiously, some preventable risk factors associated with lifestyle actually confer a protective benefit in early adulthood. The World Cancer Research Fund/American Institute for Cancer Research (WCRF/AICR) classified obesity as a cause of post-menopausal BrCa, but was deemed a protective factor in pre-menopausal BrCa (Lauby-Secretan *et al* 2016, WCRF 2017). In the UK, approximately 9% of female BrCa are linked to excess body weight (Parkin and Boyd 2011).

Furthermore, lack of physical activity has been associated with BrCa risk. Wu *et al's* (2013) meta-analysis showed that BrCa risk decreased by 5% for every 2 hours per week increment in recreational activity (both moderate and vigorous). Indeed, inadequate physical activity (less than 150 minutes moderate physical activity per week) is linked to an estimated 3% of female BrCa in the UK (Parkin 2011).

1.1.2.2 family history

Family history and genetics are linked to approximately 25% of BrCa cases. Risk of developing BrCa doubles in women with one first-degree relative with BrCa compared to women with no first-degree relatives affected by BrCa. However, to put this risk in perspective, 87% of women diagnosed with BrCa have no first-degree relatives with the disease (CR-UK 2016). It is estimated that between 5 – 10% of all breast cancers bear a hereditary component typically presenting with an early age of onset and associated with over-representation of bilateral BrCa, ovarian cancer and male BrCa (Larsen *et al* 2014, Rich *et al* 2014).

1.1.2.3 *BRCA1* and *BRCA2* genes

The most well-known genetic mutations associated with BrCa occur in the *BRCA1* and *BRCA2* tumour suppressor genes, accounting for 25 – 28% of family risk. Germline *BRCA1/2* mutations confer a high risk of ovarian and breast cancers, exhibiting high but incomplete penetrance. However, *BRCA1* and *BRCA2* mutations are relatively rare, respectively affecting 0.11% and 0.12% of the general population. These mutations are associated with approximately 2% of total BrCa cases but account for 15 – 20% of cases with a family history of BrCa amongst first-degree relatives. Risk of developing BrCa amongst *BRCA1/2* mutation carriers may be modulated by other known BrCa risk factors including family history and lifestyle choices (CR-UK 2014, Rich *et al* 2014).

1.1.2.4 other genetic factors

Several autosomal dominant hereditary syndromes are associated with a high lifetime BrCa risk, including Li-Fraumeni and PTEN multiple hamartoma syndromes caused by mutations in tumour protein p53 *(TP53)* and phosphatase and tensin homologue *(PTEN)* genes respectively. Mutations in *CHEK2*, *ATM*, *BRIP1* or *PALB2* genes reportedly confer an immediate BrCa risk to *BRCA1/2* mutation carriers but incidence amongst the general population is rare (CR-UK 2014, Larsen *et al* 2014, Rich *et al* 2014).

Goncalves *et al* (2014) reviewed literature reporting emerging genomic data generated by massively parallel DNA and RNA sequencing strategies on large BrCa genome cohorts. The authors concluded that this volume of data would not only increase our collective understanding of the genetic and epigenetic natural history of breast cancer, but also present novel challenges to established hypotheses regarding breast tumourigenesis.

For example, the emerging importance of epigenetic dysregulation in BrCa was highlighted. Notably, perturbed DNA hypermethylation of promoter CpG islands incurring stable epigenetic transcriptional silencing of tumour suppressor genes (such as the von Hippel-Lindau *(VHL)* gene) has been implicated in carcinogenesis (Tsai and Baylin 2011). Indeed, hypermethylation of CpG islands in the MutL Homologue 1 *(MLH1)* gene promoter region is known to underpin sporadic colorectal carcinomas exhibiting microsatellite instability (MSI) (Nakagawa *et al* 2001).

Goncalves *et al* (2014) urged that the combination of DNA- and RNA-based sequencing studies to unpick BrCa (epi-)genomes, should be augmented with mass-spectrometric characterisation of BrCa proteomes to characterise post-translational modifications (PTMs) occurring at the protein level, for a complete picture of genetic, epigenetic and proteomic factors driving breast tumourigenesis and metastatic disease progression. The authors believed that this holistic approach would expedite translation of genomic understanding of BrCa into demonstrably improved patient outcomes; something that Gonclaves *et al* felt was hitherto lacking in BrCa research.

Subsequently, Cutts *et al* (2015) developed the Breast Cancer Campaign Tissue Bank Bioinformatics portal (BCCTBbp), which seeks to achieve such an integrative, holistic "-omics" approach to translational BrCa research. The BCCTBbp online bioinformatics resource permits integration of genomic, methylomic, transcriptomic, microRNA and proteomic data mined from 146 literature-reported BrCa datasets. The aim of the portal is to augment existing BrCa knowledge and expedite the clinical utility of existing and emerging BrCa research to improve patient outcomes.

Furthermore, the developers hoped that the existence of such an exhaustive online repository of integrated BrCa research would refine design and implementation of future studies; eliminating unnecessary repetition of experiments where validated data already exists. Thus, the pool of scientific knowledge regarding BrCa could be more rapidly augmented through more efficient use of limited research resources to address the most pressing gaps in current knowledge and understanding.

1.1.3 BrCa pathology

1.1.3.1 BrCa natural history

Current understanding of BrCa natural history is founded in histopathological evidence that breast tumourigenesis is a prolonged, multi-step process characterised by sequential histological states, from benign hyperplastic lesions (atypical hyperplasia) through pre-invasive localised neoplastic disease (carcinoma *in situ*), culminating in malignant, invasive BrCa (Figure 1.2) (Arpino *et al* 2005, Hsiao *et al* 2010, Bertos and Park 2011, Viale 2012, Bateman and Shaw 2013, Lakhtakia and Chinoy 2014, WHO 2014, Dai *et al* 2016).

According to this model, *in situ* disease is considered an obligatory prelude to invasive, metastatic disease (Arpino *et al* 2005). Historically it was believed this multi-step model of breast carcinogenesis was driven by a gradual accumulation of genetic mutations underlying observed histological changes, that would eventually spawn cellular variants with invasive, metastatic potential responsible for disease progression and dissemination (Schmidt 2002, Crum *et al* 2003, Schedin and Elias 2004, Arpino *et al* 2005, Tan *et al* 2013, Polyak 2014, WHO 2014).

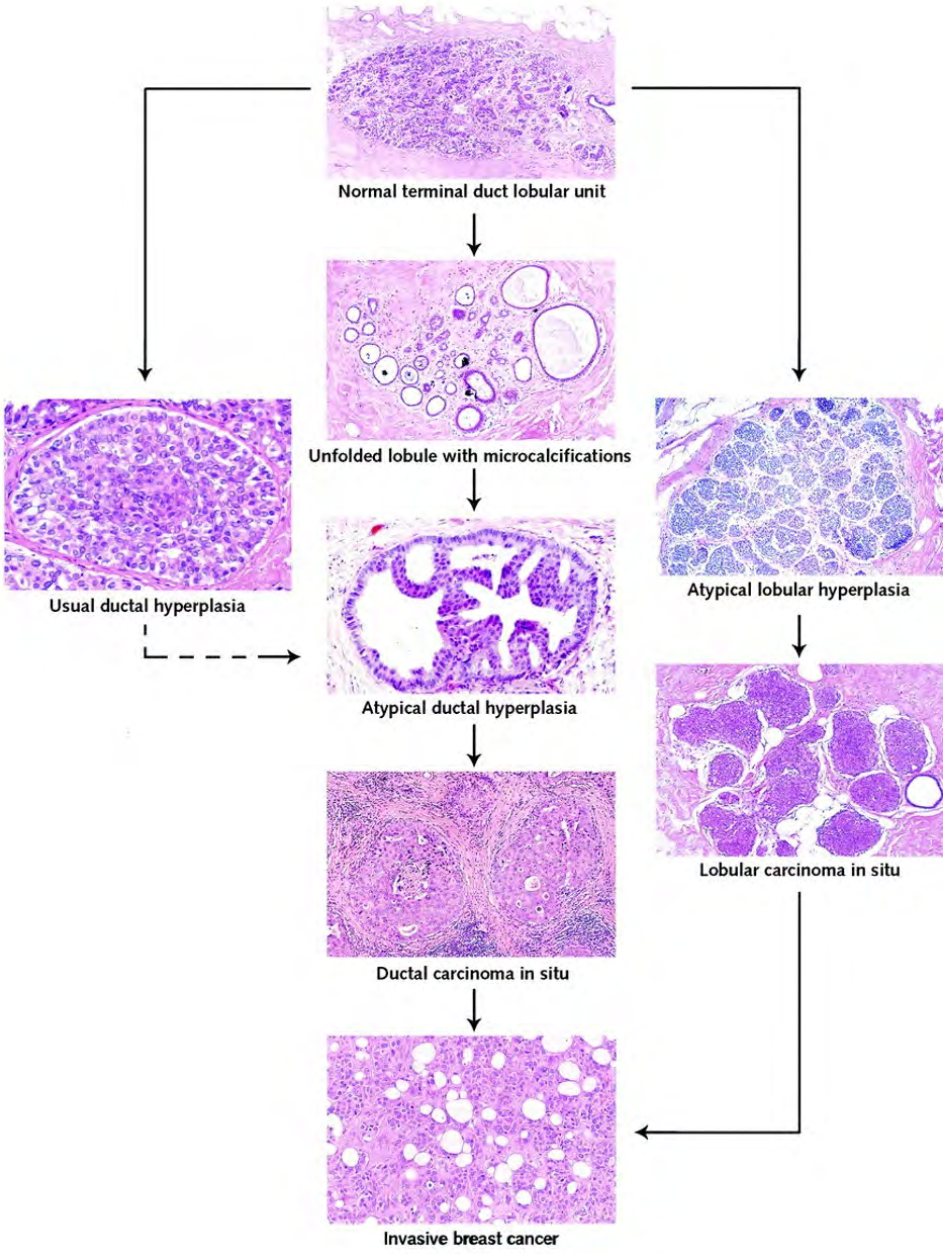

Figure 1.2
An example of the multi-step model of breast tumourigenesis represented by the development of atypical ductal hyperplasia, through DCIS culminating in invasive BrCa

Cells comprising the mammary lobules or ducts may undergo hyperplastic and proliferative changes to acquire a neoplastic phenotype. Progression from in situ to metastatic, disseminated disease is determined by acquisition of invasive potential. A localised tumour remaining bounded by its encompassing basement membrane is deemed to be in situ carcinoma due to the absence of invasion beyond its normal anatomical boundary. However, once the basement membrane delineating the epithelial-stromal interface is breached, the tumour has progressed to invasive disease with the potential for metastatic dissemination (Crum et al 2003, Schedin and Elias 2004, Bertos and Park 2011, Bateman and Shaw 2013). Image adapted from Arpino et al (2005).

1.1.3.2 diagnostics and molecular pathology: informing patient management strategies

Traditional histopathological grading and tumour-node-metastases (TNM) staging of tumours are well-established classification systems for BrCa diagnostics and prognostics, prevailing in clinical practice today (Bertos and Park 2011, Viale 2012, Sinn and Kreipe 2013, Lakhtakia and Chinoy 2014).

In accordance with National Institute of Health and Care Excellence (NICE) quality standards (NICE 2011) and clinical guidelines (NICE 2009a, NICE 2009b), grading and staging of histological features to define morphological BrCa subtype is augmented by ancilliary investigations characterising: tumour oestrogen receptor (ER), progesterone receptor (PR) and human epidermal growth factor receptor 2 (HER2) status for patient stratification and prognostication, to inform patient management by a multidisciplinary team (MDT) of healthcare professionals overseeing the patient care pathway (Crum *et al* 2003, Stevens and Lowe 2005, NICE 2011, Viale 2012, Bateman and Shaw 2013).

1.1.3.3 receptor status in BrCa

Ancillary immunohistochemical (IHC) and/or fluorescence in situ hybridisation (FISH) investigations to establish therapeutically targetable hormone receptor (ER/PR) and HER2 status are respectively vital for patient prognostication and therapeutic stratification (Bertos and Park 2011, Viale 2012, Subbiah and Gonzalez-Angulo 2014, Dai *et al* 2016) and requisite within the UK in accordance with NICE guidance (NICE 2009a, NICE 2009b, NICE 2011).

Tumour receptor status provides valuable predictive information to determine patient eligibility for established targeted therapies. Approximately 70% of sporadic BrCa cases exhibit ER-positivity and 50% are PR-positive whilst in around 15% of cases, HER2 is overexpressed (Hsiao *et al* 2010, Bertos and Park 2011). Breast tumours that do not express any of these molecular targets are classified as triple negative BrCa (TNBC) as they are ER-/PR-/HER2- negative.

In TNBC, the lack of well-defined molecular targets for biological or hormone intervention strategies limit treatment options to standard chemotherapeutics and/or surgery. TNBC tumours are aggressive and associated with poor prognosis if disease progression occurs following chemotherapy (Rodler *et al* 2010, Andre and Zielinski 2012, Engebraaten *et al* 2013, Herold and Anders 2013).

1.1.3.4 intrinsic subtypes in BrCa

Perou *et al's* (2000) landmark paper revolutionised understanding of the molecular pathology underlying BrCa subtypes. This heralded a new age in BrCa classification and molecular taxonomy based on intrinsic gene expression profiles which are continually updated, augmented and refined in accordance with the latest research (Schnitt 2010, Dieci *et al* 2014).

Recent advances in high-throughput technologies permitting molecular and proteomic dissection of BrCa subtypes in large-scale comparative studies have spawned novel molecular classification systems based upon tumour-derived gene-expression profiles. These have provided invaluable insights into the diverse natural history of BrCa and varied therapeutic response through identification of genetic and post-translational drivers inducting and sustaining tumour formation, subsequently driving disease progression and therapeutic resistance. Currently, 5 molecular subtypes are widely recognised (Table 1.1) (Perou *et al* 2000, Sorlie 2009, Hsiao *et al* 2010, Schnitt 2010, Bertos and Park 2011, Polyak 2011, Eroles *et al* 2012, Dieci *et al* 2014).

Molecular subtype	IHC signature	Treatment modality
Luminal A	HER2-; ER+ &/ PR+	Tamoxifen Endocrine therapy
Luminal B	HER2+; ER+ &/ PR+	Trastuzumab Tamoxifen
Basal-like	HER2-; ER-; PR-; HER1+; CK5/6+	Neoadjuvant therapy
HER-2(+)/ER(-)	HER2+; ER- & PR-	Neoadjuvant therapy
Normal breast-like	all markers -	no targeted molecular therapeutics available

Table 1.1
Overview of the five, established intrinsic molecular BrCa subtypes and their respective immunohistochemical (IHC) profiles
Breast tumours may be broadly classified into 5 subtypes based upon expression of oestrogen receptor (ER), progesterone receptor (PR), human epidermal growth factor receptor 1 (HER1 / EGFR), human epidermal growth factor receptor 2 (HER2) and cytokeratins (CK) 5/6. Molecular stratification of tumour type is used to inform choice of appropriate therapeutic intervention. Table adapted from (Hsiao et al 2010).

1.1.3.5 disease progression in BrCa: from *in situ* to invasive disease

It is reported that approximately 20% of all mammography-detected cases in the U.S of BrCa are pre-invasive ductal carcinoma *in situ* (Ernster et al 2002); around 5 100 cases of DCIS are diagnosed in the UK every year (CR-UK 2016). However, robustly defined predictive markers of progression to invasive disease remain elusive; their discovery compounded by the phenotypic heterogeneity exhibited by both *in situ* and invasive breast tumours in terms of clinicopathological features (such as histological grade), ER/PR/HER-2 expression and epidermal growth factor receptor (EGFR) status.

Greater understanding of the molecular, genetic and microenvironmental drivers mediating progression from *in situ* to invasive disease is critical for the identification of novel therapeutic targets to combat metastatic dissemination and alleviate its associated morbidity and mortality (Hu *et al* 2008, Chaffer and Weinberg 2011, Bateman and Shaw 2013, Almendro *et al* 2014, Polyak 2014).

In their DNA microarray analysis of primary breast tumours resected from 117 young BrCa patients (under 55 years of age at diagnosis), van 't Veer *et al* (2002) were the first to characterise a poor prognosis BrCa gene expression signature that was strongly predictive of short interval to distant metastasis that allowed for patient-tailored treatment regimens. The authors concluded that BrCa prognosis may be determined from gene expression profiling of the primary tumour. Logically, amongst the 70 prognostic classifier genes refined by van't Veer from 231 original reporter genes to determine risk of metastasis, were genes associated with rapid progression to metastatic disease; chiefly those known to govern invasion, matrix degradation, angiogenesis, cell motility and survival signalling.

Van't Veer et al's (2003) poor prognosis BrCa gene signature was found to effectively identify high-risk patients who would benefit from adjuvant therapy and also significantly reduce the number of patients subjected to unnecessary treatment. The authors proposed that using such patient-therapy-centric gene expression signatures offered a powerful genomic approach to refine use of adjuvant therapy BrCa intervention to reduce the personal and fiscal costs of BrCa treatment.

Activation of invasion and metastasis has long been deemed a seminal cancer hallmark, heralding disease progression to disseminated disease (Hanahan and Weinberg 2000, Chaffer and Weinberg 2011, Hanahan and Weinberg 2011). Van't Veer and Weigelt (2003) discussed the concept of a "roadmap to metastasis", whereby cancer cell metastatic potential is intrinsically determined early in tumourigenesis. Furthermore, the authors proposed that BrCa cells acquire a gene signature early in tumour development that is predictive of metastatic site.

Veer and Weigelt's (2003) review of gene expression profile studies highlighted that although a poor prognosis gene signature may be a common feature within the primary tumour, subpopulations of cells within the tumour display tissue-trophic gene expression profiles predictive of metastatic site. For example, the expression of osteolytic pathway genes: interleukin-11 (IL-11), chemokine receptor-4 (CXCR-4), matrix metalloprotease-1 (MMP-1) and connective tissue growth factor (CTGF) are associated with BrCa bone metastases.

In their review of emerging BrCa molecular research contextualised within Hanahan and Weinberg's cancer hallmark definitions, Dai *et al* (2016) argued that BrCa subtypes expressing basal, stem cell or epithelial-to-mesenchymal transition (EMT) markers represent tumours bearing the requisite properties for activating invasion and metastasis. Furthermore, the authors argued that these pre-metastatic markers are more likely to be enriched in TNBC and require urgent research focus to identify novel therapeutic strategies to improve patient outcomes.

Li *et al* (2015) reported CpG-island hypermethylation profiles of 7 genes *(**BRCA1**: BReast CAncer 1, **DAPK1**: Death Associated Protein Kinase 1, **MSH2**: MutS Homolgue 2, **CDKN2A**: Cyclin Dependent Kinase iNhibitor 2a, **PGR**: ProGesterone Receptor, **PRKCDBP**: Protein Kinase C Delta Binding Protein, **RANKL**: Receptor Activator of Nuclear factor Kappa-B Ligand*) showing a profound impact on patient outcomes. Analysing a multi-institutional cohort of 123 BrCa patient primary tissue samples, Li and colleagues (2015) compared gene methylation signatures of a 56-gene cancer-specific biomarker microarray in BrCa patients with metastatic cancer or metastatic relapse within 5-years post-operatively, against BrCa patients showing no disease progression. From these analyses, the authors identified a 7-gene panel *(BRCA1, DAPK1, MSH2, CDKN2A, PGR, PRKCDBP, RANKL)* deemed highly prognostic of BrCa progression and metastatic relapse. This study highlights the emerging significance of epigenetic factors, including promoter hypermethylation, during breast tumourigenesis and disease progression.

Furthermore, Lesurf *et al* (2016) compared the mRNA, microRNA (miRNA) and DNA copy-number profiles of a primary human BrCa cohort comprising 59 *in situ* lesions (DCIS) with a cohort of 85 invasive BrCa tumours (IDC). The authors deduced that some molecular features associated with metastatic disease progression in BrCa were unique to intrinsic subtypes; a similar conclusion to that drawn by Dai *et al* (2016) in their meta-analysis. The lack of universal marker(s) identified as predictors of disease progression in the Lesurf study lead the authors to conclude that each BrCa intrinsic subtype is likely to follow its own distinct evolutionary course of disease progression.

Interestingly, Lesurf *et al* (2016) also noted that Gene Ontology (GO) analyses of their dataset revealed prominent molecular traits distinguishing DCIS from IDC are related to the tumour microenvironment, namely pathways involving: cellular

adhesion, extracellular matrix (ECM)-cell receptor interactions and collagen fibril organisation; highlighting the emerging significance of the tumour microenvironment as purveyor of a metastatic niche.

Given the significance of the integrin superfamily in these processes, together with the established association of integrin $\alpha_v\beta_6$ overexpression in transformed adult tissues, it is interesting to postulate the possible role of integrin $\alpha_v\beta_6$ as a driver of tumour microenvironment establishment and regulation (Gumbiner 1996, Felding-Habermann *et al* 2001, Chen *et al* 2003, Felding-Habermann 2003, Srichai and Zent 2010, Bendas and Borsig 2012, Canel *et al* 2013, Paszek *et al* 2014, Du *et al* 2016).

1.1.3.6 the tumour microenvironment in BrCa

In addition to the intrinsic tumourigenic traits of incipient BrCa cells during invasion, the influence of the tumour microenvironment has emerged as an important concept in establishing communication networks driving metastatic disease progression (Calvo and Sahai 2011, Place *et al* 2011, Schedin and Keely 2011, Angelucci *et al* 2012, Bezdenezhnykh *et al* 2014). Indeed, Maller *et al* (2010) reviewed the role of the extracellular matrix (ECM) in driving mammary gland morphogenesis, maintenance of ductal epithelium architecture and its pro-invasive remodelling during carcinogenesis. Hu *et al* (2008) implicate the intricate interplay between tumour-trophic fibroblasts, tumour-suppressive myoepithelial and breast luminal epithelial cells potentiating transition from *in situ* to invasive BrCa. Ingthorsson *et al* (2010) highlight the importance of proliferative regulation by breast endothelial cells within the mammary microenvironment of both normal and malignant breast epithelia.

Heterotypic crosstalk amongst cell adhesion receptors and TGF-β-mediated signalling pathways has been identified as critical for breast tissue homeostasis and its derailment is associated with breast tumourigenesis. The pleiotropic cytokine TGF-β1 performs both tumour suppressive and tumour-trophic roles in the mammary microenvironment (Hu *et al* 2008, Desgrosellier and Cheresh 2010, Munger and Sheppard 2011, Bendas and Borsig 2012, Hale *et al* 2012). It is believed that the combination of epithelial-to-mesenchymal transition (EMT) and acquisition of a neoplastic phenotype in mammary epithelial cells during breast

tumourigenesis and disease progression drives the conversion of TGF-β1 from a tumour suppressor to a tumour promoter (Tang *et al* 2003, Taylor *et al* 2013, Bezdenezhnykh *et al* 2014, Zarzynska 2014, Zhang *et al* 2014).

Given the role of integrin adhesion receptors as key mediators of mechanosignal transduction between cells and their encompassing ECM, together with the reciprocity of integrin-TGF-β1 signalling, integrin-mediated regulation of invasion in BrCa remains a logical and active area of cancer research (White and Muller 2007, Van Aarsen *et al* 2008, Desgrosellier and Cheresh 2010, Margadant and Sonnenberg 2010, Allen *et al* 2011, Munger and Sheppard 2011, Aoudjit and Vuori 2012, Bendas and Borsig 2012, Allen *et al* 2014, Moore *et al* 2014, Truong *et al* 2014).

1.2 the integrin superfamily of adhesion receptors

1.2.1 an overview

The integrin superfamily of ubiquitously expressed, cell-surface type I transmembrane glycoproteins, mediate both intercellular adhesions and interactions between the cell and its encompassing ECM (Figure 1.3). They form obligate heterodimers comprising a large alpha (α) subunit (~120 – 170 kDa) non-covalently associated with a smaller beta (β) subunit (~90 – 100 kDa) (Danen 2013). There are 18 genes encoding the α subunit species and 8 genes encoding the β subunit species, giving rise to the 24 integrin heterodimer species known to exist in humans. The integrins are subclassified according to their heterodimeric constitution, which determines cognate ECM-ligand specificity and tissue distribution/restriction (Humphries *et al* 2003, Byron 2011, Campbell and Humphries 2011).

In both health and disease, many aspects of cell physiology and fate are determined by integrin signalling, including; cell survival, proliferation, differentiation, adhesion, polarity, migration (Shimaoka and Springer 2003, Campbell and Humphries 2011, Munger and Sheppard 2011) and senescence (Rapisarda *et al* 2017). Integrins are capable of modulating many aspects of cell behaviour including cell migration and invasion via physical adhesions established by binding ECM-derived cognate ligands and through bidirectional signal transduction (Bouvard *et al,* 2013; Harburger & Calderwood, 2009; Hood & Cheresh, 2002; Legate *et al,* 2009; Shattil *et al,* 2010).

1.2.2 integrin structure and regulatory motifs

Integrin receptors are typified by a large extracellular domain with short transmembrane and cytoplasmic domains, devoid of any inherent kinase activity. Owing to their lack of intrinsic enzymatic activity, the integrin receptor superfamily relies upon interactions with other intracellular mediators to induct downstream signalling and exert their functional effects. Integrin binding of adaptor proteins requisite for functional outputs is determined by defined amino acid sequences forming regulatory motifs within the cytoplasmic tail domains of the α- and β-integrin subunits (Hynes 2002, Brakebusch and Fassler 2003, Campbell and Humphries 2011, Kim *et al* 2011b).

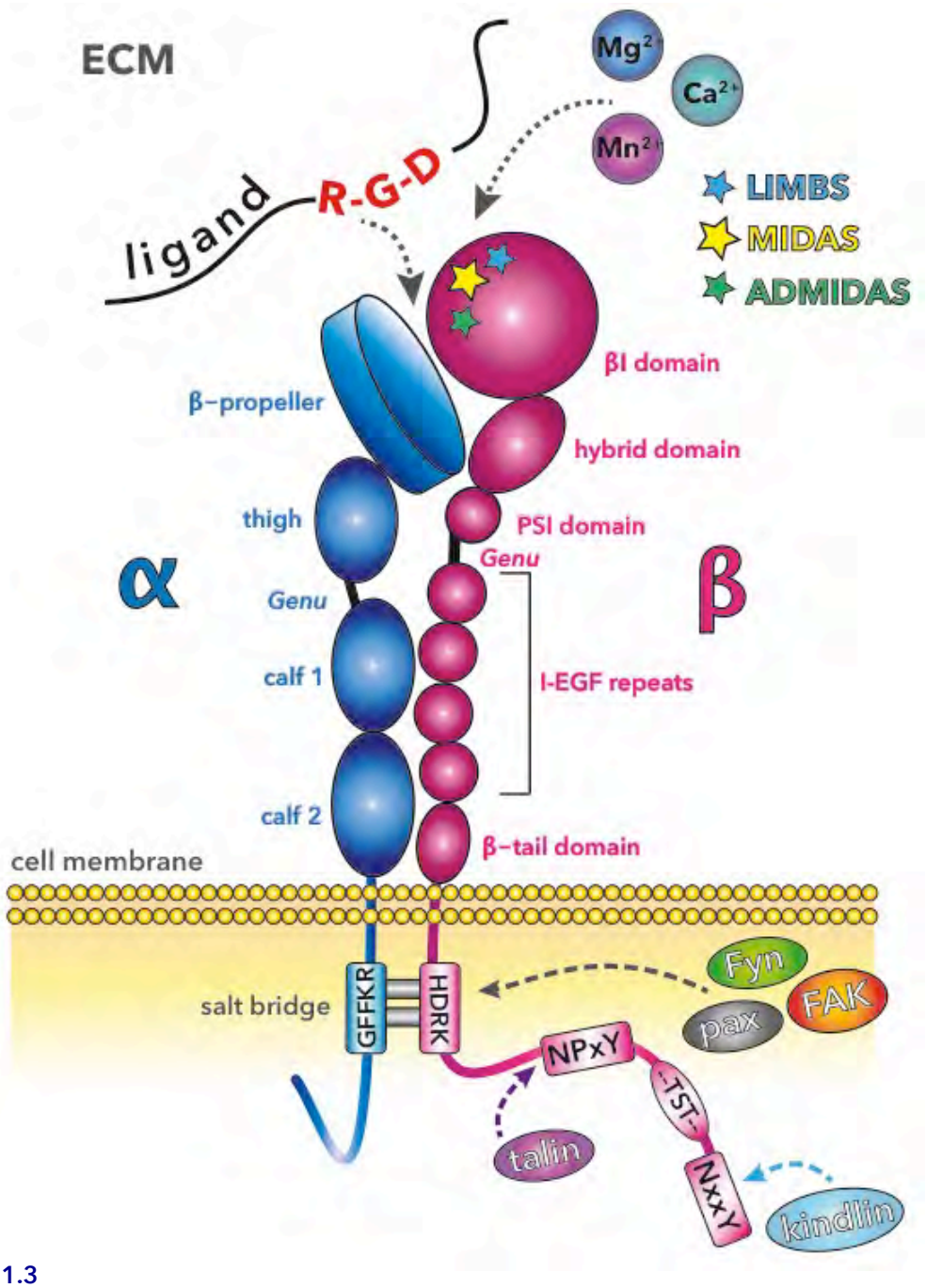

Figure 1.3
The integrin heterodimeric cellular adhesion receptor and its regulatory motifs

Schematic overview of the structure of an integrin receptor, illustrating intracellular regulatory motifs residing within the integrin cytoplasmic tail domains including the evolutionary conserved, calcium-binding repeat I-EGF (epidermal growth factor) domains within the β-subunit and PTB-binding NPxY and NxxY motifs (intersected by a serine-threonine-rich (--TST--) sequence) requisite for adaptor protein recruitment, cytoskeletal association, integrin signalling and functional output. The conserved α-subunit GFFKR and β-subunit HDRK motifs enable subunit association and stabilisation in an inactive integrin receptor conformation. Extracellular motifs residing within the head βI-domain include the divalent metal cation binding sites comprising: a metal ion-dependent adhesion site (MIDAS), adjacent to MIDAS (ADMIDAS) and a synergistic metal ion-binding site (syMBS) formerly ascribed as ligand-associated metal ion-binding site (LIMBS) that act in concert to modulate cognate ligand affinity and binding. Image adapted from Calderwood *et al* (2003).

With short cytoplasmic tails (typically less than 75 amino acids in length), notable sequence homology is shared amongst the β-subunit cytoplasmic domains (cytodomains). Conversely, the α-integrin cytoplasmic tails are markedly divergent, save for a conserved GFFKR motif proximal to the transmembrane region that is requisite for association with the β tail domain and salt bridge formation (Hughes *et al* 1996).

Integrin β cytodomain homology is most highly conserved within 3 defined regions (cytodomains-1, -2 and -3). Using point mutation studies in the avian integrin β_1-subunit, Reszka *et al* (1992) first identified these 3 regulatory amino acid clusters (cyto-1: 764-774; cyto-2:785-788; cyto-3: 797-800) that determine integrin β_1 localisation within focal adhesions (FAs) and heterodimer affinity and specificity. The authors found that membrane-proximal cyto-2 (an NPxY) motif supported structural conformation and integrin β_1 localisation within FAs; whilst membrane-distal cyto-3 (an NxxY motif) was thought to negatively regulate integrin function.

The role of these innate regulatory motifs autonomously governing integrin function is now an established concept. Takagi *et al* (1997) demonstrated the functional significance of disulphide-linked βI-domain sequences determining integrin ligand specificity. The authors found that integrin $\alpha_v\beta_1$ ligand specificity could be manipulated by replacing the integrin β_1 CTSEQNC (187 – 193) βI-domain sequence with the corresponding CYDMKTTC integrin β_3 sequence.

This $\alpha_v\beta_1$-β_3-integrin β_1 mutant variant engaged the integrin $\alpha_v\beta_3$ cognate ligands fibrinogen, von Willebrand Factor and vitronectin; ligands that integrin $\alpha_v\beta_1$ does not recognise. Reciprocal experiments manipulating integrin $\alpha_v\beta_3$ by replacing the CYDMKTTC β_3 sequence with the β_1 CTSEQNC sequence generated an $\alpha_v\beta_3$-β_1-integrin β_3 mutant incapable of binding integrin $\alpha_v\beta_3$ cognate ligands. Takagi et al (1997) therefore concluded that these 2 disulphide βI domain sequences defined a novel regulatory site within β integrin species critical for ligand specificity.

The β_3 integrin cytoplasmic tail domain is frequently used as the template sequence for mapping integrin-binding partner interactions (Legate and Fassler 2009). Firstly, the HDRK (HDRR in β_1 and β_5 integrins) membrane-proximal motif

mediates binding to: skelemin (Reddy *et al* 1998), the Src-family kinase Fyn (Reddy *et al* 2008), FAK and paxillin (Schaller *et al* 1995). For inactive integrins, this β-integrin cytoplasmic tail HDRK sequence binds to the α-integrin tail via formation of a salt bridge between the aspartate (D) residue in HDRK and the arginine (R) of the α-integrin cytodomain GFFKR motif; an interaction that is critical for stabilisation of the integrin heterodimer in the inactive conformation (Hughes *et al* 1996, Legate and Fassler 2009).

The membrane-proximal NPxY and membrane-distal NxxY motifs (flanking a Ser/Thr-rich (TST) intervening sequence) contained within the β-subunit cytoplasmic domain bind cytoskeletal and intracellular signalling proteins bearing a phosphotyrosine-binding (PTB)-domain. Some adaptor proteins bind specifically to a defined integrin species, however many binding partners are more promiscuous and associate with several different integrin cytoplasmic tails; this is particularly true of adaptor moieties binding the NPxY motif, whilst NxxY-binding proteins show more marked restriction for integrin binding (Calderwood *et al* 2003).

Alongside regulatory motifs governing integrin-protein interactions, several sites mediating association of the integrin receptor with divalent metal-cation species are known. These metal-ion binding motifs modulate integrin conformation and ligand affinity. A metal-ion-dependent adhesion site (MIDAS) residing in the α-subunit β-propellor region has been described. In non-αI integrins, a βI domain metal-ion cluster comprising an interlinked linear array of a central MIDAS flanked by the adjacent to MIDAS (ADMIDAS) and synergistic metal ion-binding site (SyMBS), formerly attributed as ligand-associated metal ion-binding site (LIMBS), is reported (Zhang and Chen 2012).

Association of calcium (Ca^{2+}), magnesium (Mg^{2+}) or manganese (Mn^{2+}) ions within these metal-ion motifs regulates integrin function in terms of conformation, ligand affinity and engagement. The ADMIDAS motif has been assigned a negative regulatory role whilst SyMBS is deemed a positive regulator of integrin function (Chen *et al* 2003), with cation occupation of the SyMBS critical for integrin activation (Valdramidou *et al* 2008, Zhu *et al* 2008). In addition to the motif site, the species of cation occupying these motifs is also known to modulate integrin function (Shimaoka *et al* 2002, Craig *et al* 2004, Zhang and Chen 2012).

During biogenesis and assembly in the endoplasmic reticulum, Ca^{2+} is requisite for subunit folding, mediating an inhibitory effect to prevent aberrant activation of nascent integrin receptors en route to the plasma lemma (Tiwari *et al* 2011). Displacement of inhibitory ions with Mg^{2+} or Mn^{2+} ions permits cognate ligand engagement; MIDAS occupation by Mg^{2+} or Mn^{2+} has been found requisite for ligand binding, permitting integrin activation and induction of downstream signalling (Dransfield *et al* 1992, Day *et al* 2002, Shimaoka *et al* 2002, Craig *et al* 2004, Pesho *et al* 2006, Campbell and Humphries 2011, Tiwari *et al* 2011, Zhang and Chen 2012).

1.2.3 integrin activation and signalling

Integrin function is allosterically regulated, whereby receptor conformation critically mediates cognate ligand affinity and downstream signalling events. The integrins are believed to exist in a continuum of conformational states relating to ligand affinity and receptor activation status (Figure 1.4) (Shimaoka *et al* 2002, Shattil *et al* 2010, Campbell and Humphries 2011, Kim *et al* 2011b).

Given their lack of intrinsic enzymatic activity, integrin β-subunit recruitment of multidomain adaptor proteins via their cytoplasmic domain regulatory motifs (NPxY; NxxY), is critical for integrin-mediated structural and signalling functions inducted upon integrin receptor activation; either by intracellular ("inside-out" signalling) or extracellular ("outside-in" signalling) mechanisms of activation (Brakebusch and Fassler 2003).

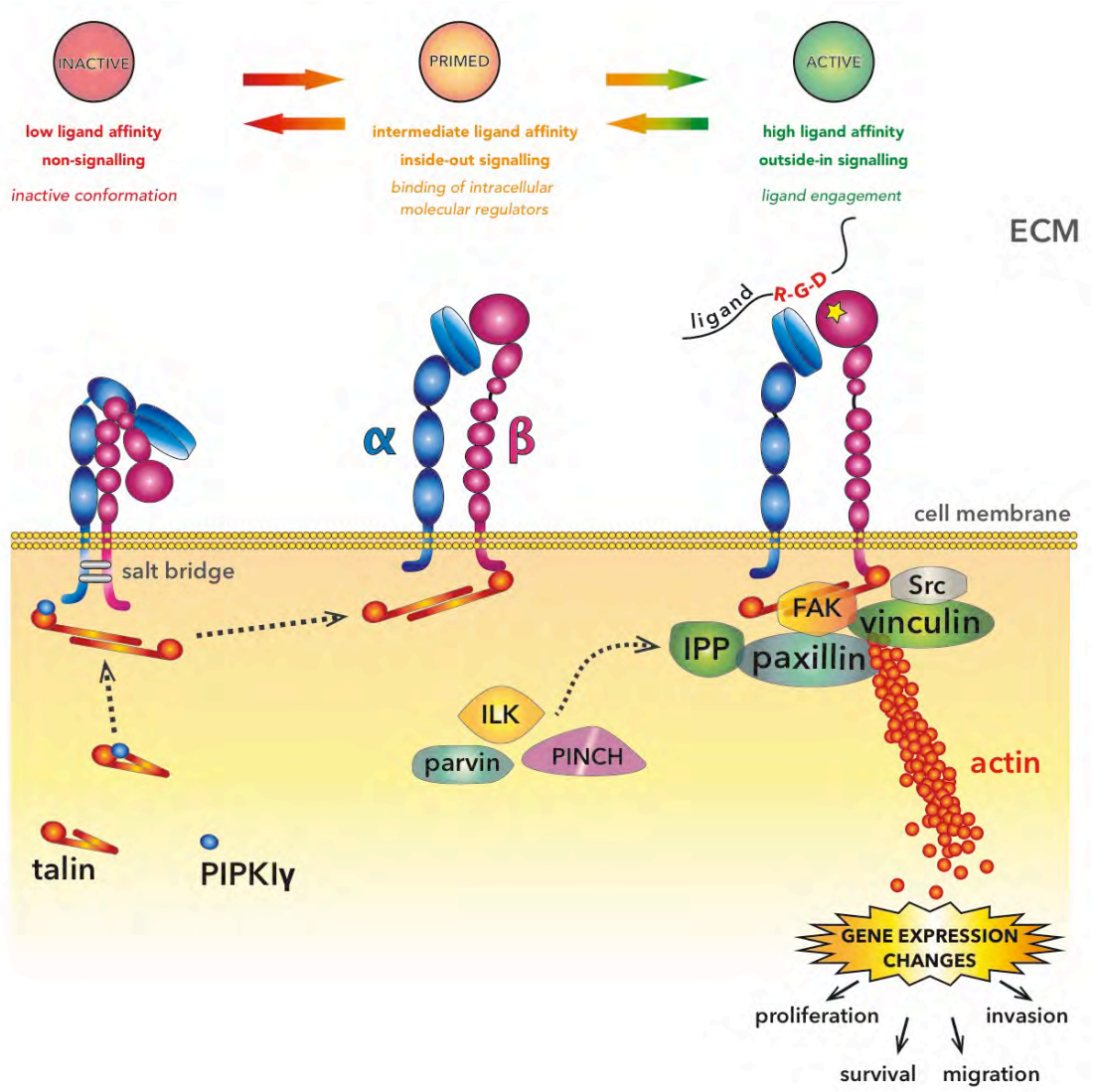

Figure 1.4
Integrins exist in a continuum of activation states (inactive [non-signalling], primed [inside-out signalling] or active [outside-in signalling]) whereby the adopted conformation determines ligand affinity and focal adhesion assembly

The integrins are classified as single-pass Type I transmembrane glycoproteins that form non-covalently associated obligate heterodimers comprising an alpha (α) and beta (β) subunit. These subunits are encoded by 18α- and 8β-integrin genes, giving rise to the 24 known integrin α/β receptor combinations. They are classified into subfamilies based upon their ligand specificity and tissue restriction. Activation and modulation of integrin "outside-in" signalling is influenced by growth factors in addition to the composition and tensile properties of the ECM. These signalling events determine a number of cell properties including survival, proliferation, differentiation, migration, polarity and adhesion. Integrin outside-in signalling determines cytoskeletal actin dynamics, including focal adhesion assembly, critical for tumour cell migration and invasion. Inside-out signalling requires recruitment of intracellular integrin activators, such as kindlins or talin, that bind to the cytoplasmic tail of the β-subunit inducing a conformational change increasing integrin affinity for extracellular ligands. Abbreviations: FAK – focal adhesion kinase; IPP – ILK/PINCH/parvin complex; ILK – integrin-linked kinase; PINCH – particularly interesting Cys-His-rich protein; PIPKIγ – phosphatidylinositol(4)phosphate 5 kinase type I gamma. Image adapted Chen et al (2013).

Integrins in their bent, inactive (non-signalling) conformation may be primed by intracellular regulators of activation (talin, kindlins) to adopt a conformation more receptive to ligand engagement ("inside-out" signalling) (Calderwood *et al* 2013); or upon exposure to extracellular activating moieties such as divalent cations or cognate ligand, adopt the active signalling-replete conformation ("outside-in" signalling) (Smith *et al* 1994, Day *et al* 2002, Chen *et al* 2003, Tiwari *et al* 2011, Zhang and Chen 2012). In both instances, integrin function is critically dependent upon multi-domain adaptor protein recruitment and assembly (Humphries 1996, Humphries 2002, Ziegler *et al* 2008, Harburger and Calderwood 2009, Legate and Fassler 2009, Shattil *et al* 2010, Campbell and Humphries 2011, Wolfenson *et al* 2013).

These adaptor proteins (requisite for integrin-mediated phenotypic outputs) may be broadly classified into 3 function-based categories: i) adaptors with a predominantly structural function coupling integrins to the cytoskeleton (talin, tensin and filamin mediating F-actin binding); ii) scaffolding adaptors bearing binding sites to facilitate recruitment of additional proteins to nascent and maturing focal adhesions (FAs); and iii) adaptor proteins with intrinsic catalytic activity (FAK, ILK) requisite for adhesion-mediated signal-transduction following adhesion complex formation (Legate and Fassler 2009).

Formation of integrin-mediated adhesion complexes is a multi-step process, driven by sequential mechanical and biochemical events. Collectively, advances in super-resolution microscopy, photo-activated localisation microscopy (PALM) and stochastic optical reconstruction microscopy (STORM), have permitted dissection and spatiotemporal characterisation of the dynamic nature of integrin-mediated adhesion complexes; distinguishing nascent from mature complexes and revealing the influence of mechanical force, as well as ligand specificity, on adhesion complex formation (Changede and Sheetz 2017).

It has been shown that upon receptor activation following ECM ligand engagement, integrins cluster to form nascent adhesions roughly 100 nm (±20 nm) in size, comprising approximately 50 integrins associated with talin (-1 or -2), FAK and paxillin (Changede *et al* 2015). Ye *et al* (2014) demonstrated that a novel lateral interaction between integrin transmembrane domains promoted integrin $\alpha_{IIb}\beta_3$ activation and clustering. Subsequent maturation of nascent integrin adhesion clusters is characterised early on by formin-mediated actin

polymerisation at the cytoplasmic interface of the cluster to permit cell spreading (Iskratsch *et al* 2013).

Several mechanisms regulating the spatiotemporal recruitment of adaptor proteins to the β-integrin cytoplasmic tail have been proposed, including: lipid-binding to the PTB domain of adaptor proteins or the direct phosphorylation of residues within the β–integrin cytodomain (Legate and Fassler 2009). The hierarchical binding of adaptor proteins modulates integrin receptor clustering and organisation at the plasma lemma, governing complete receptor activation and downstream signalling (Changede and Sheetz 2017).

The guanine nucleotide exchanger cytohesin-1 has been proposed as a proximal regulator of intracellular integrin activation (Liddington and Ginsberg 2002). Nagel *et al* (1998) reported that cytohesin-1 bound the integrin-β_2 cytoplasmic domain to regulate integrin β_2–mediated adhesion in response to phosphatidylinositol 3-kinase (PI 3-kinase) activation in Jurkat cells. Although cytohesin-1 is deemed integrin β_2–specific, other more general intracellular regulators of integrin activation have been described, including talin.

The homodimeric scaffold protein talin is known to play a critical role in integrin activation via breakage of the salt bridge formed between α and β integrin subunits when in the inactive conformation. This causes the α-β integrin heterodimer cytoplasmic tails to separate, permitting spatially favourable binding of adaptor proteins such as α-actininin, filamin and kindlins (Garcia-Alvarez *et al* 2003, Montanez *et al* 2008, Ziegler *et al* 2008, Critchley 2009, Bouaouina *et al* 2012, Atherton *et al* 2015).

Furthermore, as a structural adaptor, talin interacts with the actin cytoskeleton both directly, and indirectly via vinculin. Talin has also been shown to increase integrin clustering and promote inside-out integrin activation. Talin cooperatively binds the integrin β-subunit and PIP2 (via its FERM domain), promoting integrin clustering and activation by preventing β-integrin cytoplasmic domain interaction with its α-subunit (Ziegler *et al* 2008, Shattil *et al* 2010, Bouaouina *et al* 2012, Orlowski *et al* 2015).

Kindlins (-1, -2 and -3) show sequence homology with the talin FERM domain and demonstrably bind the integrin β-subunit cytoplasmic domain. All three kindlins have been implicated in integrin activation with studies revealing that kindlin binding to the β-integrin cytoplasmic tail is requisite but not sufficient for integrin activation (Calderwood *et al* 2013). Kindlin-2 has been shown to bind the β integrin subunit at its membrane-distal NxxY motif and was found requisite to target integrin-linked kinase (ILK) to adhesion complexes (Montanez *et al* 2008).

In addition to recruitment and binding of adaptor proteins to mediate integrin activation and downstream signalling, integrins themselves have shown the ability to be phosphorylated at serine residues by protein kinase C (PKC). Freed *et al* (1989) demonstrated that β_5 integrin phosphorylation was increased in human fibroblasts and osteosarcoma cells treated with phorbol esters (potent PKC activators). Using PKC$\varepsilon^{-/-}$ cells, Stawowy *et al* (2005) later identified that the PKCε isoform mediated β_1-integrin phosphorylation at Thr788 and Thr789 residues residing within the serine/threonine rich intervening sequence between membrane-proximal and membrane-distal NxxY motifs.

Akt and PDK1 are also thought to be mediators of direct integrin β-subunit phosphorylation. Both Akt and PDK1 have been shown to phosphorylate integrin β_3 at Thr779 in vitro to modulate Shc binding, with Akt activation correlating with β_3-integrin Thr779 phosphorylation *in vivo* (Kirk *et al* 2000). Curiously, using selective-inhibitor studies in primary human platelets, Lerea *et al* (1999) demonstrated that β_3-integrin subunit Thr779 may also be an ERK2 substrate. Later, Ahmed *et al* (2002a) reported a direct interaction between integrin $\alpha_v\beta_6$ and ERK2. Thus, direct phosphorylation of integrin cytoplasmic tail domains, in addition to canonical adaptor protein recruitment, remain areas of active research to further refine our understanding of integrin receptor activation, clustering and downstream signalling driving phenotypic changes.

In addition to molecular regulators instigating integrin activation, negative regulators of integrin activation (or rather, regulators of integrin deactivation) have also been described (Pouwels *et al* 2012). Notably, from an RNAi screen, Rantala *et al* (2011) identified SHANK Associated RH Domain Interactor (SHARPIN) as a putative molecular inhibitor of β_1-integrin activation. The authors found that siRNA-mediated gene silencing of SHARPIN promoted integrin β_1 activation in human prostate cancer (PC3) cells and human primary leucocytes. Furthermore, integrin

β_1 activity was increased in keratinocytes, leucocytes and fibrobalsts isolated from SHARPIN deficient mice but re-expression of SHARPIN rescued phenotype. Rantala and colleagues (2011) also demonstrated that SHARPIN binds a conserved region of integrin α-subunits, inhibiting recruitment of talin and kindlins to the β-subunit cytoplasmic domain thus preventing integrin receptor activation.

A Disintegrin And Metalloprotease domain (ADAM)-23, a member of the ADAM family of type I transmembrane glycoproteins, was reported to specifically interact (via its disintegrin domain) with the integrin $\alpha_v\beta_3$ (Cal *et al* 2000). Later, Verbisck *et al* (2009) demonstrated that ADAM23 negatively regulated integrin $\alpha_v\beta_3$ activation. The authors showed that loss of ADAM23 expression (using shRNA) in MDA-MB-435 BrCa cells promoted integrin $\alpha_v\beta_3$ activation (as discerned by flow cytometry using the active conformer specific anti-integrin $\alpha_v\beta_3$ monoclonal antibody AP5 in comparison with the conformation state-independent antibody LM609 to recognise total integrin $\alpha_v\beta_3$).

Furthermore, shRNA-induced loss of ADAM23 promoted a four-fold increase in MDA-MB-435 cell migration on the integrin $\alpha_v\beta_3$ cognate ligand vitronectin. Evaluation of ADAM23 promoter methylation status in human primary breast tumour samples revealed ADAM23 silencing by promoter hypermethylation was associated with disease progression (development of distal metastases) and worse patient outcomes (shorter 5-year disease-specific survival). These findings lead Verbisck and colleagues (2009) to conclude that ADAM23 negatively regulated integrin $\alpha_v\beta_3$ activation and that promoter hypermethylation-associated loss of ADAM23 expression in human BrCa is a prometastatic risk associated with worse disease outcome; highlighting the significance of aberrant regulation of integrin activation driving disease progression in BrCa.

Therefore, in addition to positive intracellular molecular regulators, it is critical to acknowledge emerging evidence pointing to the existence of counteracting negative regulators of integrin activation requisite to fine-tune the delicate balance of integrin receptor activation, priming and deactivation to maintain a healthy state. Given the critical link between integrin conformation/receptor activation status and downstream signalling capacity, cell adhesion research continues to investigate intra- and extracellular regulators of integrin activation and inactivation. Aberrant integrin activation or impaired conformation is implicated in chronic solid tissue diseases (Wehrle-Haller and Imhof 2003) such as organ fibrosis (Khan and

Marshall 2016) including pulmonary (Munger *et al* 1999) and renal fibrosis (Hahm *et al* 2007); and coagulation disorders typified by Glanzmann thrombasthaenia (Nurden 2006).

Altered integrin cellular adhesion repertoires are of emerging significance within cancer research (Desgrosellier and Cheresh 2010). Acquisition of an invasive phenotype enabled by perturbed integrin expression and activation leading to a loss of epithelial polarity and gain of motility has been hypothesised (Guo and Giancotti 2004, Mosesson *et al* 2008), and is now an established, active area of cancer research, notably in BrCa (Aoudjit and Vuori 2001, Felding-Habermann *et al* 2001, Arjonen *et al* 2012, Vazquez Rodriguez *et al* 2017).

Therefore, the ability to restore integrin function and activation status to that of a healthy state with targeted therapeutics, would alleviate the burden of chronic disease, or progression to metastatic disease dissemination in cancer, mediated by integrin conformation defects or aberrant integrin signalling. However, this requires refining our understanding of integrin activation and signalling modalities; thus ongoing research to robustly characterise mechanisms of integrin regulation is duly warranted.

1.2.4 integrins and cancer

Previous studies have demonstrated integrin overexpression frequently occurs in a variety of cancers, including BrCa. Their regulatory role modulating cellular adhesion and survival signals during migration and invasion to facilitate tumour progression continues to be investigated in the hope of identifying novel therapeutic targets (Aoudjit and Vuori 2001, Jin and Varner 2004, White and Muller 2007, Desgrosellier and Cheresh 2010, Allen *et al* 2011, Taherian *et al* 2011, Aoudjit and Vuori 2012, Allen *et al* 2014). An emerging concept is the significance of the active, signalling-replete integrin subpopulation during cancer progression (Aoudjit and Vuori 2001, Felding-Habermann *et al* 2001, Taherian *et al* 2011, Eberlein *et al* 2013, Lee *et al* 2013, Li *et al* 2013).

1.2.4.1 integrin activation status in cancer

Felding-Habermann *et al* (2001) demonstrated *in vitro* and *in vivo* that integrin $\alpha_v\beta_3$ in its active but not its inactive state, enabled tumour cell-thrombocyte interactions to circumvent anoikis facilitating establishment of a metatstatic phenotype in the MDA-MB-435 BrCa cell line. It was concluded that anomalous integrin activation may induct an adverse course of BrCa.

Lee *et al* (2013) demonstrated that β_1 integrin was constitutively active in prostate cancer cell lines with known high metastatic potential in comparison with those of low metatstatic potential. Furthermore, *in vivo* antibody-blockade of constitutively active β_1 integrin demonstrably inhibited prostate cancer metastasis and was associated with reduced phosphorylation of integrin β_1 downstream effectors focal adhesion kinase (FAK) and Akt. The authors found increased β_1 integrin activation correlated with metastatic potential *in vivo*, further implicating the significance of aberrant integrin activation states during tumour progression.

Arjonen *et al* (2012) demonstrated that distinct trafficking kinetics of the active and inactive β_1 integrin conformers modulate cell surface availability of these two receptor pools in the MDA-MB-231 BrCa cell line. Although both β_1 conformations undergo clathrin- and dynamin-dependent endocytosis, the net rate of internalisation was higher for active β_1 compared to inactive β_1, however the inactive β_1 is more rapidly recycled back to the plasma membrane via a short, Rab4-dependent trafficking route. In addition to activation-induced trafficking

routes, integrin activation status has been implicated in spatial restriction of the active integrin pool to localise and direct integrin-mediated functions. Dozynkiewicz *et al* (2012) reported Rab25 was seen to spatially restrict recycling of active, ligand-engaged integrin $\alpha_5\beta_1$ conformers to the tips of invasive protusions in ovarian cancer cells migrating through a 3D-matrix.

Collectively, these findings would suggest recognition of integrin activation status by the endocytic machinery to modulate internalisation rates and intracellular trafficking routes as determined by integrin conformation. The mechanisms by which this may occur are as yet undefined and warrant further investigation. However, Bouvard *et al* (2013) acknowledge the link between integrin activation status and endocytic regulation remains open to debate, with current evidence suggesting endocytosis of active integrins may be restricted to fibroblasts and cancer cells. Thus, integrin receptor endocytic trafficking during tumourigenesis and disease progression is a burgeoning area of research.

1.2.4.2 intracellular trafficking of integrins

In addition to integrin activation status, derailed endocytic receptor trafficking is an emerging cancer hallmark with postulated roles in both tumourigenesis and disease progression (Mosesson *et al* 2008). Rainero *et al* (2013) comprehensively reviewed current research concepts that indicate integrin internalisation, intracellular trafficking and recycling routes determine cancer cell migration and invasion. Broadly, these phenomena cooperate to control the spatial restriction of integrin receptors used by migrating (and invading) cells during physiological conditions but undergo marked derailment during tumourigenesis.

Interactions between integrin adhesion receptors and receptor tyrosine kinases (RTKs) that synergistically modulate internalisation kinetics and trafficking routes of both receptor classes is of growing research interest given the potential implications for combination targeted therapies. Muller *et al* (2009) reported the importance of p53 mutations perturbing both integrin and RTK recycling to potentiate invasion and metastasis during disease progression. Interestingly, it has been observed that the Rab-GTPase components of vesicle trafficking pathways exhibit both tumour suppressor and oncogenic functions in human cancers. It is postulated that oncogenic programming of Rabs is modulated by trafficking

events themselves. Thus, research seeking to define the mechanisms by which the aforementioned phenomena occur is ongoing. It is hoped that this will highlight novel targets for therapeutic intervention to combat the activation of invasion and metastasis associated with cancer progression (Dozynkiewicz *et al* 2012, Rainero *et al* 2012, Rainero *et al* 2013).

Active endo-exocytic cycling of fibronectin (Fn)-binding integrin receptors was first reported by Bretscher (1989). Subsequent studies have demonstrated that integrins may undergo endo-exocytic cycling via both "short-loop" and "long-loop" trafficking pathways after internalisation into early endosomes (EEs) such that the total cell surface pool of integrin receptors may be routed through the endosomal machinery once every 30 minutes (Roberts *et al* 2001, Rainero *et al* 2013). Short-loop recycling is characterised by rapid redelivery of EE receptor cargo to the plasma membrane.

Conversely, long-loop trafficking pathways are characterised by slower recycling kinetics with delivery of EE cargo to the perinuclear recycling complex (PNRC) for endosomal sorting for either degradation or recycling to the plasma membrane. Spatial redistribution of integrin receptors as determined by endocytic internalisation and intracellular trafficking is now known to be critical for maintenance of cell polarity and control of cell motility through predominantly retrograde movement (from cell front to cell rear) of integrin bulk translocation (Caswell and Norman 2006).

Integrins may endocytose via many of the established internalisation routes including macropinocytosis, caveolin-dependent pathways, clathrin-dependent pathways or via clathrin-independent carriers. The internalisation kinetics and routes of all 24-integrin species are not yet fully characterised or understood. Studies of integrin $\alpha_5\beta_1$ suggest that specific integrin heterodimers are not restricted to a single-entry route. The integrin $\alpha_5\beta_1$ has been shown to undergo both clathrin-dependent and clathrin-independent internalisation routes highlighting the complexity of endocytic integrin regulation (Teckchandani *et al* 2012, Rainero *et al* 2013).

1.2.4.3 integrin-RTK crosstalk during trafficking

Intracellular trafficking and signalling by integrins has been shown to dictate internalisation and recycling of other endocytic cargoes, such as RTKs, in an integrin-heterodimer-specific manner. This phenomenon emerged during integrin blockade studies, notably during evaluation of the cyclic pentapeptide Cilengitide (cyclo-RGDfNmeV) as an anti-angiogenic therapeutic to abrogate integrin $\alpha_v\beta_3$ and $\alpha_v\beta_5$ function. It was found that when integrin $\alpha_v\beta_3$ was able to engage cognate ligand(s), recycling of the RTK vascular endothelial growth factor receptor 2 (VEGFR2) was slow but compensated for by rapid VEGFR2 degradation upon VEGF engagement (Reynolds *et al* 2009, Millard *et al* 2011).

However, integrin $\alpha_v\beta_3$ functional blockade induced rapid recycling of VEGFR2 via a Rab4-dependent short loop, which circumvented VEGFR2 degradation, leading to an increase in the available cell-surface pool of VEGFR2. As a functional consequence of this, tumour vascularisation was promoted due to upregulation of VEGF-mediated endothelial cell migration and angiogenic sprouting. Furthermore, the proangiogenic effects of Cilengitide were seen to be dose-dependent (Reynolds *et al* 2009).

In addition to modulating RTK trafficking, integrin functional blockade has been shown to induce compensatory "integrin switching". During integrin $\alpha_v\beta_3$ blockade experiments using Cilengitide, a compensatory upregulation of other integrin species was reported. Caswell *et al* (2008) defined a Rab-coupling protein (RCP)-driven integrin $\alpha_5\beta_1$ compensatory switch inducted upon integrin $\alpha_v\beta_3$ abrogation leading to formation of an integrin $\alpha_5\beta_1$–RCP complex. The $\alpha_5\beta_1$–RCP complex recruits epidermal growth factor receptor (EGFR), an event that potentiated increased EGFR recycling and signalling to drive invasive cell migration.

The phenomena of compensatory integrin switching and perturbation of RTK-integrin synergy post integrin functional blockade has important ramifications for the development and future applications of integrin-targeted therapies. Hence, further characterisation of the complexities of integrin internalisation, trafficking and recycling remains paramount in order to expedite the translation of integrin-centric therapies from laboratory bench to bedside.

1.2.4.4 integrin-targeted therapeutics

Given the established role of integrins in both health and disease, considerable efforts have been undertaken to develop targeted therapeutics to abrogate aberrant function or harness the power of tissue-restricted integrin expression to refine specificity of drug delivery (Millard *et al* 2011, Jiang *et al* 2013, Raab-Westphal *et al* 2017). A range of therapeutic moieties have been synthesised including monoclonal antibody therapies, small molecule inhibitors and peptide-based therapeutics (summarised in Figure 1.5).

Interestingly, integrin antagonist therapies in use or successfully reaching late-stage clinical trials are directed against the ligand-binding site or the ligand itself (Hamidi *et al* 2016, Ley *et al* 2016). Best typifying the state of integrin therapeutics are those targeting the human platelet integrin $\alpha_{IIb}\beta_3$ for thrombotic disorders (Raab-Westphal *et al* 2017). Abciximab (ReoPro, clone 7E3), a Fab' fragment chimeric mouse-human monoclonal antibody targeting the human platelet integrin $\alpha_{IIb}\beta_3$ (but with specificity for $\alpha_v\beta_3$ and $\alpha_M\beta_2$) was the first integrin antagonist therapy clinically approved in 1994 for perioperative use in percutaneous coronary intervention by the US Food and Drug Administration. Its mechanism of action is direct competitive inhibition of the $\alpha_{IIb}\beta_3$ ligand-binding site, thus preventing platelet aggregation (Tam *et al* 1998).

Also targeting the platelet integrin $\alpha_{IIb}\beta_3$ are the synthetic cyclic heptapeptide Eptifibatide and the non-peptide small molecule inhibitor Tirofiban, both of which are also competitive inhibitors of fibrinogen ligand binding to ablate thrombosis formation. Apticide (Tc-99m-P280) was developed as a non-therapeutic imaging peptide that binds integrin $\alpha_{IIb}\beta_3$ to permit diagnostic imaging of deep vein thromboses (Millard *et al* 2011). Collectively, the integrin $\alpha_{IIb}\beta_3$ therapeutics exemplify the potential utility of clinical integrin targeting; their failure to gain widespread clinical application proving demonstrative of the complexities and pitfalls in translating novel molecular-based therapies into routine medical practice.

The integrin $\alpha_v\beta_6$ has also been targeted as a potential point for cancer therapy intervention strategies using monoclonal antibodies (264RAD, Oncology iMED AstraZeneca UK and STX-100, Biogen Idec); or for tumour PET-imaging using radio-labelled peptides (GSK3008348, GlaxoSmithCline Plc).

Antibody STX-100 was in a phase 2 clinical trial for nephropathy and idiopathic pulmonary fibrosis, which completed in May 2017 (ClinicalTrials.gov Identifier NCT01371305) but results are pending publication. The PET-imaging agent is currently in phase 1 clinical trials for idiopathic pulmonary fibrosis (ClinicalTrials.gov Identifier NCT03069989) (Raab-Westphal *et al* 2017). It will be interesting to evaluate the efficacy of these integrin $\alpha_v\beta_6$ targeted agents when trial results are published.

Pre-clinical data for the antibody 264RAD is promising, as a stand-alone, but more interestingly, as a component of combination therapy regimens in BrCa (Moore *et al* 2014) and pancreatic ductal adenocarcinoma (PDAC) (in-house data pending publication). Its application in conjunction with trastuzumab therapy was seen to have an augmentative effect, potentiating the efficacy of HER-2 targeting with trastuzumab in HER-2 positive BrCa *in vitro* and *in vivo* by a mechanism not yet defined but apparently mediated by Akt2 (Moore *et al* 2014). Thus, the potential utility of co-targeting relevant integrin receptor species in tandem with existing, defined therapeutics is an exciting and growing area of integrin-focussed research.

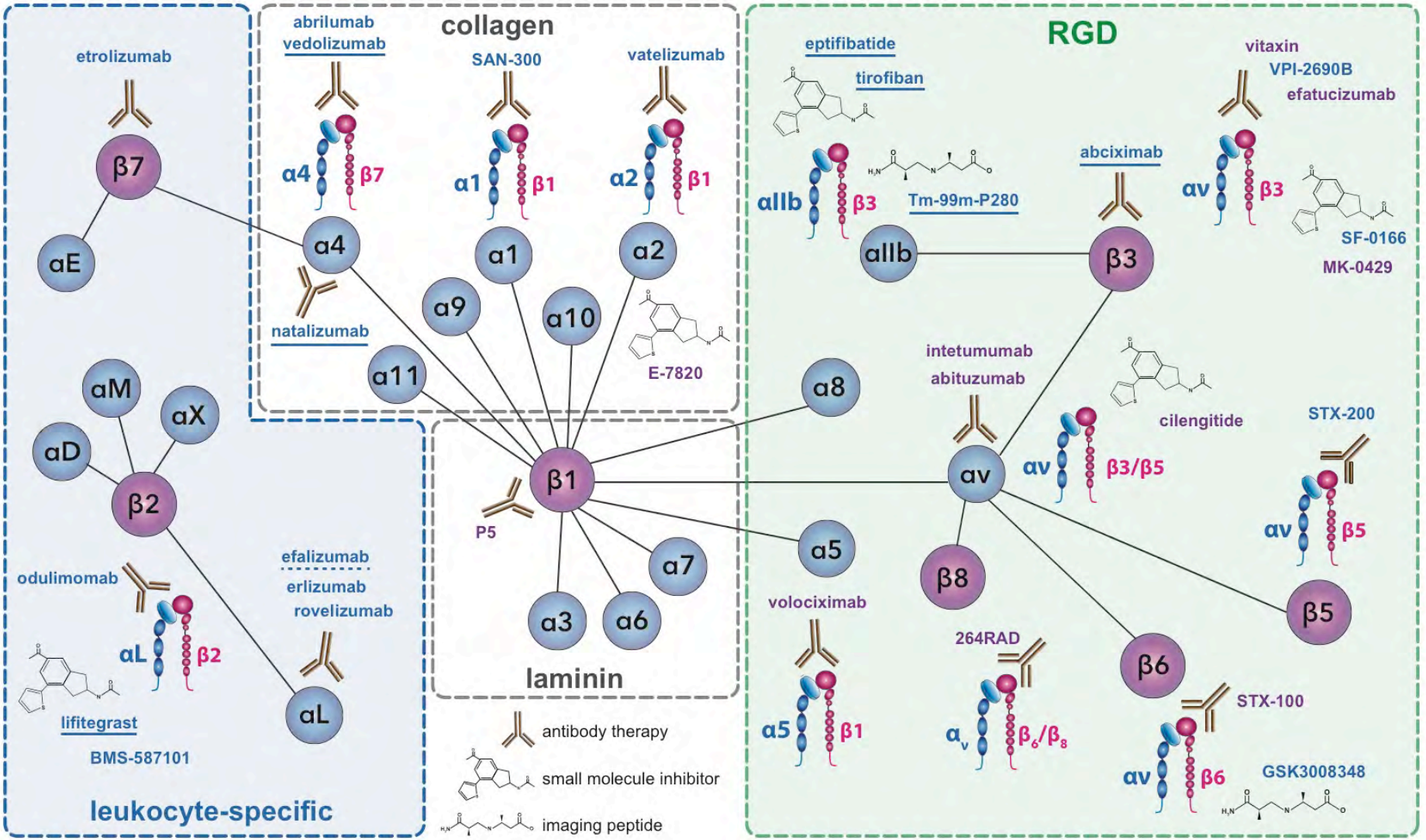

Figure 1.5

Integrin receptor classes, their ligand-specificities and targeted therapies

Figure prepared for publication in press (Raab-Westphal et al 2017). See figure legend overleaf.

Figure 1.5
Integrin receptor classes, their ligand-specificities and targeted therapies

Schematic overview of the integrin receptor classes, heterodimer subunit associations and their ligand specificities together with targeted therapies reaching clinical trials published to date. Marketed therapeutic agents currently available in clinic are underlined (abciximab, epitifibatide, lifitegrast, natalizumab, tirofiban, Tm-99m-P280, vedolizumab). Agents reaching the market but withdrawn are indicated with a dashed underline (efalizumab). Cancer therapeutics are written in purple script (abituzumab, cilengitide, efatucizumab, intetumumab, MK-0429, P5, STX-100, volociximab). Subunit-specific or heterodimer targeting is indicated. Figure prepared for publication in press (Raab-Westphal et al 2017) based on Hynes' (2002) map of integrin receptor classes and ligand specificities.

1.2.5 the integrin $\alpha_v\beta_6$

Expression of the epithelial-restricted integrin $\alpha_v\beta_6$ is low to absent in health, but is upregulated during embryogenesis, tissue morphogenesis (development), trauma, chronic inflammation and wound-healing (Khan and Marshall 2016). Integrin $\alpha_v\beta_6$ frequently localises at the invasive front of neoplastic cells implicating its involvement during cellular invasion and metastasis. Tumoural expression of integrin $\alpha_v\beta_6$ is a poor prognostic indicator in a variety of cancers, including BrCa (Nystrom *et al* 2006, Thomas *et al* 2006, Van Aarsen *et al* 2008, Margadant and Sonnenberg 2010, Saha *et al* 2010, Allen *et al* 2014, Moore *et al* 2014).

Although the α_v subunit may heterodimerise with β_1, β_3, β_5, β_6 or β_8 integrins, β_6 dimerisation is restricted to the α_v subunit. Our current mapping of integrin β_6–subunit structure is inferred from other RGD-binding β integrins (Humphries 2002, Humphries *et al* 2003, Luo *et al* 2007, Zhu *et al* 2008, Campbell and Humphries 2011). The integrin $\alpha_v\beta_6$ binds cognate ligands in the ECM bearing an RGD tripeptide motif. A metal ion-dependent adhesion site (MIDAS) provides a site for divalent cation binding, which potentiates ligand-engagement (Hynes 2002, Humphries *et al* 2003, Craig *et al* 2004, San Sebastian *et al* 2006, Bouaouina *et al* 2012, Zhang and Chen 2012).

Integrin structure as defined by X-ray crystallography has not yet been explicitly elicited for the β_6 subunit. However, research published by Dr Timothy Springer's lab (Springer Lab, Department of Biological Chemistry and Molecular Pharmacology, Harvard Medical School, Boston MA, USA) has revealed important insights into integrin β_6 structure and regulatory functional motifs. Dong *et al* (2014) defined the molecular mechanism establishing integrin $\alpha_v\beta_6$ high specificity for the RGD tripeptide motif residing in the prodomains of latent transforming growth factor (TGF)-β1 and TGF-β3.

Using a combination of crystallographic structural analysis, point mutation studies and peptide affinity measurements, Dong and colleagues demonstrated that integrin $\alpha_v\beta_6$ binds TGF-β1 and TGF-β3 with high affinity via an RGDLXXL/I motif within the TGF-β1/3 prodomains; with the LXXL/I amphipathic α-helix binding in a hydrophobic pocket within the β_6-subunit. Furthermore, the authors identified 3

distinct βI-domain loops (named "specificity-determining loops" (SDLs): SDL-1 (β1-α1 loop), SDL-2 (β2-β3 loop) and SDL-3 (α2-α3 loop) that contributed to ligand binding specificity.

To define the basis of the unparalleled high affinity of integrin $\alpha_v\beta_6$ for pro-TGF-β (and its derived peptides), Dong and colleagues (2014) elucidated the structure of the integrin $\alpha_v\beta_6$ headpiece. The authors mapped 3 proximally arranged metal ion-binding sites in the βI domain: SyMBS, MIDAS and ADMIDAS (as had been determined previously for other βI domain-bearing integrin species). In the absence of ligand, the integrin $\alpha_v\beta_6$ headpiece adopts a closed conformation. In the presence of ligand (pro-TGF-β), it was found that the aspartate residue of RGD coordinated the MIDAS-metal ion inducing headpiece opening in the presence of both Mg^{2+} or Ca^{2+}. Interestingly, the authors attributed the high affinity and selectivity of integrin $\alpha_v\beta_6$ for pro-TGF-β to the interaction between the β_6 hydrophobic pocket and TGF-β LXXL/I amphipathic α-helix motif; conferring 1000-fold selectivity for pro-TGF-β over the RGD motif present in Fn, and 1000-fold selectivity over integrin $\alpha_v\beta_3$ for pro-TGF-β engagement.

Integrin receptors typically possess a large extracellular domain for ligand engagement comprising multiple modular domains, a short single-spanning transmembrane domain of around 25 – 29 amino acid residues and a short, unstructured cytoplasmic tail devoid of any intrinsic enzymatic activity. Thus, integrin signalling is entirely dependent on the recruitment of adaptor proteins (Danen 2013). Several well-defined regulatory motifs have been identified in the β integrin C-terminus that bind many integrin-binding proteins such as talin and the kindlins. These include a membrane proximal NPxY and membrane distal NxxY motifs on the β integrin tail, which are classic phosphotyrosine-binding (PTB) domains (Legate and Fassler 2009).

Several integrin $\alpha_v\beta_6$ direct-binding partners have been reported. Using a cDNA library screen, Ramsay *et al* (2007) identified HS1-Associated Protein X-1 (HAX-1) as a novel β_6-integrin binding partner and successfully confirmed this by coimmunoprecipitation of HAX-1 and the β_6–subunit. A direct physical association between ERK2 and the β_6 subunit has also been described (Ahmed *et al* 2002a) and the Four and a Half LIM protein 2 (FHL2) was shown to associate with the cyto-3 NxxY motif of the β_6-subunit (Wixler *et al* 2000).

In addition, the β_6 tail domain bears a unique 11 amino acid sequence (EKQKVDLSTDC) requisite for integrin $\alpha_v\beta_6$-dependent invasive processes via direct association with psoriasin (S100A7) in OSCC cell lines (Morgan et al 2011). Indeed, transfection of these 11 amino acid residues into the C-terminus of the integrin β_3 subunit was previously found to promote MMP-2 or MMP-9-mediated $\alpha_v\beta_3$–dependent invasion in OSCC cells (Morgan *et al* 2004), demonstrative of the functional significance of this integrin β_6 tail motif.

Experimental studies have demonstrated that integrin $\alpha_v\beta_6$ imparts a pro-invasive and more aggressive phenotype in oral squamous carcinoma (OSCC) (Table 1.2) (Thomas *et al* 2001b, Nystrom *et al* 2006, Thomas *et al* 2006) and BrCa (Allen *et al* 2014, Moore *et al* 2014). Furthermore, functional blockade of integrin $\alpha_v\beta_6$ has been shown to reduce $\alpha_v\beta_6$–mediated proliferation, survival and tumour progression in several cancer models, highlighting its potential utility as a therapeutic target.

Both Van Aarsen *et al* (2008) and Eberlein *et al* (2013) demonstrated *in vivo* inhibition of tumour progression via functional antibody-blockade of integrin $\alpha_v\beta_6$ using antibodies 6.3G9 and 264RAD respectively. Mechanistically, abrogation of integrin $\alpha_v\beta_6$ activity was seen to modulate TGF-β1 activity in xenografts of Detroit 562 human pharyngeal cancer cell lines in both studies. Eberlein and colleagues (2013) demonstrated similar abrogation of integrin $\alpha_v\beta_6$–protumourigenic activity on orthotopic 4T-1 murine breast tumour growth in vivo.

Later, Eberlein *et al* (2015) determined that non-small cell lung carcinoma (NSCLC) cells expressing E-cadherin, EpCAM and integrin $\alpha_v\beta_6$ were able to activate normal human dermal fibroblasts via integrin $\alpha_v\beta_6$-dependent TGF-β1 signalling to modify gene expression and therapeutic response. The mechanism of activation was abrogated using 264RAD to ablate integrin $\alpha_v\beta_6$ function. The authors concluded that although tumour cell initiated fibroblast activation is integrin $\alpha_v\beta_6$ dependent, once co-opted fibroblasts acquired an active phenotype, sustenance of TGF-β1 signalling was mediated by other TGF-β pathway regulators to maintain an activation loop. Therefore, the role of tumour cell integrin $\alpha_v\beta_6$–dependent signalling (both autocrine and paracrine) during stromal modification in cancer progression warrants further investigation.

Tumour-trophic function	Comment	Cell type
TGF-β activation	Binds & activates latent TGF-β1	Keratinocytes
Invasion & migration	Promotes migration over known adhesion substrates LAP, Fn & Vn. Promotes invasion through upregulation of MMP-3 and MMP-9.	Keratinocytes OSCC
Proliferation & survival	Upregulation is protective against anoikis via activation of Akt-dependent survival signals	OSCC

Table 1.2
Summary of tumour-trophic properties of integrin $\alpha_v\beta_6$ expression demonstrated in keratinocytes and oral squamous cell carcinoma (OSCC) cells
Table content adapted from Thomas et al (2006), Thomas et al (2002) and Thomas et al (2001a). *Integrin $\alpha_v\beta_6$ expression has been implicated in tumour progression. Its tumour-trophic functions have been summarised here.* Abbreviations: Fn – *fibronectin;* MMP – *matrix metalloproteinase;* OSCC – *oral squamous cell carcinoma;* TGF-β1 – *transforming growth factor-β;* Vn – *vitronectin.*

In a large BrCa patient cohort, Moore *et al* (2014) correlated integrin $\alpha_v\beta_6$ overexpression with poor survival and increased distal metastases, demonstrative of the clinical significance of integrin $\alpha_v\beta_6$. Furthermore, using *in vivo* BrCa models the authors demonstrated that integrin $\alpha_v\beta_6$ blockade reduced tumour growth and metastasis. Of particular interest, is their finding that $\alpha_v\beta_6$ functional abrogation potentiated trastuzumab efficacy in an *in vivo* model of HER2-driven BrCa. This infers integrin $\alpha_v\beta_6$ cooperates with HER2 to modulate HER2 signalling capacity and oncogenic effects, concordant with previous hypotheses that integrins may modulate RTK endocytic fate to drive disease progression (Caswell *et al* 2008, Muller *et al* 2009, Rainero *et al* 2013).

Since Ramsay *et al* (2007) demonstrated HAX-1-dependent endocytosis of integrin $\alpha_v\beta_6$ was requisite for $\alpha_v\beta_6$-mediated invasive processes in OSCC, it is possible that the oncogenic effects of $\alpha_v\beta_6$ in BrCa may also be driven by endo-exocytic kinetics. However, little is currently known regarding regulation of integrin $\alpha_v\beta_6$ internalisation and intracellular trafficking. Several protein-binding partners have been implicated in integrin $\alpha_v\beta_6$ endocytic regulation including HAX-1 and psoriasin (Morgan *et al* 2011).

It is known that integrin $\alpha_v\beta_6$ is one of the cell surface receptors to which the foot and mouth disease virus (FMDV) binds to mediate infection of bovine epithelia. Using this mechanism as a model to study integrin $\alpha_v\beta_6$ internalisation and trafficking, Berryman *et al* (2005) demonstrated that integrin $\alpha_v\beta_6$ undergoes

clathrin-dependent endocytosis to mediate FMDV infection, a process that required endosomal acidification.

In addition to integrin-GFR synergistic interactions, integrin crosstalk with other adhesion receptors has also been identified as a regulatory checkpoint during integrin endo-exocytic cycling. Notably, Src-mediated phosphorylation of the proteoglycan ECM-receptor syndecan-4 was found to be a critical switch governing the balance between endo-exocytic cycling of integrins $\alpha_v\beta_3$ and $\alpha_5\beta_1$. Upon syndecan-4 phosphorylation by Src, integrin $\alpha_v\beta_3$ recycling was promoted at the expense of integrin $\alpha_5\beta_1$, leading to accumulation of integrin $\alpha_v\beta_3$ at the plasma membrane facilitating adhesion complex stabilisation.

In the absence of Src-mediated syndecan-4 phosphorylation, $\alpha_5\beta_1$ recycling to the plasma membrane was upregulated to promote focal adhesion turnover. Tight control of this integrin $\alpha_v\beta_3/\alpha_5\beta_1$ switching phenomenon was deemed essential for efficient cell migration (Morgan *et al* 2013). Since integrin $\alpha_v\beta_6$ has been shown to co-localise with syndecan-4 (unpublished data), it is possible that integrin $\alpha_v\beta_6$ endo-exocytic cycling kinetics may also be subject to regulation by phosphorylation of associated adhesion receptors to elicit similar integrin switching phenomena.

The pro-tumourigenic phenotypic effects imparted by integrin receptor switching were investigated by Janes and Watt (2004). Since integrin $\alpha_v\beta_5$ expression is downregulated whilst integrin $\alpha_v\beta_6$ is upregulated during transformation from healthy stratified squamous epithelia to squamous cell carcinoma (SCC), the authors sought to characterise the functional effects of this alteration in integrin receptor profile. Based on their findings, Janes and Watt (2004) proposed that integrin $\alpha_v\beta_6$ expression conferred a survival advantage over integrin $\alpha_v\beta_5$ expression by promoting Akt-dependent survival signals, enabling circumvention of anoikis. However, a mechanism was not elucidated to account for the integrin $\alpha_v\beta_6$-dependent nature of Akt signalling observed.

The protumourigenic effects of integrin $\alpha_v\beta_6$–associated Akt-dependent survival signalling is concordant with the findings of Moore *et al* (2014) that functional ablation of integrin $\alpha_v\beta_6$ using the monoclonal therapeutic antibody 264RAD

induced a significant downregulation in Akt2 expression in vivo in human HER-2-driven BrCa xenograft models. Collectively, these data would suggest functional outputs downstream of integrin $\alpha_v\beta_6$ are likely to be Akt dependent. Further characterisation of this phenomenon is warranted in light of integrin- $\alpha_v\beta_6$ targeted therapies currently in development.

The integrin $\alpha_v\beta_6$ is now of emerging significance as predictive of progression to invasive disease within the context of DCIS. Using immunohistochemical assessment of archival FFPE samples from a historical cohort of 532 ductal carcinoma *in situ* (DCIS) patients, Allen *et al* (2014), demonstrated that integrin $\alpha_v\beta_6$ expression was significantly ($p<0.006$) predictive of progression from *in situ* to invasive disease.

In addition, Allen and colleagues (2014) established that myoepithelial cell integrin $\alpha_v\beta_6$ positivity occurred with greater frequency in DCIS with associated invasion compared to pure DCIS with no evidence of microinvasion or invasion. Furthermore, their analysis of 52 case-control DCIS samples with accompanying long-term clinical follow-up data acquired from the UK, Australia and New Zealand ductal carcinoma *in situ* (UK/ANZ-DCIS) Trial (Cuzick *et al* 2011) revealed that integrin $\alpha_v\beta_6$ expression is a significant predictor ($p<0.02$) of invasive progression and disease recurrence.

In adjunctive functional investigations to elucidate a putative mechanism by which myoepithelial integrin $\alpha_v\beta_6$ expression may determine invasive risk in DCIS, Allen *et al* (2014) established that myoepithelial cells expressing integrin $\alpha_v\beta_6$ promoted tumour cell invasion *in vitro* in the MCF-7, MDA-MB-231 and T47D breast cancer cell lines when treated with conditioned media from an immortalised myoepithelial cell line transduced to constitutively and stably overexpress the integrin β_6 subunit (β_6-1089) compared to cells treated with conditioned media from non-transfected β_6 cDNA–null 1089 myoepithelial cells (N-1089).

Furthermore, myoepithelial integrin $\alpha_v\beta_6$ expression was reported to promote breast tumour growth *in vivo* when the mammary fat pads of female C.B-17 SCID mice were injected with MDA-MB-231 mixed with β_6-1089, compared to those co-injected with MDA-MB-231 and N-1089 cells. Based on MMP-9 gelatin zymography and TGF- β1 reporter assay results (subsequently corroborated by

IHC coincidental immunopositivity for both integrin $\alpha_v\beta_6$ and MMP-9 in clinical FFPE sections of DCIS with invasion), Allen *et al* (2014) concluded that myoepithelial integrin $\alpha_v\beta_6$ expression conferred a tumourigenic growth advantage. The authors proposed that integrin $\alpha_v\beta_6$–mediated MMP-9 upregulation and TGF-β1 activation established a pro-invasive tumour niche facilitating disease progression.

This study highlights the aetiopathological significance of integrin $\alpha_v\beta_6$ as a participant moiety in a regulatory hub modulating MMP-9 and TGF-β1 activity working in concert to generate and establish a pro-invasive tumour microenvironment. Indeed, integrin $\alpha_v\beta_6$ acting in concert with other MMP moieties has been implicated as a significant pro-invasive factor in other malignancies, not only BrCa.

For example, Thomas *et al* (2002) demonstrated that upregulation of integrin $\alpha_v\beta_6$ promoted MMP-3 activation and potentiated OSCC migration and invasion on fibronectin (Fn). Furthermore, Impola *et al* (2004) proposed MMP-7, MMP-9 and MMP-12 as prognostic markers (concomitant with integrin $\alpha_v\beta_6$ overexpression) at the invasive fronts of oral verrucous and OSCC cells. Al-Hazmi *et al* (2007) characterised a positive feedback loop governing MMP-2/MMP-9 activation in the VB6 OSCC cell line engineered to overexpress integrin $\alpha_v\beta_6$, whereby cell migration on Fn was enhanced by MMP-2/-9 activity which subsequently enhanced cell motility and MMP secretion.

Collectively, these studies reveal the putative significance of integrin $\alpha_v\beta_6$ as a regulatory node coordinating TGF-β1 and MMP activity, modulating ECM remodelling and protease-driven invasive processes in cancer. If integrin $\alpha_v\beta_6$ receptor activation status could be demonstrated within the context of these findings, it may be possible to define the spatiotemporal role of integrin $\alpha_v\beta_6$ activation and associated signalling within the natural history of the tumour microenvironment.

Specific discrimination between inactive (non-signalling) and active (signalling replete) integrin $\alpha_v\beta_6$ receptor pools would permit unequivocal determination of the sequential significance of integrin $\alpha_v\beta_6$ activation to elucidate its pathological role as an initiator, a driver or a responsive sequela in the invasive niche.

Collectively, there is a resounding evidence base to justify research seeking to further define the role of the integrin $\alpha_v\beta_6$ and its activation status during breast tumourigenesis and disease progression. It is hoped that this research will provide novel insights into mechanisms regulating integrin $\alpha_v\beta_6$ activation and downstream signalling pathways; in the hope that predictive biomarkers and/or potential regulatory nodes suitable for targeted therapy may be identified to improve patient outcomes.

1.3 scope and purpose of study

Given its established pro-invasive and poor-prognostic association during tumourigenesis, further characterisation of the mechanisms by which integrin $\alpha_v\beta_6$ mediates invasion and metastatic dissemination in BrCa is warranted. Indeed, therapeutic exploitation of integrin $\alpha_v\beta_6$ functional blockade using monoclonal antibodies in both stand-alone and combination treatment modalities for BrCa, is already a realistic prospect (Moore *et al* 2014).

There is a groundswell of evidence to support the hypotheses that both integrin activation status and intracellular trafficking kinetics potentiate disease progression in several *in vivo* cancer models (Arjonen *et al* 2012, Eberlein *et al* 2013), including BrCa (Felding-Habermann *et al* 2001, Moore *et al* 2014). Thus, targeting aberrant activation and/or derailed internalisation and intra-cellular trafficking kinetics may prove viable and effective aspects of integrin $\alpha_v\beta_6$ adhesion receptor biology ripe for therapeutic exploitation and intervention. However, to facilitate investigations dissecting the relevance of integrin activation status in BrCa, a robust means by which the active, signalling-replete conformer of the integrin $\alpha_v\beta_6$ may be distinguished from the inactive, non-signalling subpopulation must first be devised and validated.

Furthermore, it must be acknowledged that the mechanisms by which the downstream phenotypic effects of integrin $\alpha_v\beta_6$ are elicited both pre- and post-receptor functional abrogation, remain unknown. This impeding dearth of existing experimental evidence to define signalling events and network integration mediated by the integrin $\alpha_v\beta_6$ assuredly merits exploration of both the integrin $\alpha_v\beta_6$ adhesome and kinome to identify novel molecular regulators of the integrin $\alpha_v\beta_6$ adhesive and signalling functions respectively.

Therefore, dissecting the regulatory mechanisms governing key facets of integrin $\alpha_v\beta_6$ functional biology including; $\alpha_v\beta_6$-mediated adhesive processes, putative $\alpha_v\beta_6$-RTK cross-talk, ECM ligand-induced $\alpha_v\beta_6$-activation and ensuing internalisation, in tandem with their associated downstream signalling motifs, is critical if the clinical utility of the integrin $\alpha_v\beta_6$ in novel targeted therapies is to be realised.

1.4 hypothesis, aims and objectives

1.4.1 hypothesis

The aetiopathological significance of the cellular adhesion receptor integrin $\alpha_v\beta_6$ during neoplastic transformation and malignant progression in BrCa is dependent specifically upon its activation status and associated conformation, since this active state will permit establishment of known integrin–mediated oncogenic signalling that underpins acquisition of a malignant phenotype, including activation of invasion and metastasis. It is hypothesised that the pool of activated, signalling replete integrin $\alpha_v\beta_6$ receptors are both conformationally and functionally distinct from the inactive, non-signalling receptor pool, with the active conformers specifically mediating integrin $\alpha_v\beta_6$–derived phenotypic changes during oncogenic transformation of the breast and progression to disseminated disease.

1.4.2 aims and objectives

Within the scope and purpose of this study, this project seeks to:

i) establish a means by which the active subpopulation of integrin $\alpha_v\beta_6$ may be distinguished using monoclonal antibodies to permit further investigations into activation status

ii) once validated, employ monoclonal antibodies to evaluate the relevance of the active fraction of integrin $\alpha_v\beta_6$ during BrCa carcinogenesis using an vitro model of breast tumourigenesis and disease progression (the MCF10 isogenic model)

iii) develop, optimise and use a label-free proteomics strategy to identify novel molecular regulators modulating ligand engaged integrin $\alpha_v\beta_6$-mediated adhesions in a 2D-environment to define the integrin $\alpha_v\beta_6$ adhesome

iv) develop and apply a phosphoproteomic strategy to dissect integrin $\alpha_v\beta_6$-mediated downstream signalling events inducted upon cognate ECM ligand-engagement and subsequent receptor-ligand internalisation facilitating definition of an integrin $\alpha_v\beta_6$-kinome.

chapter II

materials & methods

II
materials & methods

2.1 cell culture

All cell lines were obtained from in-house stocks (Centre for Tumour Biology, Barts Cancer Institute, QMUL, London) and authenticated at a commercial facility by short tandem repeat (STR) profile analysis at 16 loci (PowerPlex® 16 HS 16 Loci Service, (LGC©Standards 2011)). Cell lines were cultured in the absence of antibiotics and antimycotics at 37°C in a humidified atmosphere with 8% CO_2 and passaged subconfluent (60 – 90%) to retain the exponential growth phase. Whilst in culture, cell morphology was reviewed routinely by phase contrast microscopy *(OLYMPUS IMT-2, Olympus Corp.)* for rudimentary evaluation of phenotypic stability and cell condition.

Young *et al* (2010) acknowledge the critical requirement for routine Mycoplasma spp. screening in cell culture, since infection is known to modify cellular physiology, eliciting deleterious effects on experiment validity. Therefore, all cell lines were regularly tested for *Mycoplasma spp.* infection by nested polymerase chain reaction (PCR) to ensure experimental procedures were performed on cells free from occult infection by Mycoplasma species (Dobrovolny and Bess 2011).

Derivation of cell lines used in this study together with their respective specific culture requirements are summarised in Tables 2.1 – 2.3. Details of tissue culture reagents and media supplements are given in Table 2.4.

Cell line	Aetiology & Derivation	Culture Conditions	Comment/Experimental Applications
A375puro	Tumourigenic human melanoma cell line derived from a metastatic malignant melanoma (MM) isolated from a 54-year old female engineered to express the puromycin resistance gene. Karyotype: hypotriploid (Kogelberg *et al* 2008, ATCC 2012a, Man *et al* 2013, Pisano *et al* 2013, Prat *et al* 2013).	Adherent growth DMEM/10% FBS/$_{L}$-glutamine	Used as negative control cell line for integrin $\alpha_v\beta_6$ expression.
A375β6	Derived from the A375 parent cell line and engineered to constitutively overexpress the integrin β_6 subunit. A375 cells were infected with pBabe retroviruses encoding puromycin resistance or additional cDNA for human integrin β_6 subunit. Cells were selected in 1.25 μg ml^{-1} puromycin with subsequent sorting by magnetic beads using the integrin $\alpha_v\beta_6$ specific antibody clone 10D5 (MAB2077Z, Merck Millipore) (Hausner *et al* 2007, Kogelberg *et al* 2008).	Adherent growth DMEM/10% FBS/ 2 mM $_{L}$-glutamine	Used as positive control cell line for integrin $\alpha_v\beta_6$ expression. Expression of integrin $\alpha_v\beta_6$ in this cell line is known to drift. Monthly assessment of integrin $\alpha_v\beta_6$ expression levels by flow cytometry should be undertaken for cells in continuous passage. Re-selection in puromycin or magnetic bead sorting using antibody clone 10D5 (Merck Millipore) may be undertaken as required (Hausner *et al* 2007, Kogelberg *et al* 2008).
DX3puro	Human melanoma cell line derived from a metastatic malignant melanoma engineered to express the puromycin resistance gene. Endogenously expresses several integrins but not the β_6 subunit (Hausner et al 2007).	Adherent growth DMEM/10% FBS/ 2 mM $_{L}$-glutamine	Used as negative control cell line for integrin $\alpha_v\beta_6$ expression.
DX3β6puro	Derived from the DX3 parent cell line (Albino et al 1981) and engineered to constitutively overexpress the integrin β_6 subunit. DX3 cells were infected with pBabe retroviruses encoding puromycin resistance or additional cDNA for human integrin β_6 subunit. Cells were selected in 1.25 μg ml^{-1} puromycin with subsequent sorting by magnetic beads using the integrin β_6 specific antibody clone 10D5 (MAB2077Z, Merck Millipore) (Hausner et al 2007, CRT 2013).	Adherent growth DMEM/10% FBS/ 2mM $_{L}$-glutamine	Used as positive control cell line for integrin $\alpha_v\beta_6$ expression. Expression of integrin $\alpha_v\beta_6$ in this cell line is known to drift. Monthly assessment of integrin $\alpha_v\beta_6$ expression levels by flow cytometry should be undertaken for cells in continuous passage. Re-selection in puromycin or magnetic bead sorting using antibody clone 10D5 (Merck Millipore) may be undertaken as required (Hausner et al 2007, CRT 2013)
VB6	Generated by retroviral transfection of the $\alpha_v\beta_5$ expressing human V3 cell line with β_6 integrin subunit cDNA yielding constitutive high expression of the β_6 integrin heterodimer. The V3 cell line being originally engineered from the α_v integrin subunit negative H357 oral squamous cell carcinoma cell line transfected with α_v integrin subunit DNA (Thomas *et al* 2001a, Nystrom *et al* 2006)	Adherent growth KGM: α-MEM/10% FBS/ 2mM $_{L}$-glutamine insulin [10 μg ml^{-1}] EGF [20 ng ml^{-1}] HC [500 μg ml^{-1}] CT [100 ng ml^{-1}]	Used as positive control cell line and functional model of integrin $\alpha_v\beta_6$ overexpression.

Table 2.1: Malignant melanoma (MM) and oral squamous cell carcinoma (OSCC) cell lines employed in this study as integrin $\alpha_v\beta_6$ positive and negative control cell lines.
These cell lines were previously engineered and established in-house for use as matched pair biological models of integrin $\alpha_v\beta_6$ overexpression and negative correlates. Information on cell line aetiology and derivation is provided and referenced in table text. **Abbreviations: α-MEM** – *Minimum Essential Medium alpha modifications; American* **ATCC** – *American Type Culture Collection;* **CRT** – *Cancer Research Technology© Ltd;* **DMEM** – *Dulbecco's Modified Eagle Medium;* **FBS** – *foetal bovine serum;* **KGM** – *keratinocyte growth medium*

Cell line	Aetiology	Culture Conditions	Comment
MCF-10A	Non-tumourigenic human breast cell line originating from spontaneous immortalization of non-malignant fibrocystic mammary epithelium isolated in August 1984 during reduction mammoplasty from a 36 year old Caucasian, parous premenopausal female with no family history of breast malignancy. The cell line was derived from the adherent sub-population of cells in culture in standard calcium levels (1.05 mM) (Soule *et al* 1990, Dawson *et al* 1996, ATCC 2012b). **Receptor status:** Triple negative (ER- / PR- /ERBB2/HER2-) **Subtype:** Basal B	Adherent growth. DMEM/Ham's F12 (1:1)/5% HS/ 2mM $_{L}$-glutamine insulin [10 µg ml^{-1}] EGF [20 ng ml^{-1}] HC [500 µg ml^{-1}] CT [100 ng ml^{-1}]	The MCF-10 sublines were derived by extended culture in low calcium (0.03 – 0.06 mM) with passage of floating cells (MCF-10F), or by trypsin-Versene passage of adherent cells (MCF-10A) cultured in customary calcium levels (1.05 mM). MCF-10 was deemed by Soule *et al* (1990) to possess traits of normal breast epithelium based upon the criteria: i) absence of tumourigenicity in nude mice; ii) growth in culture controlled by requisite growth factors and hormones; iii) confluent cultures exhibit dome formation; iv) absence of anchorage-independent growth and v) 3-dimensional growth in collagen.
MCF-10AT (-AT) *(formerly designated MCF10A-neoT)*	Transformed variant derived by transfection of the MCF-10A cell line with a plasmid vector (pHo6T1) containing the T24 Ha-ras oncogene and aminoglycoside phosphotransferase gene conferring resistance to geneticin enabling antibiotic selection (Basolo *et al* 1991, Dawson *et al* 1996, Heppner *et al* 2000).	Adherent growth. DMEM/Ham's F12 (1:1)/5% HS/ insulin/2mM $_{L}$-glutamine/EGF/HC/CT (concentrations as above)	Example of proliferative breast disease that is tumourigenic but not metastatic (neoplastic but non-malignant) (Tang *et al* 2003, Kadota *et al* 2010).
MCF-10AT1K.cl2 (-K.cl2)	Clone isolated from cells derived from an enzymatically dissociated xenograft of MCF-10AT1 cells (derived from a 100-day first transplant generation lesion) that produced carcinoma *in vivo* in nude/beige mice. The derived clone, MCF-10AT1K.cl2 generates premalignant lesions capable of neoplastic progression (Tang *et al* 2003).	Adherent growth DMEM/Ham's F12 (1:1)/5% HS/ insulin/2mM $_{L}$-glutamine/EGF/HC/CT (concentrations as above)	Example of proliferative breast disease that is neoplastic and may spontaneously acquire an invasive phenotype.
MCF10-DCIS.com (-DCIS.com)	Cloned from the cell culture of a xenograft generated by injection of premalignant MCF-10A cells into SCID mice that resulted in tumour growth (Heppner *et al* 2000, Miller *et al* 2000, Barnabas and Cohen 2013)	Adherent growth DMEM/Ham's F12 (1:1)/5% HS/2mM $_{L}$-glutamine	Recapitulate DCIS-like comedo lesions spontaneously progressing to IDC as xenografts in SCID mice.
MCF-10A.CA1h (-CA1h)	Derived by serial trocar passage of MCF-10AT1K.cl2 xenografts in nude/beige mice generating the MCF-10ACA1 lines giving rise to tumours directly upon transplantation. Organoids extracted from a trocar passage tumour were xenografted into nude/beige mice. The CA1h subclone was then isolated from the resulting tumour and cloned in agarose (Strickland *et al* 2000, Santner *et al* 2001, Tang *et al* 2003)	Adherent growth DMEM/Ham's F12 (1:1)/5% HS/2mM $_{L}$-glutamine	Tumourigenic, malignant. Form well-differentiated carcinomas upon xenografting.
MCF-10A.CA1a (-CA1a)	Derived by serial trocar passage of MCF-10AT1K.cl2 xenografts in nude/beige mice generating the MCF-10ACA1 lines giving rise to tumours directly upon transplantation. The CA1a subclone was isolated by *in vitro* selection, along with other variants (CA1b, CA1c, CA1d) (Strickland *et al* 2000, Santner *et al* 2001, Tang *et al* 2003).	Adherent growth DMEM/Ham's F12 (1:1)/5% HS/2mM $_{L}$-glutamine	Tumourigenic, malignant. Form poorly differentiated carcinomas upon xenografting and metastasise to lungs upon tail vein injection.

Table 2.2: The MCF-10 isogenic series of human breast cancer cell lines employed in this study.
Information compiled from references provided in text. **Abbreviations: CT** *– cholera toxin;* **DCIS** *– ductal carcinoma in situ;* **DMEM** *– Dulbecco's Modified Eagle Medium;* **EGF** *– epidermal growth factor;* **FBS** *– foetal bovine serum;* **HC** *– hydrocortisone;* **HS** *– horse serum;* **IDC** *– invasive ductal carcinoma;* **MCF** *– Michigan Cancer Foundation;* **RP MI 1640** *– Roswell Park Memorial Institute 1640 medium;* **SCID** *– severe combined immunodeficiency.*

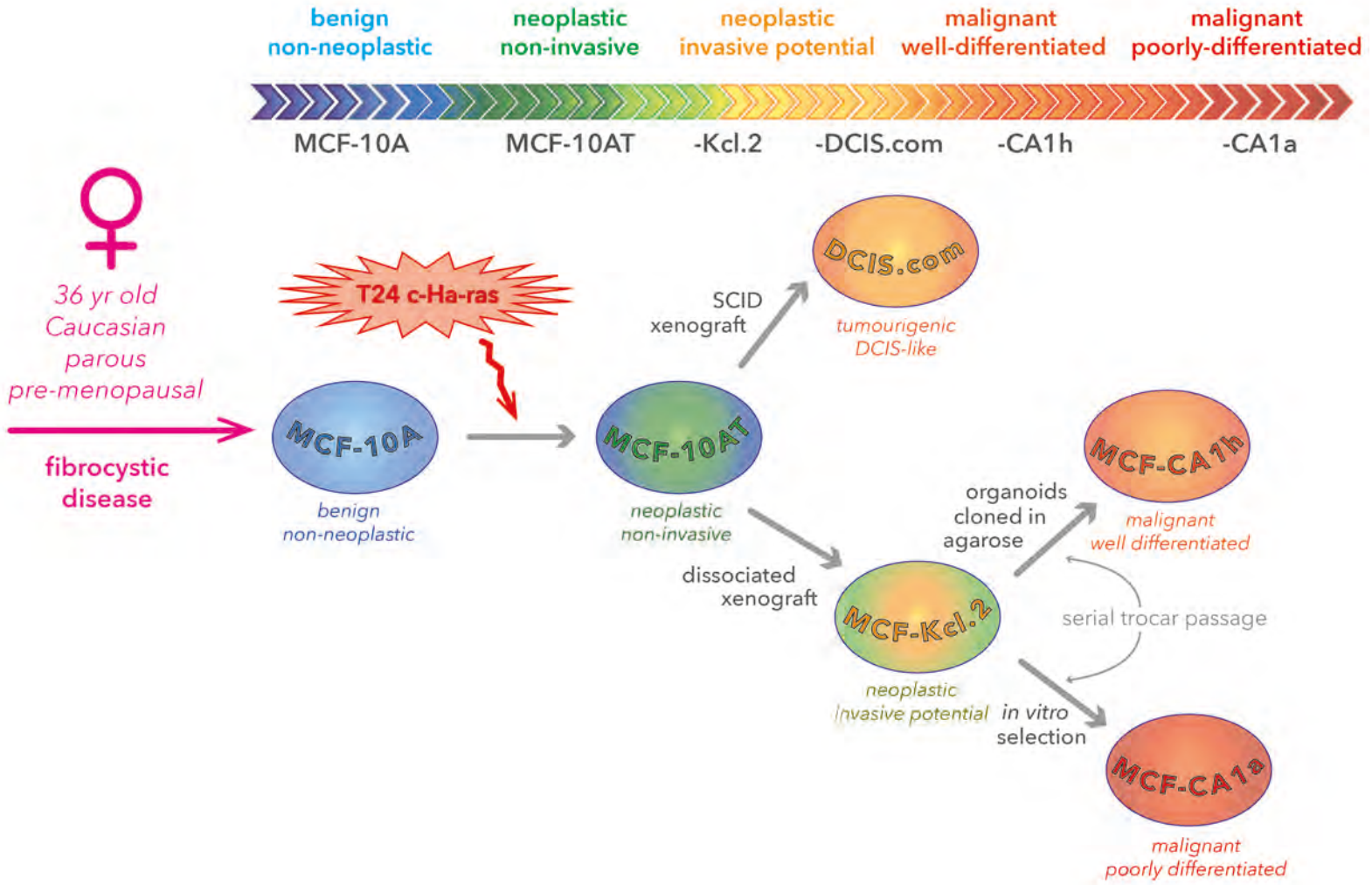

Figure 2.1: Schematic overview of the derivation of the MCF-10A series of human BrCa cell lines comprising the MCF10 isogenic model of BrCa progression.
The MCF-10A series provides a basic model of breast tumourigenesis representing the transformation of benign, non-malignant breast epithelium (MCF-10A) through neoplastic transformation following an oncogenic event (MCF-10AT) and acquisition of invasive potential (-Kcl.2 & -DCIS.com) culminating in malignant, invasive variants (MCF-10ACA1) forming well-differentiated (-CA1h) and poorly-differentiated (-CA1a) tumours upon xenografting in nude/beige mice. Details of transformation and selection processes for generation of clones are provided in Table 2.2.

Cell line	Aetiology	Culture Conditions	Receptor Status	Comment
BT-20	Tumourigenic breast adenocarcinoma cell line derived from cells isolated upon dissection of a primary IDC tumour resected from a 74 year old Caucasian female. (Lasfargues and Ozzello 1958, ATCC 2013a).	Adherent growth. α-MEM/15% FBS/2mM $_{L}$-Gln	**Triple negative** (ER- / PR- / ERBB2/HER2-)	**Subtype:** Basal A **$\alpha_v\beta_6$ status:** endogenous overexpression **Mutational status:** PIK3CA, TP53 EGFR amplification Cells express WNT3 & WNT7B oncogenes. Although negative for ER, express an exon 5-deleted ER mRNA Express WT BRCA1
SUM159	Cell line first isolated and described by Forozan *et al* (1999) from a primary anaplastic breast carcinoma from a patient who had not received chemotherapy prior to sampling.	Adherent growth. Ham's F12/10% FBS/2mM $_{L}$-Gln	**Triple negative** (ER- / PR- / ERBB2/HER2-)	**Subtype:** Basal B / claudin low **$\alpha_v\beta_6$ status:** endogenous overexpression **Mutational status:** TP53, PIK3CA, HRAS Cells express WT BRCA1
BT-474	Tumourigenic BC cell line derived from a solid, invasive ductal carcinoma isolated from a Caucasian female aged 60 years (Lasfargues *et al* 1978, ATCC 2013b).	Adherent, patchy growth. Form compact islands of multilayered colonies, rarely reaches confluence. RPMI 1640/10% FBS/ insulin (10 μg ml^{-1})/2mM $_{L}$-Gln	**Triple positive** (ER+ / PR+/ ERBB2/HER2+)	**Subtype:** Luminal **$\alpha_v\beta_6$ status:** endogenous overexpression **Mutational status:** PIK3CA Cells exhibit Her2 amplification
MDA-MB-231	Tumourigenic breast adenocarcinoma cell line derived from a metastatic site by pleural effusion from a 51 year old Caucasian female (ATCC 2012c).	Adherent growth. DMEM/10% FBS/2mM $_{L}$-Gln	**Triple negative** (ER- / PR- / ERBB2/HER2-)	**Subtype:** Basal B **$\alpha_v\beta_6$ status:** negative **Mutational status:** BRAF, CDKN2A, KRAS, TP53 Cells express *WNT7B* oncogene, EGFR and TGFαR Express WT BRCA1 & PIK3CA
MDA-MB-468	Tumourigenic breast adenocarcinoma cell line isolated from a metatstatic by pleural effusion in 1977 from a 51 year old Black female (ATCC 2012d).	Adherent growth. DMEM/10% FBS/2mM $_{L}$-Gln	**Triple negative** (ER- / PR- / ERBB2/HER2-)	**Subtype:** Basal A Cells express EGFR and TGFαR. EGFR amplification is reported; present at 1 x 10^6 per cell. Tissue donor heterozygous for G6PD alleles but cell line consistently exhibits G6PD A phenotype only. **$\alpha_v\beta_6$ status:** endogenous expression **Mutational status:** PTEN, RB1, SMAD4, TP53 Express WT BRCA1

Table 2.3: Additional human breast cancer cell lines employed in this study. *Information compiled from references as provided in text.* **Abbreviations: α-MEM** *– Minimum essential medium alpha modification;* ***BRAF*** *– V-Raf Murine Sarcoma Viral Oncogene Homolog B;* ***BRCA1*** *– Breast Cancer 1, Early Onset;* ***CDKN2A*** *– cyclin-dependent kinase inhibitor 2A;* **DMEM** *– Dulbecco's Modified Eagle Medium;* **EGFR** *– epidermal growth factor receptor;* **FBS** *– foetal bovine serum;* **G6PD** *– glucose-6-phosphate dehydrogenase;* **HRAS** *– Harvey Rat Sarcoma Viral Oncogene Homologue;* **IDC** *– invasive ductal carcinoma;* **KRAS** *– Kirsten Rat Sarcoma Viral Oncogene Homologue;* **$_{L}$-Gln** *– $_{L}$-glutamine;* **PIK3CA** *– phosphatidylinositol-4,5-bisphosphate 3-kinase, catalytic subunit alpha;* **PTEN** *– phosphatase and tensin homologue;* **RB1** *– retinoblastoma protein;* **RPMI 1640** *– Roswell Park Memorial Institute 1640 medium;* **SMAD4** *– Mothers against decapentaplegic homolog 4;* **TGFαR** *– transforming growth factor-α receptor;* **TP53** *– tumour protein 53;* **WT** *– wild type. Receptor and mutational status details compiled from (Hollestelle et al 2007, Kenny et al 2007, Kao et al 2009, Chavez et al 2010).*

Culture Component	Full Name	Product No.	Supplier	Supplied conc^{n}	Working conc^{n}	Cell Line / Experimental Application (s)
adenine	-	A2786	Sigma Aldrich©	-	18 mM	VB6 / supplement for KGM
α-MEM	minimum essential medium, alpha-modification	22571-020	Invitrogen™	-	-	base media for VB6 & BT-20
CT	cholera toxin *(Vibrio cholerae)*	227035	Calbiochem	-	100 ng ml^{-1}	supplement for KGM (VB6) & MCF-10A media (MCF-10A, -AT & Kcl.2)
DMEM	Dulbecco's minimum essential medium	D6429	Sigma Aldrich©	-	-	base media for DX3puro/β6, A375puro/β6, MDA-MB-231, MDA-MB-468 & BT-20 prepared 1:1 with Ham's F12 as base media for entire MCF-10A series
EDTA	ethylenediaminetetraacetic acid	E6758	Sigma Aldrich©	0.5 M pH8 stock	20 mM	wash step to remove residual cations during activation experiements
EGF	epidermal growth factor	E9644	Sigma Aldrich©	-	20 ng ml^{-1}	supplement for KGM (VB6) & MCF-10A media (MCF-10A, -AT & Kcl.2)
charcoal stripped FBS	foetal bovine serum (charcoal stripped)	12676029	Gibco®Invitrogen™	-	-	supplement for all complete culture media
FBS	foetal bovine serum	10500-064	Gibco®Invitrogen™	-	-	supplement for all complete culture media
$_{L}$-Glu	$_{L}$-glutamine		Sigma Aldrich©	200 mM	2 mM	supplement for all complete culture media
Ham's F12	-	N6658	Sigma Aldrich©			prepared 1:1 with DMEM as base media for entire MCF-10A series
HC	hydrocortisone	H4001	Sigma Aldrich©			supplement for KGM (VB6) & MCF-10A media (MCF-10A, -AT & Kcl.2)
HEPES	4-(2-hydroxyethyl)piperazine-1-ethanesulphonic acid	H3375	Sigma Aldrich©	1 M	20 mM 25 mM	zwitterionic organic buffer to maintain physiological pH even in variable $\%CO_2$. Used at 20 mM in low serum media & 25 mM in DMEM5
Insulin	-	I1882	Sigma Aldrich©		20 µg ml^{-1}	supplement for KGM (VB6), BT-474 media & MCF-10A media (MCF-10A, -AT & Kcl.2)
PBS-	phosphate buffered saline *without $CaCl_2$ & $MgCl_2$*	D8537	Sigma Aldrich©	-	-	standard TC washing procedures cation-free washes (activation experiments)
PBS+	phosphate buffered saline *with $CaCl_2$ & $MgCl_2$*	D8662	Sigma Aldrich©	-	-	ligand preparation for coating culture dishes
RPMI-1640	Roswell Park Memorial Institue-1640 medium	R8758	Sigma Aldrich©	-	-	base media for BT-474
Trypsin	Trypsin-EDTA	L11-004	PAA Laboratories		0.5 mg ml^{-1} trypsin 0.22 mg ml^{-1} EDTA	serine protease (trypsin) used to cleave proteins mediating cellular attachments supplemented with the chelating agent EDTA to facilitate dissociation of calcium-dependent intercellular adhesions when passaging adherent cell lines.

Table 2.4: Standard tissue culture reagents and growth media supplements.
Information compiled from supplier product details.

2.2 antibodies and reagents

A panel of integrin $\alpha_v\beta_6$-specific antibodies (see Table 2.5) was used to screen cell lines by flow cytometry and confocal immunofluorescence microscopy in order to characterise expression levels and subcellular distribution of integrin $\alpha_v\beta_6$ subpopulations previously reported to be detected by these antibodies (Desai 2011).

Summaries of additional primary, secondary and isotype-matched control antibodies used to date for flow cytometry (FCM), immunofluorescence microscopy (IMF) and Western blotting (WB) procedures are also provided in Tables 2.6 - 2.9. Details of ligands used in activation studies, functional assays and immunoprecipitation experiments are provided in Table 2.10. A list of kinase inhibitors for functional validation of putative regulators of integrin $\alpha_v\beta_6$ activation-associated signalling identified by phosphoproteomic studies is supplied in Table 2.11.

Clone	Target Epitope (integrin $\alpha_v\beta_6$)	Clonality /Isotype	Host Species	Supplier	Cat. No.	Supplied conc^n ($\mu g\ ml^{-1}$)	Working conc^n ($\mu g\ ml^{-1}$)	Application
10D5	Raised by immunisation of $\alpha_v\beta_6$ knockout mice with WT murine keratinocytes. Recognises human and murine integrin $\alpha_v\beta_6$, may recognize the receptor in other species but has not been evaluated. Antibody is specific for the intact $\alpha_v\beta_6$ heterodimer & is ligand mimetic. Does not recognise the α_v-subunit or other α_v-heterodimers.	Mono-IgG_{2a}	Mouse	Merck Millipore	MAB2077Z *Azide free*	1000	10	FB FCM IMF¶ IP
53A2	Epitope maps to the extracellular region of the heterodimer (no further details supplied). Generated by retroviral transfection of mouse fibroblasts with human β_6 subunit cDNA (3T3b6.19) resulting in expression of a mouse/human $\alpha_v\beta_6$ chimaera. Recognises the mature, fully glycosylated integrin $\alpha_v\beta_6$ heterodimer only.	Mono-IgG_{2a}	Rat	CR-UK	★	1370	10	FB FCM IMF
620W7	No datasheet available. Recognises all maturation states of integrin $\alpha_v\beta_6$ including immature non-, partially- and fully mature-glycosylated forms.	Mono-IgG_1	Rat	CR-UK	★	1370	10	FCM IMF WB°
6.2E5 (#13-1)	No datasheet available. Generated and first described by Weinreb *et al* (2004). Information regarding recognised epitope to be ascertained by communication with BioGen Idec and competitive binding assays. Protein A only, no dialysis. Data within this thesis demonstrates that 6.2E5 recognises an activation-associated epitope and ligand-induced binding site; is not ligand-mimetic and does not induce activation upon binding.	Mono-IgG_1	Mouse	Biogen Idec	PW6782-134★	2210	5	FCM IHC IMF WB°
6.2G2 (#87-1)	No datasheet available. Generated and first described by Weinreb *et al* (2004). As above for 6.2E5. Protein A only, dialysed.	Mono-IgG_1	Mouse	Biogen Idec	PW6782-142★	2100	5	FCM IHC IMF WB°

Table 2.5: Panel of anti-integrin $\alpha_v\beta_6$ unconjugated primary antibodies employed in this study to identify subpopulations of integrin $\alpha_v\beta_6$ by maturation state and activation status. *Use of antibodies for applications not indicated by the supplier are denoted*¶. *Other applications of these antibodies not utilised to date are also indicated*¤. *Information compiled from manufacturer datasheets. Where datasheets were irretrievable from online resources or unavailable from in-house records, information was taken from reagent/aliquot labels.* **Abbreviations: CDR3** *– complemenarity-determining region;* **CR-UK** *– Cancer Research UK;* **FB** *– functional blockade;* **FCM** *– flow cytometry;* **IMF** *– immunofluorescence;* **IP** *– immunoprecipitation;* **WB** *– Western (immuno-) blotting;* **WT** *– wild type.* ★**NB:** *Antibodies 620W7 (CR-UK), 6.2E5 & 6.2G2 (both Biogen Idec Ltd) were kind gifts and are not currently commercially available. Antibody 53A2 was obtained from existing stocks of the antibody first generated in-house in collaboration with CR-UK. It is acknowledged that antibody 53A2 is now commercially available (AbCam® ab97588).*

Antibody Specificity	Clone/ Product No.	Target Eptiope	Clonality Class/ Isotype	Host Species	Supplier	Cat. No.	MW (kDa)	Working conc^{n} (μg ml^{-1})	Application
α_5	-	Recognises endogenous total integrin α_5 protein. Immunogen was a synthetic peptide corresponding to residues surrounding Ser458 of human integrin α_5 protein.	Poly-IgG	Rabbit	CST	#4705S	150	1	WB
α_5	P1D6	Recognises human integrin α_5 subunit. Immunogen and antibody derivation details are not given.	Mono-IgG$_3$	Mouse	MM	MAB1956Z *Azide free*	-	10	FCM
α_v	L230	Anti-integrin α_v (CD51) antibody recognises the following α_v-bearing heterodimers: $\alpha_v\beta_1$; $\alpha_v\beta_3$; $\alpha_v\beta_5$; $\alpha_v\beta_6$. Human endothelial cells were used as the immunogen.	Mono-IgG$_1$	Mouse	in-house	-	-	10	FCM
β_1	P4C10	Recognises the integrin β_1 (CD29) subunit. Cognate epitope is not trypsin sensitive.	Mono-IgG$_{2a}$	Mouse	in-house	-	-	10	FCM
β_1	EP1041Y	Recognises the integrin β_1 (CD29) subunit. Antibody raised against a synthetic peptide corresponding to a residue proximal to the C-terminus of human integrin β_1.	Mono-IgG$_1$	Rabbit	AbCam	ab52971	140	5 (IMF) 2 (WB)	IMF WB
β_6	c-19	Epitope maps to the C-terminus of the β_6-integrin subunit of human origin. Recognises the β_6-integrin subunit of rat, mouse & human origin.	Poly-IgG	Goat	SCBT	sc-6632	97	0.2	WB
β_6	CSβ6	Antibody raised by immunising –knockout mice with recombinant secreted human integrin $\alpha_v\beta_6$. Does not recognise α_v-subunit or other α_v integrins. It is not known whether the antibody recognises the $\alpha_v\beta_6$ heterodimer or the β_6-subunit only.	Mono-IgG$_1$	Mouse	Calbio	MAB2076Z	-	5	IHC
β_8	-	Antibody raised against a synthetic peptide mapping to the C-terminal amino acids 611-660 of the human integrin subunit β_8.	Poly-IgG	Rabbit	AbCam	ab80673	-	5	WB
$\alpha_v\beta_3$	LM609	Antibody generated against a purified adhesion receptor from the human melanoma cell line M21, which was used as the immunogen.	Mono-IgG$_1$	Mouse	MM	MAB1976Z *Azide free*	-	10	FB FCM IP
$\alpha_v\beta_5$	P1F6	Antibody raised against UCLA-P3 cells derived from a human lung adenocarcinoma.	Mono-IgG$_1$	Mouse	MM	MAB1961	-	10	FCM
$\alpha_v\beta_6(\alpha_v\beta_8)$	264RAD	A recombinant human antibody generated in a Xenomouse bearing the integrin $\alpha_v\beta_6$ recognition sequence VETGRADYHFYAMDV on its CDR3. Also recognises the integrin $\alpha_v\beta_8$ (Eberlein *et al* 2013).	Mono-IgG$_1$	Human	Oncology iMED AZ	gifted	-	10	FB

Table 2.6: Additional anti-integrin antibodies employed to date in this study. *Applications of these antibodies are indicated. Clone numbers are provided for monoclonal antibodies. Product numbers are given for polyclonal antibodies. Information compiled from manufacturer datasheets or in-house records. Where datasheets were irretrievable from online resources or unavailable from in-house records, information was taken from reagent/aliquot labels.* **Abbreviations: AZ** *– Astra Zeneca UK;* **Calbio** *– Calbiochem;* **CST** *– Cell Signalling Technology;* **MM** *– Merck Millipore;* **SCBT** *– Santa Cruz BioTechnology.*

Antibody Specificity	Clone/ Product No.	Source/ Target Eptiope	Clonality Class/ Isotype	Host Species	Supplier	Cat. No.	MW (kDa)	Working conc^{n} (µg ml^{-1})	Application
Akt	-	Antibody recognises endogenous total Akt1, Akt2 & Akt3. Antibodies were raised against a synthetic peptide mapping to the carboxy-terminal sequence of murine Akt & purified by protein A & peptide affinity chromatography. Reactivity with with human Akt confirmed in QC testing. No cross-reaction with related kinases reported.	Poly-IgG	Rabbit	CST	9272S	60	1	WB
pAkt (pSer473)	D9E	Antibodies produced following immunisation of rabbits with a synthetic phosphopeptide mapping to residues flanking Ser473 of human Akt. Recognises endogenous Akt phosphorylated at the C-terminus Ser473 residue.	Mono-IgG	Rabbit	CST	4060S	60	2	WB
Akt1	D7510	Antibodies raised against a synthetic peptide mapping to a sequence flanking Leu110 of human Akt 1. Does not cross-react with Akt2 or Akt3.	Mono-IgG	Rabbit	CST	2938S	60	2	WB
pAkt1 (pSer473)	D7F10	Antibodies produced by immunising host species with a synthetic phosphopeptide mapping to residues flanking Ser473.	Mono-IgG	Rabbit	CST	9018S	60	1	WB
BAK	D4E4	Antibodies raised against a KLH-conjugated synthetic peptide corresponding to amino acids 23 – 38 of the N-terminus of human BAK.	Mono-IgG	Rabbit	CST	12105S	25	5	WB
biotin	-	Antibody generated in rabbits by multiple immunisations with biotin conjugated to KLH in Freund's adjuvant.	Poly-IgG	Rabbit	AbCam	ab1227	80	10	FCM
calnexin	-	Antibodies raised against a synthetic peptide relating to a sequence in the Ala51 region of human calnexin.	Poly-IgG	Rabbit	CST	2433BC	90	2	WB

Table 2.7 (part i): Additional unconjugated primary antibodies employed in this study.
Applications of these antibodies are indicated. For monoclonal antibodies, clone numbers are given. Product numbers are provided for polyclonal antibodies**.** *Information compiled from manufacturer datasheets. Where datasheets were irretrievable from online resources or unavailable from in-house records, information was taken from reagent/aliquot labels.* Abbreviations: BDT – *BD Transduction Laboratories;* CST – *Cell Signalling Technology;* Hsc-70 – *heat shock cognate protein;* KLH **–** *keyhole limpet haemocyanin;* MAPK – *mitogen-activated protein kinase;* MW – *molecular weight;* p – *phospho-;* SCBT – *Santa Cruz Biotechnology;* TfRC – *transferrin receptor complex;* Tyr – *tyrosine.*

Antibody Specificity	Clone/ Product No.	Source/ Target Eptiope	Clonality Class/ Isotype	Host Species	Supplier	Cat. No.	MW (kDa)	Working conc^{n} (µg ml^{-1})	Application
clathrin	23/CHC	Amino acids 4 – 171 of rat clathrin heavy chain were used as the immunogen. Antibody QC testing confirmed specificity for human clathrin heavy chain.	Mono-IgG$_1$	Mouse	BDT	BD610500	180	10 (IMF) 1 (WB)	IHC IMF WB
COT (MAP3K8 / Tpl2)	-	Antibodies raised against a recombinant fragment mapping to a region within amino acids 223-467 of human COT (MAP3K8/Tpl2).	Poly-IgG	Rabbit	AbCam	ab137589	52	1 (WB)	IHC IMF WB
pCOT (pThr290)	-	Antibodies raised against a synthetic peptide of a proprietary sequence derived from a region of human MAP3K8 flanking the Thr290 phosphorylation site.	Poly-IgG	Rabbit	AbCam	ab195706	60	1	WB
pCOT (pSer400)	-	A mixture of synthetic phosphorylated peptides mapping to residues flanking Ser400 of human, mouse & rat Tpl2 (COT/MAP3K8) were as used as the immunogen. Human species reactivity predicted based upon 100% sequence homology.	Poly-IgG	Rabbit	CST	4491S	60 / 62	1	WB
pEGFR (pTyr1068)		A synthetic phosphopeptide mapping to residues surrounding Tyr1068 of the human EGF receptor was used to immunise animals; the resulting antibodies were purified by protein A and peptide affinity chromatography	Poly-IgG	Rabbit	CST	2234S	175	2	WB
pEGFR (pTyr1086)		Antibodies were raised in animals immunised with a synthetic phosphopeptide mapping to residues flanking Tyr1086 of the human EGF receptor; and purified by protein A and peptide affinity chromatography	Poly-IgG	Rabbit	CST	2220S	175	2	WB
ERK1/2		Antibodies produced following immunisation of rabbits with a synthetic peptide corresponding a sequence located in the C-terminus of rat p44 MAP kinase (Erk1) & purified by protein A and peptide affinity chromatography.	Poly-IgG	Rabbit	CST	9102L	42 / 44	1	WB

Table 2.7 (part ii): Additional unconjugated primary antibodies employed in this study.

Antibody Specificity	Clone/ Product No.	Source/ Target Eptiope	Clonality Class/ Isotype	Host Species	Supplier	Cat. No.	MW (kDa)	Working conc^{n} (µg ml^{-1})	Application
pERK1/2 (pThr202/204)		Antibodies raised against a synthetic peptide mapping to residues encompassing Thr202/Tyr204 of human p44 MAP kinase (Erk1/2). Phospho-p44/42 MAPK (Erk1/2) (Thr202/Tyr204)	Poly IgG	Rabbit	CST	9101L	42 / 44	2	WB
pFAK (pTyr397)	(Y397)	Recognises endogenous FAK when phosphorylated at Tyr397. Antibodies raised against a synthetic phosphopeptide mapping to residues encompassing Tyr397 of human FAK. Antibody may cross-react with other tyrosine-phosphorylated RTKs.	Poly-IgG	Rabbit	CST	3283S	125	2	WB
human IgG (Fc')	ABM121	Epitope maps to the Fc' fragment of human IgG. Antibody generated using the immunogen human IgG-Fc purified by high affinity chromatography.	Mono-IgG_1	Mouse	AbCam	ab113636	-	10	FCM IMF
Hsc-70	B-6	Epitope maps between amino acids 580-601 of the C-terminus of Hsc-70 of human origin.	Mono-IgG_2a	Mouse	SCBT	sc-7298	70	0.2	WB
MAPKAPK2 (MAPK2 / MK2)	-	Antibodies raised against a synthetic peptide mapping to the C-terminus region of human MAPKAPK-2. Detects endogenous MAPKAPK-2 does not cross react with MAPKAPK-3 or -5.	Poly-IgG	Rabbit	CST	3042S	47		FCM IP WB
pMAPKAPK2 (pThr334)	27B7	A synthetic phosphopeptide corresponding to residues flanking Thr334 of human MAPKAPK-2 was used as the immunogen.	Mono-IgG	Rabbit	CST	3007S	49		
Nuak1 (ARK5)	-	A synthetic peptide corresponding to the sequence of human ARK5 (Nuak1) was used as the immunogen.	Poly-IgG	Rabbit	CST	4458S	78		WB
paxillin	H-114	Recognises α, β & γ paxillin isoforms. Epitope maps to amino acids 155 – 268 residing within an internal region of human paxillin.	Poly-IgG	Rabbit	SCBT	sc5574	68	10	IMF
PDPK1 (PDK1)	-	Antibodies were raised against a synthetic peptide mapping to residues encompassing the C-terminus of human PDK1.	Poly-IgG	Rabbit	CST	3062S	58 - 68		WB
pPDPK1 (pSer241)	-	A synthetic phosphopeptide mappingto residues flanking Ser241 of human PDK1 was used as the immunogen.	Poly-IgG	Rabbit	CST	3062S	58 - 68		WB

Table 2.7 (part iii): Additional unconjugated primary antibodies employed in this study.

Antibody Specificity	Clone/ Product No.	Source/ Target Eptiope	Clonality Class/ Isotype	Host Species	Supplier	Cat. No.	MW (kDa)	Working conc^{n} (µg ml^{-1})	Application
Smad2/3	18/Smad2/3	Amino acid residues 142 – 263 of mouse-derived Smad2 were used as the immunogen. Cross-reaction with Smad3 is predicted based on sequence homology of the immunogen.	Mono IgG$_1$ κ	Mouse	BDT	610843	58	0.2	WB
pSmad3 (pSer423/425)	C25A9	Antibody raised against a synthetic phosphopeptide mapping to residues encompassing Ser423/425 of Smad3. Antibody recognises endogenous Smad3 when phosphorylated at Ser423/425. No cross-reaction with other Smad family members.	Mono-IgG	Rabbit	CST	9520S	52	1	WB
talin	C-20	Recognises talin-1 & -2 of human origin. Epitope is mapped to the C-terminus of human talin-2.	Poly-IgG	Goat	SCBT	sc-7534	230	0.2	WB
TBK1 (NAK)	-	Antibodies were raised against a synthetic peptide mapping to residues proximal to the C-terminus of human TBK1/NAK.	Poly-IgG	Rabbit	CST	3013S	84		WB
pTBK1 (pSer172)	EPR2867(2)	Recombinant rabbit monoclonal antibody raised against a synthetic peptide mapping to residues encompassing Ser172 of human NAK.	Mono-IgG	Rabbit	AbCam	ab109272	84		IP WB
TfRC	H68.4	Recognises the human transferrin receptor complex.	Mono-IgG$_1$	Mouse	Invitrogen	136800	98	0.2 (WB)	IHC IMF IP WB
β-tubulin	-	A synthetic peptide derived from a region between residues 1 – 100 of human beta tubulin was used as the immunogen.	Poly-IgG	Goat	AbCam	ab21057	50	1	WB
pTyr	PY20	Antibody detects phosphotyrosine (pTyr) and pTyr-bearing proteins. pTyr conjugated to KLH was used as the immunogen	Mono IgG$_{2b}$	Mouse	AbCam	ab10321	multiple	2	WB IMF
vinculin	hVIN-1	Antibodies raised against the full length, native human vinculin protein which was used as the immunogen.	Mono-IgG$_1$	Mouse	AbCam	ab11194	116	0.2	WB

Table 2.7 (part iv): Additional unconjugated primary antibodies employed in this study. Applications of these antibodies are indicated. For monoclonal antibodies, clone numbers are given. Product numbers are provided for polyclonal antibodies**.** *Information compiled from manufacturer datasheets. Where datasheets were irretrievable from online resources or unavailable from in-house records, information was taken from reagent/aliquot labels.* Abbreviations: BDT – *BD Transduction Laboratories;* CST – *Cell Signalling Technology;* Hsc-70 – *heat shock cognate protein;* KLH **-** *keyhole limpet haemocyanin;* MAPK – *mitogen-activated protein kinase;* MW – *molecular weight;* p – *phospho-;* SCBT – *Santa Cruz Biotechnology;* TfRC – *transferrin receptor complex;* Tyr – *tyrosine.*

Negative Control Antibody	Clone/ Product No.	Clonality Class/ Isotype	Host Species	Supplier	Cat. No.	Supplied conc^{n} (µg ml^{-1})	Working conc^{n} (µg ml^{-1})	Application
Human IgG	N/A	Poly-IgG	Human (myeloma plasma)	ThermoFisher Invitrogen	31154	11600	10	FB
Mouse IgG $_1$	Ci4	Mono-IgG$_1$	Mouse	Merck Millipore	MABC002	500	5	FCM IMF
Mouse IgG$_{2a}$	GC270	Mono-IgG	Mouse	Merck Millipore	MABC004	500	10	FCM IMF
Non-immune Rabbit IgG	N/A	Poly-IgG	Rabbit	SCBT	sc-2027	400	10	FCM
Non-immune Rat IgG	N/A	Poly-IgG	Rat	AbCam	ab37361	5000	10	FCM
Non-immune goat serum	N/A	Poly-IgG	Goat	Vector Labs	PK-6101 (kit component)	-	-	IMF

Table 2.8: Negative control antibodies employed in this study.
Applications of these antibodies are indicated. *For monoclonal primary antibodies, isotype-matched monoclonal antibodies were employed. Polyclonal immunoglobulins served as the negative control where available. Normal goat serum used at a dilution of 1:50 (no concentration given on vial) for blocking non-specific protein interactions during IMF staining procedures. Goat serum was used as all secondary antibodies employed for IMF staining are raised in goat.*

Secondary Antibody	Host Species	Conjugate	Cat. No.	Supplier	Supplied conc^{n} (µg ml^{-1})	Working conc^{n} (µg ml^{-1})	Application
anti-goat IgG (H+L)	Donkey	AlexaFluor®680	A21084	Invitrogen™	2000	0.2	WB *(LI-COR)*
anti-mouse IgG (H+L)	Goat	AlexaFluor®488	A11029	Invitrogen™	2000	16	FCM IMF
anti-mouse IgG (H+L)	Donkey	AlexaFluor®680	A10038	Invitrogen™	2000	0.2	WB *(LI-COR)*
anti-mouse IgG (H+L)	Donkey	AlexaFluor®790	A11371	Invitrogen™	2000	0.2	WB *(LI-COR)*
anti-rabbit IgG (H+L)	Goat	AlexaFluor®488	A11034	Invitrogen™	2000	16	FCM IMF
anti-rabbit IgG (H+L)	Donkey	AlexaFluor®647	A31573	Invitrogen™	2000	16	IMF
anti-rabbit IgG (H+L)	Donkey	AlexaFluor®680	A10043	Invitrogen™	2000	0.2	WB *(LI-COR)*
anti-rabbit IgG (H+L)	Donkey	AlexaFluor®790	A11374	Invitrogen™	2000	0.2	WB *(LI-COR)*
anti-rat IgG (H+L)	Goat	AlexaFluor®488	A11006	Invitrogen™	2000	16	FCM IMF
anti-rat IgG (H+L)	Goat	AlexaFluor®546	A11081	Invitrogen™	2000	16	FCM IMF
anti-rat IgG (H+L)	Donkey	AlexaFluor®594	A21209	Invitrogen™	2000	16	IMF
anti-goat immunoglobulins	Rabbit	HRP	P0160	Dako	1300	0.2	WB (ECL)
anti-mouse immunoglobulins	Rabbit	HRP	P0260	Dako	1300	0.2	WB (ECL)
anti-rabbit immunoglobulins	Donkey	HRP	NA9340V	G E Healthcare	1000	0.2	WB (ECL)

Table 2.9: Conjugated secondary antibodies employed in this study.
Applications of these antibodies are indicated. ***Abbreviations: FCM** – flow cytometry; **HRP** – horseradish peroxidase; **IMF** – immunofluorescence; **WB** – Western (immuno)blot; **WB (ECL)** – WB electrochemiluminescence detection, **WB (LI-COR)** – WB LI-COR© Odyssey® detection system.*

Ligand	Cognate Receptor(s)	Tag	Species of origin	Supplier	Cat No.	Supplied conc^{n}	Working conc^{n}	Application
A20FMDV2	$\alpha_v\beta_6$	biotin	*synthetic peptide*	in-house (DiCara *et al* 2007)	-	2 mM	100 nM	FCM LSA
BioTJ-Ran	-	biotin	*synthetic peptide*	in-house (as above)	-	2 mM	100 nM	FCM LSA
Col I	$\alpha_2\beta_1$ [R]	-	*rat*	Corning	354236	lot specific	10 µg ml^{-1}	2D-E IMF LSA
EGF	EGFR	-	*human recombinant*	Sigma Aldrich	E9644	1 mg *(lyophilised)*	50 ng ml^{-1}	LSA
Fn	$\alpha_5\beta_1$ / $\alpha_v\beta_3$ / $\alpha_v\beta_6$ [R]	-	*human recombinant*	Sigma Aldrich	F2006	1 mg *(lyophilised)*	10 µg ml^{-1}	Func IMF
Fn	as above [R]	-	*bovine*	Sigma Aldrich	F1141	5 mg *(lyophilised)*	10 µg ml^{-1}	2D-E IMF
HGF	c-Met	-	*human recombinant*	Sigma Aldrich	H9661	1 mg *(lyophilised)*	50 ng ml^{-1}	LSA
LAP	$\alpha_v\beta_6$	-	*human recombinant*	Sigma Aldrich	L3408	25 µg *(lyophilised)*	0.5 µg ml^{-1}	2D-E Func
LAP-Fc	$\alpha_v\beta_6$	human IgG_1 (Fc') frag	*human recombinant*	Biogen Idec	-	1540 µg ml^{-1} *(in PBS)*	5 µg ml^{-1}	IMF IP
Tf-Fc	TfRC	human IgG_1 (Fc') frag	*porcine recombinant*	Hölzel Diagnostika Handels GmbH	13656-W02H	100 µg *(lyophilised)*	5 µg ml^{-1}	IMF IP

Table 2.10: Ligands utilised in this study.
Cognate integrin receptor(s) and applications are indicated. ***Abbreviations: 2D-E** – 2D-enrichment; **Col I** – collagen I; **FCM** – flow; **Fn** – fibronectin; **Func** – functional assays; **IMF** – immunofluorescence; **IP** – immunoprecipitation; **LAP** – latency-associated peptide of TGF-β1; **TfRC** – transferrin receptor complex; [R] – list of cognate receptors not exhaustive but relevant to cell lines used in this investigation.*

Target kinase	Inhibitor Name	CAS No.	Cat. No	Supplier	IC_{50} (nM)	MW (g mol^{-1})	Formula	Comment
c-MET	**PHA665752**	477575-56-7	2693	R & D Systems [Tocris]	9	641.61	$C_{32}H_{34}Cl_2N_4O_4S$	Selective ATP-competitive inhibitor of MET kinase. Anti-tumourigenic agent in murine lung cancer xenografts.
COT (MAP3K8 / Tpl2)	**TC-S 7006**	871307-18-5	5240/10	R & D Systems [Tocris]	50	404.83	$C_{21}H_{14}ClFN_6$	ATP-competitive inhibitor, selectively inhibits Tpl2 over p38, MEK, Src, MK2, PKC & EGFR.
EGFR	**Gefitinib** (IRESSA®)	184475-35-2	-	AstraZeneca	33	446.902	$C_{22}H_{24}ClFN_4O_3$	Selective ATP-competitive inhibitor of EGFR tyrosine kinase. Blocks ATP-binding site ablating autophosphorylation of C-terminal tyrosine residues (DrugBankv5.0 2017).
MAPKAPK2 (MAPK2 / MK2)	MK-2 inhibitor III	1186648-22-5	sc-221948	SantaCruz Biotech	8.5	404.83	$C_{21}H_{16}N_4O \bullet H_2O$	Selective ATP-competitive inhibitor demonstrating activity against PRAK & 3pK (IC_{50}= 81 & 210 nM respectively) with little or no activity against 8 other related kinases.
MAPKAPK2 (MAPK2 / MK2)	**PF 3644022**	1276121-88-0	4279/10	R&D Systems [Tocris]	5.2	374.46	$C_{21}H_{18}N_4OS \bullet ¾H_2O$	ATP-competitive inhibitor. Reported inhibition of TNFα (IC_{50}=160 nM) in PBMCs.
Nuak1 (ARK5)	**HTH-01-015**	1613724-42-7	5622/10	R&D Systems [Tocris]	100	468.55	$C_{26}H_{28}N_8O$	No significant inhibition against a panel of 139 kinases (including 10 AMPK family members). Blocks Nuak1-mediated phosphorylation of MYPT1. Exhibits >100-fold specificity for Nuak1>Nuak2 (Banerjee *et al* 2014).
Nuak1 (ARK5) /**TBK1**	**BX-795**	702675-74-9	204001	R&D Systems [Tocris]	5	591.50	$C_{23}H_{26}IN_7O_2S$	ATP-competitive inhibitor multi-kinase inhibitor. Also inhibits PDK1 & TBK1 (IC_{50}=111 & 6 nM respectively).

Table 2.11 (part i): Kinase inhibitors used for functional validation of phosphoproteomic hits identified as putative candidates for the molecular regulation of integrin $\alpha_v\beta_6$ signalling events inducted upon ligand-induced internalisation.

Table continues overleaf.

Target kinase	Inhibitor Name	CAS No.	Cat. No	Supplier	IC_{50} (nM)	MW (g mol^{-1})	Formula	Comment
PDPK1 (PDK1)	PDK1 inhibitor II	850717-64-5	521276	MerckMillipore [Calbiochem]	6	282.30	$C_{15}H_{14}N_4O_2$	ATP-competitive inhibitor suppressing phosphorylation of Akt at Thr308. Reported to affect PKA & 7 other kinases at higher concentrations (IC_{50}=1.6 μM & ≥600 nM)
PDPK1 (PDK1)	**GSK2334470**	1227911-45-6	4143/10	R&D Systems [Tocris]	10	462.59	$C_{25}H_{34}N_8O$	No effect on other kinases including PI3K, p38, ROCK & Aurora. Diminishes T-loop phosphorylation & downstream activation of PDPK1 substrates RSK, S6K1 & SGK but exhibits limited inhibition of Akt activation.
TBK1	**Amlexanox**	68302-57-8	4857/10	R&D Systems [Tocris]	1000	298.29	$C_{16}H_{14}N_2O_4$	Selective TBK1 & IKKε inhibitor. No activity against IKKα or IKKβ at these concentrations. Reported to bind Hsp90 & impede C-terminal chaperone function *in vitro*.

Table 2.11 (part ii): Kinase inhibitors used for functional validation of phosphoproteomic hits identified as putative candidates for the molecular regulation of integrin $\alpha_v\beta_6$ signalling events inducted upon ligand-induced internalisation. *Abbreviations: **3pK** – MAPK-protein kinase 3 (MK3/MAPKAPK3); **AMPK** – adenosine monophosphate protein kinase; **ARK5** – AMPK-related kinase 5; **ATP** – adenosine triphosphate; **COT** – Cancer Osaka Thyroid oncogene (MAP3K8/Tpl2); **EGFR** – epidermal growth factor receptor; **IKKα/β/ε** – IκB kinase α/β/ε; **MAPK** – mitogen-activated protein kinase; **MAPKAPK2** – MAPK-activated protein kinase 2; **MEK** – mitogen-activated protein kinase kinase (MKK/MAP2K); **MET** – MET kinase (hepatocyte growth factor receptor [HGFR]); **MK2** – MAPK-activated protein kinase-2 (MAPKAPK2); **MYPT1** – myosin phosphatase target subunit 1; **Nuak1** – (nua) kinase family 1; **p38** – family of 4 p38 MAPKs; **PBMCs** – peripheral blood mononuclear cells; **PDPK1** – 3-phosphoinositide dependent protein kinase 1 (PDK1); **PI3K** – phosphoinositide 3-kinase; **PKC** – protein kinase C; **PRAK** – p38-regulated/activated protein kinase (MK5/MAPKAPK5); **RSK** – ribosomal S6 kinase; **ROCK** – Rho-associated protein kinase; **S6K1** – p70 ribosomal S6 kinase 1; **SGK** – serum & glucocorticoid-inducible kinase; **Src** – non-receptor tyrosine kinase; **TBK1** – TANK-binding kinase 1; **TNFα** – tumour necrosis factor α; **Tpl2** – Tumour progression locus-2 (COT/MAP3K8). Information compiled from manufacturer and supplier's datasheets. IC_{50} values for in vitro inhibitory activity against target kinase.*

2.3 adherent cell preparation and harvesting

Adherent cells required for experiments were harvested by washing the confluent monolayer once in 10 ml phosphate buffered saline (PBS-) prior to addition of sufficient trypsin-EDTA (*[1x] (1:250) trypsin 0.5 mg ml^{-1}, ethylenediaminetetraacetic acid (EDTA) 0.22 mg ml^{-1} in PBS, L11-004 PAA Laboratories GmbH)* to cover the adherent monolayer. Upon complete detachment, trypsin was deactivated by addition of 5 – 10 ml FBS-supplemented complete medium and cells were pelleted by centrifugation [1200 rpm, 3 min; RT] *(PK121 ANNITA II Multispeed Centrifuge, ALC® International)*.

2.4 flow cytometry screening for cell-surface integrins and other moieties

Flow cytometry was performed to quantitatively demonstrate cell surface abundance of integrin receptor species, activation-induced revelation of conformation-dependent epitopes or to detect cell-surface binding of biotinylated or human IgG (Fc')-tagged ligands. As a means of robustly acquiring quantitative data at single-cell level with ease, rapidity and reliability, flow cytometry techniques have long been established (Herzenberg *et al* 2002).

2.4.1 cell preparation

After harvesting (see section 2.3), cells were washed twice by centrifugation [1200 rpm, 3 min] *(PK121 ANNITA II Multispeed Centrifuge, ALC® International)* and resuspended at 4 x 10^{6} cells ml^{-1} in DMEM/0.1/0.1 buffer [0.1% (w/v) bovine serum albumin (BSA) *(A7906, Sigma Aldrich® Co. LLC)* / 0.1% (w/v) sodium azide (NaN_3) *(S8032, Sigma Aldrich)* prepared in unsupplemented DMEM *(D6429, Sigma Aldrich)*]. Aliquots (50 µl) of the cell suspension were incubated on wet ice for 1 hour in primary antibody prepared to yield a final concentration of either 5 µg ml^{-1} (antibodies 6.2E5, 6.2G2 & mouse IgG_1 isotype control) or 10 µg ml^{-1} (all other antibodies, see Table 2.5).

Cells were washed by centrifugation prior to incubation on wet ice in the dark for 30 min in 50 µl of appropriate species-specific AlexaFluor®488-conjugated secondary antibody (see Table 2.9) prepared at 16 µg ml^{-1}. Cells were washed and resuspended to 500 µl final volume and kept on wet ice in the dark until acquisition. All washing, centrifugation and preparation of antibody solutions were performed in DMEM/0.1/0.1 buffer.

2.4.2 gating & acquisition

Data were acquired either on the BD FACSCalibur™ flow cytometer equipped with a 488 nm blue laser and a 635 nm red laser, or on the BD LSRFortessa™ equipped with 488 nm blue, 640 nm red, 405 nm violet and 561 nm yellow-green PMT lasers *(both BD Biosciences©, Becton, Dickinson & Co)*. Following instrument calibration, samples prepared with isotype-matched negative control antibodies were used to define the first logarithmic decade (10^1) of mean fluorescence intensity (MFI) signal output detected in FL-1: 530/30 (BD FACSCalibur™)/Green Channel detector array (BD LSRFortessa™) to establish the negative threshold, prior to running test samples.

A total of 1 x 10^4 gated events were acquired for each sample. All samples were acquired in the presence of 5 µg ml^{-1} propidium iodide *(P4170, Sigma Aldrich)* cell viability dye detected in FL-3 (670 LP) (BD FACSCalibur™) /Red Channel detector array (BD LSRFortessa™) to define acquisition gates ensuring data capture on viable cells only and exclusion of doublets. On board cytometer settings and acquisition metrics were monitored in-flight using either CellQuestPro™ (BD FACSCalibur™) or FACSDiva™ v8.0 (BD LSRFortessa™) software *(all BD Biosciences©, Becton, Dickinson & Co)*

2.4.3 analysis of flow cytometry data

Following acquisition, flow cytometry data were analysed using either BD CellQuestPro™ software *(BD Biosciences©, Becton, Dickinson & Co)* or FlowJo© software *(FlowJo© LLC)* to ascertain geometric mean fluorescence intensity (geoMean MFI) values as a read-out for level of cell surface-bound antibody. Test sample geoMean MFI values were normalised by subtraction of geoMean MFI

values acquired for the relevant isotype-matched negative control antibody to discount any inherent noise within the assay matrix or instrumentation.

Given the large number of data-points (1 x 10^4 events) acquired with rapidity per individual sample, it was probable that extreme outlier events not truly reflective of the sample population may be captured. Therefore the geometric mean MFI as opposed to the arithmetic mean MFI was used. Unlike the arithmetic mean, the geometric mean is less sensitive to skewing by extreme outlier values and was deemed to generate more reliable results reflecting the overall sample population more accurately (McAlister 1879).

2.5 immunofluorescence microscopy

Both non-permeabilised and permeabilised immunofluorescence (IMF) microscopy strategies were performed to evaluate distribution of epitopes recognised by a panel of anti-integrin $\alpha_v\beta_6$ antibodies at the cell-surface or subcellular level respectively. These IMF methods were also used to track the internalisation kinetics and localisation of human IgG (Fc')-tagged ligands. As outlined by Carman (2012), IMF microscopy imaging modalities remain a fundamental and highly formative technique in the study of integrin functional biology.

2.5.1 preparation of coverslips

Cells were seeded on sterile non-derivatised 13 mm diameter glass coverslips (2 x 10^4 cells per coverslip) and left to adhere overnight in complete media under standard culture conditions [8% CO_2, humidified atmosphere, 37°C]. Prior to experimental use, satisfactory cell adherence, morphology and confluence was confirmed by phase contrast microscopy *(OLYMPUS IMT-2, Olympus Corp).*

2.5.2 non-permeabilised immunofluorescence microscopy
(demonstration of cell-surface molecules)

Cell surface distribution of moieties of interest (proteins or tagged ligands) was evaluated by non-permeabilised immunofluorescence microscopy. Coverslips were washed in PBS and fixed with 4% (w/v) paraformaldehyde *(P6148, Sigma Aldrich)* for 8 min at ambient laboratory temperature (RT). After washing in PBS, coverslips were blocked for 30 min in normal goat serum *(VECTASTAIN® Elite® ABC (rabbit IgG) Kit component PK-6101, Vector Laboratories Inc)* to prohibit non-specific antibody binding, washed and incubated for 1 hr in primary antibody prepared in DMEM/0.1/0.1 before washing and labelling with the appropriate species-specific secondary antibody.

Nuclei were demonstrated with the cell membrane permeant nuclear stain Hoechst 33342 *(1 µg ml^{-1}, H3570, Life Technologies)* prior to washing and mounting coverslips *(Mowiol®4-88, 81381, Sigma-Aldrich)* ready for microscopic review and image acquisition.

NB: *Details of specific primary and secondary antibodies used in each experiment are provided in the relevant figure legends in the results chapters.*

2.5.3 permeabilised immunofluorescence microscopy
(demonstration of subcellular molecules)

To evaluate subcellular distribution of moieties of interest (proteins or tagged ligands), permeabilised immunofluorescence methods were performed. Coverslips were washed in PBS, fixed with cytoskeletal fixative buffer [4% (v/v) formaldehyde *(10170052, Fisher Scienitifc)*; 10 mM 2-(N-Morpholino)ethanesulphonic acid (MES) at pH6.1 *(M3671, Sigma Aldrich)*; 125 mM KCl *(P9333, Sigma Aldrich)*; 3 mM ($MgCl_2$) *(M8266, Sigma Aldrich)*; 2 mM ethylene-bis(oxyethylenenitrilo)tetraacetic acid (EGTA) *(03777, Fluka)*; 10% (w/v) sucrose *(10346150, Fisher Scientific)*] and permeabilised in 0.1% (v/v) Triton X-100/PBS *(AAA16046AE, Alfa Aesar© ThermoFisher Scientific Inc)* prior to washing and blocking in normal goat serum *(VECTASTAIN® Elite® ABC (rabbit IgG) Kit component PK-6101, Vector Laboratories Inc)* to inhibit non-specific antibody binding.

For single labelling, coverslips were incubated for 1 hr in primary antibody prepared in DMEM/0.1/0.1 before washing and labelling with appropriate species-specific fluorophore-conjugated secondary antibody (see Table 2.9). For dual- and triple-labelling, coverslips were incubated for 1 hr concomitantly with a cocktail of primary antibodies as required, washed and incubated simultaneously for 30 min in a cocktail of the appropriate secondary antibodies. Antibody cocktails were first validated in-house to evaluate any cross-reactivity or steric hindrance that would yield false positive or false negative results.

Nuclei were demonstrated with 4',6-diamidino-2-phenylindole at 1 µg ml^{-1} *(DAPI, D1306, Invitrogen)*. Actin filaments (F-actin) were stained using 50 µg ml^{-1}

phalloidin conjugated to either fluorescein isothiocyanate (FITC) *(P2582, Sigma Aldrich)* or tetramethylrhodamine (TRITC) *(R415, Molecular Probes© Invitrogen)*. Coverslips were then washed and mounted *(Mowiol®4-88, Sigma-Aldrich)* prior to microscopic review and image acquisition.

2.5.4 vital immunofluorescence microscopy

(capturing epitopes in live cells)

The fixation process is known to alter protein conformation and stability, potentially inducing artefacts and affecting efficacy of antibodies to detect their cognate epitope. Conformation-dependent epitopes may be particularly sensitive to biochemical or structural modification by fixation procedures (Melan 1995). To obviate this, distribution of putative conformationally distinct integrin $\alpha_v\beta_6$ subpopulations were evaluated by labelling live cells with antibody, prior to fixation with 4% (w/v) PFA or cytoskeletal fixative buffer supplemented with 4%, (v/v) formaldehyde as outlined previously, in an attempt to map subcellular localisations of integrin receptor pools as close to their *in vivo* morphological state as possible.

Cells seeded overnight on coverslips were washed twice in PBS and labelled for 15 min at RT with primary antibody prepared in an azide-free buffer [0.1% (w/v) BSA/DMEM]. Cells were washed twice with PBS and fixed with either 4% (w/v) paraformaldehyde for surface immunofluorescence or a cytoskeletal fixative buffer for permeabilised immunofluorescence as previously described (Sections 2.5.2 and 2.5.3 respectively). Following fixation, coverslips were incubated for 30 min with appropriate species-specific secondary antibody prior to washing, nuclear staining and mounting for microscopic review (as outlined previously).

NB: *Details of specific primary and secondary antibodies used in each experiment are provided in the relevant figure legends in the results chapters.*

2.5.5 immunofluorescence microscopy review & image acquisition

Immunofluorescence microscopy review and representative image acquisition were performed using either of the following instruments:

> ***i)*** Zeiss LSM710 confocal microscope *(Barts Cancer Institute Microscopy Core Facility, QMUL, London)* equipped with a laser diode [405 nm DAPI excitation], Argon laser [488 nm fluorochrome excitation], Helium Neon 543 laser [546 nm fluorochrome excitation] and interfaced with Zeiss Zen image analysis software *(all Carl Zeiss®, AG)*
>
> ***ii)*** 3i Marianas™ *(Department of Cellular & Molecular Physiology, University of Liverpool, Liverpool)* custom-built instrument equipped with SlideBook™ 5 image analysis software *(all Intelligent Imaging Innovations (3i)© Inc)*.

Microscope instrument acquisition settings were applied universally across all images for comparative analysis and acquired in a single session for each experimental procedure to ensure comparability.

The platform used for image acquisition and analysis is indicated in the relevant result figure legends. Additional image analyses and quantification where required, were performed using ImageJ software *(ImageJ64 v1.46r, National Institutes of Health)* and are also outlined in result figure legends. Images were prepared for presentation using Photoshop® for generation of composite figures in Illustrator® *(both Adobe® CreativeSuite™ CS6 v 16.0.0, Adobe Systems Software Ltd)*.

2.5.6 quantification of immunofluorescence signal intensity

Where shown, signal intensities from immunofluorescence studies were quantified by calculating corrected total cell fluorescence expressed in arbitrary units (CTCF, AU) using ImageJ software using the formula:

CTCF = Integrated Density – (Area of Selected Cell – Average Mean Background Fluorescence)

as published by McCloy *et al* (2014) and later described in technical detail by Burgess (2015).

2.6 Western blotting

First described by Towbin *et al* (1979), Western blotting (immunoblotting) is well established as a means of protein identification and quantification in biological research. Following size separation based upon molecular weight (MW, kDa) using gel electrophoresis, proteins are transferred to a solid support medium, typically a nitrocellulose membrane, to permit specific identification of blotted proteins using antibodies specific to moieties of interest (Kurien and Scofield 2006, Mahmood and Yang 2012).

Western blotting permits evaluation and quantification of many post-translational modifications (PTM) including phosphorylation, ubiquitinylation, methylation, SUMOylation and glycosylation at defined amino acid residues. This has expedited characterisation of the critical modulatory effects of PTM in both health and disease processes (Bass *et al* 2017). The longstanding utility and widespread application of the Western blotting technique remains given its ability to detect proteins of low abundance, routinely within the nanogram (ng) and reportedly down to the picogram (pg), range when using detection by peroxidase reaction products (Towbin *et al* 1979).

Two detection platforms were used for Western blotting procedures. Immunoblotting undertaken at the Centre for Tumour Biology, Barts Cancer Institute was developed by enhanced chemiluminescence (ECL) either manually using X-ray film *(BioMax XAR Film, 165-1454, Carestream Health Inc.)* or digitally using the Amersham™ Imager 600 *(GE Healthcare Life Sciences Ltd)*. An infrared (IR) detection system *(Odyssey®Sa, LI-COR© Inc)* was employed for experiments performed at the Institute of Translational Medicine, University of Liverpool. The developing and detection platform used is indicated in the relevant result figure legends.

NB: Details all of primary, secondary and loading control antibodies used in WB analyses are provided in Tables 2.6, 2.7 & 2.9. Experiment-specific details, along with protein loading quantities, are provided in the relevant result figure legends.

2.6.1 Western blotting with ECL detection

(Tumour Biology, Barts Cancer Institute)

After washing the adherent cell monolayer 3 times in TBS pre-chilled to 4°C, lysates were harvested by manual scraping in the presence of Nonidet P-40 *(FNN0021, Invitrogen™)* supplemented with protease and phosphatase inhibitors diluted 1:100 in Nonidet P-40 *(Protease Inhibitor Cocktail Set I 539131 and Phosphatase Inhibitor Cocktail Set II 524625, both Calbiochem®)*. Lysates were centrifuged [12 000 rpm; 10 min; 4°C) *(SORVAL® fresco microcentrifuge, Sorval™)* to collect supernatants and aliquoted to prevent freeze-thaw artefacts or degradation of protein moieties prior to storage at −20°C before evaluation by WB. When required, lysates were thawed on wet ice ready for protein concentration quantification.

Lysate protein concentrations were determined using a commercial modified Lowry colorimetric assay *(Bio-Rad DC™ Protein Assay Kit, 500-0116, Bio-Rad Laboratories Inc)*. Colorimetric changes correlating to protein concentrations were read at 650 nm using the TECAN Infinite® F50 microplate reader *(Tecan Trading AG)* and quantified as optical density (OD) units. Sample lysates were quantified against in-house protein standards *(0 – 2000 mg ml^{-1} BSA, A7906, Sigma Aldrich dissolved in Nonidet P-40)* tested concomitantly to yield a protein standard curve. A minimum threshold for the linear regression of the protein standard curve generated was set at R^2=0.98 to ensure accuracy of readings before the curve was used to interpolate sample lysate concentrations.

Sample and control lysate protein concentrations were equalised to yield a concentration of 1 µg ml^{-1} by dilution (where necessary) in the required volume of Nonidet P-40. Equalised lysates were mixed (1:1) in an equal volume of [2x] Laemmli buffer *(S3401, Sigma Aldrich)*. Proteins were then reduced by boiling for 5 minutes in a heat-block *(ThermoFisher)* set to 100°C in the presence of [2X] Laemmli buffer.

Proteins were resolved by SDS-PAGE in 10% acrylamide gels prepared in-house (see Section 2.6.3 for details) in the presence of Tris-Glycine-SDS running buffer *(BP1341-1, Fisher Scientific)* using the Mini-PROTEAN® Tetra Cell Module *(1658029, Bio-Rad Laboratories Inc)*. Gels were run using the at 90V for 20 min through stacking gel and at 120V for 1h30 through resolving gel, or until sample

front reached the base of the resolving gel. Once resolved, proteins were blotted onto a nitrocellulose membrane *(Amersham Hybond™ ECL™ RPN303D, GE Healthcare©)* by wet electrophoretic transfer using the BioRad Mini-PROTEAN® Trans-Blot® Module *(1658029, Bio-Rad Laboraties Inc)*. Transfer was performed overnight at 4°C running at 15 V in the presence Glycine-SDS transfer buffer *(BP1306-1, Fisher Scientific)* supplemented with 20% ethanol.

Following transfer, membranes were stained with Ponceau S *(P7170, Sigma Aldrich)* to confirm transfer success. Membranes were then rinsed in distilled H_2O to remove Ponceau S before additional washing in either 5% milk [5% (w/v) skimmed milk powder *(70166, Sigma Aldrich)* dissolved in 1% (v/v) Tween®20 *(P1379, Sigma Aldrich)* / TBS] or with 5% BSA [5% (w/v) BSA *(A2058, Sigma Aldrich)* dissolved in 1% (v/v) Tween®20/TBS] until all Ponceau S was removed. Membranes were then blocked for 30 min at RT in either 5% milk or 5% BSA to inhibit non-specific antibody binding during immunoblotting. Membranes to be probed for the β6 subunit using antibody C-19 were blocked in 5% milk. All other membranes were blocked in 5% BSA.

Once blocked, membranes were probed overnight at 4°C in primary antibody prepared in appropriate blocking buffer (please refer to Tables 2.6 – 2.9 for target and application specific antibody dilutions). After probing, membranes were washed for 30 min at RT in 5 changes of washing buffer [0.1% (v/v) Tween®20 / TBS]. Membranes were then incubated for 1h at RT with the relevant species-specific HRP-conjugated secondary antibody diluted in either 5% milk or 5% BSA blocking buffer (see Table 2.9 for details), before washing for 30 min at RT as previously described prior to detection.

Protein bands were revealed by enhanced chemiluminescence *(Amersham ECL Western Blotting Detection Kit RPN2106, GE Healthcare)* according to manufacturer's guidelines and detected by exposure to and development of conventional X-ray film *(BioMax XAR Film, 165-1454, Carestream Health Inc.)* or visualised using the Amersham™ Imager 600 *(GE Healthcare Life Sciences Ltd)* digital imaging system. Membranes were then washed and reprobed using a primary antibody to detect a suitable loading control protein.

2.6.2 Western blotting with IR detection

(Translational Medicine, University of Liverpool)

Lysates were harvested by manual scraping in [2X] RIPA buffer prepared in-house [300 mM sodium chloride (NaCl) *(10326390, Fisher Scientific)*; 2% (v/v) IGEPAL®630 *(I8896, Sigma)*; 1% (w/v) deoxycholic acid sodium salt *(10346653, Fisher Scientific)*; 0.2% (w/v) sodium dodecyl sulphate (SDS) *(10090490, Fisher Scientific)*; 100 mM Tris pH 8.0 *(Trizma®Base, 93349 Fluka)*; 0.2% (w/v) sodium azide (NaN_3) *(S8032, Sigma Aldrich)*] supplemented with protease [(10 µg ml^{-1} aprotinin *(A1153, Sigma Aldrich)* and leupeptin hemisulphate *(L2884, Sigma Aldrich*); 200 µM 4-(2-aminoethyl)benzenesulphonyl fluoride hydrochloride (AEBSF-HCl) *(1056-3165, Fisher Scientific)*] and phosphatase inhibitors [15 mM sodium fluoride (NaF) *(10244540, Fisher Scientific)*; 1.5 mM sodium orthovanadate ($NaVO_4$) *(10114740, Acros Organics)*].

Protein concentrations were determined by colorimetric assay and equalised (as previously described). Proteins were then denatured by boiling at 100°C for 5 min in a heat-block in the presence of reducing [2X] SDS sample buffer prepared in-house [50 mM Tris (Tris(hydroxymethyl)methylamine-hydrochloride) pH 6.8 *(10152400, Fisher Scientific);* 10% (v/v) glycerol *(10579570, Fisher Scientific)*; 4% (w/v) sodium dodecyl sulphate (SDS) supplemented with 0.04% β-mercaptoethanol *(M3148, Sigma Aldrich)*]. **NB:** For 2D-enrichment (2D-E) studies, samples were harvested by manual scraping directly into [2X] SDS sample buffer, prohibiting protein quantification. In these latter situations comparisons were based on identical numbers of cells plated (i.e 5 x 10^6 cells per 10 cm dish).

Proteins were resolved by SDS-PAGE in NuPAGE® 4 – 12% 1.0 mm Bis-Tris Gels *(NP0322 or NP00323, Invitrogen™)* using the Novex® XCell SureLock™ Mini-Cell Electrophoresis System *(EI0002, Invitrogen™)*. Gels were electrophoresed in the presence of NuPAGE® MES SDS running buffer *(NP002-02, Invitrogen™)* for 15 min at 90V through stacking gel, and run for 65 min at 150V through resolving gel. Transfer was achieved in the presence of Novex®Tris-Glycine Transfer Buffer *(LC3675, ThermoFisher Scientific)* using the XCell II™ Blot Module (*EI0002, Invitrogen™*) embedded in wet ice. Proteins were blotted onto a nitrocellulose membrane *(Protran® BA85, Whatman)* at 350 mA for 120 min.

After transfer, membranes were blocked for 30 min in a casein-based buffer *(B6429, Sigma Aldrich)* before probing overnight at 4°C with primary antibody. Membranes were washed [0.1% (v/v) Tween®20 / TBS] and incubated for 30 min with species-specific fluorophore-conjugated secondary antibody before scanning on the Odyssey®Sa *(LI-COR© Inc)*. Loading controls were subsequently evaluated. Digital images acquired using this detection platform were reviewed using ImageJ *(ImageJ64 v1.46r, National Institutes of Health)* software to evaluate fluorescence signal output.

2.6.3 preparation of gels for SDS-PAGE

Immediately prior to use, 10% acrylamide gels were prepared in-house according to the following protocols.

For the 10% resolving gel:

constituent	volume (ml)	cat. no.	supplier
dH_2O	20	-	-
30% (w/v) acrylamide/ methylene bisacrylamide (37.5:1)	16.6	EC-890	National Diagnostics
1.5M Tris pH 8.8	12.5	-	prepared in-house from Trizma® (TRIS base) *(T4661, Sigma Aldrich)* & pH adjusted with 5M NaOH
10% (w/v) SDS	0.5	BP2436-1	Fisher Scientific
10% (w/v) APS	0.5	-	prepared in-house from dry stock *(A3678, Sigma Aldrich)*
TEMED (N, N, N', N'-tetramethylethylene-1,2-diamine)	0.02	EC-503	National Diagnostics

Table 2.12: Preparation of 10% resolving gel solution.

For the stacking gel:

constituent	volume (ml)	cat. no.	supplier
dH_2O	6.8	-	-
30% (w/v) acrylamide/ methylene bisacrylamide (37.5:1)	1.7	EC-890	National Diagnostics
1.0M Tris pH 6.8	1.25	-	prepared in-house from Trizma® (TRIS base) *(T4661, Sigma Aldrich)* & pH adjusted with 5M NaOH
10% SDS (w/v)	0.1	BP2436-1	Fisher Scientific
10% (w/v) APS	0.1	-	prepared in-house from dry stock *(A3678, Sigma Aldrich)*
TEMED (N, N, N', N'-tetramethylethylene-1,2-diamine)	0.01	EC-503	National Diagnostics

Table 2.13: Preparation of stacking gel solution.

Gels were cast in single-use Invitrogen™ Novex™ cassettes *(ThermoFisher Scientific)*. For 10-well gels 1.0 mm cassettes *(NC2010)* were used. For 12 or 15 well gels 1.5 mm cassettes *(NC2015)* were used in order to provide ample volume for protein loading.

2.6.4 densitometric analysis of immunoblots

Where appropriate, densitometric analysis of visualised bands was performed using ImageJ software *(ImageJ64 v1.46r, National Institutes of Health)* as described by Miller (2010), with values normalised against a loading control and expressed as fold-change compared to the known positive control.

2.7 methods to evaluate the utility of antibodies 6.2E5 and 6.2G2 to recognise active integrin $\alpha_v\beta_6$

Extracellular regulation of integrin conformation and activation status by divalent cations (Smith *et al* 1994, Mould *et al* 1995b, Tiwari *et al* 2011) or by cognate ligand engagement has long been established (Mould *et al* 1995a, Humphries 1996, Luo *et al* 2007). Therefore canonical integrin activation methods utilising divalent cations or cognate ligands were performed to determine the ability of the monoclonal antibodies 6.2E5 and 6.2G2 to recognise active conformers of the integrin $\alpha_v\beta_6$.

2.7.1 integrin $\alpha_v\beta_6$ activation mediated by divalent cation species

Different species of divalent cation have been shown to elicit specific modulatory effects on integrin conformation, activation and ligand affinity. It has been reported that Ca^{2+} species elicit an inhibitory effect on integrin β_1 subunit, inducing an inactive conformation to prevent its premature activation during intracellular trafficking from the endoplasmic reticulum (ER) to the plasma lemma (Day *et al* 2002, Chen *et al* 2003, Tiwari *et al* 2011).

In contrast, both Mg^{2+} and Mn^{2+} species are now known to potentiate integrin cognate ligand engagement. Furthermore, a consensus now exists that Mn^{2+}cations are potent and universal modulators of integrin priming and activation (Shimaoka *et al* 2002, Zhang and Chen 2012). Therefore, Ca^{2+}, Mg^{2+} and Mn^{2+} cationic species were used to evaluate whether the antibodies 6.2E5 and 6.2G2 recognise epitopes revealed upon divalent cation-mediated activation of the integrin $\alpha_v\beta_6$.

2.7.1.1 evaluating divalent cation activation induced by 1 mM Ca^{2+}, Mg^{2+} or Mn^{2+} species

The DX3β6 cell line was allowed to reach 100% confluence as this promotes high levels of integrin $\alpha_v\beta_6$ expression (data not shown). After harvesting cells (previously described, section 2.3), residual cations were removed by washing and

centrifugation [1200 rpm, 3 min, 4°C] *(Avanti® J-26 RP Centrifuge, Beckman Coulter Inc)* in a chelating wash buffer [TBS pH 7.4 *(BP24711, Fisher Scientific)* supplemented with 20 mM EDTA *(E6758, Sigma Aldrich)*] that had been pre-chilled to 4°C. Following manual cell counting by phase contrast microscopy using a disposable haemocytometer *(FastRead Counting Slide, BVS100, Immune Systems Ltd)*, the cell pellet was resuspended in chelating wash buffer to yield a 1 x 10^6 cells ml^{-1} suspension. Aliquots of equal volume were transferred to 4 pre-chilled 50 ml Falcon *(CLS430829, Corning®, Sigma Aldrich)* tubes embedded in wet ice and pelleted by centrifugation (as previously described).

Solutions of divalent cations were prepared at 1 mM in TBS, chilled to 4°C and kept on wet ice. Cell pellets were resuspended in 10 ml ice-cold divalent cation solutions of either, calcium chloride ($CaCl_2$ / $\mathbf{Ca^{2+}}$) *(C7902, Sigma Aldrich)*, magnesium chloride ($MgCl_2$ / $\mathbf{Mg^{2+}}$) *(M8266, Sigma Aldrich)*, manganese (II) chloride ($MnCl_2$ / $\mathbf{Mn^{2+}}$) *(M3634, Sigma Aldrich)* or, in a chelating ion-free buffer [0.1% (w/v) BSA *(A7906 Sigma Aldrich)* / TBS pH 7.4 / 20 mM EDTA], inverted to mix thoroughly and left to incubate on wet ice for 10 min.

Cells were then centrifuged, resuspended in the appropriate 1 mM cation or ion-free chelating buffer at 4 x 10^6 cells ml^{-1} and stained for flow cytometric evaluation of putative integrin $\alpha_v\beta_6$ subpopulations (previously described, section 2.4.1) using the full panel of anti-integrin $\alpha_v\beta_6$ antibodies (see Table 2.5).

All wash steps and antibody preparations for these experiments were performed using the relevant 1 mM cation or ion-free buffer. After staining, cells were resuspended in the appropriate 1 mM cation or ion-free buffer prior to acquisition (previously described, section 2.4.2). All solutions were pre-chilled and centrifugation steps performed in a refrigerated centrifuge pre-cooled to 4°C to preserve cell viability during the course of the experiment.

2.7.1.2 evaluating Mn^{2+}-induced activation kinetics

Additional experiments were performed to characterise Mn^{2+} ion-induced activation kinetics specifically. The established cation activation protocol (outlined previously in section 2.7.1) was used to test the effects of a range of Mn^{2+}-ion

concentrations upon the binding capacity of antibodies 6.2E5 and 6.2G2. Solutions of magnesium chloride ranging from 0 mM to 10 mM were prepared in TBS as previously described.

2.7.2 integrin $\alpha_v\beta_6$ activation mediated by cognate ligand engagement

As cellular adhesion receptors, integrin engagement of cognate ligands within the ECM is critical to their extracellular activation and induction of *"outside-in"* signalling (Campbell and Humphries 2011). Therefore, the known integrin $\alpha_v\beta_6$ cognate ligands latency associated peptide (LAP) of transforming growth factor β1 (TGF- β1) and the synthetic peptide A20FMDV2 were used to characterise binding kinetics of antibodies 6.2E5 and 6.2G2 upon $\alpha_v\beta_6$ integrin ligand-engagement and assess whether these antibodies recognise a ligand-induced binding site (LIBS).

2.7.2.1 evaluating A20FMDV2-induced binding kinetics

The foot and mouth disease virus (FMDV)-derived 20mer synthetic peptide A20FMDV2 generated by DiCara *et al* (2007) is known to specifically bind the integrin $\alpha_v\beta_6$ both in vitro and in vivo (Jackson *et al* 2000, Monaghan *et al* 2005, Hausner *et al* 2007, Saha *et al* 2010). A biotinylated formulation of peptide A20FMDV2 was used for these experiments to facilitate flow cytometric detection of cell-surface bound A20FMDV2 via its biotin tag to confirm successful ligand engagement.

The VB6 cell line was harvested at 100% confluence for maximal integrin $\alpha_v\beta_6$ expression. Residual cations and ligands were removed by centrifugation in a chelating buffer (TBS/20 mM EDTA, previously described). Cells were resuspended in 100 nM biotinylated-A20FMDV2 prepared in DMEM/0.1/0.1 and kept on wet ice to permit ligand engagement. Ligand binding was quenched at designated time-points between 0 and 60 minutes, by flooding and washing with ion-free buffer.

Cells were stained for flow cytometry analysis using the panel of anti-integrin $\alpha_v\beta_6$ antibodies (previously specified). Biotinylated-A20FMDV2 was detected with an

anti-biotin antibody *(10 µg ml^{-1}, ab1227, AbCam)*. Specifications of the chelating and ion-free buffers have been given previously (section 2.7.1).

2.7.2.2 evaluating LAP-induced binding kinetics

Integrin $\alpha_v\beta_6$ binding of LAP resulting in TGF-β1 activation is well established (Thomas *et al* 2002, Munger and Sheppard 2011). Recombinant human LAP tagged with a human IgG (Fc') fragment (LAP-Fc) *(a kind gift from Biogen Idec)* was used for the purposes of these ligand-induced activation experiments.

Again, the VB6 cell line was harvested at 100% confluence and washed by centrifugation in a chelating buffer to remove residual cations or ligands. Cells were resuspended in solutions of LAP-Fc prepared at concentrations ranging from 0 – 10 µg ml^{-1} in DMEM/0.1/0.1 and incubated on wet ice for 10 minutes to permit ligand engagement.

Ligand engagement was quenched by flooding with 3 subsequent wash steps in an ion-free buffer. Cells were then stained for flow cytometry to evaluate surface integrin $\alpha_v\beta_6$ expression (previously described). Cell-surface LAP-Fc was detected using an anti-human IgG(Fc') antibody *(ab113636, AbCam)* to confirm successful engagement. Time-course activation experiments over a 30 minute period in the presence of 2 µg ml^{-1} LAP-Fc were also performed using the VB6 cell line following the method outlined above.

2.7.3 determining subcellular localisation of epitopes recognised by the antibodies 6.2E5 and 6.2G2 by immunofluorescence

To evaluate the subcellular distribution of the epitopes recognised by antibodies 6.2E5 and 6.2G2, the VB6 cell line was seeded overnight on non-derivatised 13 mm glass coverslips as previously described (section 2.5.1). Successful adherence and cell morphology was confirmed by phase contrast microscopy, prior to fixation and permeabilisation as described (section 2.5.3).

Coverslips were blocked for 30 min at RT in normal (non-immune) goat serum *(1:50, PK-6101, VECTASTAIN® Elite® ABC (rabbit IgG) Kit component, Vector Laboratories Inc)*. Cells were then labelled with either 6.2E5 or 6.2G2 *(5 µg ml^{-1})* for 1 hour at RT, prior to washing and counterstaining with antibody 53A2 *(10 µg ml^{-1})* for 1 hour at RT.

After additional washing, primary antibodies were detected with fluorophore conjugated species-specific secondary antibodies. Anti-mouse IgG-AlexaFluor®488 *(16 µg ml^{-1}, A11029, Invitrogen™)* was used to detect antibodies 6.2E5 and 6.2G2. Anti-rat IgG AlexaFluor®546 *(16 µg ml^{-1}, A11081, Invitrogen™)* was used to detect antibody 53A2. Nuclei were demonstrated with DAPI *(1 µg ml^{-1}, D1306, Invitrogen™)* and mounted in Mowiol®-4-88 *(81381, Sigma Aldrich)* ready for microscopic review as described in section 2.5.5 i).

2.7.4 evaluating the distribution of 6.2E5 and 6.2G2 cognate epitopes in cells adhering to integrin cognate ligands

Non-derivatised 13 mm glass coverslips were coated for 1 hour at RT with either human recombinant LAP of TFG-β1 (**LAP**) *(0.5 µg ml^{-1}, L3408, SigmaAldrich),* human recombinant fibronectin (**Fn**) *(10 µg ml^{-1}, F2006, SigmaAldrich)* or rat-tail collagen type I (**Col I**) *(10 µg ml^{-1}, 354236, Corning® Inc)*. Coverslips were then washed in serum-free media equilibrated to RT. A suspension of the VB6 cell line was prepared in serum-free media, seeded at 2 x 10^4 cells per coverslip and left to adhere to coverslips for 2 hours under standard tissue culture conditions.

Cells were then fixed, permeabilised (as previously described in section 2.5.3) and labelled with either 6.2E5 or 6.2G2 *(5 µg ml^{-1})* for 1 hour at RT prior to detection with anti-mouse IgG AlexaFluor®488 *(16 µg ml^{-1}, A11029, Invitrogen™)*. Actin was stained with 50 µg ml^{-1} tetramethylrhodamine phalloidin *(R415, Molecular Probes)* and nuclei demonstrated with DAPI. Coverslips were mounted *(Mowiol®-4-88)* and reviewed as described in section 2.5.5i).

2.7.5 vital staining of live cells with antibodies 6.2E5 and 6.2G2

The VB6 cell line was seeded at a density of 2 x 10^4 cells per coverslip on 13 mm non-derivatised glass coverslips and left to adhere overnight under standard tissue culture conditions. Cells were washed in serum-free media and incubated with antibody 6.2E5 or 6.2G2 *(5 µg ml^{-1})* or 620W7 *(10 µg ml^{-1})* for 10 min at 4°C. After washing off unbound antibody, cells were either fixed and permeabilised immediately (**0'** time-point) or supplemented with complete media pre-warmed to 37°C and returned to standard culture conditions for 15 minutes to permit antibody internalisation prior to fixation and permeabilisation (**15'** time-point).

Cells labelled with 6.2E5 and 6.2G2 were counterstained post-fixation with antibody 53A2 *(10 µg ml^{-1})* for 1 hour at RT. Primary antibodies were detected with fluorophore-conjugated species-specific secondary antibodies (as previously described). After DAPI nuclear staining, coverslips were mounted in Mowiol®-4-88 and microscopically reviewed as outlined as previously described.

2.7.6 immunohistochemical evaluation of antibodies 6.2E5 and 6.2G2 in FFPE and fresh frozen primary human breast tumour samples

Fourteen FFPE and 5 case-matched fresh frozen human primary breast tumour samples were obtained with kind permission from Barts Cancer Institute Breast Tissue Bank (Research Ethics Ref: 15/EE/0192). Research samples were obtained from surgical resections, formalin fixed and processed in accordance with Tissue Bank local protocols (information not provided). Case-matched fresh frozen samples were taken prior to formalin fixation and snap frozen in liquid nitrogen and stored at −80°C, again in accordance with Tissue Bank protocols and in full compliance with the requirements of the Human Tissue Act (HTA) 2004. Cases were kindly retrieved by Dr Sally Dreger (Breast Tissue Bank Co-Ordinator, Barts Cancer Institute, QMUL).

The 14 FFPE samples were sectioned at 4 µm, dewaxed and stained with haematoxylin and eosin (H&E) *(ST5010 Autostainer XL using 3801698 H&E Staining System Kit, both Leica Biosystems).* Additional 4 µm sections were dewaxed ready

for staining using the VENTANA™ BenchMark™XT automated immunohistochemistry instrument *(Ventana Medical Systems Inc).*

Endogenous peroxidases were blocked in 3% (v/v) H_2O_2 (H1009, Sigma Aldrich) diluted in methanol (1.00837, Sigma Aldrich for 10 min. For antibody CSβ6 *(MAB2076, Calbiochem/Merck Millipore)*, sections were subjected to on-board endopeptidase enzyme-induced epitope retrieval (EIER) using Protease 1 solution *(760-2018, Ventana Medical Systems Inc)* prior to labelling with CSβ6 prepared at a 1:200 dilution *(5 μg ml^{-1})*. For antibodies 6.2E5 and 6.2G2, on-board heat-induced epitope retrieval (HIER) was achieved using ULTRA™ Cell Conditioning Solution 1 (ULTRA CC1) *(950-224, Ventana Medical Systems Inc)* before labelling with antibody 6.2E5 or 6.2G2 prepared at 5 μg ml^{-1}. Primary antibodies were detected with 3,3'-diaminobenzidine (DAB) chromogen *(ultraView Universal DAB Detection Kit, 760-500, Ventana Medical Systems Inc)* and sections counterstained on-board with haematoxylin. Sections were then mounted ready for microscopic review.

The 5 fresh frozen tissue samples were equilibrated to −20°C, mounted in Optimal Cutting Temperature (OCT) compound *(O.C.T.™ 4583, Tissue-Tek® Sakura®)* and cryosectioned at 6 μm onto positively charged slides (3800211, X-tra® Slides, Leica Biosystems Nussloch GmbH). Sections were fixed briefly in 10% (v/v) neutral buffered formalin (HT501128, Sigma Aldrich) and stained immediately either with H&E (previously described) or by IHC. For IHC, fresh frozen tissue sections were not subject to endogenous peroxidase blocking nor on-board antigen retrieval protocols. Sections were labelled with CSβ6, 6.2E5 and 6.2G2 primary antibodies, detected with DAB chromogen and counterstained with haematoxylin as described above.

Clinical samples were collected by authorised members of the Barts Cancer Institute Breast Tissue Bank under the direction of Dr Sally Dreger and Dr Sally Smith. Processing, embedding, microtomy, cryotomy and staining of sections was performed by Barts Cancer Institute Pathology Core Service under the supervision of Mr George Elia (Pathology Core Services Manager, Barts Cancer Institute, QMUL).

2.8 physiomimetic 3D-mini-organotypic gels

The use of physiomimetic 3D-culture systems using ECM-based hydrogels is now widespread practice in cancer research (Froeling *et al* 2009, Li *et al* 2013, Coleman *et al* 2014a, Carapuca *et al* 2016). These 3D-culture "organotypic" models facilitate physiologically relevant characterisation of tumour cell behaviour within the context of a surrounding stromal matrix. This better recapitulates the complexities and influence of the *in vivo* tumour microenvironment on incipient, neoplastic and malignant epithelial cells (Baker and Chen 2012).

Furthermore, these organotypic models can be readily customised to address specific research themes through co-culture with tissue-specific stromal cells and modulation of the presence and concentration of extracellular mediators including cytokines, hormones or ECM ligands as required. They also prove a useful means of pre-clinical screening to determine the efficacy and putative therapeutic benefit of novel pharmacological agents, with relative ease and rapidity (Coleman *et al* 2014b).

The commercially available Matrigel® matrix *(Corning Inc®)* comprising a solubilised preparation of ECM proteins extracted from Engelbreth-Holm-Swarm mouse sarcoma cells has been applied in both 2D and 3D-culture systems (Kibbey 1994, Corning®Inc 2016).

2.8.1 precautions for experimental set-up

All reagents used to prepare collagen (I)-Matrigel®-based mini-gels for mini-organotypic assays were thawed whilst embedded in wet ice to preserve integrity. All equipment and reagents used were kept sterile, with all procedures performed in a Class II Microbiological Safety Cabinet (laminar flow tissue culture hood) to ensure aseptic experimental set-up.

2.8.2 preparation of collagen (I)-Matrigel®-based mini-gels

Mini-organotypic cultures were prepared in a 24-well plate format using 6.5 mm Transwell® 0.4 µm Pore Polycarbonate 10 µm Membrane Inserts *(#3413, Corning®)*. Transwell® membranes were pre-treated by coating each individual membrane with 300 µl of 1% (v/v) rat-tail collagen type I *(collagen (I), #354236, Corning®)* diluted in sterile ice-cold PBS. Collagen-coated membranes were placed in a standard tissue culture incubator [37°C, 8%CO_2, humidified atmosphere] for 1 hour to permit saturation of membranes with collagen (I).

Immediately prior to use, the collagen (I)-Matrigel® gel solution was prepared according to the following protocol and kept on wet ice until required to prevent degradation of components or premature gel polymerisation.

constituent	volume (µl)	cat. no.	supplier
Collagen Type I (rat tail)	525	354236	Corning®
Matrigel®	175	354248	Corning®
[10X] DMEM	100	D2429	SigmaAldrich
fibroblast culture media	100	in-house	refer to Table 2.15
filtered FBS	100	10500-064	Gibco® ThermoFisher
1M NaOH	95	S0899	SigmaAldrich *(prepared in-house from NaOH pellets)*

Table 2.14: Preparation of collagen (I)-Matrigel® gel solution for mini-organotypic culture.
The protocol yields ~1 ml 48% (v/v) collagen (I)-16% (v/v) Matrigel® gel solution sufficient for preparation of nine x 6.5 mm Transwells® each requiring 120 µl gel mix per membrane.

Depending on number of gels required, sufficient volume of organotypic gel mix was prepared to ensure 120 µl solution per Transwell® with additional redundant volume to allow for pipetting loss. On completion of pre-treatment coating of Transwell® membranes, residual 1% (v/v) collagen (I)/PBS was removed by pipetting and discarded. Ensuring that membranes did not desiccate, 120 µl of 48% (v/v) collagen (I)-16% (v/v) Matrigel® gel solution was pipetted onto each Transwell® membrane and into the base of a spare well in the 24-well plate housing the Transwells® to facilitate monitoring of gel polymerisation.

The Transwell® membranes were then returned to the tissue culture incubator for 1 hour to permit gel polymerisation. Once set, 300 µl culture media was pipetted below the Transwell® insert and 120 µl culture media added to the top of the gel

to prevent desiccation whilst cells were prepared for seeding. When cell suspensions were ready, the media was removed by pipetting from above and below Transwell® inserts bearing the organotypic gels.

2.8.3 cell seeding and BrCa cell:fibroblast co-culture

Breast cancer cells (see Tables 2.2 and 2.3) and fibroblasts (see Table 2.15) required to establish 3D-mini-organotypic cultures were grown and harvested subconfluent (as previously described). Cells were prepared to yield a final suspension of 1 x 10^5 cells per 200 µl culture media ready for seeding directly onto mini-organotypic gels.

For control cultures, 1 x 10^5 cancer cells alone suspended in 200 µl culture media were seeded per Transwell® on top of prepared mini-organotypic gels. For organotypic co-cultures, an approximate 2:1 admixture of fibroblasts:cancer cells was prepared to yield 6.7 x 10^4 fibroblasts and 3.3 x 10^4 cancer cells per 200 µl of cell suspension. Once prepared, 200 µl of the fibroblast:cancer cell admixture was seeded per organotypic gel. A 2:1 ratio of fibroblast:cancer cells has been previously established to recapitulate the tumour-stroma niche (Kadaba *et al* 2013) and adopted into in-house 3D-culture protocols.

Fibroblast	Aetiology and Isolation	Culture Conditions
1492N	Primary human breast fibroblasts derived from the reduction mammoplasty tissue obtained from a 27-year old female. Fibroblast isolation was achieved by a method adapted from Gomm *et al* (1995) and undertaken at the Barts Cancer Institute Tissue Bank. Collagenase *(1 mg ml^{-1}, C2674, SigmaAldrich)* and hyaluronidase *(1 mg ml^{-1}, H3506, SigmaAldrich)* were used to isolate fibroblasts from resected mammary tissue yielding organoids and stromal fibroblast compartments. Three successive sedimentation steps were used to harvest fibroblasts into the supernatant for propagation into cell culture. Fibroblasts were isolated and kindly gifted by Dr J Gomm, Breast Tissue Bank, Barts Cancer Institute, QMUL.	Adherent growth DMEM/10% FBS/2 mM $_L$Glu/ amphotericin B [1 µg ml^{-1}]
3137N	Primary human breast fibroblasts derived from the reduction mammoplasty tissue obtained from a 49-year old female. Fibroblasts were isolate and kindly gifted as above.	Adherent growth DMEM/10% FBS/2 mM $_L$Glu/ amphotericin B [1 µg ml^{-1}]
FSF2	Primary human foreskin fibroblasts isolated from the prepuce of a 19-day old male. De-epidermisation of skin tissue was achieved with dispase *(D4693, SigmaAldrich)*. Fibroblasts were mechanically separated in the presence of collagenase D *(11088866001, Roche Holding AG)* and filtered through cell strainers *(22363548, Fisherbrand)*. Fibroblasts were isolated and kindly gifted by Dr Su Marsh, Blizard Institute, QMUL.	Adherent growth DMEM/10% FBS/2 mM $_L$Glu/ amphotericin B [1 µg ml^{-1}]

Table 2.15: Human fibroblasts used for mini-organotypic co-culture with breast cancer cell lines.

After either cancer cells alone or the 2:1 fibroblast:cancer cell admixture were seeded, 600 µl complete culture media was added beneath each Transwell® insert containing the now seeded mini-organotypic gel. Mini-organotypic gels were cultured for 10 days under standard tissue culture conditions [37°C, 8% CO_2, humidified atmosphere].

2.8.4 feeding and maintenance of mini-organotypic cultures

Seeded cells were left to adhere to the mini-organotypic gels for 24 hours. At 24 hours post-seeding, the residual media/cell suspension on top of the mini-organotypic gel was carefully removed by pipetting and discarded. The 600 µl culture media beneath the mini-organotypic gel/Transwell® insert was also removed and discarded.

The mini-organotypic cultures were then fed by pipetting 350 µl of complete culture media beneath, and 200 µl of serum-free media on top of each mini-organotypic gel to establish a haptotactic gradient. Cultures were maintained by

feeding every 48 hours (as described above) until the required timescale was completed and gels were ready for harvesting.

2.8.5 treatment regimens using 264RAD and Gefitinib (IRESSA®)

For mini-organotypic cultures testing the efficacy of targeted therapies, the feeding and maintenance regimen was modified to include therapeutics of interest. The integrin $\alpha_v\beta_6$ function-blocking antibody 264RAD *(a kind gift from Oncology, iMED AstraZeneca, see Table 2.6)* was used to abrogate integrin $\alpha_v\beta_6$. It is also reported to block integrin $\alpha_v\beta_8$ function (Eberlein *et al* 2013). The Gefitinib (IRESSA®) small molecule inhibitor was used to ablate EGFR signalling *(AstraZeneca, see Table 2.11)*.

Mini-organotypics were treated by supplementing both complete culture media and serum-free media used for feeding and maintenance with the desired therapeutic agent(s) as previously described. The antibody 264RAD was used at 10 μg ml^{-1} final treatment concentration as previously published (Eberlein *et al* 2013, Moore *et al* 2014). An isotype-matched human IgG *(31154, Invitrogen™, ThermoFisher)* control antibody at 10 μg ml^{-1} was used as a negative control to determine treatment effect.

Based on pharmacokinetic data from Phase I clinical trials and U.S Food and Drug Administration (FDA) approved dosing of 250 mg/day, Mukohara *et al* (2005) determined that 1 μM is the maximum achievable plasma concentration of gefitinib. Therefore gefitinib treatment was administered at 1 μM. Because the lyophilised gefitinib had been dissolved in DMSO and aliquoted for long-term storage at -20°C, a control treatment of 0.1% DMSO was used to reflect the final concentration of DMSO in organotypic cultures treated with 1 μM gefitinib.

For combined therapy, complete culture and serum-free media were prepared to comprise 10 μg ml^{-1} 264RAD and 1 μM gefitinib. The corresponding control comprised 10 μg ml^{-1} human IgG and 0.1% DMSO.

2.8.6 harvesting, fixation and processing of mini-organotypic gels

After 10 days in culture, mini-organotypic gels were formalin-fixed *(10% neutral buffered formalin, BAF-0010-25A, CellStor™, CellPath Ltd)* for 24 hours before saturation in 70% ethanol for a minimum of 30 minutes. Gels were then harvested from Transwell® inserts and bisected ready for overnight vacuum-infiltration processing (VIP) *(Tissue-Tek VIP-6, Sakura®)* and paraffin wax embedding. Specimens were then sectioned at 4 μm and stained with haematoxylin and eosin (H&E) *(ST5010 Autostainer XL using 3801698 H&E Staining System Kit, both Leica Biosystems)*. Processing, embedding, microtomy and H&E staining was kindly performed by Mr George Elia (Pathology Core Services Manager, Barts Cancer Institute, QMUL).

2.9 an immunoprecipitation method to isolate integrin $\alpha_v\beta_6$ and its trafficking partners during LAP ligand-stimulated internalisation

To identify novel binding partners associated with the integrin $\alpha_v\beta_6$ during its ligand-stimulated internalisation and trafficking, an experimental method coupling a cognate ligand-induced internalisation assay with immunoprecipitation (IP) of a human IgG (Fc')-tagged cognate ligand to isolate ligand-engaged integrin $\alpha_v\beta_6$ receptor complexes for downstream proteomic interrogation by label-free LC-MS/MS was provisionally developed.

Again, the known integrin $\alpha_v\beta_6$ cognate ligand LAP was used to specifically engage integrin $\alpha_v\beta_6$ (Thomas *et al* 2002). The transferrin receptor was used as a control and stimulated with its cognate ligand, transferrin (Hopkins and Trowbridge 1983). The BT-20 TNBC cell line was used as it exhibits endogenous, stable high expression of integrin $\alpha_v\beta_6$ (data not shown).

2.9.1 validation of LAP-Fc specificity for integrin $\alpha_v\beta_6$ engagement

The specificity of an Fc-tagged LAP ligand (LAP-Fc) *(a kind gift from Biogen Idec)* for integrin $\alpha_v\beta_6$ was evaluated by flow cytometry. The BT-20 cell line was harvested from adherent culture as previously described and subjected to integrin $\alpha_v\beta_6$ functional blockade using antibody 53A2. Cells were treated with 50 µg ml^{-1} 53A2 prepared in DMEM/0.1/0.1 and incubated for 30 min on wet ice with intermittent mixing by inversion.

Cells were then washed by centrifugation in DMEM/0.1/0.1 and then incubated for 30 min on wet ice with LAP-Fc prepared at 25 µg ml^{-1}. Cells were washed by centrifugation [1200 rpm; 3 min; 4°C] *(Avanti® J-26 RP Centrifuge, Beckman Coulter Inc)*, labelled with an anti-human IgG (Fc') antibody *(10 µg ml^{-1}, ab113636, AbCam)* to demonstrate surface bound LAP-Fc and detected with anti-mouse AlexaFluor®488 antibody. Cells were analysed by flow cytometry in the presence of 5 µg ml^{-1} propidium iodide viability indicator as outlined in section 2.4.2

2.9.2 LAP-Fc ligand-induced integrin $\alpha_v\beta_6$ internalisation assay

BT-20 cells were seeded in 10 cm culture dishes *(664160, CELLSTAR® Greiner BioOne GmbH)* at a density of 5 x 10^6 cells per dish in complete culture medium and allowed to adhere overnight at 37°C in the presence of 8% CO_2. Adherence and density was first confirmed by phase contrast microscopy *(OLYMPUS IMT-2, Olympus Corp)* prior to assay.

Adherent cell monolayers were washed in calcium-/magnesium-free PBS (PBS-) *(D8537, Sigma Aldrich)* at RT prior to 4 hr serum starvation under standard tissue culture conditions in the presence of low serum media (1% FBS/α-MEM) supplemented with 25 mM HEPES pH7.0 – 7.6 *(H3375, Sigma Aldrich)*. Cells were washed with PBS- and treated for 15 min on a gyratory rocker at 4°C with Fc-tagged ligand *(LAP-Fc, Biogen Idec* or *transferrin-Fc, Hölzel Diagnostika)* prepared at 5 μg ml^{-1} in calcium-/magnesium-replete (PBS+) (*D8662, Sigma Aldrich)*.

Upon completion of Fc-tagged ligand treatment for cognate receptor engagement, cells were washed with PBS- to remove unbound ligand. Complete media (α-MEM/15% FBS) supplemented with 20 mM HEPES and pre-warmed to 37°C was added to each 10 cm dish and returned to standard tissue culture conditions to permit internalisation of Fc-ligand-engaged receptors.

At designated time points, cells were washed with PBS- and held on wet ice prior to lysis in ice cold IP lysis buffer prepared in-house: [20 mM HEPES; 1%(v/v) IGEPAL®CA-630 *(I8896, Sigma)*; 50 mM sodium chloride (NaCl) *(10326390, Fisher Scientific)*; 1 mM calcium chloride ($CaCl_2$) *(10171800, Fisher Scientific)*; 3 mM magnesium chloride ($MgCl_2$) *(10518060, Fisher Scientific)*; 300 mM sucrose *(10346150, Fisher Scientific)*; 0.1% (w/v) sodium azide (NaN_3) *(S8032, Sigma Aldrich)*] supplemented with protease [(10 μg ml^{-1} aprotinin *(A1153, Sigma Aldrich)* and leupeptin hemisulphate *(L2884, Sigma Aldrich*); 200 μM 4-(2-aminoethyl)benzenesulphonyl fluoride hydrochloride (AEBSF-HCl) *(1056-3165, Fisher Scientific)*] and phosphatase inhibitors [15 mM sodium fluoride (NaF) *(10244540, Fisher Scientific)*; 1.5 mM sodium orthovanadate ($NaVO_4$) *(10114740, Acros Organics)*].

Given the highly labile nature of receptor-protein interactions, stabilisation of ligand-receptor-protein complexes was tested using the membrane permeant cross-linker dimethyl 3,3'dithiobispropionimidate•2HCl (DTBP) *(20665, Pierce/Thermo Scientific)* (Corgiat *et al* 2014). On completion of internalisation assay, the cell monolayer was treated with 3 mM DTBP for 30 min, before washing and harvesting lysates for IP as described above.

2.9.3 receptor-ligand complex isolation by IP

Lysates were tumbled overnight with unconjugated protein G beads *(101243, Invitrogen™)* at 4°C to immunoprecipitate Fc-tagged ligand/receptor complexes. Beads were then washed by centrifugation [3 000 rpm; 1 min; 4°C] *(eppendorf® 5417R centrifuge, Eppendorf AG)* in a series of stringency IP wash buffers at 4°C. First in a high salt buffer [1M NaCl; 0.1M Tris pH 8.0 *(Trizma®Base, 93349 Fluka)*; 0.1% (v/v) IGEPAL®CA-630; 0.1% (v/v) NaN_3] and then in a high detergent buffer [0.1M NaCl; 0.1M Tris pH 8.0; 1% (v/v) IGEPAL®CA-630; 0.3% (w/v) SDS; 0.1% (v/v) NaN_3]. Wash cycles were repeated with a final wash in a salt-free buffer [0.1M Tris pH 8.0; 0.1% (v/v) IGEPAL®CA-630; 0.1% (v/v) NaN_3].

On completion of stringency washing, supernatant was removed and beads were boiled in an equal volume of [2X] reducing SDS sample buffer (previously described) at 100°C for 5 min. Beads were pelleted by centrifugation [3 000 rpm; 1 min; RT] *(eppendorf® 5417R centrifuge, Eppendorf AG)* and the supernatant kept for Western blot validation prior to SDS-PAGE protein separation for LC-MS/MS sample preparation.

2.9.4 preparation of IP samples for LC-MS/MS

Immunoprecipitation samples were not prepared for proteomic analysis (as intended) owing to inconsistency of IP yields. Therefore, a proteomic dataset for bioinformatic analysis of IP-experiments was not generated. However, results from IP experiments were used to validate use of LAP-Fc to interrogate the integrin $\alpha_v\beta_6$ during LAP ligand-induced internalisation in the BT-20 cell line, as LAP-Fc successfully and reproducibly immunoprecipitated the integrin β_6 subunit detected by WB.

2.10 defining an integrin $\alpha_v\beta_6$–dependent "adhesome" using 2D-enrichment for adhesion complexes

In order to define an integrin $\alpha_v\beta_6$-dependent adhesion environment ("*adhesome*"), an established method for the isolation, enrichment and proteomic interrogation of transmembrane receptor-ligand complexes first reported by Humphries *et al* (2009) was adopted. This protocol permits stabilisation of notoriously labile integrin-mediated adhesion complexes facilitating their enrichment by sonication in an astringent detergent extraction buffer compatible with downstream proteomic investigation.

Again, the concept of integrin receptor-ligand specificity was exploited in order to modulate the species of integrin engaged upon different cognate ligands designed to simulate distinct, integrin-specific 2-dimensional (2D) adhesion environments. Since ligand-engagement induces integrin activation, these experiments will provide valuable insight into the nature of the adhesome downstream of integrin $\alpha_v\beta_6$ activation. The endogenous integrin $\alpha_v\beta_6$ overexpressing BT-20 TNBC cell line was also employed for the purpose of these investigations.

2.10.1 experimental work up: *determining specificity of $\alpha_v\beta_6$–mediated LAP-engagement*

The ability of BT-20 cells to bind LAP was evaluated following integrin $\alpha_v\beta_6$ functional abrogation using the integrin $\alpha_v\beta_6$ blocking rat monoclonal antibody (clone 53A2) as previously described (Section 2.9.1).

2.10.2 adhesion assay

Cell culture dishes *(100mm, 664160, CELLSTAR® Greiner BioOne GmbH)* were coated overnight at 4°C with the ligands LAP (**LAP**) *(0.5 µg ml^{-1}; L3408, Sigma Aldrich)*, fibronectin (**Fn**) *(10 µg ml^{-1}; L3408, Sigma Aldrich)* or collagen I (**Col I**) *(10 µg ml^{-1}; 354236, Corning® Inc)* prepared in ice-cold PBS+ *(D8862, Sigma Aldrich).* After coating, dishes were washed in PBS- *(D8537, Sigma Aldrich)* and blocked in 10 mg ml^{-1} BSA *(A7906, Sigma Aldrich)* for 1 hr at 4°C on a gyratory rocker. Dishes

were washed again in PBS- before adding DMEM5 [25 mM HEPES prepared in unsupplemented DMEM] to each dish and left to equilibrate at 37°C in the presence of 5% CO_2 in preparation for the adhesion assay.

After harvesting, cells were washed twice by centrifugation [1400 rpm, 4 min; RT] in PBS- pre-warmed to 37°C, resuspended in pre-warmed DMEM5 and held in suspension for 30 min at 37°C with 5% CO_2 to permit internalisation of cell surface receptor pool. Cells were washed again by centrifugation in PBS-, resuspended in pre-warmed DMEM5 and seeded on ligand-coated dishes (prepared as described above) at 5 x 10^6 cells per dish. Cells were left to adhere for 2 hr 30 under standard culture conditions. Successful cellular adhesion to ligand-coated surfaces was confirmed by phase contrast microscopy *(AxioVert.A1, Carl Zeiss® AG)*.

2.10.3 2D-enrichment for adhesion complexes

Upon completion of the assay, formed adhesion complexes were stabilised with the membrane permeant cross-linker dimethyl 3,3'dithiobispropionimidate•2HCl (DTBP) *(20665, Pierce/Thermo Scientific)* prepared in DMEM5. Cells were treated with 3mM DTBP pre-warmed to 37°C and left to incubate for 30 min under standard culture conditions. Cross-linkage was then quenched with 20 mM Tris at pH 8.0 for 5 min at RT. Cells were washed in ice cold PBS- and held at 4°C ready for adhesion complex enrichment by sonication.

Dishes were sonicated in the presence of ice cold extraction buffer [20 mM ammonium hydroxide (NH_4OH) *(221228, Sigma Aldrich)*, 0.5 % (v/v) TritonX-100 prepared in PBS-] for 1 min per dish using a SONICS® Vibra-Cell™ sonicator *(Sonics & Materials Inc.)* set to 20% amplitude and equipped with a 13 mm tapered tip probe. Cells were washed in ice cold PBS- and lysis efficiency confirmed by phase contrast microscopy. Dishes were kept at 4°C until adhesion complex harvesting by manual scraping in the presence of [2X] SDS sample buffer prepared in-house (previously described).

2.10.4 proteomic analysis of 2D-E samples by LC-MS/MS

Peptides were prepared and interrogated by tandem mass-spectrometry (LC-MS/MS) using the LTQ Orbitrap XL™ ETD Hybrid Ion Trap-Orbitrap Mass Spectrometer *(Thermo Scientific)* as outlined below.

2.10.4.1 peptide preparation

Adhesion complex-enriched samples for proteomic analysis were separated by SDS-PAGE in NuPAGE® 4 – 12% Bis-Tris Gels *(Invitrogen™)* and allowed to run 16 mm into the gel permitting dissection of gel lanes into 16 x 1 mm slices per sample. After staining with InstantBlue *(ISB1L, Expedeon)* for 60 min at ambient laboratory temperature, gels were destained in Milli-Q® ultra-pure water *(EMD Millipore, Merck KGaA)* before excision of gel lanes for manual slicing into 1 mm bands using single edge blades *(12443170/YSJ-762-Q, Fisher Scientific)*. Samples were then subject to in-gel tryptic digestion using a 96-well plate format (Humphries *et al* 2009, Jacquemet *et al* 2013) adapted from established methods (Shevchenko *et al* 1996).

Perforated 96-well *(CB0801, Proxeon/Thermo Scientific)* and U-shaped collection plates *(AB-0796 AbGene/ThermoScientific)* were assembled for the procedure. Briefly, gel bands were further diced into 1mm^3 cubes and subjected to chemical washing and dehydration. Samples were washed twice for 30 min at RT in 50% (v/v) acetonitrile (ACN) *(14261 Fluka/LC-MS Ultra CHROMASOLV®, Sigma Aldrich)* prepared in 25 mM ammonium bicarbonate (NH_4HCO_3) *(09830 Fluka, Sigma Aldrich)* with removal of wash by centrifugation [1500 rpm, 2 min]. Next, gel pieces were chemically dehydrated in 100% ACN and subsequently dried by vacuum centrifugation at 45°C *(V-AQ mode, Vacufuge®, Eppendorf AG)* until dry.

Proteins were then reduced by 60 min incubation with 10 mM dithiothreitol (DTT) *(D5545, BioXtra, Sigma Aldrich)* at 56°C prior to alkylation in the presence of 55 mM iodoacetamide (IAA) *(I1149, BioUltra, Sigma Aldrich)* at 37°C for 45 min. Gel pieces were successively washed and dehydrated by respective, alternate incubations for 5 min at RT in 25 mM NH_4HCO_3 (washing) and 100% ACN (dehydration) before drying by vacuum centrifugation as previously described. Once gel pieces were dry, proteins underwent overnight tryptic digest at 37°C in

the presence of 1.25 ng μl^{-1} trypsin *(V511A, Promega Corp.)* prepared in 25 mM NH_4HCO_3.

Following digestion, peptides were extracted by incubating gel pieces for 30 min at RT first with 0.2% (v/v) formic acid (FA)/99.8% (v/v) ACN, and then 0.1% FA/50% ACN. Peptides were collected by centrifugation [1500 rpm, 2 min] and evaporated to dryness by vacuum centrifugation (as previous). Desiccated peptides were resuspended in 5% ACN prepared in 0.1% FA, transferred to glass sample vials *(186000385C, Waters Ltd)* and stored at -20°C until acquisition.

2.10.4.2 LC-MS/MS data acquisition

Peptides were analysed by ultra performance liquid chromatography (UPLC) tandem mass spectrometry (LC-MS/MS) on a nanoACQUITY UPLC® ultra performance liquid chromatography system *(Waters Ltd)* coupled to an LTQ Orbitrap XL™ ETD Hybrid Ion Trap-Orbitrap Mass Spectrometer *(Thermo Scientific)*. Peptides were concentrated, desalted and separated on a 75-minute linear gradient from 1% to 25% (v/v) ACN in 0.1% (v/v) FA. Peptides were automatically selected for fragmentation by data-dependent analysis.

2.10.4.3 proteomic data analysis

Raw SEQUEST.dta data files from LC-MS/MS runs were searched using Mascot Daemon *(version 2.2.2, Matrix Science©)* for peptide identification based on peak intensities against entries held in the International Protein Index (IPI) Human database (version 3.70, released 4th March 2010). Searches were submitted to a Mascot server located at the Wellcome Trust Centre for Cell Matrix Research, University of Manchester *(http://msct.smith.man.ac.uk/mascot/home.html; Matrix Science)*.

Cysteine (C) residue carbamidomethylation was set as a fixed modification. Phosphorylation of serine (S), tyrosine (Y) and threonine (T) residues was permitted as variable modifications. Additionally, oxidation of methionine (M) residues and hydroxylation of proline (P) residues were also assigned permissible as variable

modifications. Only tryptic peptides were considered with allowance for up to 2 miscleavages. Both peptide and fragment ion tolerance were set at 0.5 Da with only double and triply charged fragment ions considered.

Mascot (.mgf) files were reviewed in Scaffold™ v4.3.2 *(Proteome Software© Inc, USA)* for data pre-processing to exclude ambiguities in peptide assignment and validate spectral count data. For all LC-MS/MS datasets, identification threshold criteria were set to ≥99% at the protein level and ≥50% at the peptide level with identification of ≥ 2 unique validated peptides. Once validated, peptides were quantified using an established spectral counting method reported for analysis of label free proteomic strategies (Kito and Ito 2008). Spectral counts for each identified protein were normalised against both the total number of spectra detected in a given sample and molecular weight (kDa) of the protein of interest.

Network mapping of protein-protein interactions was performed using the well-established open source software Cytoscape v3.1.1 *(Cytoscape Consortium©, National Resource for Network Biology)* for visualizing molecular interaction networks and biological pathways (Shannon *et al* 2003, Cline *et al* 2007, Smoot *et al* 2011, Saito *et al* 2012). A human protein interaction network comprising entries curated by the Protein Interaction Network Analysis (PINA, 10th December 2012) (Wu *et al* 2009, Cowley *et al* 2012) with adaptations to encompass the Integrin Adhesome (Zaidel-Bar *et al* 2007) and Matrisome Project (Hynes and Naba 2012, Naba *et al* 2012a, Naba *et al* 2012b).

2.10.5 bioinformatic analysis of 2D-E/LC-MS/MS datasets

After data pre-processing and spectral count validation, 2D-E datasets were provisionally analysed using a logic-gating strategy in Microsoft®Excel® for Mac 2011 v.14.2.5. Inclusion criteria for validated peptides for PPI network mapping were set at a ≥ 2-fold enrichment with ≥5 unweighted spectral counts (USC) in a single experiment, or ≥4 unweighted spectral counts in at least two biological replicate experiments. Peptides compliant with these criteria were mapped as previously described.

2.11 phosphoproteomic definition of active, LAP ligand-engaged integrin $\alpha_v\beta_6$–mediated signalling

Little is currently known regarding specific downstream signalling events inducted upon integrin $\alpha_v\beta_6$ ligand engagement and subsequent receptor activation. The integrin $\alpha_v\beta_6$ is known to recognise and engage the LAP sequence of TGF-β1, leading to TGF-β1 activation and signalling (Thomas *et al* 2002, Munger and Sheppard 2011, Khan and Marshall 2016). Therefore, to define integrin $\alpha_v\beta_6$–dependent signalling, phosphoproteomic interrogation of lysates generated from a LAP-ligand stimulation assay was undertaken to characterise the active integrin $\alpha_v\beta_6$ kinome. Time-points were selected to capture early (5'), intermediate (15') and late (30') signalling events, in addition to a baseline control time-point (0').

Acknowledgements and thanks are given to Dr Pedro Cutillas and Dr Edmund Wilkes *(Cell Signalling & Proteomics Group, Centre for Haemato-Oncology, Barts Cancr Institute, QMUL)* for their collaboration with the phosphoproteomic investigations. Particular thanks are extended to Dr Wilkes who kindly supervised solid-phase extraction and phosphoenrichment of peptides and performed bioinformatic analyses.

2.11.1 LAP-ligand stimulation assay

The TNBC BT-20 cell line was seeded in 10 cm culture dishes *(664160, CELLSTAR® Greiner BioOne GmbH)* at 5 x 10^6 cells per dish in complete culture medium and left to adhere overnight under standard culture conditions (37°C/8% CO_2). Immediately prior to assay, adherence and density were confirmed by phase contrast microscopy *(OLYMPUS IMT-2, Olympus® Corp)* to ensure sufficient cell volume for protein yield.

Adherent cell monolayers were washed in TBS *(BP24711, Fisher Scientific)* at RT prior to 4 hr serum starvation under standard tissue culture conditions in the presence of low serum media comprising charcoal-stripped FBS *(126760929, Gibco™, ThermoFisher Scientific)* supplemented with 25 mM HEPES pH 7.0 – 7.6 *(H3375, Sigma Aldrich)* (1%FBS/α-MEM/25 mM HEPES) Following serum starvation, cell monolayers were treated with human recombinant LAP *(0.5 μg ml^{-1},*

L3408, Sigma Aldrich) for 10 min whilst buried on wet ice and placed on an orbital shaker in a walk-in cold room at 4°C. Monolayers were washed (x3) in pre-chilled serum-free α-MEM to remove all unbound ligand. Complete media (15% charcoal-stripped FBS/α-MEM) supplemented with 25 mM HEPES was equilibrated to 37°C and added to the 30', 15' and 5' time-point dishes respectively (5 ml per dish) and returned to standard culture conditions (8%CO_2/37°C /humidified atmosphere) to permit ligand internalisation. The baseline control time-point was not subject to internalisation.

Ligand internalisation was quenched by flooding with TBS pre-chilled to 4°C and supplemented with phosphatase inhibitors: 1 mM sodium orthovandate (Na_3VO_4; *450243, Sigma Aldrich*) and 0.5 mM sodium fluoride (NaF; *01151, Sigma Aldrich*).

A total of four biological replicates were performed across two experiments; each experiment comprised two biological replicates run in tandem.

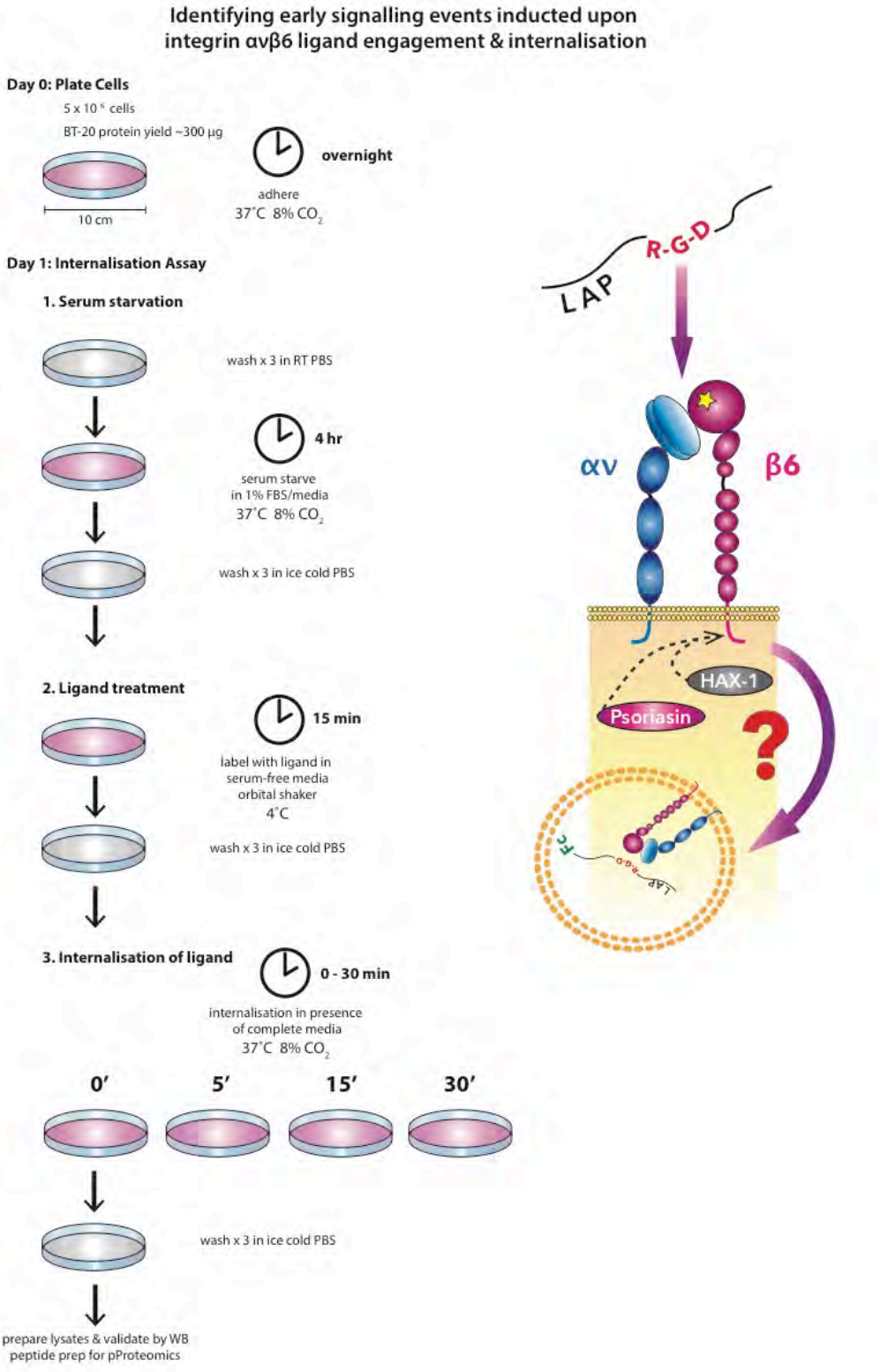

Figure 2.2
Schematic overview of LAP-ligand stimulation and internalisation assay for phosphoproteomic characterisation of LAP-engaged integrin $\alpha_v\beta_6$ activation and downstream signalling events

2.11.2 cell lysis, peptide digestion and solid-phase extraction

Cells were lysed and manually harvested by scraping on wet ice in the presence of pre-chilled (4°C) phosphoproteomic lysis buffer comprising 8 M urea/20mM HEPES pH 8.0 *(U4883 and H3375 respectively, both Sigma Aldrich)* supplemented with: 0.5 M NaF, 0.1 M Na_3VO_4, 1M disodium β-glycerophosphate ($CH_3H_7Na_2O_6P$; *50020, Sigma Aldrich*) and 0.25 M disodium pyrophosphate ($Na_2H_2P_2O_7$; *71501, Sigma Aldrich*). Lysates were sonicated at 20% intensity for 3 x 10 s *(SONICS® Vibra-Cell™ Ultrasonic Liquid Processor VCX750, Sonics & Materials Inc.)* whilst buried in ice, prior to centrifugation at 13 000 rpm for 10 min at 4°C *(eppendorf® 5417R, Eppendorf AG)*.

Lysis supernatants were decanted into pre-labelled, pre-chilled 2 ml Eppendorf® Protein Lo-bind microcentrifuge tubes *(Z666513, Sigma Aldrich)* using low-binding pipette tips *(Corning® DeckWorks™)* to preserve protein yield. Lysates were then stored at −80°C prior to protein concentration assay in preparation for peptide desalting, titanium oxide (TiO_2) phosphoenrichment, solid-phase extraction and interrogation of phosphopeptides by LC-MS/MS.

Lysates were thawed on wet ice and protein concentrations determined using a Pierce™ BCA Protein Concentration Assay *(23227, ThermoFisher Scientific)* in accordance with manufacturer's guidelines. Samples were then normalised to a final concentration of 250 µg protein in 250 µl sample volume (1 µg μl^{-1}) in pre-chilled phosphoproteomic lysis buffer.

Cysteine residues were reduced in the presence of 10 mM dithiothreitol (DTT; *D5545, Sigma Aldrich)* for 30 min in the dark at RT prior to alkylation in the presence of 40 mM iodoacetamide (IA; *I1149, Sigma Aldrich)*, again for 30 min in the dark at RT. Proteins were digested in suspension using $_L$-(tosylamido-2-phenyl) ethyl chloromethyl ketone (TPCK)-treated trypsin immobilised on agarose resin beads *(20230, ThermoFisher Scientific)* which had been pre-conditioned by washing and centrifugation (2000 g, 5°C, 5 min) in 20 mM HEPES pH 8.0. Samples were incubated with immobilised trypsin beads for 16 hr at 37°C with constant agitation to facilitate protein digestion.

Trypsin beads were then removed by centrifugation [2000 g, 5°C, 5 min] *(eppendorf® 5430R, Eppendorf AG)*. The resulting peptide solutions were desalted by reversed solid-phase extraction (SPE) using OASIS® HLB (Hydrophilic-Lipophilic Balance) Extraction Cartridges *(186000383, Waters Corp)* rigged to a 12-port Visiprep™ SPE Vacuum Manifold *(57030-U SUPELCO, Sigma Aldrich)* to control flow rate (P=5.0 inHg ±0.5 inHg).

Columns within the cartridge were first conditioned each with 1 ml 100% acetonitrile (ACN; *1.00029, EMD Millipore)* before equilibration with 1 ml 1% ACN/0.1% TFA *(trifluoroacetic acid; 302031-M EMD Millipore, Sigma Aldrich)* (v/v) prepared in molecular grade water (mH_2O; *W4502, Sigma Aldrich)* and washing with 500 µl 1% ACN/0.1% TFA (v/v) in mH_2O. Peptide samples were then loaded into conditioned, equilibrated cartridge columns and purged at a low flow rate. Columns (with peptides now bound to sorbent) were washed in 1 ml 1% ACN/0.1% TFA (v/v) in mH_2O prior to elution of desalted peptides in 250 µl 1 M glycolic acid *(G8284, Sigma Aldrich)* prepared in a solution of 50% ACN/5% TFA (v/v) ready for phosphopeptide enrichment.

2.11.3 TiO_2 metal oxide affinity chromatography (MOAC)

Samples were enriched for phosphopeptides by metal oxide affinity chromatography (MOAC) using titanium dioxide (TiO_2). Desalted peptides were normalised to 500 µl with 1 M glycolic acid/80%ACN/5%TFA. Next, 125 mg dry weight of Titansphere® TiO 10 µm particles *(5020-75010, GL Sciences Inc)* (equivalent to 12.5 mg particles per sample) was reconstituted in 250 µl 1% TFA and vortexed to ensure a homogenous suspension of Titansphere® particles.

Normalised peptide samples were then incubated with 25 µl of this Titansphere® slurry (equivalent to 12.5 mg Titansphere® particles per sample) for 5 min at RT with constant agitation. Next, the enriched phosphopeptides were eluted by centrifugation [2 min, 1500 rcf] *(eppendorf® 5430R, Eppendorf AG)* using TopTip™ micro-spin columns *(TT3, Glygen Corp)* previously washed with 100% ACN. Titansphere® particles were sequentially washed on a gradient accordingly: 1 M glycolic acid/80% ACN/5% TFA (x 1), 100 mM ammonium acetate ($NH_4CH_3CO_2$)/25% ACN (x 1) and 10% ACN (x 3).

Bound phosphopeptides were eluted from Titansphere® particles by washing with 50 µl 5% NH_4OH/10% ACN/mH_2O per elution and centrifuging for 2 min at 1500 rcf. A total of 5 elutions were performed. Once eluted, phosphopeptide samples were immersed in dry ice to permit sublimation of NH_4OH and desiccated overnight using a Vacufuge® Vacuum Concentrator *(Eppendorf Ltd)*. Samples were then stored at −80°C ready for mass spectrometry.

2.11.4 nanoflow-liquid chromatography tandem mass spectrometry

Immediately prior to use, samples for analysis were reconstituted with 20 µl 50 nM enolase peptide digest *(MassPREP™ Enolase Digest Phosphopeptide Mix, 186003286, Waters Corp)* dissolved in 5% ACN/0.1% TFA, subjected to bath sonication (15 min, RT) and centrifugation (5 min, 5°C) to recover supernatants for LC-MS analysis.

Phosphopeptide liquid chromatography (LC) separations were performed using a Dionex UltiMate™ 3000 RSLCnano UHPLC system *(ThermoFisher Scientific)* with an Acclaim™ PepMap™ 100 C18 RSLC Analytical Column (75 µm x 25 cm, 3 µm, 100Å) *(164261, ThermoFisher Scientific)* and Acclaim™ PepMap™ 100 C18 Trap Column (100 µm x 5 cm, 5 µm, 100Å) *(160434, ThermoFisher Scientific)*. Solvents used for LC separation comprised; solvent A: 2% ACN/0.1% formic acid (FA) and solvent B: 80% ACN/0.1% FA. Sample injections of 3 µl were loaded onto the trap column at a flow rate of 8 µl min^{-1} over 5 min. After loading, samples were eluted along an 85 min gradient from 6.3% to 43.8% solvent A prior to column cleaning in 90% solvent B for 10 min and equilibration with 6.3% solvent A for 10 min.

All analyses were performed on the Thermo Scientific LTQ Orbitrap™-Velos™ Hybrid FT spectrometer. The instrument was operated in data-dependent acquisition (DDA) mode, whereby a full MS^1 survey scan (m/z 350 – 1500) was completed at a resolution of 30 000 FWHM (m/z 400) and ions were analysed in the Orbitrap™. The top 7 most intense multiply charged precursor ions detected in the MS^1 survey scan were automatically mass-selected for fragmentation by collision-induced dissociation (CID) with multi-stage activation enabled and analysed in the LTZ-Velos™ linear ion trap (m/z 190 – 2000). Dynamic exclusion

was enabled to prevent repeat analysis of identical precursor ions within a 60 min window).

2.11.5 identification and quantification of phosphopeptides

Mascot Daemon and Distiller software *(v2.3.0.0 and v2.4.2.0 respectively, both Matrix Science)* were used to convert exported LTQ Orbitrap™-Velos™ .raw files into .mgf files for peak list searches against the UniProtKB/SwissProt human proteome database (UniProtConsortium 2017). Data were searched according to the following criteria: ±10 ppm precursor and ±600 mmu fragment ion m/z tolerances; digestion enzyme = trypsin (2 missed cleavages tolerated); fixed modification: carbamidomethyl (C); variable modifications: oxidation (M), phospho (ST), phospho (Y) and gln −> pyro-glu (glutamine −> pyroglutamate) (Q) at N-terminus.

Mascot search engine results for phosphopeptide identification were collated using Perl script *(Perl® 5, Perl.org)* and Post Analysis Data Acquisition v1.1 (PAnDA) software (Hoopmann *et al* 2009). Data were curated algorithmically to include only unique phosphopeptide ions with a q-value ≤0.05, calculated by comparison to searches against a randomised database. All phosphopeptides assigned a Mascot delta score ≥10 were reported as the specific phosphorylation site.

Phosphopeptides were quantified using PEak Statistical CALculator (PESCAL) *(Barts Cancer Institute, QMUL)* (Cutillas and Vanhaesebroeck 2007) to generate extracted ion chromatograms for the first three isotopes of each phosphopeptide ion within the database (±7 ppm m/z tolerance, ±1.5 min retention time tolerance, isotope correlation >0.8) enabling calculation of peak height for each constructed extracted ion chromatogram.

Using the R statistical programming environment *(R 3.2.5, The R Foundation)*, the peak heights for each phosphopeptide ion were then $\log_2$-transformed, quantile normalised and fitted to a linear model where difference in magnitude and statistical significance between time-points was calculated using Bayes shrinkage of standard deviations (Smyth 2004). The p-values generated were then subject to Benjamini-Hochberg post-hoc analyses to correct for multiple testing. Kinase

Substrate Enrichment Analysis (KSEA) was performed on the dataset as previously described (Casado *et al* 2013a), in order to infer phosphoproteomic network activity and plasticity.

2.12 kinase inhibition studies to investigate putative mechanisms regulating integrin $\alpha_v\beta_6$ activation

Putative regulatory nodes of kinase activity downstream of integrin $\alpha_v\beta_6$ LAP ligand-mediated activation were identified by both raw and inferential KSEA analyses of the phosphoproteomic dataset. To evaluate the role of the identified kinases during LAP-mediated integrin $\alpha_v\beta_6$ activation and downstream signalling, preliminary kinase inhibition studies were undertaken.

Commercial small molecule kinase inhibitors (listed in Table 2.11) were used to ablate kinase function prior to stimulation assays with known integrin cognate ligands. The effects of a functional loss of the targeted kinase on integrin $\alpha_v\beta_6$–mediated functions and signalling, were evaluated by flow cytometry and Western blotting respectively.

2.12.1 kinase inhibition assay to dissect integrin $\alpha_v\beta_6$–dependent signalling

Breast cancer cell lines (BT-20, MDA-MB-468 and SUM159) were seeded in 6 cm tissue culture dishes at a density of 3 x 10^6 cells per dish in complete media and allowed to adhere overnight under standard culture conditions. Prior to assay, cell condition, adherence and confluence were confirmed by phase contrast microscopy *(OLYMPUS IMT-2, Olympus® Corp)*.

Cell monolayers were washed in serum free media (3 x 2 ml per dish) to remove all residual FBS and growth factors, prior to serum starvation in the presence of low-serum culture media (1% (v/v) FBS/20 mM HEPES/cell line-specific media; 2 ml per dish) for 4 hr under standard culture conditions.

Kinase inhibitors (**EGFR**: *gefitinib (IRESSA®)*; **c-MET**: *PHA665752*; **COT**: *TC-S7006*) were prepared to yield 1 µM treatment concentration in the appropriate low-serum culture media. Vehicle control treatments (**veh**) were also prepared comprising 0.1% DMSO. Upon completion of serum starvation, media was removed from culture dishes and replaced with 2 ml per dish of required kinase inhibitor or control treatment prepared in low serum media and equilibrated to

37°C. Cells were subject to inhibitor or vehicle control treatments for 30 min under standard culture conditions.

At the end of inhibition treatments, human recombinant ligands were spiked in at the final stimulating concentrations as follows: LAP *(0.5 µg ml^{-1}, L3408, Sigma Aldrich)*, EGF *(50 ng ml^{-1}, E9644, Sigma Aldrich)* or HGF *(50 ng ml^{-1}, H9661, Sigma Aldrich)*. In the unstimulated dishes, an equivalent volume of serum-free media alone was spiked in, in lieu of inhibitor volume. Cells were ligand stimulated for 10 min under standard culture conditions.

Ligand stimulation was quenched by burying dishes in wet ice and flooding with pre-chilled (4°C) TBS supplemented with: 1 mM sodium orthovandate (Na_3VO_4; *450243, Sigma Aldrich*) and 0.5 mM sodium fluoride (NaF; *01151, Sigma Aldrich*). Lysates from each sample and treatment condition were harvested manually by scraping in the presence of pre-chilled Nonidet P-40 *(FNN0021, Invitrogen™)* supplemented with protease and phosphatase inhibitors diluted 1:100 in Nonidet P-40 *(Protease Inhibitor Cocktail Set I 539131 and Phosphatase Inhibitor Cocktail Set II 524625, both Calbiochem®)*.

Lysates were aliquoted to prevent freeze-thaw artefacts or degradation of protein moieties prior to storage at −20°C before evaluation by WB. When required, lysates were thawed on wet ice ready for protein concentration quantification and immunoblotting (as previously described, Section 2.6.1) to evaluate changes in protein phosphorylation signatures.

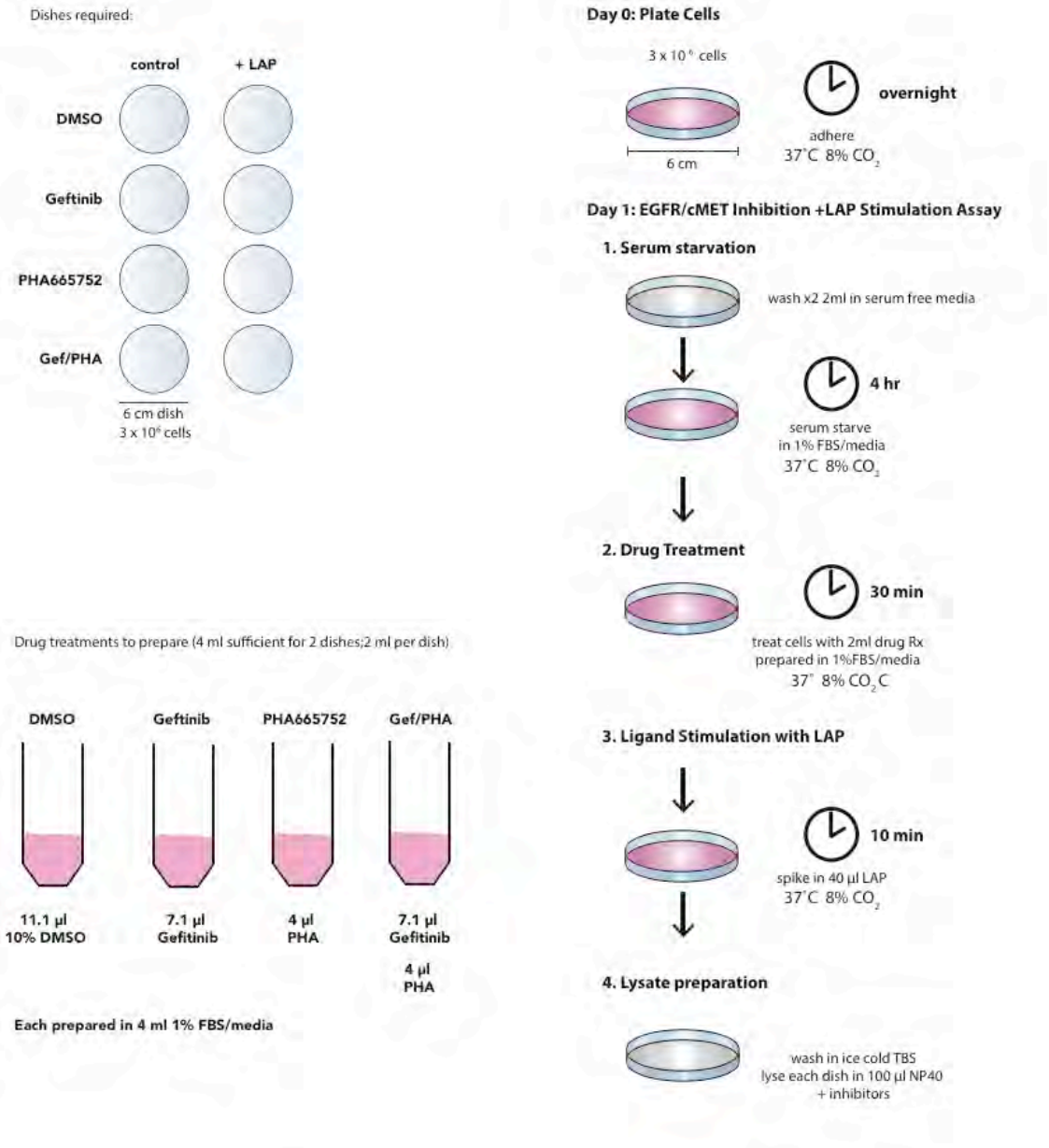

Figure 2.3
Schematic overview of kinase inhibition/LAP-ligand stimulation assay to investigate the regulatory effects of targeted kinases during LAP-mediated integrin $\alpha_v\beta_6$ activation and downstream signalling events

2.12.2 kinase inhibition assay to dissect integrin $\alpha_v\beta_6$–ligand engagement and cell surface receptor activation

The BT-20 and VB6 cell lines were cultured to 80% confluence prior to harvesting by trypsinisation (as previously described, section 2.4). Cells were manually counted, resuspended to 4 x 10^6 cells ml^{-1} and serum starved in low-serum media (1% FBS (v/v)/20 mM HEPES/media) in suspension in a vented 50 ml Falcon tube for 4 hr under standard culture conditions.

Following serum starvation, aliquots of the cell suspension were subject to 1 μM kinase inhibition or 0.1% DMSO vehicle control treatment for 30 min, again in suspension and under standard culture conditions. Cell/treatment preparations were inverted to mix thoroughly to ensure a homogenous cell suspension prior to commencement of treatment time.

Next, cells were subject to canonical integrin $\alpha_v\beta_6$ activation methods by stimulation with either: 1 mM Mn^{2+} ions *($MgCl_2$ / Mg^{2+}: M8266, Sigma Aldrich)* or cognate ligand LAP-Fc *(2 μg ml^{-1}, Biogen Idec)*, as previously described in sections 2.7.1.2 and 2.7.2.2 respectively.

Cells were then labelled for flow cytometric evaluation of: integrin $\alpha_v\beta_6$ activation status *(demonstrated by antibody clone 6.2E5, Biogen Idec)*, cell-surface bound LAP *(demonstrated by an anti-Fc antibody, ab113636, AbCam)* and total surface integrin $\alpha_v\beta_6$ expression *(demonstrated by antibody clone 53A2, CR-UK)* in the presence and absence of functional kinase moieties targeted by the small molecule inhibitors used.

Labelling, gating, acquisition and analysis of samples by flow cytometry was undertaken as previously described (Section 2.4).

2.12.3 metabolic MTT cell viability assay to compare target kinase requirement for cell proliferation in an integrin β_6 positive and an integrin β_6 negative cell line

The A375puro (integrin $\alpha_v\beta_6$ null) and A375B6 (integrin $\alpha_v\beta_6$ positive) malignant melanoma (MM) cell lines were seeded in complete media at 3.6 x10^4 cells per well in a 96-well tissue culture plate *(3595, Corning® Inc)* and left to adhere overnight. Adherence and cell density were checked by phase contrast microscopy *(OLYMPUS® TM-2, Olympus Corp)* before treatment with small molecule inhibitors (SMI) of kinase activity.

An inhibitor targeting MAP3K8/COT kinase *(TC-S 7006, 5240/10, Tocris, R&D Systems)* and an inhibitor targeting MAPKAPK2 kinase *(MK-II, sc-221948, Santa Cruz Biotechnology)* were prepared in serum-free media. Cells were treated (6 replicate wells per concentration) with TC-S7006 or MK-II over a concentration range of 0 – 1000 nM (0 – 1 µM) for 72 hours under standard culture conditions.

On completion of 72-hour culture in the presence of SMI, media was removed and replaced with 100 µl 3-(4,5-dimethyl-2-thiazolyl)-2,5-diphenyl-2H-tetrazolium bromide *(MTT, M5655, Sigma Aldrich)* prepared at 0.2 mg ml-1 in serum free media. Cells were incubated in the presence of MTT at 37°C for 1 hr in the dark. At the end of incubation, MTT was removed and replaced with 100 µl 100% DMSO to solubilise the MTT-formazan reaction product ready for reading optical density (OD) per well at 570 nm using the Infinite®F-50 *(Tecan Trading AG)* platereader to determine cell viability per well.

Values for OD (AU) readings were normalised against assay matrix background OD values and converted to % viability values based on OD values for 0 nM SMI being equivalent to 100% cell viability. Values for % viability for each concentration were plotted using GraphPad Prism Software to generate curves of best fit using the non-linear regression curve analysis *(log(inhibitor) vs normalised response – variable slope)* function.

2.13 quality control procedures

To ensure biological and technical validity of results, all methods employed were subject to quality control procedures. For biological validation, matched pair cell lines known to be positive and negative for integrin $\alpha_v\beta_6$ expression (see Table 2.1, section 2.1) were prepared in conjunction with target BrCa cell lines of interest for FCM, WB and IMF procedures.

Technical validation was achieved by inclusion of isotype-matched negative control antibodies (see Table 2.8, section 2.2). Untreated controls were included where methodologically appropriate. Cross-reactivity and off-target binding of antibodies were evaluated by IMF microscopy before undertaking double or triple antibody labelling.

2.14 other considerations

2.14.1 ethical considerations

The established human cell lines utilised in this study (outlined in Tables 2.1 – 2.3) are not deemed "*relevant material*" under the terms of the Human Tissue Act (HTA) 2004 and are not subject to statutory regulation therein (HTA 2004). Primary human breast tissue samples were obtained from the Breast Cancer Now Tissue Bank (R02/16), Barts Cancer Institute, QMUL, London. Informed consent for storage and research use was given (Ethics Code: 15/EE/0192). No animal procedures were undertaken, obviating requirements for personal licensure under the terms of the Animals (Scientific Procedures) Act (ASPA) 1986 (ASPA 1986).

2.14.2 health & safety considerations

All national and local guidelines governing Health & Safety, Control of Substances Hazardous to Health (COSHH), Manual Handling, Risk Assessments (Equipment & Reagents) and use of personal protective equipment (PPE) were reviewed prior to, and strictly adhered to, whilst undertaking experimental work at both host research institutions.

2.15 statistical analyses

Graphical representation of data and their accompanying statistical analyses were undertaken using GraphPad Prism® 5.0b for MacOSX *(GraphPad Software Inc.)* unless otherwise stated. Details of statistical tests, where applied, and significance levels are given within the relevant methods sections and/or results figure legends.

chapter III

results part I

establishing the utility of antibodies 6.2E5 & 6.2G2 to study the active subpopulation of integrin $\alpha_v\beta_6$

III

identifying the active conformer of integrin $\alpha_v\beta_6$ using monoclonal antibodies

antibodies 6.2E5 & 6.2G2 recognise active conformers of the integrin $\alpha_v\beta_6$

3. introduction

Bidirectional signalling is an irrefutable tenet of integrin functional biology. Regulatory modulation of integrin activation via recruitment of intracellular molecular regulators to the β–subunit cytoplasmic tail (*"inside-out"* signalling), or by exposure of the extracellular domain to extracellular regulators including growth factors, cognate ligands, presence of divalent cations or changes in ECM spatio-tensile forces (*"outside-in"* signalling) have been extensively characterised and validated as canonical integrin activation modalities (Humphries 1996, Shimaoka *et al* 2002, Shattil *et al* 2010, Campbell and Humphries 2011, Kim *et al* 2011a, Kim *et al* 2011b, Pouwels *et al* 2012, Welf *et al* 2012, Bouvard *et al* 2013, Calderwood *et al* 2013).

Since extracellular regulation of integrin activation mediated by the presence of divalent cations (Smith *et al* 1994, Mould *et al* 1995b, Tiwari *et al* 2011) or by cognate ligand engagement (Humphries 1996, Luo et al 2007) are such well-established concepts, canonical *"outside-in"* integrin activation methods utilising divalent cations or cognate ligands were performed to evaluate the ability of 2 novel monoclonal antibodies, clones 6.2E5 and 6.2G2 *(Biogen Idec),* to recognise

the integrin $\alpha_v\beta_6$ in its active conformation. Following their generation, these clones were first briefly described by Weinreb *et al* (2004) as non-blocking anti-integrin $\alpha_v\beta_6$ antibodies, based on their inability to abrogate integrin $\alpha_v\beta_6$ ligand engagement in solid phase LAP-binding and cell adhesion assays.

However, unpublished data previously generated in-house provided a rationale for considering the possibility that antibodies 6.2E5 and 6.2G2 may recognise active conformers of the integrin $\alpha_v\beta_6$. DiCara and Saha (2006) conducted preliminary experiments screening the binding affinities of antibodies 6.2E5 and 6.2G2 in comparison with the well-characterised ligand-mimetic antibody 10D5 (data not published). Flow cytometry results indicated that antibodies 6.2E5 and 6.2G2 bound less cell surface integrin $\alpha_v\beta_6$ than antibody 10D5. To ascertain whether differences in antibody affinity were the cause of this observed difference in binding kinetics, ELISA screens were performed.

Binding kinetics were evaluated against purified, secreted recombinant full-length integrin $\alpha_v\beta_6$ and a truncated variant lacking the transmembrane and cytoplasmic domains of the β_6-subunit as first engineered in CHO cells by Weinacker *et al* (1994). The antibodies 6.2E5 and 6.2G2 bound both full length and truncated recombinant integrin $\alpha_v\beta_6$ by ELISA more abundantly than had been observed for native cell surface integrin $\alpha_v\beta_6$ in flow cytometry experiments. These findings excluded affinity as the reason for observed differences in binding kinetics (data not shown).

Furthermore, since recombinant integrins immobilised in an ELISA assay are unable to modify conformation, they are deemed to mimic constitutively active integrins. Since the antibodies 6.2E5 and 6.2G2 bound immobilised recombinant integrin $\alpha_v\beta_6$ with greater efficacy than native cell surface integrin $\alpha_v\beta_6$, it was hypothesised that these antibodies may recognise an activation epitope. Therefore, further characterisation of the properties of antibodies 6.2E5 and 6.2G2 was deemed prudent to fully evaluate their potential efficacy in future investigations into the biological and pathological functions of the integrin $\alpha_v\beta_6$.

Validation of the utility of antibodies 6.2E5 and 6.2G2 to discriminate the active subpopulation of integrin $\alpha_v\beta_6$ would permit future research into the biological significance of integrin $\alpha_v\beta_6$ activation status using a monoclonal antibody-based

approach, as discussed by Byron *et al* (2009) and successfully employed by Arjonen *et al* (2012) to unpick the complexities of the distinct, differential trafficking kinetics of the active and inactive conformers of β_1 integrin. Thus, it is hoped that the antibody clones 6.2E5 and 6.2G2 will prove valuable, novel tools to dissect the putative aetiological relevance of integrin $\alpha_v\beta_6$ activation status during breast tumourigenesis and disease progression.

overview of key findings

To summarise the key findings, results from canonical integrin activation experiments demonstrate that both antibodies 6.2E5 and 6.2G2 each recognise a cation-induced activation-associated epitope and a ligand-induced binding site (LIBS) on the integrin $\alpha_v\beta_6$ revealed respectively by extracellular activation methods including treatment with manganese ions (Mn^{2+}) (Figures 3.1.1 and 3.1.2) or cognate ligands bearing an RGD motif (Figures 3.2.1 and 3.2.2).

Comparison of these results with activation kinetics of a ligand-mimetic (clone 10D5) and a non-ligand mimetic (clone 53A2) anti-integrin $\alpha_v\beta_6$ functional blocking antibody suggests the antibodies 6.2E5 and 6.2G2 are non-ligand mimetic and do not bind via the RGD cleft requisite for ligand binding (Figure 3.2.3). Antibody binding kinetics were quantified by flow cytometry using the geometric mean fluorescence intensity (geoMean MFI) of surface-bound antibody as a read out for cell surface abundance of integrin $\alpha_v\beta_6$ sub-populations recognised by each anti- integrin $\alpha_v\beta_6$ specific antibody.

Qualitative, observational immunofluorescence (IMF)-based characterisation of antibodies 6.2E5 and 6.2G2 confirmed their efficacy for *in vitro* studies to visualise the subcellular distribution of the active subpopulation of integrin $\alpha_v\beta_6$ in adherent cells (Figure 3.3.1), cells adhering to and spreading on integrin cognate ligands (Figure 3.3.2) and live cells (Figure 3.3.3).

Finally the utility of these antibodies to distinguish the active fraction of integrin $\alpha_v\beta_6$ in clinical samples was evaluated by comparison of the tissue-distribution of

the 6.2E5 and 6.2G2 epitopes in both fresh frozen and FFPE integrin $\alpha_v\beta_6$–positive primary breast tissue samples from 5 patients kindly supplied by Barts Cancer Institute Breast Tissue Bank (Ethics code 15/EE/0192) (Figures 3.4.1 and 3.4.2).

After initial IHC screening for integrin $\alpha_v\beta_6$ expression to identify suitable cases (Figure 3.4.1), subsequent IHC analysis of the immunopositive distribution of epitopes recognised by antibodies 6.2E5 and 6.2G2 in FFPE versus fresh frozen tissue samples (Figure 3.4.2) did not conclusively demonstrate their ability to recognise a unique integrin $\alpha_v\beta_6$ subpopulation definitively distinct from gross integrin β_6-subunit expression revealed by antibody CSβ6 *(Calbiochem)*.

3.1 antibodies 6.2E5 and 6.2G2 each recognise an activation-associated epitope revealed by canonical extracellular activation of integrin $\alpha_v\beta_6$ using divalent Mn^{2+} cations

Both the species of divalent cation and the metal-ion binding site within the integrin that it occupies have been widely reported to modulate integrin activation and affinity for cognate ligand (Day *et al* 2002, Chen *et al* 2003, Shimaoka and Springer 2003). Several metal-ion binding motifs that modulate integrin conformation and ligand affinity have been mapped to specific regions of integrin heterodimers.

In their review, Zhang and Chen (2012) comprehensively précised current understanding of integrin metal-ion binding motifs. A metal-ion-dependent adhesion site (MIDAS) has been described in the α-subunit β-propeller region. Specifically, this MIDAS is located in the αI domain of αI-bearing integrins, and in the βI domain of non-αI domain integrin species. In non-αI integrins, a βI domain metal ion cluster has been characterised. It comprises an interlinked linear array of a central MIDAS flanked by two distinct metal-ion binding motifs; the adjacent to MIDAS (ADMIDAS) and synergistic metal ion-binding site (SyMBS), the latter formerly being named ligand-associated metal-ion binding site (LIMBS).

Both the αI and βI domain MIDAS critically regulate metal ion coordination and subsequent ligand engagement. Mutational abrogation of MIDAS metal-ion coordination abolished integrin ligand interactions in both αI and non-αI bearing integrin species, demonstrative of the essential role of MIDAS in integrin-ligand engagement (Michishita *et al* 1993, Kamata *et al* 1994, Valdramidou *et al* 2008). Regarding ligand engagement, current literature assigns a negative regulatory role to ADMIDAS, and a positive regulatory role to SyMBS (Chen *et al* 2003). Indeed, integrin activation is now deemed dependent upon SyMBS occupation by a metal ion (Valdramidou *et al* 2008, Zhu *et al* 2008). Thus integrin conformation, ligand-affinity and engagement may be modulated by the presence of divalent cation species and the metal ion-binding motif that they occupy.

Within the α-subunit β-propeller region between blades 4 to 7, three to four Ca^{2+}-binding sites have been mapped in the integrin $\alpha_v\beta_3$ and $\alpha_{IIb}\beta_3$ integrin species. A

further Ca^{2+}-binding site has been determined on the α-subunit *genu*, although its biological function remains unclear (Xie *et al* 2004).

The inhibitory effect of Ca^{2+} binding has been found requisite for β subunit folding during biogenesis and assembly in the endoplasmic reticulum, remaining bound during trafficking to prevent premature activation of the nascent integrin receptor or untimely induction of intracellular integrin-mediated signalling en route to the plasma lemma (Tiwari *et al* 2011). Displacement of Ca^{2+} ions with Mg^{2+} or Mn^{2+} ions facilitates cognate ligand engagement and thus, cell surface integrin activation. Indeed, integrin ligand binding is dependent upon MIDAS occupation by Mg^{2+} or Mn^{2+} cations (Leitinger *et al* 2000, Chen *et al* 2003, San Sebastian *et al* 2006, Valdramidou *et al* 2008, Tiwari *et al* 2011, Zhang and Chen 2012).

Thus, it is thought that Ca^{2+} ions mediate an inhibitory effect upon integrin-ligand interactions, whilst Mg^{2+} and Mn^{2+} prime integrin ligand engagement and subsequent activation. Notably, Mn^{2+} is deemed to universally and potently support ligand binding, requiring the presence of Mn^{2+} ions in only the low μM range to potentiate integrin-mediated adhesive phenomena (Smith *et al* 1994). Cation sequestration by means of a chelating agent such as EDTA ablates integrin-ligand binding, demonstrative of divalent cations as critical intrinsic and extrinsic regulators of integrin activation, function and associated downstream signalling induction (Dransfield *et al* 1992, Shimaoka *et al* 2002, Zhang and Chen 2012).

Given the established biological relevance and significance of Ca^{2+}, Mg^{2+} and Mn^{2+} cations as canonical modulators of integrin activation, it was deemed appropriate to utilise these cationic species specifically to evaluate the ability of antibodies 6.2E5 (Figure 3.1.1) and 6.2G2 (Figure 3.1.2) to recognise the integrin $\alpha_v\beta_6$ in its active conformation. Treatment with 1 mM divalent cations (Ca^{2+}, Mg^{2+} or Mn^{2+}) or a chelating ion-free buffer (TBS-20mM EDTA) demonstrated that although binding of both antibodies 6.2E5 (Figure 3.1.1C) and 6.2G2 (Figure 3.1.2C) to their respective cognate epitopes is cation-independent, their respective binding affinities are significantly increased in the presence of physiomimetic concentrations of cations across all treatment groups compared to a chelating ion-free buffer (Kruskall-Wallis test with Dunn's multiple comparison post-hoc test; 6.2E5: $p<0.05$, p=0.0064; 6.2G2: $p<0.001$, p=0.0003).

Concordant with literature reporting Mn^{2+}-ions as a potent, universal integrin activation modality (Shimaoka et al 2002), a significant increase in antibody binding was observed in the presence of 1 mM Mn^{2+}-ions compared with TBS for both 6.2E5 (Figure 3.1.1C) and 6.2G2 (Figure 3.1.2C) (Kruskall-Wallis test with Dunn's multiple comparison post-hoc test, adjusted *p* values; 6.2E5: *p<0.05,* p=0.0194; 6.2G2: *p<0.05,* p=0.0194).

The biphasic nature of Ca^{2+}-ion–mediated allosteric regulation of integrin conformation and ligand affinity has been widely reviewed (Leitinger *et al* 2000, San Sebastian *et al* 2006, Zhang and Chen 2012). Interestingly, the presence of Ca^{2+}-ions did not inhibit binding of antibody 6.2E5 to its cognate epitope in comparison with Mg^{2+}-ions. Conversely, the epitope recognised by antibody 6.2G2 proved sensitive to the reported inhibitory effects of Ca^{2+}-ions, again in comparison with Mg^{2+}-ions (Kruskall-Wallis test with Dunn's multiple comparison post-hoc test, adjusted *p* values; 6.2E5: p=0.8462; 6.2G2: p=>0.ġ).

Antibody binding kinetics for clone 6.2E5 (Figure 3.1.1D) and clone 6.2G2 (Figure 3.1.2D) performed in the presence of assay buffer alone confirmed that intrinsic cations present within the assay matrix did not markedly alter binding affinity of these antibodies over a 30 min timescale. It was therefore deduced that binding of antibodies 6.2E5 and 6.2G2 to their cognate epitopes did not itself induce integrin $\alpha_v\beta_6$ activation and thus could be eliminated as a confounding factor for future activation studies utilising these antibodies.

Furthermore, titration of antibody 6.2E5 (Figures 3.1.1E – G) binding across a range of Mn^{2+}-ion concentrations elicited canonical integrin activation kinetics yielding a significant correlation between levels of surface-bound 6.2E5 (represented by detected geometric MFI, AU) and Mn^{2+}-ion concentration ranging from (Figure 3.1.1F) 0 to 1 mM Mn^{2+} (Spearman's correlation r=0.782, *p<0.01,* p=0.0053) and (Figure 3.1.1G) 0 to 200 μM Mn^{2+} (Spearman's correlation r=0.943, *p<0.01,* p=0.0083).

Similarly, titration of antibody 6.2G2 binding over a range of Mn^{2+}-ion concentrations exhibited archetypal integrin activation kinetics (Figure 3.1.2E – G), comparable to the activation profiles discerned using antibody 6.2E5 (Figure

3.1.1E – G). In both the presence of 0 to 1 mM Mn^{2+} (Figure 3.1.2F) and 0 to 200 µM Mn^{2+} (Figure 3.1.2G), a significant correlation between surface-bound 6.2G2 and Mn^{2+} concentration was observed (Spearman's rank correlation; **0 to 1 mM**: r=0.927, *p<0.001,* p=0.0002; **0 to 200 µM:** r=1, *p<0.002,* p=0.0014). Collectively, the findings from divalent cation-induced activation studies (Figures 3.1.1 and 3.1.2) confirm that both clones 6.2E5 and 6.2G2 each recognise an activation-associated epitope, which is revealed upon treatment with Mn^{2+}-ions.

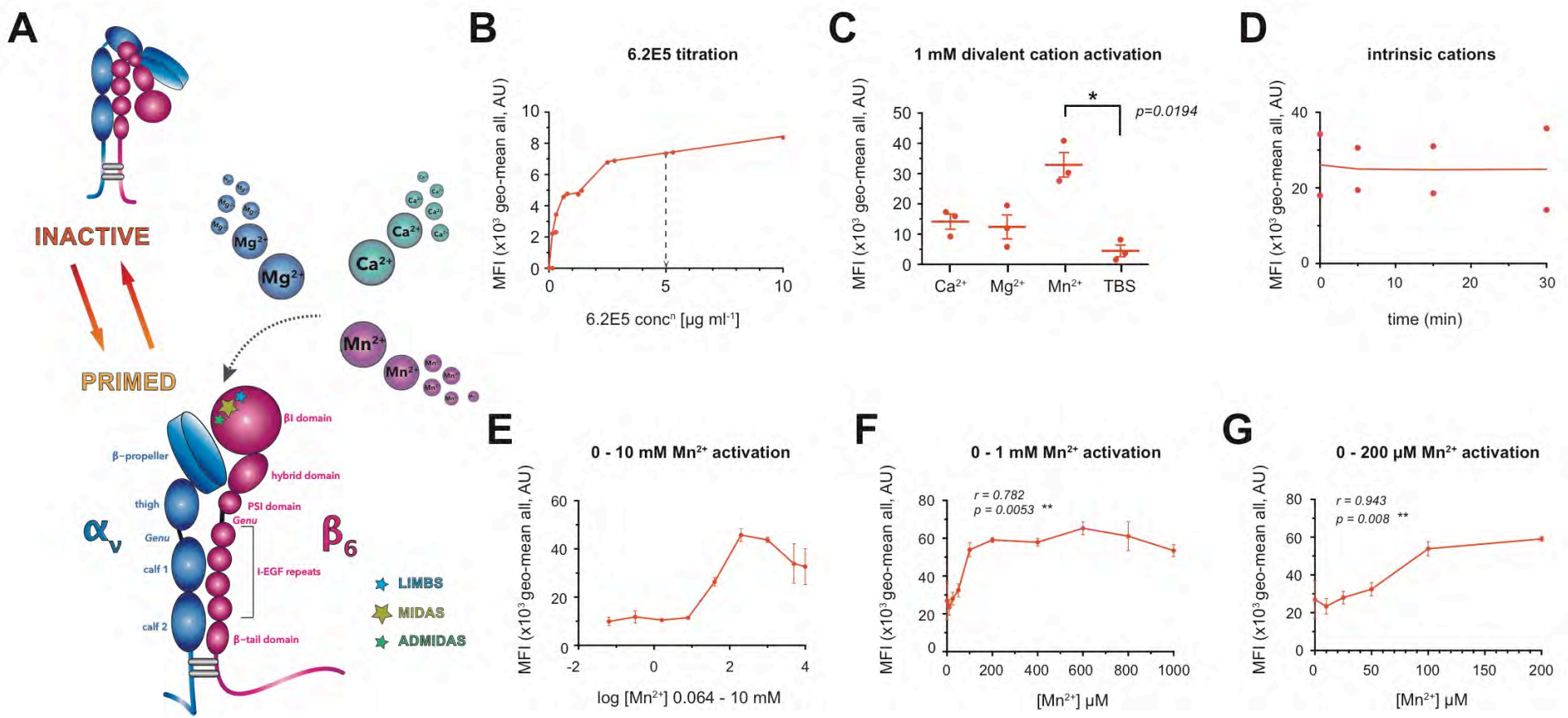

Figure 3.1.1

The antibody 6.2E5 recognises an activation-associated epitope located on integrin $\alpha_v\beta_6$ that is revealed by treatment with divalent manganese (Mn^{2+}) cations

Abbreviations: ADMIDAS – adjacent to MIDAS; AU – arbitrary units; conc^n – concentration; LIMBS – ligand-associated metal-binding site; MIDAS – metal-ion dependent adhesion site; MFI – mean fluorescence intensity; TBS – Tris-buffered saline.

Figure 3.1.1

The antibody 6.2E5 recognises an activation-associated epitope located on integrin $\alpha_v\beta_6$ that is revealed by treatment with divalent manganese (Mn^{2+}) cations

(3.1.1 A) Divalent cation regulation of integrin conformation, activation status and signalling capacity is well established. Thus, canonical divalent cation activation experiments using the known integrin-regulatory species of divalent cations Ca^{2+}, Mg^{2+} & Mn^{2+}, were performed and compared with a chelating ion-free buffer (Tris-buffered saline/20 mM EDTA – TBS) to evaluate the ability of the antibody 6.2E5 to recognise the active conformer of integrin $\alpha_v\beta_6$. **(3.1.1 B)** Antibody 6.2E5 was titrated at doubling dilutions ranging from 10 to 0 µg ml^{-1} to determine a suitable concentration for labelling surface integrin $\alpha_v\beta_6$ on live DX3β6 cells to permit detection by flow cytometry (n=2). A concentration of 5 µg ml^{-1} was deemed both suitably economical and efficient for surface labelling and flow cytometric detection of integrin $\alpha_v\beta_6$ using antibody 6.2E5. **(3.1.1 C)** Canonical integrin activation in the presence of 1 mM divalent cations (Ca^{2+}, Mg^{2+}, Mn^{2+}) or a chelating ion free buffer supplemented with 20 mM EDTA (TBS) was performed on the DX3β6 cell line (n=3). Flow cytometric analysis of treated cells subsequently labelled with 6.2E5 (Biogen Idec, 5 µg ml^{-1}) revealed a statistically significant difference in detected mean fluorescence intensity (MFI) across all treatment groups (Kruskall-Wallis test with Dunn's multiple comparison test, p=0.0064) and a statistically significant increase in 6.2E5 binding post treatment with 1 mM Mn^{2+} compared to TBS (Dunn's multiple comparison test, p=0.0194). **(3.1.1 D)** Binding kinetics of 6.2E5 in the presence of DMEM/0.1/0.1 flow cytometry buffer alone was evaluated briefly to determine effects of intrinsic cations within this assay buffer that may confound activation studies, but no observable change was noted (n=2). **(3.1.1 E - G)** Titration of 6.2E5 binding over a range of Mn^{2+}-ion concentrations, again using the DX3β6 cell line, demonstrated classical activation kinetics **(3.1.1 E)**, yielding a significant positive correlation between concentration of Mn^{2+} ions and MFI from **(3.1.1 F)** 0 to 1 mM (Spearman's correlation r=0.782, p=0.0053, n=3) and **(3.1.1 G)** 0 to 200 µM (Spearman's correlation r=0.943, p=0.0083, n=3). Graphs show mean with error bars for s.e.m for triplicate experiments **(3.1.1 C, E, F & G).** All other graphs show individual replicates with a line transecting the mean average **(3.1.1 B & D).** All data were acquired on live cells only by flow cytometry acquisition (BD FACSCalibur™, BD Biosciences) in the presence of a cell viability indicator (propidium iodide, P4170, Sigma Aldrich, 5 µg ml^{-1}). Following normalisation against isotype matched control antibodies, geometric-MFI values were obtained by analysis in BD CellQuestPro™ software (BD Biosciences). Statistical analyses were performed using GraphPad Prism® 5.0b for MacOSX (Graphpad Software Inc., CA, USA).

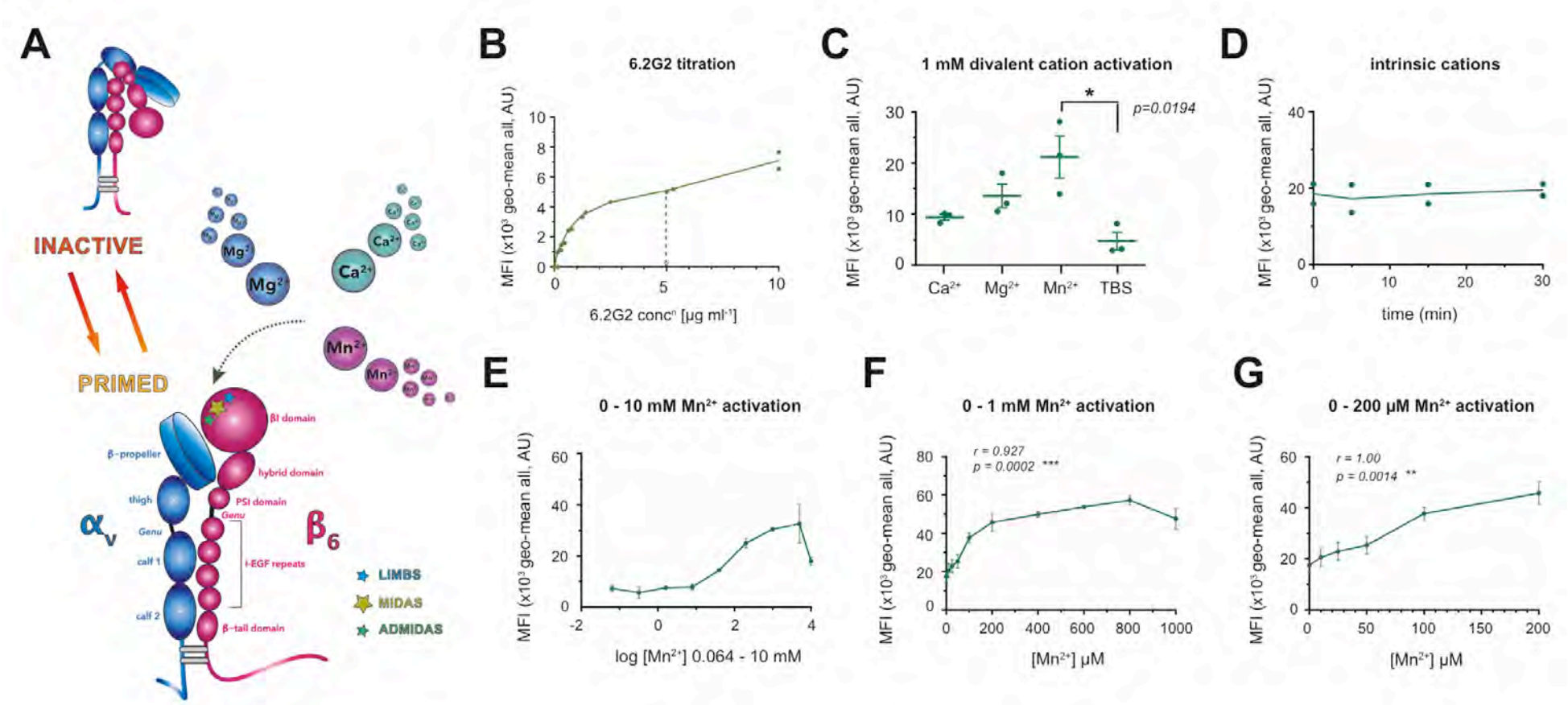

Figure 3.1.2

Treatment with divalent manganese (Mn^{2+}) cations reveals an activation-associated epitope located on integrin $\alpha_v\beta_6$ that is recognised by antibody 6.2G2

Abbreviations: ADMIDAS – adjacent to MIDAS; AU – arbitrary units; conc^n – concentration; LIMBS – ligand-associated metal-binding site; MIDAS – metal-ion dependent adhesion site; MFI – mean fluorescence intensity; TBS – Tris-buffered saline.

Figure 3.1.2
Treatment with divalent manganese (Mn^{2+}) cations reveals an activation-associated epitope located on integrin $\alpha_v\beta_6$ that is recognised by antibody 6.2G2

(3.1.2 A) Divalent cation regulation of integrin conformation, activation status and signalling capacity is well established. Thus, canonical divalent cation activation experiments using the known integrin-regulatory species of divalent cations Ca^{2+}, Mg^{2+} & Mn^{2+}, were performed and compared with a chelating ion-free buffer (Tris-buffered saline/20 mM EDTA – TBS) to evaluate the ability of the antibody 6.2G2 to recognise the active conformer of integrin $\alpha_v\beta_6$. **(3.1.2 B)** Antibody 6.2G2 was titrated at doubling dilutions ranging from 10 to 0 µg ml^{-1} to determine a suitable concentration for labelling surface integrin $\alpha_v\beta_6$ on live DX3β6 cells to permit detection by flow cytometry (n=2). A concentration of 5 µg ml^{-1} was deemed both suitably economical and efficient for surface labelling and flow cytometric detection of integrin $\alpha_v\beta_6$ using antibody 6.2G2. **(3.1.2 C)** DX3β6 cells were treated with either a chelating ion free buffer supplemented with 20 mM EDTA (TBS) or 1 mM divalent cations (Ca^{2+}, Mg^{2+}, Mn^{2+}) to induce integrin activation (n=3). Flow cytometric analysis of cells subsequently labelled with 6.2G2 (Biogen Idec, 5 µg ml^{-1}) revealed a statistically significant difference in detected mean fluorescence intensity (MFI) across all treatment groups (Kruskall-Wallis test with Dunn's multiple comparison test, p=0.0003) and a statistically significant increase in 6.2G2 binding post treatment with 1 mM Mn^{2+} compared to TBS (Kruskall-Wallis test with Dunn's multiple comparison test, p=0.0194). **(3.1.2 D)** Binding kinetics of 6.2G2 in the presence of DMEM/0.1/0.1 flow cytometry buffer alone was evaluated briefly to determine effects of intrinsic cations within this assay buffer that may confound activation studies, but no observable change was noted (n=2). **(3.1.2 E - G)** Titration of 6.2G2 binding over a range of Mn^{2+}-ion concentrations, again using the DX3β6 cell line, demonstrated classical activation kinetics **(3.1.2 E)**, yielding a significant positive correlation between concentration of Mn^{2+} ions and MFI from **(3.1.2 F)** 0 to 1 mM (Spearman's correlation r=0.927, p=0.0002, n=3) and **(3.1.2 G)** 0 to 200 µM (Spearman's correlation r=1, p=0.0014, n=3). Graphs show mean with error bars for s.e.m for triplicate experiments **(3.1.2 C, E, F & G).** All other graphs show individual replicates with a line transecting the mean average **(3.1.2 B & D).** All data were acquired on live cells only by flow cytometry acquisition (BD FACSCalibur™, BD Biosciences) in the presence of a cell viability indicator (propidium iodide, P4170, Sigma Aldrich, 5 µg ml^{-1}). Following normalisation against isotype matched control antibodies, geometric-MFI values were obtained by analysis in BD CellQuestPro™ software (BD Biosciences). Statistical analyses were performed using GraphPad Prism® 5.0b for MacOSX (Graphpad Software Inc., CA, USA).

3.2 antibodies 6.2E5 and 6.2G2 are non-ligand mimetic and each recognise a LIBS revealed upon engagement of the integrin $\alpha_v\beta_6$ with its cognate ligands A20FMDV2 or LAP

Results from ligand-induced activation experiments qualitatively indicate that antibodies 6.2E5 (Figure 3.2.1) and 6.2G2 (Figure 3.2.2) each recognise a LIBS. In the presence of integrin $\alpha_v\beta_6$–cognate ligands A20FMDV2 or LAP, the antibodies 6.2E5 (Figure 3.2.1B and D) and 6.2G2 (Figure 3.2.2B and D) bound with an observable increasing affinity to an epitope revealed upon RGD-ligand-induced integrin $\alpha_v\beta_6$ activation. This suggests that the respective epitopes for 6.2E5 and 6.2G2 are each ligand-inducible. However, only a significant positive correlation between antibody binding and ligand-engagement was yielded for clone 6.2G2 following A20FMDV2-engagement (Spearman's correlation, 6.2E5: $r=0.8$, $p>0.05$, $p=0.1667$; 6.2G2: $r=1$, $p<0.05$, $p=0.0417$).

Concordant with literary evidence that integrin-mediated binding of their cognate ligands is cation-dependent; the presence of cations within the assay matrix was found requisite for integrin $\alpha_v\beta_6$ engagement of the synthetic peptide and non-physiological ligand A20FMDV2 (Figures 3.2.1C and 3.2.2C). Furthermore, in these experiments where cation sequestration using a chelating ion-free buffer ablated integrin $\alpha_v\beta_6$-A20FMDV2 interaction, binding kinetics of both 6.2E5 and 6.2G2 were unaltered in the absence of ligand-engagement.

This lack of an observable increase in 6.2E5 or 6.2G2 antibody binding in the absence of ligand-engagement adds credence to the conclusion that these antibodies each recognise a LIBS. Furthermore, the ability of antibodies 6.2E5 and 6.2G2 to bind integrin $\alpha_v\beta_6$ even in its ligand-free conformation fits with Humphries (2004) explanation that epitopes comprising LIBS are present even in the absence of cognate ligand.

However, it is only when the integrin adopts a primed or ligand-engaged conformation that the LIBS is revealed permitting favourable steric interaction with its cognate anti-LIBS monoclonal antibody. As acknowledged by Humphries (2004) the term LIBS may not be an entirely accurate description as expression of the LIBS is not induced upon ligand engagement as it is already present within the integrin amino acid sequence. Rather, it is the ability of an anti-LIBS antibody to detect an

increase in the abundance of its cognate epitope residing within the LIBS that is revealed due to the favourable sterics induced once the integrin is ligand-engaged. Thus, since adoption of a primed or ligand-engaged conformation favours revelation and detection of LIBS, the anti-LIBS class of monoclonal antibodies may be used to demonstrate integrin activation status.

Divalent cation-mediated and ligand-induced activation studies were also performed concomitantly using the well characterised, commercially available integrin $\alpha_v\beta_6$ function blocking antibody clones 10D5 (ligand mimetic) and 53A2 (non-ligand mimetic) for technical validation of experiments (Figure 3.2.3), and to serve as comparators for the kinetics observed for clones 6.2E5 and 6.2G2.

Activation experiments performed in the presence of 1 mM divalent cations (Ca^{2+}, Mg^{2+} or Mn^{2+}) or a chelating ion-free buffer (TBS/20 mM EDTA) demonstrated that the ligand mimetic, integrin $\alpha_v\beta_6$ heterodimer specific antibody 10D5 did not bind in the absence of divalent cations (Figure 3.2.3A). Concordant with literature, cation modulation of integrin $\alpha_v\beta_6$ ligand (or ligand-mimetic antibody) binding affinity was also observed for clone 10D5. Notably, Mn^{2+}-ions yielded a significant increase in 10D5 binding (Kruskall Wallis with Dunn's multiple comparison test, $p<0.05$, p=0.0372) compared to ion-free buffer.

As anticipated, sequestration of cations in a chelating ion-free buffer ablated the ability of antibody 10D5 to bind integrin $\alpha_v\beta_6$. In contrast, binding of the function blocking antibody 53A2 was not significantly altered in the presence or absence of divalent cations (Kruskall Wallis with Dunn's multiple comparison test, $p>0.05$, p=0.4747) (Figure 3.1.3B) inferring expression of its cognate epitope is not determined by integrin $\alpha_v\beta_6$ conformation nor activation status.

The antibody 10D5 is known to be ligand-mimetic, binding via the RGD-recognising cleft of the integrin $\alpha_v\beta_6$ heterodimer (Lawrence et al 2015). As anticipated, canonical competitive inhibition kinetics were generated for 10D5 binding in experiments where $\alpha_v\beta_6$–positive cells were pre-treated with known integrin $\alpha_v\beta_6$ cognate ligands A20FMDV2 or LAP (Figure 3.2.3C and D respectively). A significant negative correlation between abundance of surface-bound ligand and 10D5 binding was discerned for both A20FMDV2 (Figure

3.2.3C; Spearman's correlation r=-1, *p<0.05*, p=0.0417) and LAP (Figure 3.2.3D; Spearman's correlation r=-1, *p<0.01*, p=0.0083).

Given the cation-sensitivity of clone 10D5, binding kinetics in the presence of intrinsic cations within the assay buffer was briefly evaluated (Figure 3.2.3E). No observable increase in 10D5 binding was observed, thus eliminating cations inherent within the assay matrix as a potential confounding factor in the evaluation of antibody binding kinetics.

As previously noted, antibody-binding kinetics elicited post-integrin $\alpha_v\beta_6$ ligand occupancy for clone 6.2E5 (Figure 3.2.1B and D) and clone 6.2G2 (Figure 3.2.2B and D) show an observable positive correlation between ligand-engagement and surface antibody binding. This contrasts with the corresponding classic inhibition profiles obtained for the ligand-mimetic antibody clone 10D5 (Figure 3.2.3C and D). Therefore, it may be concluded that clones 6.2E5 and 6.2G2 not only each recognise a LIBS, but are also non-ligand mimetic antibodies.

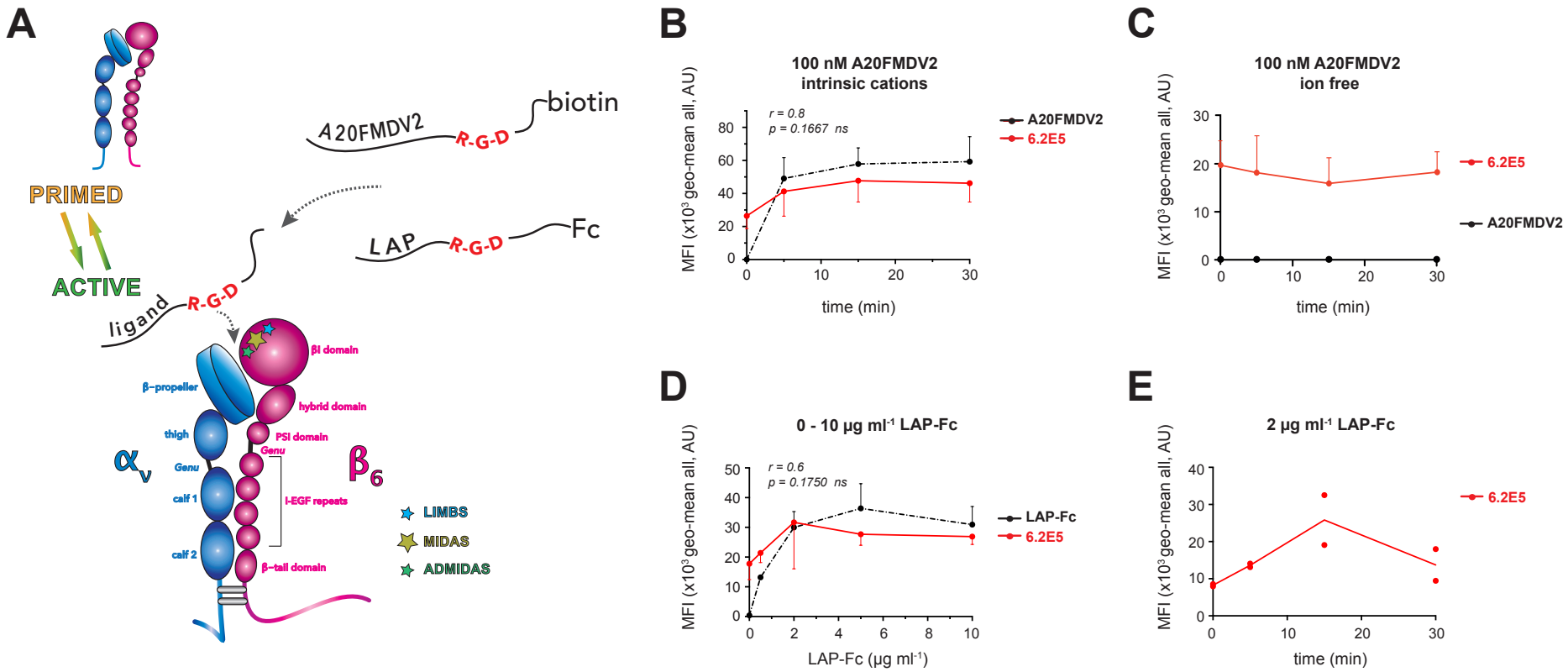

Figure 3.2.1

The antibody 6.2E5 recognises a LIBS on integrin $\alpha_v\beta_6$ that is revealed upon engagement of the cognate ligands A20FMDV2 and LAP

Abbreviations: ADMIDAS – adjacent to MIDAS; AU – arbitrary units; conc^n – concentration; LAP-Fc – latency associated peptide bearing an Fc-tag; LIBS – ligand-induced binding site; LIMBS – ligand-associated metal-binding site; MIDAS – metal-ion.

Figure 3.2.1
The antibody 6.2E5 recognises a LIBS on integrin $\alpha_v\beta_6$ that is revealed upon engagement of the cognate ligands A20FMDV2 and LAP

(3.2.1 A) It is believed that like other integrin moieties, upon engagement of an RGD-bearing cognate ligand, the integrin $\alpha_v\beta_6$ undergoes ligand-induced activation, adopting a signalling replete, fully active conformation permitting induction of downstream signalling events. Two well established integrin $\alpha_v\beta_6$ cognate ligands (the biotin-tagged 20mer synthetic peptide A20FMDV2 and a human IgG (Fc')-tagged human recombinant LAP) were therefore used to perform ligand-induced activation experiments on the known $\alpha_v\beta_6$–positive VB6 cell line to evaluate the ability of antibody 6.2E5 to recognise the ligand-induced active conformation of integrin $\alpha_v\beta_6$ **(3.2.1 B – E)**. Ligand-engagement was confirmed by flow cytometric detection of their respective tags using either an anti-biotin antibody (ab1227, AbCam, 10 µg ml^{-1}) or an anti-human IgG (Fc') antibody (ab113636, AbCam, 10 µg ml^{-1}). Although binding of 6.2E5 (Biogen Idec, 5 µg ml^{-1}) observably increased in the presence of **(3.2.1 B)** 100 nM biotin-tagged A20FMDV2 (n=3) and **(3.2.1 D)** 0 – 10 µg ml^{-1} Fc-tagged LAP (n=3), neither ligand elicited a statistically significant difference in detected geometric MFI (AU) representative of surface-bound 6.2E5 (Spearman's correlation; **A20FMDV2:** r=0.8, p>0.1, p=0.1667 and **LAP-Fc:** r=0.6, p>0.1, p=0.1750). Binding kinetics of 6.2E5 in the presence of 100 nM A20FMDV2 in a chelating ion free buffer (TBS supplemented with 20 mM EDTA) was evaluated briefly (n=2) **(3.2.1 C)** and confirmed that the observed increase in 6.2E5 binding was attributable to ligand binding and not the presence of intrinsic cations within the assay buffer used in **(3.2.1 B)**. Activation timecourse experiments in the presence of 2 µg ml^{-1} LAP-Fc **(3.2.1 E)** elicited an increase in 6.2E5 binding reaching maxima at 15 min (n=2). Graphs show mean with error bars for s.d for triplicate experiments **(3.2.1 B & D)**. All other graphs show individual replicates with a line transecting the mean average **(3.2.1 C & E)**. All data were acquired on live cells only by flow cytometry acquisition (BD FACSCalibur™, BD Biosciences) in the presence of a cell viability indicator (propidium iodide, P4170, Sigma Aldrich, 5 µg ml^{-1}). Following normalisation against isotype matched control antibodies, geometric-MFI values were obtained by analysis in BD CellQuestPro™ software (BD Biosciences). Statistical analyses were performed using GraphPad Prism® 5.0b for MacOSX (Graphpad Software Inc., CA, USA).

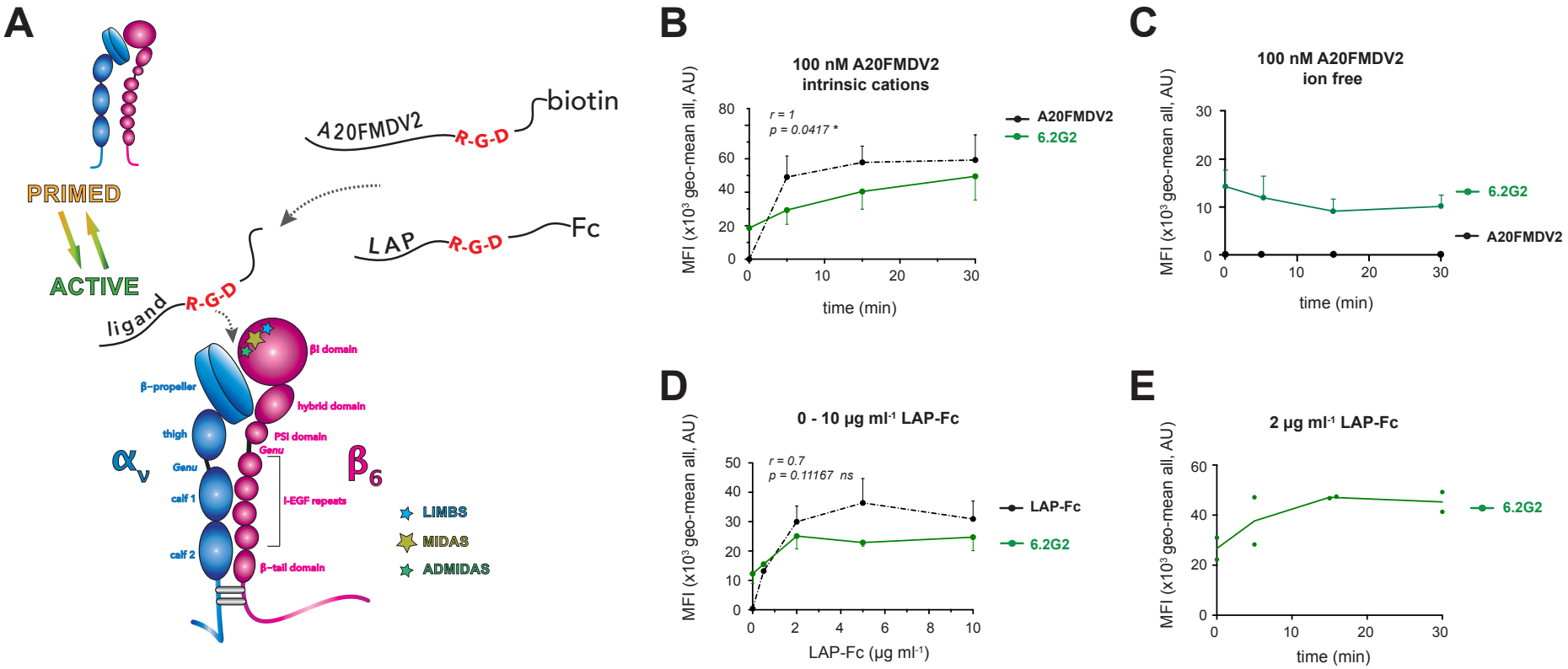

Figure 3.2.2

Engagement of the cognate ligand A20FMDV2 or LAP reveals a LIBS located on the integrin $\alpha_v\beta_6$ that is recognised by antibody 6.2G2

Abbreviations: ADMIDAS – adjacent to MIDAS; AU – arbitrary units; conc^n – concentration; LAP-Fc – latency associated peptide bearing an Fc-tag; LIBS – ligand-induced binding site; LIMBS – ligand-associated metal-binding site; MIDAS – metal-ion.

Figure 3.2.2
Engagement of the cognate ligand A20FMDV2 or LAP reveals a LIBS located on the integrin $\alpha_v\beta_6$ that is recognised by antibody 6.2G2

(3.2.2 A) Following cognate ligand-engagement, the integrin $\alpha_v\beta_6$ undergoes ligand-induced activation, adopting a signalling replete, fully active conformation permitting induction of downstream signalling events. Two well established integrin $\alpha_v\beta_6$ cognate ligands (the 20mer synthetic peptide A20FMDV2 bearing a biotin tag and human recombinant LAP tagged with a human IgG (Fc') fragment) were therefore used to perform ligand-induced activation experiments on the known $\alpha_v\beta_6$–positive VB6 cell line to evaluate the ability of antibody 6.2G2 to recognise the ligand-induced active conformation of integrin $\alpha_v\beta_6$ **(3.2.2 B – E)**. Ligand-engagement was confirmed by flow cytometric detection of their respective tags using either an anti-biotin antibody (ab1227, AbCam, 10 µg ml^{-1}) or an anti-human IgG (Fc') antibody (ab113636, AbCam, 10 µg ml^{-1}). **(3.2.2 B)** Binding of 6.2G2 (Biogen Idec, 5 µg ml^{-1}) significantly increased in the presence of 100 nM biotin-tagged A20FMDV2 (n=3) (Spearman's correlation r=1, $p<0.05$ p=0.0417). **(3.2.2 C)** Binding kinetics of 6.2G2 in the presence of 100 nM A20FMDV2 in a chelating ion free buffer (TBS supplemented with 20 mM EDTA) was evaluated briefly (n=2). In the absence of divalent cations, binding of antibody 6.2G2 appeared to decline over the 30 min timecourse. However the significance of this observable decrease could not be statistically evaluated as only duplicate experiments were performed. Furthermore, these experiments confirmed that the observed increase in 6.2G2 binding was attributable to ligand binding and not the presence of intrinsic cations within the assay buffer used in **(3.2.2 B)** nor attributable to the process of 6.2G2 binding its cognate epitope in the manner of an integrin activating antibody**. (3.2.2 D)** Titration of antibody 6.2G2 binding against concentrations of LAP-Fc ranging from 0 to 10 µg ml^{-1} yielded an observable, but not significant, increase in 6.2G2 binding (Spearman's correlation r=0.7, $p>0.1$, p=0.1167, n=3). **(3.2.2 E)** Activation timecourse experiments in the presence of 2 µg ml^{-1} LAP-Fc elicited an observable increase in 6.2G2 binding reaching maxima at 15 min (n=2). Graphs show mean with error bars for s.d for triplicate experiments **(3.2.2 B & D).** All other graphs show individual replicates with a line transecting the mean average **(3.2.2 C & E).** All data were acquired on live cells only by flow cytometry acquisition (BD FACSCalibur™, BD Biosciences) in the presence of a cell viability indicator (propidium iodide, P4170, Sigma Aldrich, 5 µg ml^{-1}). Following normalisation against isotype matched control antibodies, geometric-MFI values were obtained by analysis in BD CellQuestPro™ software (BD Biosciences). Statistical analyses were performed using GraphPad Prism® 5.0b for MacOSX (Graphpad Software Inc., CA, USA).

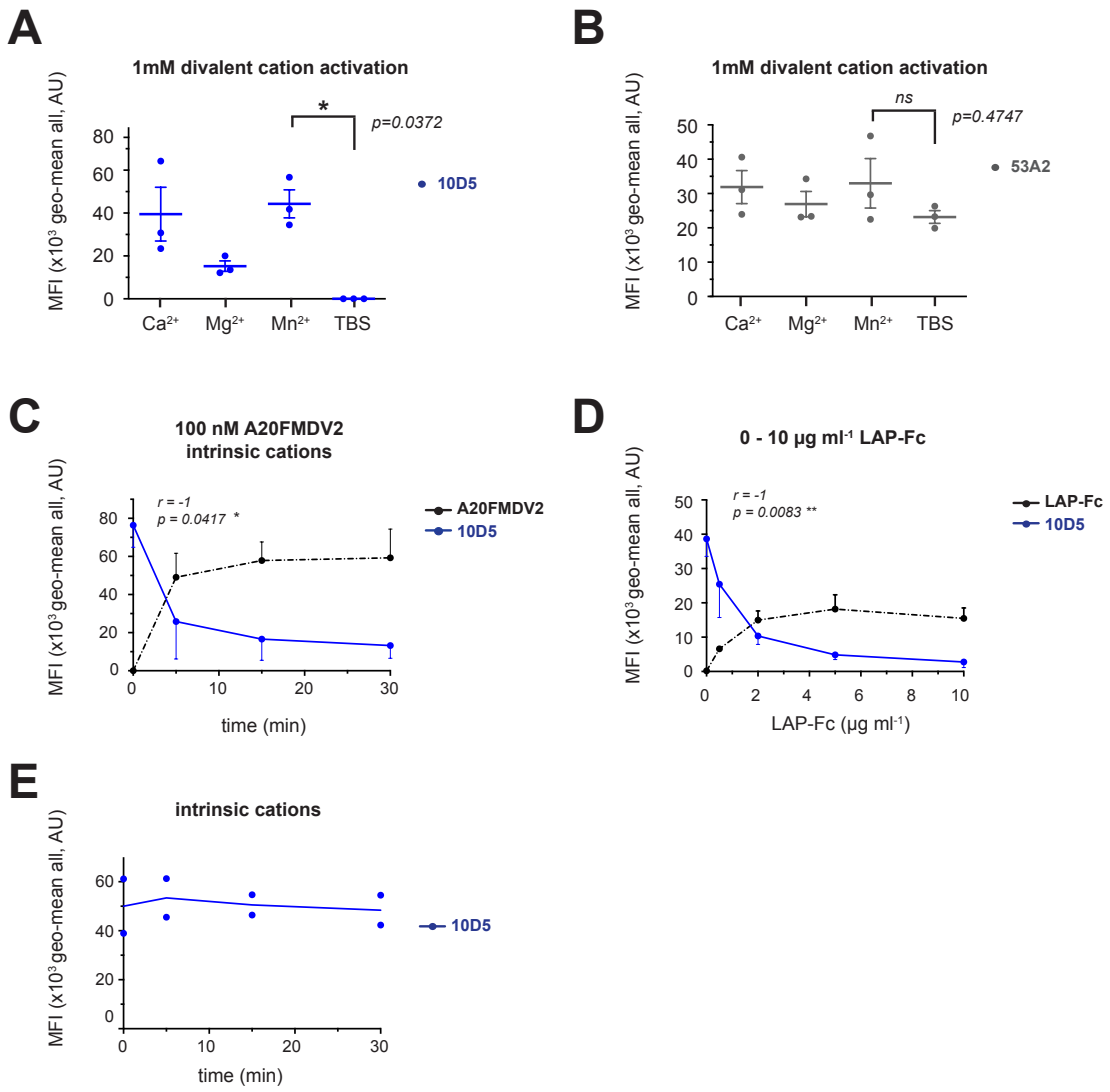

Figure 3.2.3

The ligand-mimetic (clone 10D5) and non-ligand mimetic (clone 53A2) integrin $\alpha_v\beta_6$ function blocking antibodies evaluated in tandem with antibodies 6.2E5 and 6.2G2 during integrin activation experiments suggest that 6.2E5 and 6.2G2 are not ligand-mimetic

As previously described, DX3β6 cells were treated with either a chelating ion free buffer supplemented with 20 mM EDTA (TBS) or 1 mM divalent cations (Ca^{2+}, Mg^{2+} or Mn^{2+}) to induce integrin activation (n=3). Flow cytometric analysis of cells subsequently labelled with either **(3.2.3 A)** 10D5 (MAB2077Z, Merck Millipore, 10 µg ml^{-1}) or **(3.2.3 B)** 53A2 (CR-UK, 10 µg ml^{-1}) revealed ligand-mimetic antibody 10D5 binding is cation-dependent but binding of non-ligand mimetic antibody 53A2 is cation-independent. Classic competitive inhibition kinetics were observed for ligand-mimetic 10D5 binding on VB6 cells pre-treated with integrin cognate ligands biotin-tagged-A20FMDV2 (100 nM) **(3.2.3 C)** or human IgG (Fc')-tagged-LAP (0 - 10 µg ml^{-1}) **(3.2.3 D)** (both n=3), eliciting a significant negative correlation between surface-bound and 10D5 binding capacity (Spearman's correlation; **A20FMDV2:** r=-1, p<0.05, p=0.0417; **LAP-Fc:** r=-1, p<0.01, p=0.083). Bound ligand was detected by means of their respective tags using either an anti-biotin antibody (ab1227, AbCam, 10 µg ml^{-1}) or an anti-human IgG (Fc') antibody (ab113636, AbCam, 10 µg ml^{-1}). **(3.2.3 E)** Binding kinetics of antibody 10D5 in the presence of assay buffer alone was briefly evaluated and confirmed that intrinsic cations present within the assay matrix used for ligand-induced activation studies did alter cation-sensitive 10D5 binding kinetics (n=2). All graphs show mean and s.d where n=3. For n=2, individual replicates with a line transecting the mean average is shown. All flow cytometric data were acquired, analysed and statistically evaluated as previously described.

3.3 antibodies 6.2E5 and 6.2G2 may be used to visually discriminate the subcellular localisation of the active population of the integrin $\alpha_v\beta_6$ by immunofluorescence microscopy

The spatiotemporal properties of cognate epitopes each recognised by antibodies 6.2E5 and 6.2G2 were evaluated by permeabilised immunofluorescence microscopy in a 2D-environment to determine their subcellular localisation (Figure 3.3.1), ligand-engaged distribution (Figure 3.3.2) and ability to trace the integrin $\alpha_v\beta_6$ active subpopulation in live cells using these antibodies (Figure 3.3.2).

In untreated adherent cells unexposed to integrin $\alpha_v\beta_6$–specific cognate ligands, immunopositivity for antibody 6.2E5 was observed at the cell periphery and in filopodial structures but was excluded from cell-cell contacts (Figure 3.3.1A). Interestingly, immunopositivity for antibody 6.2G2 under the same conditions was also observed at the peripheral edges of spreading cells and was also absent from cell-cell junctions. However, in contrast with 6.2E5, antibody 6.2G2 was not detected in filopodial structures (Figure 3.3.1B).

Given that both antibodies 6.2E5 and 6.2G2 were each found to recognise a LIBS by flow cytometry (Figure 3.2), their respective subcellular distributions in a 2D-environment were evaluated in both the presence and absence of ligand (Figure 3.3). The subcellular distributions of antibody 6.2E5 in cells spreading in the absence of ligand (**nil**) or in the presence of an integrin $\alpha_v\beta_6$–specific ligand (**LAP**) or a non-integrin $\alpha_v\beta_6$–binding ligand (**col I**) were compared (Figure 3.3.2A). The antibody 6.2E5 was excluded from cell-cell junctions. Marked vesicular accumulations of 6.2E5 immunopositivity were observed in cells spreading on the integrin $\alpha_v\beta_6$ cognate ligand LAP. This vesicular staining pattern was not observed on collagen type I (**col I**), a ligand that does not engage integrin $\alpha_v\beta_6$, nor under ligand-free conditions (**nil**). This may suggest that in the presence of LAP, the integrin $\alpha_v\beta_6$ is subject to LAP ligand-induced regulatory internalisation and trafficking events.

Under ligand-free conditions (**nil**), the antibody 6.2E5 appears to localise at actin fibre-rich protusions at the edges of spreading cells. This is concordant with previous observations that 6.2E5 was observed in filopodial structures in cells adhering to untreated non-derivatised glass coverslips (Figure 3.3.1A).

Interestingly, in the presence of either LAP or collagen type I, the antibody 6.2E5 was absent from such actin-rich protusions or filopodial structures.

In the case of LAP-ligand binding, the role of integrin $\alpha_v\beta_6$–mediated LAP-engagement is predominantly one of mechano-tensile *"traction"*-induced TGF-β1-activation, as opposed to stable ECM-adhesion formation and may account for its exclusion from filopodial structures (Munger and Sheppard 2011). With regard to collagen type I, the integrin $\alpha_v\beta_6$ is not known to mediate adhesion to collagens. Instead, binding to ECM collagens is dependent on integrin β_1 species, notably $\alpha_1\beta_1$ and $\alpha_2\beta_1$ (Jokinen *et al* 2004). Since adhesion to collagen type I is an integrin $\alpha_v\beta_6$–independent process, it is logical that in cells spreading on collagen type I, no 6.2E5 immunopositivity was observed either at the peripheral edges of cells, in filopodial structures nor in vesicular accumulations given that ligand-induced activation of integrin $\alpha_v\beta_6$ would not be expected.

The subcellular distribution of antibody 6.2G2 in cells spreading either in the absence of ligand (**nil**), or in the presence of the RGD motif-bearing ECM ligand fibronectin (**Fn**), were reviewed by permeabilised immunofluorescence (Figure 3.3.2B). As observed previously in Figure 3.3.1B, antibody 6.2G2 was again excluded from cell-cell junctions and appeared to localise at the periphery of cells adhering in the absence of ligand (**nil**). Upon fibronectin engagement (**Fn**), marked and abundant immunopositivity for antibody 6.2G2 was observed at the tips of actin-rich protusions of the plasma lemma. This contrasted with an absence of 6.2G2 immunopositivity in filopodial structures under ligand-free conditions. Thus, fibronectin-engagement appears to reveal the integrin $\alpha_v\beta_6$-LIBS recognised by antibody 6.2G2.

Surface distribution of the 6.2E5 cognate epitope in unstimulated live cells labelled with was briefly evaluated by non-permeabilised immunofluorescence (Figure 3.3.2C). The antibody 6.2E5 was seen to localise in clusters at the cell periphery in what appear to be membrane ruffles. This phenomenon of integrin clustering is associated with activated, high-affinity integrin conformers (Cluzel et al 2005, Welf et al 2012), which the antibody 6.2E5 may recognise. (Figure 3.3.2C).

Collectively, these observations from immunofluorescence studies infer that the antibodies 6.2E5 and 6.2G2 each recognise a distinct subpopulation of integrin $\alpha_v\beta_6$ that is involved in dynamic cellular processes associated with integrin activation including cell spreading, ligand-engagement, filopodia formation and in the case of antibody 6.2E5, integrin $\alpha_v\beta_6$ receptor clustering.

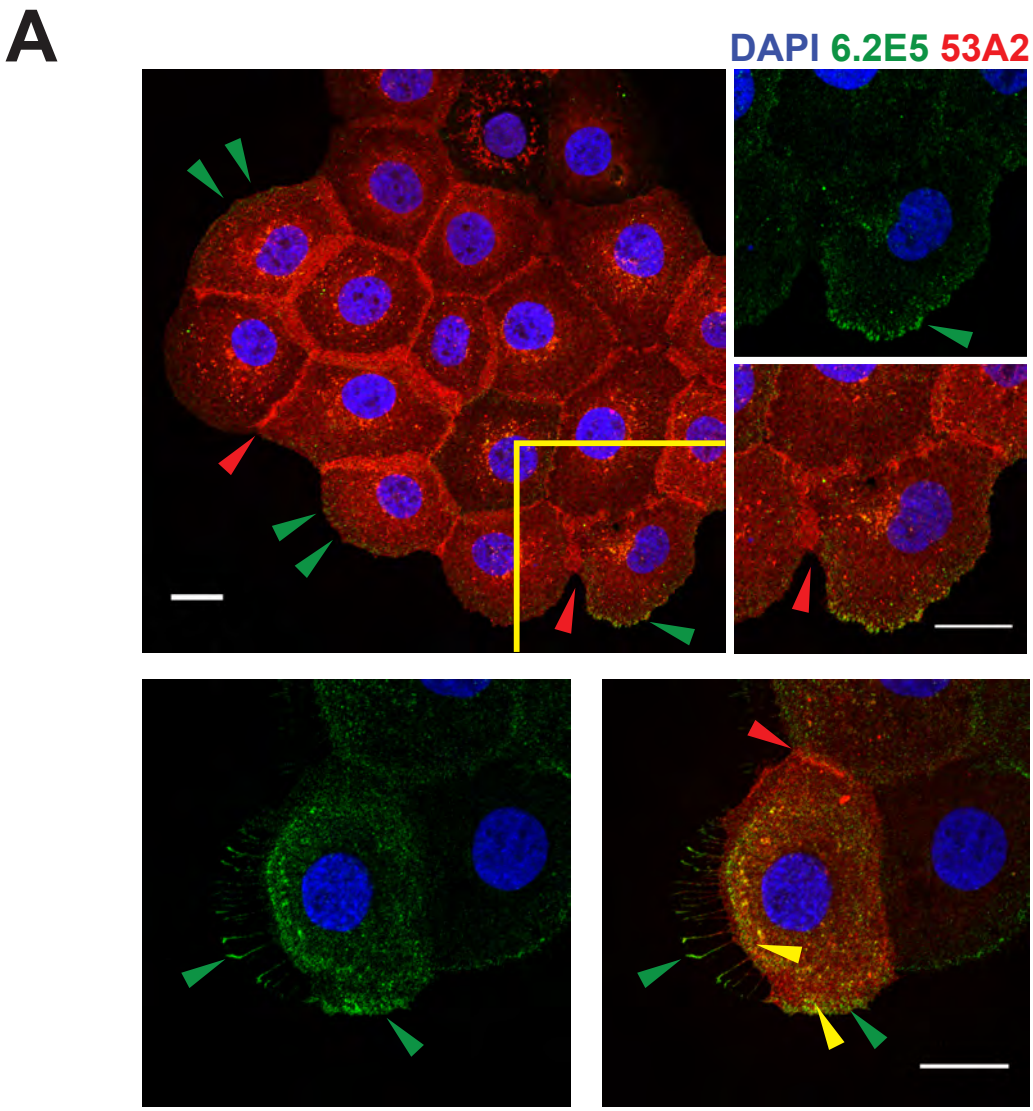

Figure 3.3.1 (A)
The antibody 6.2E5 localises at the peripheral edges of cells spreading in 2D and is observed at the distal tips of filopodial projections, but is excluded from cell-cell junctions where the antibody 53A2 predominates

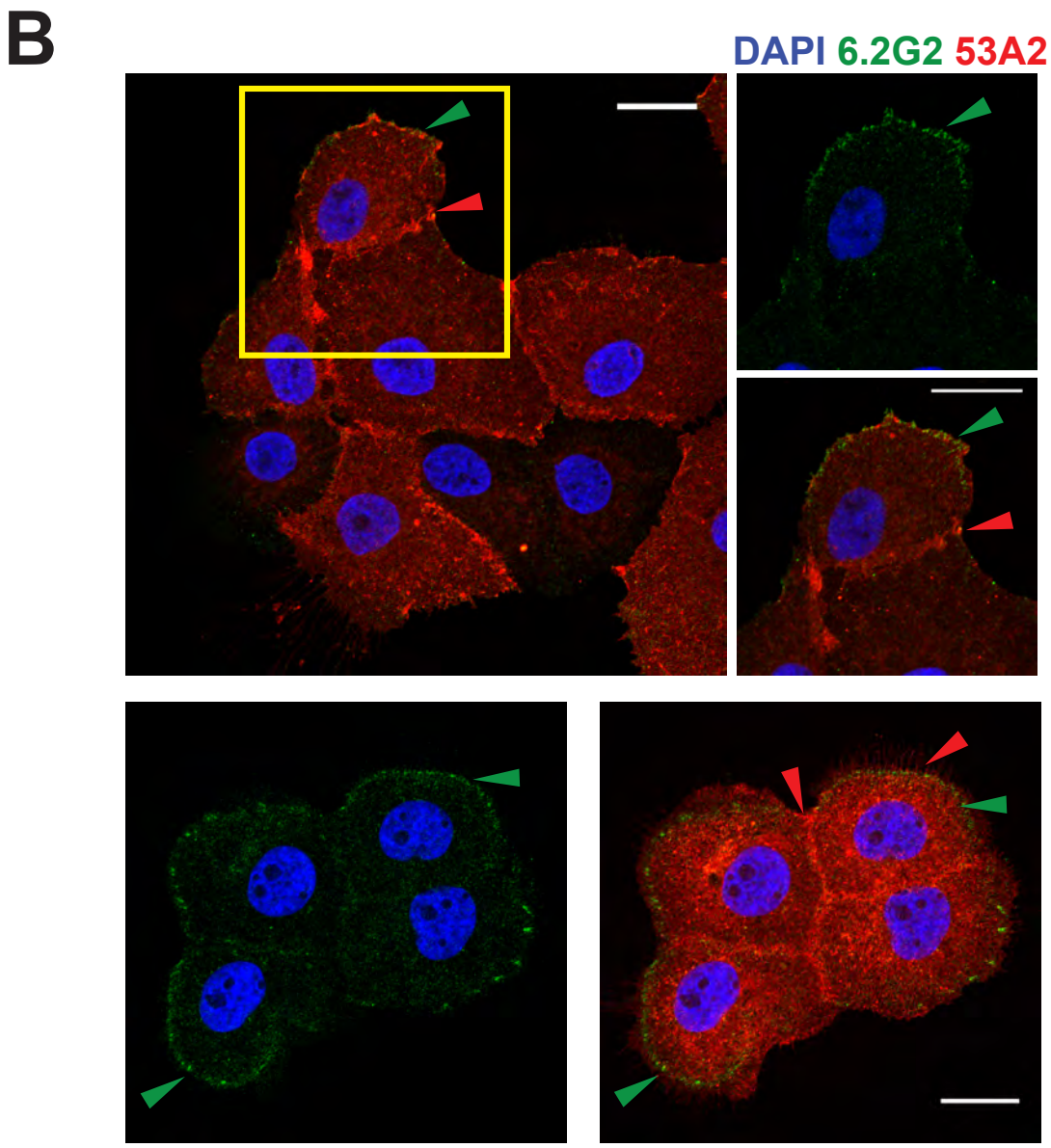

Figure 3.3.1 (B)
The antibody 6.2G2 localises at the peripheral edges of cells spreading in 2D but is absent from the distal tips of filopodial projections, and is excluded from cell-cell junctions where the antibody 53A2 predominates

Figure 3.3.1

The antibodies 6.2E5 and 6.2G2 may be used to discriminate and visualise the subcellular localisations of the active subpopulation of the integrin $\alpha_v\beta_6$ by immunofluorescence microscopy

(3.3.1 A & B) The utility of antibodies 6.2E5 **(3.3.1 A)** and 6.2G2 **(3.3.1 B)** to study the subcellular distribution of the active subpopulation of $\alpha_v\beta_6$ by immunofluorescence methods was evaluated in the VB6 cell line. Cells were seeded on non-derivatised 13 mm glass coverslips (2 x 10^4 cells per coverslip) and left to adhere overnight in complete media under standard culture conditions prior to fixation and permeabilisation in cytoskeletal fixative buffer supplemented with 4% (w/v) formaldehyde. Total integrin $\alpha_v\beta_6$ was demonstrated with antibody 53A2 (CR-UK, 10 µg ml^{-1}) whilst the active subpopulations of integrin $\alpha_v\beta_6$ were labelled with either antibody 6.2E5 or 6.2G2 (both Biogen Idec, 5 µg ml^{-1}). Nuclei were labelled with DAPI (Invitrogen, 1 µg ml^{-1}). **(3.3.1 A)** In contrast with 53A2, an antibody established to recognise the mature fully glycosylated form of $\alpha_v\beta_6$ which was prevalent at cell-cell junctions (red arrows), the antibody 6.2E5 localised at the leading edge of spreading cells and was observed at the tips of filopodia (green arrows) where 53A2 was not detected by permeabilised immunofluorescence. Some co-localisation with 53A2 was observed (yellow arrows). The antibody 6.2E5 appeared to be excluded from cell-cell junctions where 53A2 predominated. **(3.3.1 B)** As observed for antibody 6.2E5, the antibody 6.2G2 was also excluded from cell-cell junctions where antibody 53A2 predominated (red arrows). The antibody 6.2G2 localised at leading edges of spreading cells (green arrows), but unlike antibody 6.2E5 was not observed in filopodia and did not appear to co-localise with antibody 53A2. Images were acquired by confocal microscopy using the ZEISS LSM710 equipped with ZEISS Zen image analysis software (all Carl Zeiss AG, DE). Images were prepared for presentation using Image J (National Institutes of Health) and Adobe® Photoshop© CS6, with composites generated in Adobe® Illustrator© CS6 (Adobe Systems Software© Ltd).

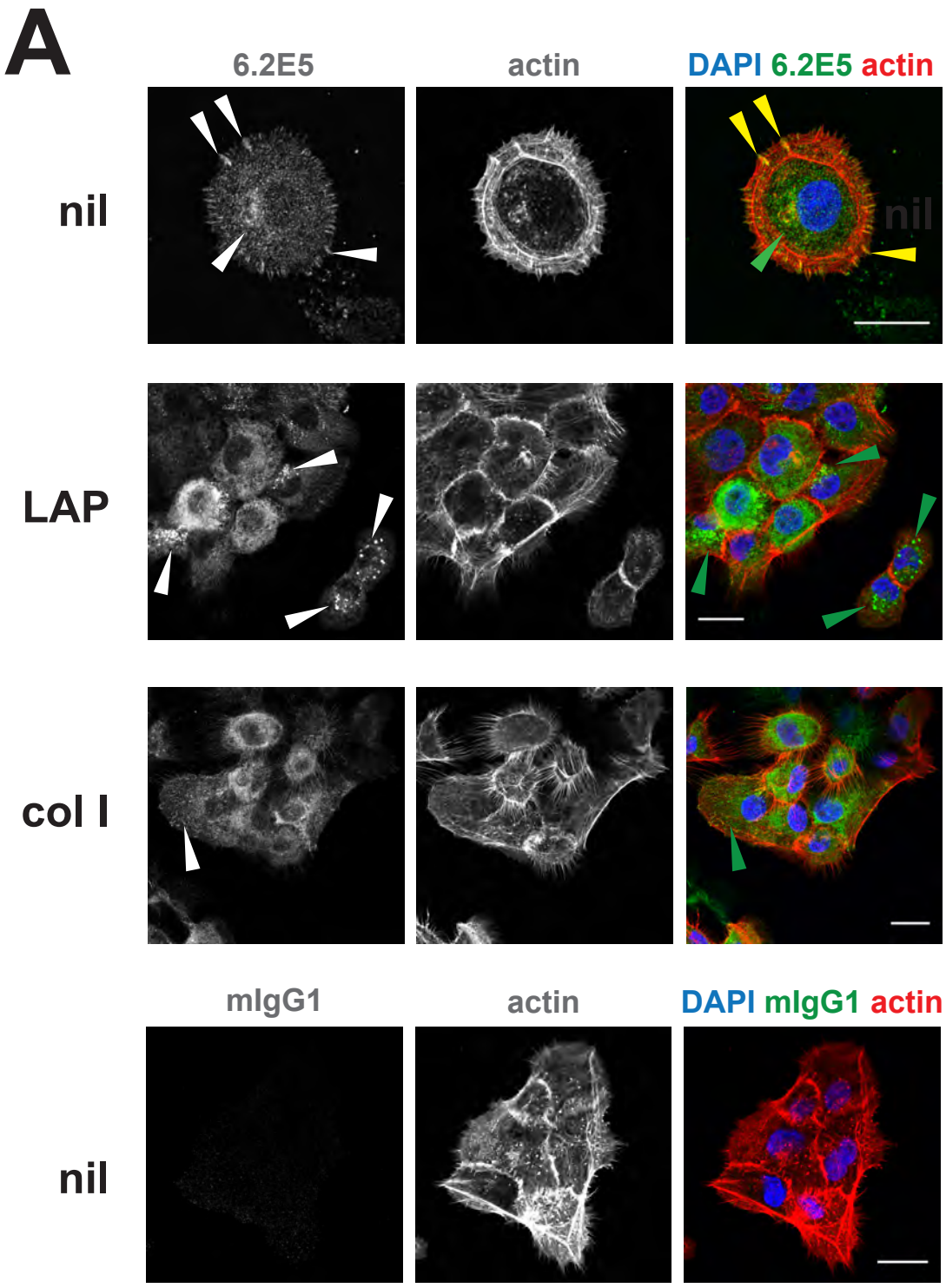

Figure 3.3.2 (A)
The antibody 6.2E5 reveals the subcellular distribution of the active integrin $\alpha_v\beta_6$ subpopulation during 2D ligand engagement on LAP and collagen type I

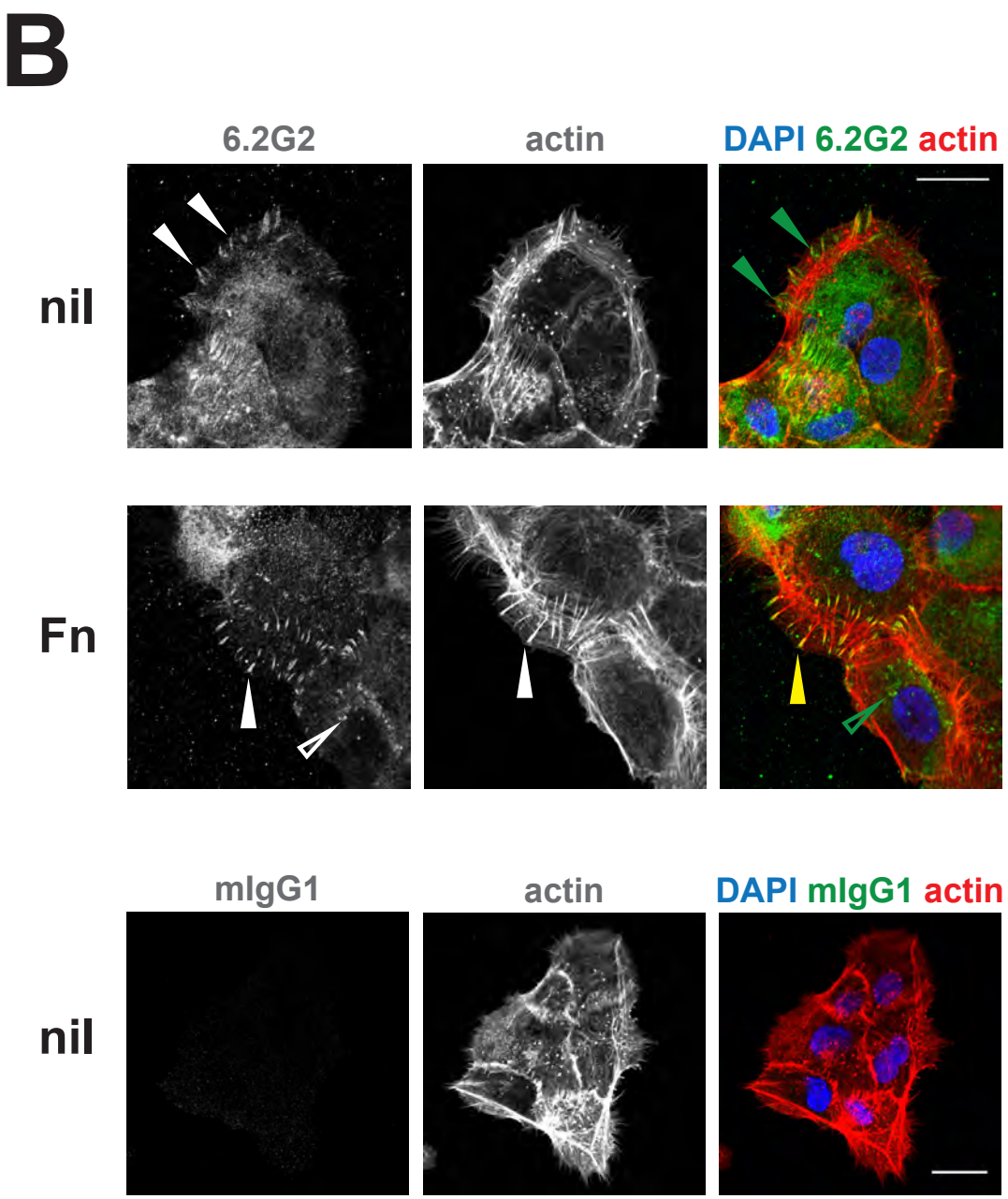

Figure 3.3.2 (B)
The antibody 6.2G2 reveals the subcellular distribution of the active integrin $\alpha_v\beta_6$ subpopulation during 2D-ligand engagement on fibronectin

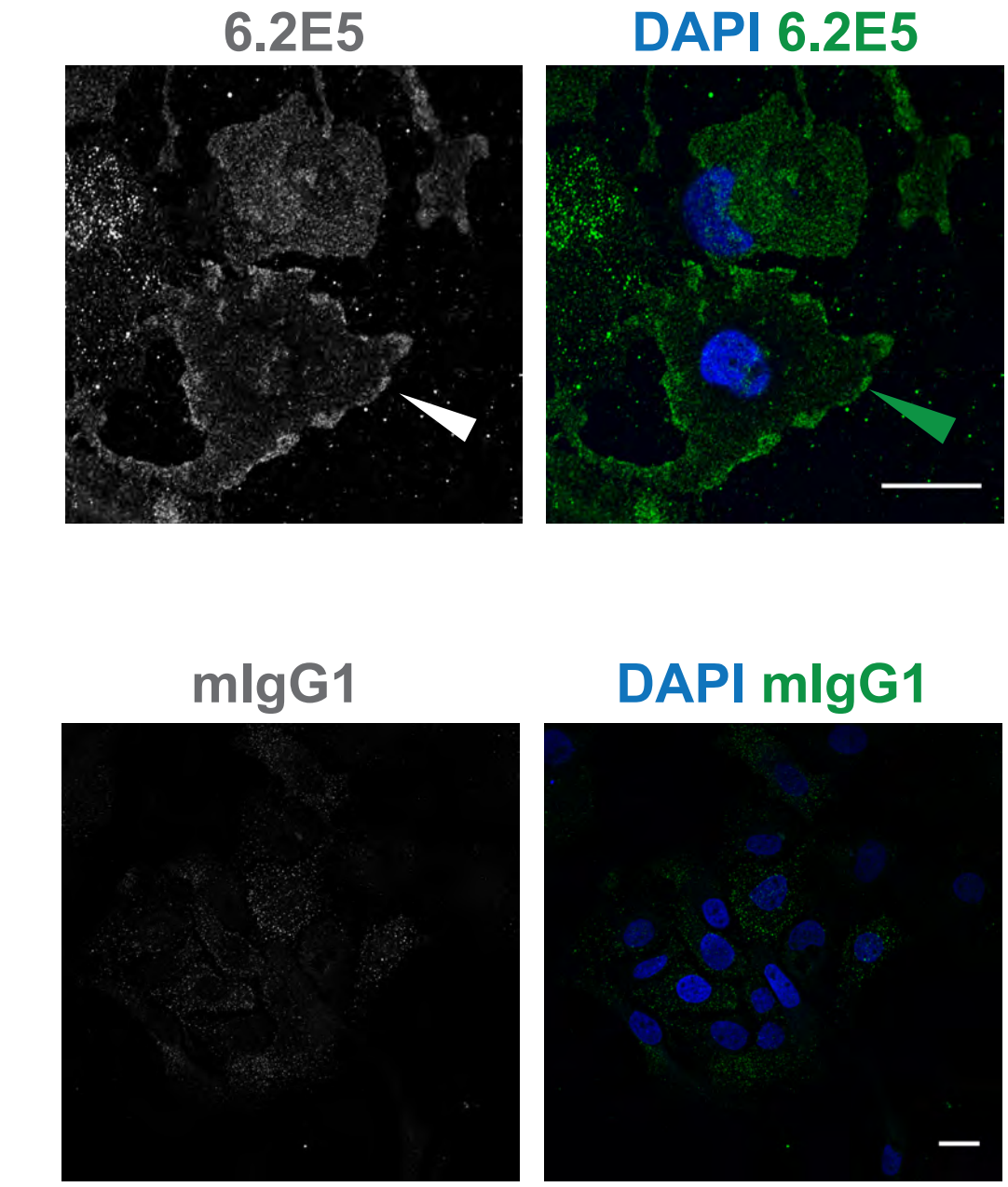

Figure 3.3.2 (C)
The antibody 6.2E5 reveals the cell surface distribution of the active integrin $\alpha_v\beta_6$ localising in clusters at the cell periphery

Figure 3.3.2
The antibodies 6.2E5 and 6.2G2 reveal the subcellular distribution of the active integrin $\alpha_v\beta_6$ subpopulation during ligand engagement

(3.3.2 A & B) The utility of antibodies 6.2E5 **(3.3.2 A)** and 6.2G2 **(3.3.2 B)** to study the subcellular distribution of the active subpopulation of ligand-engaged integrin $\alpha_v\beta_6$ was evaluated in the VB6 cell line by permeabilised immunofluorescence. In addition, the ability of antibody 6.2E5 to characterise the cell-surface distribution of active integrin $\alpha_v\beta_6$ was briefly evaluated **(3.3.2 C)**, again in the VB6 cell line, by non-permeabilised immunofluorescence. **(3.3.2 A & B)** Non-derivatised 13 mm glass coverslips were coated overnight at 4°C with either; serum-free media (**nil**), human recombinant LAP (**LAP**, L3408, Sigma Aldrich, 0.5 µg ml^{-1}), human recombinant fibronectin (**Fn**, F2006, Sigma Aldrich, 10 µg ml^{-1}) or murine collagen I (**col I**, 354236, Corning, 10 µg ml^{-1}). Cells were then seeded (2 x 10^4 cells per coverslip) and left to adhere for 2 hours in serum-free media under standard culture conditions prior to fixation and permeabilisation in cytoskeletal fixative. The integrin $\alpha_v\beta_6$ was labelled with either antibody 6.2E5 or 6.2G2 (both Biogen Idec, 5 µg ml^{-1}), cytoskeletal actin was demonstrated with tetramethylrhodamine-phalloidin (R415, Molecular Probes, 50 µg ml^{-1}) and nuclei were stained with DAPI (Invitrogen, 1 µg ml^{-1}). **(3.3.2 A)** Marked vesicular clustering of 6.2E5 immunopositivity was observed in VB6 cells spreading on the integrin $\alpha_v\beta_6$ cognate ligand LAP (**LAP**), distinct from the peripheral pattern of 6.2E5 immunopositivity observed on untreated (**nil**) coverslips (white and green arrows). In the absence of cognate ligand, 6.2E5 appears to localise at the tips of actin rich projections at the cell periphery, which may be filopodia or possibly invadopodia, given the propensity of the VB6 cell line to form the latter. In cells spreading on the non-$\alpha_v\beta_6$ cognate ligand collagen I (**col I**), no distinct pattern of 6.2E5 immunopositivity was observed. Instead, 6.2E5 positivity was diffusely cytoplasmic, proximal to cell nuceli. In contrast with LAP, no vesicular accumulations nor localisation at actin fibre tips were discernible for 6.2E5 in the presence of collagen I. **(3.3.2 B)** In VB6 cells spreading on fibronectin (**Fn**), 6.2G2 immunopositivity (white and green arrows) was predominantly localised at actin fibre tips (filopodia) protruding at the leading edges of spreading cells. Some vesicular accumulations of 6.2G2 immunopositivity were also observed. As with antibody 6.2E5, the antibody 6.2G2 was seen to localise at the periphery of cells spreading in the absence of ligand (**nil**). Accumulations at actin fibres were less marked in the absence of ligand (**nil**) compared to in the presence of fibronectin (**Fn**). Owing to technical failure and limited supply of antibodies 6.2G2 and 6.2E5 complete evaluation of each antibody on VB6 cells spreading on a panel of cognate **(3.3.2 C)** Cells (2 x 10^4 cells per coverslip) were left to adhere overnight on uncoated glass coverslips. Surface integrin $\alpha_v\beta_6$ was labelled on live cells using antibody 6.2E5 (Biogen Idec, 5 µg ml^{-1}) for 10 min at 4°C prior to fixation in 4% PFA. Nuclei were demonstrated with membrane-permeant Hoechst 33342 (H3570, Life Technologies, 1 µg ml^{-1}). Cell-surface labelling revealed a clustered pattern of immunopositivity for antibody 6.2E5 at the cell periphery in what appear to be membrane ruffles (white arrow and green arrows). Images were acquired by confocal microscopy using the ZEISS LSM710 equipped with ZEISS Zen image analysis software (all Carl Zeiss AG, DE). Images were prepared for presentation using Image J (National Institutes of Health) and Adobe® Photoshop© CS6, with composites generated in Adobe® Illustrator© CS6 (Adobe Systems Software© Ltd).

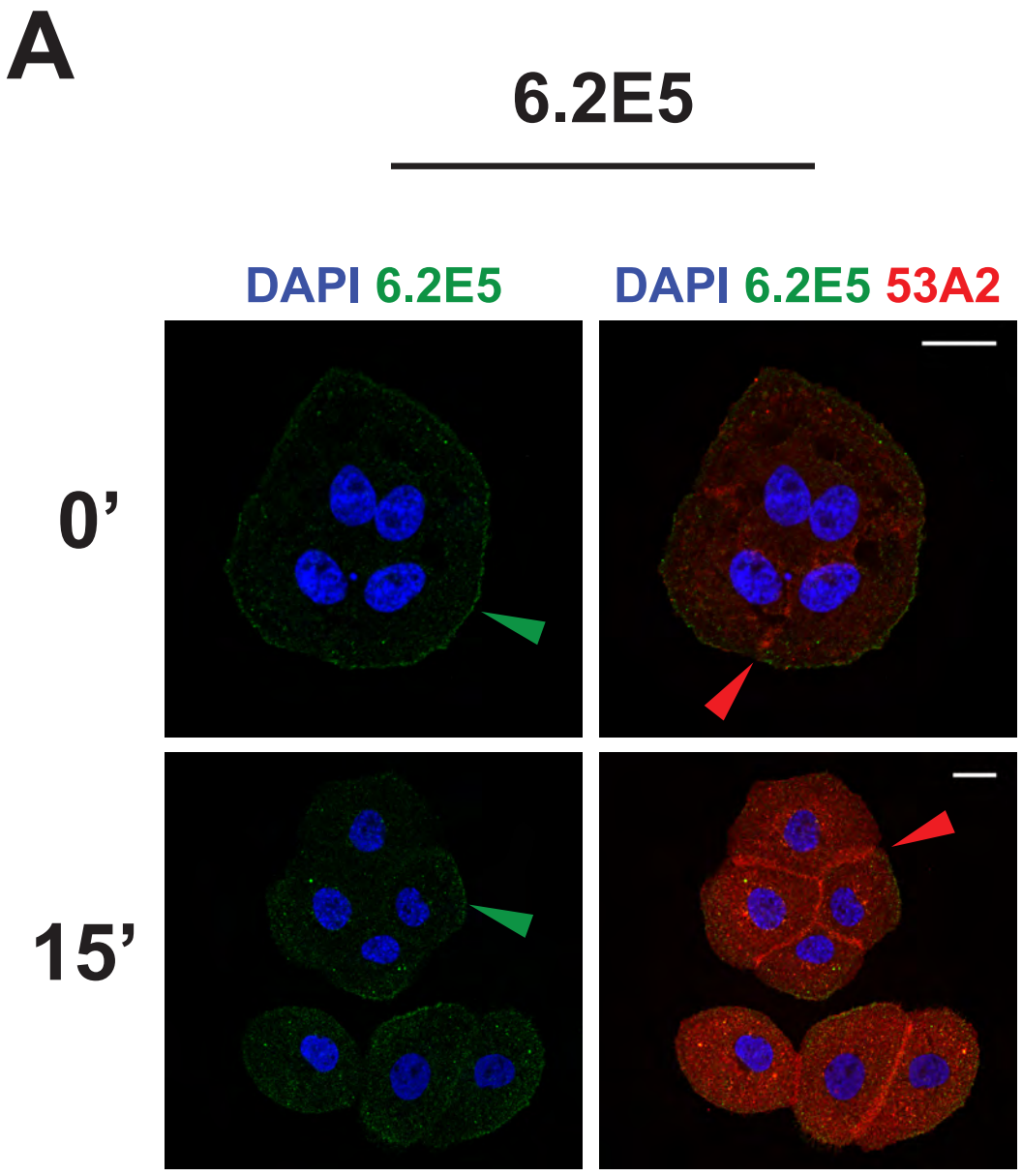

Figure 3.3.3 (A)
The antibodies 6.2E5 and 6.2G2 may be used to label the active subpopulation of integrin $\alpha_v\beta_6$ in live cells to demonstrate the spatiotemporal distribution of activation-associated epitopes

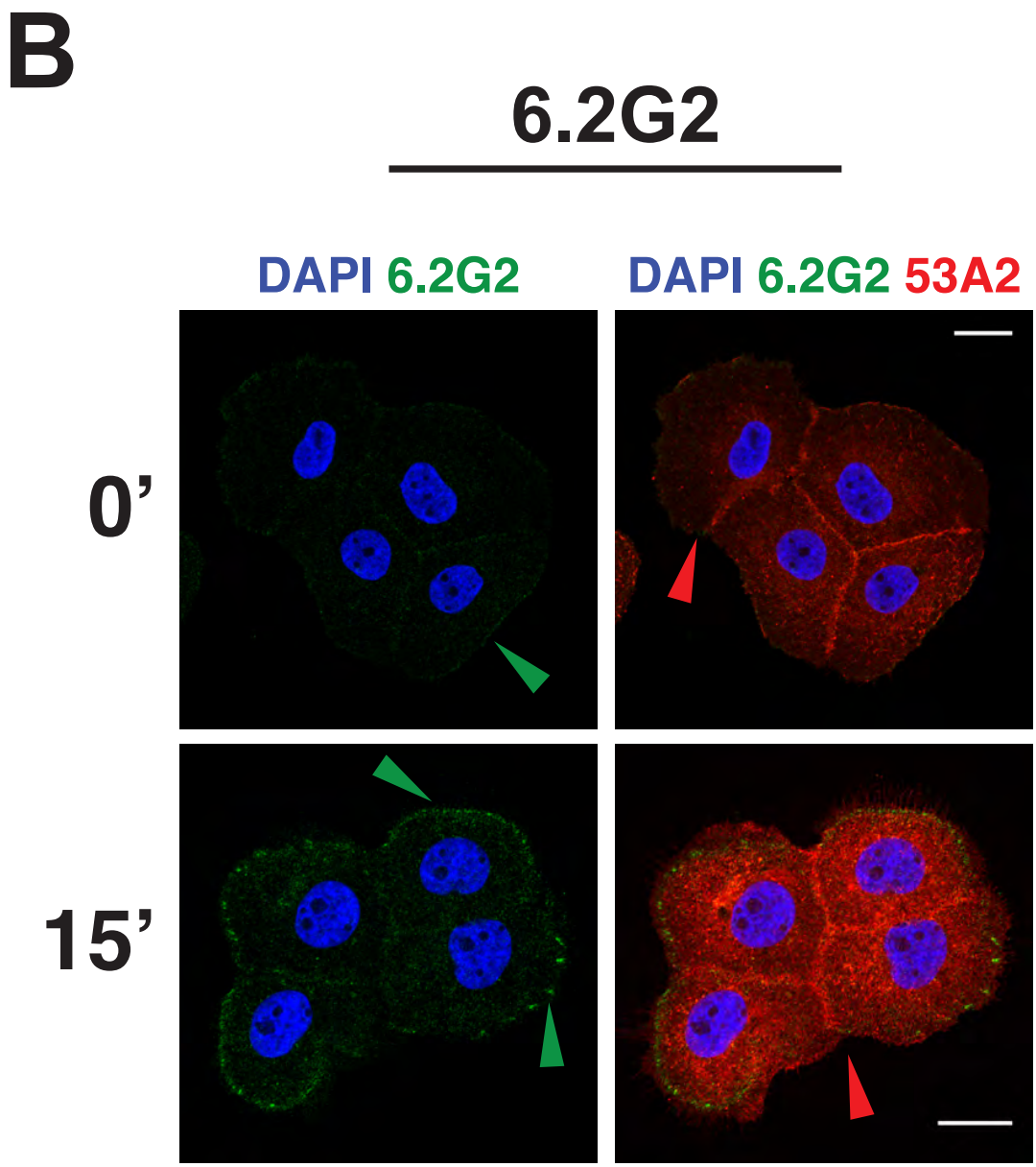

Figure 3.3.3 (B)
The antibodies 6.2E5 and 6.2G2 may be used to label the active subpopulation of integrin $\alpha_v\beta_6$ in live cells to demonstrate the spatiotemporal distribution of activation-associated epitopes

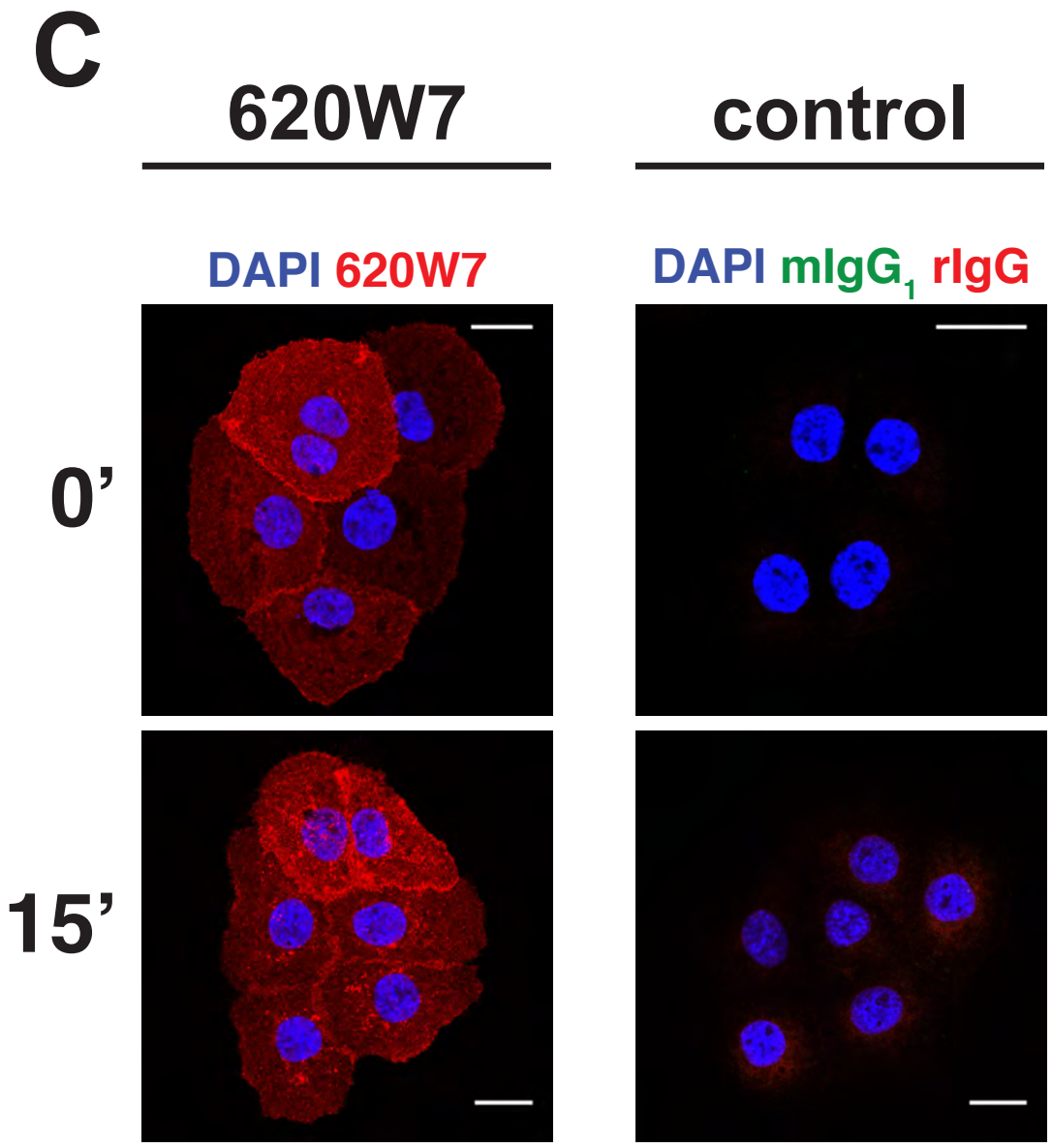

Figure 3.3.3 (C)
The antibodies 6.2E5 and 6.2G2 may be used to label the active subpopulation of integrin $\alpha_v\beta_6$ in live cells to demonstrate the spatiotemporal distribution of activation-associated epitopes

Figure 3.3.3

The antibodies 6.2E5 and 6.2G2 may be used to label the active subpopulation of the integrin $\alpha_v\beta_6$ in live cells to demonstrate the spatiotemporal subcellular distribution of activation-associated epitopes

(3.3.3 A - C) The utility of antibodies 6.2E5 **(3.3.3 A)** and 6.2G2 **(3.3.3 B)** to determine the spatiotemporal distribution of integrin $\alpha_v\beta_6$ activation-associated epitopes in live cells was performed by vital staining and permeabilised immunofluorescence using the VB6 cell line. The localisations of 6.2E5 and 6.2G2 cognate epitopes were compared concomitantly with the distribution of the cognate epitope for antibody 53A2 (CR-UK, 10 µg ml^{-1}), a function-blocking antibody with no association to integrin $\alpha_v\beta_6$ activation status or conformation. The antibody 620W7, an anti-integrin $\alpha_v\beta_6$ antibody that recognises total integrin $\alpha_v\beta_6$ (both mature and immature-data not shown) in its various glycosylation states, was also evaluated **(3.3.3 C)**. Live cells allowed to adhere overnight on uncoated non-derivatised 13 mm glass coverslips were labelled with antibody 6.2E5, 6.2G2 (both Biogen Idec, 5 µg ml^{-1}) or antibody 620W7 (CR-UK, 10 µg ml^{-1}) for 10 min at 4°C. Cells were either washed, fixed and permeabilised immediately post-labelling (**0'**) or supplemented with complete media and returned to standard culture conditions for 15 min to permit early internalisation events (**15'**). After 15 min, cells were washed, fixed and permeabilised as previously described. Cells that had been live-labelled with 6.2E5 and 6.2G2 were post-labelled with antibody 53A2. After labelling with appropriate fluorophore-conjugated secondary antibodies and addition of DAPI nuclear stain (Invitrogen, 1 µg ml^{-1}), coverslips were mounted and reviewed by immunofluorescence microscopy. **(3.3.3 A)** The antibody 6.2E5 was seen to predominate at the peripheral edges of spreading cells and was excluded from cell-cell junctions where 53A2 localised in abundance. After 15 min, punctate cytoplasmic immunopositivity was observed for 6.2E5. **(3.3.3 B)** The antibody 6.2G2 demonstrated weak, punctate immunopositivity at the peripheral edges of spreading cells and diffusely throughout the cytoplasm. Following 15 min of internalisation, marked clusters of vesicular-like accumulations of 6.2G2 were noted at the peripheral edges of cells which did not appear to co-localise with 53A2, which again predominated at cell-cell junctions and whose localisation at cell-cell junctions was not observably altered following 15 minutes internalisation. **(3.3.3 C)** Cells live-labelled with antibody 620W7 revealed the distribution of 620W7 cognate epitopes were not visibly altered following internalisation. Isotype and species-matched negative control antibodies (mouse IgG_1: MABC002, Merck Millipore, 5 µg ml^{-1} or rat IgG: ab37361, AbCam, 10 µg ml^{-1}) were also reviewed for technical validation. Images were acquired by confocal microscopy using the ZEISS LSM710 equipped with ZEISS Zen image analysis software (all Carl Zeiss AG, DE). Images were prepared for presentation using Image J (National Institutes of Health) and Adobe® Photoshop© CS6, with composites generated in Adobe® Illustrator© CS6 (Adobe Systems Software© Ltd).

3.4 antibodies 6.2E5 and 6.2G2 may be used in FFPE and fresh frozen human primary breast cancer tissue samples to demonstrate integrin $\alpha_v\beta_6$ histological distribution but may not reliably discriminate receptor activation status

To ascertain whether the antibodies 6.2E5 and 6.2G2 may be used to histologically distinguish the integrin $\alpha_v\beta_6$ active subpopulation by immunohistochemistry (IHC), their distribution was evaluated in match-paired FFPE and fresh frozen sections of human primary breast tumour samples kindly obtained from the Barts Cancer Institute Breast Tissue Bank (Research Ethics Code 15/EE/0192). Discrimination between the spatiotemporal distributions of active versus inactive integrin $\alpha_v\beta_6$ receptor populations in primary human BrCa samples would permit novel evaluation of the relevance of integrin $\alpha_v\beta_6$ activation status and $\alpha_v\beta_6$–mediated downstream signalling specifically during breast tumourigenesis and disease progression.

To date, only IHC appraisal and histological analysis of gross integrin $\alpha_v\beta_6$ expression without delineation of receptor activation status has been published. This approach has successfully demonstrated that total integrin $\alpha_v\beta_6$ is overexpressed in a variety of cancers including pancreatic (Sipos *et al* 2004), ovarian (Ahmed *et al* 2002b) and oral squamous cell carcinoma (Thomas *et al* 2001b); and is a poor prognostic indicator in colorectal (Bates *et al* 2005), lung (Elayadi *et al* 2007), cervical (Hazelbag *et al* 2007) and breast (Moore *et al* 2014) cancers. However, this strategy has failed to demonstrate a robust, definitive link between integrin $\alpha_v\beta_6$ receptor activation specifically and disease progression.

Thus, it was deemed prudent to ascertain whether the antibody clones 6.2E5 and 6.2G2 could discriminate between active and inactive pools of integrin $\alpha_v\beta_6$ in histopathological human BrCa samples. This characterisation was particularly prescient given that all of the studies described above (excluding Sipos and colleagues' (2004) pancreatic cancer study), utilised antibody 6.2G2 to histologically demonstrate integrin $\alpha_v\beta_6$ expression.

Therefore, ability to demonstrate integrin $\alpha_v\beta_6$ activation status within clinical samples of known grade, stage, therapeutic responsiveness and long-term patient outcome would refine our understanding of the causal, effective or reciprocal

function of integrin $\alpha_v\beta_6$–mediated phenotypic outputs during neoplastic transformation, tumourigenesis and progression to invasive and metastatic disease.

Data presented earlier in this chapter have shown that the antibodies 6.2E5 and 6.2G2 each recognise an activation-associated epitope and LIBS at a single-cell level by flow cytometry (Figures 3.1 and 3.2) and immunofluorescence (Figure 3.3). However, given the conformational-dependency of these epitopes inferred from these data, the ability of these antibodies to recognise active integrin $\alpha_v\beta_6$ conformers in excised, formalin-fixed or snap frozen human tissue samples required evaluation.

Formalin fixation, tissue processing and subsequent antigen retrieval by heat-induced epitope retrieval (HIER) or enzyme-induced epitope retrieval (EIER) techniques are known to alter protein gross conformation, induce disulphide cross-linkage formation and modify critical residues which will determine the accurate and successful detection of retrieved epitopes by their cognate antibody (Shi *et al* 2011). These factors render FFPE-IHC application of conformer-specific antibodies particularly problematic since the conformational epitope may be lost, or revealed in artefact, by the FFPE process. Therefore, case-matched fresh frozen tumour samples were compared in tandem since these snap-frozen tissues are more likely to capture the integrin $\alpha_v\beta_6$ *in vivo* conformational state at time of resection.

To obviate any sample selection bias, 14 anonymised breast cancer cases were screened by FFPE-IHC to determine their integrin $\alpha_v\beta_6$ status using the CSβ6 *(Calbiochem)* monoclonal anti-integrin β_6–subunit antibody well established in-house for use in FFPE human tissue samples (Figure 3.4.1). Five cases were selected for additional staining and review based upon their strong integrin $\alpha_v\beta_6$ expression and superior histological preservation of tissue morphology (Figure 3.4.1B). Human placental tissue, known to express the integrin $\alpha_v\beta_6$ (Ahmed *et al* 2004), was used as a positive control to validate IHC detection of integrin $\alpha_v\beta_6$ expression by this method.

Each of the five FFPE cases (Figure 3.4.2A, C, E, G & I), along with their respective fresh frozen counterpart samples (Figure 3.4.2B, D, F, H & J) were sectioned and

stained using the antibodies 6.2E5 and 6.2G2 to evaluate and compare the immunopositive distributions of epitopes recognised by each antibody in FFPE versus fresh frozen human BrCa tissue (Figure 3.4.2A – J).

Both the antibodies 6.2E5 and 6.2G2 clearly delineated integrin $\alpha_v\beta_6$-positive mammary ductal structures in a similar pattern to antibody CSβ6 in both FFPE and fresh frozen samples. Furthermore, like the antibody CSβ6, the antibodies 6.2E5 and 6.2G2 each distinguished integrin $\alpha_v\beta_6$-positive breast parenchyma even in the absence of ductal morphology (or the vestiges thereof) in transformed breast tissues as shown in Figure 3.4.2H. Collectively this confirms the suitability of antibodies 6.2E5 and 6.2G2 to demonstrate gross morphological detail of integrin $\alpha_v\beta_6$–positive structures within human breast tissue architecture.

However, the marked membranous localisation of integrin $\alpha_v\beta_6$ expression principally observed in fresh frozen tissue samples (Figures 3.4.2B, D, F, H and J) contrasted with predominantly diffuse cytoplasmic immunopositivity in FFPE matched samples (Figures 3.4.2A, C, E, G and I) revealed by each of the antibodies CSβ6, 6.2E5 and 6.2G2. The exquisite cell surface membrane immunopositivity demonstrated by each of these antibodies is clearly shown in frozen tissue samples presented in Figures 3.4.2D and F.

Notably, Figure 3.4.2D highlights that no marked observable difference in patterns of immunopositivity for the epitopes recognised by antibodies CSβ6, 6.2E5 and 6.2G2 is appreciable in fresh frozen tissue. Here, the vestiges of the same mammary gland may be compared directly for the localisation of CSβ6, 6.2E5 and 6.2G2. A distinct and prominent membranous pattern of immunopositive localisation of integrin $\alpha_v\beta_6$ is observed for each of these antibodies. Indeed their respective IHC staining patterns appear identical.

To date, the antibody CSβ6 has not been screened to determine whether it recognises an activation-associated or conformation-specific epitope. Therefore, it may be possible that this antibody detects an epitope revealed upon integrin $\alpha_v\beta_6$ activation or conformational priming. This would account for the similarity in immunopositive tissue and cellular distribution shared between antibodies CSβ6, 6.2E5 and 6.2G2 observed in fresh frozen tissue sections. Therefore, it would be informative to define antibody kinetics for clone CSβ6 following canonical modes

of integrin activation to ascertain whether its cognate epitope is conformation-dependent. Until the nature of the epitope recognised by antibody CSβ6 has been more clearly defined, it must be concluded that the antibodies 6.2E5 and 6.2G2 do not robustly discriminate conformation-specific integrin $\alpha_v\beta_6$ receptor pools, even in fresh frozen human tissue samples more likely to capture tertiary and quaternary protein structures reflective of their *in vivo* biochemical and ultrastructural state at the time of tissue excision.

The observation of a predominantly diffuse cytoplasmic IHC appearance of integrin $\alpha_v\beta_6$ in FFPE samples compared to a markedly membranous localisation of integrin $\alpha_v\beta_6$ in fresh frozen samples infers that the exquisite cellular localisation of epitopes recognised by each of these antibodies is altered by FFPE processing. Therefore, integrin $\alpha_v\beta_6$ cellular distribution observed in FFPE samples may not accurately reflect the *in vivo* subcellular morphological fine detail requisite to robustly characterise the precise spatiotemporal role of integrin $\alpha_v\beta_6$ in neoplastic transformation and malignant progression using histopathological samples.

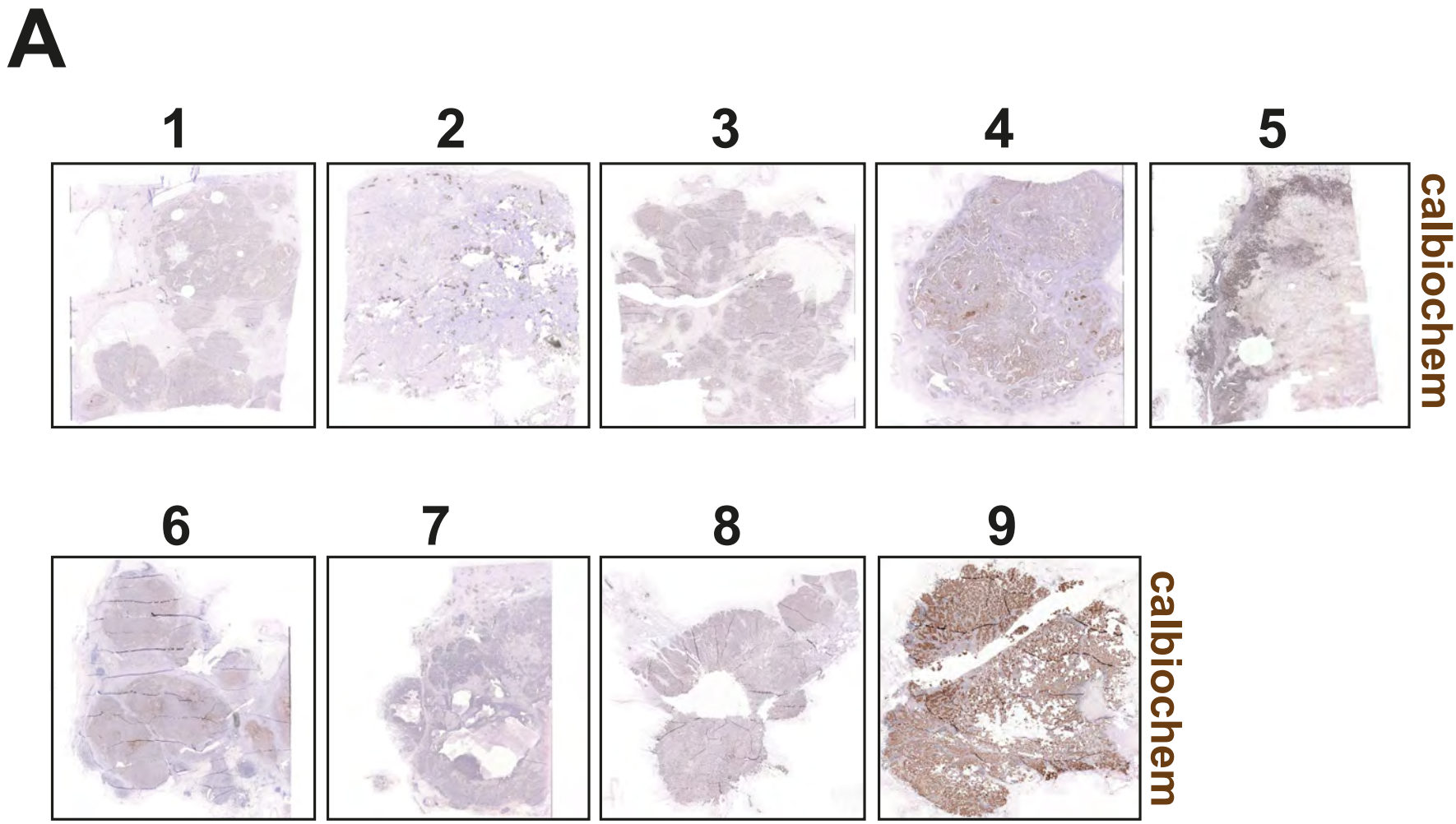

Figure 3.4.1 (A)
Identifying integrin $\alpha_v\beta_6$ positive human primary breast cancer tissue samples to histologically evaluate the utility of antibodies 6.2E5 and 6.2G2 to discriminate activation specific receptor subpopulations

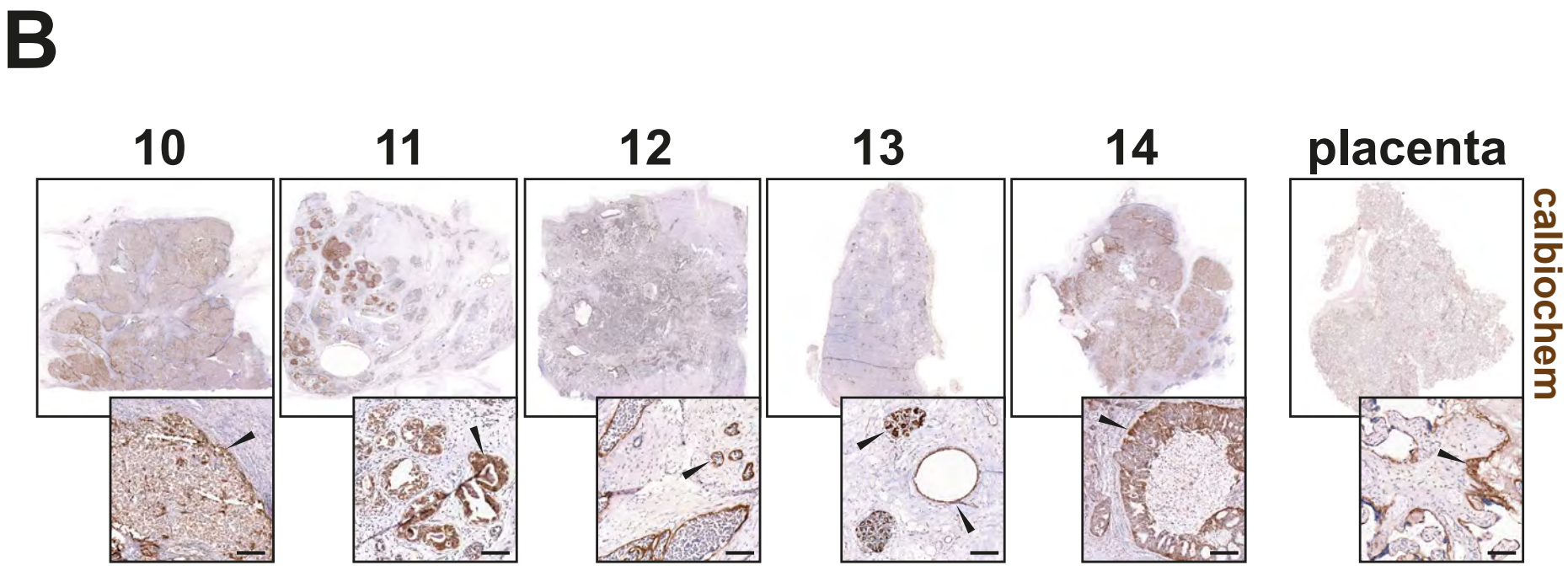

Figure 3.4.1 (B)
Identifying integrin $\alpha_v\beta_6$ positive human primary breast cancer tissue samples to histologically evaluate the utility of antibodies 6.2E5 and 6.2G2 to discriminate activation specific receptor subpopulations

Figure 3.4.1

Identifying integrin $\alpha_v\beta_6$ positive human primary breast cancer tissue samples to evaluate the utility of antibodies 6.2E5 and 6.2G2 to histologically discriminate activation specific receptor subpopulations

In order to identify suitable cases of human-derived primary breast cancer tissue samples to permit evaluation of the ability of antibodies 6.2E5 and 6.2G2 to histologically discriminate the active and inactive conformers of integrin $\alpha_v\beta_6$, FFPE samples from 14 cases kindly donated by Barts Cancer Institute Breast Tissue Bank (Research Ethics Code: 15/EE/0192) were screened by IHC for gross integrin $\alpha_v\beta_6$ expression using an antibody directed against the integrin β_6 subunit (CSβ6 (Calbiochem), MAB2076Z, Merck Millipore, 1:200). **(3.4.1 A)** Following review by brightfield microscopy, 9 cases were excluded based upon their; integrin β_6 negative status (anonymised case no. 1, 5 and 7), weak integrin β_6 expression (cases 3, 6, 8) or poor morphological preservation (cases 2, 4, 9) which was confirmed by second independent review. **(3.4.1 B)** The 5 cases selected for additional evaluation exhibited strong integrin β_6 expression and satisfactory morphological preservation. Integrin β_6 immunopositivity localised at and clearly delineated mammary ductal structures (black arrows) distinct from surrounding stroma and inflammatory infiltrate where present. At a cellular level, diffuse cytoplasmic pattern of integrin β_6 immunopositivity was observed using antibody CSβ6 (Calbiochem) in FFPE tissues evaluated. Human placental tissue, known to express integrin $\alpha_v\beta_6$ was included as a positive control sample. Following endopeptidase protease antigen retrieval with VENTANA™ Protease 1 solution (#760-2018), immunohistochemistry was performed using the VENTANA™ BenchMark GX using the VENTANA™ ultraView Universal DAB Detection Kit (#760-500) (all Ventana Medical Systems Inc, Roche Holdings AG). Slides were scanned and images acquisitioned on Pannoramic 250 Flash II digital scanner prior to review using Panoramic Viewer Software (both 3DHISTECH Ltd, Hungary). Scale bars represent 100 μm.

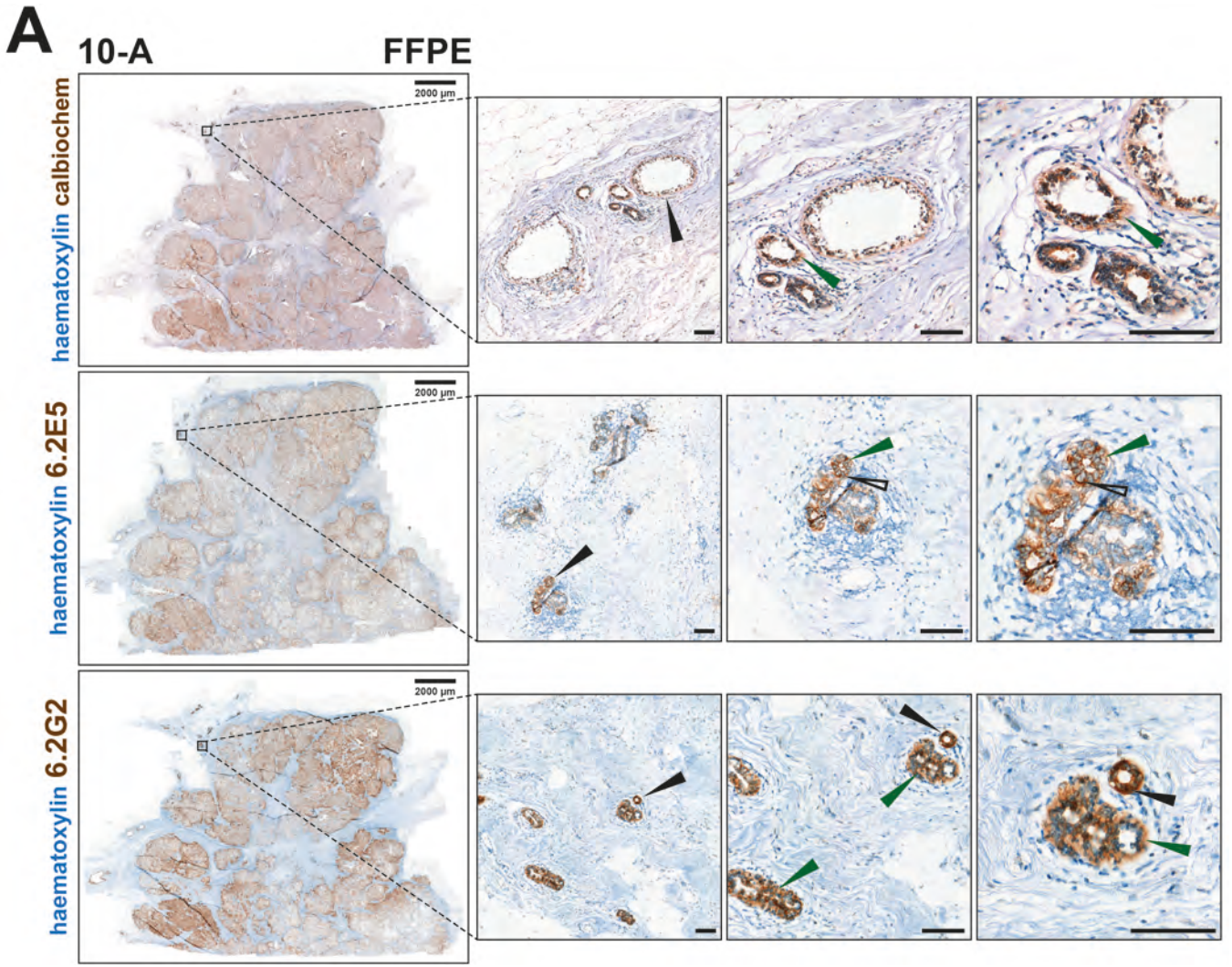

Figure 3.4.2 (A)
Evaluating the utility of antibodies 6.2E5 and 6.2G2 to histologically study the active population of integrin $\alpha_v\beta_6$ in FFPE and matched frozen clinical samples of human breast cancer specimens

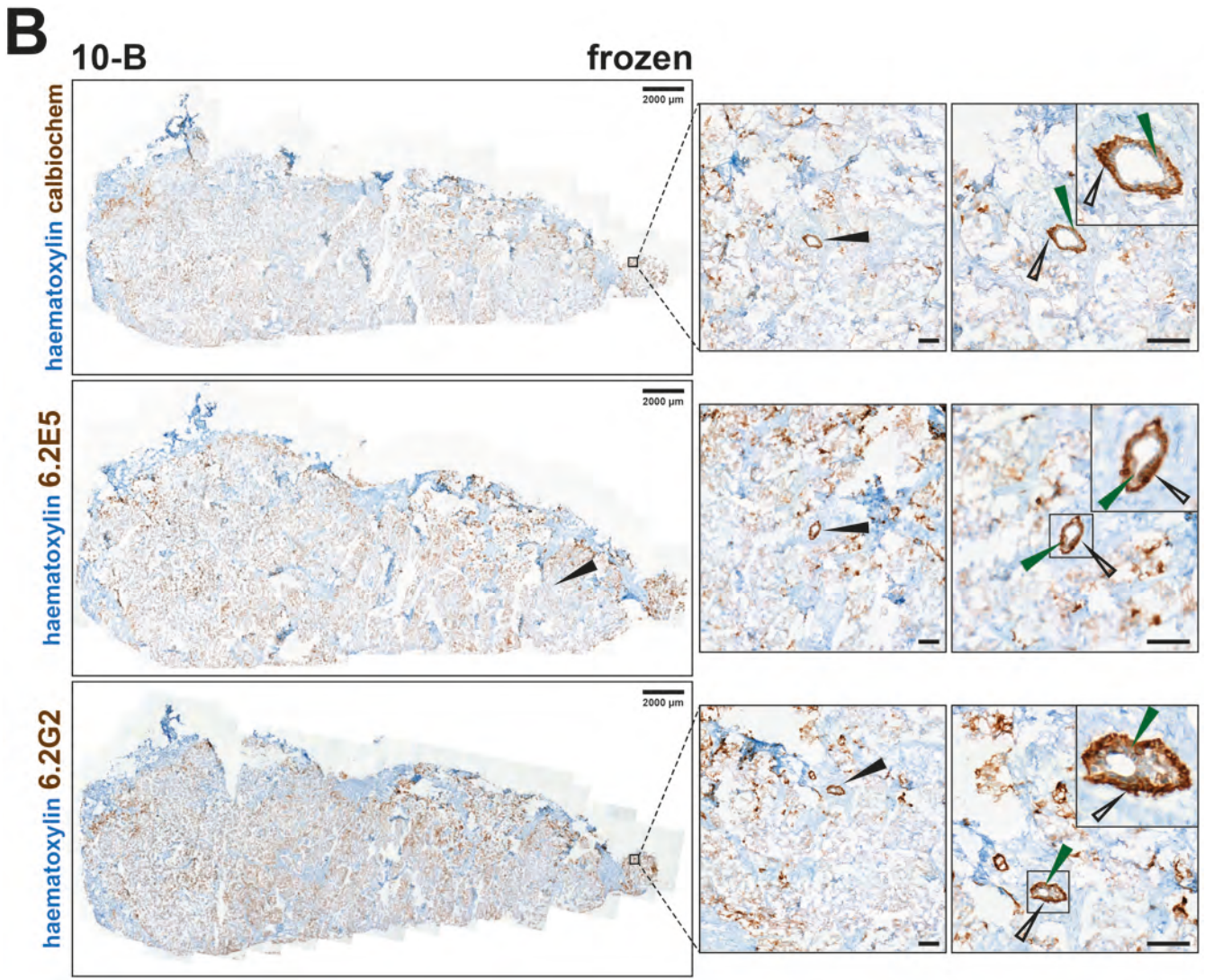

Figure 3.4.2 (B)
Evaluating the utility of antibodies 6.2E5 and 6.2G2 to histologically study the active population of integrin $\alpha_v\beta_6$ in FFPE and matched frozen clinical samples of human breast cancer specimens

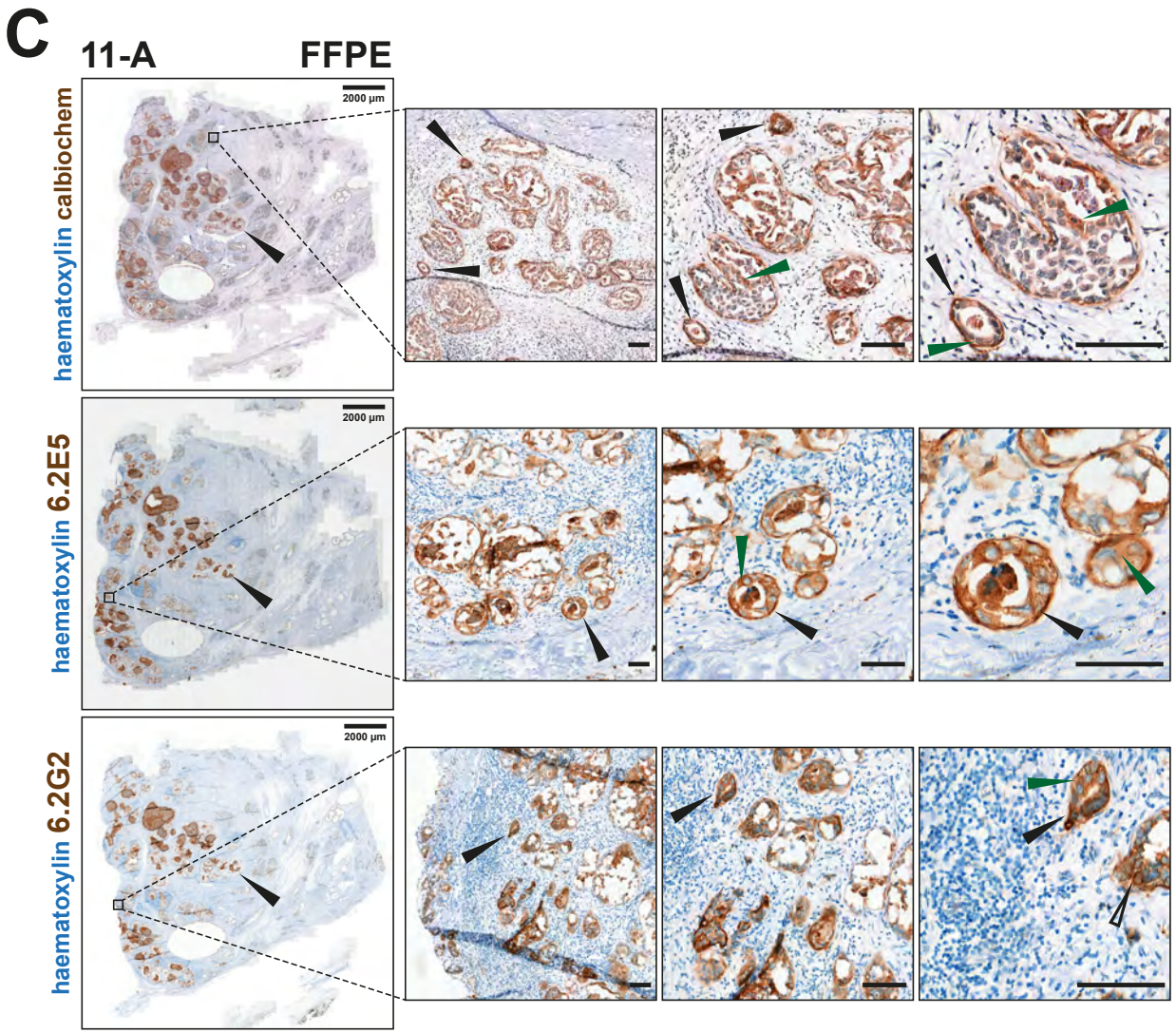

Figure 3.4.2 (C)
Evaluating the utility of antibodies 6.2E5 and 6.2G2 to histologically study the active population of integrin $\alpha_v\beta_6$ in FFPE and matched frozen clinical samples of human breast cancer specimens

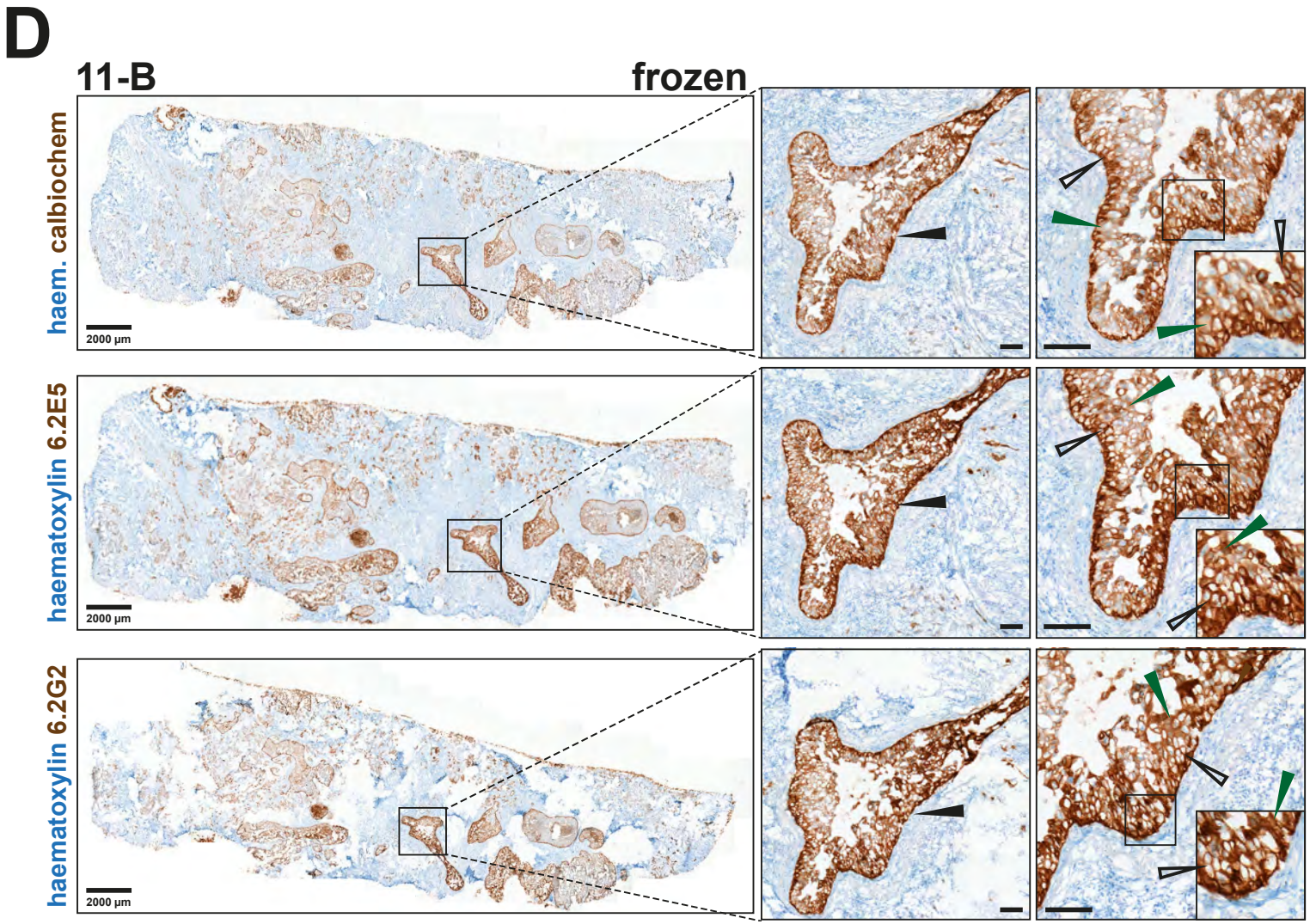

Figure 3.4.2 (D)
Evaluating the utility of antibodies 6.2E5 and 6.2G2 to histologically study the active population of integrin $\alpha_v\beta_6$ in FFPE and matched frozen clinical samples of human breast cancer specimens

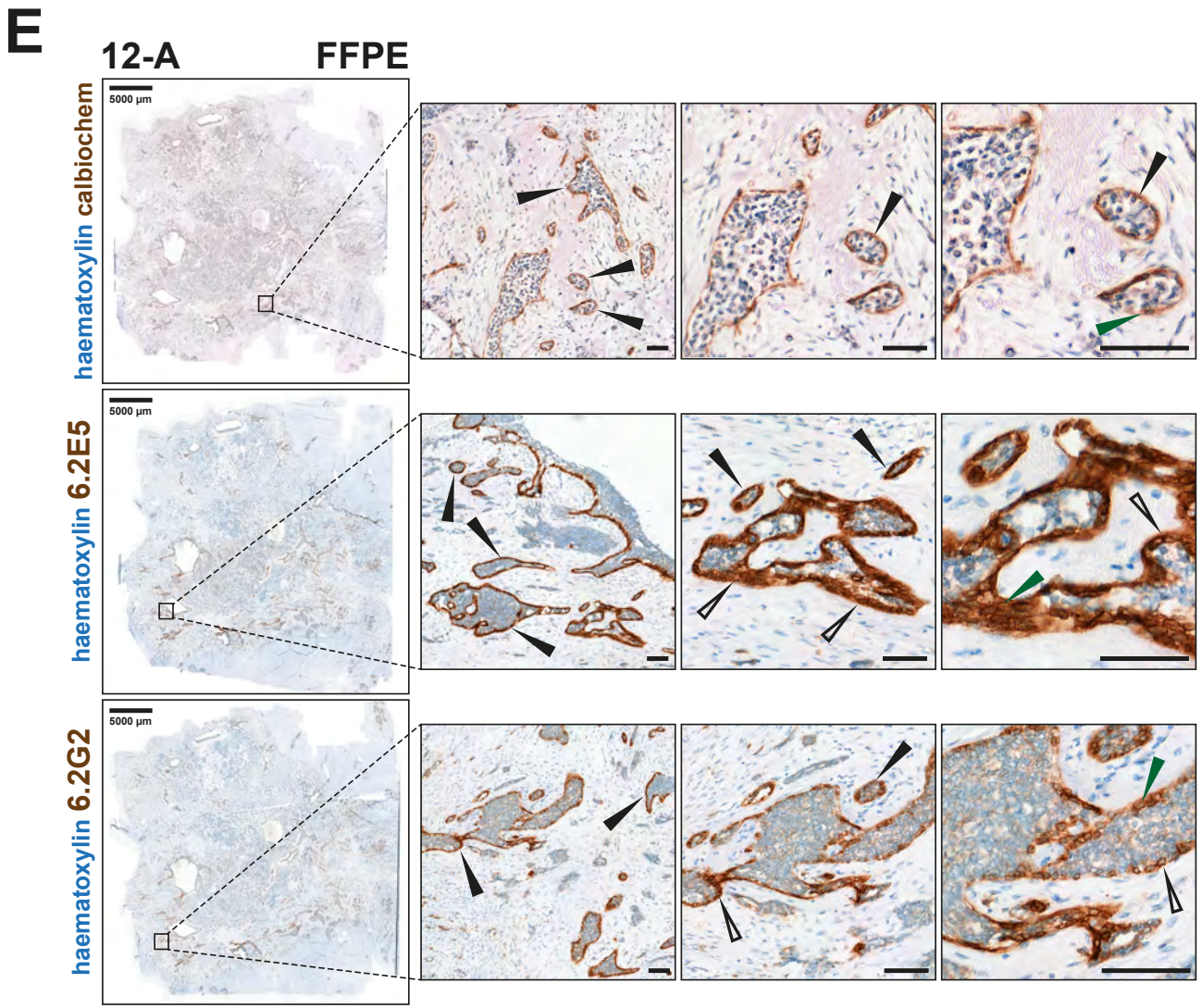

Figure 3.4.2 (E)
Evaluating the utility of antibodies 6.2E5 and 6.2G2 to histologically study the active population of integrin $\alpha_v\beta_6$ in FFPE and matched frozen clinical samples of human breast cancer specimens

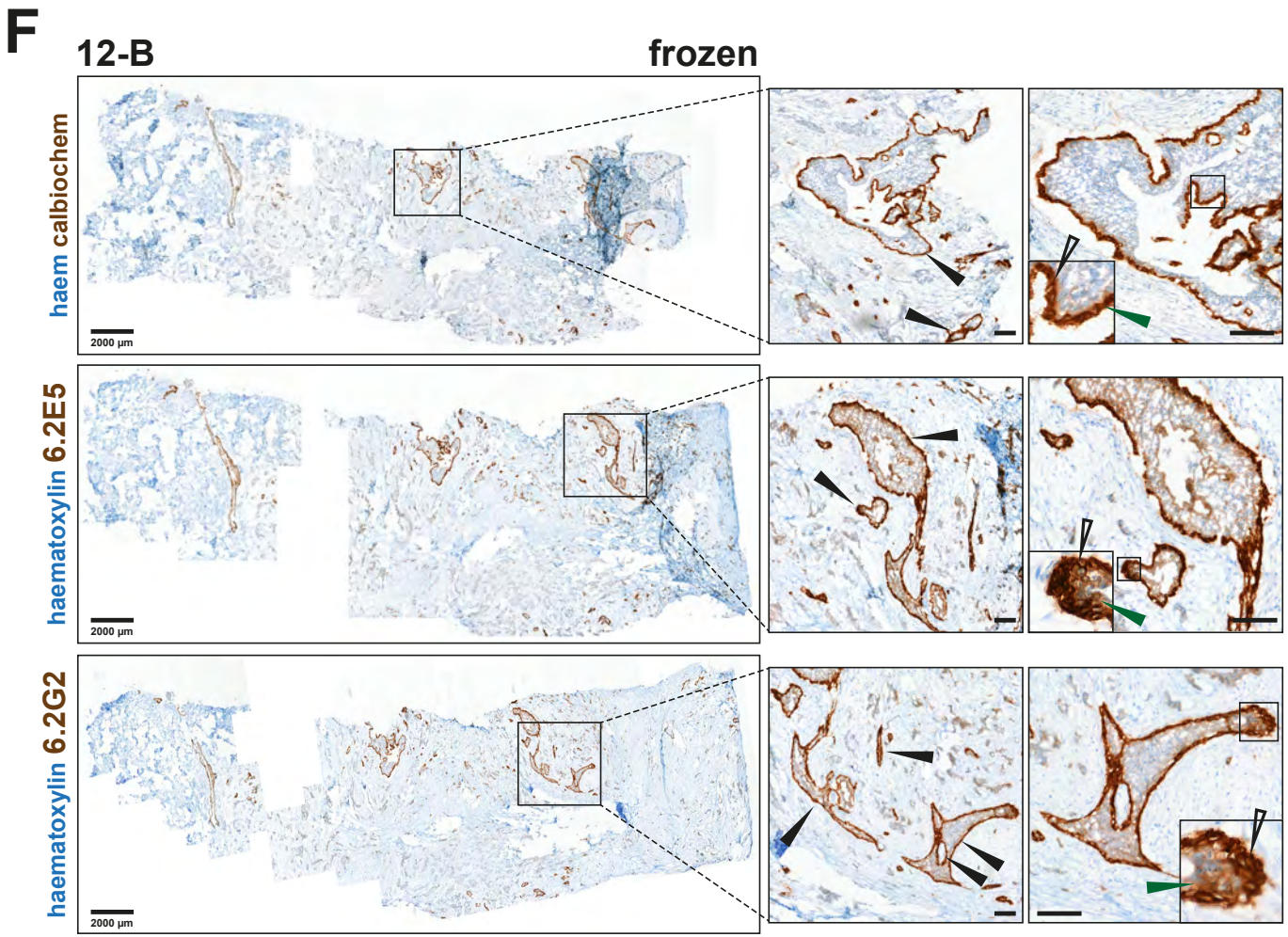

Figure 3.4.2 (F)
Evaluating the utility of antibodies 6.2E5 and 6.2G2 to histologically study the active population of integrin $\alpha_v\beta_6$ in FFPE and matched frozen clinical samples of human breast cancer specimens

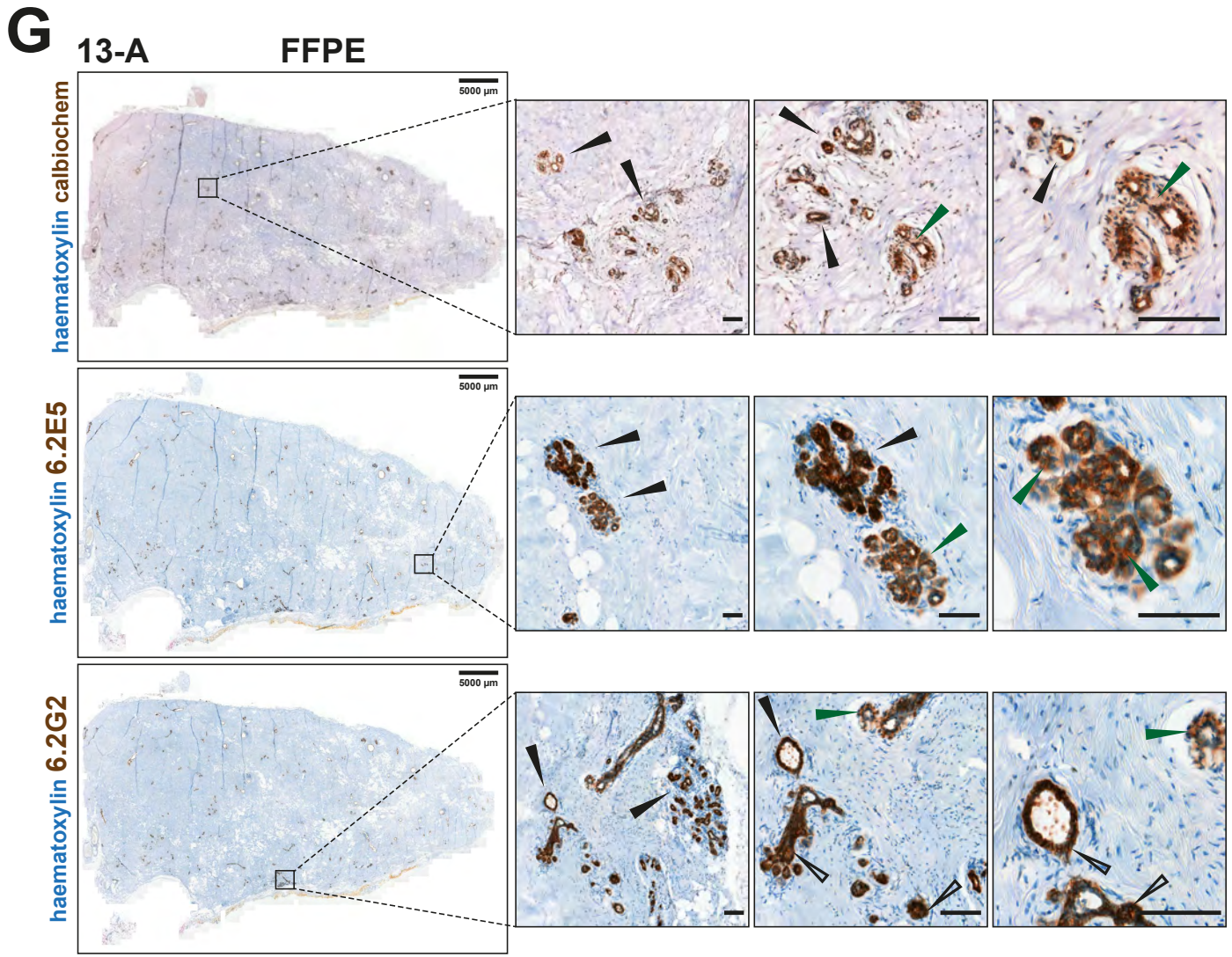

Figure 3.4.2 (G)
Evaluating the utility of antibodies 6.2E5 and 6.2G2 to histologically study the active population of integrin $\alpha_v\beta_6$ in FFPE and matched frozen clinical samples of human breast cancer specimens

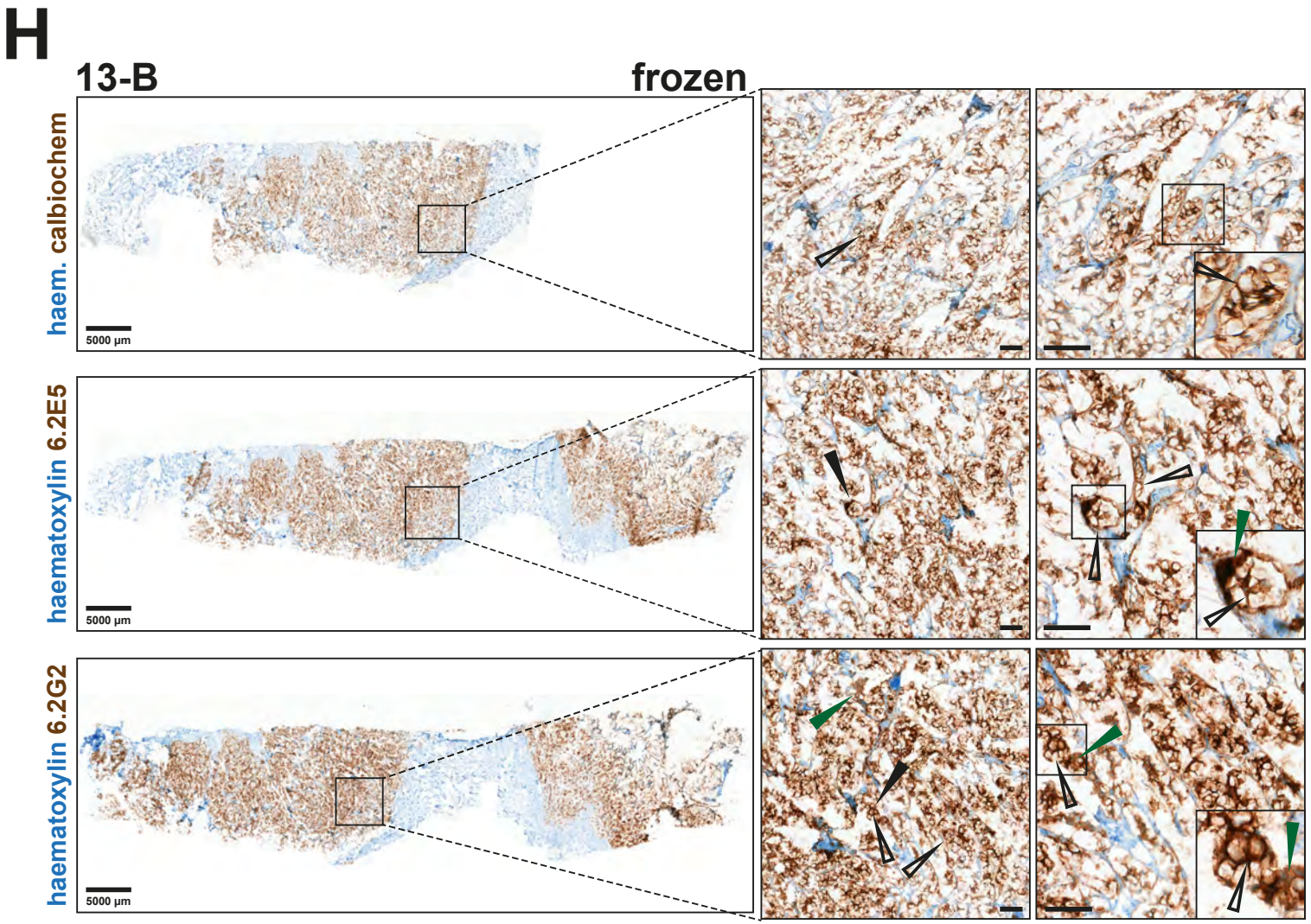

Figure 3.4.2 (H)
Evaluating the utility of antibodies 6.2E5 and 6.2G2 to histologically study the active population of integrin $\alpha_v\beta_6$ in FFPE and matched frozen clinical samples of human breast cancer specimens

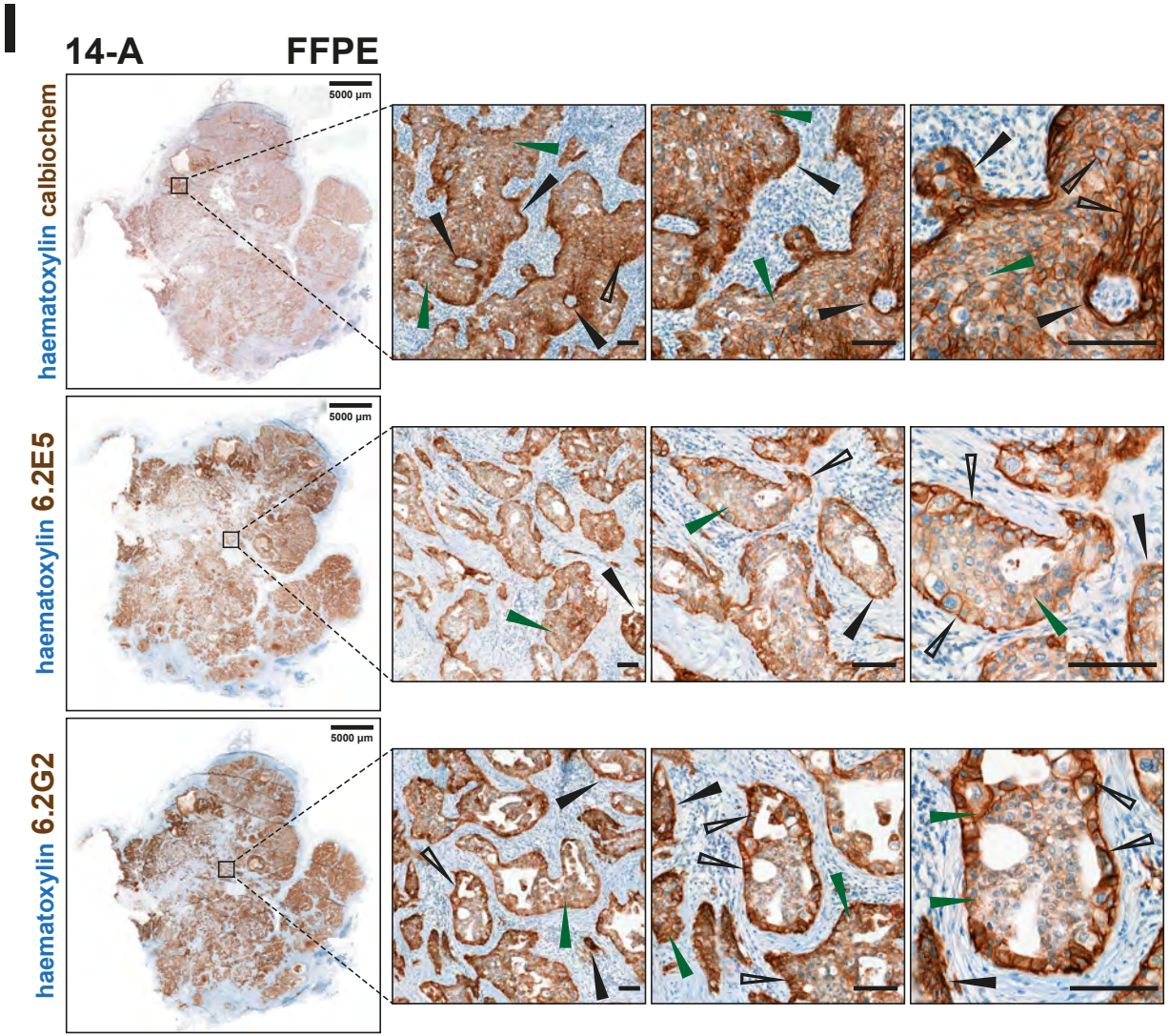

Figure 3.4.2 (I)
Evaluating the utility of antibodies 6.2E5 and 6.2G2 to histologically study the active population of integrin $\alpha_v\beta_6$ in FFPE and matched frozen clinical samples of human breast cancer specimens

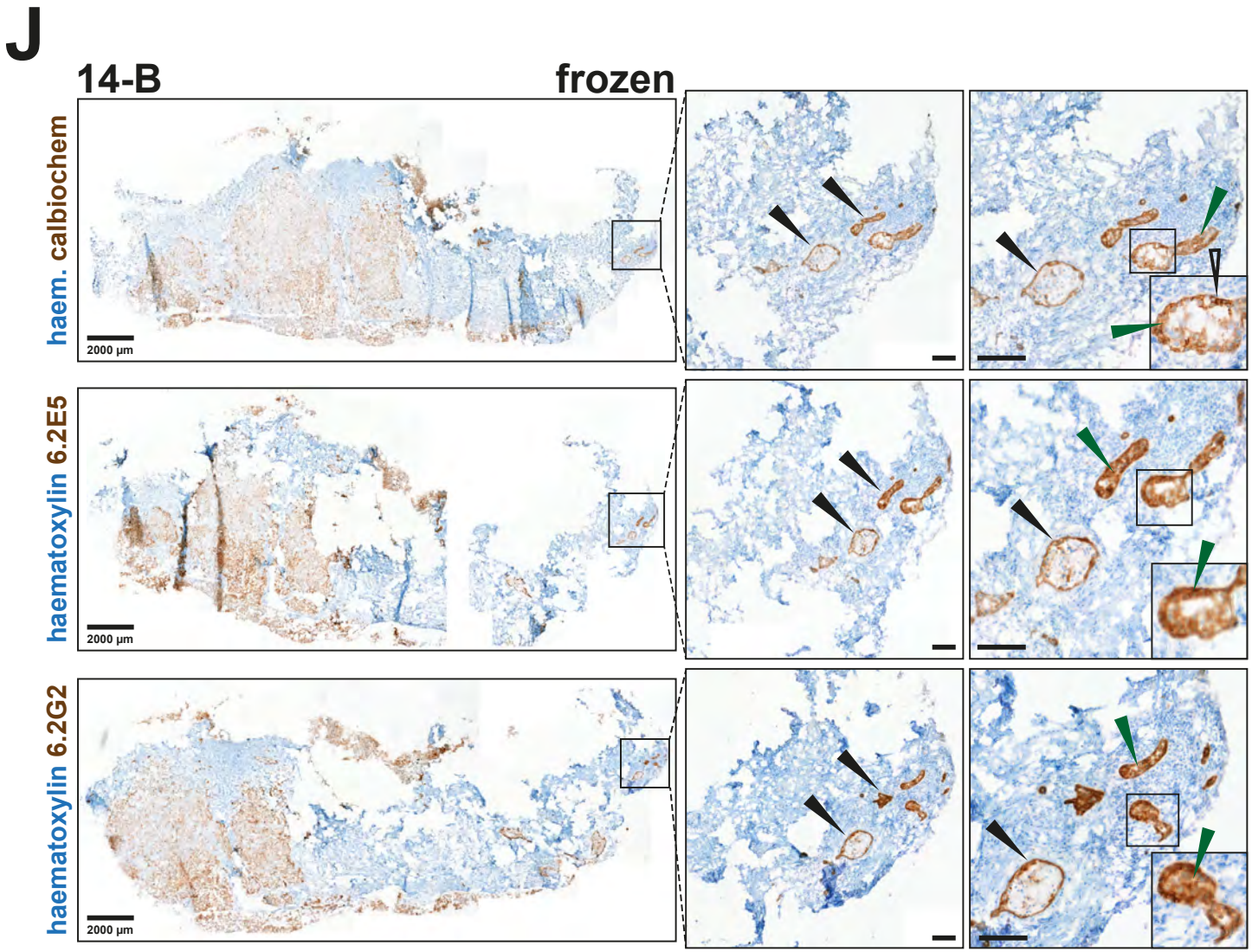

Figure 3.4.2 (J)
Evaluating the utility of antibodies 6.2E5 and 6.2G2 to histologically study the active population of integrin $\alpha_v\beta_6$ in FFPE and matched frozen clinical samples of human breast cancer specimens

Figure 3.4.2

Evaluating the utility of antibodies 6.2E5 and 6.2G2 to histologically study the active population of integrin $\alpha_v\beta_6$ in FFPE and matched frozen clinical samples of human breast cancer specimens

The ability of antibodies 6.2E5 and 6.2G2 to histologically distinguish the integrin $\alpha_v\beta_6$ active subpopulation in human clinical breast cancer samples was evaluated by immunohistochemistry in matched FFPE and frozen tissue sections from 5 anonymised cases kindly obtained from the Barts Cancer Institute Breast Tissue Bank (Research Ethics Code: 15/EE/0192). Following formalin fixation and VIP-processing (**FFPE**) or snap freezing (**frozen**), samples were sectioned at 4 μm. FFPE samples **(3.4.2 A, C, E, G & I)** only were subject to on-board endopeptidase protease antigen retrieval using VENTANA™ Protease 1 solution (#760-2018). Fresh frozen samples **(3.4.2 B, D, F, H & J)** were not subject to antigen retrieval protocols. Sections were stained with the following anti-integrin $\alpha_v\beta_6$ antibodies: Calbiochem-CSβ6 (MAB2076Z, Merck Millipore, 1:150), 6.2E5 and 6.2G2 (both Biogen Idec, 1:200) using the VENTANA™ BenchMark GX automated IHC stainer (Ventana Medical Systems Inc, Roche Holdings AG) and detected using the biotin-free polymer system Novolink™ DAB (polymer) chromogen (RE7230-K, Novocastra, Leica Microsystems UK Ltd). Integrin $\alpha_v\beta_6$ delineation of mammary ducts was demonstrated immunohistochemically (block black arrows) by all antibodies across both the FFPE and frozen tissue panels. Diffuse, intracellular cytoplasmic immunopositivity for integrin $\alpha_v\beta_6$ (green arrows) was observed in parenchymal cells, again across all tissue samples and with all antibody moieties. Distinct localisation of integrin $\alpha_v\beta_6$ immunopositivity at parenchymal cell surface membranes and at cell-cell junctions (black outline arrows) was observed most frequently in fresh frozen tissue samples and occasionally in FFPE sections. Slides were scanned and images acquired using the Pannoramic™ 250 Flash II digital scanner and reviewed using Panoramic Viewer Software (both 3DHISTECH Ltd, Hungary). Scale bars represent 100 μM unless otherwise stated in figures.

3.5 discussion

The use of monoclonal antibodies to discriminate specific integrin conformers and their associated activation status is now a well-established method in the field of integrin research (Mould *et al* 1995a, Humphries 1996, Mould *et al* 1996, Humphries 2004, Byron *et al* 2009, Campbell and Humphries 2011). The application of such monoclonal antibody-based approaches has proven the critical link between receptor activation and integrin-mediated functional biology driving phenotypic cellular responses to; cognate ligand engagement, crosstalk with GFR-mediated signalling and ECM remodelling as reviewed by Kim *et al* (2011a).

Validated, conformer specific anti-integrin antibodies have been successfully employed previously to delineate activation-specific integrin internalisation and trafficking kinetics (Arjonen et al 2012), ligand engagement, adhesion complex formation and associated signalling (Mould *et al* 1995b, Askari *et al* 2009, Askari *et al* 2010, Yu *et al* 2012). Furthermore, antibodies as functional probes to specifically and reversibly modulate integrin activation or inhibition have revealed novel insights into the significance of aberrant integrin activation and downstream signalling in the aetiopathology of various human diseases (Humphries 1996, Wehrle-Haller and Imhof 2003, Humphries 2004) including early characterisation of thrombasthaenic disorders (Ginsberg *et al* 1990), periodontal disease (Larjava *et al* 2014) and many cancer types (Thomas *et al* 2001a, Thomas *et al* 2006, White and Muller 2007, Virtakoivu *et al* 2012, Yang *et al* 2012), recently permitting refinement of subtypes and invasive-risk stratification (Allen *et al* 2014).

Excitingly, two monoclonal antibodies 6.2E5 and 6.2G2 (Biogen Idec) have demonstrated their novel utility to recognise the integrin $\alpha_v\beta_6$ in its active conformation *in vitro*. Based upon the results of canonical extracellular integrin activation experiments using divalent cations and cognate ligands they have each been found to recognise a conformationally-dependent activation-associated epitope and LIBS. Thus, they may be used to study the active subpopulation of integrin $\alpha_v\beta_6$ in future *in vitro* investigations. However, their ability to discriminate active from inactive populations of integrin $\alpha_v\beta_6$ could not be validated in a panel of FFPE and matched-pair fresh frozen primary human breast cancer tissue samples. This precludes their use to histopathologically study integrin $\alpha_v\beta_6$ activation status at present.

It is not claimed that these antibodies recognise exquisitely specific activation epitopes, rather that they recognise activation-associated epitopes based upon the fact that these antibodies still engage integrin $\alpha_v\beta_6$ in the absence of known activating moieties such as divalent cations (Figures 3.1.1 and 3.1.2) or cognate ligands (Figures 3.2.1 and 3.2.2). This may be attributable to the presence of a base-line pool of integrin $\alpha_v\beta_6$ adopting the active conformation to which these antibodies favourably bind. This would fit with the hypothesis that integrins exist in a continuum of activation states and may continually flux between inactive, primed and high-affinity conformations (Humphries 1996, Shimaoka *et al* 2002, Shimaoka and Springer 2003, Arnaout *et al* 2007, Campbell and Humphries 2011, Bouvard *et al* 2013).

Furthermore, based upon results from ligand-mediated integrin activation experiments, it was concluded that antibodies 6.2E5 (Figures 3.2.1) and 6.2G2 (Figure 3.2.2) each recognise a LIBS. As acknowledged by Humphries (2004), the term LIBS is not entirely accurate, given that the epitope comprising the LIBS is not in the strictest sense *"expressed"* upon ligand-engagement. Because the constituent amino acid sequence comprising the LIBS is already present within the integrin homodimers' amino acid sequences, it therefore may be bound by its cognate epitope even in the absence of ligand. This is concordant with the ability of antibodies 6.2E5 and 6.2G2 to engage the integrin $\alpha_v\beta_6$ even in the absence of ligand, lending further credence to the conclusion that these may be deemed anti-LIBS monoclonal antibodies.

Frelinger *et al* (1990) first described the concept of LIBS and outlined the generation of a panel of specific anti-LIBS monoclonal antibodies that could be used to dissect the complexities of integrin-mediated functional biology post ligand occupancy. Using these monoclonal anti-LIBS antibodies they identified two distinct LIBS on GPIIb (α_{IIb}) and one on GPIIIa (β_3). In combination with function-blocking antibodies, Frelinger *et al* (1990) further deduced that certain LIBS they identified modulate integrin $\alpha_{IIb}\beta_3$ function. Abrogation of a LIBS was found to ablate fibrin clot contraction even when ligand-occupied $\alpha_{IIb}\beta_3$ engaged fibrin.

Later, Ginsberg et al (1990) used this panel of anti-LIBS antibodies recognising resting, primed or ligand occupied integrin $\alpha_{IIb}\beta_3$ receptor forms to refine the

hierarchical ontogeny of defects in thrombocytic pathways resulting in haemostatic disorders. They successfully characterised the key $\alpha_{IIb}\beta_3$–mediated events determining thrombocyte aggregation as being; i) $\alpha_{IIb}\beta_3$ receptor priming by an agonist to reveal the fibrinogen binding site, ii) ligand (fibrin)-engagement itself and iii) effects inducted post-occupancy (downstream signalling). Using these antibodies in a flow cytometry screen of patient platelet-rich plasma or peripheral whole blood samples, Ginsberg *et al* (1990) first identified a defect in $\alpha_{IIb}\beta_3$ ligand-engagement in a variant of Glanzmann's thrombasthaenia and deficient agonist-induced $\alpha_{IIb}\beta_3$ activation in myelofibrosis as the causative deficiencies resulting in pathologically diminished platelet aggregation.

This early example of the clinical utility and application of anti-LIBS antibodies to refine classifications of human disease and identify specific pathway defects that may be exploited for targeted therapeutic intervention is demonstrative of the significance of identifying novel anti-LIBS antibodies. Their ongoing contribution to our understanding of integrin activation and signalling will only expedite the possibility to explore the translatability of integrin functional biology research into new screening, stratification, imaging and therapeutic strategies to improve clinical intervention and patient management strategies. Thus, the potential significance of the antibodies 6.2E5 and 6.2G2 to dissect the role of integrin $\alpha_v\beta_6$ activation status and downstream signalling during breast tumourigenesis and disease progression, amongst other integrin $\alpha_v\beta_6$–associated pathologies, should not be underestimated.

Several fundamental limitations are acknowledged with the antibody characterisation data presented here. Firstly, the activation methods employed only relate to extracellular modes of integrin activation and do not truly reflect the bidirectional nature of integrin activation. For completeness, a more robust validation of the specificity of these antibodies to discriminate active conformers of the integrin $\alpha_v\beta_6$ could encompass characterisation of the binding kinetics and spatiotemporal distribution of the antibodies 6.2E5 and 6.2G2 following intracellular modes of integrin activation and inhibition targeting the array of emergent molecular regulators modulating integrin function.

For example, genetic silencing or overexpression of molecular regulators reported in literature to activate or inhibit integrin function (see Table 3.1) and/or downstream signalling would provide additional data with which the utility of

antibodies 6.2E5 and 6.2G2 to recognise activated or primed integrin $\alpha_v\beta_6$ conformers could be evaluated with greater physiological relevance.

Admittedly, molecular regulators of integrin activation have been demonstrated for specific integrin species, not yet including the integrin $\alpha_v\beta_6$, which may add complexity to antibody validation data as these molecular regulators themselves would require validation as intracellular modulators of integrin $\alpha_v\beta_6$ function. However, a review of integrin literature highlights several strong candidates, outlined in Table 3.1, that warrant additional investigation.

molecular regulator	action	reported regulatory mechanism
PIPKIγ	INHIBITOR	overexpression suppresses integrin activation bind talin F3 PTB domain (competitive inhibition)
FILAMIN	"	filamin binds β-tail at site overlapping talin binding site also thought to compete with kindlin for β-tail binding
SHARPIN	"	inhibits talin & kindlin binding to β-tail – mechanism unknown
ICAP-1	"	binds distal kindlin NpxY motif & inhibits talin binding in β1 integrin. Inhibitory effect not via direct competition
TALIN	ACTIVATOR	talin F3 domain complexes with membrane-proximal NpxY motif β-tail requisite for talin-mediated integrin activation FAK mediates recruitment of talin
KINDLIN	"	degree of homology with talin head but bears inserted PH domain and preferentially bind membrane-distal NpxY motif
MIGFILIN	"	filamin-binding protein – expression enhances integrin activation
α-actinin	PLEIOTROPIC	binding site overlaps talin binding site. Competitive inhibition reported in β3; enhances talin binding to β1

Table 3.1: Published intracellular molecular regulators of integrin activation exhibiting inhibitory, activating or pleiotropic effects. Abbreviations: FAK – focal adhesion kinase; ICAP-1 – integrin cytoplasmic domain associated protein-1; Sharpin – SHANK-associated RH-domain interacting protein; PIPKIγ – phosphatidylinositol 4-phosphate 5-kinase type Iγ; PTB - phosphotyrosine binding domain. Information compiled from: (Humphries 1996, Hynes 2002, Shimaoka *et al* 2002, Luo *et al* 2007, Campbell and Humphries 2011, Pouwels *et al* 2012, Bouvard *et al* 2013, Calderwood *et al* 2013)

The antibody validation dataset presented here focuses on extracellular integrin activation modalities using cognate ligands and divalent cations that come with their own inherent limitations. In their review of experimental strategies to reconstruct integrin activation *in vitro*, Ye *et al* (2012) highlight the ongoing debate concerning the physiological relevance of data acquired from Mn^{2+}-induced integrin activation studies. Admittedly, this strategy alone may prove of limited physiological significance to dissect the complexities of integrin receptor activation, induction of downstream functional sequelae including signal activation and integration into other signalling networks *in vivo*.

Therefore, it is acknowledged that using divalent cations alone as an activation-agonist, in the absence of a truly physiomimetic integrin-ECM ligand interaction reflective of the *in vivo* context of integrin behaviour and function, is undoubtedly of limited relevance to characterise integrin-ECM or integrin-GFR mediated signalling. However, for the purposes of antibody validation to evaluate whether an antibody specifically or preferentially recognises an active integrin conformer, use of divalent Mn^{2+}-cations as a proven and expedient method of exogenous integrin activation was deemed appropriate given its successful application for this purpose in previous studies generating and characterising conformer-specific anti-integrin antibodies (Frelinger *et al* 1990, Weinreb *et al* 2004).

In their structural biochemistry modelling and analyses of the Lymphocyte Function-Associated Antigen-1 (LFA-1) (integrin $\alpha_L\beta_2$) MIDAS and its interactions with a ligand-mimetic acetate molecule, San Sebastian *et al* (2006) acknowledged that although Mg^{2+}-ions may be the most physiologically abundant divalent cation species, they are not necessarily the biochemically optimal species for favourable MIDAS occupation to potentiate ligand-integrin interactions. Indeed, the authors acknowledged that Zn^{2+} or Mn^{2+} ions exhibited the most favourable coordination to MIDAS facilitating ligand engagement, further demonstrative of the utility of Mn^{2+}-activation studies for the defined purposes of conformer-specific antibody validation as used here.

Furthermore, since the allosteric regulation of integrin conformation and ligand affinity by Ca^{2+}-ion species is known to be biphasic with elicited effects varying as a function of Ca^{2+} concentration (San Sebastian *et al* 2006), the evaluation of 6.2E5 and 6.2G2 binding kinetics in the presence of a single (1 mM) concentration of Ca^{2+}-ions hinders additional interpretations regarding the location and nature of the epitopes recognised by these antibodies.

In their review, Leitinger *et al* (2000) summarise the existence of 1 high affinity and 3 – 4 low affinity Ca^{2+}-ion binding sites as characterised using equilibrium dialysis studies on purified platelet integrin $\alpha_{IIb}\beta_3$ first published by Rivas and Gonzalez-Rodriguez (1991). The authors outline how the high affinity Ca^{2+}-binding site is sensitive to μM Ca^{2+} concentrations and promotes ligand binding in $\alpha_5\beta_1$ and β_3 integrins. Conversely, the low affinity binding sites responsive to mM Ca^{2+}

concentrations allosterically compete for Mg^{2+} occupation eliciting an inhibitory effect on ligand engagement.

Additional evaluation of antibody binding kinetics in the presence of Ca^{2+}-ion concentrations ranging from the μM to mM for clones 6.2E5, but more presciently 6.2G2, which already appears Ca^{2+} sensitive (Figure 3.1.2C), would determine with greater acuity whether these epitopes are truly Ca^{2+}-dependent or independent. If either antibody 6.2E5 or 6.2G2 were found to recognise Ca^{2+}-dependent epitopes, they would prove useful tools to further probe modulation of integrin $\alpha_v\beta_6$ conformational arrangement.

Xie *et al* (2004) successfully employed two murine monoclonal anti-human α_L antibodies (clones NKI-L16 and AO3) that each recognise a Ca^{2+}-ion and activation-dependent epitope to study the cell-surface conformational arrangement of integrin $\alpha_L\beta_2$. The authors mapped the cognate epitopes of these antibodies to the α_L-thigh domain and hypothesised that conformational rearrangements during priming, activation and α_L–leg extension occur between the *genu* and thigh domains, not the *genu* and calf-1 domain. Thus if similar epitope mapping studies and evaluation of Ca^{2+}-ion dependency could be completed for 6.2E5 and 6.2G2 cognate epitopes, these antibodies may be used to characterise the conformational arrangement and cation regulation of activation of cell-surface integrin $\alpha_v\beta_6$, about which is little currently known.

The use of synthetic peptide A20FMDV2 to evaluate ligand-induced binding kinetics of antibodies 6.2E5 and 6.2G2 was deemed suitable for the defined purpose of antibody validation, given its established high affinity and specificity for integrin $\alpha_v\beta_6$ and previous application in integrin $\alpha_v\beta_6$–specific investigations, including *in vivo* tumour imaging (Saha *et al* 2010). It is acknowledged that this is not a natural ECM ligand and so may prove to be of limited physiological relevance if seeking to define the complexities of integrin $\alpha_v\beta_6$–ECM interactions *in vivo*.

However, to establish whether antibodies 6.2E5 and 6.2G2 recognise a LIBS, the use of a high affinity, specific ligand, although synthetic, is deemed justifiable. Ligand-induced activation studies were also performed using human recombinant LAP of TGF-β1 in order to provide antibody characterisation data within the

context of a physiologically relevant integrin $\alpha_v\beta_6$ ligand known to be present within the ECM.

Furthermore, it is noted that epitope-mapping for the residues recognised by these antibodies has not yet been performed, but some inferences as to their location have been deduced based on observations to date. Flow cytometric evaluation of 6.2E5 and 6.2G2 binding kinetics on live, non-permeabilised cells suggests logically that they bind the extracellular integrin $\alpha_v\beta_6$ domain. Since they are non-ligand mimetic and are capable of binding integrin $\alpha_v\beta_6$ in its ligand-engaged state (Figures 3.2.1 and 3.2.2), it is inferred that these epitopes do not lie within, or proximal to the RGD ligand binding cleft. If either were the case, these antibodies would not bind ligand-engaged integrin $\alpha_v\beta_6$ either due to direct competitive inhibition with ligand or due to steric hindrance about the binding site once ligand is bound.

It is possible that the LIBS recognised by antibodies 6.2E5 and 6.2G2 may reside on the β_6 subunit. Indeed, previous publications have used antibody 6.2E5 to detect the integrin $\alpha_v\beta_6$ by Western blot, indicating its cognate epitope must reside within the β_6 subunit sequence (Azare *et al* 2007). The marked similarity in immunopositive distribution of the epitope recognised by the β_6-subunit specific antibody CSβ6 with the immunohistochemical localisation of epitopes recognised by antibodies 6.2E5 and 6.2G2 in fresh frozen primary breast tissue (Figure 3.4.2D) would infer this. Other LIBS monoclonal antibodies have been mapped to integrin β-subunits. Mould *et al* (1995a) first identified that the antibody clone 12G10 recognised a LIBS on the β_1 subunit. They conducted epitope mapping by competitive inhibition studies using a panel of antibodies directed against β_1-bearing integrin species previously characterised by Takada and Puzon (1993).

A similar competitive inhibition strategy using the known RGD-ligand mimetic and $\alpha_v\beta_6$ heterodimer-specific antibody clone 10D5 would permit confirmation that the antibodies 6.2E5 and 6.2G2 do not bind via, or proximal to, the heterodimeric RGD cleft. It would be useful to identify the specific extracellular portion of integrin $\alpha_v\beta_6$ to which these antibodies bind to further understand the nature of conformational regulation of integrin $\alpha_v\beta_6$ activation status.

This could be achieved by combining mutational analysis of the β_6 subunit with evaluation of antibody binding kinetics, in a strategy recapitulating that successfully employed by Takada and Puzon (1993) and later by Bazzoni *et al* (1995) to characterise antibody clone 9EG7 and Faull *et al* (1996) to define antibody clone QE.2E5. Using CHO cells as a host, Takada and Puzon (1993) generated chimaeras transfected with human β_1 cDNA to express either WT human β_1 or variants bearing known mutations in the β_1 subunit amino sequence. Flow cytometric analysis of antibody binding characteristics in the presence of these known β_1-subunit mutations was then performed.

This permitted successful epitope mapping for a panel of anti β_1-antibodies studied to specific regions of the β_1 subunit, including mapping the cognate epitope recognised by antibody A1A5 to a region mapping to residues 207 – 218 of the human β_1 subunit domain. Such an approach using WT β_6 cDNA and β_6 cDNA variants bearing known mutations generated by site directed mutagenesis, prior to flow cytometric evaluation of antibody binding capacity, the location of epitopes recognised by antibodies 6.2E5 and 6.2G2 could be mapped. Knowledge of the precise regions where these epitopes reside would provide further insight into mechanisms governing integrin $\alpha_v\beta_6$ conformation and the elicitation of downstream phenotypic and functional responses inducted upon integrin $\alpha_v\beta_6$ activation.

Immunofluorescence studies provided useful preliminary insights into the utility of antibodies 6.2E5 and 6.2G2 to track spatiotemporal distributions of active integrin $\alpha_v\beta_6$ conformers. However, the inferences from this observational dataset are limited, requiring additional follow up in order to deduce more robust conclusions regarding the application of antibodies 6.2E5 and 6.2G2 to dissect mechanisms and sequelae of integrin $\alpha_v\beta_6$ activation.

For example, integrin clustering associated with activated, high-affinity integrin conformers was observed when live cells were surface labelled with 6.2E5 (Figure 3.3.2C). Confirmation that 6.2E5 is detecting integrin in high-affinity clusters could be obtained by co-labelling for markers associated with integrin activation, high-affinity state clustering and signalling such as pFAK, talin, vinculin and α-actinin (Cluzel *et al* 2005, Welf *et al* 2012, Roca-Cusachs *et al* 2013, Hirata *et al* 2014).

It is also regrettable that the immunofluorescence dataset for antibodies 6.2E5 and 6.2G2 is incomplete owing to technical errors and prohibitively limited availability of these antibodies. Thus, completion of each dataset to ensure both antibodies are fully evaluated is necessary for fair comparisons.

Immunohistochemical assessment of antibodies 6.2E5 and 6.2G2 in human primary breast tumour histopathology samples was limited to only 5 cases due to restricted availability of these antibodies and access to human primary tissues. Undoubtedly this small sample size would prohibit broader interpretation of the utility of antibodies 6.2E5 and 6.2G2 to stratify or refine breast cancer subtypes in terms of their integrin $\alpha_v\beta_6$ activation status, or abundance of 6.2E5 or 6.2G2 cognate epitopes, within the context of histopathological diagnosis and patient outcome. However, for the defined purpose of preliminary evaluation of the ability of antibodies 6.2E5 and 6.2G2 may be used to discriminate the integrin $\alpha_v\beta_6$ active subpopulation in clinically derived tissues, this sample size was deemed sufficient, if limited.

Disappointingly it has not been possible to validate the use of antibodies 6.2E5 and 6.2G2 to distinguish a conformationally distinct integrin $\alpha_v\beta_6$ receptor subpopulation in either FFPE or fresh frozen histological samples. It is likely that the protein-modifying biochemical processes involved in FFPE-processing and protease-mediated EIER protocols employed in this investigation partially ablate the finer detail of epitope distribution as would be found *in vivo*.

This is best exemplified by the predominantly cytoplasmic immunopositivity for antibody CSβ6 observed in FFPE samples, compared to the abundance of a membranous distribution of CSβ6 in fresh frozen tissues. The phenomenon of epitope instability has been widely reported (Dabbs 2008, Shi *et al* 2008, Shi *et al* 2011) and informed the inclusion of fresh frozen tissues as it was anticipated that FFPE and EIER protocols may either destroy or unmask the putative conformation-dependent 6.2E5 and 6.2G2 epitopes in artefact.

If it were possible to identify an antibody capable of reliably detecting active integrin $\alpha_v\beta_6$ conformers within clinical histopathological samples, large-scale screening of human primary breast tumour cases may be undertaken to

investigate any correlation between expression of the active integrin $\alpha_v\beta_6$, histopathological classification, tumour staging and patient outcome, as successfully undertaken for total integrin $\alpha_v\beta_6$ (Moore *et al* 2014). If a positive correlation were to be established between integrin $\alpha_v\beta_6$ activation status, metastatic potential and patient outcomes, this would refine current understanding of the epidemiological role of aberrant integrin $\alpha_v\beta_6$ activation in breast tumourigenesis and disease progression.

Indeed, Felding-Habermann *et al* (2001) successfully demonstrated *in vitro* and *in vivo* the functional significance of integrin $\alpha_v\beta_3$ activation status in human breast cancer. The authors demonstrated that integrin $\alpha_v\beta_3$ in its active state was requisite for tumour cell-thrombocyte attachments to circumvent anoikis in the MDA-MB-435 human breast cancer cell line and also in freshly isolated primary human metatstatic breast cancer cells (PE02JA cells).

In addition, using MDA-MB-435 mutant variants transfected to stably overexpress constitutively active integrin $\alpha_v\beta_{3\mathbf{D723R}}$, the authors showed that activated integrin $\alpha_v\beta_3$ strongly promoted metastasis when injected into SCID mice, compared to their $\alpha_v\beta_{3\mathbf{WT}}$ counterpart MDA-MB-435 cells. A similar strategy could be employed to determine the biological role of active integrin $\alpha_v\beta_6$ in human breast cancer, utilising the antibodies 6.2E5 and 6.2G2 to distinguish the active forms of integrin $\alpha_v\beta_6$. If such studies could be augmented with demonstration of functionally distinct activation integrin $\alpha_v\beta_6$ states within clinically-derived human tissue samples of known histopathological grade and status, a robust case for integrin $\alpha_v\beta_6$ activation status in breast tumourigenesis and disease progression could be made.

It is acknowledged that variegation in digital scan quality and inter-batch variance in IHC staining intensity compounded any attempts at direct quantification of signal strength as a read out for integrin $\alpha_v\beta_6$ expression levels in the FFPE and fresh frozen histopathological sample set evaluated. Furthermore, direct comparisons between histological distributions of epitopes recognised by antibodies 6.2E5 and 6.2G2 in comparison with antibody CSβ6 could not be accurately made. In order to characterise the specific immunohistochemical subcellular localisation or abundance of epitopes recognised by these antibodies with greater confidence, serial sections would need to be prepared. This would

enable review of the localisation of these epitopes within a defined region of tissue and within a 4 μm to 8 μm spatial range to facilitate direct comparison.

At present, studies have only characterised integrin $\alpha_v\beta_6$ gross expression without demonstrating receptor activation status. This is largely due to a hitherto lack of available biological means to distinguish integrin $\alpha_v\beta_6$ conformers. Now, the antibodies 6.2E5 and 6.2G2 may be used to address this gap in our current understanding of the significance of integrin $\alpha_v\beta_6$ activation status in the natural history of human breast cancer.

The critical caveat to their use is acknowledgement that recognition of a conformation-dependent epitope is sensitive to certain experimental procedures that may reveal the epitope in a manner that does not truly recapitulate the *in vivo* morphological status of integrin $\alpha_v\beta_6$. But with this in mind to guide selection of suitable experimental techniques and to temper data interpretation, these antibodies will undoubtedly prove prized assets in the armoury of integrin $\alpha_v\beta_6$ research tools.

To conclude, it has been demonstrated for the first time that the antibodies 6.2E5 and 6.2G2 each recognise a primed or active integrin $\alpha_v\beta_6$ conformer. Furthermore, they may be classified as anti-LIBS antibodies and excitingly shall facilitate future investigations seeking to dissect the complexities of integrin $\alpha_v\beta_6$ activation, downstream signalling and functional sequelae *in vitro*.

chapter IV

results part II

evaluating the role of integrin $\alpha_v\beta_6$ activation status during breast cancer progression using the isogenic MCF-10A in vitro model of breast tumourigenesis

IV

evaluating integrin $\alpha_v\beta_6$ activation state-specific subpopulations in the MCF-10 isogenic model of breast tumourigenesis and disease progression

derailed internalisation and trafficking of the integrin $\alpha_v\beta_6$ in its active state is implicated in breast cancer progression

4. introduction

Activation of invasion and metastasis is a seminal cancer hallmark (Hanahan and Weinberg 2000, Hanahan and Weinberg 2011). Dysregulation of cellular adhesive repertoires facilitating acquisition of an invasive phenotype as a critical event promoting progression from localised *in situ* disease to disseminated, metastatic malignancy is now well established and widely reviewed (Behrens 1993, Van't Veer and Weigelt 2003, Duffy *et al* 2008, Aoudjit and Vuori 2012, Bendas and Borsig 2012, Hale *et al* 2012, Zhong and Rescorla 2012, Quail and Joyce 2013).

Cellular adhesion profiles determining cell-cell interactions and cell-ECM (including cell-basal lamina) anchorage are established by a variety of adhesion receptor family classes including: cadherins, selectins, immunoglobulins, proteoglycans (syndecans) and integrins (Gumbiner 1996, Maller *et al* 2010, Kim *et al* 2011a, Lu *et al* 2012, Oskarsson 2013, Pickup *et al* 2014).

As the predominant cell-ECM receptor superfamily, the integrins are known to regulate a wide array of phenotypic traits in both health and disease (Felding-Habermann 2003). These include: cellular proliferation (Moreno-Layseca and Streuli 2014), senescence (Rapisarda *et al* 2017), cell fate via anchorage-dependent survival signalling or induction of anoikis (Guadamillas *et al* 2011); growth factor receptor (GFR) signalling integration (Ivaska and Heino 2010, Hamidi *et al* 2016); modulation of cell-ECM interactions and coordination of ECM remodelling (Bonnans *et al* 2014, Oudin *et al* 2016).

Given the diversity of cellular functions subject to integrin-mediated regulation, it is logical that different integrin heterodimer species may mediate distinct tumour suppressive or oncogenic functions, driving tumourigenesis and facilitate disease dissemination. Indeed, literature reviewed by Hurst and Welch (2011) highlighted the importance of integrin repertoire modulation during tumour progression. Broadly, previous studies have shown tumour suppressive integrin moieties ($\alpha_2\beta_1$, $\alpha_3\beta_1$) promoting stable adhesions and a differentiated, quiescent phenotype are down regulated (Zutter *et al* 1995, Varzavand *et al* 2016), whilst oncogenic moieties driving proliferation and migration ($\alpha_v\beta_3$, $\alpha_v\beta_6$, $\alpha_6\beta_4$) are up-regulated, by incipient tumour cells (Petitclerc *et al* 1999, Diaz *et al* 2005, Sloan *et al* 2006). However, the cell-type specific nature and pleiotropy of integrin function is also acknowledged (Desgrosellier and Cheresh 2010, Shattil *et al* 2010, Hurst and Welch 2011).

Taherian *et al* (2011) investigated the phenotypic effects of differential integrin expression and resultant alterations in integrin-mediated signalling in BrCa cells that determined their tumourigenic and metastatic potential. Their study revealed that BrCa cells vary in their integrin expression profiles, ability to form focal adhesions and capacity for integrin-mediated signalling. This was concordant with findings previously published by Havaki *et al* (2007) who also investigated the phenotypic role of distinct integrin $\alpha_v\beta_3$ expression using human primary cancer cells derived from clinical breast tumour biopsies.

In addition to overexpression of gross (total) integrin $\alpha_v\beta_3$, high expression of integrin $\alpha_v\beta_3$ specifically in its active conformation has been linked to breast tumourigenesis. The functional significance of activated integrin $\alpha_v\beta_3$ driving a pro-metastatic phenotype in human BrCa both *in vitro* and *in vivo,* was first reported by Felding-Habermann *et al* (2001) using the MDA-MB-435 cell line

model. The authors demonstrated that active integrin $\alpha_v\beta_3$ enabled tumour cell-thrombocyte interactions that circumvented anoikis, establishing a favourable metastatic niche.

Later, Verbisck *et al* (2009) identified the type I transmembrane glycoprotein disintegrin and metalloproteinase domain-containing protein 23 (ADAM23) as a negative regulator of integrin $\alpha_v\beta_3$ activation that was perturbed in BrCa. ADAM23 was previously shown to directly, physically interact with integrin $\alpha_v\beta_3$ in human astrocytoma and blastoma cell lines via its disintegrin domain (Cal *et al* 2000, White 2003). Verbisck *et al* (2009) confirmed the direct $\alpha_v\beta_3$/ADAM23 physical interaction in the MDA-MB-435 cell line using a glutathione S-transferase (GST)-pull down assay. Since $\alpha_v\beta_3$ is the only β_3 integrin expressed in this cell line, the authors concluded that ADAM23 directly binds integrin $\alpha_v\beta_3$ via its disintegrin domain in MDA-MB-435 cells.

Furthermore, molecular rescission of ADAM23 through shRNA silencing in MDA-MB-435 cells was found to promote integrin $\alpha_v\beta_3$ activation by up to 4-fold, enhancing adhesion to and migration on the canonical integrin $\alpha_v\beta_3$ ligands fibronectin and vitronectin. To evaluate the clinical relevance of ADAM23 during disease progression, Verbisck and colleagues evaluated a cohort of 94 primary human invasive ductal carcinomas (IDC) of the breast. They demonstrated that DNA promoter hypermethylation-induced silencing of ADAM23 significantly correlated with reduced distal metastases-free and disease-specific survival rates. In addition, loss of ADAM23 expression was found to be an independent prognostic factor for poor disease outcome within this IDC cohort.

The specific significance of active rather than inactive integrin species facilitating metastatic potential and disease progression has also been demonstrated in prostate cancer. Using the activation conformer-specific anti-integrin β_1 monoclonal antibody 9EG7, Lee *et al* (2013) showed that integrin β_1 was constitutively active in the PC3 and PC3-mm2 human prostate cancer cell lines of known high metastatic potential, in comparison with the LNCaP and C4-2B4 prostate cancer cell lines of low metastatic potential. Immunohistochemical assessment of total integrin β_1 and FAK phosphorylation at tyrosine 397 ($pFAK^{Y397}$) in 58 human primary prostate cancer tissues revealed that integrin β_1 and associated integrin-induced FAK autophosphorylation levels were elevated in samples of primary prostate cancer tissue (20 cases) and prostate cancer

secondary lymph node metastases (18 cases), in comparison with normal prostate tissue (20 cases). Thus, Lee *et al* (2013) deduced that integrin β_1 activation occurred during metastatic disease progression in prostate cancer.

The authors evaluated the effects of integrin β_1 activation on prostate cancer metastasis *in vivo* by orthotopic injection of SCID mice with PC3-mm2 cells. Mice were treated with control antibody IgG or the integrin β_1–specific neutralising monoclonal antibody 33B6 first described by Bednarczyk *et al* (1993). Two-week systemic therapy with antibody 33B6 significantly reduced lymph node metastasis in comparison with IgG treatment ($p<0.001$).

In a separate study cohort of SCID mice with metastatic tumours derived from disseminated PC3-mm2 cells already established in distal lymph nodes, 33B6 therapy was seen to significantly slow rate of tumour growth and reduce tumour volume in comparison with the IgG-treated control arm. The authors concluded that activation of β_1 integrin species promotes tumour cell survival and extravasation, enabling dissemination to distal sites establishing increased metastatic disease burden and poor survival (Bednarczyk et al, 1993).

Based on previous studies reporting the significance of integrin $\alpha_v\beta_3$ and integrin β_1 activation state during tumourigenesis, it is clear that both the nature of integrin species grossly expressed, along with their associated activation status, elicit significant effects determining tissue transformation, tumourigenesis and disease progression to disseminated, metastatic disease. Of growing clinical interest is the relevance of integrin species activation during tumour initiation and disease progression for therapeutic intervention (Jin and Varner 2004, Staunton 2006, Eberlein *et al* 2013, Lee *et al* 2013, Parvani *et al* 2013, Moore *et al* 2014, Truong *et al* 2014). Indeed, Felding-Habermann *et al* (2001) demonstrated the importance integrin activation during BrCa progression over a decade ago.

Unusually, expression of the epithelial-restricted integrin $\alpha_v\beta_6$ is not constitutive in healthy adult tissues. It is upregulated during tissue remodelling associated with wound-healing responses and carcinogenesis (Breuss *et al* 1995, Thomas *et al* 2006). In breast cancer, overexpression of the integrin $\alpha_v\beta_6$ (Allen *et al* 2014), together with its efficacy as a target in multi-agent combination therapy modalities (Moore *et al* 2014) is now well established.

Given the importance of integrin $\alpha_v\beta_6$ expression during breast tumourigenesis, it was deemed pertinent to investigate whether the integrin $\alpha_v\beta_6$ in its active, signalling-replete state is requisite for establishing a neoplastic phenotype and pro-metastatic niche during mammary cell transformation and disease progression in breast cancer.

overview of key findings

Integrin $\alpha_v\beta_6$ expression is associated with poor prognosis and risk of progression in BrCa (Allen *et al* 2014, Moore *et al* 2014). Therefore, gross (total) and active integrin $\alpha_v\beta_6$ conformations were screened in breast cancer cell lines comprising the MCF10 isogenic *in vitro* model of breast tumourigenesis to investigate the relevance of integrin $\alpha_v\beta_6$ activation status at each stage of breast carcinogenesis from neoplastic transformation through to malignant progression.

A series of monoclonal antibodies validated in house for the detection of distinct integrin $\alpha_v\beta_6$ subpopulations were used to define the population of total integrin $\alpha_v\beta_6$: clones 10D5, 53A2 and 620W7, (Desai 2011) in addition to antibody clones 6.2E5 and 6.2G2 now established to recognise the pool of active integrin $\alpha_v\beta_6$ (see Chapter 3: Results Part I). Using this monoclonal antibody-based approach, relative cell surface abundance of total and active integrin $\alpha_v\beta_6$ conformers was quantified by flow cytometry, with their respective subcellular distributions defined by confocal immunofluorescence microscopy.

Critically, it was found that in the presence of a relatively stable cell surface pool of active integrin $\alpha_v\beta_6$, the activation-associated epitopes recognised by antibodies 6.2E5 and 6.2G2 underwent notable subcellular redistribution upon neoplastic transformation and malignant progression in the MCF-10AT and MCF-10CA1h variants respectively, where large vesicular-like accumulations of active integrin $\alpha_v\beta_6$ were observed. This implicated derailed integrin $\alpha_v\beta_6$ receptor internalisation and intracellular trafficking kinetics as oncogenic drivers during breast tumourigenesis, as opposed to cell surface overexpression of the active integrin $\alpha_v\beta_6$ subpopulation alone.

4.1 cell surface and whole cell abundance of total integrin $\alpha_v\beta_6$ varies demonstrably across the MCF10 model, but the relative surface fraction of active integrin $\alpha_v\beta_6$ is not significantly altered

The MCF-10 isogenic cell line series has been used extensively in breast cancer research to provide a simple, *in vitro* 2D-model recapitulating breast tumourigenesis and disease progression (Soule *et al* 1990, Dawson *et al* 1996, Heppner *et al* 2000, Santner *et al* 2001).

The MCF-10 panel, derived from the non-neoplastic MCF-10A parent cell line, subsequent neoplastic variants (MCF-10AT, MCF-10Kcl.2), malignant variants (MCF-10CA1a, MCF-10CA1h) together with a variant recapitulating *in situ* ductal disease (MCF-10DCIS.com), was deemed appropriate for preliminary investigations into integrin $\alpha_v\beta_6$ expression and activation status. Exemplifying the utility of the MCF-10 cell line model, Tang *et al* (2003) successfully used this panel previously to highlight TGF-β1 pleiotropy during breast tumourigenesis, defining a novel switch from tumour suppressor in early stage disease, to a prometastatic factor in advanced disease.

Cell surface abundance of distinct integrin $\alpha_v\beta_6$ receptor populations (both total and activated) were quantified by flow cytometry using a panel of anti-integrin $\alpha_v\beta_6$ monoclonal antibodies (as outlined previously in *Chapter 3: Results Part I*). Geometric mean fluorescence intensity (geoMean MFI, AU) values were detected for each of the antibodies used and subsequently normalised against geoMean MFI values obtained for the relevant species-specific isotype-matched negative control antibodies evaluated in tandem.

These data served as a quantitative readout of cell surface total integrin $\alpha_v\beta_6$ expression (demonstrated by antibody clones 10D5, 53A2 and 620W7; Figure 4.1A) or the activated integrin $\alpha_v\beta_6$ receptor pool (labelled using antibody clones 6.2E5 and 6.2G2; Figure 4.1C and D respectively). Whole cell integrin subunit protein was determined by Western blotting (Figure 4.1B).

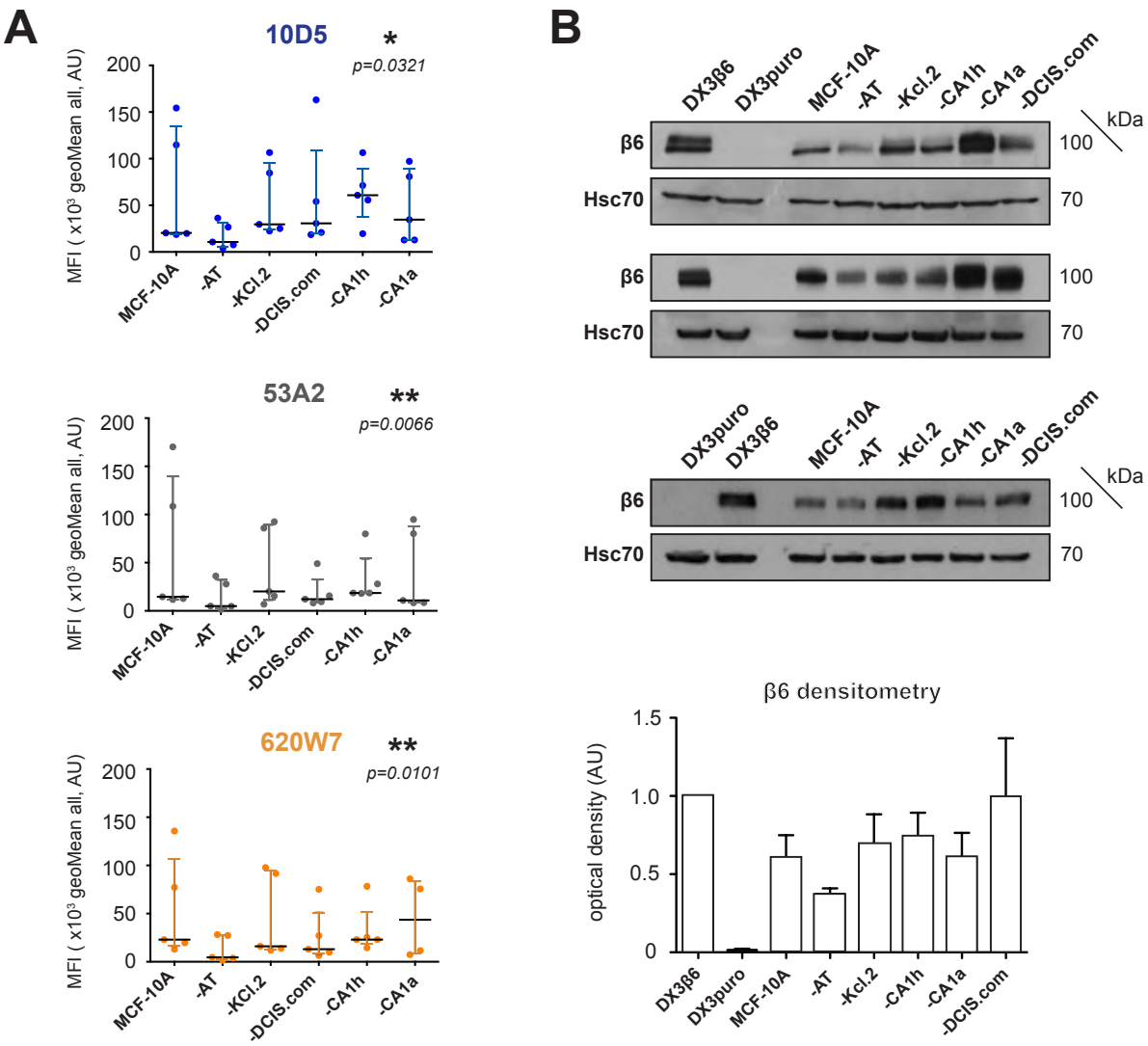

Figure 4.1 (A & B)
Total surface expression of the integrin $\alpha_v\beta_6$ is significantly altered across the MCF-10 isogenic model of breast tumourigenesis and disease progression, however, relative surface abundance of the active subpopulation of integrin $\alpha_v\beta_6$ recognised by antibodies 6.2E5 and 6.2G2 is not significantly altered

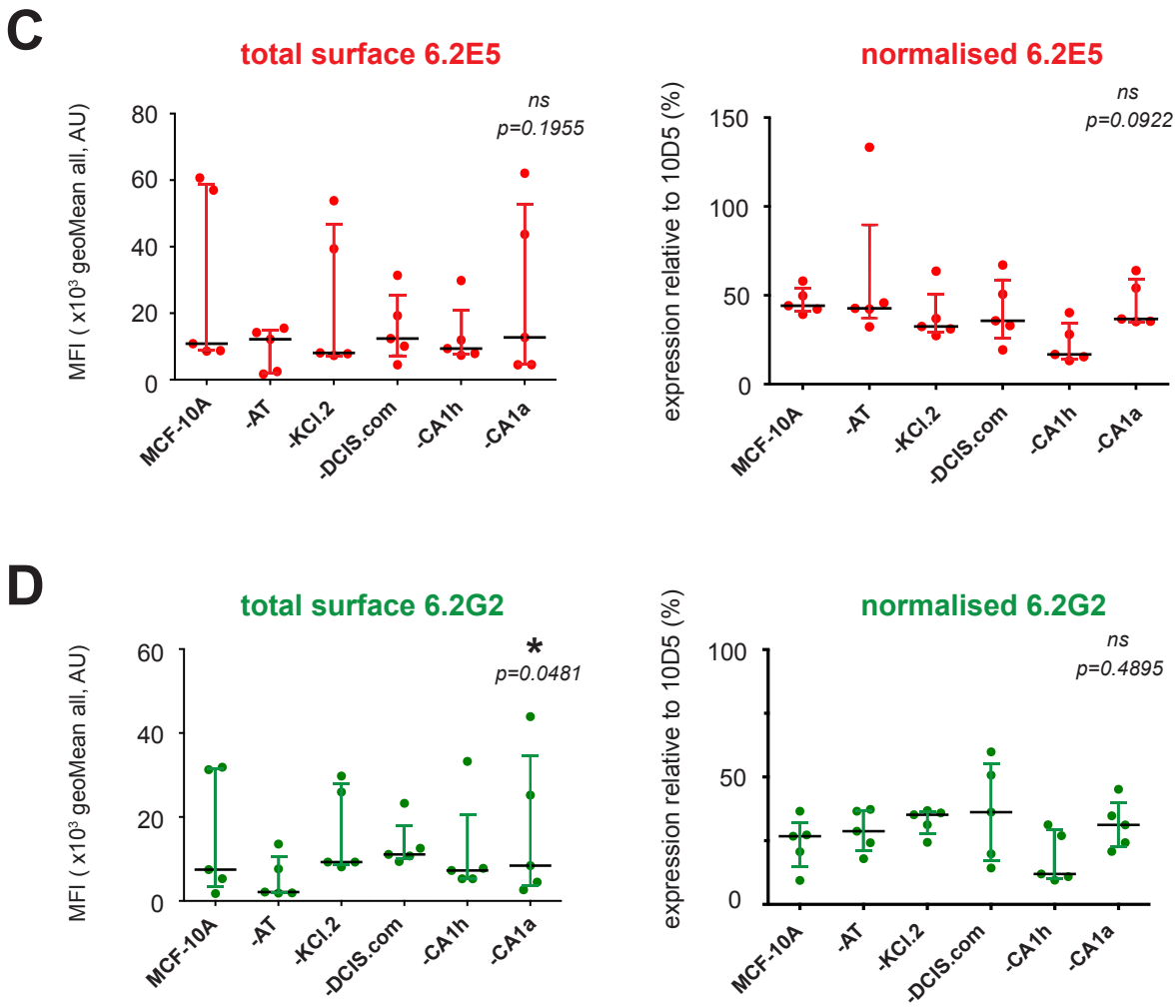

Figure 4.1 (C & D)
Total surface expression of the integrin $\alpha_v\beta_6$ is significantly altered across the MCF-10 isogenic model of breast tumourigenesis and disease progression, however, relative surface abundance of the active subpopulation of integrin $\alpha_v\beta_6$ recognised by antibodies 6.2E5 and 6.2G2 is not significantly altered

Figure 4.1

Total surface expression of the integrin $\alpha_v\beta_6$ measured by flow cytometry is significantly altered across the MCF-10 isogenic model of breast tumourigenesis and disease progression, however, relative surface abundance of the active subpopulation of integrin $\alpha_v\beta_6$ recognised by antibodies 6.2E5 and 6.2G2 is not significantly altered

The MCF-10A series of breast cancer cell lines (MCF10 isogenic model) generated to recapitulate neoplastic transformation and malignant progression were used to explore the putative role of active integrin $\alpha_v\beta_6$ during breast tumourigenesis. Cell surface abundance of total integrin $\alpha_v\beta_6$ recognised by antibodies 10D5, 53A2 and 620W7 was determined by flow cytometry **(4.1 A)** and total cellular integrin $\alpha_v\beta_6$ evaluated by Western blot **(4.1 B)**. The active subpopulation of integrin $\alpha_v\beta_6$ was assessed by flow cytometry in terms of total cell surface abundance using antibodies 6.2E5 **(4.1 C)** and 6.2G2 **(4.1 D)** and as a relative fraction of total integrin $\alpha_v\beta_6$ by normalising MFI values against values for 10D5. **(4.1 A)** The ligand mimetic antibody 10D5 (10 μg ml^{-1}, Merck Millipore) which was used to identify the total surface pool of integrin $\alpha_v\beta_6$ by flow cytometry was significantly altered across the MCF-10A series (n=5, Friedman Test with Dunn's multiple comparison test, $p<0.05$, $p=0.0321$). Surface binding of antibodies 53A2 and 620W7 (both 10 μg ml^{-1}, CR-UK) was also used to identify the total pool of integrin $\alpha_v\beta_6$ and was again significantly altered across the MCF-10A panel ($p=0.0066$ and $p=0.0101$ respectively, Friedman Test with Dunn's multiple comparison test). **(4.1 B)** Total cell expression of the integrin β6 subunit was determined across the MCF10 model by immunoblot (antibody C-19, 0.2 μg ml^{-1}, SCBT), technically validated against known integrin $\alpha_v\beta_6$ positive (DX3β6) and negative (DX3puro) control cell lines and quantified by densitometry (n=3). Protein was loaded at 25 μg per well. Blots were developed using ECL and exposed manually onto X-ray film (CARESTREAM, Carestream Health Ltd) before scanning blot hardcopies to digitise images (Epson PERFECTION V39 Scanner, Seiko Epson Corp.). **(4.1 C)** Neither total surface bound (MFI values) nor relative fraction (% of total $\alpha_v\beta_6$) of 6.2E5 (5 μg ml^{-1}, Biogen Idec) normalised against 10D5 MFI values were significantly altered across the MCF-10A series (n=5, Friedman Test with Dunn's multiple comparison test $p=0.1955$ and $p=0.0922$ respectively). **(4.1 D)** Total surface abundance of 6.2G2 measured by detected MFI was significantly altered across the MCF-10A panel (n=5, Friedman test with Dunn's multiple comparison $p=0.0481$). However, the relative fraction of 6.2G2 (5 μg ml^{-1}, Biogen Idec) normalised against 10D5 MFI values were not significantly altered across the panel (n=5, Friedman test with Dunn's multiple comparison, $p=0.4895$). Graphs represented in **(4.1 A**, **C** and **D)** show median with interquartile range, except for graphs representing relative expression of 6.2E5 & 6.2G2 normalised to 10D5, which show means and error bars for s.e.m. Densitometry graph in **(4.1B)** shows mean with error bars for s.d. All flow cytometry data was acquired on live cells in the presence of a cell viability indicator (5 μg ml^{-1} propidium iodide, P4170, Sigma Aldrich) using the BD FACSCalibur™ (BD Biosciences). Following normalisation against isotype matched negative control antibodies, geometric MFI values were determined by analysis in BD CellQuestPro™ software (BD Biosciences). Statistical analyses were performed using GraphPad Prism® 5.0b for MacOSX (Graphpad Software Inc, CA, USA).

It was consistently found that cell surface abundance of the total pool of integrin $\alpha_v\beta_6$ receptors recognised by antibodies 10D5, 53A2 and 620W7, was visibly altered across the MCF10 cell line series (Figure 4.1A). Statistical analyses revealed this variation in cell surface expression of total integrin $\alpha_v\beta_6$ amongst the MCF10 panel to be significant (n=5, Friedman test with Dunn's multiple comparison: 10D5 p=0.0321; 53A2 p=0.0066; 620W7 p=0.0101).

When compared to a variant representing neoplastic but non-invasive disease (MCF-10AT), total integrin $\alpha_v\beta_6$ expression was notably increased in MCF10A derived cell lines representing: a neoplastic variant with invasive potential (MCF10-Kcl.2), invasive variants representing either well differentiated (MCF10-CA1h) or poorly differentiated (MCF10-CA1a) disease and a variant recapitulating in situ ductal disease (MCF10-DCIS.com). This suggested an association between increased integrin $\alpha_v\beta_6$ surface expression during breast cancer cell transformation and acquisition of a more invasive phenotype.

Next, it was deemed pertinent to establish whether the observed variation in total integrin $\alpha_v\beta_6$ expression across the MCF10 panel (as defined by flow cytometric evaluation) was specifically a cell-surface receptor spatial restriction phenomenon, or attributable to altered whole cell (gross) expression. Therefore, whole cell abundance of integrin $\alpha_v\beta_6$ was determined in the MCF10 panel by Western blotting using a β_6–subunit specific antibody (Figure 4.1B).

Across three independent biological replicates, whole cell integrin β_6–subunit expression was seen to vary in a similar pattern to that observed for cell-surface abundance. Densitometric analysis of blots was reviewed to aid comparison of enhanced chemiluminescence signal strength as a read-out for whole cell β_6–subunit abundance. This revealed that again, in comparison with the neoplastic but non-invasive MCF-10AT variant, integrin β_6–subunit expression was markedly upregulated in both the neoplastic with invasive potential MCF-10Kcl.2 variant and the malignant variants MCF10-CA1h, MCF-10CA1a and MCF-10DCIS.com.

Concordant with flow cytometric data, the Western blotting results also suggested an association between total integrin β_6-subunit (and thus, integrin $\alpha_v\beta_6$) expression during breast cancer cell transformation and acquisition of a more

invasive phenotype. However, it was not confirmed from these data alone whether spatial restriction of the integrin $\alpha_v\beta_6$ receptor pool was implicated as a driving factor during breast tumourigenesis or progression to metastatic disease.

Interestingly, data obtained for the MCF10-DCIS.com cell line did point to the possible aetiopathological significance of integrin $\alpha_v\beta_6$ spatial distribution during breast tumour progression. Western blotting revealed that amongst the entire MCF10 panel, the MCF10-DCIS.com cells expressed the highest levels of whole cell integrin-β_6 subunit. Notably, this whole cell abundance was not translated to cell surface abundance of the total integrin $\alpha_v\beta_6$ receptor pool. Flow cytometry data had revealed that the MCF10-CA1h and MCF10-CA1a malignant, invasive variants expressed the highest levels of total integrin $\alpha_v\beta_6$ receptor at their cell surface. Therefore, it was postulated that upregulation of the integrin $\alpha_v\beta_6$ receptor at the cell surface, rather than whole cell overexpression, may drive acquisition of the invasive phenotype requisite for breast cancer disease progression.

Curiously, it was noted that the MCF-10A parent cell line (derived from benign, fibrocystic breast tissue) which is intended to represent benign, non-neoplastic, non-tumourigenic, non-invasive mammary epithelial cells, consistently expressed more integrin $\alpha_v\beta_6$ than the transformed, neoplastic but non-invasive MCF-10AT variant. This finding (for both cell surface and whole cell abundance) was unexpected. It had been anticipated that the MCF-10A cells would express little integrin $\alpha_v\beta_6$, since this integrin moiety is only expressed in healthy adult tissues during wound healing. Therefore it was hypothesised that total integrin $\alpha_v\beta_6$ expression (already associated with neoplastic transformation and invasive progression during breast carcinogenesis) would show a successive increase in expression across the MCF10 panel, from benign (MCF10A) through neoplastic (MCF-10AT, MCF10-Kcl.2) to malignant (MCF10-CA1h, MCF-10CA1a, MCF10-DCIS.com) variants, positively correlating with neoplastic transformation and malignant progression concordant with the established multi-step model of breast tumourigenesis (Crum *et al* 2003, Schedin and Elias 2004, Bateman and Shaw 2013, Lakhtakia and Chinoy 2014, WHO 2014).

It was postulated that integrin $\alpha_v\beta_6$ expression in the MCF-10A cell line could be an artefact from 2D-culture on rigid, uncoated plastic tissue culture vessels inducting a wound healing response. It is now established that ECM stiffness regulates many epithelial cell phenotypic traits including differentiation, survival, polarisation and

migration (Butcher *et al* 2009, Allen *et al* 2012, Du *et al* 2016). These physical ECM forces generate specific tensile biomechanical cues that are transduced into meaningful intracellular signals by mechanotransduction receptor classes, such as the integrin superfamily (Sun *et al* 2016). Therefore, it may be that the rigid tissue culture vessel surface recapitulated a stiffened ECM-environment known to occur during fibrosis (Saneyasu *et al* 2016), inducing a fibrotic or wound healing phenotypic response in MCF10A cells during culture. The integrin $\alpha_v\beta_6$ is known to regulate fibrosis via TGF-β1 signalling (Sheppard 2015) in: lung (Tatler and Jenkins 2012) and renal (Hahm *et al* 2007) tissues.

Indeed, the primacy of integrin $\alpha_v\beta_6$-mediated TGF-β1 activation and signalling in inflammatory diseases such as idiopathic pulmonary fibrosis (Porte and Jenkins 2014) is indicative of the importance of this integrin moiety within a fibrotic environment, and potentially in the pseudo-fibrotic environment of culture on stiff, uncoated plastic. In addition, it may be that the spontaneously immortalised MCF10A parent cell line natively expresses integrin $\alpha_v\beta_6$, given its isolation from resected fibrocystic mammary epithelium (Soule *et al* 1990), where pro-fibrotic integrin $\alpha_v\beta_6$/TGF-β1 signalling pathways would be anticipated and account for its expression in this cell line.

After evaluating cell surface expression of the total integrin $\alpha_v\beta_6$ receptor, the abundance of integrin $\alpha_v\beta_6$ in its activated conformation was quantitatively determined across the MCF10 panel by flow cytometry using antibody clones 6.2E5 (Figure 4.2C) and 6.2G2 (Figure 4.2D). Again, geoMean MFI values for antibodies 6.2E5 and 6.2G2 were normalised against geoMean MFI values obtained for a species-specific isotype-matched control antibody (mouse IgG_1).

Cell surface abundance of active integrin $\alpha_v\beta_6$ recognised by antibody 6.2E5 (Figure 4.1C) was not significantly altered across the MCF10 panel (n=5, Friedman test with Dunn's multiple comparison, p=0.1955). In contrast, the cell surface pool of active integrin $\alpha_v\beta_6$ detected by antibody 6.2G2 (Figure 4.1D) was significantly altered amongst the MCF10 isogenic breast cancer cell lines (n=5, Friedman test with Dunn's multiple comparison p=0.0481).

It was acknowledged that cell surface expression of active integrin $\alpha_v\beta_6$ would be affected by the total abundance of gross integrin $\alpha_v\beta_6$ present at the cell surface capable of activation. For a fairer comparison of the role of the active fraction of integrin $\alpha_v\beta_6$ (i.e what proportion of integrin $\alpha_v\beta_6$ being expressed is activated), geoMean MFI values for total surface 6.2E5 or 6.2G2 were then expressed as a relative percentage of gross surface integrin $\alpha_v\beta_6$ expression.

This was achieved by normalising expression of epitopes recognised by antibodies 6.2E5 and 6.2G2 (representing the active integrin $\alpha_v\beta_6$) against the epitope recognised by antibody 10D5 (representing total integrin $\alpha_v\beta_6$ surface expression). Given that the ligand-mimetic inhibitory antibody 10D5 is a commercial, well-characterised inhibitory antibody known to detect an intact heterodimeric-dependent epitope, it was deemed most suitable for labelling the total pool of integrin $\alpha_v\beta_6$ without inducting canonical downstream activation owing to the function blocking properties of this antibody.

The relative surface fraction of active integrin $\alpha_v\beta_6$ expression ("normalised 6.2E5" and "normalised 6.2G2"; Figures 4.2C & 4.2D respectively) proportional to total integrin $\alpha_v\beta_6$ expression (10D5) was not significantly altered across the MCF10A panel (n=5, Friedman test with Dunn's multiple comparison: 6.2E5 p=0.0922; 6.2G2 p=0.4895). However, it was observed that between the malignant, invasive variants (MCF-10CA1h and MCF10-CA1a), the poorly differentiated MCF-10CA1a cells expressed a greater proportion of active integrin $\alpha_v\beta_6$ recognised by antibodies 6.2E5 and 6.2G2, in comparison with the well-differentiated MCF10-CA1h variants. Therefore, it may be that integrin $\alpha_v\beta_6$ activation is a driving factor in advanced disease, determining differentiation status and tumour grade.

This suggested that in isolation, the abundance of activated integrin $\alpha_v\beta_6$ at the cell surface may not be a significant factor during breast tumourigenesis and disease progression. Therefore, the possibility of alternative integrin $\alpha_v\beta_6$–mediated mechanisms driving neoplastic transformation and malignant progression warranted investigation.

4.2 total integrin $\alpha_v\beta_6$ is stably expressed at cell-cell junctions and the cell periphery across the MCF10 in vitro model of breast tumourigenesis, but active integrin $\alpha_v\beta_6$ undergoes cytoplasmic subcellular redistribution upon neoplastic transformation and malignant progression

Given the emerging importance of derailed adhesion receptor internalisation kinetics and intracellular trafficking routes during carcinogenesis (Mosesson *et al* 2008), it was deemed pertinent to next characterise the subcellular localisation of integrin $\alpha_v\beta_6$ receptor populations (total and active) in the MCF10 cell line panel. Indeed, the work of Arjonen *et al* (2012) characterised distinct intracellular trafficking routes for active and inactive integrin β_1, highlighting the importance of not just integrin receptor activation status, but also subcellular localisation and internalisation kinetics.

Evaluating three independent lung, prostate and breast cancer cell lines (NCI-H460, PC-3 and MDA-MB-231 respectively), Arjonen *et al* (2012) found that integrin β_1 in its inactive form (recognised by antibodies mAB13 and 4B4) predominated at the cell surface, where only 20% of cell surface integrin β_1 were active conformers (recognised by antibodies 12G10 and 9EG7); which was concordant with the previous findings of Tiwari *et al* (2011). Furthermore, confocal microscopy revealed that active integrin β_1 was predominantly cytoplasmic in localisation, whilst inactive predominated at cell edges and was enriched at cell membrane protusions, suggesting differential trafficking routes for active versus inactive integrin β_1 (Arjonen et al, 2012).

Arjonen and colleagues (2012) also determined that active integrin β_1 is endocytosed more efficiently and co-traffics with cognate ligand. In addition, it was shown that both active and inactive β_1 integrins traffic to the same early endosomes (Rab5-, Rab4a and Rab21-GTPase positive compartments) within 30 minutes from initial endocytosis. Interestingly, only active β_1 integrin was present in Rab7-positive compartments 30 minutes post-internalisation. Inactive integrin β_1 recycling was found to be Rab-4 dependent mechanism requiring F-actin polymerisation.

Therefore, Arjonen et al (2012) concluded that active integrin β_1 exhibits higher net internalisation kinetics and recycles at a slower rate than inactive integrin β_1;

and although both inactive and active integrin β_1 conformers initially share the same early endosomal trafficking routes, active β_1 integrin is directed to a Rab7-GTPase endosomal compartment whilst inactive integrin internalisation is equilibrated with rapid Rab-4/F-actin-dependent recycling shunting β_1 integrins back to ARF6-positive plasma lemma protrusions. Collectively their findings provide evidence that integrin traffic is differentially regulated and dependent upon integrin receptor activation status.

Thus, confocal immunofluorescence (IMF) microscopy was performed on the MCF10 panel of cell lines to characterise the subcellular localisation of the total integrin $\alpha_v\beta_6$ population labelled with antibody 10D5 (Figure 4.2B), in comparison with active integrin $\alpha_v\beta_6$ demonstrated by antibodies 6.2E5 (Figure 4.2C) and 6.2G2 (Figure 4.2D). The MCF10 isogenic variants were routinely monitored in culture by phase microscopy (Figure 4.2A) to assess their phenotypic appearance and condition prior to experimental use.

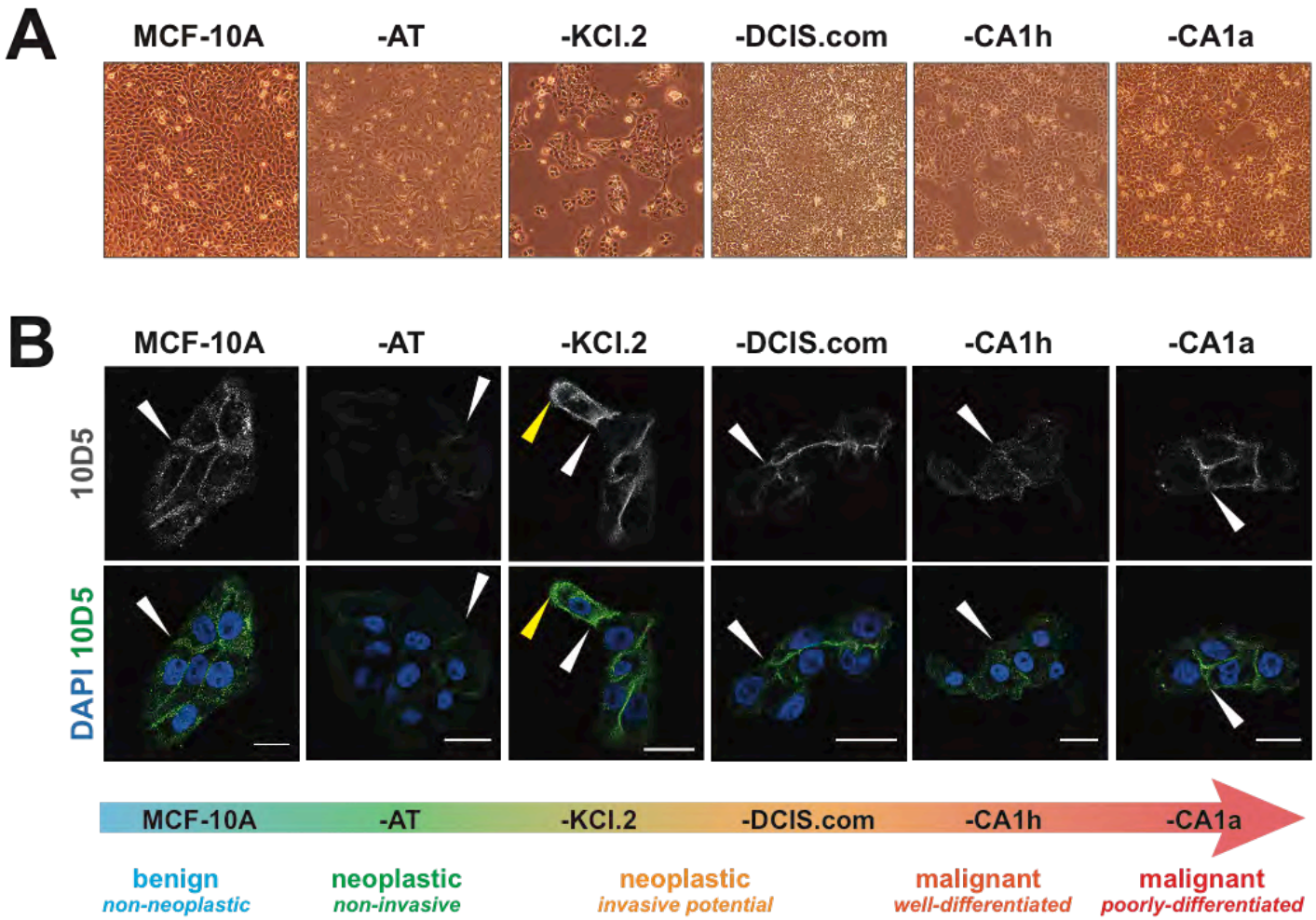

Figure 4.2 (A & B)
Total integrin $\alpha_v\beta_6$ demonstrated by antibody 10D5 appears to stably localise at cell-cell junctions in all MCF-10 isogenic variants but the active subpopulation of integrin $\alpha_v\beta_6$ recognised by antibodies 6.2E5 and 6.2G2 undergoes subcellular redistribution upon neoplastic transformation and malignant progression as represented by the MCF-10 cell line series

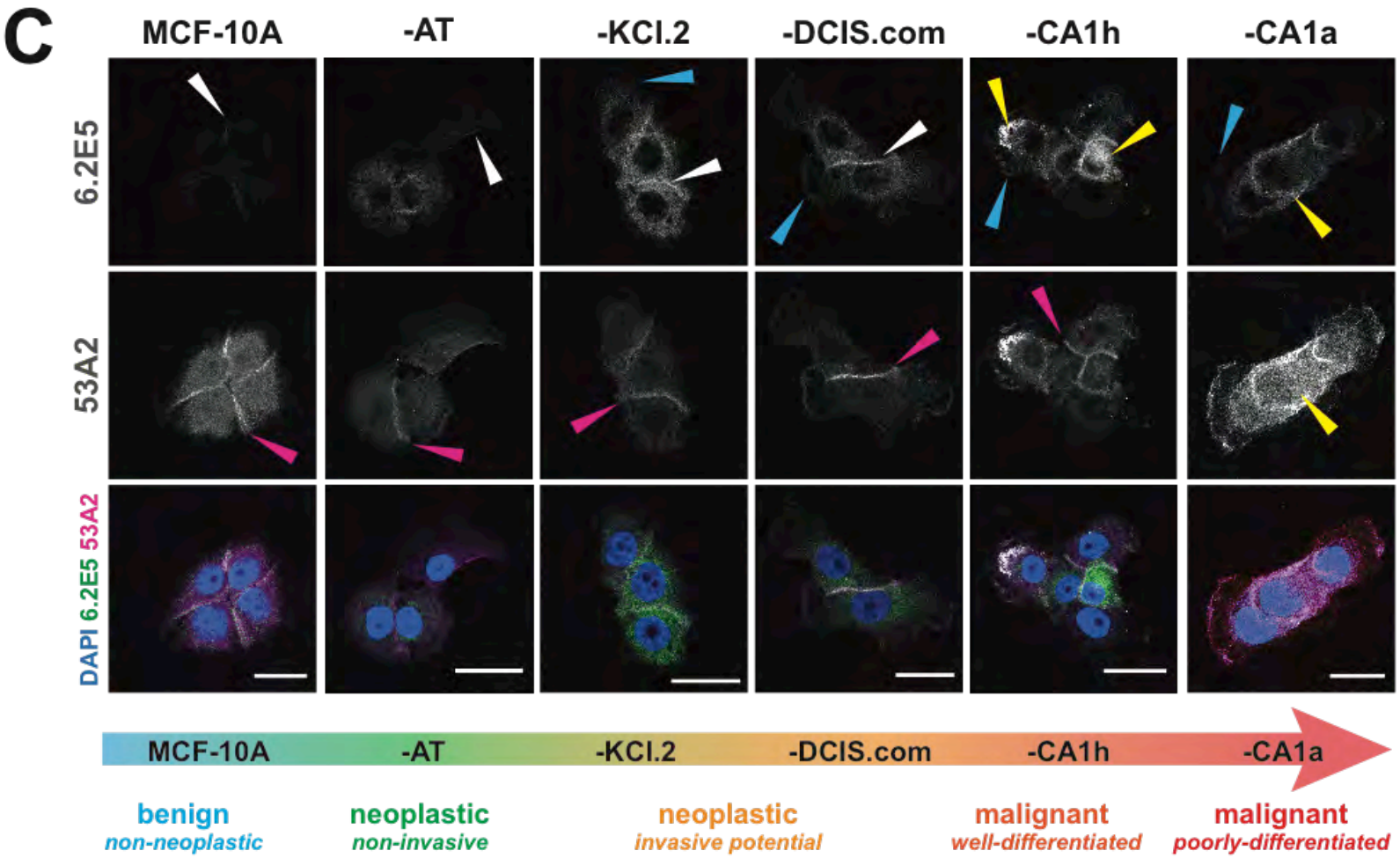

Figure 4.2 (C)
Total integrin $\alpha_v\beta_6$ demonstrated by antibody 10D5 appears to stably localise at cell-cell junctions in all MCF-10 isogenic variants but the active subpopulation of integrin $\alpha_v\beta_6$ recognised by antibodies 6.2E5 and 6.2G2 undergoes subcellular redistribution upon neoplastic transformation and malignant progression as represented by the MCF-10 cell line series

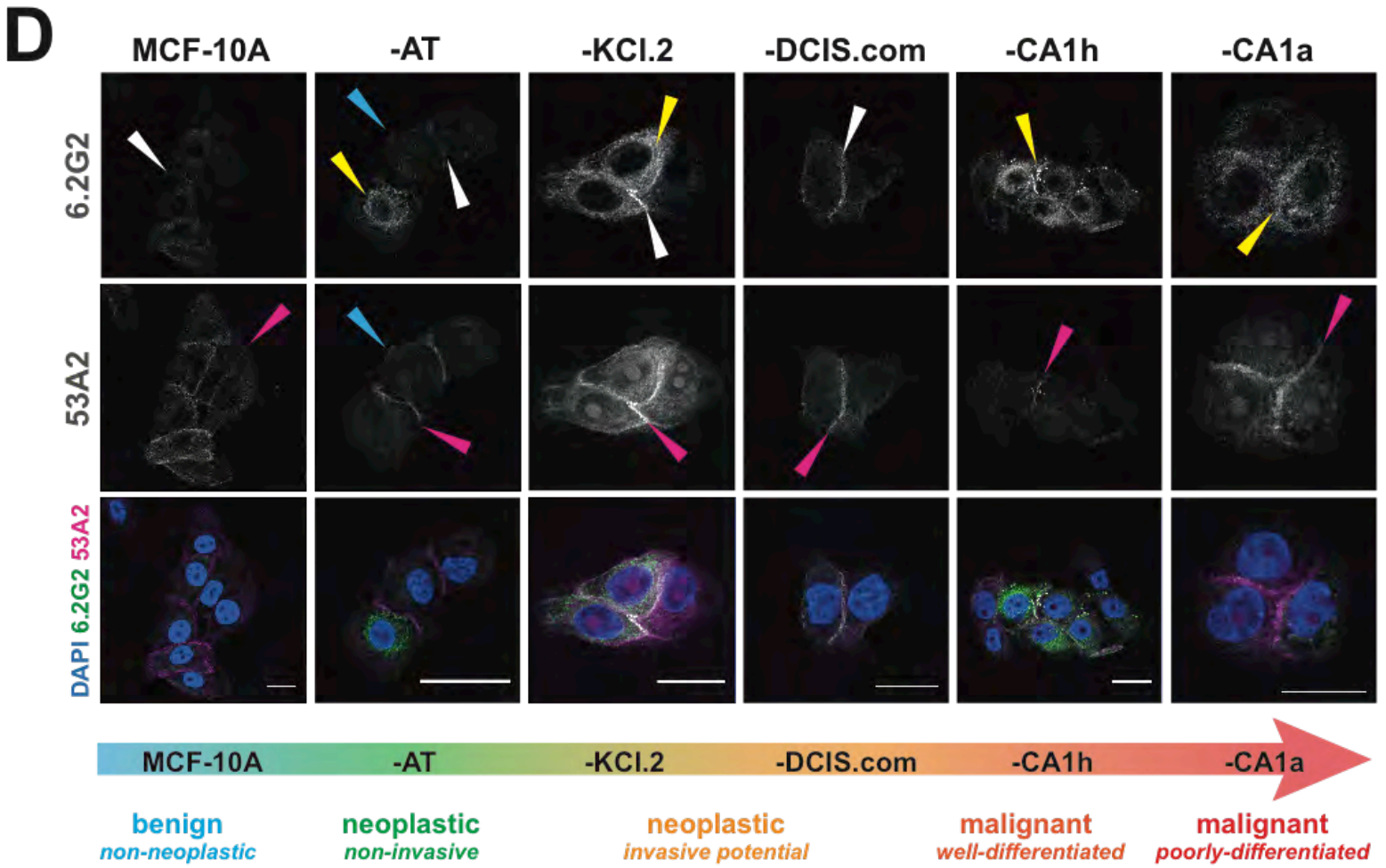

Figure 4.2 (D)
Total integrin $\alpha_v\beta_6$ demonstrated by antibody 10D5 appears to stably localise at cell-cell junctions in all MCF-10 isogenic variants but the active subpopulation of integrin $\alpha_v\beta_6$ recognised by antibodies 6.2E5 and 6.2G2 undergoes subcellular redistribution upon neoplastic transformation and malignant progression as represented by the MCF-10 cell line series

Figure 4.2

Total integrin $\alpha_v\beta_6$ demonstrated by antibody 10D5 appears to stably localise at cell-cell junctions in all MCF-10 isogenic variants but the active subpopulation of integrin $\alpha_v\beta_6$ recognised by antibodies 6.2E5 and 6.2G2 undergoes subcellular redistribution upon neoplastic transformation and malignant progression as represented by the MCF-10 cell line series

The MCF-10A series of breast cancer cell lines (MCF10 isogenic model) generated to recapitulate neoplastic transformation and malignant progression **(4.2 A)** were used to explore the putative role of active integrin $\alpha_v\beta_6$ during breast tumourigenesis. The subcellular localisation and surface abundance of integrin $\alpha_v\beta_6$ recognised by antibodies 10D5, 6.2E5 and 6.2G2 were evaluated by permeabilised immunofluorescence **(4.2 B**, **C** and **D)** respectively. **(4.2 A)** The MCF-10 isogenic variants were routinely phenotypically monitored in culture by phase contrast microscopy morphological assessment (OLYMPUS™ IMT-2, Olympus® Corp). **(4.2 B)** The antibody 10D5 (10 µg ml^{-1}, Merck Millipore) was used to identify the total pool of integrin $\alpha_v\beta_6$ and was seen to localise at cell-cell junctions (white arrows) across the entire MCF-10A panel of cell lines. Occasional cytoplasmic, vesicular accumulations (yellow arrow) were observed in the MCF-10A-KCl.2 neoplastic with invasive potential isogenic variant. **(4.2 C)** Antibody 6.2E5 (5 µg ml^{-1}, Biogen Idec) was seen to localise at cell-cell junctions (white arrows) in non-transformed (MCF-10A) and neoplastic cells (MCF-10AT, -KCl.2 and –DCIS.com) but this pattern of immunopositivity was deregulated in malignant variants (MCF-10A-CA1h and –CA1a). In neoplastic variants with invasive potential (-KCl.2 and –DCIS.com) 6.2E5 was seen to localise at leading edges of spreading cells (blue arrows). This was also observed in the malignant variants, where marked intracellular vesicular accumulations (yellow arrows) were noted. **(4.2 D)** Antibody 6.2G2 (5 µg ml^{-1}, Biogen Idec) was observed at cell-cell junctions (white arrows) in the non-transformed and neoplastic variants, but not in the malignant variants. In the neoplastic variant MCF-10AT, 6.2G2 was seen to localise at the edges of spreading cells (blue arrows) and intracellular vesicular accumulations (yellow arrows) were also observed. Intracellular accumulations of 6.2G2 immunopositivity were present in both the –CA1h and –CA1a malignant variants, as had been observed for antibody 6.2E5. Images were acquired by confocal microscopy using the ZEISS LSM710 equipped with ZEISS Zen image analysis software (both Carl Zeiss AG, DE). Images were prepared for presentation in Image J software (National Institutes of Health) and Adobe®Photoshop©CS6 with composites generated in Adobe®Illustrator©CS6 (Adobe Systems Software© Ltd).

The total pool of integrin $\alpha_v\beta_6$ recognised by antibody 10D5 was seen to predominate at cell-cell interfaces across the MCF10 model when evaluated by permeabilised IMF microscopy (Figure 4.2B), but only weakly expressed at the cell periphery. Similarly, the antibody 53A2 (Figures 4.2C and 4.2D) was also seen to localise most markedly at cell-cell junctions, and weakly at the cell periphery. Occasional cytoplasmic accumulations of 53A2 immunopositivity were observed in the malignant variants MCF10-CA1h and MCF-10CA1a.

Interestingly, the integrin $\alpha_v\beta_6$ activation-associated epitopes recognised by antibodies 6.2E5 (Figure 4.2C) and 6.2G2 (Figure 4.2D) underwent subcellular redistribution following neoplastic transformation and malignant progression. In the non-tumourigenic, non-invasive MCF-10A benign parent cell line, these activation-associated epitopes were weakly expressed and localised at cell-cell junctions. However, in the MCF-10AT neoplastic variant, these epitopes appeared weakly immunopositive and predominantly cytoplasmic in localisation. This suggested that although the active integrin $\alpha_v\beta_6$ was only present at low levels, it had undergone visible cytoplasmic redistribution upon neoplastic transformation in the MCF-10AT variant in comparison with the non-neoplastic MCF-10A parent cell line.

Furthermore, vesicular-like cytoplasmic accumulations of the active integrin $\alpha_v\beta_6$ (as demonstrated by antibodies 6.2E5 and 6.2G2) were apparent in variants with invasive potential (MCF10-Kcl.2) and invasive, malignant variants (MCF10-CA1h, MCF10-CA1a). The most marked alteration in subcellular localisation was observed in the MCF-10CA1h malignant variant, where notably large cytoplasmic accumulations of active integrin $\alpha_v\beta_6$ were observed. This may suggest that derailed internalisation and trafficking of the active integrin $\alpha_v\beta_6$ are implicated in advanced stages of breast cancer, facilitating an invasive phenotype requisite for metastatic dissemination.

Curiously, the MCF10-DCIS.com variant recapitulating in situ disease, exhibited little or no cytoplasmic integrin $\alpha_v\beta_6$, either in its active or inactive state. Instead, both the active and inactive integrin $\alpha_v\beta_6$ conformers were seen to stably localise at cell-cell interfaces in a similar patter to that observed for the MCF-10A parent cell line. The notable absence of cytoplasmic integrin $\alpha_v\beta_6$ active conformers in the non-invasive, in situ disease variant (MCF10-DCIS.com) contrasts with the marked

vesicular, cytoplasmic abundance of active integrin $\alpha_v\beta_6$ conformers in the malignant, highly invasive variants (MCF10-CA1h, MCF10-CA1a).

Collectively, these observations indicate that subcellular redistribution of active integrin $\alpha_v\beta_6$ may be necessary during invasion in late-stage disease. However, the mechanism driving this cellular re-localisation is unclear. It may be attributable to: increased internalisation kinetics for the active conformer resulting in greater cytoplasmic abundance; slower recycling kinetics yielding an accumulation of active conformers awaiting lysosomal degradation or perhaps aberrant intracellular receptor activation due to perturbed molecular regulation of integrin $\alpha_v\beta_6$ activation.

Undoubtedly these findings warrant further investigation to define whether this subcellular redistribution of the active $\alpha_v\beta_6$ conformer is a cause or effect during acquisition of an invasive phenotype; what regulates integrin $\alpha_v\beta_6$ internalisation and trafficking and how this may be perturbed during the course of breast tumourigenesis.

4.3 isogenic variants comprising the MCF10 in vitro model of breast tumourigenesis may be successfully co-cultured with human fibroblasts employed in physiomimetic 3D-miniorganotypic gel assays, but their phenotypic instability in routine culture hinders their utility

The seminal importance of integrin adhesion receptors as the nexus integrating bidirectional signalling cues exchanged between cells and their encompassing three-dimensional (3D) environment has long been established (Hood and Cheresh 2002, Hynes 2002, Luo *et al* 2007, Harburger and Calderwood 2009, Campbell and Humphries 2011, Kim *et al* 2011a, Welf *et al* 2012, Byron *et al* 2014).

Given that integrins modulate many aspects of cell-fate in response to cognate ligand-patterning, composition and tensile forces determined by the ECM, many

researchers seek to establish biomimetic models that better recapitulate the structural and biochemical complexities of the native 3D cellular-environment than conventional 2D-culture systems alone permit (Baker and Chen 2012).

Zutter *et al* (1995) published an early example of the utility of even a rudimentary 3D model to characterise the critical role of integrin-mediated ECM cues during tissue morphogenesis. The authors demonstrated integrin $\alpha_2\beta_1$ expression is critical during murine mammary morphogenesis using natural ECM-based hydrogels comprising unsupplemented commercial Matrigel® preparation to recapitulate basal laminae 3D-matrices.

They observed that α_2–null Mm5MT murine mammary epithelial cells cultured within these gels formed aggregates mesenchymal in appearance and devoid of any discernible structural organisation. In contrast, Mm5MT cells transfected to stably express the α_2-subunit formed highly organised, branching 3D alveolar and ductal structures within 3 to 4 days of in-gel culture.

Subsequently, 3D-physiomimetic culture models have been refined to better recapitulate the emerging complexities of the tumour microenvironment. Parenchymal cells may be co-cultured with tissue-specific stromal cells to reflect the importance of tumour-stroma cellular crosstalk now known to initiate, enable and enhance established cancer hallmarks in many malignancies (Hanahan and Weinberg 2011, Quail and Joyce 2013), including breast cancer (Criscitiello *et al* 2014, Bussard *et al* 2016).

Furthermore, these 3-D assay matrices may be customised by treatment with physiological and/or pharmaceutical supplements to study the effects of defined extracellular mediators including cytokines and growth factors, or evaluate the efficacy of novel therapeutics, on tumour cell behaviour (Coleman *et al* 2014b). Therefore it was deemed pertinent to establish the utility of the MCF10 isogenic panel in an established 3D-miniorganotypic gel fibroblast co-culture assays (Figure 4.4) to further investigate the role of integrin $\alpha_v\beta_6$ activation.

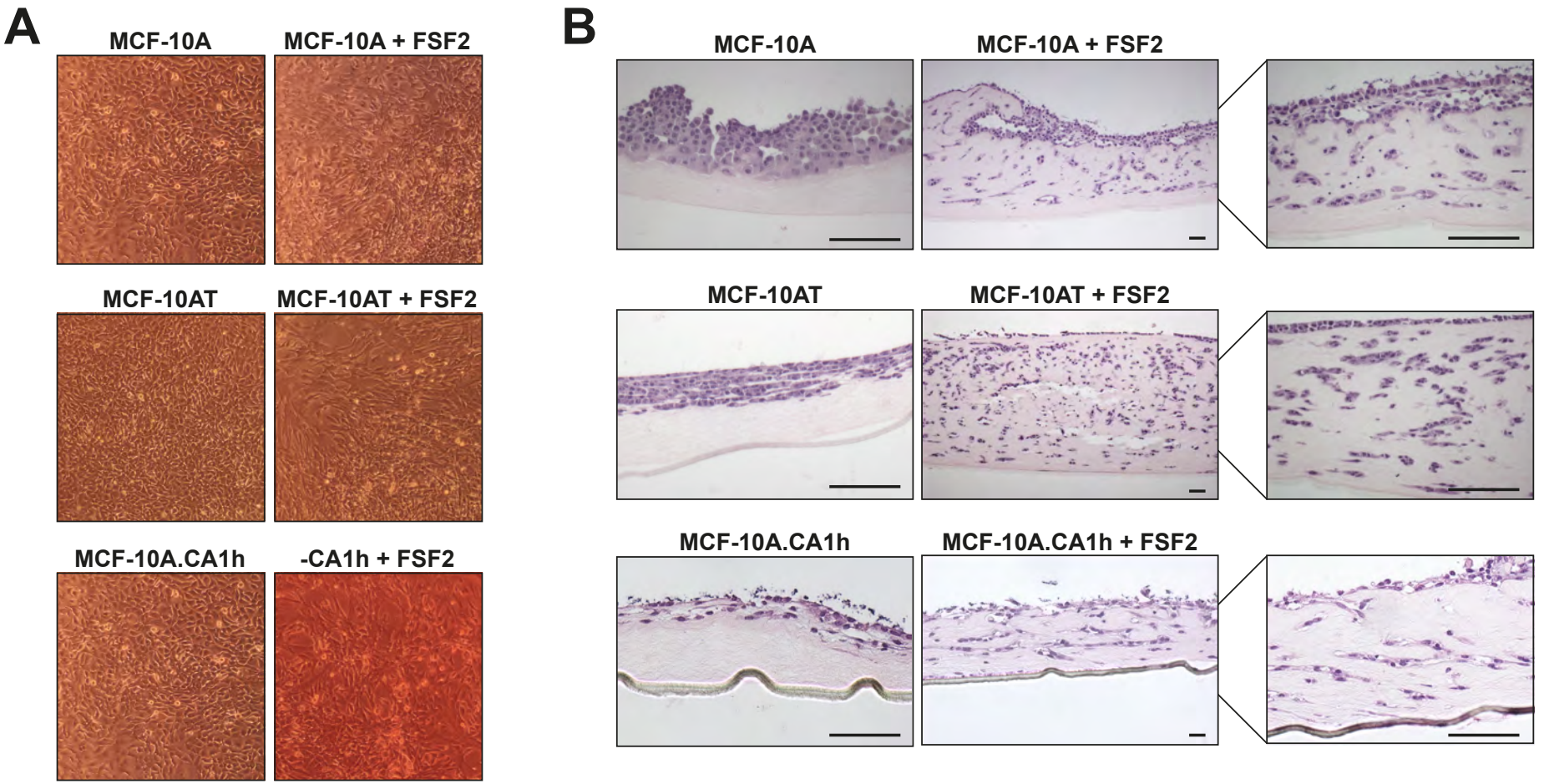

Figure 4.3 (A & B)
Establishing the utility of cells comprising the MCF-10 isogenic model of breast tumourigenesis and disease progression in 3D-organotypic cultures

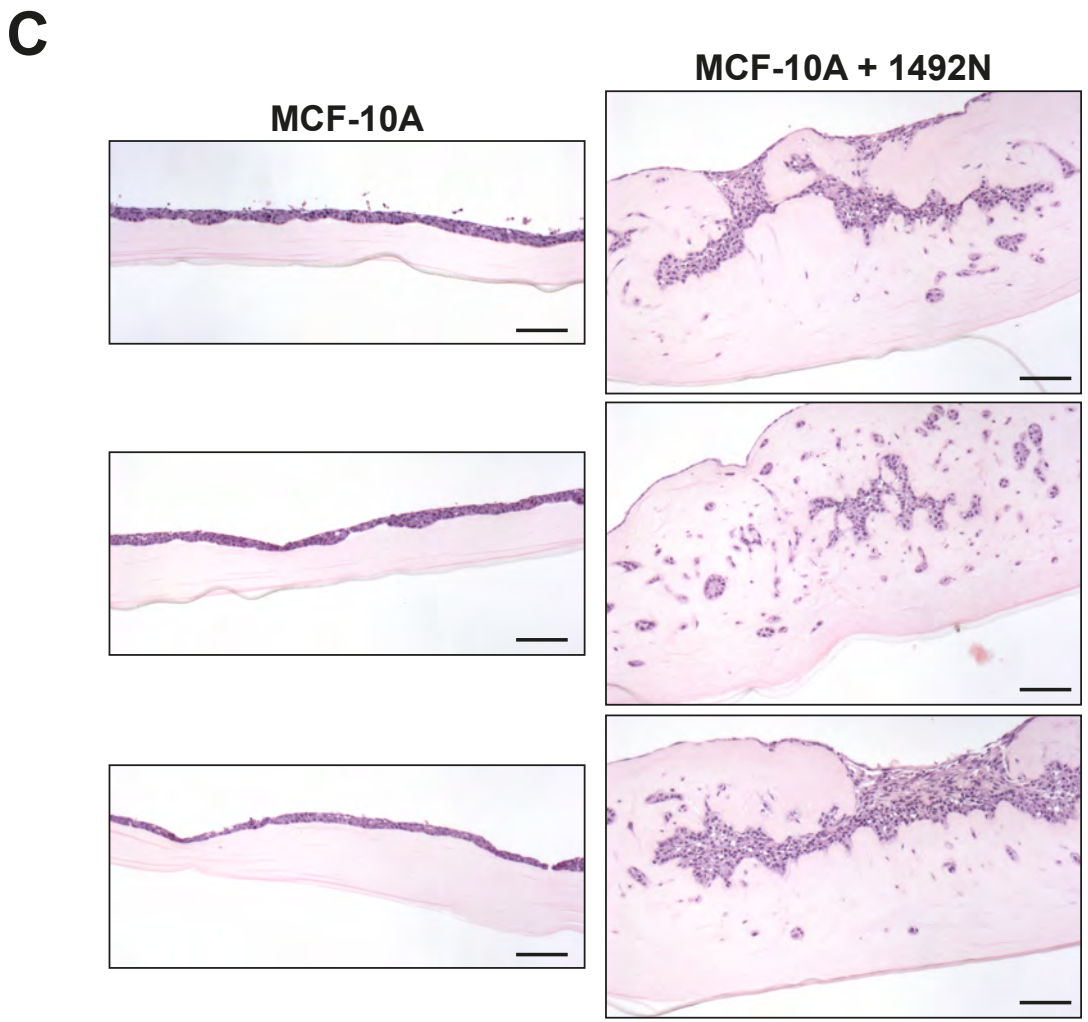

Figure 4.3 (C)
Establishing the utility of cells comprising the MCF-10 isogenic model of breast tumourigenesis and disease progression in 3D-organotypic cultures

Figure 4.3

Establishing the utility of cells comprising the MCF-10 isogenic model of breast tumourigenesis and disease progression in 3D-organotypic cultures

Organotypic cultures using the MCF-10A, MCF-10AT and MCF-10A.CA1h alone, or co-culture in a 2:1 ratio with **(4.3 B)** human foreskin fibroblasts (FSF2) or **(4.3 C)** primary human fibroblasts isolated from a reduction mammoplasty (1492N) were prepared to evaluate the potential utility and feasibility of this model in future investigations seeking to characterise the role of the active integrin $\alpha_v\beta_6$ subpopulation in neoplastic transformation of mammary epithelium and malignant progression within a physiomimetic 3D-context. **(4.3 A)** An aliquot of cell suspensions used to prepare organotypic cultures were seeded in spare wells of the 24-well tissue culture plate housing the organotypics to confirm adherent morphology by phase contrast microscopy (OLYMPUS IMT-2, Olympus® Corp). **(4.3 B** and **C)** Organotypic cultures were maintained over a 10-day period, and media replenished every 48 hours. **(4.3 B)** As previously reported, cancer cells alone did not invade, but in the presence of human foreskin fibroblasts (FSF2), invasion into the gel was observed even with the benign, non-invasive MCF-10A parental cell line. **(4.3 C)** Similar observations were made for organotypic cultures established with human mammary fibroblasts isolated from a reduction mammoplasty (1492N). Following completion of 10-day culture, organotypic gels were harvested, formalin fixed overnight and immersed in 70% ethanol for a minimum of 12 hours prior to processing. Sections from FFPE samples were stained with haematoxylin and eosin (H&E) and images acquired using the ZEISS AxioPlan brightfield microscope equipped with ZEISS AxioVision v4.8.1 imaging software (both Carl Zeiss AG, DE). Scale bars represent 50 µm.

It was hoped this approach would contextualise the role of integrin $\alpha_v\beta_6$ activation during breast tumourigenesis and disease progression within a biomimetic, 3D-environment that would better recapitulate the complexities of the tumour microenvironment than in vitro 2D studies alone. However, the phenotypic instability of the MCF10 variants in routine culture (Figure 4.4) hindered their successful application for the purposes of this investigation.

To establish the suitability of the MCF10 panel to characterise integrin $\alpha_v\beta_6$ activation within a 3D physiomimetic environment, mini-organotypic gel cultures were prepared using co-culture with FSF2 normal human foreskin fibroblasts (Figure 4.3A and B), or tissue-specific 1492N normal breast fibroblasts derived from reduction mammoplasty tissue (Figure 4.3C). Concordant with previous literature (Wang *et al* 2002), the presence of fibroblasts promoted breast cancer cell invasion. Invasion into the mini-organotypic gels was not observed in the presence of cancer cells alone.

Concordant with the findings of Qu *et al* (2015), MCF-10A cells in 2D-culture exhibited a cuboidal epithelial morphology. In 3D-organotypic cultures in the presence of Matrigel and collagen type I, MCF-10A cells formed spheroid structures as previously described by Qu and colleagues. A similar formation of spheroid, pseudo-ductal structures were seen to form in MCF-10A co-cultures with both FSF2 and 1492N fibroblasts. However staining for epithelial and mesenchymal markers to distinguish the MCF-10A cell compartment from the co-cultured fibroblast component of the organotypic model would need to be undertaken to establish whether these spheroid, ductal-like structures were formed by MCF-10A cells, as described by Qu et al (2015).

Curiously, seeded cells were seen to invade gels when the benign, non-invasive MCF10A cell line was co-cultured with FSF2 normal human foreskin fibroblasts (Figure 4.3B) and 1492N normal human breast fibroblasts (Figure 4.3C). Similarly, co-cultures of the reportedly neoplastic but non-invasive MCF-10AT cell line with FSF2 fibroblasts, also exhibited unexpected invasion into mini-organotypic gels. Invasion was observed for the well differentiated, invasive MCF-10CA1h variant co-cultured with FSF2 fibroblasts, although this appeared to be to a lesser extent than for the MCF-10A and MCF-10AT variants.

It had been anticipated that little or no invasion would be observed for the MCF-10A and MCF-10AT cell lines. It is possible that the observed invasion is attributable to the fibroblast component in the absence of cancer cell invasion for mini-organotypics using these non-invasive breast cancer cell lines. In the absence of robust immunohistochemical confirmation of the epithelial (cancer cell) versus mesenchymal (fibroblast) cellular compartments to conclusively determine location of cancer cells and fibroblasts within the gel, it is difficult to draw meaningful conclusions.

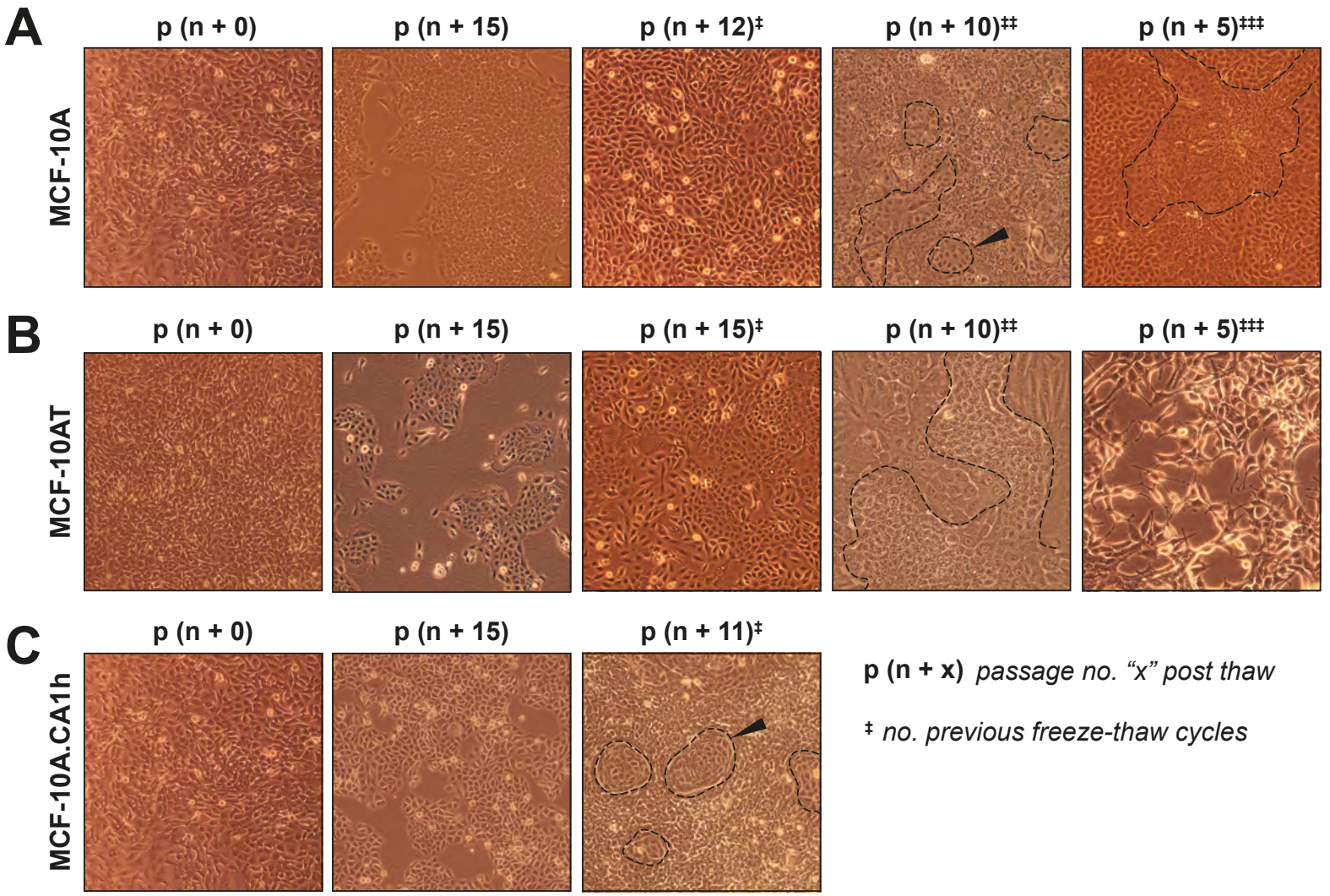

Figure 4.4
Instability of integrin $\alpha_v\beta_6$ expression and phenotypic loss of the MCF-10 isogenic cell line series in routine culture

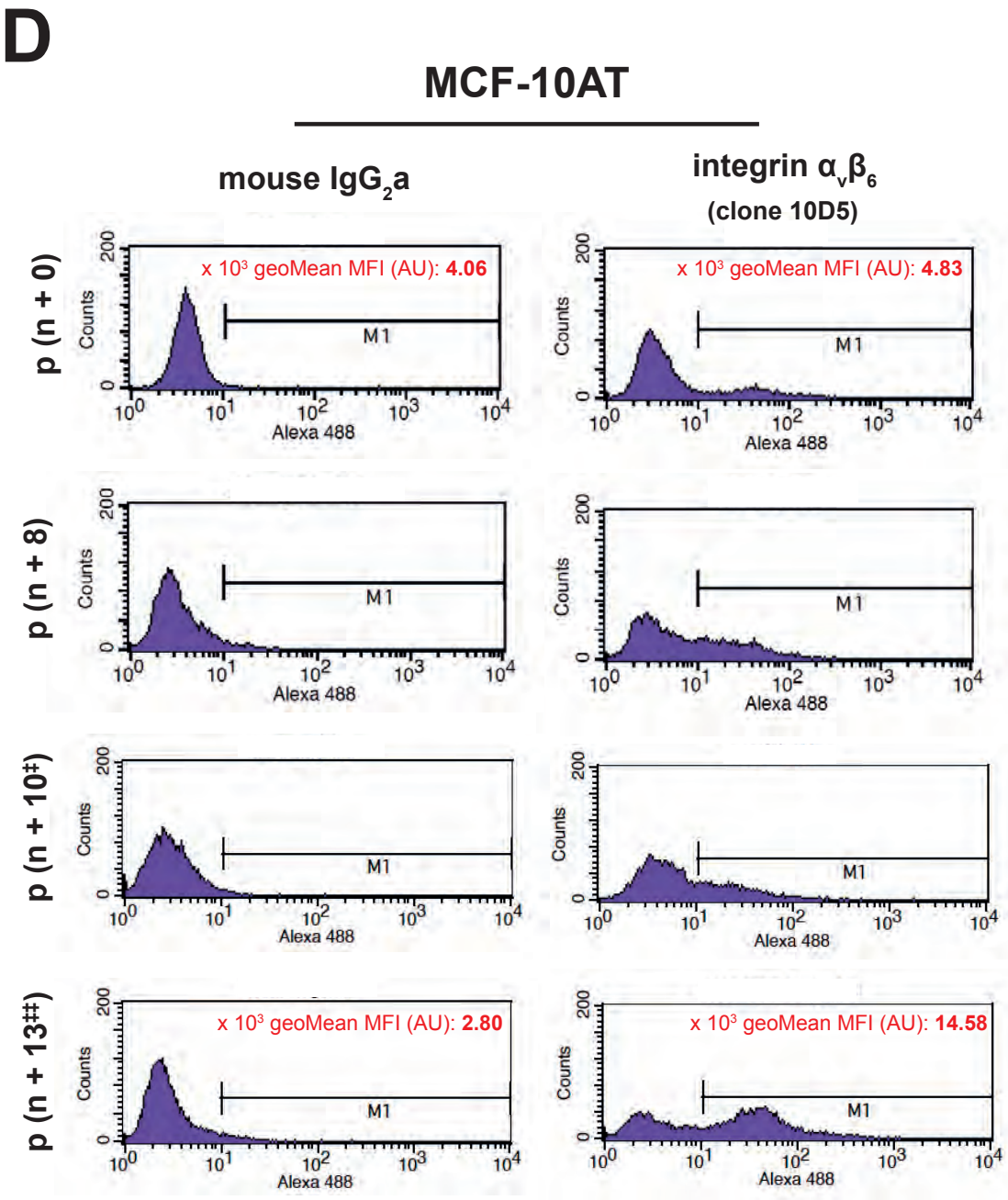

Figure 4.4 (D)
Instability of integrin $\alpha_v\beta_6$ expression and phenotypic loss of the MCF-10 isogenic cell line series in routine culture: Emergence of two morphologically distinct subpopulations within the MCF-10AT cell line coincided with acquisition of integrin $\alpha_v\beta_6$ weakly and highly positive populations

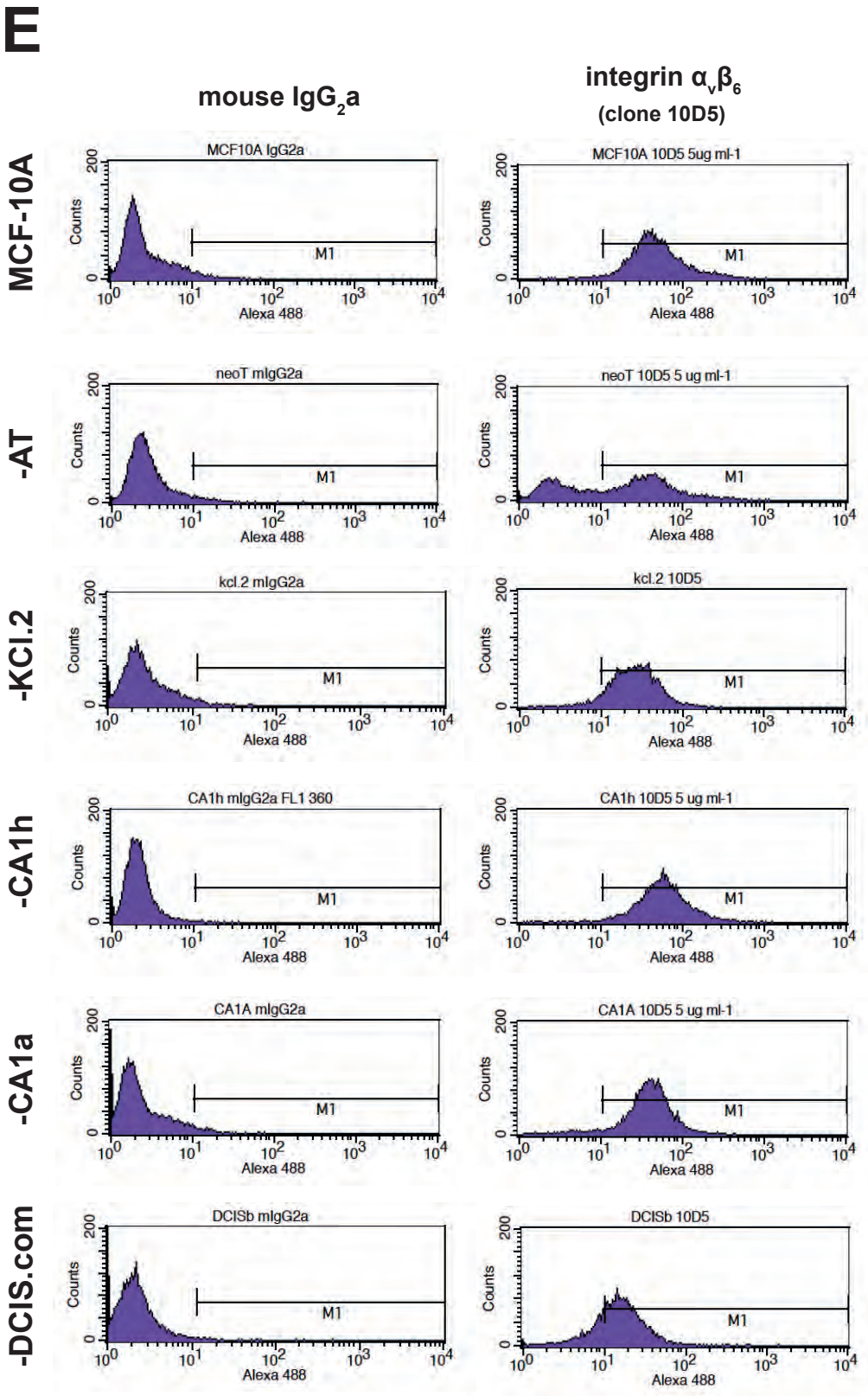

Figure 4.4 (E)
Instability of integrin $\alpha_v\beta_6$ expression and phenotypic loss of the MCF-10 isogenic cell line series in routine culture: Uniformity of integrin $\alpha_v\beta_6$ expression in MCF-10 variants in comparison with distinct weak and strong positive subpopulations observed in the MCF-10AT cells

Figure 4.4

Instability of integrin $\alpha_v\beta_6$ expression and phenotypic loss of the MCF-10 isogenic cell line series in routine culture

The MCF10 panel of isogenic cell lines were monitored daily by phase contrast microscopy during routine culture. Representative images for the **(4.4 A)** MCF10A, **(4.4 B)** MCF-10AT and **(4.4 C)** MCF-10CA1h variants are shown. Passage numbers **(p)** indicate the number of passages after thawing **(n + 11)** frozen cells. It was observed that the morphological appearance of these cell lines drifted notably during the course of routine tissue culture. **(4.4 A)** MCF10A cells appeared to lose their epithelial morphology and differentiate into two distinct morphological subtypes (outlined in black dashed line and highlighted with block arrows), suggesting a mixed population of cells. **(4.4 B)** Similarly, the MCF-10AT and **(4.4 C)** MCF-10CA1h variants appeared to differentiate into two distinct morphological subtypes indicating loss of cell line clonal homogeneity. With progressive passage in culture, the phenotypic loss observed coincided with the emergence of two distinct populations within the MCF-10AT cell line in terms of integrin $\alpha_v\beta_6$ expression (weak and high) observed on FCM histogram plots **(4.4 D)**, which contrasted with uniformity of integrin expression observed in the other MCF-10 isogenic variants **(4.4 E)** Disappointingly, the phenotypes were not recovered. Phase contrast images were acquired using the OLYMPUS™ IMT-2 phase contrast microscope (Olympus® Corp). All images were acquired at x20 magnification. All flow cytometry data was acquired on live cells labelled with clone 10D5 (10 µg ml^{-1}, Merck Millipore) in the presence of a cell viability indicator (5 µg ml^{-1} propidium iodide, P4170, Sigma Aldrich) using the BD FACSCalibur™ (BD Biosciences). Following normalisation against isotype matched negative control antibodies, geometric MFI values were determined by analysis in BD CellQuestPro™ software (BD Biosciences). Statistical analyses were performed using GraphPad Prism® 5.0b for MacOSX (Graphpad Software Inc, CA, USA).

Based upon altered microscopic appearance and the emergence of two distinct morphological phenotypes observed by phase contrast microscopy during routine tissue culture, the in-house stocks of the MCF-10A cell line and its derived variants were deemed to be phenotypically unstable (Figure 4.4). The MCF-10AT variants were phenotypically unstable in routine culture. The observation of distinct morphological phenotypes coincided with a shift in integrin $\alpha_v\beta_6$ expression which suggested the emergence of two subpopulations that were either weakly, or strongly integrin $\alpha_v\beta_6$ positive (Figure 4.4D). In light of phenotypic instability and loss of stable integrin $\alpha_v\beta_6$ expression, the continued experimental use of the MCF-10 model was not deemed justifiable for the purposes of this study.

The spontaneous emergence of distinct morphological subpopulations in the MCF-10A variants has been previously published. Zantek *et al* (2001) reported the emergence of a spontaneous novel variant arising during routine culture of the T24 human bladder carcinoma Ha-Ras-oncogene transformed MCF-10AT (previously designated MCF-10NeoT). The authors described the differentiation of MCF-10NeoT cells into a novel variant of spindled mesenchymal morphology. Naming this novel, spontaneously arising variant "NeoST", Zantak and colleagues noted that this acquired phenotype was irreversible.

Furthermore, functional characterisation of the MCF-10NeoST revealed their in vitro recapitulation of traits ascribed to metastatic breast cancer cells including: loss of plasmalemma E-cadherin, invasiveness in 3D assays, anchorage-independent growth (circumvention of anoikis) and increased activity of FAK tyrosine kinase. Zantak and colleagues concluded that the spontaneously arising NeoST represented a novel, distinct phenotypic variant in both functional traits and morphological appearance.

Therefore, given previous reports of a novel variant arising spontaneously in culture from the MCF10 panel that was both morphologically and functionally distinct in phenotype, it was deemed inadvisable to continue experimental work with the MCF10 panel in light of this emerging morphological phenotypic instability. In addition, further immunohistochemical or molecular characterisation of the emergent morphological subpopulations observed was not undertaken as it was not deemed of potential value to the aims of this project.

4. discussion

In summary, it was found that in the presence of a relatively stable cell surface pool of active integrin $\alpha_v\beta_6$ (quantified by flow cytometry), the activation-associated epitopes recognised by antibodies 6.2E5 and 6.2G2 underwent subcellular redistribution upon neoplastic transformation and malignant progression in the MCF-10AT and MCF-10CA1h variants respectively (as demonstrated by confocal IMF microscopy).

Based upon these observations, it is postulated that derailed internalisation kinetics and intracellular trafficking routes of active integrin $\alpha_v\beta_6$ may be involved in tumour initiation and acquisition of an invasive, metastatic phenotype in mammary epithelial cells undergoing transformative changes. This theory fits with Ramsay *et al* (2007) observation that HAX-1-mediated clathrin-dependent endocytosis of integrin $\alpha_v\beta_6$ was requisite for carcinoma cell invasion in an OSCC model. In addition, emerging evidence suggests that it is the active integrin conformer that mediates invasive and metastatic potential (Lee *et al* 2013). Collectively, this would justify further investigation into a putative role for aberrant active integrin $\alpha_v\beta_6$ internalisation determining invasive potential in BrCa cells.

It is acknowledged that additional data would strengthen the case for such investigations, which so far are based predominantly on observational data. Characterisation of active versus inactive integrin $\alpha_v\beta_6$ internalisation kinetics could be quantitatively determined using a biochemical surface-biotinylation endocytosis assay established by Roberts *et al* (2001), or using a flow cytometric, activation-specific monoclonal antibody approach as employed by Arjonen *et al* (2012). Furthermore, it would be valuable to characterise and compare specific mechanisms of internalisation and intracellular trafficking routes for the active and inactive integrin $\alpha_v\beta_6$ conformers. It would be interesting to investigate whether the integrin $\alpha_v\beta_6$ is subject to distinct activation-specific internalisation, trafficking and recycling kinetics in cancer, as defined by Arjonen *et al* (2012) in breast, lung and prostate cancer cell lines.

Definition of differential trafficking and recycling of distinct receptor conformations, could be achieved by IMF co-labelling of integrin $\alpha_v\beta_6$ conformers with endosomal compartment markers at defined time-points. Results from such

investigations would inform whether integrin $\alpha_v\beta_6$ trafficking routes are activation-status dependent and/or altered during the course of breast tumourigenesis and progression to malignant disease.

It was observed that between the malignant, invasive variants (MCF-10CA1h and MCF10-CA1a), the poorly differentiated MCF-10CA1a cells expressed a greater proportion of active integrin $\alpha_v\beta_6$ recognised by antibodies 6.2E5 and 6.2G2, in comparison with the well-differentiated MCF10-CA1h variants. This may indicate that integrin $\alpha_v\beta_6$ activation is a driving factor in advanced disease, determining differentiation status and tumour grade. Indeed, this would fit with the findings of Tang *et al* (2003) who defined a pleiotropic TGF-β1 signalling switch during breast tumourigenesis and malignant progression using the MCF10 isogenic model.

The authors concluded that TGF-β1 signalling was tumour suppressive in early stage disease, but switched to a prometastatic factor in advanced disease. Given that the integrin $\alpha_v\beta_6$ is known to regulate TGF- β1 activation (Thomas *et al* 2002, Margadant and Sonnenberg 2010, Munger and Sheppard 2011, Khan and Marshall 2016), it is logical that integrin activation may play a role in establishing this TGF-β1 signalling prometastatic switch in late-stage disease observed in the MCF10 model.

Felding-Habermann *et al* (2001) proposed a "two hit hypothesis" for the role of integrin $\alpha_v\beta_3$ during breast carcinogenesis and metastatic dissemination. The authors suggested that integrin $\alpha_v\beta_3$ expression was necessary, but on its own insufficient, for breast cancer metastasis. Instead, they argued that additional factors governing the activation state of integrin $\alpha_v\beta_3$ were requisite for metastatic dissemination. However, these factors were as yet undefined. Felding-Habermann and colleagues concluded that tumours (and their microenvironments) favouring aberrant integrin activation would elicit an adverse effect on the course and outcome of human breast cancer.

This hypothesis of a "two-hit" model for integrin-mediated outcomes in breast cancer is concordant with results discussed in this chapter. Flow cytometry data suggested that relative cell surface abundance of integrin $\alpha_v\beta_6$ expression alone may be insufficient to drive neoplastic transformation or malignant progression in the human breast. Instead, the requisite "second hit" determining an unfavourable

outcome in the course of breast cancer may arise from perturbed intracellular trafficking of the active integrin $\alpha_v\beta_6$ receptor pool, as intimated from the subcellular redistribution of 6.2E5 and 6.2G2 epitopes upon neoplastic transformation and malignant progression demonstrated by confocal immunofluorescence studies.

A notable limitation is acknowledged regarding the use of the MCF10 isogenic 2D model of breast tumourigenesis and disease progression. In light of the phenotypic complexities of human mammary epithelium, the suitability of the MCF-10A series to characterise the mechanisms by which normal breast cell functions are perturbed during neoplastic transformation, has been increasingly called into question. Given the abundance of BrCa research published using the MCF-10 isogenic cell line series as a surrogate pathogenetic model recapitulating breast tumourigenesis *in vitro*, Qu *et al* (2015) evaluated the biological relevance and reliability of the parent MCF-10A cell line itself to represent "normal" human mammary epithelial cells.

It was demonstrated that MCF-10A cells exhibit unique, culture dimension-specific phenotypes. In 2D culture, MCF-10A cells comprising a well-established monolayer expressed markers for luminal, basal and progenitor phenotypes. Strong expression of the basal markers alpha smooth muscle actin (α-SMA), vimentin and N-cadherin suggest MCF-10A cells are of basal ontogeny. Myoepithelial markers showed mixed expression with strong CK5 expression observed in approximately 50% of cells, moderate expression of CK17 in 10% of cells and less than 1% of cells expressing CK14.

In 2D-culture, concomitant expression of luminal markers was also observed, with 50% of cells showing positivity for CK8, but less than 10% of cells exhibiting expression of other luminal markers including mucin-1, CK18 and CK7. Furthermore, expression of breast-tissue specific milk proteins α-lactalbumin and β-casein was absent in the MCF-10A 2D-monolayer. Interestingly, Qu *et al* (2015) also found that a sub-population of MCF-10A cells in 2D-culture highly expressed the stem cell-associated transcription factors Sox-2 and Oct4.

However, MCF-10As in mammospheres and 3D-culture expressed both luminal and basal markers. It was observed that MCF-10A cells formed acinar structures in 3D culture demonstrating positivity for basal and luminal markers in addition to

expression of the milk proteins α-lactalbumin and β-casein. It is argued that the although MCF-10A cells in 3D-culture recapitulate some features of human luminal epithelial cells in terms of structure and function, the co-localisation of milk proteins and basal markers alongside luminal markers in branches and acini has not yet been robustly demonstrated in normal human mammary gland tissue.

Qu *et al* (2015) concluded that the differentiated MCF-10A phenotype uniquely observed in 3D-culture is unlikely to exist in normal human breast tissue *in vivo*; which restricts the biological relevance and translational applications of this cell line. Although the MCF10 isogenic cell line series may still have merit as a basic in vitro model, the ontogeny of transformative events and clonal selection criteria for neoplastic and malignant variants, culture-specific and highly variable phenotypes exhibited by the MCF-10A cell line and its derivatives, mean that interpretation of experimental data should be appropriately contextualised within the limitations of this adequate, but imperfect model of breast tumourigenesis and disease progression.

However, this model was deemed suitable for the purposes of preliminary investigations to justify future investigations into the putative role of integrin $\alpha_v\beta_6$ activation during breast tumourigenesis and metastatic disease progression. Using this model, an exciting avenue for future research was successfully identified. It was observed that the active integrin conformer underwent subcellular redistribution upon neoplastic transformation and malignant progression across the MCF10 panel. Given that cell surface abundance of the active integrin $\alpha_v\beta_6$ remained stable across cell lines comprising the MCF10 model, it was hypothesised that derailed internalisation and intracellular trafficking, rather than overexpression of active integrin $\alpha_v\beta_6$, may be critical oncogenic and metastatic drivers in BrCa.

Attempts were made to dissect this hypothesis further, including development of an internalisation assay to co-immunoprecipate LAP-ligand-engaged integrin $\alpha_v\beta_6$ internalisation complexes for proteomic interrogation to identify novel regulators of integrin $\alpha_v\beta_6$ endocytic regulation that may be derailed in BrCa. Although this assay could not be satisfactorily optimised for proteomics, it was used to validate subsequent experimental strategies developed to define th integrin –kinome associated with LAP-ligand internalisation (Chapter VI: Results Part IV; Figures 6.1.1 and S6.1).

A flow cytometry-based internalisation assay was developed to characterise internalisation kinetics (broadly defined as downregulation from the cell surface) for the active versus inactive integrin $\alpha_v\beta_6$ conformers. Disappointingly this assay performed in suspension could not be robustly validated as a biologically relevant read-out for the internalisation of an adhesion receptor and development was halted (Supplementary Figure S4.1).

Although a method to mechanistically dissect the putative derailed internalisation of the active integrin $\alpha_v\beta_6$ associated with neoplastic transformation and malignant progression could not be established within this body of work, this interesting finding most assuredly warrants further investigation. Indeed, definitions of integrin $\alpha_v\beta_6$ endocytic regulation and intracellular trafficking routes would be informative as this adhesion receptor is of emerging clinical significance in a variety of human pathologies, including BrCa.

supplementary information

S4

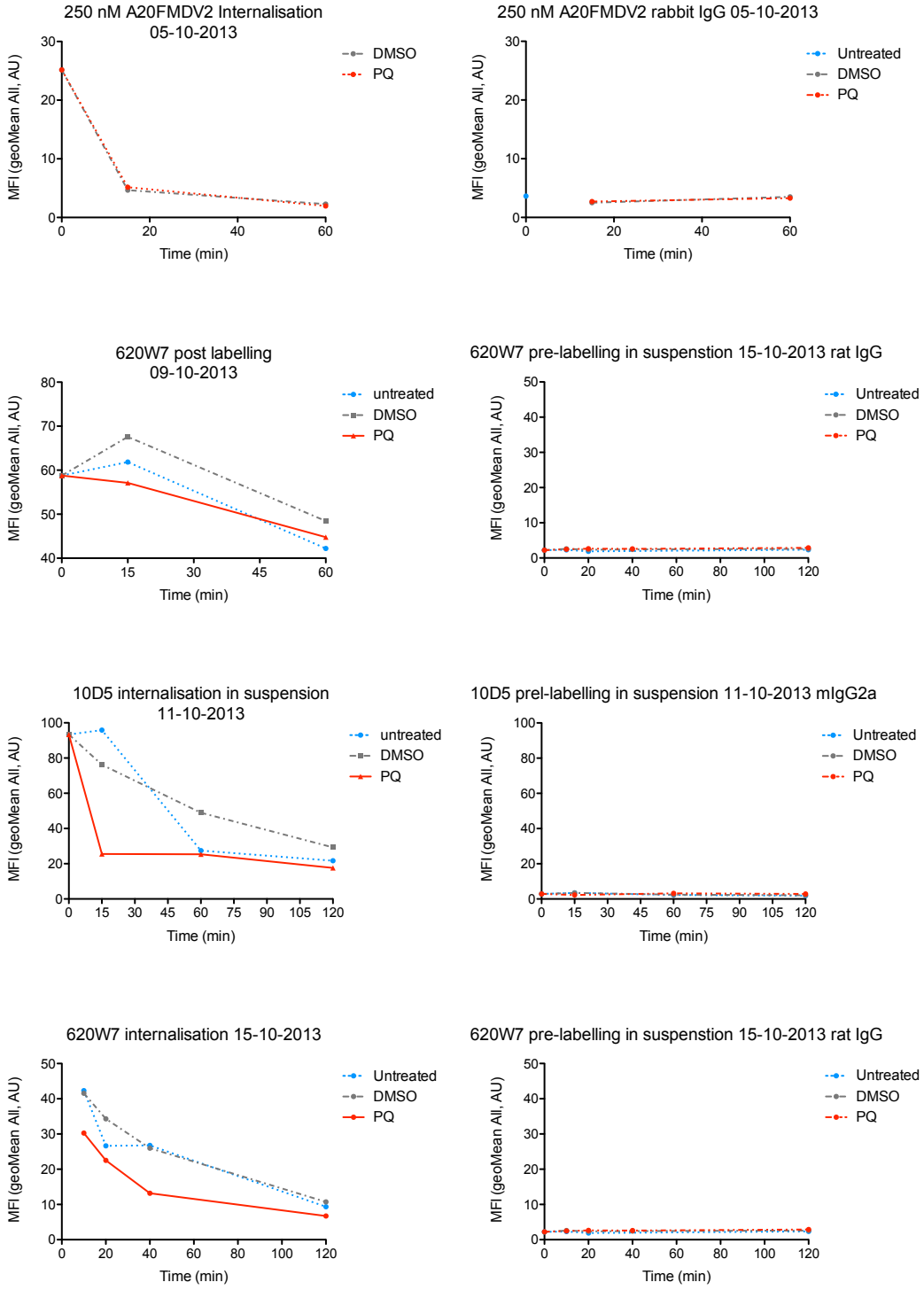

Supplementary Information (Figure) S4.1

Optimisation attempts for a flow cytometry-based internalisation assay to quantitatively define internalisation kinetics of integrin $\alpha_v\beta_6$ conformers

Supplementary Information (Figure) S4.1

Optimisation attempts for a flow cytometry-based internalisation assay to quantitatively define internalisation kinetics of integrin $\alpha_v\beta_6$ conformers

To characterise putative integrin $\alpha_v\beta_6$ conformer-specific internalisation kinetics, a flow cytometry (FCM)-based internalisation was tested using monoclonal antibodies or a synthetic peptide to specifically label cell-surface integrin $\alpha_v\beta_6$ populations. Representative examples of experiments using MCF10-CA1a cells are shown. Cells were labelled in suspension on wet ice for **10'** with anti-integrin $\alpha_v\beta_6$ moieties including the 20mer synthetic –RGD- motif bearing peptide A20FMDV2 (250 nM, in-house), a ligand mimetic antibody (clone 10D5, 10 µg ml^{-1}, Merck Millipore) or a non-ligand mimetic antibody (clone 620W7, 10 µg ml^{-1}, CR-UK). Cells were then washed and immersed in pre-warmed (37°C) complete media and returned to standard culture conditions to permit internalisation. At designated time-points internalisation was quenched by flooding and washing with ice-cold DMEM/0.1/0.1 FACS buffer prior to labelling residual surface bound antibody with fluorophore-conjugated secondary antibody to permit detection by FCM. Inclusion of 0.6 mM primaquine (PQ), a known-reversible inhibitor of integrin endocytic recycling (Reid and Watts 1990, van Weert AW 2000), was tested to prevent recycling of internalised antibody-bound integrin $\alpha_v\beta_6$ back to the plasmalemma. The "in-suspension' internalisation assay was not pursued given concerns regarding the biological relevance of characterising the properties of a cellular adhesion receptor in the absence of physiologically relevant adhesion cues. Flow cytometry was performed as previously described.

chapter V

results part III

proteomic definition of a ligand-engaged integrin $\alpha_v\beta_6$-dependent adhesion environment (β_6 "adhesome") using a 2D-enrichment strategy with downstream interrogation by label free-LC-MS/MS

V

proteomic definition of a ligand-engaged integrin $\alpha_v\beta_6$-dependent adhesion environment using a 2D-enrichment approach

DMBT-1, MARCKS, MXRA5, MYH9, MYH10, SEPT6 and SEPT9 are implicated in the BT-20 LAP-engaged β_6-adhesome; whilst EGFR is uniquely enriched in the MDA-MB-468 β_6-adhesome

5. introduction

Integrin activation induced by cognate ligand-engagement during adhesive processes is well established (Humphries 1996, Shimaoka *et al* 2002, Humphries 2004, Luo *et al* 2007, Shattil *et al* 2010, Campbell and Humphries 2011, Kim *et al* 2011b). Thus, characterisation of an integrin $\alpha_v\beta_6$–driven adhesion environment *("β_6-adhesome")* would provide valuable insights into putative molecular mediators of ligand-induced integrin $\alpha_v\beta_6$ activation and subsequent signalling induction. Proteomic dissection of the *β_6-adhesome* was undertaken by coupling a two-dimensional enrichment (2D-E) method for adhesion complexes to downstream label-free mass-spectrometry (LC-MS/MS) and bioinformatic interrogation (summarised schematically in Figure 5.1). Kind thanks are extended to Dr Mark R Morgan, *(Principal Investigator at the Receptor Dynamics in Cancer Laboratory, Institute of Translational Medicine, Centre for Molecular Physiology,*

University of Liverpool), who hosted and supervised experimental 2D-E work undertaken in his laboratory and presented here.

The 2D-E/LC-MS/MS method employed was first described by Humphries *et al* (2009) and later refined by Byron *et al* (2011) to successfully: characterise integrin $\alpha_4\beta_1$–mediated adhesion complexes (Byron *et al* 2012), refine tissue-specific ECM definitions (Rashid *et al* 2012, Byron *et al* 2013, Lennon *et al* 2014), identify novel glomerular cell cross-talk during renal ECM assembly and modification (Byron *et al* 2014), reveal integrin activation state-dependent regulation of cortical microtubule arrays (Byron *et al* 2015) and define a fibronectin (Fn)-induced integrin-dependent phospho-adhesome (Robertson *et al* 2015).

In order to define an integrin $\alpha_v\beta_6$-dependent adhesion environment *("β_6-adhesome")*, an established method for the isolation, enrichment and proteomic interrogation of transmembrane receptor-ligand complexes first reported by Humphries *et al* (2009) was adopted. This protocol permits stabilisation of notoriously labile integrin-mediated adhesion complexes via biochemical cross-linkage using the membrane permeant cross-linker dimethyl 3,3'-dithiobispropionimidate•2HCl (DTBP) (Corgiat *et al* 2014) to facilitate adhesion complex enrichment by sonication in an astringent detergent extraction buffer compatible with downstream proteomic investigation.

Successful application of this 2D-enrichment (2D-E) method to elucidate novel molecular (Byron *et al* 2011, Byron *et al* 2012, Jacquemet *et al* 2013) and phosphorylation (Paul 2014, Robertson 2014) signatures associated with integrin activation and signalling at sites of integrin-mediated adhesions is clearly now well-established. Recently this strategy has enabled characterisation of distinct, cell-type specific extracellular matrix (ECM) environments that modulate adhesion receptor crosstalk, matrix assembly and organisation within the renal glomerulus (Byron *et al* 2014, Lennon *et al* 2014) and to define novel integrin-associated multi-protein complexes isolated from mesenchymal stem cells (Ajeian *et al* 2016). Such investigations will be of growing importance given the emerging aetiological significance of the cellular microenvironment and ECM constitution as regulators of disease outcome in a variety of pathologies, including cancer (Lu *et al* 2012, Pickup *et al* 2014).

Byron and Frame (2016) recently reviewed the significance and impact that this strategy for proteomic analysis of integrin-mediated adhesion complexes has had on expanding our previously limited understanding of protein-protein-interaction (PPI) networks and associated signalling induction downstream of focal adhesion (FA) assembly. Indeed, Eke and Cordes (2015) highlight the importance of FA-mediated signalling as a driver of therapeutic resistance in cancer within the context of both cell adhesion-mediated drug resistance (CAMDR) and cell adhesion-mediated radiotherapy-resistance (CAMRR). The authors acknowledge that due to their upstream localisation and role as nexūs integrating adhesion- and growth factor (GF)-mediated signals within the complex network of ECM-derived signalling, FA appear a logical place to initiate therapeutic intervention.

However, citing their previous studies characterising signalling events associated with chemoresistance to the anti-EGFR agent cetuximab (Eke *et al* 2013a, Eke *et al* 2013b), Eke and Cordes highlight network plasticity, complexity and redundancy as confounding factors limiting the efficacy of single-agent therapeutic strategies. Instead, the authors postulate that multi-agent/multi-modal treatment regimens may provide a more effective means of administering targeted therapies; limiting the capacity for resistance to develop if network redundancy and by-pass mechanisms are simultaneously targeted.

Given the established cross-talk between integrin receptor classes and receptor tyrosine kinase (RTK) moieties, the possibility of establishing effective multi—modal cancer therapies targeting known tumourigenic growth factor receptors (GFRs) in tandem with modulation of synergistic integrin signalling (and ergo function), appears a logical area to focus integrin-based cancer therapy research (Jin and Varner 2004, Desgrosellier and Cheresh 2010). For example, functional abrogation of integrin $\alpha_v\beta_6$ using the therapeutic inhibitory antibody 264RAD *(Oncology iMED, AstraZeneca UK Ltd)* has already been shown to potentiate trastuzumab efficacy in an *in vivo* murine model of HER-2 positive BrCa (Moore *et al* 2014).

Interestingly, Lesniak *et al* (2009) demonstrated that integrin β_1 expression is an independent prognostic factor for tumour progression in human epidermal growth factor-2 (HER-2) positive metastatic breast cancer (MBC) patients treated with trastuzumab-based therapy. The authors immunohistochemically evaluated integrin β_1 expression in a cohort of HER-2 positive MBC patients, of whom 83 had received trastuzumab-based therapy and 30 had received chemotherapy without

trastuzumab (vinorelbine, capecitabine or docetaxel). Kaplan-Meier analysis revealed that integrin β_1 overexpression showed a strong and significant correlation with short time-to-tumour progression (TTP) in the trastuzumab cohort *(HR 2.04; 95% CI 1.02 – 3.4; p=0.0081)* but not the treated without trastuzumab cohort *(p=0.75)*.

To define the mechanism by which integrin β_1 overexpression accelerates TTP in trastuzumab treated MBC patients, Lesniak *et al* (2013) performed *in vitro* studies using the trastuzumab-sensitive, HER-2 positive, integrin β_1 low/null SKBR-3 cell line transfected with a Flag-tagged human integrin β_1-subunit vector. In comparison with untransfected SKBR-3 cells and cells transfected with empty vector, expression of integrin β_1 was associated with increased phosphorylation of Akt^{S473} and ERK1/2. Interestingly, the authors also demonstrated that functional abrogation of integrin β_1 using a blocking monoclonal antibody (clone AIIB2) in tandem with trastuzumab therapy, decreased Akt^{S473} and ERK1/2 phosphorylation and also inhibited cell proliferation and colony forming ability *in vitro*. Lesniak and colleagues concluded that integrin β_1 is a driver of chemoresistance, facilitating circumvention of the anti-proliferative effects of trastuzumab via integrin β_1–mediated increased phosphorylation of Akt^{S473} and ERK1/2.

Collectively, this research points to the potential clinical benefit of combination therapy strategies exploiting both established molecular targets (such as HER-2) and novel regulators of specific resistance mechanisms (for example integrin β_1). Therefore, exploration of integrin $\alpha_v\beta_6$–mediated adhesion complex signalling in tumour establishment, progression – and even chemotherapeutic resistance – may be of similar value to improve outcomes in BrCa patients.

The concept of integrin receptor-ligand specificity (Hynes 2002, Kapp *et al* 2017) was exploited in order to modulate the species of integrin engaged upon different cognate ligands designed to simulate distinct, physiologically relevant integrin-specific 2-dimensional (2D) adhesion environments. Since ligand-engagement induces integrin activation, the experiments outlined in this chapter were intended to provide valuable insight into the nature of the adhesion environment *(adhesome)* assembled downstream of activated integrin $\alpha_v\beta_6$ engaged in adhesion to its cognate LAP ligand *(β_6-adhesome)*.

overview of key findings

To characterise the molecular nature of an integrin $\alpha_v\beta_6$–dependent adhesion environment *("β_6-adhesome")* a 2D-E strategy (Figure 5.1.1A) first described by Humphries *et al* (2009) was modified to specifically address the research intention to specifically characterise a ligand-engaged integrin $\alpha_v\beta_6$–dependent adhesion environment (Figure 5.1.1B).

Owing to loss of reliably stable phenotypes amongst variants comprising the MCF-10 isogenic cell line series (outlined in Chapter IV: *Results part II*), the use of this *in vitro* model of breast tumourigenesis and disease progression was excluded from future studies. Therefore, a panel of known integrin $\alpha_v\beta_6$-positive BrCa lines comprising: the triple negative BT-20, SUM159 and MDA-MB-468; and triple positive BT-474 cell lines, were screened by flow cytometry (FCM) to evaluate stability of endogenous cell surface integrin $\alpha_v\beta_6$ expression and identify a cell line suitable for 2D-E/LC-MS/MS-experimental work-up (Figure 5.1.2).

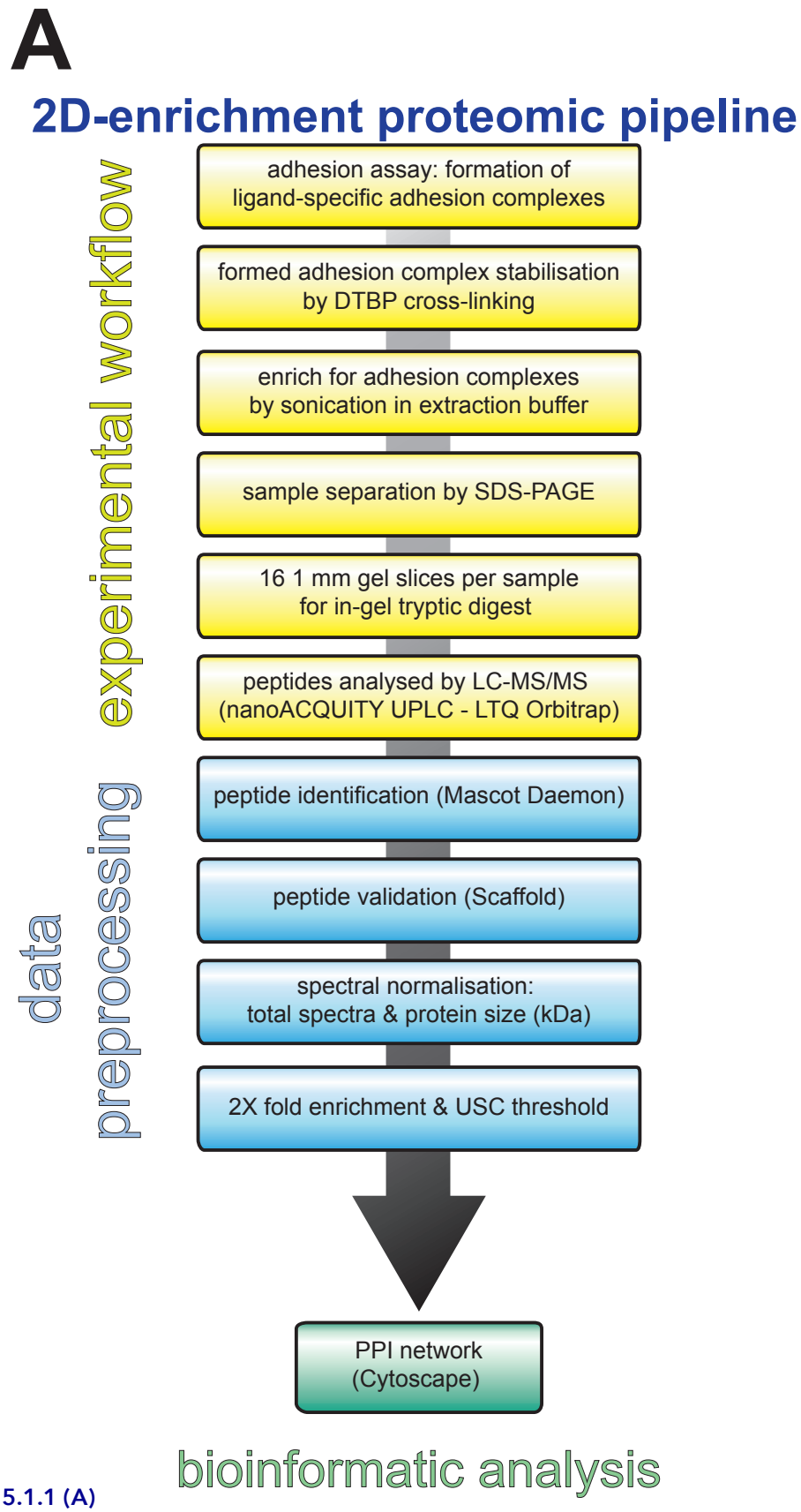

Figure 5.1.1 (A)
Proteomic pipeline for the definition of a ligand-engaged integrin $\alpha_v\beta_6$-dependent adhesion environment ("β_6-adhesome") using a 2D-enrichment adhesion assay coupled to label-free LC-MS/MS interrogation

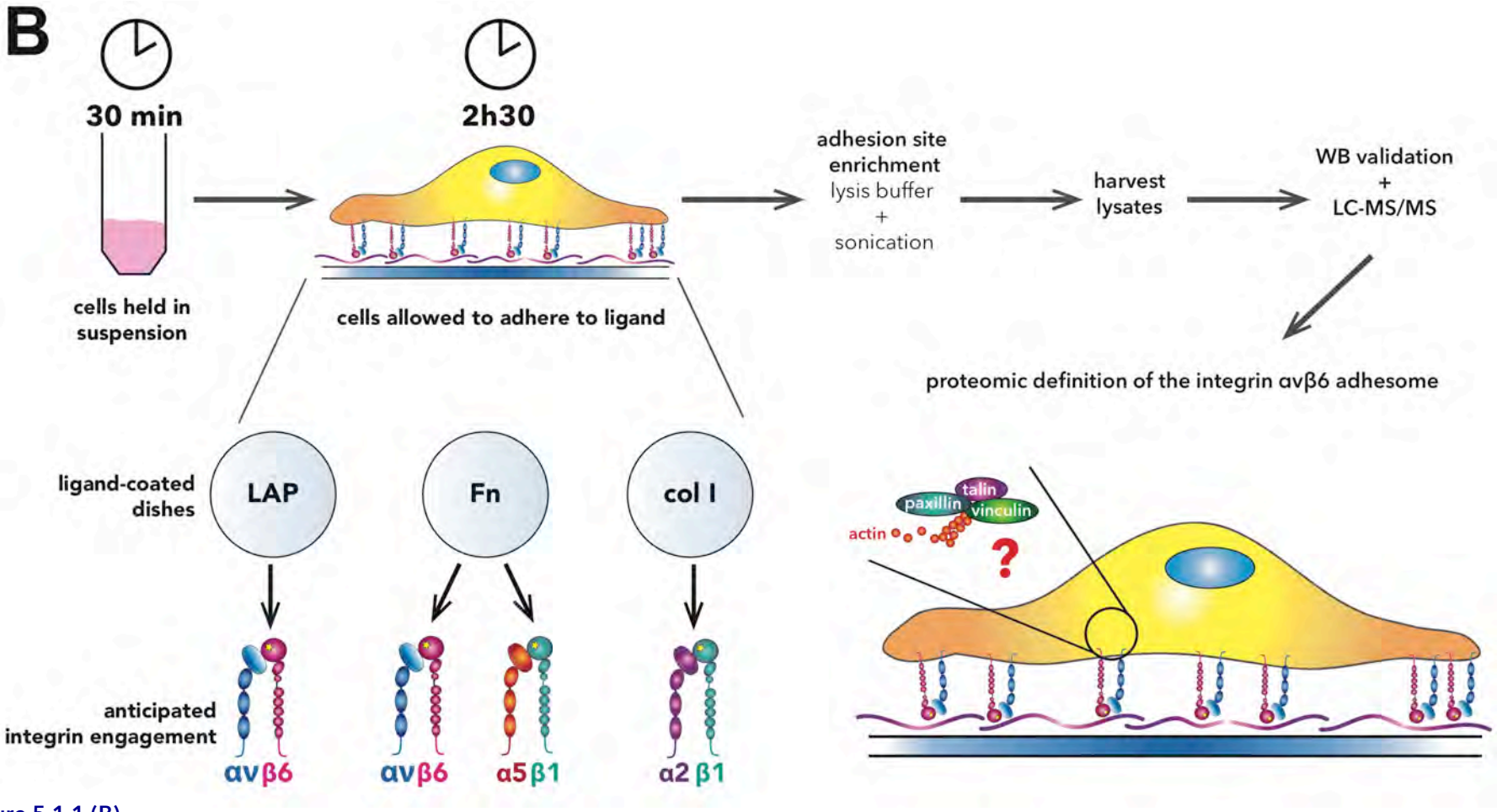

Figure 5.1.1 (B)
Schematic overview of the 2D-enrichment protocol to isolate ligand-engaged integrin $\alpha_v\beta_6$-mediated adhesion complexes for proteomic dissection of the β_6-adhesome

Figure 5.1.1
Summary of the proteomic pipeline and schematic overview of the 2D-enrichment protocol used to isolate ligand-engaged integrin $\alpha_v\beta_6$–mediated adhesion complexes for proteomic definition of the β_6-adhesome

(5.1.1 A) A proteomics pipeline based upon that described by Humphries *et al* (2009) and Byron *et al* (2011) was modified for the purposes of defining a ligand-engaged integrin $\alpha_v\beta_6$ adhesion environment (β_6-adhesome) by label-free tandem mass spectrometry (LC-MS/MS). **(5.1.1 B)** A method permitting 2D-enrichment of integrin $\alpha_v\beta_6$–mediated adhesion complexes ready for isolation and downstream interrogation by LC-MS/MS was followed. Briefly, adherent cells are trypsinised, washed to remove residual trypsin and held in suspension in complete media for 30 min under standard culture conditions to permit internalisation of surface integrin receptor pools and dissociation from cognate ligand (if still bound), prior to assay. Next, cells are left to adhere for 2h30 (again under standard culture conditions) to ligand coated 10 cm culture dishes (human recombinant **LAP**: 0.5 µg ml^{-1}; bovine **Fn**: 10 µg ml^{-1}; rat tail **Col I**: µg ml^{-1}). Three known integrin cognate ligands were used to promote differential integrin receptor species engagement to compare differences, or indeed similarities, between integrin receptor-specific adhesion environments. The process of adhesion in 2D was checked by phase contrast microscopy throughout the course of assay and confirmed at the 2h30 end-point. Adhesion complexes were enriched and isolated by sonication in the presence of a 2D-E extraction buffer (prepared in-house). Adhesion complexes were then manually harvested by scraping in 5X Lysis Buffer (prepared in-house) ready for validation by Western blot and interrogation by LC-MS/MS. A detailed description of the 2D-E protocol and reagents/buffers used is provided in the relevant Material & Methods section.

Given the woeful lack of therapeutic molecular targets in TNBC (Herold and Anders 2013), it was deemed pertinent to focus the remaining body of research presented here on TNBC; with the intent of identifying putative candidates for novel therapeutic strategies to improve patient outcomes. The BT-20 TNBC cell line was selected due to its stable, high endogenous integrin $\alpha_v\beta_6$ cell surface expression (Figure 5.1.2A), expedient tissue culture and triple negative receptor status. Functional abrogation of the integrin $\alpha_v\beta_6$ receptor using the blocking antibody 53A2 abolished binding of LAP, confirming that the integrin $\alpha_v\beta_6$ is the predominant LAP receptor in BT-20 cells (Figure 5.1.2C).

With LAP specificity for integrin $\alpha_v\beta_6$ validated, 2D-enrichment (2D-E) experiments were performed to isolate ligand-specific adhesion complexes formed on latency-associated peptide of TGF-β1 (**LAP**), fibronectin (**Fn**) and collagen type I (**Col I**) for proteomic interrogation. Adhesion to ligand was confirmed by phase contrast microscopy and evaluated by confocal immunofluorescence (IMF) microscopy; isolated adhesion complexes for proteomic analysis were validated by Western blot (WB) (Figure 5.2).

The integrin $\alpha_v\beta_6$ was reproducibly enriched during adhesion to its cognate ligand LAP across four biological replicate 2D-E experiments. Engagement of other integrin species on the Fn and Col I conditions could not be reliably validated by WB. Technical validation markers to confirm specificity of technique were identified by WB with varying success. The proteins talin and vinculin associated with integrin-mediated adhesion complexes (Hirata *et al* 2014, Atherton *et al* 2015, Atherton *et al* 2016) were observed on the LAP condition only. The pro-apoptotic mitochondrial membrane protein Bak, excluded from integrin adhesion complexes was used as a non-specific marker to confirm purity of adhesion enrichment as previously described (Paul 2014, Robertson 2014).

Adhesion complex-enriched samples from the four-biological replicate 2D-E experiments were subject to in-gel tryptic digest to generate peptides for label-free LC-MS/MS analysis *(Institute of Translational Medicine Mass Spectrometry Core Facility, Centre for Molecular Physiology, University of Liverpool)*. Following proteomic analysis, peptides were identified, validated and quantified by unweighted spectral counting using Mascot Daemon v2.2.2 *(Matrix Science©)* and

Scaffold™ v4.3.2 *(Proteome Software© Inc, USA)* open source software programmes. A total of 24 410 spectra were identified, with sequences mapping to 196 proteins.

Protein-protein-interaction (PPI) networks of proteins showing a two-fold or greater (≤2-fold) enrichment to LAP in comparison with Fn (Figure 5.3A) or Col I (Figure 5.3B) were mapped in Cytoscape v3.1.1 *(Cytoscape Consortium©, National Resource for Network Biology)* using a literature-curated database of the human adhesome comprising entries curated by Protein Interaction Network Analysis *(PINA, 10th December 2012)* (Wu *et al* 2009, Cowley *et al* 2012, Soteriou *et al* 2013) with adaptations to encompass the Integrin Adhesome (Zaidel-Bar *et al* 2007) and Matrisome Project (Hynes and Naba 2012, Naba *et al* 2012a, Naba *et al* 2012b). Based on these PPI networks, 7 candidate proteins of interest (Table 5.1) deemed putative molecular regulators of a LAP-ligand-engaged integrin $\alpha_v\beta_6$–dependent adhesion environment *(β_6-adhesome)* characterised in the BT-20 TNBC cell line were selected for functional validation based on a combination of existing GO entries, available peer-reviewed literature and unpublished in-house data.

Seeking to investigate the broader biological relevance of the LAP-engaged *β_6-adhesome* in TNBC, it was intended to conduct further enrichment experiments in additional TNBC cell lines for comparison. A single 2D-E experiment comprising 2 technical replicates was performed using the MDA-MB-468 TNBC cell line and used to generate a PPI network of LAP versus Fn enrichment which interestingly revealed the epidermal growth factor receptor (EGFR) is uniquely enriched to integrin $\alpha_v\beta_6$ mediated adhesions to LAP in comparison with Fn-induced adhesions in the MDA-MB-468 cell line (Figure 5.4).

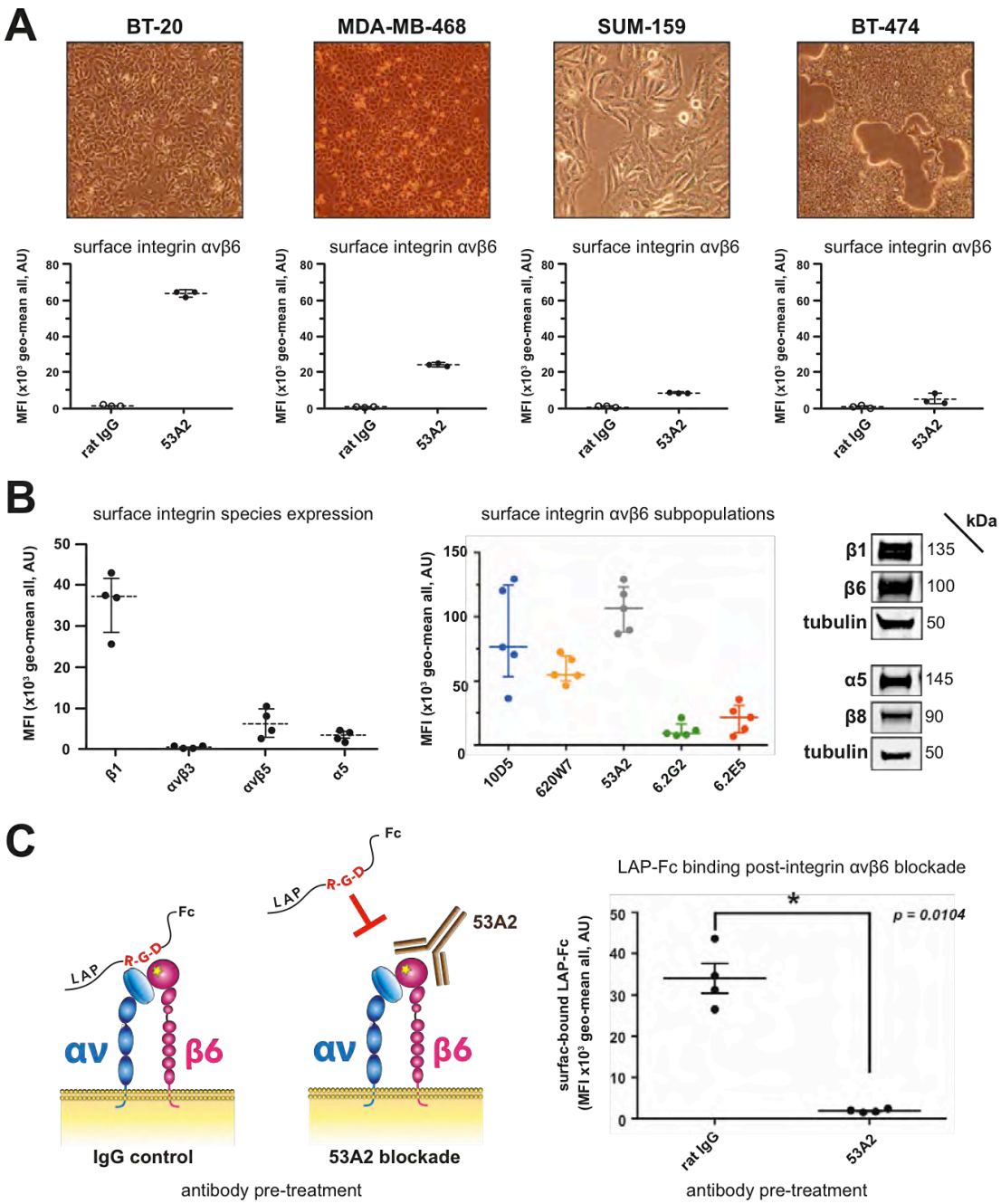

Figure 5.1.2
2D-enrichment experimental work up: Cell line selection and validation of LAP ligand specificity for the integrin $\alpha_v\beta_6$

Figure 5.1.2
2D-enrichment experimental work up: Cell line selection and validation of LAP ligand specificity for the integrin $\alpha_v\beta_6$

(5.1.2 A) A panel of known integrin $\alpha_v\beta_6$ positive TNBC cell lines were screened to identify a cell line with stable, endogenous high integrin $\alpha_v\beta_6$ expression suitable 2D-E/LC-MS/MS definition of a ligand-engaged integrin $\alpha_v\beta_6$–mediated adhesion environment. Cell lines were screened by flow cytometry using antibody clone 53A2 (10 µg ml^{-1}, CR-UK) to demonstrate cell surface abundance of integrin $\alpha_v\beta_6$; an isotype matched rat IgG antibody was also included in the screen as a negative control (n=3; three biological repeats). **(5.1.2 B)** Owing to reliability of culture and stably high integrin $\alpha_v\beta_6$ expression, the BT-20 cell line was selected for experimental work up for 2D-E proteomic interrogation. The BT-20 cell line was screened by flow cytometry for surface expression of other RGD-binding integrin species reported as putative LAP-ligand cognate receptors including: **β_1** (clone P4C10, 10 µg ml^{-1}, in-house), **$\alpha_v\beta_3$** (clone LM609, 10 µg ml^{-1}, MAB1976Z, Merck Millipore), **$\alpha_v\beta_5$** (clone P1F6, 10 µg ml^{-1}, MAB1961Z, Merck Millipore) and **α_5** (clone P1D6, 10 µg ml^{-1}, MAB1956Z, Merck Millipore). Four biological repeats were performed (n=4). In addition, the BT-20 cell line was also screened for integrin $\alpha_v\beta_6$ receptor populations using the panel of anti-integrin $\alpha_v\beta_6$ antibodies (previously described). Five biological repeats (n=5) were performed to assess stability of expression. Where suitable antibodies were available, integrin species expression was also confirmed by Western blot: **β_1** (clone EP1041Y, 2 µg ml^{-1}, ab52971, AbCam), **β_6** (c-19, 10 µg ml^{-1}, sc-6632, SantaCruz Biotechnology), **α_5** (1 µg ml^{-1}, 4705S, Cell Signalling Technology) and **β_8** (5 µg ml^{-1}, ab80673, AbCam). β-tubulin was used as a loading control (1 µg ml^{-1}, ab21057, AbCam). Finally, to confirm integrin $\alpha_v\beta_6$ specificity for LAP-engagement in the BT-20 cell line, functional abrogation studies using the blocking antibody 53A2 were performed **(5.1.2 C)**. Cells were treated with either antibody 53A2 (40 µg ml^{-1}, CR-UK) or non-immune rat IgG negative control antibody (40 µg ml^{-1}, ab37361, AbCam) for 30 min to abrogate surface integrin $\alpha_v\beta_6$. Next, cells were incubated with an Fc-tagged LAP ligand for 10 min and washed prior to evaluation of surface bound LAP-Fc abundance by flow cytometry using an anti-Fc antibody (clone ABM121, 10 µg ml^{-1}, ab113636, AbCam). Across four biological repeats, functional abrogation of integrin $\alpha_v\beta_6$ significantly abolished binding of LAP ligand in comparison with the rat IgG negative control treatment (one-tailed 2-sample t-test; $p<0.05$, $p=0.0104$) confirming LAP ligand specificity for the integrin $\alpha_v\beta_6$ receptor in the BT-20 cell line. Flow cytometry experiments were performed on the BD LSRFortessa™ equipped with FACSDiva™ v8.0 acquisition software to gate 10^4 events per sample and analysed using FlowJo® to obtain geoMean MFI values. Propidium iodide cell viability indicator (10 µg ml^{-1}) was used to define gating strategy to ensure data were obtained on live cells only. Each plot on flow cytometry graphs show mean values of technical triplicates performed for each biological replicate. Mean of the biological repeats are shown with error bars indicating s.d. Western blotting was performed at the University of Liverpool using the LI-COR© Odyssey®Sa System (as described in detail in the relevant Materials & Methods section); 20 ng protein per well was loaded. Statistical analyses were performed using GraphPad Prism® 5.0b for MacOSX (GraphPad Software Inc). **Abbreviations: AU** – arbitrary units.

5.1 cell line selection and proof of concept for an adhesion assay to define an integrin $\alpha_v\beta_6$–dependent adhesion environment

The lack of defined, molecular targets suitable for therapeutic intervention in TNBC is a known significant limiting factor and impediment to patient outcomes burdened with this disease (Herold and Anders 2013). Therefore, the prescient need to augment the existing knowledge base regarding the aetiopathology of TNBC informed the decision to focus this initial characterisation of the *"β_6-adhesome"* within the context of TNBC.

A panel of BrCa cell lines comprising: the triple negative BT-20, MDA-MB-468 and SUM159 cell lines, together with the triple positive BT-474 cell line, were screened for cell surface integrin $\alpha_v\beta_6$ expression by FCM; stability of morphological phenotype was monitored in culture by phase contrast microscopy (Figure 5.1.2A). The antibody clone 53A2 (CR-UK) was used to detect total cell surface integrin $\alpha_v\beta_6$ in an activation-state/conformation-independent manner (as previously outlined in Chapter 3: *results part I*). Three biological repeat screens, each comprising intra-assay technical triplicates, were performed. Detected geometric mean fluorescence intensity (geoMean MFI, AU) values (normalised against an isotype, species-matched negative rat IgG control antibody) served as a read-out for surface integrin $\alpha_v\beta_6$ expression (as previously described).

The BT-20 cell line exhibited consistently high and stable endogenous cell surface integrin $\alpha_v\beta_6$ expression, which remained in the order of ~6 $x10^4$ geoMeanMFI, AU across three biological replicates. Therefore, the BT-20 cell line was selected for 2D-E assays given its stably high, endogenous integrin $\alpha_v\beta_6$ expression and relatively expedient culture to yield sufficient cell volume for assay.

In order to specifically engage integrin $\alpha_v\beta_6$–mediated adhesion complexes, it was hypothesised that use of the known integrin $\alpha_v\beta_6$ cognate ligand LAP (Munger *et al* 1999, Thomas *et al* 2002) would elicit the desired specific integrin $\alpha_v\beta_6$ receptor engagement and thus, β_6–mediated adhesion complex formation on 2D-immobilised LAP. However, an emerging body of literature, reviewed by Munger and Sheppard (2011), suggest that other RGD integrin receptor species may interact with LAP inducing activation of ECM-bound latent TGF-β1 by mechanical

traction; the integrins $\alpha_v\beta_3$, $\alpha_v\beta_5$ (Wipff *et al* 2007) and $\alpha_v\beta_8$ (Mu *et al* 2008) are also reported to bind LAP and mediate TGF- β1 activation.

Therefore, to establish the specificity of integrin $\alpha_v\beta_6$ for LAP-ligand, the BT-20 cell line was screened by FCM (Figure 5.1.2B) for integrin species reported to bind LAP (integrins $\alpha_v\beta_3$, $\alpha_v\beta_5$); in addition to the RGD-binding integrin β_1-subunit and α_5-subunit, known to engage the comparator ligand-specific adhesion complexes that would be elicited during adhesion to Fn (integrins $\alpha_v\beta_3$, $\alpha_5\beta_1$) and Col I (integrins $\alpha_1\beta_1$, $\alpha_2\beta_1$). Four biological replicates each comprising intra-assay technical triplicates were performed.

Integrin $\alpha_v\beta_6$ cell-surface subpopulations were also characterised by flow cytometry using a panel of anti-integrin $\alpha_v\beta_6$ antibodies (previously described). Here, five biological repeats were performed, again with each comprising intra-assay technical triplicates. Finally, whole cell expression of the integrin subunits: α_5, β_1, β_6 and β_8, were evaluated by WB.

It was found by FCM that the BT-20 cell line expressed relatively high levels ($\bar{x} \approx 38 \times 10^3$ geoMean MFI, AU) of cell surface integrin β_1, with marked whole cell integrin β_1 expression confirmed by WB. Interestingly, integrin α_5 surface abundance was low ($\bar{x} \approx 5 \times 10^3$ geoMean MFI, AU) in comparison with whole cell abundance demonstrated by WB.

Cell surface abundance of integrin $\alpha_v\beta_3$ was negligible ($\bar{x} \leq 0.1 \times 10^3$ geoMean MFI, AU) but integrin $\alpha_v\beta_5$ was moderately expressed ($\bar{x} \approx 65 \times 10^3$ geoMean MFI, AU). Whole cell expression of the integrins β_3 and β_5 could not be confirmed by WB as application-appropriate antibodies were unavailable. Integrin β_8 whole cell expression was confirmed by WB only using a commercially available antibody tested in-house (Supplementary Information S5.1); cell surface screening could not be performed, again owing to a lack of application-appropriate antibodies.

Screening of integrin $\alpha_v\beta_6$ subpopulations revealed high cell surface expression of total integrin $\alpha_v\beta_6$ recognised by antibodies 10D5 ($\bar{x} \approx 75 \times 10^3$ geoMean MFI, AU), 53A2 ($\bar{x} \approx 110 \times 10^3$ geoMean MFI, AU) and 620W7 ($\bar{x} \approx 60 \times 10^3$ geoMean MFI,

AU). As anticipated, active integrin $\alpha_v\beta_6$ conformers recognised by antibodies 6.2E5 and 6.2G2 were present at lower levels than total integrin $\alpha_v\beta_6$ (**6.2E5**: $\bar{x} \approx 25$ x 10^3 geoMean MFI, AU; **6.2G2:** $\bar{x} \approx 10$ x 10^3 geoMean MFI, AU). Whole cell abundance of integrin β_6 was also confirmed by WB.

Since the presence of non-β_6 integrin species reported to engage LAP (notably $\alpha_v\beta_5$ and $\alpha_v\beta_8$) were detected in the BT-20 cell line, it was deemed pertinent to test the specificity of LAP for integrin $\alpha_v\beta_6$ engagement before commencing 2D-E assays (Figure 5.2C). Functional abrogation of cell surface integrin $\alpha_v\beta_6$ using the inhibitory antibody clone 53A2 significantly abolished binding of a human IgG (Fc')-tagged LAP ligand in comparison with an isotype-matched rat IgG negative antibody control treatment (one-tailed 2-sample t-test; p=0.0104). This demonstrated that integrin $\alpha_v\beta_6$ is the predominant LAP receptor in BT-20 cells, validating the use of LAP ligand to specifically target integrin $\alpha_v\beta_6$–mediated adhesion complexes to define a β_6-adhesome using the TNBC BT-20 cell line.

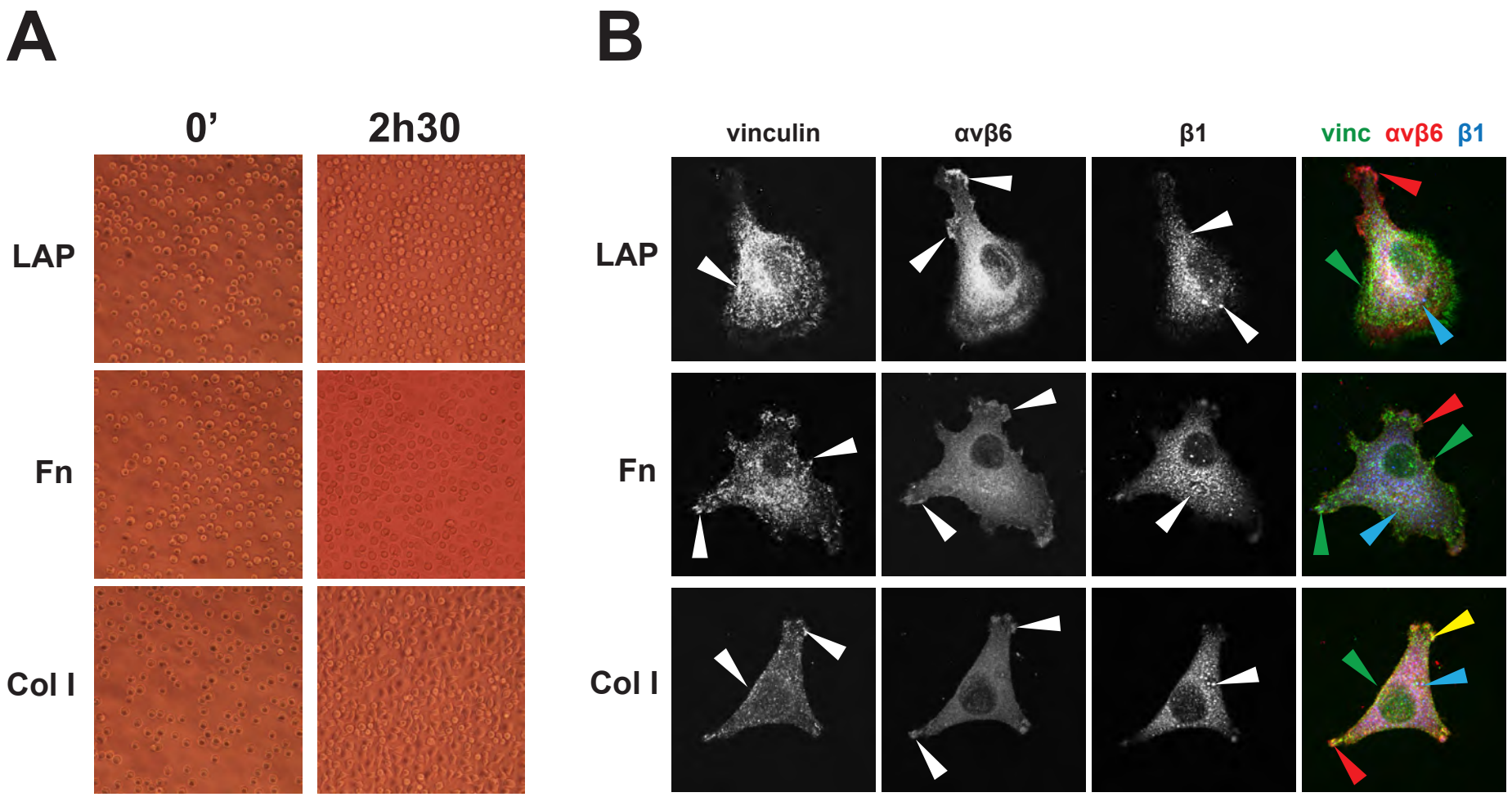

Figure 5.2 (A & B)
Technical validation of 2D-enrichment assays performed to enrich, isolate and extract integrin $\alpha_v\beta_6$-mediated adhesion complexes ready for label-free LC-MS/MS proteomic interrogation to define an integrin $\alpha_v\beta_6$ adhesome: Evaluation by microscopy methods

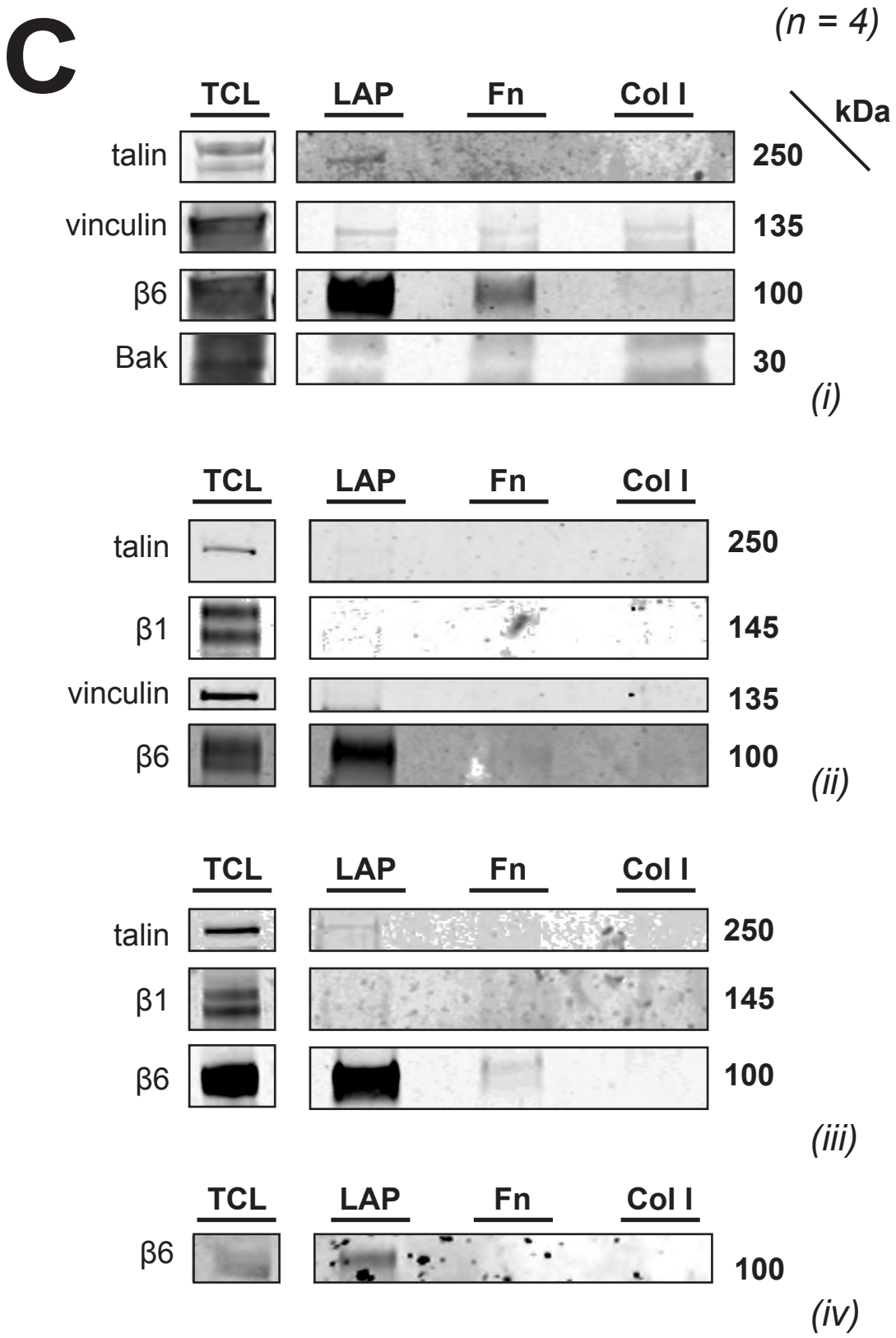

Figure 5.2 (C)
Technical validation of 2D-enrichment assays performed to enrich, isolate and extract integrin $\alpha_v\beta_6$-mediated adhesion complexes ready for label-free LC-MS/MS proteomic interrogation to define an integrin $\alpha_v\beta_6$ adhesome: Evaluation by Western blotting

Figure 5.2

Technical validation of 2D-enrichment assays performed to enrich, isolate and extract integrin $\alpha_v\beta_6$-mediated adhesion complexes ready for label-free LC-MS/MS proteomic interrogation to define an integrin $\alpha_v\beta_6$ adhesome

Adhesion assays were performed using BT-20 cells adhering in 2D under standard culture conditions to the integrin cognate ligands LAP (**LAP** - 0.5 µg ml^{-1}, L3408, Sigma Aldrich), fibronectin (**Fn** - 10 µg ml^{-1}, F1141, Sigma Aldrich) & collagen I (**Col I** - 10 µg ml^{-1}, 354236, Corning®) (four biological repeats were performed; n=4). **(5.2 A)** Adherence was checked by phase contrast microscopy (OLYMPUS IMT-2, Olympus® Corp) during the adhesion assay. Representative images of cell morphology at the start (**0'**) and end of assay (**2h30**) are shown. Although adhered, BT-20 cells binding to LAP maintained a rounded morphology suggesting ligand adhesion in the absence of cell spreading on ligand. This contrasted with the flattened appearance of BT-20 cells adhered to Fn and Col I where it appeared cells had both adhered to and spread upon ligand. **(5.2 B)** Morphology of adhesion complexes and subcellular distribution of the integrins $\alpha_v\beta_6$ (red arrows) and integrin β_1 (blue arrows) together with the adhesion complex-associated protein vinculin (green arrows), were evaluated by permeabilised IMF. Proteins of interest were labelled accordingly: integrin $\alpha_v\beta_6$ (antibody clone 620W7, 10 µg ml^{-1}, CR-UK), integrin β_1 (antibody clone EP1041Y, 10 µg ml^{-1}, ab52971, AbCam) in addition to the adhesion complex protein, vinculin (antibody clone hVIN-1, 10 µg ml^{-1}, ab11194, AbCam). The integrin $\alpha_v\beta_6$ was seen to localise at the cell periphery across all ligand treatments. Curiously, the subcellular localisation of integrin β_1 showed a marked intracellular, vesicular distribution pattern, even on cells adhered to known integrin β_1 cognate ligands Fn and Col I. Vinculin clusters at the cell periphery were observed across ligand treatments, but appeared most marked in BT-20 cells adhered to Fn. **(5.2 C)** Following stabilisation of formed adhesion complexes by DTBP cross-linking and adhesion complex enrichment by sonication in 2D-extraction buffer, lysates were prepared for LC-MS/MS interrogation and evaluated by WB for integrin engagement and technical validation markers. Across four biological replicates, the integrin $\alpha_v\beta_6$ was successfully and reproducibly enriched in BT-20 cells adhered to LAP. Integrin $\alpha_v\beta_6$ enrichment was also observed for cells adhered to Fn, but to a visibly lesser extent than on LAP. No enrichment for integrin $\alpha_v\beta_6$ was observed on cells exposed to Col I. Markers to validate adhesion complex formation (FA proteins talin and vinculin) were demonstrated with varying success. A protein not known to associate with adhesion complexes (the mitochondrial protein Bak) was used as an additional control to demonstrate specificity of adhesion complex enrichment. The integrin β_1 was not detected by Western blotting. Antibodies were used as follows: **$\alpha_v\beta_6$**: c-19 (0.2 µg ml^{-1}, sc-6632, SantaCruz Biotech); **β_1**: EP1041Y (2 µg ml^{-1}, ab52971, AbCam); **Bak**: D4E4 (0.2 µg ml^{-1}, 12105S, Cell Signalling Technology); **talin**: c-20 (0.2 µg ml^{-1}, sc-7534, SantaCruz Biotech); **vinculin**: hVIN-1 (0.2 µg ml^{-1}, ab11194, AbCam). All experiments were performed at the Institute for Translational Medicine, University of Liverpool. Confocal IMF microscopy was undertaken using the 3i© Marianas™ microscope equipped with SlideBook™ 5 image analysis software (both Intelligent Imaging Innovations (3i)© Inc). Western blotting was performed using the LI-COR® ODYSSEY-Sa© system.

5.2 technical validation of 2D-E/LC-MS/MS experiments to proteomically define the β_6-adhesome

Having established the utility of LAP to specifically bait the integrin $\alpha_v\beta_6$ receptor in the BT-20 cell line, four biological replicate 2D-E adhesion assays were performed on immobilised ligand substrates to preferentially engage specific integrin species accordingly: **LAP:** – $\alpha_v\beta_6$, **Fn:** – $\alpha_5\beta_1$ / $\alpha_v\beta_6$ and **Col I:** – $\alpha_1\beta_1$ / $\alpha_2\beta_1$.

Reyes *et al* (2008) highlight the need to extend characterisation of ECM ligand-integrin interactions beyond single ligand-receptor analyses (which have been the focus to date) in order to reflect ECM complexity. Therefore, it was hoped that formation and analysis of Fn and Col I ligand-specific integrin adhesion complexes would provide physiologically relevant comparators when defining the LAP ligand-engaged, integrin $\alpha_v\beta_6$–dependent adhesion environment.

Cell morphology and successful adhesion to substrate ligand was confirmed by phase contrast microscopy during the adhesion assays (Figure 5.2A). Adhesion assays were stopped at 2h30 in order to isolate mature adhesion complexes as opposed to nascent adhesive structures; such as the spreading initiation centres first described by de Hoog *et al* (2004), and later reported by Serrels *et al* (2010) to modulate cancer cell polarity.

Successful cell adherence was again confirmed by phase contrast microscopy following initial wash steps at the assay end-point prior to adhesion complex enrichment by sonication in 2D-E extraction buffer. It was noted that BT-20 cells adhered to LAP maintained a rounded morphology (indicated by plasmalemma refringence upon phase contrast microscopy review) even at the 2h30 assay end-point; suggesting cellular adhesion with minimal spreading upon LAP ligand. This contrasted with the flattened appearance of BT-20 cells adhered to Fn and Col I that was reminiscent of an established epithelial monolayer at the 2h30 end-point.

Adhesion complex morphology was also evaluated by permeabilised confocal IMF (Figure 5.3B) to evaluate subcellular localisation of the integrins $\alpha_v\beta_6$ and β_1, alongside the known integrin adhesion-complex protein vinculin (Humphries *et al*

2007, Ziegler *et al* 2008, Carisey *et al* 2013, Hirata *et al* 2014, Atherton *et al* 2015, Atherton *et al* 2016) during adhesion to LAP, Fn and Col I ligands.

Carisey *et al* (2013) demonstrated that vinculin modulates transmission of ECM-derived mechanotensile signals into the actomyosin cytoskeletal machinery via its association with integrin-talin complexes and F-actin. The authors showed that vinculin interaction with integrin-talin complexes is necessary for both recruitment and release of core FA proteins including: FAK, ILK, parvin, p130Cas, zyxin and tensin. Therefore, given its established role in formation of integrin-mediated adhesion complexes, vinculin colocalisation with integrin receptors visible by IMF was deemed a suitable marker of formed adhesion complexes.

Vinculin was seen to localise at the cell periphery, exhibiting marked clusters of immunopositivity believed to be adhesion complexes. The canonical, published pattern of vinculin immunopositivty associated with adhesion complex formation (Humphries *et al* 2007, Kanchanawong *et al* 2010, Carisey *et al* 2013) was most notable in BT-20 cells adhered to immobilised Fn. These adhesion complex-associated clusters of vinculin immunopositivity were observed to a lesser extent in BT-20 cells spreading on LAP and Col I. This may indicate fewer, or less mature, adhesion complexes were formed on these immobilised substrate ligands compared to Fn.

However, it is acknowledged that the majority of literature dissecting integrin-mediated adhesion complexes focuses on the integrin $\alpha_v\beta_3$ receptor adhering to Fn in fibroblasts, or integrin $\alpha_5\beta_1$–mediated adhesions to Fn in monocytes. Therefore, it may be that the TNBC BT-20 cell line, although basal in molecular subtype (Chavez *et al* 2010), may inherently form fewer and or/smaller integrin-mediated complexes on substrate ligand compared to those published for integrin $\alpha_v\beta_3$– and integrin $\alpha_5\beta_1$–mediated adhesions formed on Fn in fibroblasts and monocytes respectively.

Therefore, the variation in vinculin appearance observed in IMF results shown here may not necessarily indicate poor adhesion complex assembly. Instead it may be attributable to ligand and cell-type specific adhesion complex formation; and so remain experimentally valid for the purposes of the specific research aim to characterise the β_6-adhesome.

It had been intended that the ligand substrates Fn and Col I would elicit integrin β_1–mediated adhesions. It was anticipated that Fn would partially engage β_1–species in addition to the integrin $\alpha_v\beta_6$ that was first reported to engage Fn by Busk *et al* (1992); Col I was expected to exclusively engage integrin β_1 moieties (Leitinger 2011).

However, IMF revealed a distinct intracellular, vesicular pattern of immunopositivity for β_1 integrin on all ligand substrates. The absence of integrin β_1 at the cell periphery and lack of co-localisation at vinculin-rich structures (presumed to be adhesion complexes) in BT-20 cells adhered to Fn, suggested that β_1 species were not mediating adhesion to Fn as expected. Integrin β_1 colocalisation with vinculin, and curiously with integrin $\alpha_v\beta_6$, was only observed on Col I substrate ligand, but appeared limited.

An activation/conformation-independent anti-integrin β_1 antibody was used to label integrin β_1 for IMF evaluation of adhesion complexes. It may have been pertinent to use an activation-state specific antibody that does not bind the heterodimer cleft, such as clone 9EG7 (Byron *et al* 2009), in order to detect activated (presumed ligand-engaged) integrin β_1 without eliciting ligand-mimetic antibody activation that would confound immobilised substrate engagement studies.

The integrin $\alpha_v\beta_6$ (demonstrated by clone 620W7; an antibody recognising both mature fully-glycosylated and immature partially-glycosylated integrin $\alpha_v\beta_6$ receptors) was seen to cluster at the periphery of cells adhering to LAP and Fn, suggesting integrin $\alpha_v\beta_6$ cognate ligand-engagement as anticipated. On all ligand substrates, integrin $\alpha_v\beta_6$ appeared to cluster at vinculin-rich lamellipodia-like membrane protrusions. The observation of integrin $\alpha_v\beta_6$ co-localisation with vinculin and integrin β_1 on Col I was curious, given that the integrin $\alpha_v\beta_6$ is not known to engage this ligand.

It may be that integrin $\alpha_v\beta_6$ was recruited to Col I adhesion complexes following ligand engagement and adhesion initiation by another Col I cognate receptor expressed in BT-20 cells, for example an integrin β_1 species. Indeed, integrin

receptor lateral clustering following ligand activation is an established concept (Welf *et al* 2012). Cluzel *et al* (2005) extensively characterised mechanisms of integrin $\alpha_v\beta_3$ lateral clustering in live mouse and hamster melanoma cell lines (B16F1 and CS-1 respectively). The authors reported that the head domain of the cytoskeletal protein talin was requisite for integrin clustering; concluding that talin's anti-parallel dimer conformation favours its role as a putative intracellular integrin cross-linker.

Using *in silico* atomistic molecular dynamic simulations based upon existing crystallographic mapping of integrin $\alpha_{II}\beta_3$, Orlowski *et al* (2015) later hypothesised that the membrane phospholipid phosphatidylinositol 4,5-bisphosphate (PIP2) works in concert with talin to induce integrin activation. PIP2 has been shown to enforce conformational changes in talin, exposing talin's integrin β–cytoplasmic tail binding region that resides within its head domain; thus enabling talin-integrin interaction and induction of intracellular priming and/or activation concordant with the *"inside-out"* model of integrin signalling.

This *in silico* evidence is concordant with Cluzel *et al's* (2005) earlier *in vitro* finding that specific PIP2-dependent recruitment of talin to active integrins demonstrated that the cytoplasmic tail domain of the integrin β_3-subunit is essential for lateral integrin $\alpha_v\beta_3$ clustering. Therefore, it may be possible that ligand-engagement, receptor activation and lateral clustering of one integrin receptor species, may orchestrate intracellular activation and recruitment of other integrin moieties.

For example, given that the talin N-terminal FERM domain binds the integrin C-terminal NPxY motif (Garcia-Alvarez *et al* 2003, Critchley 2009, Kim *et al* 2012), it is possible that activation of talin mediated either by extracellular integrin-ligand engagement, or by conducive changes in membrane phospholipid composition at sites of integrin clustering facilitating PIP2-dependent talin activation, may induce intracellular activation and recruitment of other integrin species to nascent ligand-adhesions.

Therefore, Col I ligand-engaged integrin β_1-activation inducing intracellular recruitment of talin and membrane phospholipid PIP2 may act in concert to drive sequential recruitment of other proximal integrin species, such as integrin $\alpha_v\beta_6$, via talin engagement of the β_6–cytoplasmic tail NPxY motif. This hypothesis may

account for the observation of integrin $\alpha_v\beta_6$ at sites of vinculin enrichment on Col I, presumed to be sites of adhesion.

Similar to demonstration of the integrin β_1, an antibody recognising total integrin $\alpha_v\beta_6$ was used. Again, it may have proved informative to use an antibody recognising the active integrin $\alpha_v\beta_6$ (such as 6.2E5 or 6.2G2) to robustly confirm the presence of active, ligand-engaged integrin $\alpha_v\beta_6$ at clusters of vinculin immunopositivity presumed to be sites of adhesion.

It is also possible that the unexpected observation of integrin $\alpha_v\beta_6$ at adhesion sites on Col I may be a technical artefact. Any conformational or protein degradation of substrate ligand Col I fibrils during ligand coating procedures or the adhesion assay itself, may liberate or expose Col I RGD-motif bearing regions in a spatially favourable presentation for integrin $\alpha_v\beta_6$ RGD-recognition and engagement. The concept of stoichiometric regulation of cognate RGD motif binding by integrin species was explored and validated by Davidenko *et al* (2016) using collagen and gelatin gel-based methods, and should be considered a possibility when critiquing data discussed here.

Despite the curious and unanticipated IMF findings regarding subcellular localisation of $\alpha_v\beta_6$ and β_1 integrin species on the immobilised substrate ligands LAP, Fn and Col I (Figure 5.2B); four biological replicate 2D-E adhesion assays yielded successful, specific and reproducible enrichment for the integrin $\alpha_v\beta_6$ receptor on its cognate ligand LAP, that was demonstrably validated by WB (Figure 5.2C). This confirmed the specificity of the assay to address the research aim of characterising a β_6–dependent adhesion environment and so justified subsequent peptide preparation for LC-MS/MS analysis and bioinformatic PPI network mapping.

Partial enrichment of the integrin $\alpha_v\beta_6$ on Fn substrate ligand was also detected by WB. However, integrin $\alpha_v\beta_6$ enrichment on Fn was markedly less than enrichment on LAP. This is concordant with reports that although integrin $\alpha_v\beta_6$ binds Fn, integrin $\alpha_5\beta_1$ is the predominant Fn-binding integrin species (Busk *et al* 1992, Hynes 2002).

Indeed, Bharadwaj *et al* (2017) recently reported the novel phenomenon of dual roles for α_v–integrins and integrin $\alpha_5\beta_1$ in MEFs and mouse kidney fibroblasts attaching to Fn; the duality of integrin species characterised by initial ligand competition and subsequent receptor cooperation to: establish stable adhesions, induct integrin clustering and initiate downstream signal activation.

The authors demonstrated that α_v–integrins initially outcompete $\alpha_5\beta_1$ for Fn engagement, but once engaged, signal recruitment of $\alpha_5\beta_1$ integrins to establish additional complexes. If a similar phenomenon of integrin-switching occurs in mammary-derived epithelial cells, this could account for the partial enrichment of integrin $\alpha_v\beta_6$ in BT-20 cells adhered to Fn demonstrated by WB probing of adhesion complexes isolated for LC-MS/MS.

Disappointingly, technical validation of the 2D-E procedure to robustly confirm purity of adhesion complex isolation and extraction, using markers specific for integrin-mediated adhesion complexes (talin and vinculin), alongside proteins excluded from adhesion complexes (the mitochondrial protein Bak), was inconsistent. Attempts to trouble-shoot this problem identified several possible technical causes including: inefficient protein transfer conditions during immunoblotting, insufficient stabilisation of highly labile multi-protein adhesion complexes by DTBP cross-linkage and primary antibody inter-batch variation.

The possibility of a biological explanation to account for the inconsistency of WB adhesion complex validation was also considered. Critically, adhesion complexes formed in BT-20 cells under 2D-E experimental conditions and reviewed by IMF (Figure 5.3B) appear to be smaller and fewer in abundance than published data on canonical adhesion complexes as studied in U-2 OS osteosarcoma cells and MEFs (Kanchanawong *et al* 2010, Carisey *et al* 2013).

Thus the low yield or absence of certain adhesion complex proteins may be attributable to fundamental, and as yet unpublished, variations between the size and constitution of adhesomes derived from cells of mammary epithelial origin (BT-20) compared to those as being formed in cells of mesenchymal origin (MEFs and U-2 OS).

Furthermore, IMF review of the adhesion complexes formed in BT-20 cells under 2D-E experimental conditions indicated that integrin β_1 moieties were not discernibly redelivered to the plasma lemma to engage the $\alpha_5\beta_1$ cognate ligand Fn. Regarding the $\alpha_1\beta_1/\alpha_2\beta_1$ cognate ligand Col I, integrin β_1 was detected by IMF in a few regions of the plasma lemma and at a lower abundance than anticipated. Instead, integrin β_1 predominated in intracellular vesicular structures during the adhesion phase of the protocol.

This observation (and inference that integrin β_1 was not abundantly redelivered to the plasmalemma to mediate substrate ligand engagement) was concordant with a failure to demonstrate integrin β_1 in isolated adhesion complex lysates by WB. For technical validation of WB procedures, total cell lysates (TCL) samples were loaded and probed in tandem with their corresponding 2D-E isolated adhesion complex samples.

Where probed, integrin β_1 expression was clearly confirmed in TCL. However, presence of the integrin β_1 in isolated adhesion complexes was not demonstrated in any of the four biological replicate experiments. It had been anticipated that integrin β_1 would be partially enriched on Fn (signifying $\alpha_5\beta_1$-Fn engagement) and markedly enriched on Col I (signifying $\alpha_1\beta_1/\alpha_2\beta_1$-Col I engagement). The absence of this enrichment pattern in WB results was concordant and consistent with IMF findings.

Although the four replicate 2D-E experiments could not be robustly validated for exquisite purity of adhesion complex enrichment and isolation using established markers (Paul 2014, Robertson 2014), the successful, reproducible and marked LAP-mediated enrichment of integrin $\alpha_v\beta_6$ was deemed sufficiently convincing and reliable to proceed with peptide preparation for LC-MS/MS analysis and PPI network mapping to explore the nature of an integrin $\alpha_v\beta_6$–dependent adhesion environment.

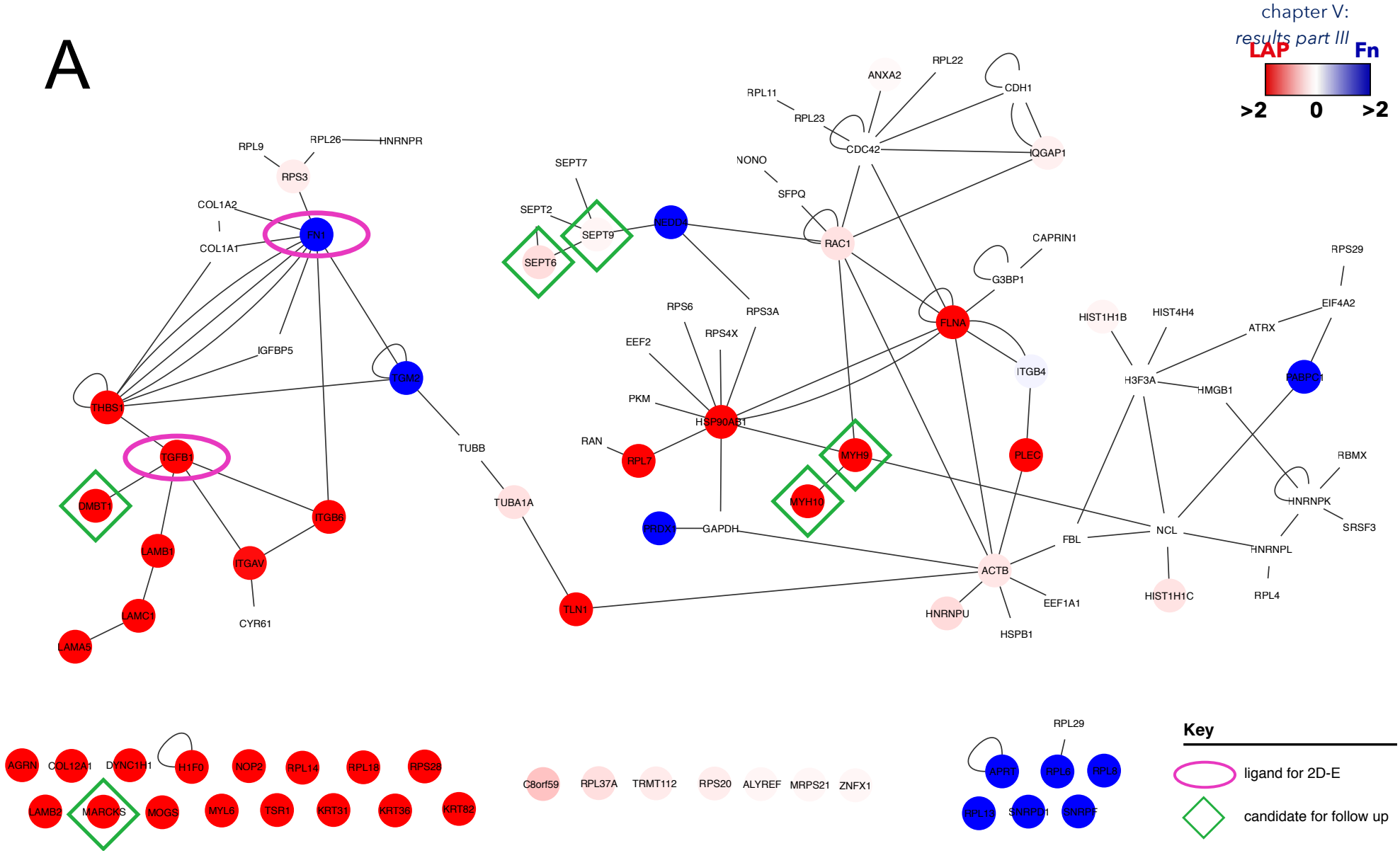

Figure 5.3 (A)
Protein-protein interaction network mapping proteins ≥2-fold enriched to a LAP-ligand induced β_6–adhesome compared to a Fn-ligand induced adhesion environment in the BT-20 cell line.

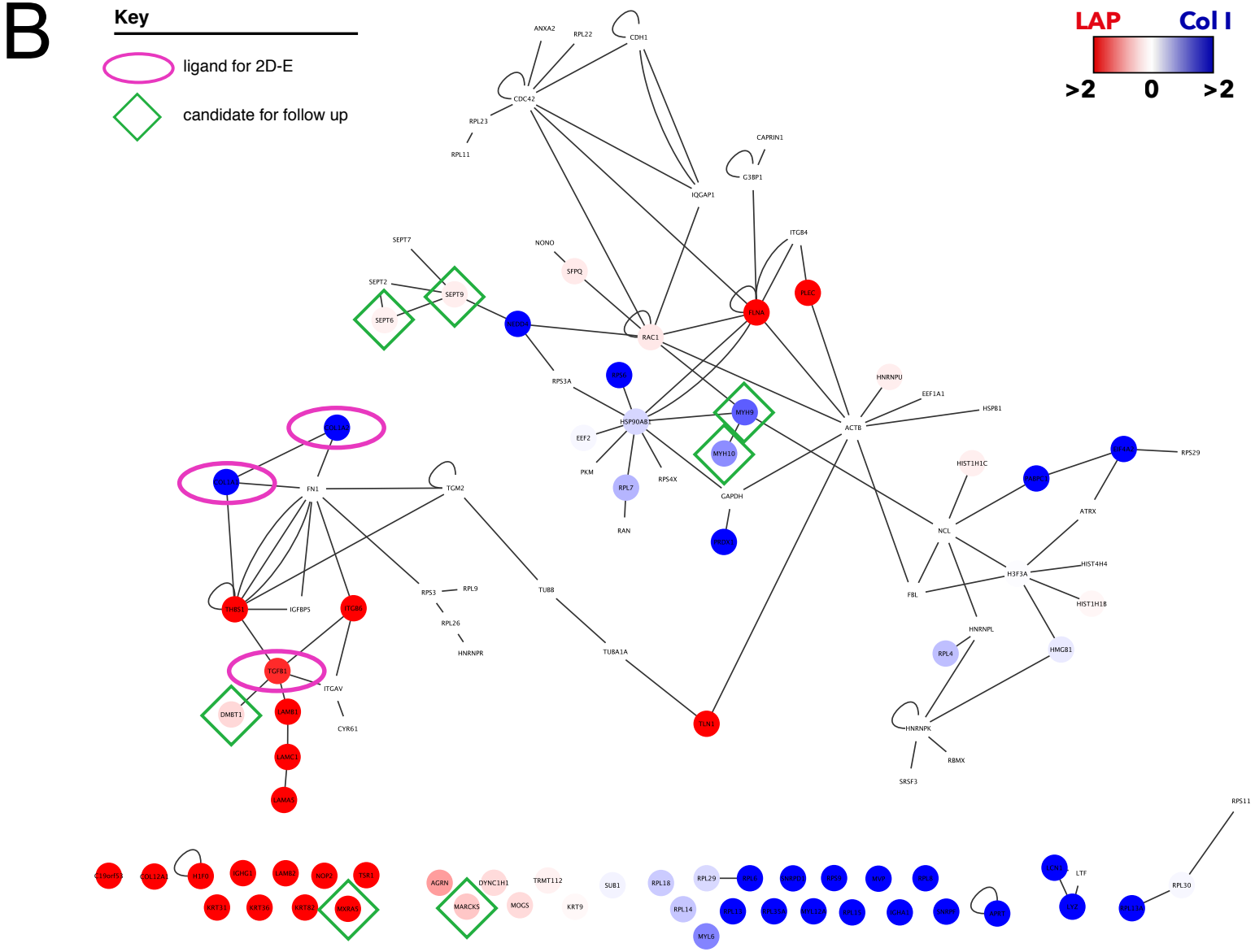

Figure 5.3 (B)
Protein-protein interaction network mapping proteins ≥2-fold enriched to a LAP-ligand induced β_6–adhesome compared to a Col I-ligand induced adhesion environment in the BT-20 cell line

Figure 5.3

Protein-protein interaction networks mapping proteins ≥2-fold enriched to a LAP-ligand induced β_6–adhesome compared to a Fn or a Col I-ligand induced adhesion environment in the BT-20 cell line

Following enrichment and isolation of adhesion complexes formed on LAP, Fn and Col I immobilised substrate ligands, peptides were prepared for LC-MS/MS analysis using the nanoACQUITY UPLC® ultra performance liquid chromatography system (Waters Ltd) coupled to an LTQ-Orbitrap XL™ ETD Hybrid Ion Trap-Orbitrap Mass Spectrometer (Thermo Scientifc Inc). Peptides were identified from raw SEQUEST (.dta) files using Mascot Daemon (v2.2.2, Matrix Science®) software and searched against entries held in the International Protein Index (IPI) Human Database (v3.70 released 4th March 2010). Mascot (.mgf) files were reviewed in Scaffold™ (v4.3.2, Proteome Software© Inc) for data pre-processing to exclude ambiguous peptide assignments and validate spectral count data. Identification threshold criteria were set to ≥99% at the protein level and ≥50% at the peptide level, with ≥2 unique validated peptides detected. Protein-protein interaction (PPI) networks for LAP-ligand engaged, integrin $\alpha_v\beta_6$–dependent adhesions were mapped using Cytoscape open source software (v3.1.1, Cytoscape Consortium©) in comparison with **(5.3 A)** Fn-induced and **(5.3 B)** Col I-induced adhesomes. Nodes (circles) represent proteins labelled with gene names. Node colour represents fold enrichment to either LAP compared to Fn or Col I (a minimum threshold of 2-fold enrichment was set). Block colour represents unique enrichments to either condition. Edges (lines) represent reported interactions between 2 proteins based on a literature-curated PPI database detailed by Jacquemet et al (2013).

5.3 PPI network maps comparing fold-enrichment of proteins during BT-20 cell adhesion to LAP, Fn and Col I ligands identify candidate proteins that putatively define the β_6-adhesome

Following enrichment and isolation of adhesion complexes formed on LAP, Fn and Col I immobilised substrate ligands, peptides were prepared for LC-MS/MS analysis *(Institute of Translational Medicine Mass Spectrometry Core Facility, Centre for Molecular Physiology, University of Liverpool)*. Peptides were then identified *(Mascot Daemon, v2.2.2, Matrix Science®)* and validated against entries held in the International Protein Index (IPI) Human Database *(v3.70 released 4th March 2010)*.

Mascot (.mgf) files were reviewed in Scaffold™ *(v4.3.2, Proteome Software© Inc)* for data pre-processing to exclude ambiguous peptide assignments and validate spectral count data. Identification threshold criteria were set to ≥99% at the protein level and ≥50% at the peptide level, with ≥2 unique validated peptides detected. A total of 24 410 spectra were analysed, mapping to 196 identified proteins (summarised in Supplementary Information S5.2).

Peptides were then quantified using an unweighted spectral count (USC) method established for label-free proteomics (Kito and Ito 2008), prior to mapping protein interaction networks incorporating fold-enrichment data (Figure 5.3) using Cytoscape v3.1.1 *(Cytoscape Consortium©)*.

Proteomic analysis of each ligand-specific proteomic dataset consistently identified the cognate ligand substrate used to elicit integrin engagement (LAP assigned TGF-β1; Fn assigned FN1; Col I assigned COL1A1/COL1A2), serving as an internal positive control for technical validation of sample specificity. Peptide sequences identified as TGF-β1-derived were checked against TGF-β1 amino acid sequence data to confirm that all detected peptide species specifically mapped to the LAP sequence residing within TGF-β1 complete sequence (UniProtKB – P01137 (TGFB1_HUMAN) online database entry).

Furthermore, USC data showed that both integrin α_v (ITGAV) and integrin β_6 (ITGB6) were specifically, and uniquely enriched to adhesion complexes formed on LAP; ITGAV and ITGB6 spectra were not detected in either Fn- or Col I-

mediated adhesion complexes isolated for proteomic analysis. This conferred additional confidence in LAP specificity for the integrin $\alpha_v\beta_6$ receptor in the BT-20 cell line, validating the use of this dataset to address the specific research intent of identifying novel molecular mediators associated with an integrin $\alpha_v\beta_6$–dependent adhesion environment.

However, the absence of ITGB6 spectra in samples isolated from Fn-mediated adhesion complex samples was inconsistent with findings from WB sample validation prior to LC-MS/MS analysis (Figure 5.2C). The presence of integrin β_6 was clearly demonstrated by WB in at least 3 of the 4 replicates sent for proteomic interrogation, yet were not detectable by more sensitive LC-MS/MS methods.

Curiously, vinculin spectra were not detected in any samples across the four biological repeats, which again was inconsistent with validation WB data where vinculin was detected in 2 replicates. Interestingly, talin (assigned TLN1) spectra were uniquely identified in LAP-mediated adhesion complex samples and were concordant with validation WBs. Furthermore, other anticipated integrin-mediated adhesion complex proteins (e.g kindlin, paxillin, FAK, ILK) were not successfully identified by proteomic analysis of 2D-E samples.

These inconsistencies between validation WB and LC-MS/MS spectral data, together with identification of fewer protein moieties than had been anticipated (protein underestimation), elicited concerns regarding LTQ Orbitrap XL™ ETD Ion Trap-Orbitrap *(ThermoScientific)* instrument efficacy and calibration.

With the kind assistance of Dr Edmund Wilkes *(Barts Cancer Institute)*, RAW LC-MS/MS data files were reviewed using the RAWMeat data quality diagnostic opensource software tool *(RawMeat, Vast Scientific)*. Disappointingly it was found that contrary to information supplied by the Mass Spectrometry Core Facility, the instrument was set to fragment the single most abundant ion in MS^1, rather than selecting the top 6 ions in MS^1 for MS^2 fragmentation.

This would account for the overall underestimation of identified protein species and may explain why proteins demonstrated by WB were not detected by proteomics. However, despite the obvious limitations this technical issue presents

when interpreting the 2D-E/LC-MS/MS dataset, it was felt that the specific enrichment of integrin $\alpha_v\beta_6$ to LAP-mediated adhesions (demonstrated by both validation WB and spectral analysis), sufficiently justified additional PPI network analyses to putatively and cautiously define a preliminary *β_6-adhesome*.

PPI networks were mapped comparing LAP-mediated adhesions with Fn-mediated adhesions (Figure 5.3A), and LAP-mediated adhesions with Col I-mediated adhesions (Figure 5.3B). It was intended that these analyses would identify proteins specifically enriched to LAP to characterise the *β_6-adhesome* and permit physiologically relevant exploration of integrin receptor switching through comparison with Fn and Col I adhesion environments.

Given that integrin switching has been observed previously *in vitro* (Caswell *et al* 2008), has subsequent to this study been shown to occur amongst α_v- and $\alpha_5\beta_1$ integrins during Fn-attachment (Bharadwaj *et al* 2017), and is associated with establishing metastatic competence (Parvani *et al* 2013, Madamanchi *et al* 2014) ; the 2D-E experiments were performed using 3 different ECM substrates known to preferentially engage different integrin species (LAP – $\alpha_v\beta_6$; Fn – $\alpha_5\beta_1/\alpha_v\beta_6$; col I – β_1 species) with the intention of exploring this integrin switching phenomenon in the BT-20 BrCa cell line.

However, WB to validate isolated adhesion complex lysates used for peptide preparation failed to demonstrate integrin β_1 enrichment on Fn and Col I substrates. Concordant with this, integrin β_1 spectra were not detected, even in the Fn and Col I sample datasets, as had been anticipated. Thus the anticipated integrin-switching phenomenon was not demonstrable by WB or proteomics. However, this does not categorically preclude the possibility of integrin switching occurring in the BT-20 cell line, nor within the wider context of TNBC.

Interestingly, integrin β_4 (ITGB4) spectra were identified. The integrin β_4 is deemed a basal marker in BrCa and was shown to be frequently overexpressed in TNBC patient tissue samples and associated with poorer prognosis (Lu *et al* 2008); rendering detection of integrin β_4 spectra in the BT-20 TNBC cell line a logical finding. Furthermore, integrin β_4 comprises the $\alpha_6\beta_4$ receptor for laminins (Stewart and O'Connor 2015).

Based on a ≥2 fold or unique enrichment to LAP versus Fn or Col I, together with published GO entries and existing in-house data (not published), a total of 7 candidate proteins for functional characterisation were identified from the 2D-E/LC-MS/MS dataset (summarised in Table 5.1).

Gene Name	UniProt ID	MW (kDa)	LAP unique v. Fn	LAP unique v. Col I	≥2X LAP v. Fn	≥2X LAP v. Col I
DMBT1	Q9UGM3	261	DMBT1		DMBT1	DMBT1
MARCKS	P22966	32	MARCKS		MARCKS	MARCKS
MXRA5	Q9NR99	312		MXRA5		MXRA5
MYH9	P33579	233	MYH9		MYH9	MYH9
MYH10	P33580	227	MYH10		MYH10	MYH10
SEPT6	Q14141	50			SEPT6	SEPT6
SEPT9	Q9UHD8	65			SEPT9	SEPT9

Table 5.1
Summary of seven candidate proteins implicated in establishing a LAP ligand-induced integrin $\alpha_v\beta_6$-dependent adhesion environment (β_6-adhesome) that were identified by proteomic interrogation of isolated adhesion complexes
Table summarises USC findings; indicating whether the candidate protein was uniquely enriched on LAP-ligand or showed a ≥2-fold enrichment to LAP compared to Fn- or Col I-induced adhesion complexes.

5.4 strategy for functional validation of seven candidate proteins that putatively define the β_6-adhesome

Proteomics-based studies exploring mechanisms of chemotherapeutic resistance in BrCa have successfully employed established siRNA gene-silencing strategies to investigate the functional role of candidate proteins identified in preliminary proteomic screens (Derycke *et al* 2011, Boyer *et al* 2013, Browne *et al* 2013). Therefore it was deemed appropriate to use similar siRNA-screening to functionally interrogate the role of 7 candidate proteins identified as putative mediators of the *β_6-adhesome*.

It was intended that candidates would be silenced in a panel of TNBC cell lines using siRNA and subject to functional assays to define the effect of a functional loss of target candidate on: integrin β_6 expression (to establish any co-regulatory link), cell proliferation, adhesion, invasion and migration characteristics.

Owing to a lack of published, reliable, commercially available antibodies to candidates of interest at the time of study, confirmation of knockdown was to be performed at the nucleic rather than protein level by quantitative real-time polymerase chain reaction (qPCR) *(SYBR®Green, Qiagen)*.

Disappointingly, stable siRNA silencing was not demonstrable by qPCR within the timescale remaining on this study arm (Supplementary Figures S5.3 to S5.5). It is hoped that with additional troubleshooting to address issues encountered with primer efficiency and off-target effects of siRNA hindering reliable target knockdown, the candidate proteins identified in 2DE-LC-MS/MS experiments will receive the requisite functional validation to establish their role in the *β_6-adhesome*.

5.5 PPI network maps comparing fold-enrichment of proteins during MDA-MB-468 cell adhesion to LAP with adhesion to Fn reveal EGFR is uniquely enriched to the LAP-induced MDA-MB-468 β_6-adhesome

Proteomic interrogation of a single 2D-E experiment (comprising two technical replicates) performed using MDA-MB-468 cells permitted PPI network mapping of the LAP versus Fn-induced adhesomes in an alternative TNBC in vitro model (Figure 5.4). Although lacking the accompanying validation WB data, spectral analyses of LC-MS/MS data confirmed specific and unique enrichment of integrin α_v (ITGAV) and integrin β_6 spectra (ITGB6) in LAP-mediated adhesion complexes. Similar to results obtained using the BT-20 cell line, the integrin $\alpha_v\beta_6$ was not engaged during Fn-mediated adhesions in the MDA-MB-468 cell line as neither ITGAV nor ITGB6 spectra were detected.

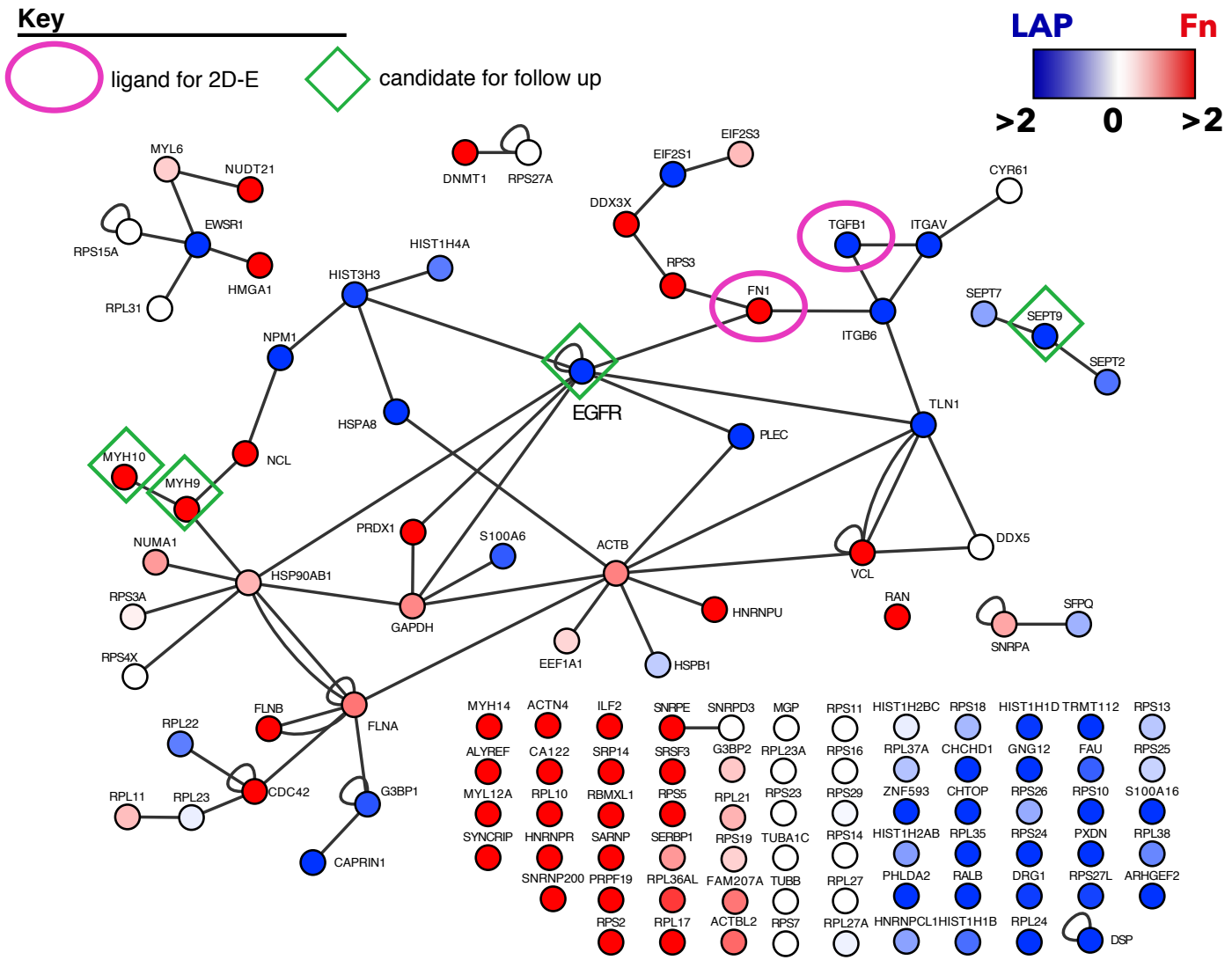

Figure 5.4
Protein-protein interaction networks mapping proteins ≥1.5-fold enriched to a LAP-ligand induced β_6-adhesome compared to a Fn induced adhesion environment in the MDA-MB-468 cell line (n=1)

Figure 5.4

Protein-protein interaction networks mapping proteins ≥1.5-fold enriched to a LAP-ligand induced β_6–adhesome compared to a Fn induced adhesion environment in the MDA-MB-468 cell line (n=1)

Following enrichment and isolation of adhesion complexes formed on LAP and Fn immobilised substrate ligands, peptides were prepared for LC-MS/MS analysis using the nanoACQUITY UPLC® ultra performance liquid chromatography system (Waters Ltd) coupled to an LTQ-Orbitrap XL™ ETD Hybrid Ion Trap-Orbitrap Mass Spectrometer (Thermo Scientifc Inc). Peptides were identified from raw SEQUEST (.dta) files using Mascot Daemon (v2.2.2, Matrix Science®) software and searched against entries held in the International Protein Index (IPI) Human Database (v3.70 released 4th March 2010). Mascot (.mgf) files were reviewed in Scaffold™ (v4.3.2, Proteome Software© Inc) for data pre-processing to exclude ambiguous peptide assignments and validate spectral count data. Identification threshold criteria were set to ≥99% at the protein level and ≥50% at the peptide level, with ≥2 unique validated peptides detected. Protein-protein interaction (PPI) networks for LAP-ligand engaged, integrin $\alpha_v\beta_6$–dependent adhesions were mapped using Cytoscape open source software (v3.1.1, Cytoscape Consortium©) in comparison with Fn-induced adhesomes. Nodes (circles) represent proteins labelled with gene names. Node colour represents fold enrichment to either LAP (blue) compared to Fn (red) (a minimum threshold of ≥1.5-fold enrichment was set). Block colour represents unique enrichments to either condition. Edges (lines) represent reported interactions between 2 proteins based on a literature-curated PPI database detailed by Jacquemet et al (2013). Data shown is a composite from a merged report of two technical replicates analysed on two separate LC-MS/MS runs using peptides prepared from a single 2D-E experiment.

Excitingly, EGFR was uniquely enriched in LAP-mediated, integrin $\alpha_v\beta_6$–specific adhesion complexes in comparison with Fn-induced, integrin $\alpha_v\beta_6$-null adhesion complexes. Although the significance of this finding must be tempered by its observation in a single biological experiment comprising two technical replicates, this preliminary finding assuredly warrants validation with additional biological repeats to confirm whether unique EGFR enrichment within the *β_6-adhesome* is reproducible.

5.6 discussion

To address our limited understanding of signalling events inducted downstream of integrin $\alpha_v\beta_6$ activation upon ligand engagement and adhesion complex formation, a proteomic strategy to characterise the molecular nature of an integrin $\alpha_v\beta_6$–dependent adhesion environment *("β_6-adhesome")* in the BT-20 TNBC cell line was developed and employed using the 2D-E strategy first described by Humphries *et al* (2009) and refined by Byron *et al* (2011).

Functional abrogation of the integrin $\alpha_v\beta_6$ receptor using inhibitory monoclonal antibody blockade abolished LAP ligand engagement in comparison with an isotype, species-matched negative control antibody treatment (one-tailed 2-sample t-test; p=0.0104). This successful validation of apparent exquisite LAP specificity for integrin $\alpha_v\beta_6$ in the BT-20 cell line (Figure 5.1.2C) firmly established the utility of LAP ligand to specifically target the integrin $\alpha_v\beta_6$ in a physiologically relevant manner for studies seeking define $\alpha_v\beta_6$–dependent functions. It is acknowledged that this is not a universal validation of LAP-integrin $\alpha_v\beta_6$ specificity but rather demonstrates that the integrin $\alpha_v\beta_6$ is the predominant LAP receptor in BT-20 cells. Therefore, use of integrin $\alpha_v\beta_6$ targeting via LAP engagement in other cell line models would first need to be validated as cell-type specific integrin-ligand dynamics are reported (Sakamoto *et al* 1996, Heino 2000).

Despite a failure to robustly validate purity of isolated adhesion complexes using established markers of integrin-mediated complexes by WB (Paul 2014, Robertson 2014, Robertson *et al* 2015), the four-biological replicate 2D-E experiments successfully yielded specific and reproducible enrichment for the integrin $\alpha_v\beta_6$ receptor on its cognate ligand LAP (Figure 5.2). It was concluded that this LAP-mediated integrin $\alpha_v\beta_6$-enrichment was sufficient to justify proceeding with proteomic interrogation of integrin $\alpha_v\beta_6$–dependent adhesion complexes; provided the limitations rendered by less stringent validation than desired were considered during interpretation and contextualisation of findings.

Although some results generated were unexpected, they did exhibit a degree of consistency. For example, the anticipated integrin β_1 enrichment to Fn and Col I immobilised ligands was not demonstrated by validation WBs (Figure 5.2C). This was concordant with an absence of ITGB1 spectra detected by LC-MS/MS. These findings were consistent with the IMF observation that integrin β_1 remained bounded in an intracellular, vesicular pattern of immunopositivity on all substrate ligands; suggesting that integrin β_1 was not trafficked to the plasma lemma for ligand engagement. Although integrin β_1 was seen to co-localise with the adhesion complex-associated protein vinculin and the integrin $\alpha_v\beta_6$ on Col I, these regions of integrin β_1 at the plasma lemma were sparse.

The curious lack of integrin β_1 engagement to Fn and Col I may be an artefact, but given the emerging significance of derailed internalisation and endocytic trafficking of integrin receptors in cancer (Mosesson *et al* 2008, Rainero *et al* 2013), the perturbed surface membrane delivery of integrin β_1 species observed in BT-20 cells adhering to β_1–cognate ligands may warrant additional dissection. Published integrin-centric mechanisms governing differential integrin intracellular traffic and recycling kinetics may prove a logical starting point for future experiments (such as those presented later in Chapter VI, Results Part IV).

For example, Src-mediated syndecan-4 phosphorylation was shown to suppress Arf6 activity, promoting integrin $\alpha_v\beta_3$ delivery to the plasma lemma leading to preferential engagement of integrin $\alpha_v\beta_3$ over integrin $\alpha_5\beta_1$ for cellular adhesion to Fn (Morgan *et al* 2013). It would prove interesting to determine whether syndecan-4 phosphorylation is also a regulatory checkpoint for other α_v integrin species.

Previous in-house data (unpublished) has demonstrated that syndecan-4 co-localises with integrin $\alpha_v\beta_6$ in OSCC cells and HaCaT keratinocytes. Therefore it would be logical to establish whether integrin $\alpha_v\beta_6$ is also subject to Src-mediated syndecan-4 regulation. It may be that integrin $\alpha_v\beta_6$ is preferentially delivered to the plasma lemma for initial Fn engagement at the expense of integrin $\alpha_5\beta_1$, in a similar manner to that described by Morgan *et al* (2013) for the integrin $\alpha_v\beta_3$.

Given that integrin switching has been observed previously *in vitro* (Caswell *et al* 2008, Morgan *et al* 2013) and is associated with establishing metastatic competence (Parvani *et al* 2013, Madamanchi *et al* 2014), the 2D-E experiments were performed using 3 different ECM substrates known to preferentially engage different integrin species (LAP – $\alpha_v\beta_6$; Fn – $\alpha_5\beta_1/\alpha_v\beta_6$; Col I – β_1 species). The intention of this experimental design was to permit exploration of the integrin switching phenomenon within the context of TNBC using the BT-20 BrCa cell line.

Although it is disappointing that the postulated integrin switching mechanism was not observed in these experiments, the primary remit of the 2D-E/LC-MS/MS assays to yield specific and reproducible enrichments for the integrin $\alpha_v\beta_6$ receptor during engagement to its cognate ligand LAP was resoundingly achieved. Across the four biological replicates, validation WBs showed that integrin $\alpha_v\beta_6$ was demonstrably enriched in LAP-engaged adhesion complexes; and so validates the relevance of this dataset to begin characterisation of an integrin $\alpha_v\beta_6$–dependent adhesion environment.

Curiously, results from proteomic investigation of an integrin $\alpha_v\beta_6$–dependent adhesion environment utilising the 2D-E strategy did not yield consistent hits for several canonical integrin-mediated adhesion complex proteins, notably: **talin** (Garcia-Alvarez *et al* 2003, Critchley 2009, Orlowski *et al* 2015), **vinculin** (Humphries *et al* 2007, Ziegler *et al* 2008, Carisey *et al* 2013, Hirata *et al* 2014, Atherton *et al* 2015, Atherton *et al* 2016), **kindlin** (Shattil *et al* 2010, Calderwood *et al* 2013), **FAK** (Serrels *et al* 2010, Duperret *et al* 2015) and **paxillin** (Crowe and Ohannessian 2004, Brown *et al* 2005). This may be attributable to several factors.

Current understanding of integrin-dependent adhesion processes is based predominantly on integrin receptors other than $\alpha_v\beta_6$, notably $\alpha_v\beta_3$ or β_1–bearing species, during adhesion to Fn; typically characterised in fibroblasts (Huttenlocher

and Horwitz 2011). Critically, adhesion complexes formed in BT-20 cells under 2D-E experimental conditions and reviewed by IMF appeared to be smaller and fewer in abundance than published data on canonical adhesion complexes. Thus the low yield or absence of certain adhesion complex proteins may be attributable to fundamental variations between the size and constitution of adhesomes derived from cells of mammary epithelial origin compared to those formed in other cell lineages.

For example, published tandem characterisation of proteomic constitution in concert with IMF nanostructural organisation of integrin-driven adhesion complexes has been undertaken in: K562 human chronic myelogenous leukaemia cells and B16-F10 mouse melanoma cells (Humphries *et al* 2009, Byron *et al* 2012), A375 human melanoma cells (Robertson *et al* 2015), human bone marrow-derived mesenchymal stem cells (MSC) (Ajeian *et al* 2016), MEF fibroblasts and U2-OS osteosarcoma cells (Kanchanawong *et al* 2010, Carisey *et al* 2013); not mammary epithelial cells, as has been attempted in this study, rendering appropriate literature-based comparisons for observational validation challenging.

Adhesion complex morphology observed by IMF in BT-20 cells (Figure 5.2B) was subsequently compared with unpublished data characterising murine primary mammary epithelial cells adhering to laminin-111 or collagen type I (Paul 2014). These comparisons suggested the nature of presumed adhesion complexes formed in BT-20 cells (based on clusters of vinculin immunopositivity) adhered to immobilised substrate ligands, was indeed comparable to those established and validated by Paul (2014); lending credence to the 2D-E assays performed for proteomic investigation of the *β_6-adhesome*.

Disappointingly, technical validation of the 2D-E procedure by WB using markers specific for integrin-mediated adhesion complexes (talin and vinculin) was inconsistent (Figure 5.2C). Attempts to trouble-shoot this problem identified several possible technical causes including inefficient protein transfer conditions and primary antibody inter-batch variation. Furthermore, the mitochondrial protein Bak (its absence used to confirm purity of adhesion-complex enrichment) was only probed in one biological replicate owing to insufficient residual sample volume.

In addition, it is possible that suboptimal stabilisation of notoriously labile adhesion complexes using the biochemical cross-linker DTBP, may account for the underestimation of proteins detected by WB and LC-MS/MS. Although the use of such biochemical cross-linkers is well established (Corgiat *et al* 2014), it would have been pertinent to specifically optimise and validate cross-linkage conditions (time, DTBP concentration) alongside adhesion complex isolation by sonication in the BT-20 cell line to ensure adhesions were suitably stabilised.

Inefficient cross-linkage would not sufficiently stabilise adhesion complexes leading to dissociation of protein interactions during extraction by sonication; resulting in an underestimation or absence of adhesion-associated moieties, as observed here. In the interests of time during limited secondment tenure, a 2D-E protocol previously established and validated by the host institution for MEFs was followed. However, it is acknowledged that this fails to account for cell line-specific idiosyncracies often encountered when translating an established protocol to a different cell line.

Furthermore, owing to time constraints of secondment to complete experiments, WB validation of 2D-E lysates was undertaken simultaneously with peptide preparation and LC-MS/MS analysis. Therefore, the 2D-E lysate aliquot retained for WB (the bulk being used for peptide preparation) proved insufficient to allow for technical issues with WB and requirements for additional blots to complete more robust, convincing validation. Ideally (and logically) WB validation would be performed prior to peptide preparation and LC-MS/MS interrogation.

However, it is also acknowledged that the low abundance, or absence of certain adhesion-complex markers detected by WB and LC-MS/MS may not necessarily be technical artefacts. It is possible that integrin $\alpha_v\beta_6$–mediated adhesion complexes in TNBC BT-20 cells differ in constitution to published adhesion complex published for other integrin receptor species and cell types (as previously discussed).

Thus, as these 2D-E experiments were an exploratory exercise to define a hitherto uncharacterised integrin $\alpha_v\beta_6$–dependent adhesion environment *(β_6-adhesome)*, the use of published, peer-reviewed, experimentally validated markers for integrin $\alpha_v\beta_6$ adhesions, was not possible. Therefore, the use of talin and vinculin to

validate adhesion complex formation during 2D-E assays was inferred from literature characterising other integrin species during adhesion.

In addition to possible biological causes, technical limitations resulting in low abundance, or absence of anticipated protein moieties detected, must also be considered. For example, known technical limitations associated with label-free LC-MS/MS techniques for quantitative proteomics may also account for the absence of anticipated proteins identified from 2D-E samples. Although label-free quantitative proteomic strategies are experimentally simpler in comparison with conventional stable isotope labelling with amino acids in cell culture (SILAC) methods, there are several key limitations with label-free systems that must be considered during data processing (Patel *et al* 2009).

Label-free methods are less accurate than their SILAC counterparts but yield high coverage, making them amenable to large-scale, exploratory proteomic workflows (Kito and Ito 2008, Patel *et al* 2009), such as that employed in this study arm. Furthermore, label-free methods are more error prone owing to systematic inter-run variability and stochasticity of indices used for quantitation calculations (Wong and Cagney 2010). Typically, peptide quantification methods using label-free data are based on peptide ion characteristics such as peak intensity or identification frequency (spectral count). Thus label-free methods permit relative quantification of any protein from which a peptide has been unambiguously identified. Spectral counting reportedly shows highest correlation with relative protein abundance so is more often used for relative protein quantification than ion peak intensity (Kito and Ito 2008).

Spectral counting based on MS/MS spectra has been shown to generate good estimates of protein abundance, but is limited by instrument MS/MS sampling frequency. Thus, for low-abundance proteins yielding solitary peptide identifications, low quantitative resolution using this method cannot be overcome (Domon and Aebersold 2010, Sandin *et al* 2014). However, since larger proteins will generate a larger number of peptides, precursor ions and MS/MS spectra (and so will be detected at greater frequency than smaller proteins), sampling bias must be overcome by spectral normalisation prior to calculation of relative protein abundance (Kito and Ito 2008, Patel *et al* 2009, Wong and Cagney 2010).

In this study, unweighted spectral counts (USC) were normalised against protein size (kDa), since linear correlation of spectral count per molecular weight with protein stoichiometry has been shown (Liu *et al* 2004) . Samples were analysed in data-dependent acquisition (DDA) mode, whereby the most abundant peptide peaks are selected for MS/MS fragmentation (Wong and Cagney 2010). A caveat to USC-based proteomic analyses is the fact that proteins of low abundance may be masked in the presence of contaminant proteins that may mask peak ion characteristics, precluding selection in MS^1 for fragmentation in MS^2 (Liu *et al* 2004, Kito and Ito 2008, Domon and Aebersold 2010, Sandin *et al* 2014).

Indeed, post-acquisition analysis of RAW files using RAWmeat data quality diagnostic software revealed that contrary to assurances from the Mass Spectrometry Core Facility *(Institute for Translational Medicine, University of Liverpool)*, the LTQ Orbitrap XL™ ETD Ion Trap-Orbitrap *(ThermoScientific* instrument used was calibrated to fragment the **single** most abundant ion, not the top 6 most abundant ion species in MS^1 for fragmentation in MS^2. This would account for a gross underestimation of identified peptides and thus a markedly smaller number of protein species comprising the final dataset merged from the four biological replicates.

In stark contrast with previous proteomic (Humphries *et al* 2009, Byron *et al* 2011, Jacquemet *et al* 2013, Byron *et al* 2015, Ajeian *et al* 2016) and phosphoproteomic (Robertson *et al* 2015) analyses of integrin-mediated adhesion complexes that identified proteins in the 10^3 or 10^4 order of magnitude, only 196 proteins were identified in this study. Therefore, it is most probable that key mediators of the *β_6-adhesome* would not have been identified owing to the lack of requisite instrument sensitivity. Curiously, the technical limitations of fragmenting only the single most abundant ion in MS^1 may in fact confer a modicum of confidence in the validity of candidate proteins identified. For example, in light of the inherent underestimation of peptides due to instrument limitations, it is more likely that false negative (i.e no peptide detection) rather than false positive results would be obtained.

However, even in light of technical limitations and unanticipated findings, the demonstrable, reproducible and reliable enrichment of integrin $\alpha_v\beta_6$ to LAP-mediated adhesions demonstrated by both validation WBs and spectra identified by LC-MS/MS should not be discounted entirely. Across four biological replicate

experiments, samples were successfully generated and validated that permit specific (albeit preliminary in light of protein underestimation) characterisation of an integrin $\alpha_v\beta_6$–mediated adhesion environment in the BT-20 cell line (Figure 5.3).

For a more exhaustive, robustly validated dataset to define the *β_6-adhesome* in more detail with greater confidence, experiments would need to be repeated for analysis on an appropriately calibrated mass-spectrometer as a minimum. Furthermore, in-depth validation of adhesion-complex formation by IMF (to characterise structural composition) and WB (to confirm purity of isolation) using a broader panel of established markers of adhesion-complex proteins would be required.

In spite of the limitations acknowledged thus far, it is important to reiterate the reproducible and specific integrin $\alpha_v\beta_6$–enrichment in LAP-induced adhesion complexes; sufficient to undertake provisional characterisation of the *β_6–adhesome*. Bioinformatic analysis and PPI networking enabled identification of 7 candidate proteins showing ≥2-fold enrichment (**DMBT-1**, **MARCKS**, **MXRA5**, **MYH9**, **MYH10**, **SEPT6**, **SEPT9**) for functional interrogation of their putative role in integrin $\alpha_v\beta_6$–mediated adhesions using a gene silencing siRNA screening strategy successfully employed elsewhere to validate proteomic datasets (Boyer *et al* 2013, Browne *et al* 2013).

Within the LC-MS/MS dataset, it was curious that β_1 integrin was not detected in either Fn or Col I ligand conditions. However, spectra mapping to β_4 integrin (ITGB4) were detected. This is of interest as spectra mapping to laminin moieties were consistently detected. Laminins are integral components of basal lamina providing structural support for the overlying epithelium. Disease progression from *in situ* to invasive disease is marked by epithelial cell acquisition of an invasive phenotype facilitating breach of the basal lamina to invade surrounding tissues with the potential for metastatic dissemination (Hamill *et al* 2009, Iorio *et al* 2015). Interestingly, derailed endo-exocytic trafficking of laminins has been reported in aggressive cancer subtypes (Leonoudakis *et al* 2014).

Curiously, several laminin subunits were uniquely enriched to the LAP condition including: α5, β1, β2 and γ1 (assigned LAMA5, LAMB1, LAMB2 and LAMBC1 respectively). Kim *et al* (2012) demonstrated that invasive BrCa induced laminin-

332 upregulation and neoexpression of integrin β_4 in myofibroblasts, conferring an anoikis-resistant survival advantage during tissue remodelling. Indeed, Terranova *et al* (1983) first reported expression of high-affinity laminin receptors in human MCF-7 BrCa cells.

Recently, Vieira *et al* (2014) demonstrated that the integrin $\alpha_6\beta_4$ laminin receptor modulates P-cadherin signalling to induct stemness and an invasive phenotype in basal-like BrCa cells. The cell-cell adhesion molecule P-cadherin has been shown to promote BrCa progression and is associated with poor prognosis. Using the BT-20 and MDA-MB-468 TNBC cell lines, Vieira *et al* (2014) demonstrated *in vitro* that: expression of P-cadherin regulated integrin $\alpha_6\beta_4$ expression with P-cadherin ablation downregulating integrin $\alpha_6\beta_4$; and integrin $\alpha_6\beta_4$ was requisite for P-cadherin signalling. *In vivo* studies using TNBC tumour xenografts revealed that integrin $\alpha_6\beta_4$/P-cadherin protumourigenic crosstalk was mediated by pFAK and pSrc.

Demonstrative of the emerging significance of laminin-integrin coordination in BrCa cancer, Carpenter *et al* (2017) reported the pulmonary endothelial laminin-332 was a tropic motility factor for BrCa dissemination to the lung; with tumour cell motile arrest dependent upon integrin $\alpha_3\beta_1$ expression, as previously described by Zhou *et al* (2014). Therefore, the presence of both integrin β_4 and laminin subunit spectra within the context of a *β_6-adhesome* defined by proteomics may warrant further characterisation of the role of integrin $\alpha_v\beta_6$ LAP-ligand engagement, activation and adhesion complex formation within the context of TNBC matrix-mediated metastatic dissemination.

Interestingly, in line with the concept of matrix-associated responses in cancer, the ECM remodelling moiety matrix-remodelling associated protein-5 (MXRA5) was found to be uniquely enriched to LAP-mediated, integrin $\alpha_v\beta_6$–dependent adhesions in comparison with Col I-mediated adhesions and showed a >2-fold enrichment to LAP-mediated adhesions in comparison with Fn-induced adhesion complexes.

MXRA5 is a protein of relatively unknown function. Proteomic biomarker discovery undertaken by Wang *et al* (2013) revealed MXRA5 to be a novel tissue biomarker in human colorectal carcinoma (CRC); utility as a serum marker was not evaluated.

The authors evaluated a cohort of human tissue samples comprising 20 colorectal adenomas, 156 CRC tumours, alongside their corresponding adjacent normal mucosa.

IHC evaluation showed that MXRA5 was overexpressed in CRC tissues in comparison with corresponding normal mucosa. Furthermore, intensity of MXRA5 expression positively and significantly correlated with lesion site, TNM staging and metastasis, with the highest observed MXRA5 positivity in omental metastasis. Wang and colleagues concluded that MXRA5 was of potential clinical value for CRC disease detection and prediction of omental metastasis, but would require additional validation.

Recently (and subsequent to termination of this study arm), Poveda *et al* (2017) demonstrated that MXRA5 was subject to TGF-β1 regulation and exhibited anti-inflammatory and anti-fibrotic properties within the context of human chronic kidney disease. Given that the integrin $\alpha_v\beta_6$ is known to activate latent TGF- β1 via engagement of LAP, it is possible that the integrin $\alpha_v\beta_6$ may be implicated in this MXRA5-TGF-β1-axis and may prove an interesting lead to investigate; especially given the association between integrin $\alpha_v\beta_6$-dependent adhesions and MXRA5 as defined by the 2D-E proteomic dataset.

Other proteins identified as putative components of the *β_6-adhesome*, showing unique enrichment to LAP-mediated adhesion complexes in comparison with either Fn- or Col I-mediated adhesions include known regulators of actin cytoskeletal dynamics. Notably the filamentous (F)-actin crosslinking protein myristolated alanine-rich protein kinase C (MARCKS) known to regulate cell motility via actin cytoskeleton regulation (Aderem 1992) was identified; the filament forming cytoskeletal small GTPases septin-6 (SEPT6) and septin-9 (SEPT9) requisite for cytokinesis were also detected. In their proteomic interrogation of signalling networks associated with acquired tamoxifen resistance in MCF-7 BrCa cells, Browne *et al* (2013) demonstrated that MARCKS expression was upregulated eight-fold in tamoxifen resistant MCF-7 cells compared to tamoxifen-sensitive MCF-7 cells.

Furthermore, the authors reported that siRNA silencing of MARCKS significantly decreased cell motility. In addition, MARCKS IHC staining in a TMA constructed

from samples from a 292 cohort of primary IDC breast tumours was significantly higher in basal-like and HER-2 tumours, compared to luminal cancers. Tissue-expression of MARCKS was also found to be independently predictive of poor patient outcome in multivariate analysis of the entire primary BrCa cohort studied.

Subsequently, Chen *et al* (2015) demonstrated that phosphorylation of MARCKS at serine 159/163 (pMARCKS$^{S159/163}$) was (at least in part) contributing to paclitaxel resistance in BrCa taxane therapy-based regimens. Inhibition of MARCKS phosphorylation using an inhibitory peptide elicited restitution of paclitaxel efficacy *in vivo* in nude mice orthotopically injected with MDA-MB-468 BrCa cells.

Most recently, Manai *et al* (2017) performed IHC evaluation of MARCKS expression in pre-therapeutic tissue samples obtained from a cohort of 133 inflammatory breast cancer (IBC) patients in comparison with a 369 non-IBC patient cohort. The authors found that MARCKS expression was associated with poor metastasis-free survival rates. Collectively this literature (Browne *et al* 2013, Chen *et al* 2015, Manai *et al* 2017) is indicative of the emerging significance of MARCKS in BrCa, justifying additional characterisation of MARCKS within the context of an integrin $\alpha_v\beta_6$-dependent adhesion environment in a TNBC model.

The septins -6 and -9 (SEPT6 and SEPT9) were also identified; showing a ≥2-fold enrichment to LAP compared either Fn or Col I. The septins are of emerging importance in cancer (Pous *et al* 2016). High mutation frequency of SEPT6 has been reported in endometrial cancers (Angelis and Spiliotis 2016); whilst SEPT9 overexpression has been demonstrated in a variety of solid tumours including: serous ovarian cancer (Scott *et al* 2006), high-grade prostate cancer (Gilad *et al* 2015) and breast cancer (Connolly *et al* 2011).

Integrin-septin crosstalk has been reported to modulate ECM-stiffness regulated endothelial cell proliferation. Yeh *et al* (2012) demonstrated integrin $\alpha_v\beta_3$ inactivation upregulated SEPT9 expression in human umbilical vein endothelial cells (HUVECs) adhered on high-stiffness hydrogels. This in turn attenuated Src phosphorylation and inhibited RhoA-dependent HUVEC proliferation. Therefore, it is possible that the integrin $\alpha_v\beta_6$ may also act in concert with SEPT6 or SEPT9 to modulate proliferative signalling and warrants further functional characterisation.

In addition, the non-muscle myosin II (NM-II) isoforms myosin-9 (II-A) and -10 (II-B) (assigned MYH9 and MYH10 respectively) were specifically enriched during integrin $\alpha_v\beta_6$–mediated adhesions to LAP in comparison with Fn-derived adhesions (Figure 5.4A), and showed partial enrichment to Col I adhesions over LAP (Figure 5.4B). The role of non-muscle myosin motor proteins during BrCa progression, promoting invasion and metastasis, is of growing research interest (Derycke *et al* 2011, Arjonen *et al* 2014, Ouderkirk and Krendel 2014, Li and Yang 2016).

In a comparative proteomic analysis of invasive (MCF-7/6) and non-invasive (MCF-7/AZ) MCF-7 BrCa cell variants, Derycke *et al* (2011) discovered a single, significant difference between their proteomes. The authors identified NM II-A (MYH9) expression was restricted to the invasive MCF-7/6 variant, suggesting MYH9 may confer an invasive phenotype. MYH9 blockade, using genetic silencing with stable shRNA transduction or pharmacological functional abrogation with blebbistatin, successfully abolished MCF-7/6 invasion in embryonic chick heart fragments or Col I gels serving as invasion 3D-substrata. Derycke and colleagues thus concluded that MYH9 is a decisive protein for MCF-7 invasion and may prove a useful molecular target for anti-invasive therapy in BrCa.

Recently, high expression of MYH9 (as determined by IHC in primary patient cohorts) has been associated with poorer clinicopathological features of malignancy and poor survival probability in: resected non-small cell lung carcinoma (NSCLC) (Katono *et al* 2015), osteosarcoma (Zhou *et al* 2016) and colorectal cancer (CRC) (Liu *et al* 2017). Given the emerging clinical significance of MYH9 expression in malignant disease, evaluation of MYH9 expression in BrCa and correlation with disease manifestation and patient outcome would prove informative.

Indeed, MYH10 (NM II-B) has also been reported to potentiate invasion in BrCa. It has been shown that MYH10 promotes invasion in BrCa via directing integrin traffic to filopodial tips and is requisite for invadopodial formation and ECM degradation via engagement of the MYH10 pleckstrin homology domain with the membrane phospholipid phosphatidylinositol (3,4,5)-triphosphate (PtdIns(3,4,5)P3) (Arjonen *et al* 2011).

Later, Arjonen *et al* (2014) concluded that MYH10 upregulation is requisite for mutant p53-driven BrCa invasion. Gene expression profiling of 2 BrCa clinical datasets revealed MYH10 was highly expressed in aggressive BrCa subtypes. Furthermore, *in vitro* expression of mutant p53 upregulated MYH10 expression in BrCa cells, but suppression of endogenous mutant p53 constrained MYH10 expression; suggesting mutant p53 modulates MYH10 expression in BrCa cells.

The authors also conducted mutational studies using MYH10 mutants lacking their integrin-binding domain. This revealed MYH10-mediated delivery of integrin β_1 to filopodial tips was necessary for invasion. These findings highlight the importance of integrin-synergy with other molecular mediators to drive disease progression in BrCa, and justify further investigation of proinvasive MYH10-integrin transport within the context of other integrin species, such as the integrin $\alpha_v\beta_6$.

The mucin-like protein deleted in malignant brain tumours-1 (DMBT1) was also found to be specifically and uniquely enriched to LAP-mediated integrin $\alpha_v\beta_6$–dependent adhesions. Research into the role of DMBT1 in cancer has revealed it to be pleiotropic; with dual roles in epithelial protection and differentiation, it cannot be categorically termed a classical tumour suppressor (Mollenhauer *et al* 2002). Early studies reported DMBT1 is down-regulated in BrCa (Braidotti *et al* 2004) and is a candidate for mammary tumour modification and BrCa risk (Blackburn *et al* 2007).

Tchatchou *et al* (2010) identified 5'-region polymorphisms in DMBT1 that resulted in loss of DMBT1 promoter activity conferring increased risk of BrCa in a cohort of 1 195 BRCA1/2 mutation-negative BrCa families and 1 466 unrelated controls that were analysed. This was concordant with previous studies associating decrease of DMBT1 with BrCa risk. In their evaluation of the functional role of DMBT1 in vascular endothelial cells, Muller *et al* (2012) reported a coincidental finding that integrin β_3 expression was attenuated in DMBT$^{-/-}$ mice; leading to the authors tentatively proposing a functional link between integrin β_3 and DMBT1. In light of this, and given that DMBT1 was uniquely enriched to the LAP-mediated *β_6-adhesome* in BT-20 cells, it would be logical to explore the functional role of DMBT1 during integrin $\alpha_v\beta_6$–mediated adhesions.

Therefore, it is disappointing that siRNA functional screening targeting these exciting candidate proteins implicated during establishment of an integrin $\alpha_v\beta_6$–adhesion-mediated proteome environment (*β_6-adhesome*), could not be validated and developed within the time constraints of this study. However, it is hoped that this work will be continued, particularly in light of emerging research that appears to independently validate the significance of these moieties in malignant disease: **DMBT-1** (Mollenhauer *et al* 2002, Mollenhauer *et al* 2002, Braidotti *et al* 2004, Blackburn *et al* 2007, Tchatchou *et al* 2010, Muller *et al* 2012); **MARCKS** (Aderem 1992, Chen *et al* 2015, Manai *et al* 2017); **MXRA5** (Wang *et al* 2013, Poveda *et al* 2017); **MYH9** (Derycke *et al* 2011, Katono *et al* 2015, Zhou *et al* 2016, Liu *et al* 2017); **MYH10** (Arjonen *et al* 2014, Cao *et al* 2014, Ouderkirk and Krendel 2014, Li and Yang 2016); **SEPT6** (Angelis and Spiliotis 2016, Pous *et al* 2016) and **SEPT9** (Scott *et al* 2006, Connolly *et al* 2011, Yeh *et al* 2012, Gilad *et al* 2015).

The preliminary identification of EGFR specificity within the MDA-MB-468 LAP-mediated *β_6-adhesome* is exciting, suggesting the possibility of integrin $\alpha_v\beta_6$/EGFR cross-talk during ECM-ligand-mediated adhesions, which is concordant with previous findings (Caswell et al 2008). Undoubtedly this warrants further investigation to provide sufficient evidence to determine whether EGFR/integrin $\alpha_v\beta_6$ receptor cooperation is a cell line specific phenomenon (as observed here in the MDA-MB-468 cell line but not the BT-20 cell line) or has broader relevance within the context of TNBC.

Validation of EGFR/integrin $\alpha_v\beta_6$ reciprocity would offer the potential for therapeutic intervention and possible receptor co-targeting in a manner similar to that described by Moore *et al* (2014) who successfully abrogated integrin $\alpha_v\beta_6$ function using 264RAD to potentiate trastuzumab efficacy in HER-2 driven BrCa.

Therefore, this body of data represents a springboard from which additional exploration of the TNBC *β_6-adhesome* may be launched; in the hope of identifying cancer-specific, intracellular regulators of integrin $\alpha_v\beta_6$–mediated adhesions and putative EGFR-integrin $\alpha_v\beta_6$ cross-talk that may be therapeutically targeted in multi-modal treatment regimens to prevent disease progression and metastatic dissemination, and ultimately improve TNBC BrCa patient outcomes.

supplementary information S5

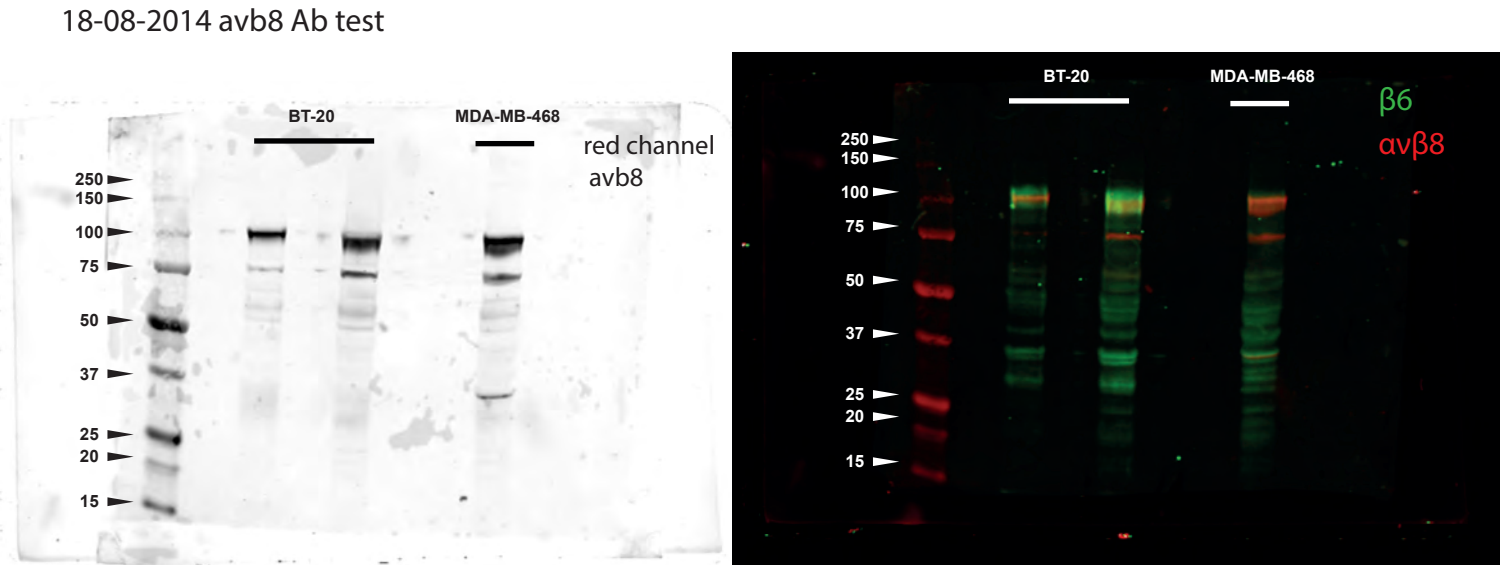

Supplementary Information (Figure) S5.1

Immunoblots to test an integrin β_8 antibody by dual probing for integrin β_8 (red channel) and integrin β_6 (green channel)

To test an integrin antibody not previously used in-house, lysates from integrin β_6 high expressors (BT-20) and a moderate-to-low expressor (MDA-MB-468) were probed for integrin β_6 subunit (c-19, 0.2 µg ml^{-1}, sc-6632, SantaCruz BioTech) and integrin β_8 (5 µg ml^{-1}, ab80673, AbCam) subunit using the LI-COR ODYSSEY®Sa dual immunofluorescence WB system. A distinct band at the anticipated MW was observed in accordance with manufacturer's datasheet.

Identified Proteins (196)	Reviewed UniProt Acc No	UniProtKB ID	Gene Name	Molecular Weight (kDa)
Actin, cytoplasmic 1 OS=Homo sapiens GN=ACTB PE=1 SV=1	P60709	ACTB_HUMAN	ACTB	42
Agrin OS=Homo sapiens GN=AGRN PE=1 SV=5	O00468	AGRIN_HUMAN	AGRN	217
Serum albumin OS=Homo sapiens GN=ALB PE=1 SV=2	P02768	ALBU_HUMAN	ALB	69
Annexin A2 OS=Homo sapiens GN=ANXA2 PE=1 SV=2	P07355	ANXA2_HUMAN	ANXA2	39
Adenine phosphoribosyltransferase OS=Homo sapiens GN=APRT PE=1 SV=2	P07741	APT_HUMAN	APRT	20
Isoform 1 of Transcriptional regulator ATRX OS=Homo sapiens GN=ATRX	P46100	ATRX_HUMAN	ATRX	260
Guanine nucleotide-binding protein G(I)/G(S)/G(T) subunit beta-2 (Fragment) OS=Homo sapiens GN=GNB2 PE=2 SV=1	C9JIS1	C9JIS1_HUMAN	GNB2	26
Cadherin-1 OS=Homo sapiens GN=CDH1 PE=1 SV=3	P12830	CADH1_HUMAN	CDH1	97
Caprin-1 OS=Homo sapiens GN=CAPRIN1 PE=1 SV=2	Q14444	CAPR1_HUMAN	CAPRIN1	78
Cell division control protein 42 homolog OS=Homo sapiens GN=CDC42 PE=1 SV=2	P60953	CDC42_HUMAN	CDC42	21
Uncharacterized protein C8orf59 OS=Homo sapiens GN=C8orf59 PE=1 SV=2	Q8N0T1	CH059_HUMAN	C8orf59	11
Coiled-coil-helix-coiled-coil-helix domain-containing protein 1 OS=Homo sapiens GN=CHCHD1 PE=1 SV=1	Q96BP2	CHCH1_HUMAN	CHCHD1	13
Collagen alpha-1(I) chain OS=Homo sapiens GN=COL1A1 PE=1 SV=5	P02452	CO1A1_HUMAN	COL1A1	139
Collagen alpha-2(I) chain OS=Homo sapiens GN=COL1A2 PE=1 SV=7	P08123	CO1A2_HUMAN	COL1A2	129
Isoform 4 of Collagen alpha-1(XII) chain OS=Homo sapiens GN=COL12A1	Q99715	COCA1_HUMAN	COL12A1	325
Ubiquinone biosynthesis monooxygenase COQ6 OS=Homo sapiens GN=COQ6 PE=1 SV=2	Q9Y2Z9	COQ6_HUMAN	COQ6	51
Cancer/testis antigen family 45 member A1 OS=Homo sapiens GN=CT45A1 PE=2 SV=1	Q5HYN5	CT451_HUMAN	CT45A1	21
Protein CYR61 OS=Homo sapiens GN=CYR61 PE=1 SV=1	O00622	CYR61_HUMAN	CYR61	42
Deleted in malignant brain tumors 1 protein OS=Homo sapiens GN=DMBT1 PE=1 SV=2	Q9UGM3	DMBT1_HUMAN	DMBT1	261

Supplementary Information (Table) S5.2

Scaffold™ merged report of proteins identified by LC-MS/MS interrogation of adhesion complexes isolated from BT-20 cells adhering to LAP, Fn or Col I to characterise the β_6-adhesome (n=4)

Summary table of proteins identified from LC-MS/MS analysis. Peptides were identified and validated using Mascot Daemon and exported to Scaffold for worklist analysis. Candidate proteins are highlighted in blue.

Developmentally-regulated GTP-binding protein 1 OS=Homo sapiens GN=DRG1 PE=1 SV=1	Q9Y295	DRG1_HUMAN	DRG1	41
Cytoplasmic dynein 1 heavy chain 1 OS=Homo sapiens GN=DYNC1H1 PE=1 SV=5	Q14204	DYHC1_HUMAN	DYNC1H1	532
Nascent polypeptide-associated complex subunit alpha OS=Homo sapiens GN=NACA PE=2 SV=1	E9PAV3	NACAM_HUMAN	NACA	205
Serine/arginine repetitive matrix protein 1 OS=Homo sapiens GN=SRRM1 PE=2 SV=2	E9PCT1	E9PCT1_HUMAN	SRRM1	104
Heat shock cognate 71 protein (Fragment) OS=Homo sapiens GN=HSPA8 PE=2 SV=1	E9PI65	E9PI65_HUMAN	HSPA8	18
Elongation factor 1-alpha 1 OS=Homo sapiens GN=EEF1A1 PE=1 SV=1	P68104	EF1A1_HUMAN	EEF1A1	50
Elongation factor 2 OS=Homo sapiens GN=EEF2 PE=1 SV=4	P13639	EF2_HUMAN	EEF2	95
rRNA 2'-O-methyltransferase fibrillarin OS=Homo sapiens GN=FBL PE=1 SV=2	P22087	FBRL_HUMAN	FBL	34
Fibronectin OS=Homo sapiens GN=FN1 PE=1 SV=4	P02751	FINC_HUMAN	FN1	263
Filamin-A OS=Homo sapiens GN=FLNA PE=1 SV=4	P21333	FLNA_HUMAN	FLNA	281
Ras GTPase-activating protein-binding protein 1 OS=Homo sapiens GN=G3BP1 PE=1 SV=1	Q13283	G3BP1_HUMAN	G3BP1	52
Isoform B of Ras GTPase-activating protein-binding protein 2 OS=Homo sapiens GN=G3BP2	Q9UN86	G3BP2_HUMAN	G3BP2	51
Glyceraldehyde-3-phosphate dehydrogenase OS=Homo sapiens GN=GAPDH PE=1 SV=3	P04406	G3P_HUMAN	GAPDH	36
Translational activator GCN1 OS=Homo sapiens GN=GCN1L1 PE=1 SV=6	Q92616	GCN1L_HUMAN	GCN1L1	293
Uncharacterized protein (Fragment) OS=Homo sapiens PE=4 SV=1	H0YHG0	H0YHG0_HUMAN	H0YHG0	59
Histone H1.0 OS=Homo sapiens GN=H1F0 PE=1 SV=3	P07305	H10_HUMAN	H1F0	21
Histone H1.2 OS=Homo sapiens GN=HIST1H1C PE=1 SV=2	P16403	H12_HUMAN	HIST1H1C	21
Histone H1.5 OS=Homo sapiens GN=HIST1H1B PE=1 SV=3	P16401	H15_HUMAN	HIST1H1B	23
Histone H2A type 1-J OS=Homo sapiens GN=HIST1H2AJ PE=1 SV=3	Q99878	H2A1J_HUMAN	HIST1H2AJ	14
Histone H2B type 1-B OS=Homo sapiens GN=HIST1H2BB PE=1 SV=2	P33778	H2B1B_HUMAN	HIST1H2BB	14
Histone H2B type 1-D OS=Homo sapiens GN=HIST1H2BD PE=1 SV=2	P58876	H2B1D_HUMAN	HIST1H2BD	14
Histone H3.3 OS=Homo sapiens GN=H3F3A PE=1 SV=2	P84243	H33_HUMAN	H3F3A	15
Histone H4 OS=Homo sapiens GN=HIST1H4A PE=1 SV=2	P62805	H4_HUMAN	HIST4H4	11
High mobility group protein HMG-I/HMG-Y OS=Homo sapiens GN=HMGA1 PE=1 SV=3	P17096	HMGA1_HUMAN	HMGA1	12
High mobility group protein B1 OS=Homo sapiens GN=HMGB1 PE=1 SV=3	P09429	HMGB1_HUMAN	HMGB1	25
Heterogeneous nuclear ribonucleoproteins C1/C2 OS=Homo sapiens GN=HNRNPC PE=1 SV=4	P07910	HNRPC_HUMAN	HNRNPC	34

Heterogeneous nuclear ribonucleoprotein K OS=Homo sapiens GN=HNRNPK PE=1 SV=1	P61978	HNRPK_HUMAN	HNRNPK	51
Heterogeneous nuclear ribonucleoprotein L OS=Homo sapiens GN=HNRNPL PE=1 SV=2	P14866	HNRPL_HUMAN	HNRNPL	64
Heterogeneous nuclear ribonucleoprotein R OS=Homo sapiens GN=HNRNPR PE=1 SV=1	O43390	HNRPR_HUMAN	HNRNPR	71
Heterogeneous nuclear ribonucleoprotein U OS=Homo sapiens GN=HNRNPU PE=1 SV=6	Q00839	HNRPU_HUMAN	HNRNPU	91
Heat shock protein HSP 90-beta OS=Homo sapiens GN=HSP90AB1 PE=1 SV=4	P08238	HS90B_HUMAN	HSP90AB1	83
Heat shock protein beta-1 OS=Homo sapiens GN=HSPB1 PE=1 SV=2	P04792	HSPB1_HUMAN	HSPB1	23
Insulin-like growth factor-binding protein 5 OS=Homo sapiens GN=IGFBP5 PE=1 SV=1	P24593	IBP5_HUMAN	IGFBP5	31
Eukaryotic translation initiation factor 2 subunit 1 OS=Homo sapiens GN=EIF2S1 PE=1 SV=3	P05198	IF2A_HUMAN	EIF2S1	36
Eukaryotic translation initiation factor 2 subunit 3 OS=Homo sapiens GN=EIF2S3 PE=1 SV=3	P41091	IF2G_HUMAN	EIF2S3	51
Isoform 2 of Eukaryotic initiation factor 4A-II OS=Homo sapiens GN=EIF4A2	Q14240	IF4A2_HUMAN	EIF4A2	46
Ig alpha-1 chain C region OS=Homo sapiens GN=IGHA1 PE=1 SV=2	P01876	IGHA1_HUMAN	IGHA1	38
Ig gamma-1 chain C region OS=Homo sapiens GN=IGHG1 PE=1 SV=1	P01857	IGHG1_HUMAN	IGHG1	36
Ras GTPase-activating-like protein IQGAP1 OS=Homo sapiens GN=IQGAP1 PE=1 SV=1	P46940	IQGA1_HUMAN	IQGAP1	189
Integrin alpha-V OS=Homo sapiens GN=ITGAV PE=1 SV=2	P06756	ITAV_HUMAN	ITGAV	116
Integrin beta-4 OS=Homo sapiens GN=ITGB4 PE=1 SV=5	P16144	ITB4_HUMAN	ITGB4	202
Integrin beta-6 OS=Homo sapiens GN=ITGB6 PE=1 SV=2	P18564	ITB6_HUMAN	ITGB6	86
Probable ATP-dependent RNA helicase DDX5 OS=Homo sapiens GN=DDX5 PE=3 SV=1	J3KTA4	J3KTA4_HUMAN	DDX5	69
Keratin, type I cytoskeletal 10 OS=Homo sapiens GN=KRT10 PE=1 SV=6	P13645	K1C10_HUMAN	KRT10	59
Keratin, type I cytoskeletal 14 OS=Homo sapiens GN=KRT14 PE=1 SV=4	P02533	K1C14_HUMAN	KRT14	52
Keratin, type I cytoskeletal 18 OS=Homo sapiens GN=KRT18 PE=1 SV=2	P05783	K1C18_HUMAN	KRT18	48
Keratin, type I cytoskeletal 19 OS=Homo sapiens GN=KRT19 PE=1 SV=4	P08727	K1C19_HUMAN	KRT19	44
Keratin, type I cytoskeletal 9 OS=Homo sapiens GN=KRT9 PE=1 SV=3	P35527	K1C9_HUMAN	KRT9	62
Keratin, type I cuticular Ha1 OS=Homo sapiens GN=KRT31 PE=2 SV=3	Q15323	K1H1_HUMAN	KRT31	47
Keratin, type II cytoskeletal 2 epidermal OS=Homo sapiens GN=KRT2 PE=1 SV=2	P35908	K22E_HUMAN	KRT2	65
Keratin, type II cytoskeletal 1 OS=Homo sapiens GN=KRT1 PE=1 SV=6	P04264	K2C1_HUMAN	KRT1	66
Keratin, type II cytoskeletal 5 OS=Homo sapiens GN=KRT5 PE=1 SV=3	P13647	K2C5_HUMAN	KRT5	62

Keratin, type II cytoskeletal 7 OS=Homo sapiens GN=KRT7 PE=1 SV=5	P08729	K2C7_HUMAN	KRT7	51
Isoform 2 of Keratin, type II cytoskeletal 8 OS=Homo sapiens GN=KRT8	P05787	K2C8_HUMAN	KRT8	57
Pyruvate kinase isozymes M1/M2 OS=Homo sapiens GN=PKM PE=1 SV=4	P14618	KPYM_HUMAN	PKM	58
Keratin, type I cuticular Ha6 OS=Homo sapiens GN=KRT36 PE=1 SV=1	O76013	KRT36_HUMAN	KRT36	52
Keratin, type II cuticular Hb2 OS=Homo sapiens GN=KRT82 PE=1 SV=3	Q9NSB4	KRT82_HUMAN	KRT82	57
Keratin, type II cuticular Hb3 OS=Homo sapiens GN=KRT83 PE=1 SV=2	P78385	KRT83_HUMAN	KRT83	54
Keratin, type II cuticular Hb5 OS=Homo sapiens GN=KRT85 PE=1 SV=1	P78386	KRT85_HUMAN	KRT85	56
Leydig cell tumor 10 protein homolog OS=Homo sapiens GN=C19orf53 PE=1 SV=1	Q9UNZ5	L10K_HUMAN	C19orf53	11
Laminin subunit alpha-5 OS=Homo sapiens GN=LAMA5 PE=1 SV=8	O15230	LAMA5_HUMAN	LAMA5	400
Laminin subunit beta-1 OS=Homo sapiens GN=LAMB1 PE=1 SV=2	P07942	LAMB1_HUMAN	LAMB1	198
Laminin subunit beta-2 OS=Homo sapiens GN=LAMB2 PE=1 SV=2	P55268	LAMB2_HUMAN	LAMB2	196
Laminin subunit gamma-1 OS=Homo sapiens GN=LAMC1 PE=1 SV=3	P11047	LAMC1_HUMAN	LAMC1	178
Lipocalin-1 OS=Homo sapiens GN=LCN1 PE=1 SV=1	P31025	LCN1_HUMAN	LCN1	19
Lysozyme C OS=Homo sapiens GN=LYZ PE=1 SV=1	P61626	LYSC_HUMAN	LYZ	17
U1 small nuclear ribonucleoprotein A (Fragment) OS=Homo sapiens GN=SNRPA PE=4 SV=1	M0R2B8	M0R2B8_HUMAN	SNRPA	17
Myristoylated alanine-rich C-kinase substrate OS=Homo sapiens GN=MARCKS PE=1 SV=4	P29966	MARCS_HUMAN	MARCKS	32
Pyrin OS=Homo sapiens GN=MEFV PE=1 SV=1	O15553	MEFV_HUMAN	MEFV	86
Matrix Gla protein OS=Homo sapiens GN=MGP PE=1 SV=2	P08493	MGP_HUMAN	MGP	12
Myosin regulatory light chain 12A OS=Homo sapiens GN=MYL12A PE=1 SV=2	P19105	ML12A_HUMAN	MYL12A	20
Mannosyl-oligosaccharide glucosidase OS=Homo sapiens GN=MOGS PE=1 SV=5	Q13724	MOGS_HUMAN	MOGS	92
Major vault protein OS=Homo sapiens GN=MVP PE=1 SV=4	Q14764	MVP_HUMAN	MVP	99
Matrix-remodeling-associated protein 5 OS=Homo sapiens GN=MXRA5 PE=2 SV=3	Q9NR99	MXRA5_HUMAN	MXRA5	312
Isoform 4 of Myosin-10 OS=Homo sapiens GN=MYH10	P35580	MYH10_HUMAN	MYH10	233
Myosin-9 OS=Homo sapiens GN=MYH9 PE=1 SV=4	P35579	MYH9_HUMAN	MYH9	227
Myosin light polypeptide 6 OS=Homo sapiens GN=MYL6 PE=1 SV=2	P60660	MYL6_HUMAN	MYL6	17
Isoform 4 of E3 ubiquitin-protein ligase NEDD4 OS=Homo sapiens GN=NEDD4	P46934	NEDD4_HUMAN	NEDD4	104

Non-POU domain-containing octamer-binding protein OS=Homo sapiens GN=NONO PE=1 SV=4	Q15233	NONO_HUMAN	NONO	54
Putative ribosomal RNA methyltransferase NOP2 OS=Homo sapiens GN=NOP2 PE=1 SV=2	P46087	NOP2_HUMAN	NOP2	89
Nucleolin OS=Homo sapiens GN=NCL PE=1 SV=3	P19338	NUCL_HUMAN	NCL	77
Polyadenylate-binding protein 1 OS=Homo sapiens GN=PABPC1 PE=1 SV=2	P11940	PABP1_HUMAN	PABPC1	71
Plasminogen activator inhibitor 1 RNA-binding protein OS=Homo sapiens GN=SERBP1 PE=1 SV=2	Q8NC51	PAIRB_HUMAN	SERBP1	45
Protein piccolo OS=Homo sapiens GN=PCLO PE=1 SV=4	Q9Y6V0	PCLO_HUMAN	PCLO	553
Isoform 4 of Plectin OS=Homo sapiens GN=PLEC	Q15149	PLEC_HUMAN	PLEC	516
Peroxiredoxin-1 OS=Homo sapiens GN=PRDX1 PE=1 SV=1	Q06830	PRDX1_HUMAN	PRDX1	22
60S ribosomal protein L5 OS=Homo sapiens GN=RPL5 PE=2 SV=1	Q5T7N0	Q5T7N0_HUMAN	RPL5	14
Ras-related protein Ral-B OS=Homo sapiens GN=RALB PE=2 SV=1	P11234	RALB_HUMAN	RALB	26
Ras-related C3 botulinum toxin substrate 1 OS=Homo sapiens GN=RAC1 PE=1 SV=1	P63000	RAC1_HUMAN	RAC1	21
Radixin OS=Homo sapiens GN=RDX PE=1 SV=1	P35241	RADI_HUMAN	RDX	69
RNA-binding protein Raly OS=Homo sapiens GN=RALY PE=1 SV=1	Q9UKM9	RALY_HUMAN	RALY	32
GTP-binding nuclear protein Ran OS=Homo sapiens GN=RAN PE=1 SV=3	P62826	RAN_HUMAN	RAN	24
RNA-binding motif protein, X chromosome OS=Homo sapiens GN=RBMX PE=1 SV=3	P38159	RBMX_HUMAN	RBMX	42
60S ribosomal protein L10 OS=Homo sapiens GN=RPL10 PE=1 SV=4	P27635	RL10_HUMAN	RPL10	25
60S ribosomal protein L11 OS=Homo sapiens GN=RPL11 PE=1 SV=2	P62913	RL11_HUMAN	RPL11	20
60S ribosomal protein L13 OS=Homo sapiens GN=RPL13 PE=1 SV=4	P26373	RL13_HUMAN	RPL13	24
60S ribosomal protein L13a OS=Homo sapiens GN=RPL13A PE=1 SV=2	P40429	RL13A_HUMAN	RPL13A	24
60S ribosomal protein L14 OS=Homo sapiens GN=RPL14 PE=1 SV=4	P50914	RL14_HUMAN	RPL14	23
60S ribosomal protein L15 OS=Homo sapiens GN=RPL15 PE=1 SV=2	P61313	RL15_HUMAN	RPL15	24
60S ribosomal protein L17 OS=Homo sapiens GN=RPL17 PE=1 SV=3	P18621	RL17_HUMAN	RPL17	21
60S ribosomal protein L18 OS=Homo sapiens GN=RPL18 PE=1 SV=2	Q07020	RL18_HUMAN	RPL18	22
60S ribosomal protein L21 OS=Homo sapiens GN=RPL21 PE=1 SV=2	P46778	RL21_HUMAN	RPL21	19
60S ribosomal protein L22 OS=Homo sapiens GN=RPL22 PE=1 SV=2	P35268	RL22_HUMAN	RPL22	15
60S ribosomal protein L23 OS=Homo sapiens GN=RPL23 PE=1 SV=1	P62829	RL23_HUMAN	RPL23	15

60S ribosomal protein L23a OS=Homo sapiens GN=RPL23A PE=1 SV=1	P62750	RL23A_HUMAN	RPL23A	18
60S ribosomal protein L24 OS=Homo sapiens GN=RPL24 PE=1 SV=1	P83731	RL24_HUMAN	RPL24	18
60S ribosomal protein L26 OS=Homo sapiens GN=RPL26 PE=1 SV=1	P61254	RL26_HUMAN	RPL26	17
60S ribosomal protein L27 OS=Homo sapiens GN=RPL27 PE=1 SV=2	P61353	RL27_HUMAN	RPL27	16
60S ribosomal protein L27a OS=Homo sapiens GN=RPL27A PE=1 SV=2	P46776	RL27A_HUMAN	RPL27A	17
60S ribosomal protein L29 OS=Homo sapiens GN=RPL29 PE=1 SV=2	P47914	RL29_HUMAN	RPL29	18
60S ribosomal protein L30 OS=Homo sapiens GN=RPL30 PE=1 SV=2	P62888	RL30_HUMAN	RPL30	13
60S ribosomal protein L31 OS=Homo sapiens GN=RPL31 PE=1 SV=1	P62899	RL31_HUMAN	RPL31	14
60S ribosomal protein L35 OS=Homo sapiens GN=RPL35 PE=1 SV=2	P42766	RL35_HUMAN	RPL35	15
60S ribosomal protein L35a OS=Homo sapiens GN=RPL35A PE=1 SV=2	P18077	RL35A_HUMAN	RPL35A	13
60S ribosomal protein L36a-like OS=Homo sapiens GN=RPL36AL PE=1 SV=3	Q969Q0	RL36L_HUMAN	RPL36AL	12
60S ribosomal protein L37a OS=Homo sapiens GN=RPL37A PE=1 SV=2	P61513	RL37A_HUMAN	RPL37A	10
60S ribosomal protein L38 OS=Homo sapiens GN=RPL38 PE=1 SV=2	P63173	RL38_HUMAN	RPL38	8
60S ribosomal protein L4 OS=Homo sapiens GN=RPL4 PE=1 SV=5	P36578	RL4_HUMAN	RPL4	48
60S ribosomal protein L6 OS=Homo sapiens GN=RPL6 PE=1 SV=3	Q02878	RL6_HUMAN	RPL6	33
60S ribosomal protein L7 OS=Homo sapiens GN=RPL7 PE=1 SV=1	P18124	RL7_HUMAN	RPL7	29
60S ribosomal protein L8 OS=Homo sapiens GN=RPL8 PE=1 SV=2	P62917	RL8_HUMAN	RPL8	28
60S ribosomal protein L9 OS=Homo sapiens GN=RPL9 PE=1 SV=1	P32969	RL9_HUMAN	RPL9	22
39S ribosomal protein L34, mitochondrial OS=Homo sapiens GN=MRPL34 PE=1 SV=1	Q9BQ48	RM34_HUMAN	MRPL34	10
40S ribosomal protein S10 OS=Homo sapiens GN=RPS10 PE=1 SV=1	P46783	RS10_HUMAN	RPS10	19
40S ribosomal protein S11 OS=Homo sapiens GN=RPS11 PE=1 SV=3	P62280	RS11_HUMAN	RPS11	18
40S ribosomal protein S13 OS=Homo sapiens GN=RPS13 PE=1 SV=2	P62277	RS13_HUMAN	RPS13	17
40S ribosomal protein S14 OS=Homo sapiens GN=RPS14 PE=1 SV=3	P62263	RS14_HUMAN	RPS14	16
40S ribosomal protein S15 OS=Homo sapiens GN=RPS15 PE=1 SV=2	P62841	RS15_HUMAN	RPS15	17
40S ribosomal protein S15a OS=Homo sapiens GN=RPS15A PE=1 SV=2	P62244	RS15A_HUMAN	RPS15A	15
40S ribosomal protein S16 OS=Homo sapiens GN=RPS16 PE=1 SV=2	P62249	RS16_HUMAN	RPS16	16

40S ribosomal protein S17-like OS=Homo sapiens GN=RPS17L PE=2 SV=1	P0CW22	RS17L_HUMAN	RPS17L	16
40S ribosomal protein S18 OS=Homo sapiens GN=RPS18 PE=1 SV=3	P62269	RS18_HUMAN	RPS18	18
40S ribosomal protein S19 OS=Homo sapiens GN=RPS19 PE=1 SV=2	P39019	RS19_HUMAN	RPS19	16
40S ribosomal protein S2 OS=Homo sapiens GN=RPS2 PE=1 SV=2	P15880	RS2_HUMAN	RPS2	31
40S ribosomal protein S20 OS=Homo sapiens GN=RPS20 PE=1 SV=1	P60866	RS20_HUMAN	RPS20	13
40S ribosomal protein S23 OS=Homo sapiens GN=RPS23 PE=1 SV=3	P62266	RS23_HUMAN	RPS23	16
40S ribosomal protein S24 OS=Homo sapiens GN=RPS24 PE=1 SV=1	P62847	RS24_HUMAN	RPS24	15
40S ribosomal protein S25 OS=Homo sapiens GN=RPS25 PE=1 SV=1	P62851	RS25_HUMAN	RPS25	14
40S ribosomal protein S26 OS=Homo sapiens GN=RPS26 PE=1 SV=3	P62854	RS26_HUMAN	RPS26	13
Ubiquitin-40S ribosomal protein S27a OS=Homo sapiens GN=RPS27A PE=1 SV=2	P62979	RS27A_HUMAN	RPS27A	18
40S ribosomal protein S27-like OS=Homo sapiens GN=RPS27L PE=1 SV=3	Q71UM5	RS27L_HUMAN	RPS27L	9
40S ribosomal protein S28 OS=Homo sapiens GN=RPS28 PE=1 SV=1	P62857	RS28_HUMAN	RPS28	8
40S ribosomal protein S29 OS=Homo sapiens GN=RPS29 PE=1 SV=2	P62273	RS29_HUMAN	RPS29	7
40S ribosomal protein S3 OS=Homo sapiens GN=RPS3 PE=1 SV=2	P23396	RS3_HUMAN	RPS3	27
40S ribosomal protein S30 OS=Homo sapiens GN=FAU PE=1 SV=1	P62861	RS30_HUMAN	FAU	7
40S ribosomal protein S3a OS=Homo sapiens GN=RPS3A PE=1 SV=2	P61247	RS3A_HUMAN	RPS3A	30
40S ribosomal protein S4, X isoform OS=Homo sapiens GN=RPS4X PE=1 SV=2	P62701	RS4X_HUMAN	RPS4X	30
40S ribosomal protein S5 OS=Homo sapiens GN=RPS5 PE=1 SV=4	P46782	RS5_HUMAN	RPS5	23
40S ribosomal protein S6 OS=Homo sapiens GN=RPS6 PE=1 SV=1	P62753	RS6_HUMAN	RPS6	29
40S ribosomal protein S7 OS=Homo sapiens GN=RPS7 PE=1 SV=1	P62081	RS7_HUMAN	RPS7	22
40S ribosomal protein S8 OS=Homo sapiens GN=RPS8 PE=1 SV=2	P62241	RS8_HUMAN	RPS8	24
40S ribosomal protein S9 OS=Homo sapiens GN=RPS9 PE=1 SV=3	P46781	RS9_HUMAN	RPS9	23
28S ribosomal protein S21, mitochondrial OS=Homo sapiens GN=MRPS21 PE=1 SV=2	P82921	RT21_HUMAN	MRPS21	11
Small nuclear ribonucleoprotein F OS=Homo sapiens GN=SNRPF PE=1 SV=1	P62306	RUXF_HUMAN	SNRPF	10
Septin-2 OS=Homo sapiens GN=SEPT2 PE=1 SV=1	Q15019	SEPT2_HUMAN	SEPT2	41
Septin-6 OS=Homo sapiens GN=SEPT6 PE=1 SV=4	Q14141	SEPT6_HUMAN	SEPT6	50

Septin-7 OS=Homo sapiens GN=SEPT7 PE=1 SV=2	Q16181	SEPT7_HUMAN	SEPT7	51
Septin-9 OS=Homo sapiens GN=SEPT9 PE=1 SV=2	Q9UHD8	SEPT9_HUMAN	SEPT9	65
D-3-phosphoglycerate dehydrogenase OS=Homo sapiens GN=PHGDH PE=1 SV=4	O43175	SERA_HUMAN	PHGDH	57
Splicing factor, proline- and glutamine-rich OS=Homo sapiens GN=SFPQ PE=1 SV=2	P23246	SFPQ_HUMAN	SFPQ	76
Small nuclear ribonucleoprotein Sm D1 OS=Homo sapiens GN=SNRPD1 PE=1 SV=1	P62314	SMD1_HUMAN	SNRPD1	13
Small nuclear ribonucleoprotein Sm D3 OS=Homo sapiens GN=SNRPD3 PE=1 SV=1	P62318	SMD3_HUMAN	SNRPD3	14
Serine/arginine-rich splicing factor 2 OS=Homo sapiens GN=SRSF2 PE=1 SV=4	Q01130	SRSF2_HUMAN	SRSF2	25
Serine/arginine-rich splicing factor 3 OS=Homo sapiens GN=SRSF3 PE=1 SV=1	P84103	SRSF3_HUMAN	SRSF3	19
Tubulin alpha-1A chain OS=Homo sapiens GN=TUBA1A PE=1 SV=1	Q71U36	TBA1A_HUMAN	TUBA1A	50
Tubulin beta chain OS=Homo sapiens GN=TUBB PE=1 SV=2	P07437	TBB5_HUMAN	TUBB	50
Activated RNA polymerase II transcriptional coactivator p15 OS=Homo sapiens GN=SUB1 PE=1 SV=3	P53999	TCP4_HUMAN	SUB1	14
Transforming growth factor beta-1 OS=Homo sapiens GN=TGFB1 PE=1 SV=2	P01137	TGFB1_HUMAN	TGFB1	44
Protein-glutamine gamma-glutamyltransferase 2 OS=Homo sapiens GN=TGM2 PE=1 SV=2	P21980	TGM2_HUMAN	TGM2	77
THO complex subunit 4 OS=Homo sapiens GN=ALYREF PE=1 SV=3	Q86V81	THOC4_HUMAN	ALYREF	27
Talin-1 OS=Homo sapiens GN=TLN1 PE=1 SV=3	Q9Y490	TLN1_HUMAN	TLN1	270
tRNA methyltransferase 112 homolog OS=Homo sapiens GN=TRMT112 PE=1 SV=1	Q9UI30	TR112_HUMAN	TRMT112	14
Lactotransferrin OS=Homo sapiens GN=LTF PE=1 SV=6	P02788	TRFL_HUMAN	LTF	78
Thrombospondin-1 OS=Homo sapiens GN=THBS1 PE=1 SV=2	P07996	TSP1_HUMAN	THBS1	129
Pre-rRNA-processing protein TSR1 homolog OS=Homo sapiens GN=TSR1 PE=1 SV=1	Q2NL82	TSR1_HUMAN	TSR1	92
Zinc finger protein 593 OS=Homo sapiens GN=ZNF593 PE=1 SV=2	O00488	ZN593_HUMAN	ZNF593	15
NFX1-type zinc finger-containing protein 1 OS=Homo sapiens GN=ZNFX1 PE=1 SV=2	Q9P2E3	ZNFX1_HUMAN	ZNFX1	220

Gene	siGENOME SMARTpool [5 nmol] product code
DMBT1	M-007883-01-0005
MARCKS	M-004772-03-0005
MXRA5	M-013988-01-0005
MYH10	M-023017-00-0005
MYH9	M-007668-01-0005
SEPT6	M-019260-01-0005
SEPT9	M-006373-04-0005
siGENOME non-targetting control pool #2 [20 nmol]	D-001810-10-20

Supplementary Information (Table) S5.3

Table summarising siRNA purchased to silence candidate proteins identified by proteomics as putative molecular regulators of an integrin $\alpha_v\beta_6$ adhesion environment ("adhesome"). *To functionally validate candidate proteins, siRNA were purchased (siGENOME, Dharmacon, GE Healthcare). Cells were transfected with siRNA using the INTERFERin® regent protocol (Polyplus). Knockdowns were evaluated by qRT-PCR.* **Abbreviations: DMBT-1 –** *deleted in malignant brain tumours;* **MARCKS –** *myristoylated alanine-rich C-kinase substrate;* **MXRA5 –** *matrix-remodelling associated protein 5;* **SEPT-6 –** *septin-6;* **SEPT-9 –** *septin-9;* **MYH-9 –** *myosin 9;* **MYH-10 –** *myosin 10.*

Gene	Primer	Sequence (5' -> 3')	PrimerBank ID	Strand	Length (bp)	T_m (°C)	GC content (%)
DMBT-1	F	GCCAACCTCTCGTGCATCAA	148539843c2	PLUS	20	68.6	55
	R	TGTCCCAGTAGTCATCACACAC		MINUS	22	62.6	50
MARCKS	F	AGCCCGGTAGAGAAGGAGG	153070259c1	PLUS	19	64.5	63.2
	R	TTGGGCGAAGAAGTCGAGGA		MINUS	20	69.3	55
MXRA5	F	CCTTGTGCCTGCTACGTCC	201860266c2	PLUS	19	65.8	63.2
	R	TTGGTCAGTCCTGCAAATGAG		MINUS	21	65.1	47.7
MYH-9	F	CCTCAAGGAGCGTTACTACTCA	225703132c2	PLUS	22	62.3	50
	R	CTGTAGGCGGTGTCTGTGAT		MINUS	20	62.8	55
MYH-10	F	GCTTCAAGATCGTGAGGACCA	367460089c3	PLUS	21	66.6	52.4
	R	ACTGGTTTAGGCGATTCCTGAG		MINUS	22	65.3	50
SEPT-6	F	ATGGCAGCGACCGATATAGC	156071509c1	PLUS	21	65.1	47.7
	R	GGCTGACGGACTTATTCACCA		MINUS	21	66.1	52.4
SEPT-9	F	GTCCATCACGCACGATATTGA	164698495c3	PLUS	21	65.8	47.7
	R	TGCAGGTATTTCTCGTACTGGT		MINUS	22	62.4	45.5

Supplementary Information (Table) S5.4

Primers used for qPCR validation of candidates identified by 2D-enrichment LC-MS/MS strategies as putative molecular regulators of an integrin $\alpha_v\beta_6$ adhesion environment ("adhesome"). To validate siRNA knockdown of candidates identified by LC-MS/MS analysis of 2D-enrichment experiments to evaluate their functional putative regulatory role(s) in mediating integrin $\alpha_v\beta_6$-dependent adhesions, the primers described above were used. Primers were designed using NCBI Primer-BLAST, primer sequences confirmed using NCBI BLAST and compared with primers logged in the Harvard PrimerBank repository (PrimerBank ID numbers are provided). **Abbreviations: DMBT-1 –** deleted in malignant brain tumours; **MARCKS –** myristoylated alanine-rich C-kinase substrate; **MXRA5 –** matrix-remodelling associated protein 5; **SEPT-6 –** septin-6; **SEPT-9 –** septin-9; **MYH-9 –** myosin 9; **MYH-10 –** myosin 10.

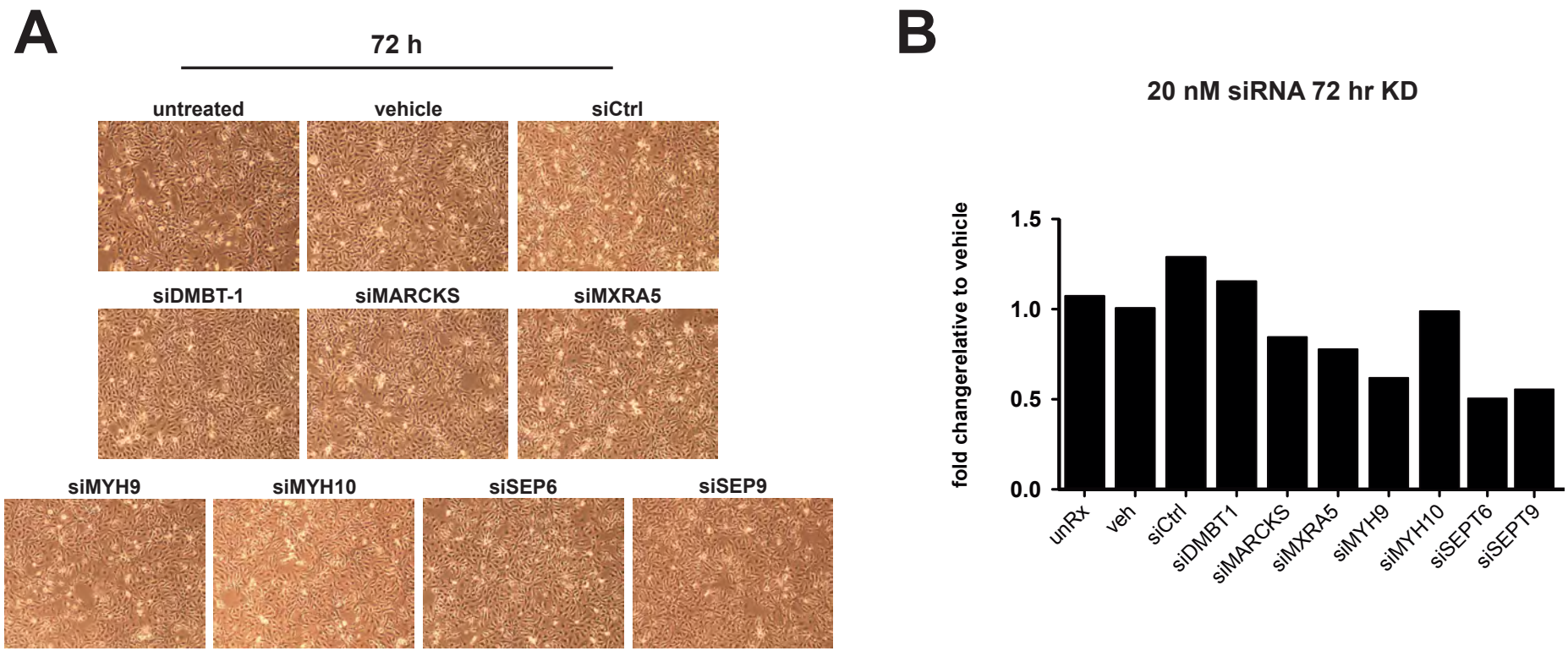

Supplementary Information (Figure) S5.5

Preliminary attempts to establish siRNA-mediated genetic silencing of the 7 candidate proteins identified for functional validation did not yield stable knockdowns of target proteins

Attempts to genetically silence the 7 candidate proteins of interest identified by LC-MS/MS failed to establish stable knockdowns of target proteins in the BT-20 cells to permit functional interrogation of their role in mediating the β_6–adhesome. Cells were transfected with 20 nM siRNA for 72 hr using the INTERFERin© protocol (Polyplus). **(S5.5 A)** Cell morphology was reviewed by phase contrast microscopy prior to RNA harvesting, cDNA synthesis and **(S5.5 B)** qPCR analysis using SYBR® Green which highlighted off-target effects of siRNA moieties.

chapter VI

results part IV

phosphoproteomic dissection of early signalling events inducted upon integrin $\alpha_v\beta_6$ engagement with its cognate ligand latency-associated peptide (LAP), ensuing activation & subsequent internalisation

VI

phosphoproteomic dissection of early signalling events inducted upon integrin $\alpha_v\beta_6$ engagement with its cognate ligand LAP, ensuing activation and subsequent internalisation

LAP-engaged integrin $\alpha_v\beta_6$-dependent signalling mediated by ERK1/2 phosphorylation is EGFR-dependent in the BT-20 TNBC model; inferential network analyses suggest Akt1 isoform predominance in Akt mediated signalling inducted during LAP/integrin $\alpha_v\beta_6$-internalisation

6. introduction

Allosteric regulation of integrin receptor activation and consequent integrin-mediated signalling events has long been established. Indeed, integrin signalling and receptor conformation are virtually synonymous; with integrin receptor signalling capacity intrinsically linked to activation status (Humphries 1996, Humphries 2002, Shimaoka *et al* 2002, Humphries *et al* 2003, Humphries 2004, Shattil *et al* 2010, Campbell and Humphries 2011, Kim *et al* 2011b, Ye *et al* 2012). Steric availability of regulatory motifs enables direct physical interactions between integrins and other protein moieties requisite for lateral integrin clustering (avidity regulation), adhesion complex microdomain formation via recruitment and assembly of adaptor proteins (notably talin, vinculin, Fyn, FAK and the kindlins)

necessary for downstream signal induction and actin cytoskeleton association (Cluzel *et al* 2005, Askari *et al* 2009, Harburger and Calderwood 2009, Shattil *et al* 2010, Margadant *et al* 2011, Roca-Cusachs *et al* 2013).

The strict spatiotemporal control of integrin receptor class expression, ligand specificity, affinity, activation, endocytic trafficking and consequent signalling underpins solid tissue morphogenesis and homeostasis in health, wound healing and tissue repair (Gumbiner 1996, Mosesson *et al* 2008, Huttenlocher and Horwitz 2011, Ivaska and Heino 2011, Margadant *et al* 2011, Arjonen *et al* 2012, Danen 2013, Alanko *et al* 2015). Logically, aberrant integrin receptor expression and activation has already been implicated in the aetiopathology of a variety of fibrotic disorders (Margadant and Sonnenberg 2010, Khan and Marshall 2016) and solid tumours (Ahmed *et al* 2002b, Bates *et al* 2005, Elayadi *et al* 2007, Havaki *et al* 2007, Hazelbag *et al* 2007, Yang *et al* 2012, Zhou *et al* 2014); including during breast tumourigenesis and disease progression (White and Muller 2007, Lambert *et al* 2012).

Of growing clinical significance, integrin-mediated signalling events are now thought to modulate tumour cell pro-invasive behaviour and therapeutic responses, notably during acquisition of chemoresistance (Aoudjit and Vuori 2012). Aberrant gross integrin receptor class expression as a poor prognostic factor in BrCa has been demonstrated for integrins: β_1 (Lesniak *et al* 2009, Zhou *et al* 2014), β_4 (Vieira *et al* 2014), $\alpha_v\beta_3$ (Havaki *et al* 2007) and $\alpha_v\beta_6$ (Allen *et al* 2014, Moore *et al* 2014). In addition, integrin receptor activation status has also been implicated in neoplastic transformation and malignant progression to metastatic disease.

The protumourigenic effects of constitutive integrin β_1 activation were reported by Lee *et al* (2013), who found that integrin β_1 was constitutively active in prostate cancer cell lines of high metastatic potential (PC3, PC3-mm2) in comparison with those of low metastatic potential (LNCaP, C4-2B4). Using the inhibitory anti-β_1 monoclonal antibody 33B6 to ablate integrin β_1 activation in vivo, the authors noted SCID mice systemically treated with 33B6 following intra-prostatic orthotopic injection with metastatic PC3-mm2 cells exhibited fewer distal lymph node metastases in comparison with SCID mice in the control IgG antibody treatment cohort.

To characterise the underlying prometastatic mechanism of integrin β_1 activation observed in their prostate cancer model, Lee and colleagues (2013) established that shRNA silencing of integrin β_1 in PC3-mm2 cells reduced FAK^{397} and Akt^{473} phosphorylation, sensitising cells to anoikis as demonstrated by increased cleavage of the DNA damage repair protein, poly (ADP-ribose) polymerase (PARP). The authors concluded that integrin β_1 activation is associated with increased FAK^{397} and Akt^{473} phosphorylation, generatng survival and mitogenic signals that circumvent anoikis and promote a prometastatic phenotype; findings that are concordant with Lesniak et al's (2009) earlier proposed mechanism of integrin β_1–driven trastuzumab resistance in BrCa.

Similarly, Moore *et al* (2014) demonstrated a putative role for integrin $\alpha_v\beta_6$–mediated trastuzumab insensitivity in HER-2 positive BrCa. The authors found that functional abrogation of integrin $\alpha_v\beta_6$ using the therapeutic antibody 264RAD (Oncology iMED, AstraZeneca UK) potentiated treatment efficacy of trastuzumab (Herceptin®, Genentech USA Inc) HER-2 blockade in an in vivo model of HER-2-driven BrCa. Co-targeting of both HER-2 (trastuzumab) and integrin $\alpha_v\beta_6$ (264RAD) was seen to reduce both tumour growth and metastasis. Preliminary mechanistic dissection of this integrin $\alpha_v\beta_6$-HER-2 RTK cross talk revealed a reduction of total Akt2 in trastuzumab/264RAD dual-therapy tumour samples in comparison with trastuzumab monotherapy, suggesting integrin $\alpha_v\beta_6$–derived Akt2-signalling compensation of trastuzumab downstream effects; again, a mechanism similar to that proposed by Lesniak *et al* (2009) for integrin β_1 within the context of trastuzumab therapy in MBC. Indeed, Janes and Watt (2004) had earlier described that integrin $\alpha_v\beta_6$ expression conferred a survival advantange over integrin $\alpha_v\beta_5$ expression during malignant transformation of stratified squamous epithelia to squamous cell carcinoma. The authors attributed this integrin $\alpha_v\beta_6$–mediated survival advantage to Akt-dependent survival signals permitting circumvention of anoikis.

Derailed endocytic regulation of integrin receptors (Mosesson *et al* 2008), integrin signalling within endosomes (Alanko *et al* 2015) and integrin-RTK crosstalk during intracellular trafficking (Soung *et al* 2010, Ivaska and Heino 2011) have all been implicated as pro-tumourigenic and pro-metastatic determinants in human malignancy; with demonstrable links to generation of anoikis-resistant signalling. Thus, exploration of integrin receptor activation status and endocytic dynamics is of growing research interest.

Integrin $\alpha_v\beta_6$ expression within the myoepithelial compartment has already been associated with risk of progression to invasive disease in human primary DCIS (Allen *et al* 2014). This finding, in conjunction with the demonstrable treatment benefit achieved with integrin $\alpha_v\beta_6$ functional blockade in tandem with trastuzumab administration in HER-2 driven BrCa (Moore *et al* 2014), implicate integrin $\alpha_v\beta_6$–mediated signalling during BrCa progression to metastatic disseminated disease which warrants further investigation.

Furthermore, given the emerging significance of integrin-mediated signalling compensating the antiproliferative effects of established therapeutics (Lesniak *et al* 2009, Aoudjit and Vuori 2012), integrin $\alpha_v\beta_6$–derived signals may also play a role in stromal remodelling (Marsh *et al* 2008) and the development of chemoresistance. However, current definitions of integrin $\alpha_v\beta_6$–mediated signalling events following ligand engagement, receptor activation, subsequent internalisation and intracellular trafficking are presently limited; although several intracellular proteins have been shown to directly bind the integrin β_6-cytoplasmic domain to modulate integrin $\alpha_v\beta_6$–dependent invasive functions in cancer including HS-1 Associated Protein X-1 (HAX-1) (Ramsay *et al* 2007) and psoriasin (S100A7) (Morgan *et al* 2011_.

Other binding partners acting in concert with integrin $\alpha_v\beta_6$ to mediate its pro-invasive effects have also been described. Jones *et al* (2013) reported that ADAM10 was overexpressed in oral cancer and may modulate progression to invasive disease. Jones and colleagues (2013) concluded that ADAM10 is an important regulator of invasion and migration in malignant cells by an as yet undefined mechanism. The authors hypothesised that crosstalk between integrin $\alpha_v\beta_6$ and ADAM10 may promote MMP expression to permit stromal remodelling and degradation thus imparting an invasive and migratory phenotype.

Therefore, in light of the established biological importance of integrin $\alpha_v\beta_6$ expression and localisation during tumour cell migration and invasion, it is evident that characterisation of integrin $\alpha_v\beta_6$–mediated signalling events that drive acquisition of a pro-metastatic phenotype is duly warranted to determine its aetiopathological significance within the context of BrCa progression to disseminated disease. Greater understanding of the mechanisms by which the integrin $\alpha_v\beta_6$ facilitates cellular invasion may elucidate novel targets for therapeutic

intervention, either as new monotherapy strategies or to potentiate the efficacy of existing agents in dual targeting regimens.

overview of key findings

To characterise signalling-associated phosphorylation events inducted upon integrin $\alpha_v\beta_6$ receptor activation following cognate ligand engagement and subsequent internalisation, a phosphoproteomics strategy was developed. A LAP-ligand internalisation assay targeting the integrin $\alpha_v\beta_6$ receptor was first developed to generate peptides for phosphoenrichment and LC-MS/MS interrogation. As previously demonstrated (Chapter V: Results Part III, Figure 5.2C), LAP ligand specifically engages the integrin $\alpha_v\beta_6$ in BT-20 TNBC cells and was therefore used to interrogate integrin $\alpha_v\beta_6$–dependent processes in the BT-20 cell line.

Using human IgG (Fc')-tagged ligands, proof of concept experiments performed using the VB6 cell line showed that LAP-Fc (a surrogate marker for active, ligand-engaged integrin $\alpha_v\beta_6$) internalises from the plasmalemma over a 60 min timeframe reaching the perinuclear region within 30 min, but the integrin function blocking antibody 53A2 does not internalise (Figure 6.1.1A - D). An Fc-tagged transferrin ligand (Tf-Fc) was used as a control to validate internalisation assays (Figure 6.1.1E).

Given the purpose of the ligand engagement and internalisation assay was to generate phosphopeptides for downstream phosphoproteomic identification of novel integrin $\alpha_v\beta_6$–dependent signalling events, a panel of integrin $\alpha_v\beta_6$ cognate ligands comprising the synthetic peptide A20FMDV2 (-**TJ**) alongside natural ECM ligands LAP (**LAP**) and fibronectin (**Fn**) were evaluated in tandem with the non-integrin β_6 ligands collagen I (**Col I**) and epidermal growth factor (**EGF**), for their utility to stimulate downstream phosphorylation events in the BT-20 cell line (Figure 6.1.3).

Once validated, four replicate LAP-ligand engagement and internalisation assays using an unconjugated human recombinant LAP ligand were performed from which phospho-enriched peptides were generated for LC-MS/MS interrogation. Phosphoproteomic LC-MS/MS analysis identified 88 533 tandem mass spectra corresponding to 8 874 unique peptide ions; of which 6 491 were phosphopeptides containing 7 129 phosphorylation sites mapping to 2 073 proteins identified (Figure 6.2).

Inferential network analysis using a kinase substrate enrichment analysis (KSEA) method pioneered by Casado *et al* (2013a) was used to characterise kinase-mediated signalling events inducted or downregulated at defined LAP-ligand internalisation timepoints (Figure 6.3). Five kinases (**MAP3K8**; **MAPKAPK2**; **Nuak1**; **PDK1**; **TBK1**) identified by KSEA as putative regulators of early (5', t=5: **MAP3K8**; **MAPKAPK2**; **PDK1**; **TBK1**) and late (30', t=30: **Nuak1**) integrin $\alpha_v\beta_6$–mediated signalling following LAP ligand engagement and internalisation were selected for additional investigation using commercially available small molecule inhibitors (SMI) of kinase activity (Supplemental Figure S6.2).

KSEA indicated that MAP3K8/COT kinase activity was upregulated upon integrin $\alpha_v\beta_6$/LAP internalisation (Figure 6.4A). Review of KSEA results for known MAP3K8 downstream effectors (ERK1/2, JNK and p38) also exhibited upregulation in activity (Figure 6.4B), further implicating upstream activity of MAP3K8. Preliminary investigations into the regulatory role of MAP3K8 (COT) in the BT-20 cell line suggested MAP3K8 inhibition using the commercial SMI TC-S 7006 (Tocris, R&D Systems) dampened ERK1/2 phosphorylation downstream of LAP ligand stimulation, but did not appear to modulate Akt1 phosphorylation motifs nor EGFR phosphorylation at Tyr1068 (Figure 6.4C).

Curiously, MAP3K8 inhibition was seen to promote the active integrin $\alpha_v\beta_6$ conformer (recognised by FCM evaluation of surface bound antibody 6.2E5) in the presence of canonical integrin activation methods using Mn^{2+} ions and cognate LAP ligand (Figure 6.4D and E) in the BT-20 TNBC cell line. A similar effect in response to LAP activation in the presence of TC-S 7006 was observed in the VB6 cell line (Figure 6.4F). Using the A375 matched pair cell lines, expression of integrin β_6 appeared to sensitise A375β6 cells to the anti-proliferative effects of MAP3K8 targeting using TC S-7006, in comparison with integrin β_6 null A375puro cells.

KSEA results also indicated that downstream LAP-ligand induced integrin $\alpha_v\beta_6$–mediated signalling events in the BT-20 TNBC cell line are driven by Akt1 ($p \leq 0.01$**) (Figure 6.5.1) and ERK1/2 (Figure 6.5.2) phosphorylation; with ERK1 phosphorylation heavily implicated in late (30'; t=30) integrin $\alpha_v\beta_6$–associated signalling events ($p \leq 0.001$***). Attempts to functionally interrogate the five kinases identified by KSEA were hindered by a lack of reliable antibodies to confirm siRNA knockdown (Supplemental Figure S6.3) or SMI ablation of activating phosphorylation motifs (Supplemental Figure S6.4).

Several phosphopeptides mapping to EGFR phosphorylation residues were strongly enriched and directly identified by LC-MS/MS; implicating EGFR-mediated signalling downstream of LAP-ligand integrin $\alpha_v\beta_6$-engagement and internalisation in the BT-20 cell line (Figure 6.5.3A).

To further investigate the putative role of RTK crosstalk during integrin $\alpha_v\beta_6$ LAP-ligand engagement, LAP-sitmulation assays were performed in the BT-20, SUM159 and MDA-MB-468 TNBC cell lines in the presence of EGFR and/or c-MET blockade (Figure 6.5.3B and C). Results from these assays suggested that LAP-induced ERK1/2 phosphorylation is EGFR-dependent but independent of c-MET in the BT-20 and SUM159 cell lines, but is unaffected in the MDA-MB-468 cell line bearing constitutively active ERK1/2.

Preliminary investigations seeking to define LAP-internalisation kinetics and downstream signalling in the presence of EGFR and/or integrin $\alpha_v\beta_6$ blockade to investigate putative EGFR/integrin co-regulatory cross talk met with limited success and require additional optimisation (Supplementary Figure S6.5).

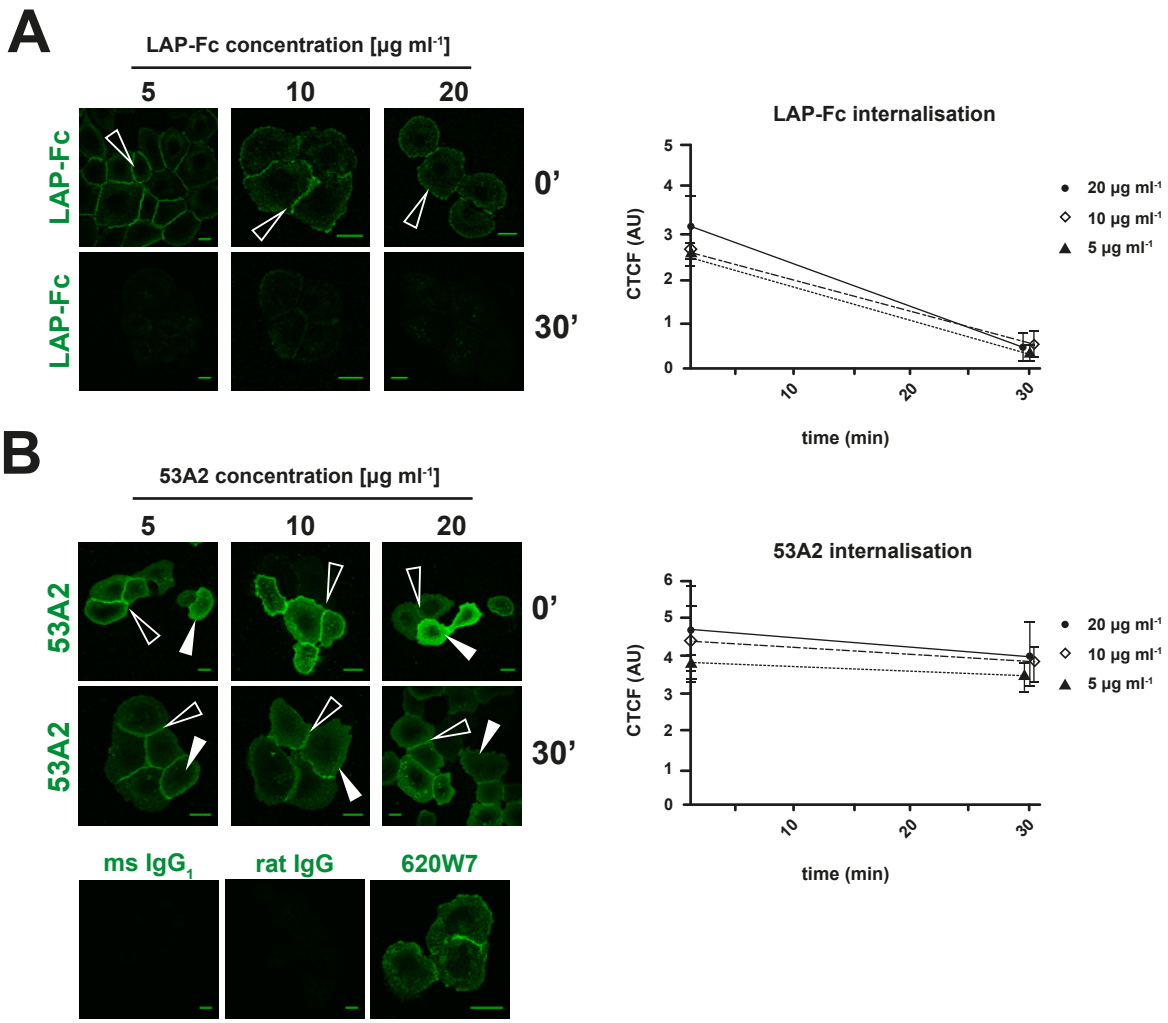

Figure 6.1.1 (A & B)
LAP-ligand stimulation experimental work up: Immunofluorescence microscopy validation of LAP ligand-stimulated internalisation kinetics in comparison with the integrin $\alpha_v\beta_6$ function-blocking antibody clone 53A2

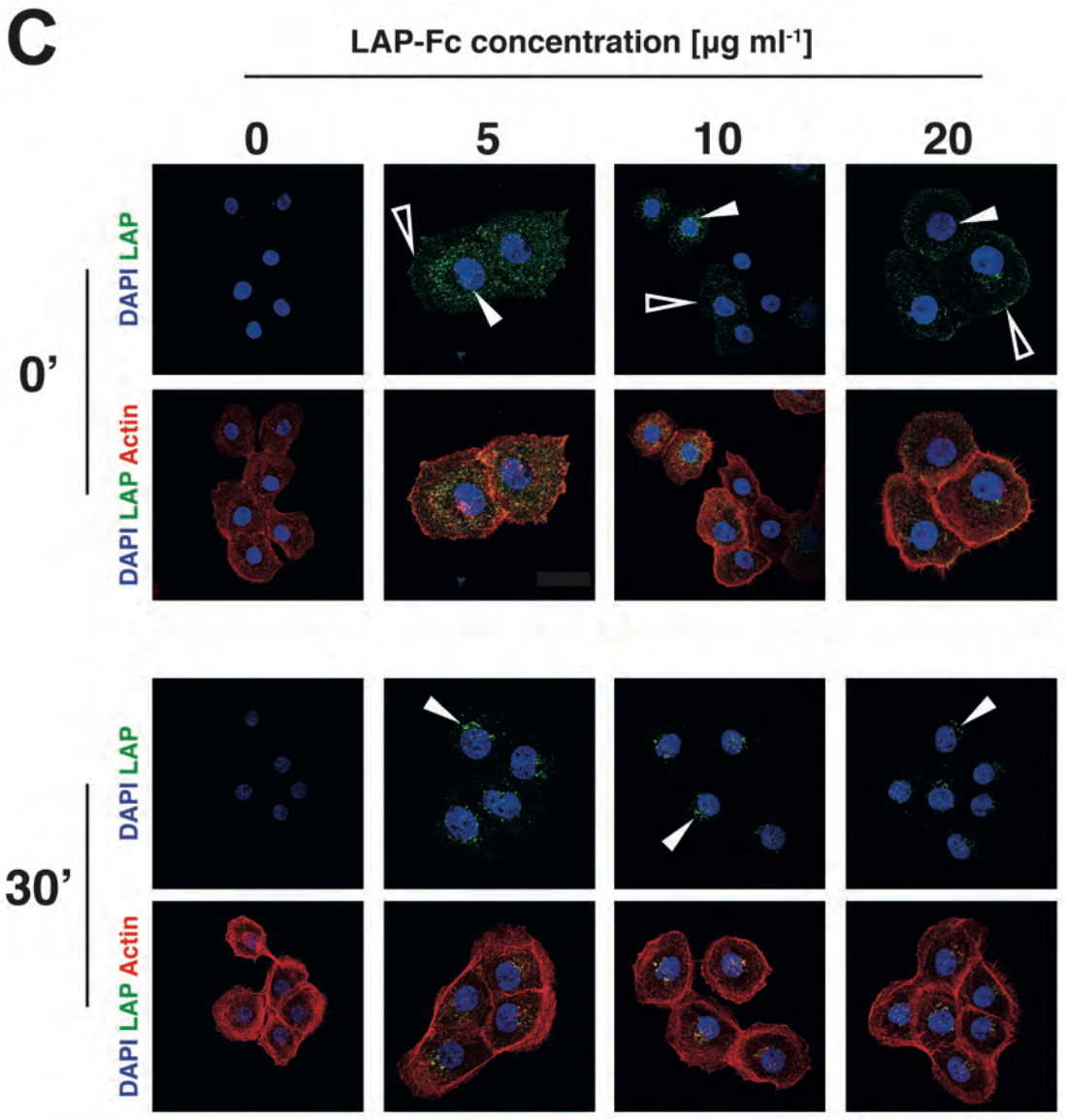

Figure 6.1.1 (C)
LAP-ligand stimulation experimental work up: Immunofluorescence microscopy validation of LAP ligand-stimulated internalisation kinetics in comparison with the integrin $\alpha_v\beta_6$ function-blocking antibody clone 53A2

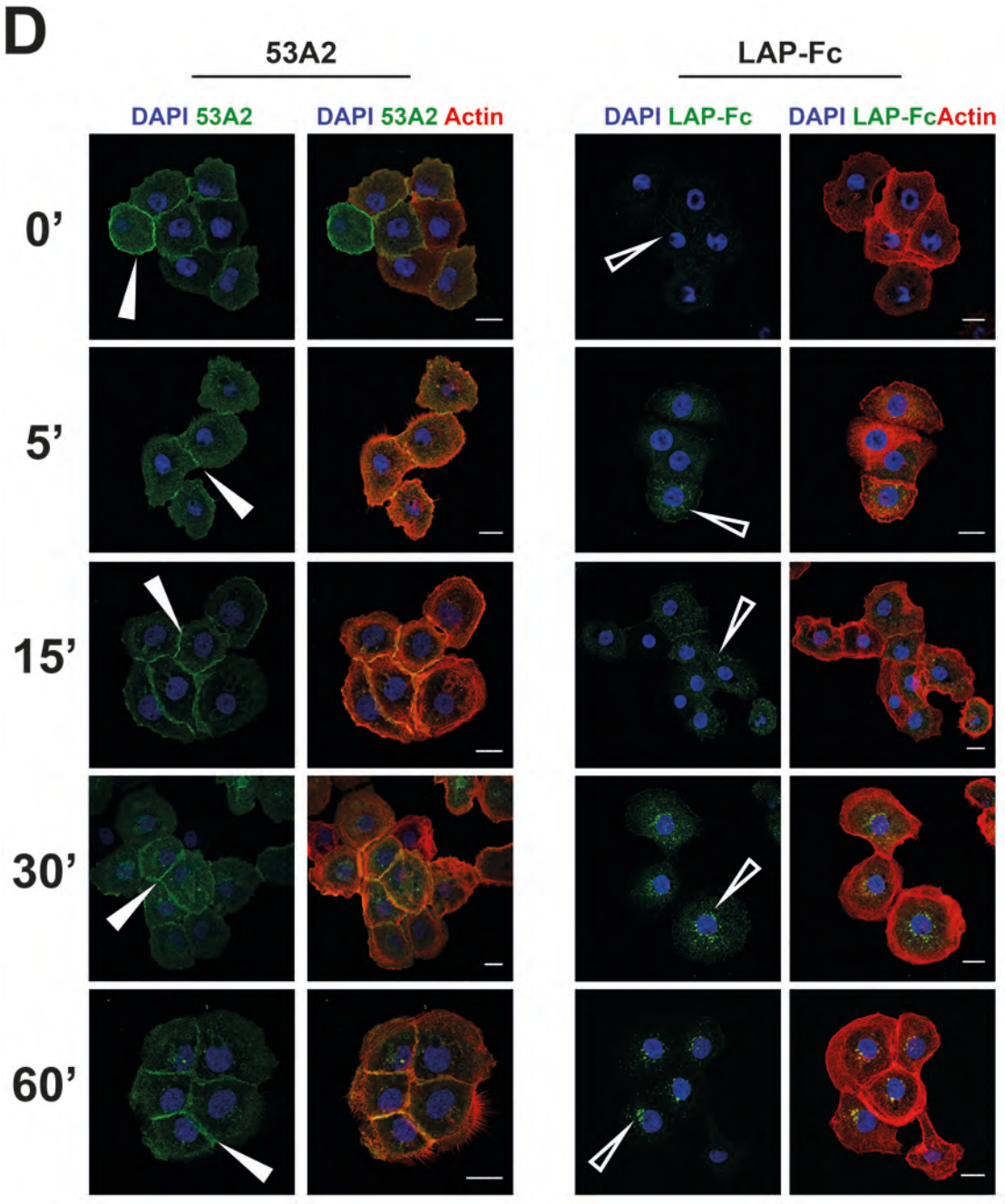

Figure 6.1.1 (D)
LAP-ligand stimulation experimental work up: Immunofluorescence microscopy validation of LAP ligand-stimulated internalisation kinetics in comparison with the integrin $\alpha_v\beta_6$ function-blocking antibody clone 53A2

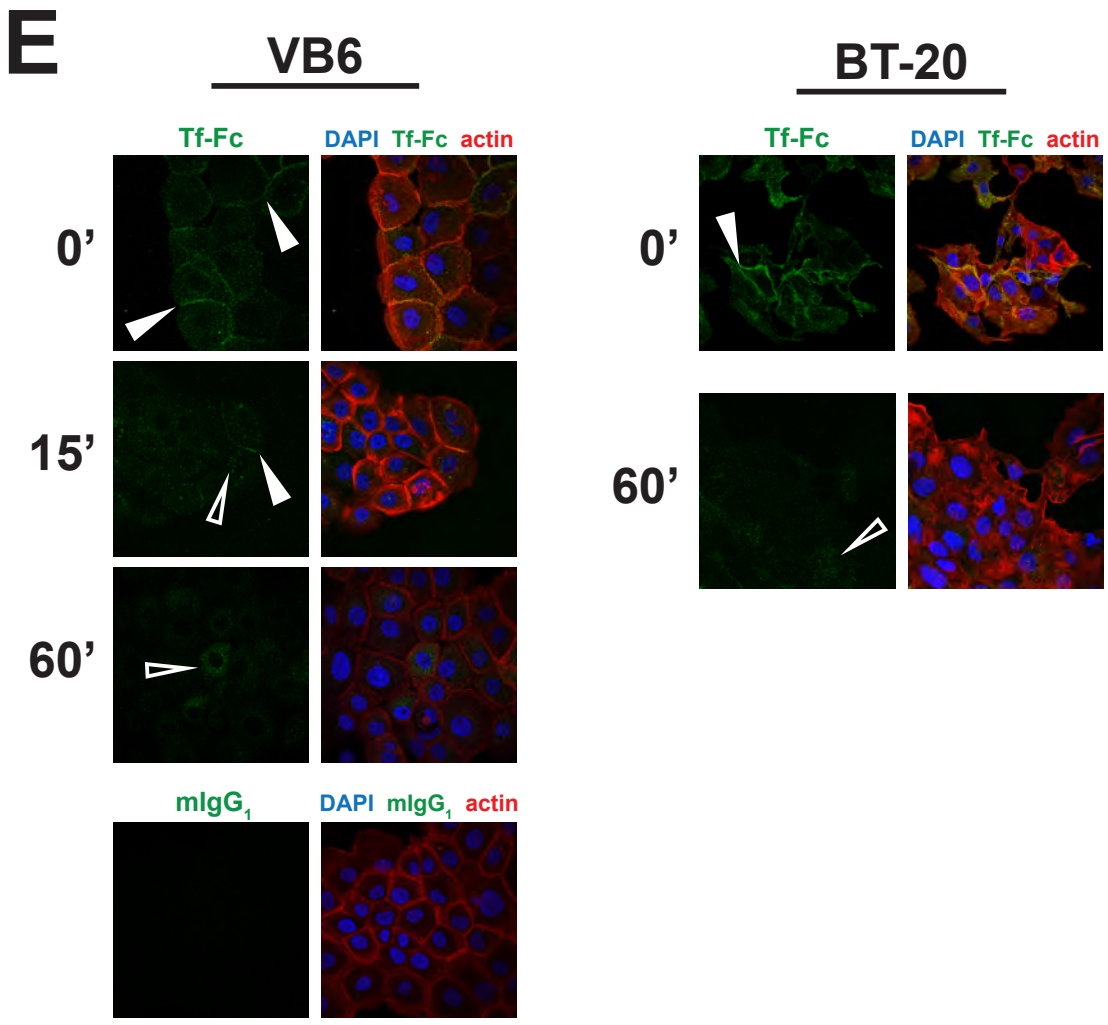

Figure 6.1.1 (E)
LAP-ligand stimulation experimental work up: Immunofluorescence microscopy validation of a human IgG (Fc')-tagged transferrin control ligand-stimulated internalisation kinetics in the VB6 and BT-20 cell lines

Figure 6.1.1

LAP-ligand stimulation experimental work up: Immunofluorescence microscopy validation of LAP ligand-stimulated internalisation kinetics in comparison with the integrin $\alpha_v\beta_6$ function-blocking antibody clone 53A2

To permit phosphoproteomic dissection of integrin $\alpha_v\beta_6$-mediated signalling inducted upon cognate LAP-ligand engagement, the upstream ligand-stimulation/internalisation assay was first validated by IMF. Cells were seeded onto 13 mm non-derivatised glass coverslips at 2 x10^4 cells per coverslip and left to adhere overnight ready for assay. Cells were serum-starved for 4 hours in low serum media (1% FBS), cell monolayers washed and treated with ligand or antibody for 10 min at 4°C prior to washing to remove unbound ligand. Complete media was added and cells returned to standard culture conditions to permit ligand internalisation. The surface abundance of a human IgG (Fc')-tagged LAP ligand (**LAP-Fc**; Biogen Idec) or transferrin ligand (**Tf-Fc**; Hölzel Diagnostika) undergoing internalisation were first evaluated by non-permeabilised IMF. VB6 cells were live-labelled with either **(6.1.1 A)** LAP-Fc ligand (Biogen Idec) or **(6.1.1 B)** the integrin $\alpha_v\beta_6$–function blocking antibody clone 53A2 (CR-UK) at concentrations of 5, 10 and 20 μg ml^{-1} to compare cell surface labelling efficacy and internalisation kinetics over a 30' time period. At 0' or 30' internalisation timepoints cells were fixed with 4% (w/v) PFA (P6148, Sigma Aldrich) for 8'. LAP-Fc was labelled with a monoclonal mouse anti-human (Fc') antibody (10 μg ml^{-1}, ab113636, AbCam) and detected with a tertiary AlexaFluor®488-fluorophore conjugated anti-mouse IgG antibody (16 μg ml^{-1}, A11029, Invitrogen™). An anti-rat IgG AlexaFluor®488 antibody (16 μg ml^{-1}, A11006, Invitrogen™) was used to detect surface-bound antibody 53A2. Corrected total cell fluorescence (CTCF) was determined using ImageJ software to quantify cell surface fluorescence as a read out for abundance of surface-bound LAP-Fc ligand or antibody 53A2 to determine their respective internalisation kinetics. Five fields of view were evaluated for each condition and timepoint across 3 biological replicates (n=3) each comprising intra-assay technical triplicates. Mean CTCF values were plotted in GraphPad Prism with error bars showing s.d. Isotype matched negative controls were prepared (mouse IgG and rat IgG) along with an integrin $\alpha_v\beta_6$ positive control antibody (620W7). Representative images are shown. **(6.1.1 A)** LAP-Fc predominated at the cell periphery or cell-cell junctions at the 0' starting timepoint (white outline arrows). Surface abundance of LAP-Fc ligand visibly and markedly decreased over a 30' time period, suggesting internalisation. No discernible difference in labelling efficacy was observed between the concentrations 5, 10 and 20 μg ml^{-1}. **(6.1.1 B)** The antibody 53A2 localised at the peripheral edges of cells and cell-cell junctions (white outline arrows). A diffuse cell surface distribution was also observed (block white arrows). Surface abundance of antibody 53A2 appeared relatively unaltered across the 30' time period studied, with no discernible difference in labelling efficacy or internalisation kinetics across the different concentrations evaluated. **(6.1.1 C)** To confirm that the loss of fluorescence signal for LAP-Fc observed in **(6.1.1 A)**, was attributable to ligand-stimulated internalisation and not physical dissociation, permeabilised IMF was performed to assess subcellular distribution of LAP-Fc ligand over a 30' time period. Again, VB6 cells were used to compare concentrations of LAP-Fc ranging from 0 - 20 μg ml^{-1}. At 0', LAP-Fc was seen to localise at the cell periphery and cell-cell junctions (white outline arrows), with a punctate cytoplasmic distribution (block white arrows) most notable at 5 and 20 μg ml^{-1}. By 30', the cell periphery, cell-cell junction and more diffuse cytoplasmic LAP-Fc distributions were lost. Instead, LAP-Fc was observed in a vesicular, perinuclear pattern. **(6.1.1 D)** The subcellular distribution of LAP-Fc (5 μg ml^{-1}) was next characterised by permeabilised IMF over a 60' time period in comparison with antibody 53A2 to optimise time points for phosphoproteomic interrogation. The antibody 53A2 (10 μg ml^{-1}) predominated at cell-cell junctions (block white arrows). This subcellular distribution pattern was unaltered across the 0', 5', 15' 30' and 60' time points evaluated, suggesting that the function blocking antibody 53A2 remains bound to the integrin $\alpha_v\beta_6$ in a steady state and does not undergo receptor-engaged internalisation. In contrast, LAP-Fc underwent subcellular redistribution from the plasma lemma to the cytoplasm in a vesicular pattern (white outline arrows). By 60', LAP-Fc appeared completely downregulated from the cell surface and predominated in large vesicular perinuclear clusters. **(6.1.1 E)** Binding and internalisation of a Tf-Fc ligand (5 μg ml^{-1}) were also evaluated (as described for LAP-Fc) for utility as a control ligand/receptor biological comparator. The Images were acquired on the ZEISS LSM710 equipped with ZEISS Zen image analysis software (all Carl Zeiss AG, DE). Images were prepared for presentation using Image J (National Institutes of Health).

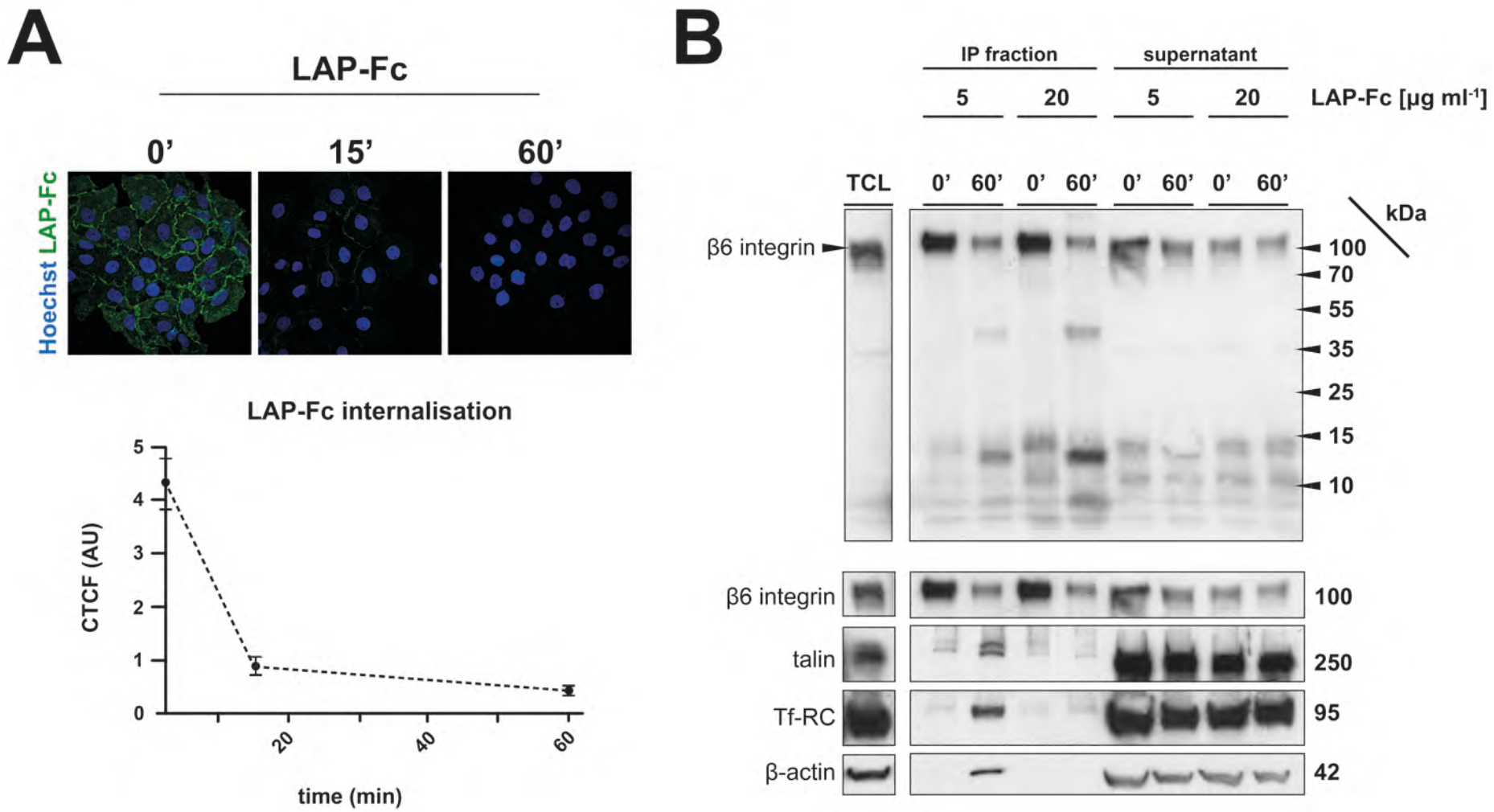

Figure 6.1.2 (A & B)
LAP-ligand stimulation experimental work up (validation of LAP-ligand-integrin $\alpha_v\beta_6$ direct association in the BT-20 cell line): Non-permeabilised immunofluorescence microscopy validation of LAP ligand-stimulated internalisation kinetics and confirmation of LAP-integrin $\alpha_v\beta_6$ direct protein-protein interaction during internalisation by co-immunoprecipitation of integrin $\alpha_v\beta_6$ using a human IgG (Fc')-tagged LAP-ligand

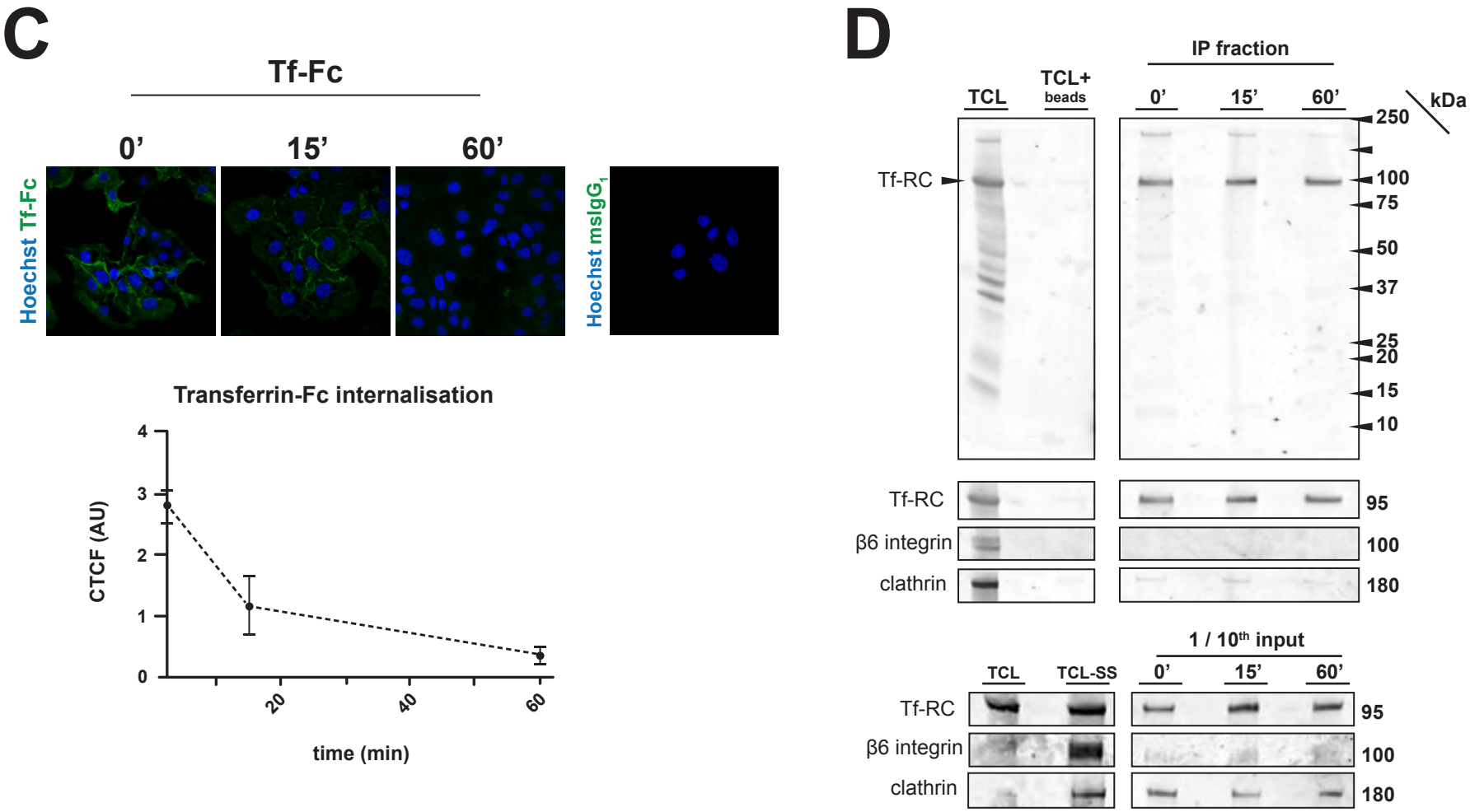

Figure 6.1.2 (C & D)
LAP-ligand stimulation experimental work up (validation of LAP-ligand-integrin $\alpha_v\beta_6$ direct association in the BT-20 cell line): Non-permeabilised immunofluorescence microscopy validation of transferrin (Tf) ligand-stimulated internalisation kinetics and confirmation of Tf-Transferrin Receptor Complex (Tf-RC) direct ligand-receptor protein-protein interaction during internalisation by co-immunoprecipitation of Tf-RC using a human IgG (Fc')-tagged Tf-ligand

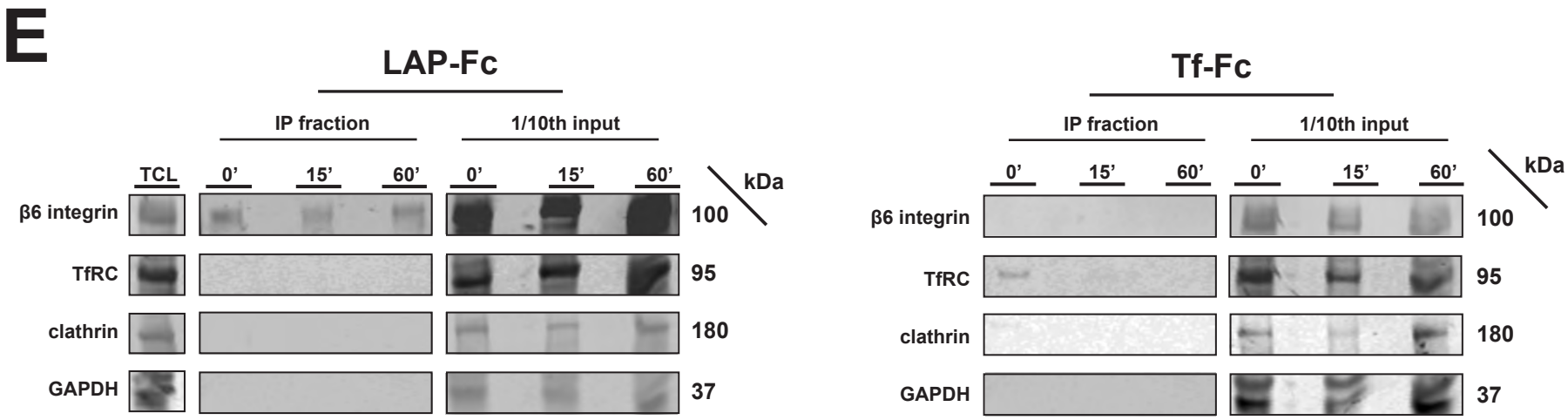

Figure 6.1.2 (E)
LAP-ligand stimulation experimental work up (validation of LAP-ligand-integrin $\alpha_v\beta_6$ direct association in the BT-20 cell line): Confirming reproducibility of LAP-integrin $\alpha_v\beta_6$ direct protein-protein interaction during internalisation by co-immunoprecipitation of integrin $\alpha_v\beta_6$ using a human IgG (Fc')-tagged LAP-ligand

Figure 6.1.2

LAP-ligand stimulation experimental work up (validation of LAP-ligand-integrin $\alpha_v\beta_6$ direct association in the BT-20 cell line): Non-permeabilised immunofluorescence microscopy validation of LAP ligand-stimulated internalisation kinetics and confirmation of LAP-integrin $\alpha_v\beta_6$ direct protein-protein interaction during internalisation by co-immunoprecipitation of integrin $\alpha_v\beta_6$ using a human IgG (Fc')-tagged LAP-ligand

Following proof of concept that the integrin $\alpha_v\beta_6$ is the predominant LAP receptor and may be used to specifically interrogate ligand-engaged integrin $\alpha_v\beta_6$–mediated functions in the BT-20 TNBC cell line (see Chapter V: results part III), non-permeabilised immunofluorescence (IMF) was used to confirm that surface-bound LAP ligand is internalised over a 60 min time frame **(6.1.2 A)** in comparison with transferrin (**Tf**) control ligand **(6.1.2 C).** Additional co-immunoprecipitation (co-IP) validation experiments were performed to confirm direct LAP-integrin $\alpha_v\beta_6$ protein-protein interaction, demonstrating that LAP-ligand engages and remains directly associated with integrin $\alpha_v\beta_6$ during LAP-ligand internalisation **(6.1.2 B)**, as verified against transferrin ligand (**Tf**)-transferrin receptor complex (**Tf-RC**) co-IP **(6.1.2 D)**; reproducibility of co-IP was assessed **(6.1.2 E)**. For non-permeabilised IMF, BT-20 cells were plated on 13 mm non-derivatised glass coverslips at 2 x 10^4 cells per coverslips and left to adhere overnight under standard culture conditions. Cell monolayers were washed (x3) in serum-free α-MEM equilibrated to 37°C prior to 4-hour serum starvation in low serum media (1% charcoal-stripped FBS/α-MEM) supplemented with 25 mM HEPES, prior to human IgG (Fc')-tagged-ligand pre-treatments using either **(6.1.2 A) LAP-Fc** (5µg ml^{-1}, Biogen Idec) or **(6.1.2 C) Tf-Fc** (5µg ml^{-1}, 13656-W02H, Hölzel-Diagnostika GmbH) for 10 min at 4°C. Unbound ligand was removed by washing, complete media supplemented with 25 mM pre-equilibrated to 37°C was added and coverslips returned to standard culture conditions to permit ligand internalisation. At designated time-points, coverslips were fixed (4% (v/v) paraformaldehyde; 8 min) ready for labelling with a mouse anti-human IgG (Fc') antibody (10 µg ml^{-1}, ab113636, AbCam) to detect Fc-tagged ligands and detected with AlexaFluor®488-fluorophore conjugated anti-mouse IgG antibody (16 µg ml^{-1}, A11029, Invitrogen™). Nuclei were demonstrated with membrane permeant Hoechst 33342 (H3570, Life Technologies). Corrected total cell fluorescence (CTCF) was determined using ImageJ software to quantify cell surface fluorescence as a read out for abundance of surface-bound LAP-Fc or Tf-Fc ligand determine their respective internalisation kinetics. Five fields of view were evaluated for each condition and timepoint across 3 biological replicates (n=3) each comprising intra-assay technical triplicates. Mean CTCF values were plotted with error bars showing s.d. Both **(6.1.2 A)** **LAP-Fc** and **(6.1.2 C)** **Tf-Fc** ligands were seen to internalise over a 60 minute time-period, most rapidly in the first 15 min. To confirm that integrin $\alpha_v\beta_6$ remains bound to LAP during the ligand internalisation observed by IMF, co-IP experiments were performed **(6.1.2 B, D & E)**. BT-20 cells were seeded in 10 cm dishes at 5 x 10^6 cells per dish and left to adhere overnight, prior to ligand labelling and internalisation (as previously described). At designated time-points, lysates were harvested in IP lysis buffer (prepared in-house). Lysates were tumbled overnight at 4°C with unconjugated protein G beads (101243, Invitrogen™) to co-IP Fc'-tagged ligand/cognate receptor complexes. Beads were washed by centrifugation in a series of stringency IP wash buffers (prepared in-house): first in a high salt buffer, then a high detergent buffer with final washing in a salt-free buffer prior to boiling (100°C; 5 min) beads in an equal volume of [2X] reducing SDS sample buffer (prepared in-house). Beads were pelleted by centrifugation and supernatants kept for validation by Western blot (WB). **(6.1.2 B & E)** Integrin $\alpha_v\beta_6$ was successfully IP'd using LAP-Fc at specified internalisation time-points, confirming direct association of LAP undergoing internalisation with the integrin $\alpha_v\beta_6$ receptor. Control IP experiments using Tf-Fc to isolate Tf-RC provided technical validation **(6.1.2 D & E)**. IP samples were probed by WB for: **integrin β6** (c-19, 0.2 µg ml^{-1}, sc-6632, Santa Cruz BioTech); **Tf-RC** (0.2 µg ml^{-1}, S); alongside the endocytic vesicle coating protein **clathrin** (1 µg ml^{-1}, BD610500, BDT); the integrin-associated protein **talin** (0.2 µg ml^{-1}, sc-7534, SCBT) was probed to evaluate the presence of additional known integrin binding partners; **GAPDH** (0.1 µg ml^{-1}, 2118L, CST) was used to assess purity and specificity of ligand/receptor complexes co-IP'd.

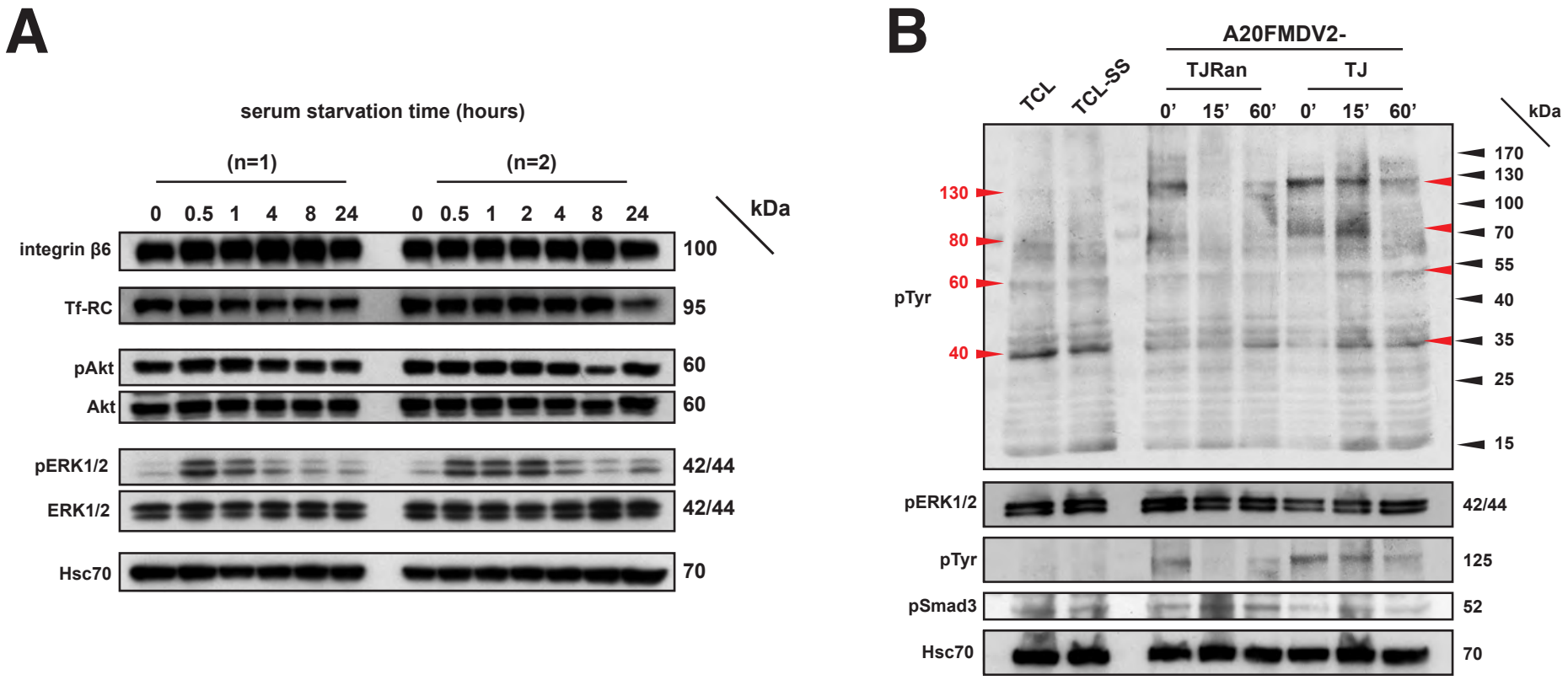

Figure 6.1.3 (A and B)
Development and protein-level validation of a ligand-stimulated internalisation assay to investigate and define downstream signalling pathways inducted upon integrin $\alpha_v\beta_6$ ligand-engagement, activation and internalisation

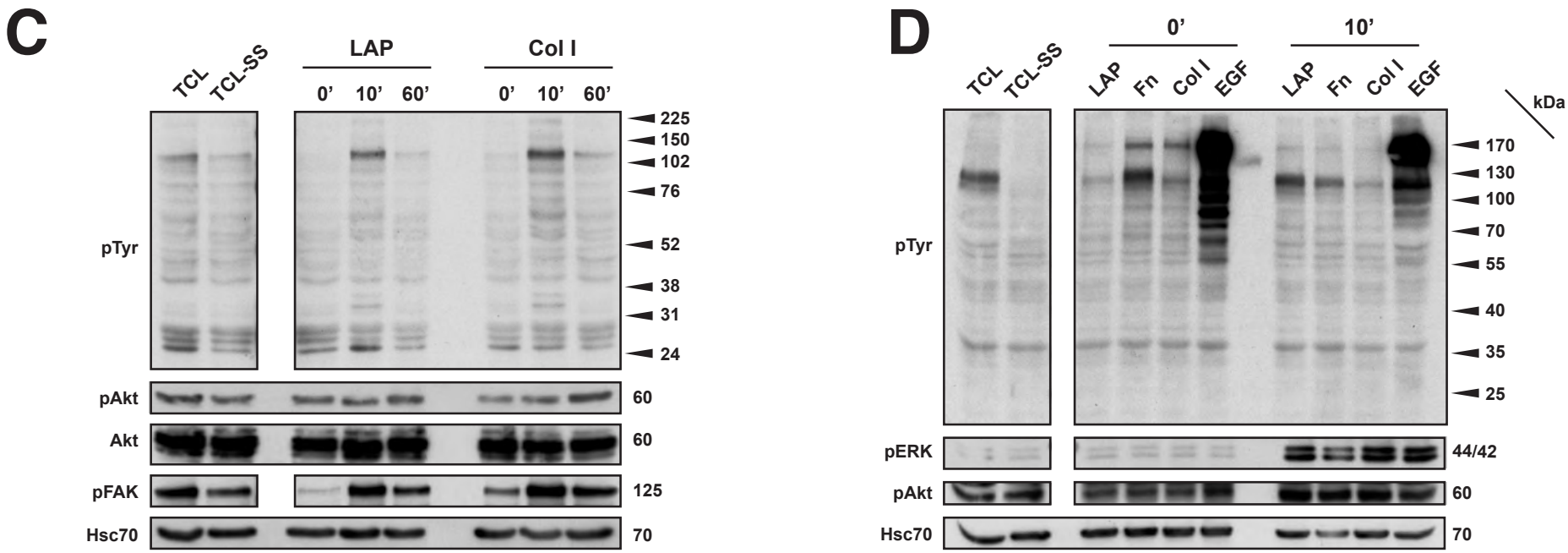

Figure 6.1.3 (C and D)
Development and protein-level validation of a ligand-stimulated internalisation assay to investigate and define downstream signalling pathways inducted upon integrin $\alpha_v\beta_6$ ligand-engagement, activation and internalisation

Figure 6.1.3

Development and protein-level validation of a ligand-stimulated internalisation assay to investigate and define downstream signalling pathways inducted upon integrin $\alpha_v\beta_6$ ligand-engagement and internalisation

Following proof of concept that surface-bound LAP ligand is internalised over a 60 min time frame, additional proof of concept experiments were performed to validate that integrin $\alpha_v\beta_6$-mediated signalling could be dissected using LAP-ligand engagement of integrin $\alpha_v\beta_6$ in the BT-20 cell line. **(6.1.3 A)** The effect of a 4-hour serum starvation step (performed prior to ligand-engagement/ internalisation assay) upon downstream signalling, was reviewed by WB. BT-20 cells were seeded in 3 cm dishes at 3 x 10^6 cells per dish and left to adhere overnight. Cell monolayers were washed (x3) in serum-free α-MEM equilibrated to 37°C prior to serum starvation in low serum media (1% FBS/α-MEM) for serial time-points as indicated. On completion of serum starvation, lysates were manually harvested at designated time-points by scraping in NP-40 lysis buffer supplemented with protease and phosphatase inhibitors. Lysates were normalised and samples evaluated by WB (20 ng loading protein) for surface receptor moieties to evaluate stability of surface receptor pools during serum starvation: **integrin β6** (c-19, 0.2 µg ml^{-1}, sc-6632, Santa Cruz BioTech); transferrin receptor complex (**Tf-RC**) (0.2 µg ml^{-1}, S); alongside the known integrin downstream signalling mediators **pAkt** (pSer473, 2 µg ml^{-1}, 4060S, CST), **pERK1/2** (pThr202/204, 2 µg ml^{-1}, 9101L, CST); together with their corresponding total protein **Akt** (1 µg ml^{-1}, 9272S, CST) and **ERK1/2** (1 µg ml^{-1}, 9102L, CST). A loading control was also performed (**Hsc-70**, 0.2 µg ml^{-1}, S). Two biological repeats were performed (n=2). Notably, pERK1/2 was upregulated in the 2 hours immediately post induction of serum starvation however, pERK levels were restored to baseline (0 time-point) by 4 hours in both biological repeats. This validated the use of a 4-hour serum starvation step in low serum media (1% FBS), confirming that pERK1/2 signalling is not aberrantly upregulated due to low serum conditions which would confound use of pERK1/2 as a readout for induction of downstream signalling in the LAP-ligand/integrin $\alpha_v\beta_6$ stimulation and internalisation assay being developed. **(6.1.3 B - D)** Evaluation of ligand species to be used for ligand-induced stimulation and internalisation of integrin $\alpha_v\beta_6$ was performed comparing signalling motifs inducted by a natural integrin ligands (**LAP**) in comparison with a synthetic peptide (**A20FMDV2-TJ**) and random sequence negative control peptide (**BioTJ-Ran**) alongside another integrin $\alpha_v\beta_6$ cognate ligand (**Fn**). An integrin β_1 ligand (**Col I**) and an RTK ligand (**EGF**) were also evaluated. In all experiments shown, BT-20 cells were seeded in 3 cm dishes at 3 x 10^6 cells per dish, left to adhere overnight prior to 4-hour serum starvation and exposed to ligand for 10 min at 4°C (**A20FMDV2-TJ** or **BioTJ-Ran** (a kind gift from Prof T Jackson) 100 nM; **LAP** (L3408, Sigma) – 0.5 µg ml^{-1}; **Fn** (F2006, Sigma) – 10 µg ml^{-1}; **Col I** (354236, Corning® – 10 µg ml^{-1}; **EGF** (E9644, Sigma) – 50 ng ml^{-1}) pior to internalisation at 37°C in complete media for designated times (as indicated in WB figure labels), when lysates were manually harvested in NP-40 supplemented with protease and phosphatase inhibitors. Lysates were probed by WB (20 ng loading protein) using a pan-phospho-tyrosine antibody (**pTyr**: 2 µg ml^{-1}; ab10321, AbCam) to evaluate global changes in tyrosine phosphorylation residues. Samples were also probed for: **pAkt** and **pERK1/2** (as previously described), and where available, **pFAK** (pTyr397, 2 µg ml^{-1}, 3283S, CST). All blots were revealed using Amersham ECL Detection Kit (RPN2106, GE Healthcare) and manually developed on X-Ray film (BioMax XAR Film, 165-1454, Carestream Health Inc.), prior to scanning to digitise image (Epson Scanner).

6.1 development of a LAP-ligand internalisation assay to characterise integrin $\alpha_v\beta_6$–mediated signalling associated with receptor activation upon cognate ligand engagement and internalisation

To characterise integrin $\alpha_v\beta_6$-mediated signalling events following cognate ligand engagement, receptor activation and internalisation, a phosphoproteomics strategy was adopted. First, a LAP-ligand internalisation assay was developed in the VB6 cell line (Figure 6.1.1) and validated for use in the BT-20 cell line (Figure 6.1.2). Lysates from LAP-internalisation assays performed in the BT-20 TNBC cell line would then be used to generate peptides for phosphoenrichment and LC-MS/MS interrogation. Previous experiments had shown that integrin $\alpha_v\beta_6$ is the predominant LAP receptor in BT-20 cells (Chapter V: Results Part III, Figure 5.2C) and may be used to specifically target the integrin $\alpha_v\beta_6$ in this cell line, although the utility of other ligands was also evaluated (Figure 6.1.3).

Internalisation kinetics of a human IgG (Fc')-tagged LAP ligand (**LAP-Fc**) were characterised over a 30 min time-period by non-permeabilised surface IMF in the VB6 cell line (Figure 6.1.1A) and compared to internalisation kinetics of the integrin $\alpha_v\beta_6$ function blocking antibody 53A2 (Figure 6.1.1B). A range of ligand concentrations was evaluated to optimise the protocol in development.

Prior to internalisation at the 0' time point, LAP-Fc was seen to predominate at the plasmalemma, showing intense immunopositivity at cell-cell interfaces. A similar pattern was observed for 53A2 at 0', although antibody 53A2 also exhibited some diffuse cell surface immunopositivity. Following 30' internalisation, an almost total loss of surface fluorescence was observed LAP-Fc, suggesting internalisation/downregulation from the plasmalemma. In contrast, cell surface fluorescence for antibody 53A2 was retained.

Quantification of corrected total cell fluorescence (CTCF) indicated no significant difference in labelling efficacy or internalisation kinetics between the concentrations of LAP-Fc ligand or antibody 53A2 used, validating the use of LAP-Fc at 5 µg ml^{-1} in future experiments. Permeabilised IMF was performed to determine the subcellular distribution of LAP-Fc (Figure 6.1.1C) which showed that LAP-Fc redistributes from the plasmalemma at 0' to the perinuclear region by 30'. These findings confirmed that loss of cell surface fluorescence observed in Figure

6.1.1A was due to LAP-ligand internalisation and not ligand and/or antibody dissociation.

With the ability of LAP-Fc to internalise now confirmed, additional permeabilised IMF was performed to characterise its internalisation kinetics over a 60' min time period, again in comparison with the integrin $\alpha_v\beta_6$ function blocking antibody 53A2 (Figure 6.1.1D). Results demonstrated that at 5' and 15' internalisation, LAP-Fc begins subcellular redistribution from the plasmalemma, exhibiting a vesicular like cytoplasmic distribution with occasional residual cell-cell membrane immunopositivity. By 30' LAP-Fc predominates in the perinuclear region with occasional cytoplasmic immunopositivity, with total localisation at the perinuclear region by 60' internalisation.

To biologically validate internalisation assays against a canonical cell surface receptor/cognate ligand complex (Hopkins and Trowbridge 1983, Ponka and Lok 1999, Vercauteren *et al* 2010), a human IgG (Fc')-tagged transferrin ligand (**Tf-Fc**) was also evaluated for use as a biological control in both the VB6 and BT-20 cell lines (Figure 6.1.1E). Permeabilised IMF confirmed that Tf-Fc redistributes from the plasma lemma to the cytoplasm and perinuclear region by 30' and 60' min.

Having established proof of concept in the integrin $\alpha_v\beta_6$ overexpressing VB6 cell line, LAP-ligand internalisation assays were next validated in the high endogenous integrin $\alpha_v\beta_6$ expressing BT-20 TNBC cell line, using Tf-Fc as a biological comparator (Figure 6.1.2). Non-permeabilised IMF confirmed internalisation of both LAP-Fc (Figure 6.1.2A) and Tf-Fc (Figure 6.1.2C) ligands over a 60' time period; LAP-Fc appeared to be more rapidly downregulated from the plasma lemma between 0' and 15' minutes than Tf-Fc.

A previous experiment (Chapter V: Results Part III, Figure 5.2C) had demonstrated by FCM that integrin $\alpha_v\beta_6$ functional abrogation using antibody 53A2 abolished LAP-Fc binding; confirming LAP ligand specificity for the integrin $\alpha_v\beta_6$ in the BT-20 cell line and its utility to interrogate integrin $\alpha_v\beta_6$–mediated process in this particular TNBC model. However, more robust validation of the association between LAP and integrin $\alpha_v\beta_6$ during internalisation rather than at the cell surface at a lone time-point was deemed necessary.

Owing to technical failings, co-localisation of LAP-Fc/integrin $\alpha_v\beta_6$ complexes undergoing internalisation in BT-20 cells could not be demonstrated by IMF methods. However, results from co-immunopreciptation (co-IP) experiments originally intended to isolate LAP/integrin $\alpha_v\beta_6$ complexes undergoing internalisation for proteomic interrogation, were used to confirm the direct physical interaction between integrin $\alpha_v\beta_6$ and LAP at defined internalisation time points (Figure 6.1.2B and E) and were validated by successful co-IP of the transferrin receptor complex (**Tf-RC**) using Tf-Fc ligand in tandem control experiments (Figure 6.1.2D and E). The repeated, reproducible and successful co-IP of integrin β_6 using LAP-Fc in 3 biological replicate internalisation experiments using the BT-20 cell line (Figure 6.1.2D and E; Supplemental Figure S6.1A) was deemed to sufficient to validate the use of LAP ligand to interrogate the LAP-engaged integrin $\alpha_v\beta_6$ receptor undergoing internalisation.

Next, features of the internalisation protocol were validated including a serum starvation step (Figure 6.1.3A) and use of ligands to stimulate signalling-associated downstream phosphorylation events (Figure 6.1.3B – D). Serum starvation of BT-20 cells in low serum (1% charcoal-stripped FBS) conditions was evaluated over 24 hours to determine a suitable timescale to ablate basal phosphorylation of downstream signalling mediators prior to ligand treatment and internalisation assay (Figure 6.1.3A). Two biological replicates revealed that levels of pERK1/2 were diminished after 4 hours, validating use of a preceding 4-hour serum starvation step prior to ligand-based stimulation and/or internalisation assays.

The synthetic 20mer peptide A20FMDV2 (**A20FMDV2-TJ**) known to specifically engage the integrin $\alpha_v\beta_6$ was assessed alongside a random sequence negative (non-RGD-motif) control 20mer peptide (**A20FMDV2-TJRan**) to broadly characterise downstream signalling events inducted upon ligand engagement and internalisation at 15′ and 60′ timepoints by Western blotting using a pan-phospho-tyrosine (p-Tyr) antibody (Figure 6.1.3B).

Few notable differences in p-Tyr motifs were observed. Probing for known integrin receptor signalling mediators pERK1/2 and pSmad3 revealed similar downstream phosphorylation signatures for these proteins inducted by both the negative (non-RGD-motif) peptide (**A20FMDV2-TJRan**) and the integrin $\alpha_v\beta_6$–specific peptide

(**A20FMDV2-TJ**); obviating the use of A20FMDV2 to define integrin $\alpha_v\beta_6$–mediated signalling by these methods.

The ability of the integrin $\alpha_v\beta_6$ natural ligand LAP to stimulate downstream signalling in the BT-20 cell line following ligand engagement and internalisation was evaluated alongside the β_1 integrin ligand collagen I (**Col I**) (Figure 6.1.3C), in addition to fibronectin (**Fn**) and the epidermal growth factor receptor (EGFR) RTK ligand epidermal growth factor (**EGF**) (Figure 6.1.3D).

Collectively, these results (Figure 6.1.3) indicated that LAP induced FAK phosphorylation at 10′ and 60′ following internalisation and ERK1/2 phosphorylation at 10′ following internalisation but Akt phosphorylation appeared unaltered; confirming that LAP ligand may be used to induce detectable changes in signalling-associated downstream phosphorylation motifs.

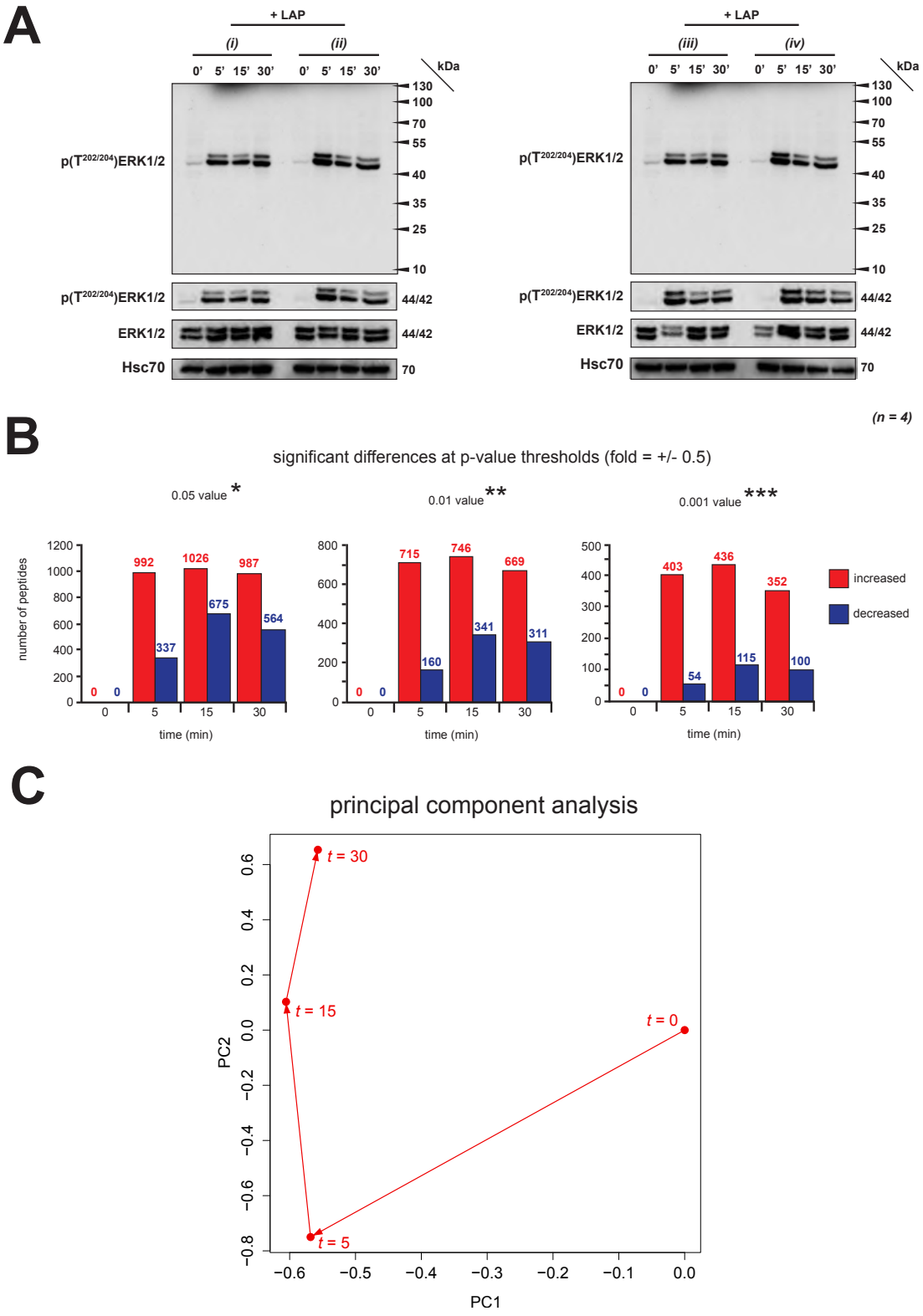

Figure 6.2
Mass spectrometry sample validation and dataset key metrics overview for the phosphoproteomic characterisation of downstream signalling events inducted upon LAP ligand-stimulated activation and internalisation of the integrin $\alpha_v\beta_6$

Figure 6.2

Mass spectrometry sample validation and dataset key metrics overview for the phosphoproteomic characterisation of downstream signalling events inducted upon LAP ligand-stimulated activation and internalisation of the integrin $\alpha_v\beta_6$

To characterise integrin $\alpha_v\beta_6$–mediated signalling inducted upon LAP-ligand engagement and subsequent internalisation, a LAP-ligand internalisation assay (development thereof shown previously) was performed using the BT-20 cell line to generate lysates for peptide preparation and LC-MS/MS interrogation; four biological replicates were performed (n=4). The TNBC BT-20 cell line was seeded in 10 cm dishes at 5 x 10^6 cells per dish in complete culture media and left to adhere overnight. Cell monolayers were washed and serum starved in low serum-media (1% charcoal-stripped FBS/α-MEM) supplemented with 25 mM HEPES for 4 hours prior to LAP ligand pre-treatment (0.5µg ml^{-1}, 10 min, 4°C). Monolayers were washed and the 30', 15' and 5' time-point dishes replenished with complete media (15% charcoal-stripped FBS/α-MEM) supplemented with 25 mM HEPES before returning to standard culture conditions (8%CO_2/37°C/humidified atmosphere) to permit ligand internalisation. The 0' baseline time-point was not subject to ligand internalisation. At the designated time-points, dishes were buried in wet ice and monolayers washed by flooding in pre-chilled (4°C) TBS supplemented with 1 mM Na_3VO_4 and 0.5 mM NaF. Lysates were manually harvested by scraping in the presence of pre-chilled (4°C) phosphoproteomic lysis buffer comprising: 8 M urea/20 mM HEPES supplemented with 0.5 M NaF, 0.1 M Na_3VO_4, 1 M $CH_3H_7Na_2O_6P$ (disodium β–glycerophosphate), 0.25 M $Na_2H_2P_2O_7$ (disodium pyrophosphate); prior to sonication at 4°C (20% intensity for 3 x 10 s, SONICS® Vibra-Cell™ Ultrasonic Liquid Processor VCX750, Sonics & Materials Inc). A total of four biological replicates were performed across two experiments; each experiment comprised two biological replicates run in tandem. **(6.2 A)** Harvested lysates were validated by WB (25 ng loading protein) prior to peptide preparation and TiO_2 enrichment. Samples were probed to determine **pERK1/2** (pThr202/204, 2 µg ml^{-1}, 9101L, CST) signature as a read out of downstream signalling induction. Total **ERK1/2** (1 µg ml^{-1}, 9102L, CST) and **Hsc-70** (0.2 µg ml^{-1}, sc-7298, Santa Cruz Bio Tech) were also probed. Blots were revealed using Amersham ECL Detection Kit (RPN2106, GE Healthcare) and manually developed on X-Ray film (BioMax XAR Film, 165-1454, Carestream Health Inc.), prior to scanning to digitise image (Epson Scanner). Following TiO_2 enrichment, phosphopeptides were analysed by LC-MS/MS (LTQ Orbitrap™-Velos™ Hybrid FT mass spectrometer, Thermo Scientific). LC-MS/MS analysis identified a total of 88 533 tandem mass spectra corresponding to 8 874 unique peptide ions; of these unique ions, 6 491 were phosphopeptides containing 7 129 phosphorylation sites. A total of 7 368, 5 505 and 3 683 unique peptides showed expectation scores <0.05, <0.01 and <0.001 respectively; collectively these peptides mapped to 2 073 identified proteins. **(6.2 B)** Summary histograms showing the number of statistically significant differences in peptide abundance, either increase (red) or decrease (blue), across each experimental time-point at p-value thresholds p<0.05*****, p<0.01****** and p<0.001******* with Benjamini-Hochberg correction for multiple testing (n=4). **(6.2 C)** Two dimensional (2D) principal component analysis (PCA) summarising data variance between time-points revealed the similarity between phosphopeptide profiles characterised for the 5' (t=5), 15' (t=15) and 30' (t=30) time-points, which show marked variation from phosphopeptides characterising the 0' (t=0) baseline. Histograms and multivariate PCA plots were prepared in the R statistical programming environment (R 3.2.5, The R Foundation) with the kind assistance of Dr Edmund Wilkes (Centre for Haemato-Oncology, Barts Cancer Institute, QMUL).

6.2 phosphoproteomic interrogation of LAP-ligand, integrin $\alpha_v\beta_6$-mediated signalling events inducted during ligand engagement and subsequent internalisation in the BT-20 TNBC cell line

Following successful development and validation of a LAP ligand-based internalisation assay (Figures 6.1.1 to 6.1.3), four biological replicate LAP-ligand internalisation experiments were performed using the BT-20 cell line to permit phosphoproteomic interrogation of phosphorylation signatures associated with the LAP-ligand-engaged integrin $\alpha_v\beta_6$ receptor undergoing internalisation (Figure 6.2).

Before peptide preparation and TiO_2 phosphoenrichment, lysates from four biological replicate experiments were initially validated by WB (Figure 6.2A) to confirm changes in ERK1/2 phosphorylation signatures (**pERK1$^{T202/Y204}$/ERK2$^{T185/Y187}$**), as had been observed in previous LAP-ligand stimulation assays (Figure 6.1.3). Prior to internalisation (**0'**; t=0), ERK1/2 was not discernibly phosphorylated. However, ERK1/2 phosphorylation was inducted by **5'** (t=5) post-internalisation and sustained throughout the 30 min internalisation time-course (Figure 6.2A); validating success of the assay to generate downstream changes in phosphorylation signatures for LC-MS/MS interrogation.

Lysates were then used to generate peptides that were subsequently TiO_2-phosphoenriched and subject to LC-MS/MS analysis. Phosphoproteomic interrogation of the four replicate LAP-ligand internalisation experiments successfully identified 88 533 tandem mass spectra corresponding to 8 874 unique peptide ions; of which, 6 491 were phosphopeptides containing 7 129 phosphorylation sites collectively mapping to 2 073 identified proteins. Summary histograms (Figure 6.2B) showed the number of statistically significant differences in peptide abundance, either an increase (red) or decrease (blue), across each experimental time-point at p-value thresholds $p<0.05$*, $p<0.01$** or $p<0.001$***.

Two dimensional (2D) principal component analysis (PCA) summarising dataset-wide variance between internalisation time-points (Figure 6.2C) indicated broad similarity between phosphopeptide profiles characterising the **5'** (t=5), **15'** (t=15) and **30'** (t=30) time-points, which collectively showed marked variation from phosphopeptides characterising the **0'** (t=0) time-point.

Thus, the greatest changes in the dataset are between the pre-internalisation (**0'**) and post-internalisation (**5'**, **15'**, **30'**) time-points. This broad dataset analysis would suggest that the biggest changes in phosphorylation signatures are associated with internalisation as a broad process as no significant shift in variance between internalisation time-points was observed by PCA.

6.3 kinase substrate enrichment analysis (KSEA) reveals putative regulatory kinases and associated pathways governing integrin $\alpha_v\beta_6$-mediated signalling events inducted during LAP-ligand engagement and subsequent internalisation in the BT-20 TNBC cell line

The phosphoproteomic dataset was interrogated using the kinase substrate enrichment analysis (KSEA) computational method first developed by Casado *et al* (2013a) to infer kinase pathway activation from LC-MS/MS-based phosphoproteomic analysis of human acute myeloid leukaemia cells (AML). The KSEA model utilises a repository of 330 PhosphoSitePlus® (Cell Signalling Technology Inc) kinases and literature-curated kinase(s)/kinase inhibitor activity studies. Based upon direct identification of phosphopeptides within the LC-MS/MS dataset that are known substrates of the 330 specified kinase(s) species curated in the KSEA repository, this analytical approach permitted inference of specific kinase activity and associated signalling network modulation during integrin $\alpha_v\beta_6$ LAP-engagement and internalisation in the BT-20 TNBC cell line (Figure 6.3.1).

The KSEA inferential approach evaluated the activity of these 330-curated kinases within the LC-MS/MS dataset to identify putative regulatory kinases and their inferred activity in terms of $\log_2$-fold-ratio enrichment across LAP-internalisation time-points; the KSEA results are summarised in a heatmap (Figure 6.3.1A).

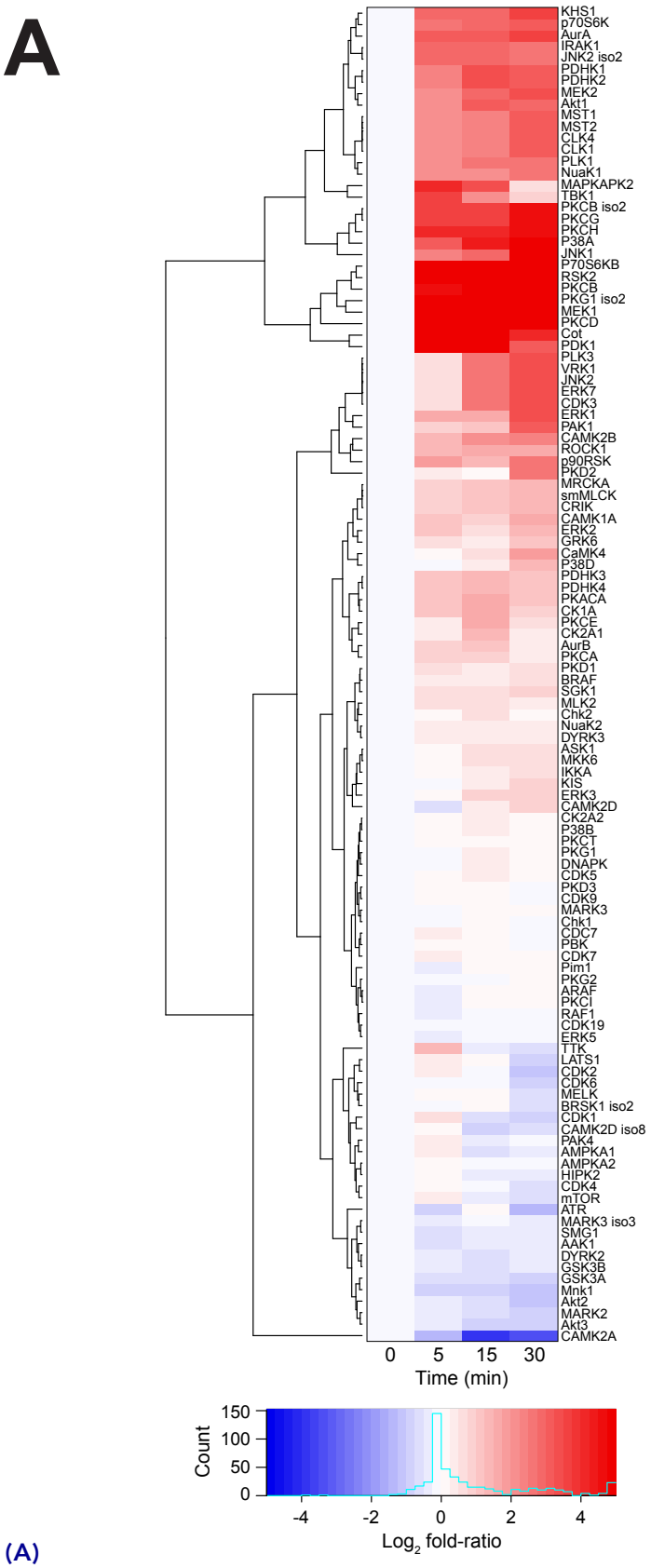

Figure 6.3.1 (A)
Summary of kinase substrate enrichment analysis (KSEA): Heatmap summarising fold-changes in kinase activity (z-score) during integrin $\alpha_v\beta_6$ LAP-ligand engagement and internalisation, inferred from analysis of respective kinase substrates identified within the LC-MS/MS dataset

B

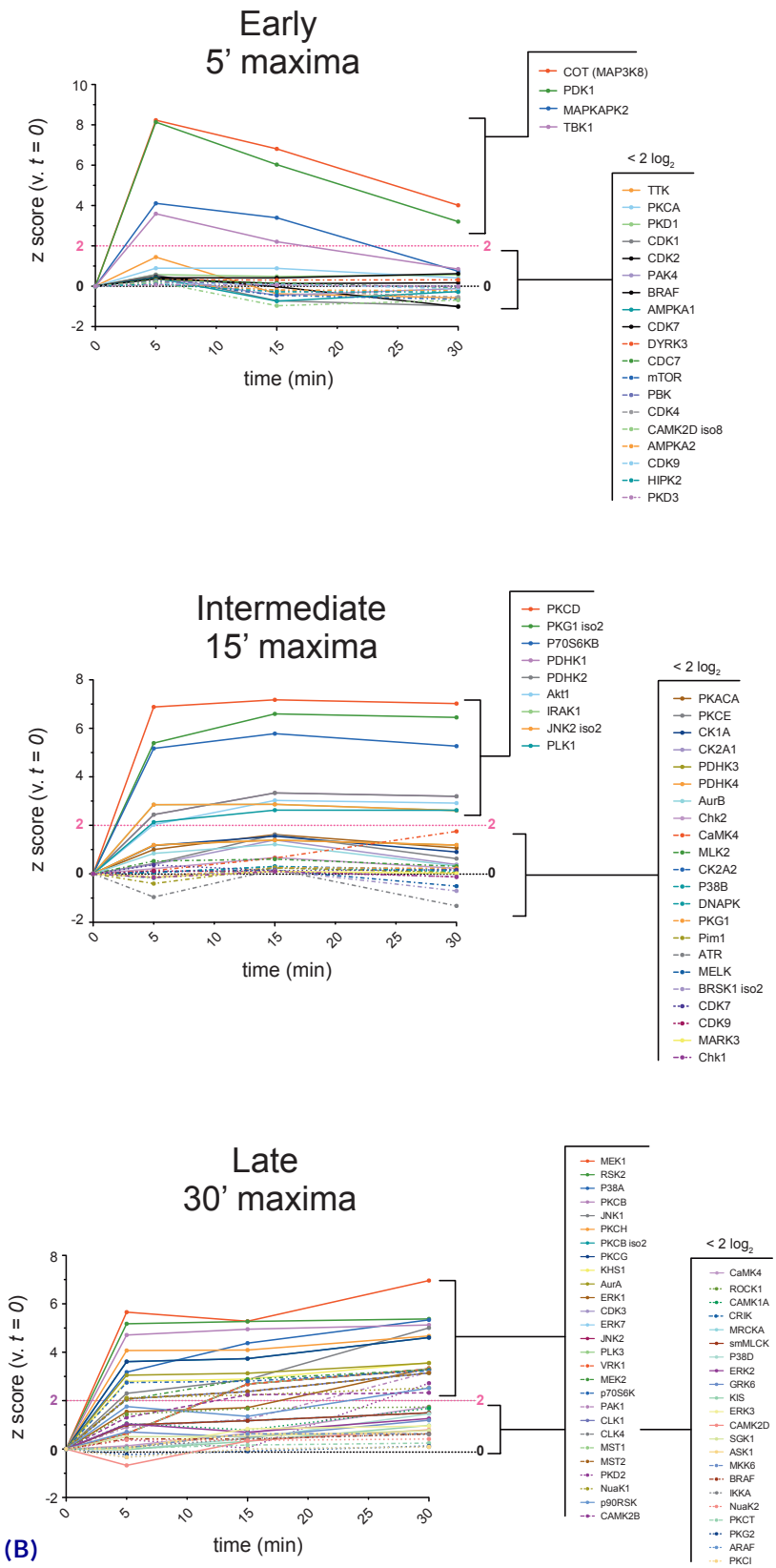

Figure 6.3.1 (B)
Summary of kinase substrate enrichment analysis (KSEA): Time-point stratification of maximal kinase activation events (z-score) inducted during integrin $\alpha_v\beta_6$ LAP-ligand engagement and internalisation, inferred from analysis of respective kinase substrates identified within the LC-MS/MS dataset

C

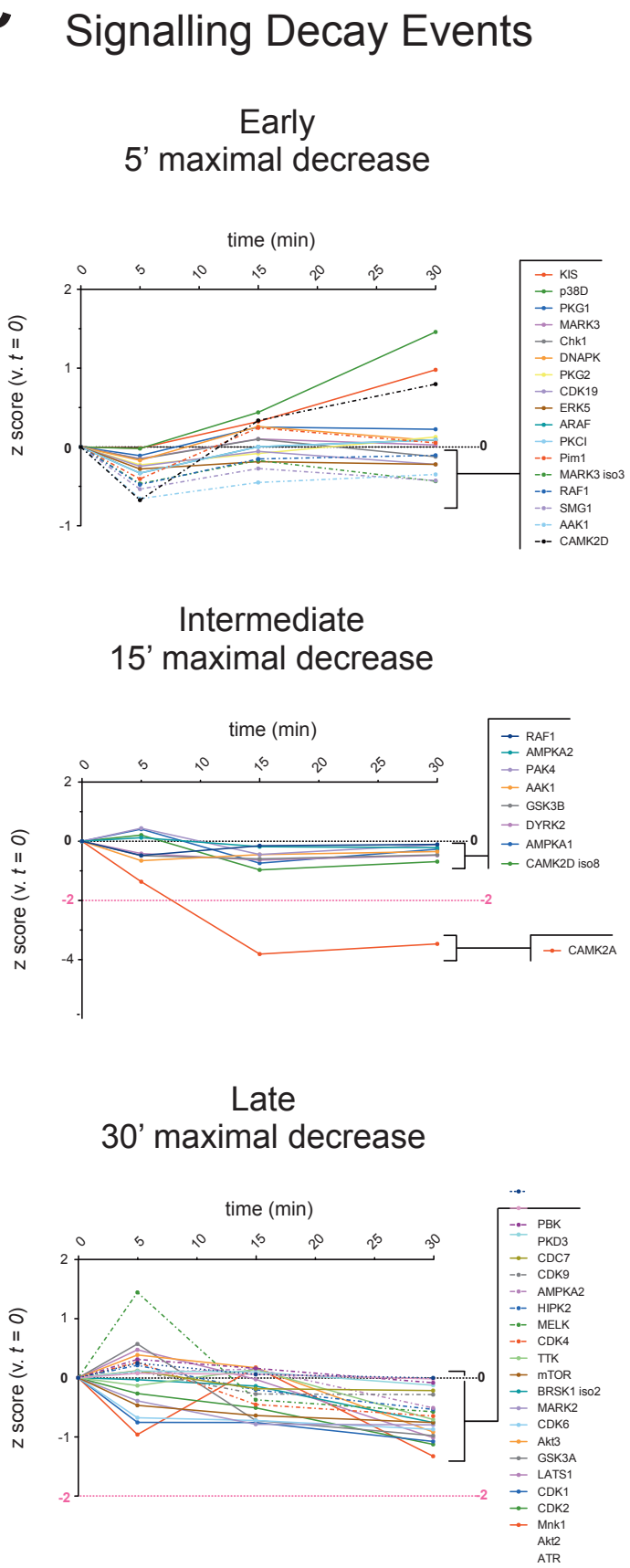

Figure 6.3.1 (C)
Summary of kinase substrate enrichment analysis (KSEA): Time-point stratification of kinase deactivation (signal decay) events (z-score) inducted during integrin $\alpha_v\beta_6$ LAP-ligand engagement and internalisation, inferred from analysis of respective kinase substrates identified within the LC-MS/MS dataset

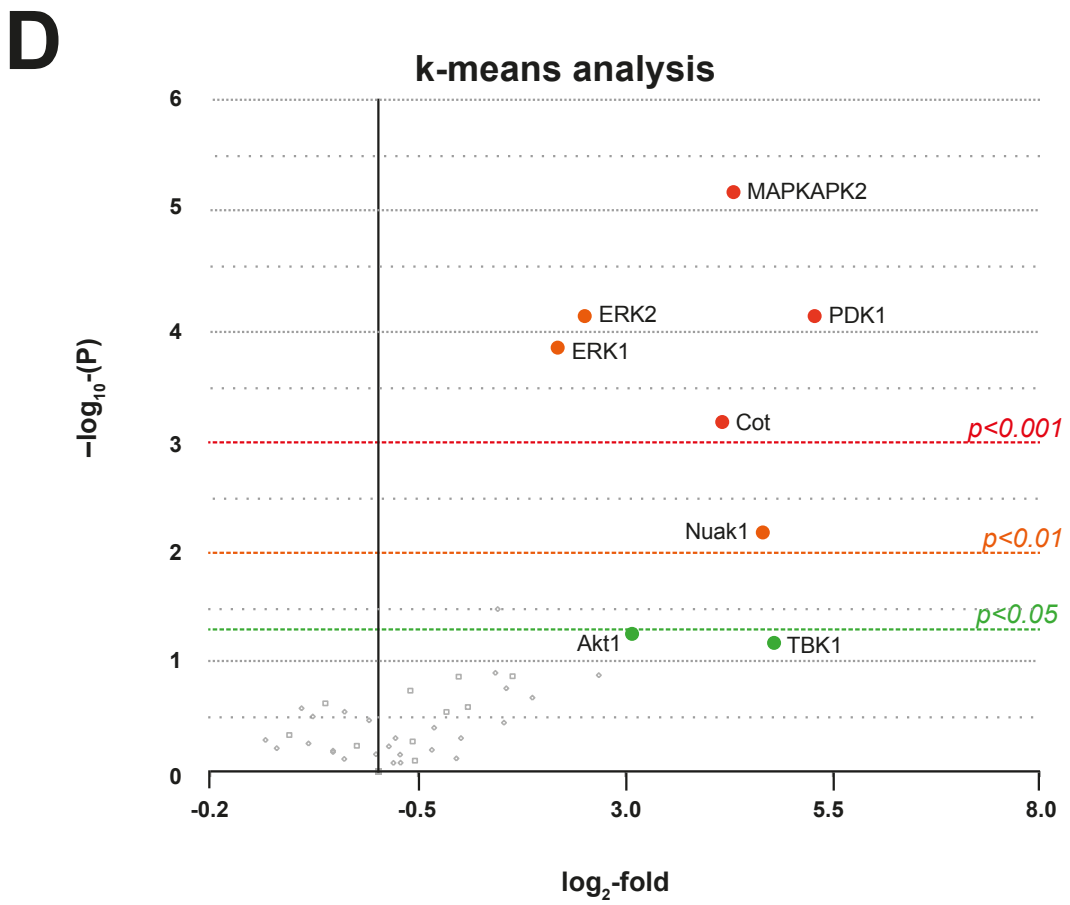

Figure 6.3.1 (D)
Summary of kinase substrate enrichment analysis (KSEA): k-means analysis plot indicating kinases identified for functional validation as putative regulators of changes in the phosphoproteome (signalling events) downstream of integrin $\alpha_v\beta_6$ LAP-ligand engagement and internalisation

Figure 6.3.1

Summary of kinase substrate enrichment analysis (KSEA): Heatmap (A), time-point stratifications of kinase modulation (activation and deactivation) events (B & C) and k-means analysis (D) of kinases inducted during integrin $\alpha_v\beta_6$ LAP-ligand engagement and internalisation, inferred from analysis of respective kinase substrates directly identified within the LC-MS/MS dataset

Phosphopeptide data was interrogated using a kinase substrate enrichment analysis (KSEA) method developed by Casado *et al* (2013a) to infer kinase activity based upon identified phosphopeptides that are known to be substrates of specified kinase(s) moieties; permitting inference of signalling pathway activation, deactivation or neutrality in response to integrin $\alpha_v\beta_6$ LAP-ligand engagement and internalisation in the BT-20 TNBC model. **(6.3.1 A)** A summary heatmap of kinases and their activity (log_2 fold-ratio enrichment) identified (based on their known substrate phosphopeptides identified within the LC-MS/MS dataset) was mapped (R 3.5.2, The R Foundation), highlighting which of the 330 PhosphoSitePlus® (Cell Signalling Technology Inc) and literature-curated kinases entered in the KSEA model exhibited alteration in activity in response to time of LAP-ligand internalisation. KSEA results were then stratified to identify which kinases maximally deviated from t=0 at each time point to identify early (5'), mid (15') and late (30') signalling events in terms of **(6.3.1 B)** activation (positive deviation of z-score adjusted to t=0) or **(6.3.1 C)** decay (negative deviation of z-score adjusted to t=0) to characterise signalling pathways inducted downstream of LAP-ligand internalisation; where z=0 no deviation in kinase activity from t=0 is inferred, where z=2 a deviation of 2 s.d from t=0 is inferred for kinase activity. **(6.3.1 D)** Results summary from k-means score analysis highlighting kinases identified for functional validation, showing log_2-fold enrichment versus $-log_{10}$ of the corresponding adjusted p-value for each kinase shown.

The KSEA results were used to infer specific kinase pathway activation and associated signalling network modulation inducted upon integrin $\alpha_v\beta_6$ LAP-ligand engagement and subsequent internalisation. The KSEA-algorithm-derived z-score denotes how many standard deviations (s.d) a component within the dataset deviates from the mean ($\bar{\chi}$). Here, a z-score (adjusted against **0'**, t=0) was used as a measure of alteration in kinase activity at each time-point in comparison with its baseline activity (taken as **0'**, t=0).

The z-score values were then plotted to more clearly distinguish kinases according to signalling activation (upregulation in kinase activity from baseline; Figure 6.3.1B) or signalling decay (downregulation in kinase activity from baseline; Figure 6.3.1C); and stratify their temporal relevance (in terms of maximal increase or decrease) as early (**5'**), middle (**15'**) or late (**30'**) signalling mediators.

Based on these temporal plots and k-means analysis (Figure 6.3.1D), in conjunction with a literature review, five kinases were identified as putative mediators of signalling derived from integrin $\alpha_v\beta_6$–dependent LAP-ligand engagement and internalisation in the BT-20 TNBC model (Supplementary Figure S6.2). Four early mediators (**5'**, (t=5): **MAP3K8**; **MAPKAPK2**; **PDK1**; **TBK1**) and a late mediator (30', (t=30): **Nuak1**) were selected for subsequent functional validation using siRNA and commercially available SMIs (Chapter II: Materials and Methods, Table 2.11), to explore their putative role in regulating integrin $\alpha_v\beta_6$–driven LAP-ligand derived signalling associated with ligand engagement and internalisation.

Following temporal analyses of kinase activity based on *z*-score $\log_2$-fold enrichment or depletion (Figure 3.3.1), the KSEA dataset was subject to supervised hierarchical clustering analysis to group kinases according to correlation with Gene Ontology (GO) Biological Pathway annotations (Spearman's correlation: $\rho \geq 0.8$ correlation with GO Biological Pathway annotation terms). These analyses (Figure 6.3.2) were kindly devised and performed by Dr Mark R Morgan (University of Liverpool) to provide novel insights into biological pathways that may be regulated (enriched or depleted) by the β_6-kinome during integrin $\alpha_v\beta_6$ LAP-engagement and internalisation.

Amongst the 330 literature- and PhosphoSitePlus®-curated kinases comprising KSEA analysis, a total of 10 clusters (assigned Ontology Clusters A – J) were mapped based on individual kinase correlation ($\rho \geq 0.8$) with GO Biological Pathway terms (Figure 6.3.2A). Networks were plotted for each internalisation time-point (Figures 6.3.2B to F) to map alterations in the β_6-kinome during integrin $\alpha_v\beta_6$ LAP-engagement and internalisation in terms of ontological cluster to identify putative biological pathway regulation.

Interestingly, the 5 kinases identified for further functional validation (Figure 6.3.1D) were also validated as viable target kinases based on GO analyses. Within the most active (enriched) ontology clusters A – C: MAP3K8/COT, MAPKAPK2, TBK1 and PDK1 kinases were identified within cluster A and Nuak1 identified within cluster B; suggesting commonality between regulation of phenotypic outputs in terms of biological pathways regulated by these kinases.

Global pathway analyses using the Kyoto Encyclopædia of Genes and Genomes (KEGG) database (Kanehisa Laboratories, GenomeNet) revealed enrichment for pathway annotations corresponding to: i) inositol phosphate metabolism, ii) endocytosis and iii) MAPK signalling; whilst depletion for terms relating to: i) autophagy, ii) cell cycle and iii) JAK/STAT signalling were associated with the β_6-kinome during integrin $\alpha_v\beta_6$ LAP-engagement and internalisation.

Disappointingly, antibodies intended to validate siRNA knockdown of target protein kinase expression (Supplementary Figure S6.3) or to evaluate phosphorylation status to confirm SMI efficacy (Supplementary Figure S6.4), could not be reliably validated by WB to permit robust functional interrogation of the 5 target kinases identified by KSEA (Figures 6.3.1 and 6.3.2). However, preliminary experiments targeting MAP3K8/COT kinase were performed as an exploratory exercise (Figure 6.4), even though SMI kinase inhibition could not be confirmed.

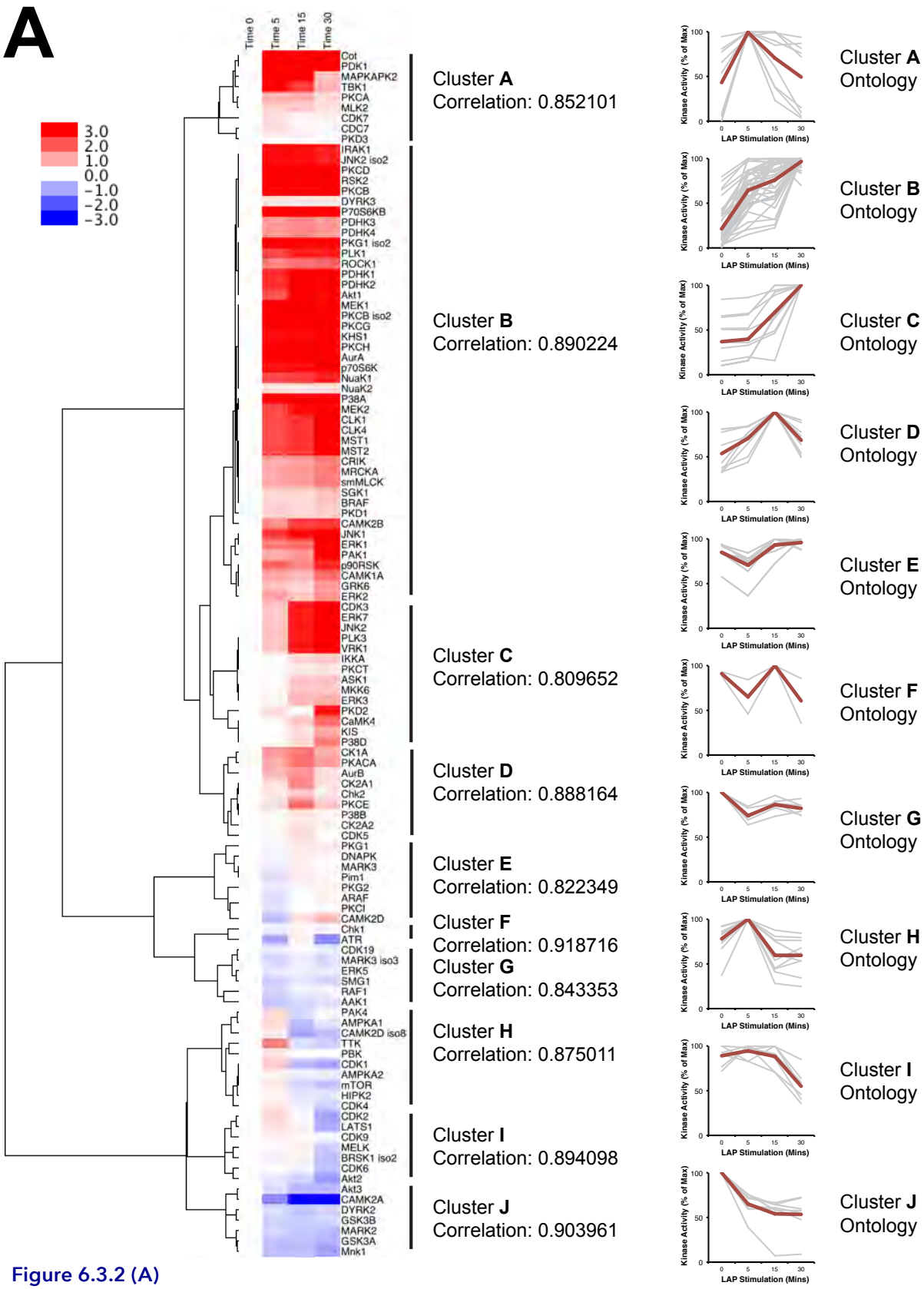

Figure 6.3.2 (A)
Summary of supervised hierarchical cluster analyses grouping the 330 individual kinases within the KSEA repository into ontological clusters based on their shared GO Pathway Activity to infer network plasticity during integrin $\alpha_v\beta_6$ LAP-engagement and internalisation in the BT-20 TNBC model

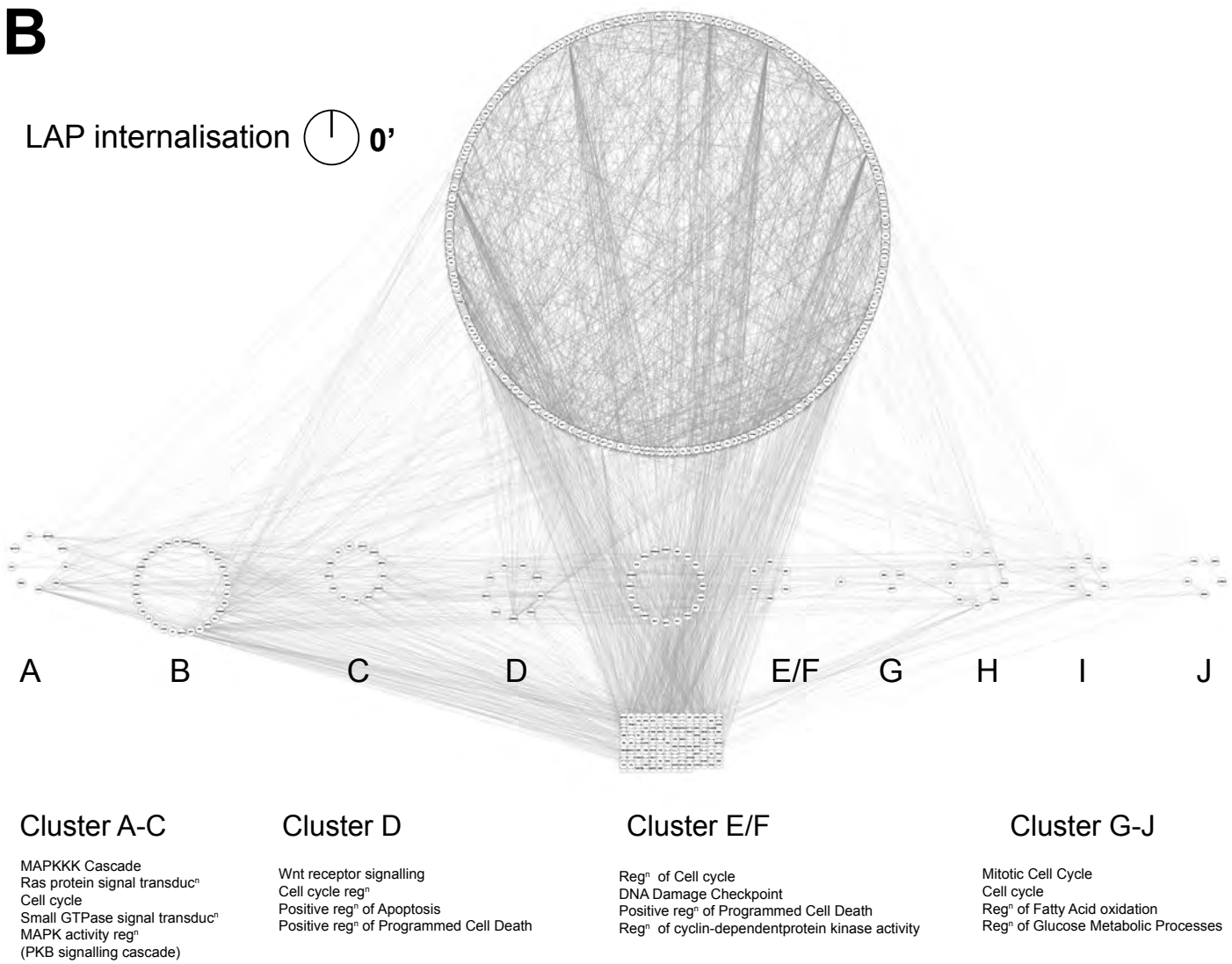

Figure 6.3.2 (B)
Network analysis with supervised ontological clustering (GO Pathway Analysis) to infer network plasticity in the β_6-mediated kinome during integrin $\alpha_v\beta_6$ LAP-engagement and internalisation in the BT-20 TNBC model: Mapping the baseline (0') KSEA-inferred network

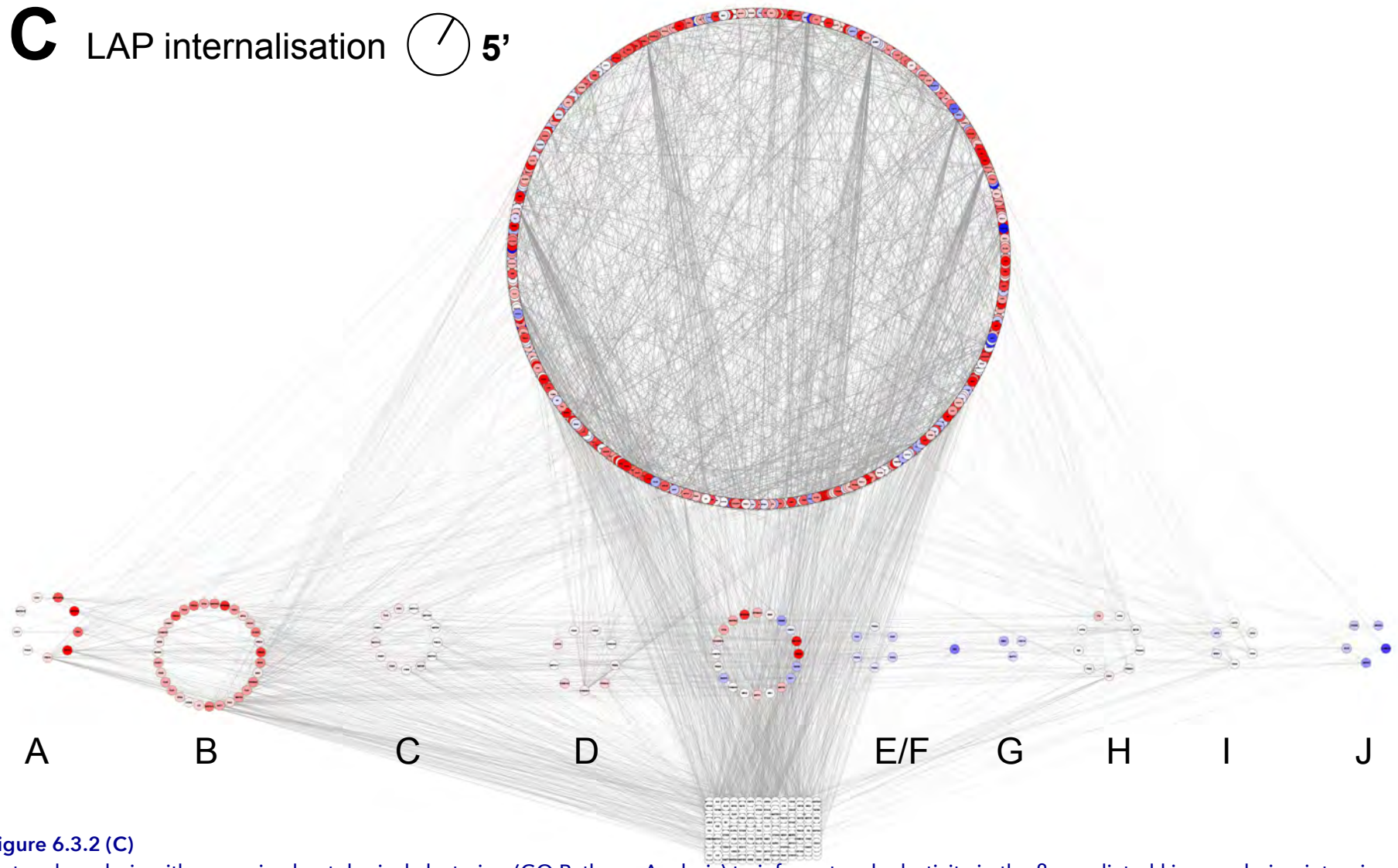

Figure 6.3.2 (C)
Network analysis with supervised ontological clustering (GO Pathway Analysis) to infer network plasticity in the β_6-mediated kinome during integrin $\alpha_v\beta_6$ LAP-engagement and internalisation in the BT-20 TNBC model: Mapping the early (5') KSEA-inferred network

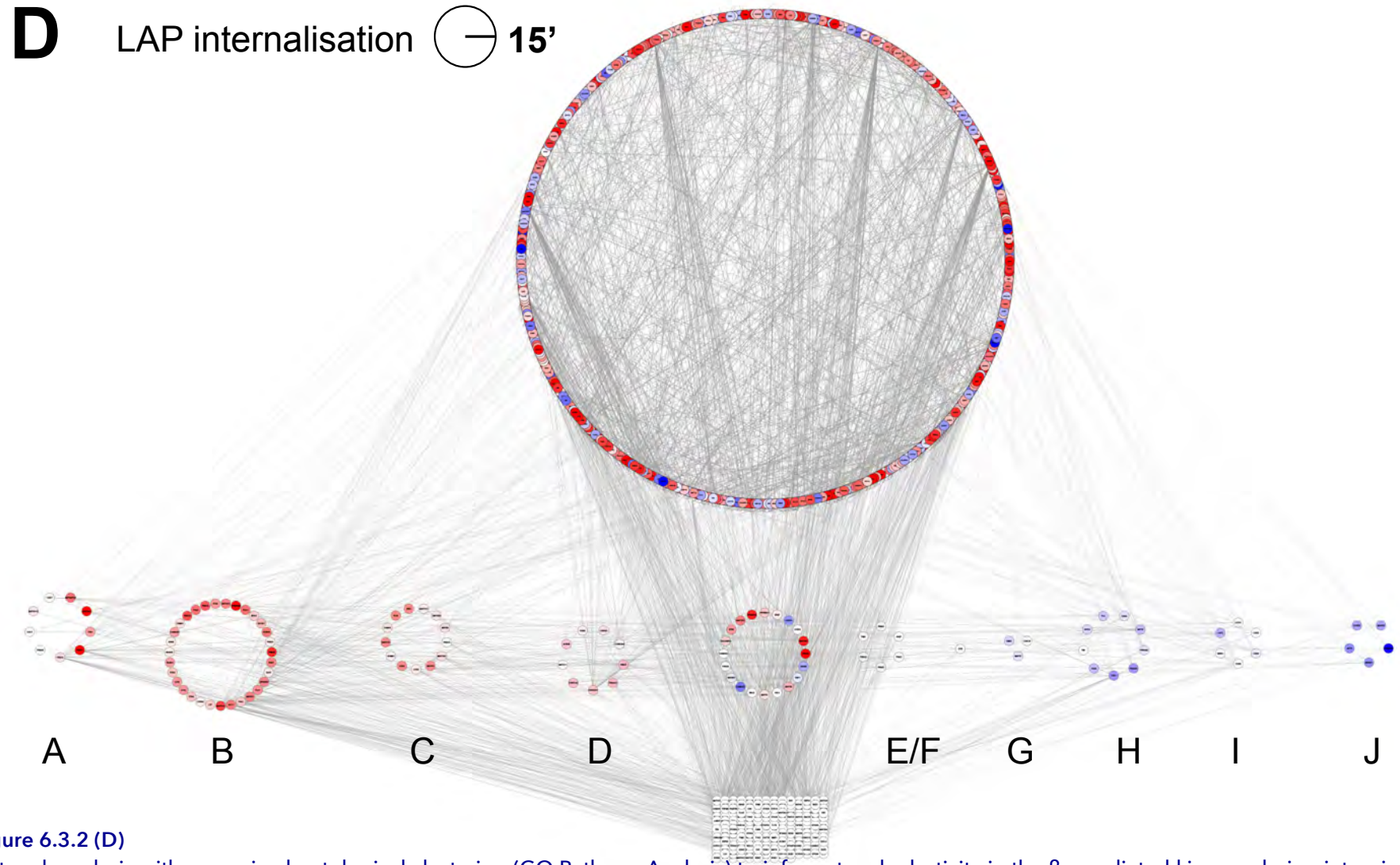

Figure 6.3.2 (D)
Network analysis with supervised ontological clustering (GO Pathway Analysis) to infer network plasticity in the β_6-mediated kinome during integrin $\alpha_v\beta_6$ LAP-engagement and internalisation in the BT-20 TNBC model: Mapping the intermediate (15’) KSEA-inferred network

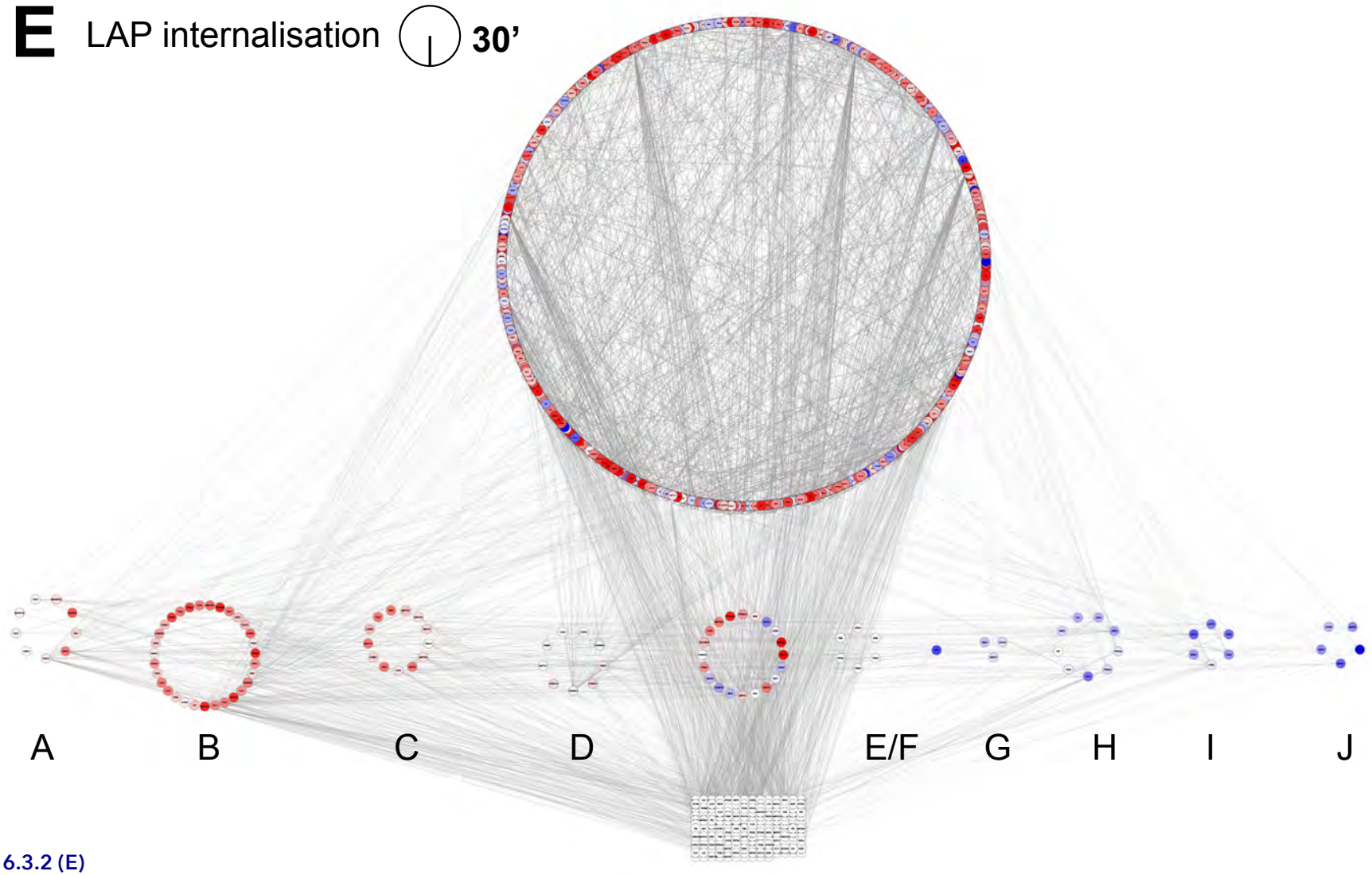

Figure 6.3.2 (E)
Network analysis with supervised ontological clustering (GO Pathway Analysis) to infer network plasticity in the β_6-mediated kinome during integrin $\alpha_v\beta_6$ LAP-engagement and internalisation in the BT-20 TNBC model: Mapping the late (30’) KSEA-inferred network

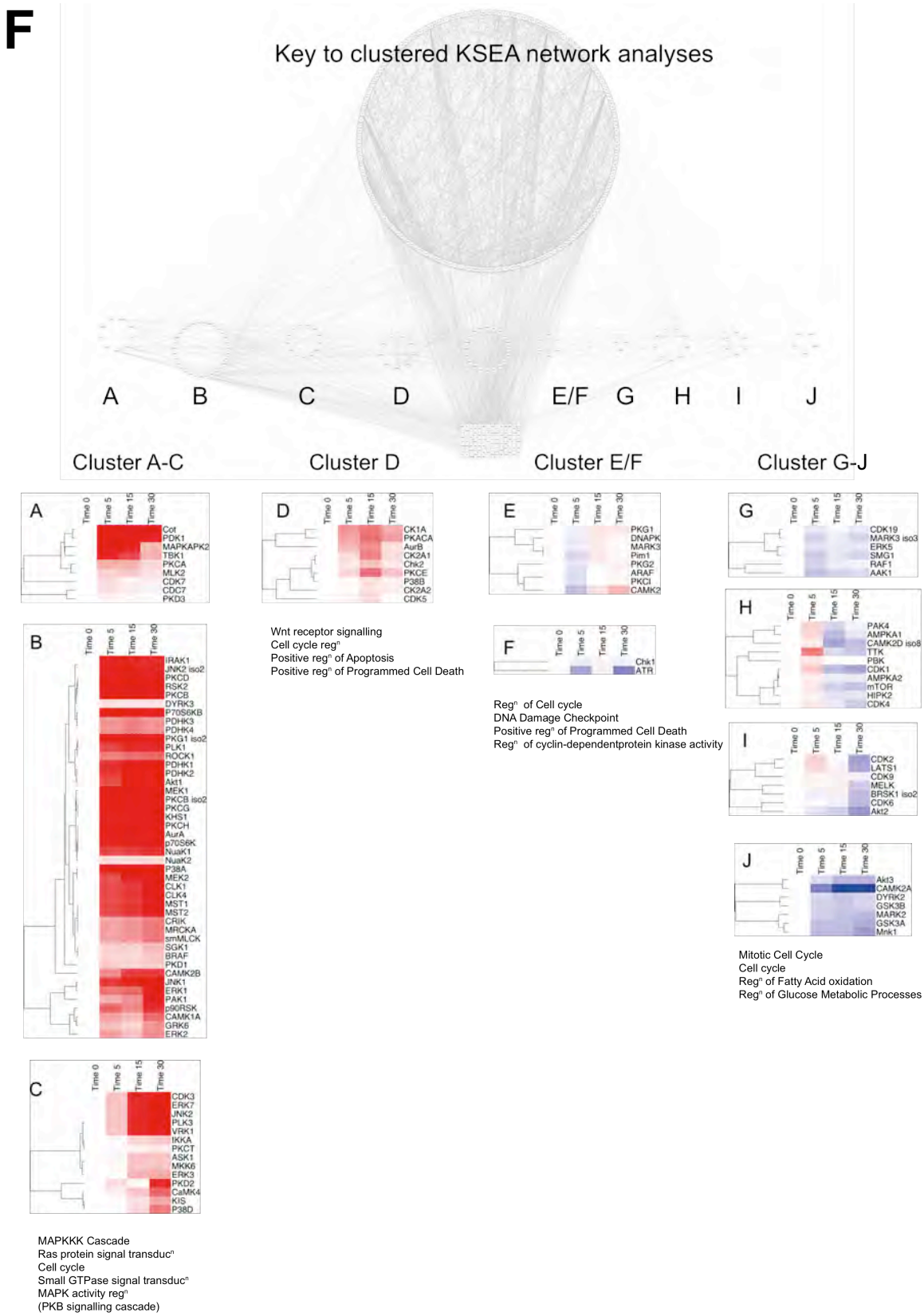

Figure 6.3.2 (F)

Network analysis with supervised ontological clustering (GO Pathway Analysis) to infer network plasticity in the β_6-mediated kinome during integrin $\alpha_v\beta_6$ LAP-engagement and internalisation in the BT-20 TNBC model: Key to clustered KSEA network maps indicating kinases by ontological cluster

Figure 6.3.2

Network analyses with supervised ontological clustering to infer network plasticity in the β_6-mediated kinome during integrin $\alpha_v\beta_6$ LAP-engagement and internalisation in the BT-20 TNBC model

Phosphopeptide data were first interrogated using a kinase substrate enrichment analysis (KSEA) method developed by Casado *et al* (2013a) to infer kinase activity based upon identified phosphopeptides that are known to be substrates of specified kinase(s) moieties as outlined in Figure 6.3.1. Courtesy of Dr Mark R Morgan (Receptor Dynamics in Cancer Laboratory, University of Liverpool), the KSEA dataset was subject to Gene Ontology (GO) Biological Pathway Analysis to cluster kinases (Ontology Clusters A – J) according to correlation with GO annotations to assigned pathway activity **(6.3.2 A)** (minimum threshold for cluster analysis: Spearman's rank correlation coefficient $\rho \geq 0.8$) and used to plot clustered kinase activity networks for each internalisation time point **(6.3.2 B - E)**. **(6.3.2 A)** A summary heatmap of kinase activity clustered according GO Pathway Analysis with corresponding ontological kinase cluster activity plots showing mean average kinase activity (% of maximal activity) of kinases grouped within each cluster according to correlation with GO Pathway Analysis terms (Spearman's rank correlation coefficient $\rho \geq 0.8$). Network maps highlighting kinase activity by ontology cluster (clusters A – J) were generated for **(6.3.2 B)** baseline activity **0'** (t=0) alongside each time point to review changes in the β_6-mediated kinome at **(C) 5'** (t=5), **(6.3.2 D) 15'** (t=15), and **(6.3.2 E) 30'** (t=30) during LAP internalisation. A summary key to identify network-mapped kinases within each cluster is provided **(6.3.2 F)**. Cluster analysis and networks were generated using Cytoscape v3.1.1 with ClueGO v2.3.4 plug in (Bindea *et al* 2009) (Cytoscape Consortium, National Resource for Network Biology). **Acknowledgements:** Analyses presented in this figure were devised and performed by, and reproduced here with the kind permission of, Dr Mark R Morgan (Principal Investigator, Receptor Dynamics in Cancer Laboratory, University of Liverpool).

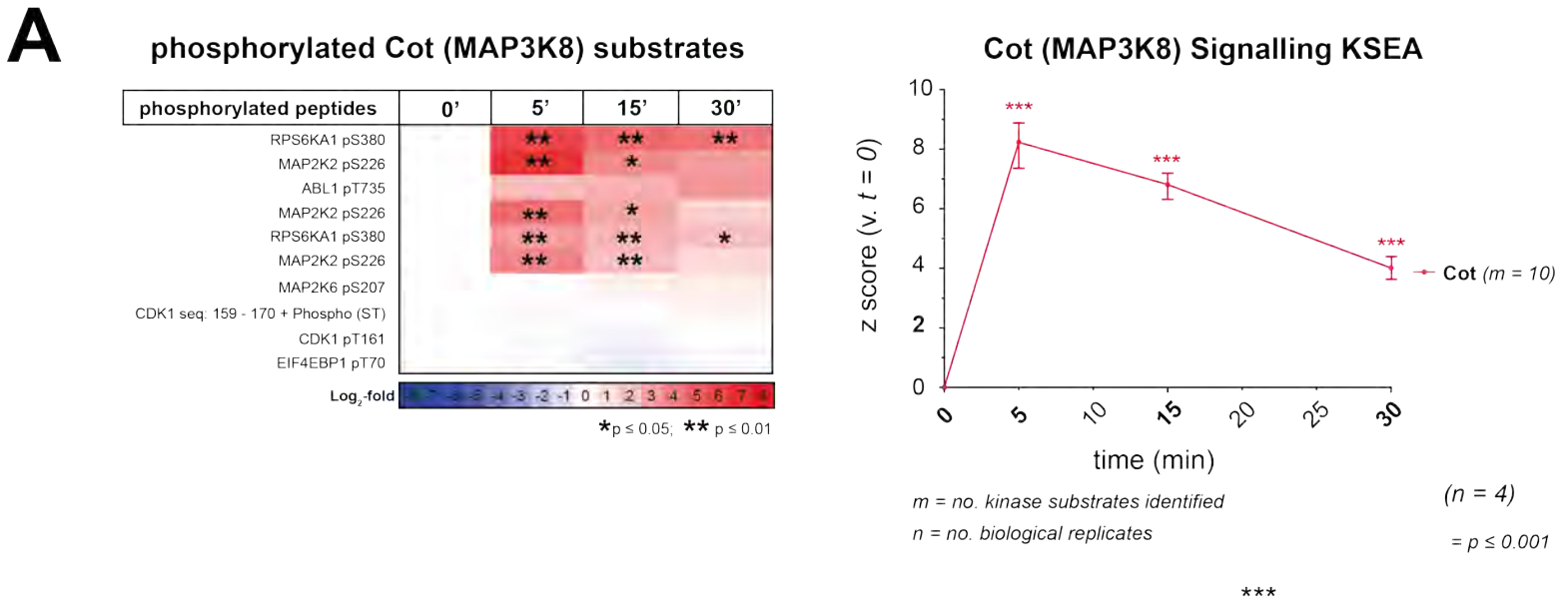

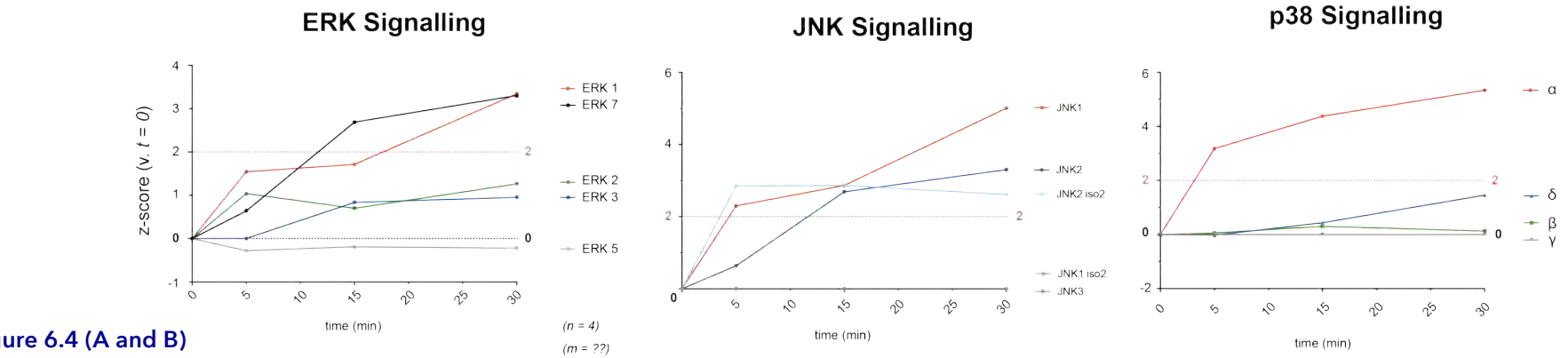

Figure 6.4 (A and B)
KSEA identifies significant upregulation of **(A)** the kinase COT (MAP3K8) and **(B)** its downstream pathway effectors implicating MAP3K8 activity as a putative mediator of integrin $\alpha_v\beta_6$/LAP ligand-derived signalling in the BT-20 cell line

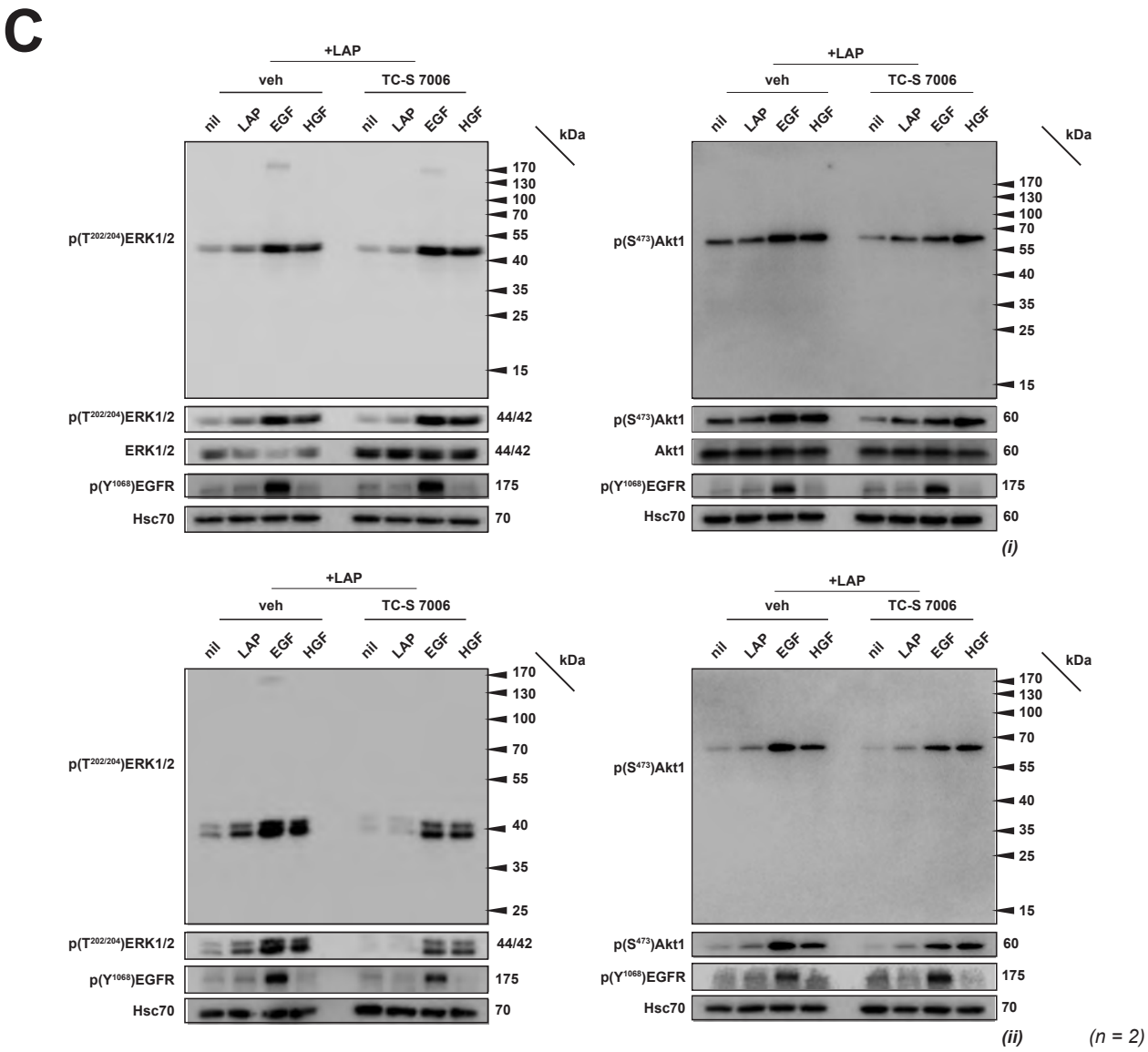

Figure 6.4 (C)
Investigating the regulatory role of the kinase COT (MAP3K8) during signalling inducted upon integrin $\alpha_v\beta_6$ LAP ligand engagement and internalisation using the COT kinase inhibitor TC-S 7006

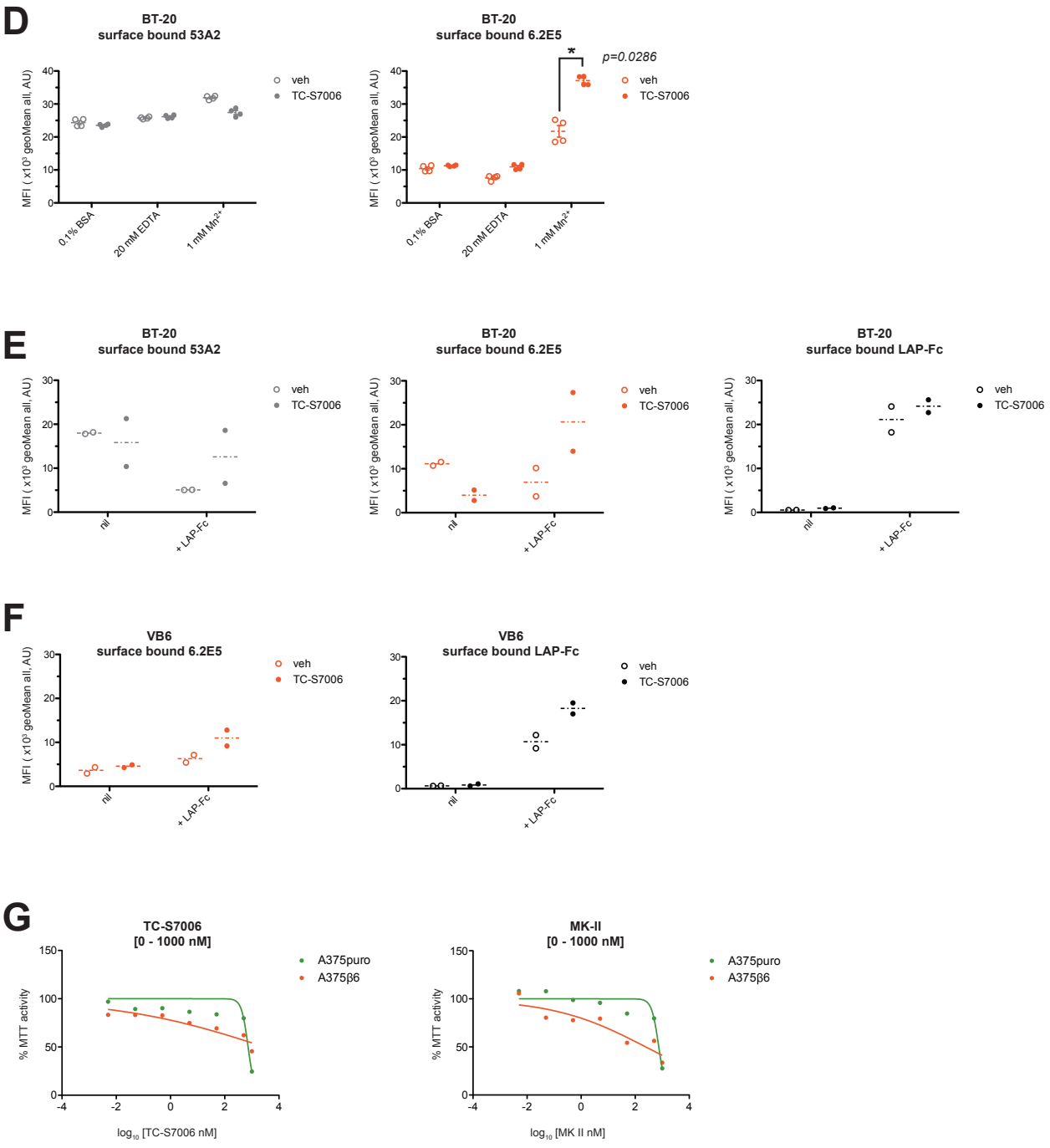

Figure 6.4 (D – G)
Investigating the regulatory role of the kinase COT (MAP3K8) during signalling inducted upon integrin $\alpha_v\beta_6$ LAP ligand engagement and internalisation using the COT kinase inhibitor TC-S 7006: treatment with TC-S7006 potentiates integrin activation in response to canonical integrin activation methods using Mn^{2+} ions **(D)** and LAP ligand **(E, F)**

Figure 6.4

Investigating the regulatory role of the kinase COT (MAP3K8) during signalling inducted upon integrin $\alpha_v\beta_6$ LAP ligand engagement and internalisation using the COT kinase inhibitor TC-S 7006

Results from KSEA analysis identified kinases that may potentially mediate signalling inducted downstream of integrin $\alpha_v\beta_6$ LAP ligand-engagement and internalisation in the BT-20 TNBC model. **(6.4 A)** COT (MAP3K8) kinase was identified based on its known substrates identified from phosphopeptide data in terms of both substrate moiety and specific phosphorylation site. A summary heatmap of identified phosphopeptides is shown, indicating $\log_2$-fold enrichment and statistical significance of identified phosphopeptide. KSEA plot showing inferred COT activity (z score v. t = 0) based on statistically significant abundance of 10 known COT substrates (m=10) identified within the dataset ($p \leq 0.05$*****, $p \leq 0.01$******, $p \leq 0.001$*******) and **(6.4 B)** upregulation of its downstream pathway effectors ERK1/2, Jnk and p38. **(6.4 C)** Given the apparent significance of COT, kinase inhibition assays were performed to dissect its putative role in integrin $\alpha_v\beta_6$–mediated signalling. The COT (MAP3K8) inhibitor TC-S7006 (Tocris, R&D Systems) was used to target COT activity. BT-20 cells were serum starved for 4-hr in low serum media (1% charcoal-stripped FBS) prior to treatment with 1 μM TC-S7006 for 30 min under standard culture conditions (all in low serum media) prior to challenge with ligand spiked in at: **LAP** (0.5 μg ml^{-1}, L3408, Sigma); **EGF** (50 ng ml^{-1}, E9644, Sigma); **HGF** (50 ng ml^{-1}, H9661, Sigma). Cells were stimulated for 10 min; ligand stimulation was quenched by flooding prior to harvesting lysates in NP-40 supplemented with protease and phosphatase inhibitors. Samples were probed by WB for: **pEGFR** (pTyr1068, 2234S, 2 μg ml^{-1}, 9018S, CST); **pAkt1** (pSer473, 2 μg ml^{-1}, 9018S, CST) and **pERK1/2** (pThr202/204, 2 μg ml^{-1}, 9101L, CST) alongside corresponding total proteins **Akt1** (1 μg ml^{-1}, 2938S, CST) and **ERK1/2** (1 μg ml^{-1}, 9102L, CST). A loading control was also performed (**Hsc-70**, 0.2 μg ml^{-1}, sc-7298, Santa Cruz Bio Tech). WBs were developed using Amersham ECL Detection Kit (RPN2106, GE Healthcare) and visualised using the Amersham™ Imager 600 (GE Healthcare Life Sciences Ltd) digital imaging system. To determine the effect of COT inhibition on integrin $\alpha_v\beta_6$ activation and LAP-ligand binding, **(6.4 D)** canonical Mn^{2+} cation (n=4) and **(6.4 E)** ligand-induced (n=2) activation assays were performed in the presence of TC-S7006. In brief, BT-20 **(6.4 D, E)** or VB6 cells **(6.4 F)** were treated in suspension with either vehicle (0.1% DMSO) or 1μM TC-S7006 for 30 min in low serum media prior to assay. Cells were washed and treated for 10 minutes in the presence of vehicle or 1μM TC-S7006 with either: **(6.4 D)** 0.1% BSA, 20 mM EDTA or 1 mM Mn^{2+}-ions; or **(6.4 E, F)** 0.5 μg ml^{-1} LAP-Fc (Biogen Idec), prior to washing, antibody labelling and detection by flow cytometry. To determine cell surface integrin $\alpha_v\beta_6$ activation, cells were labelled for an activation sensitive integrin $\alpha_v\beta_6$ epitope (**6.2E5**, 5 μg ml^{-1}, Biogen Idec) or an activation refractory integrin $\alpha_v\beta_6$ epitope (**53A2**, 5 μg ml^{-1}, CR-UK). Successful cell surface binding of LAP-Fc was demonstrated using an anti-Fc antibody (ABM121, 5 μg ml^{-1}, ab113636, AbCam) to detect the human IgG (Fc') tag of the LAP-Fc ligand. Surface antibody levels were determined by flow cytometry (BD LSRFortessa™, BD Biosciences) in the presence of a cell viability dye (propidium iodide, 5 μg ml^{-1}, Sigma Aldrich) to ensure gated events comprised live cells only. A significant difference in 6.2E5 binding (active integrin $\alpha_v\beta_6$ conformer) was found in the presence of TC-S7006 in comparison with vehicle alone (paired t-test: $p<0.05$, $p=0.0286$). **(6.4 G)** A preliminary screen of the potential effect of COT inhibition on integrin $\alpha_v\beta_6$–dependent proliferation was performed using 3-(4,5-dimethyl-2-thiazolyl)-2,5-diphenyl-2H-tetrazolium bromide *(MTT, M5655,* Sigma Aldrich) based assays in the A375puro (integrin β_6 negative) and A375β6 (integrin β_6 positive) cell lines in the presence of 0 - 1000 nM COT SMI TC-S7006 (as previous) or 0 – 1000 nM MAPKAPK2 SMI MK II (EMD Millipore). Cells were seeded in 96 well plates at 3.6 x 10^4 cells per well in complete media and left to adhere overnight prior to 72 hour treatment with kinase inhibitors under standard culture conditions. On completion of treatment, cells were incubated with 0.2 mg ml^{-1} MTT (M2003, Sigma Aldrich) for 1 hr in the dark at 37°C, insoluble formazan-products were liberated in the presence of 100% DMSO before optical density (OD) readings were taken at 550 nm using the Infinite®F50 platereader (TECAN Trading AG). OD values were normalised against assay matrix only background readings and converted to %MTT activity values normalised against 100% MTT activity/cell survival using Microsoft Excel. Graphs were plotted using GraphPad Prism software following $\log_{10}(x)$ data transformation and curve-fitting using the agonist-response (variable slope) analysis function.

6.4 MAP3K8 (COT) kinase inhibition appears to downregulate LAP-induced ERK1/2 phosphorylation and modulates divalent Mn^{2+}-cation and cognate LAP-ligand-induced integrin $\alpha_v\beta_6$ activation

Based upon LC-MS/MS detection of 10 phosphopeptides (m=10) mapping to its known substrates, mitogen-activated protein kinase kinase kinase 8 (MAP3K8) was significantly identified by KSEA (Figure 6.4A) as a putative regulator of integrin $\alpha_v\beta_6$–mediated signalling associated with LAP ligand engagement and subsequent internalisation at **5'** (t=5; z-(score)=8.231; p<0.001***), **15'** (t=15; z-(score)=6.811; p<0.001***) and **30'** (t=30; z-(score)=4.014; p<0.001***).

Furthermore, Gene Ontology (GO) Biological Pathway analysis of the inferential KSEA dataset revealed enrichment for MAPK Signalling annotations associated with integrin $\alpha_v\beta_6$ LAP engagement and internalisation. This was validated by National Cancer Institute (NCI) Ontological Pathway Analysis of phosphopeptides directly detected by LC-MS/MS which revealed enrichment for GO terms corresponding to the MAPK Cascade (GO (Process): 0000165P: MAPK Cascade and GO (Function): 0004707F: MAPK Activity). Therefore, interrogation of MAPK signalling downstream of integrin $\alpha_v\beta_6$ LAP-ligand engagement and internalisation was justified.

MAP3K8, also known as Cancer Osaka Thyroid (COT) or tumour progression locus 2 (TPL2), is a member of the serine/threonine protein kinase family involved in ERK1/2, JNK, p38 and NF-κB signalling nodes (Lee *et al* 2015). Its expression has been implicated as an oncogenic factor in several cancers, including BrCa (Sourvinos *et al* 1999). Review of KSEA results for MAP3K8/COT downstream effector kinase activity revealed upregulation in mediators of MAP3K8 derived signalling (Figure 6.4B), further implicating MAP3K8 activity during integrin $\alpha_v\beta_6$/LAP internalisation-associated signalling events.

A commercial MAP3K8/COT-targeting SMI (**TC-S 7006**, Tocris, R&D Systems) was used to functionally interrogate the role of MAP3K8/COT during integrin $\alpha_v\beta_6$–mediated processes including: LAP-stimulated downstream signalling (Figure 6.4C; n=2), integrin $\alpha_v\beta_6$ receptor activation using Mn^{2+} ions (Figure 6.4D; n=4) or LAP-ligand (Figure 6.4E; n=2) in the BT-20 cell line and VB6 cell line (Figure 6.4F; n=2). The effect of MAP3K8/COT inhibitor treatment on integrin $\alpha_v\beta_6$–dependent

proliferation/survival was briefly evaluated using a 1-(4,5-dimethylthiazol-2-yl)-3,5-diphenylformazan (MTT)-based metabolic assay in the A375puro (integrin β_6 null) and A375β6 (integrin β_6 positive) matched pair human malignant melanoma (MM) cell lines (Figure 6.4F; n=1).

To investigate the effects of MAP3K8/COT on integrin $\alpha_v\beta_6$–derived signalling downstream of LAP-ligand engagement, BT-20 cells were pre-treated (30') with 1 μM TC-S7006 (**TC-S 7006**) prior to stimulation (10') with **LAP**, or the EGFR and c-MET RTK cognate ligands **EGF** and **HGF** respectively (Figure 6.4C). Probing of lysates by WB revealed treatment with **TC-S 7006** reduced LAP-induced ERK1/2 phosphorylation and EGFR phosphorylation at Tyr1068 in comparison with vehicle (**veh**); the effect on LAP-mediated Akt1 phosphorylation at Ser473 was negligible. Treatment with TC-S 7006 elicited no discernible alteration in EGFR phosphorylation levels at Tyr1068 downstream of **EGF** stimulation.

The effect of TC-S 7006 treatment on integrin $\alpha_v\beta_6$ extracellular "outside-in" receptor activation via divalent $\mathbf{Mn^{2+}}$ cation exposure (Figure 6.4D) and cognate **LAP** ligand engagement (Figure 6.4E) in the BT-20 cell line, and **LAP** ligand engagement in the VB6 cell line (Figure 6.4F) were evaluated by FCM using canonical integrin activation experiments as previously described (Chapter III: Results Part I, Figures 3.1.1 – 3.2.2).

Curiously, the presence of 1 μM TC-S 7006 (**TC-S 7006**) potentiated BT-20 cell surface abundance of integrin $\alpha_v\beta_6$ in its active conformer (recognised by the conformation-sensitive antibody 6.2E5) upon exposure to 1 mM $\mathbf{Mn^{2+}}$ ions (Figure 6.4D), which was found to be significant in comparison with vehicle (**veh**) alone (paired t-test; $p<0.05$, $p=0.0286$; n=4). Treatment with TC-S 7006 exhibited no significant alteration in cell surface abundance of total integrin $\alpha_v\beta_6$ (recognised by the conformer-insenstive antibody 53A2); eliciting only a marginal reduction in 53A2 binding in comparison with vehicle (**veh**) alone.

The presence of TC-S 7006 also appears to potentiate the integrin $\alpha_v\beta_6$ active conformer (demonstrated by antibody 6.2E5) following engagement with a human IgG (Fc')-tagged LAP-ligand (Figure 6.4E). This finding was replicated in experiments using the VB6 cell line (Figure 6.4F), suggesting this result may be of

biological significance. However, only 2 biological replicate (n=2) experiments were performed in each cell line, obviating statistical analyses.

Finally, the possible effects of MAP3K8/COT and MAPKAPK2 (another KSEA-identified target kinase), on integrin $\alpha_v\beta_6$–dependent cell survival were evaluated by MTT-proliferation assay using the A375puro (integrin $\alpha_v\beta_6$ negative) and A375β6 (integrin $\alpha_v\beta_6$ positive) matched pair MM cell lines (Figure 6.4G). Preliminary, single experiments using a MAP3K8/COT inhibitor (**TC-S 7006**) and a MAPKAPK2 inhibitor (**MK II**) over a range of 0 – 1 μM suggest that proliferation of integrin $\alpha_v\beta_6$ expression may sensitise A375β6 MM cells to the anti-proliferative effects mediated by MAP3K8/COT and MAPKAPK2 inhibition, in comparison with integrin $\alpha_v\beta_6$ null A375puro MM cells.

Although successful inhibition of MAP3K8/COT kinase activity could not be demonstrated, these preliminary findings in the presence of a MAP3K8 inhibitor (TC-S 7006) implicate this kinase in integrin $\alpha_v\beta_6$ receptor extracellular activation and downstream ligand-stimulated signalling; warranting further investigation.

6.5 integrin $\alpha_v\beta_6$–mediating signalling events downstream of LAP-ligand engagement and internalisation are characterised by ERK1/2$^{T202/204}$ and Akt1^{S473} phosphorylation; LAP-induced ERK1/2 activation is pEGFR^{Y1068}-dependent

KSEA results indicated Akt1^{S473} (Figure 6.5.1) and ERK1/2$^{T202/204}$ (Figure 6.5.2) phosphorylation are inducted during integrin $\alpha_v\beta_6$ LAP-ligand engagement and internalisation, which was confirmed by WB. Direct identification of EGFR phosphopeptides implicated EGFR phosphorylation motifs as key mediators of LAP-induced integrin $\alpha_v\beta_6$ signalling (Figure 6.5.3A); functional validation using the anti-EGFR SMI gefitinib (**Gef**) (IRESSA®, AstraZeneca UK Ltd) and anti-cMET SMI PHA665752 (**PHA**) (Tocris, R&D Systems) revealed that ERK1/2 phosphorylation downstream of LAP-ligand stimulation in the integrin $\alpha_v\beta_6$–positive BT-20 and SUM159 TNBC cell lines is EGFR-dependent but independent of c-MET (Figure 6.5.3B and C).

Activity of Akt isoforms during integrin $\alpha_v\beta_6$ LAP-ligand engagement and internalisation was evaluated by KSEA. Curiously, phosphopeptides mapping to Akt1 phosphorylation sites were not directly detected with significance or abundance (Figure 6.5.1A). However, based on the presence of 45 phosphopeptides detected by LC-MS/MS (m=45) mapping to known Akt1 substrates (Figure 6.5.1B), KSEA inferred that Akt1 activity is significantly and rapidly upregulated following integrin $\alpha_v\beta_6$ LAP-ligand engagement and internalisation reaching maximal activity at **15'** (t=5; z-(score)=3.027; p<0.01**).

Conversely, KSEA indicated Akt2 and Akt3 isoforms were gradually downregulated during integrin $\alpha_v\beta_6$ LAP-ligand engagement and internalisation, reaching maximal signalling decay at **30'** post-internalisation (t=30; **Akt2**: z-(score)=−1.125; **Akt3**: z-(score)=−0.796). To validate Akt1 activity inferred by KSEA, parental lysates used to prepare peptides for phosphoenrichment and LC-MS/MS were analysis were probed for the Akt1 isoform phosphorylated at Ser473 (**p(S^{473})Akt1**), total Akt1 (**Akt1**) and pan-Akt (all isoforms) phosphorylated at Ser473 (**p(S^{473})Akt**) (Figure 6.5.1C).

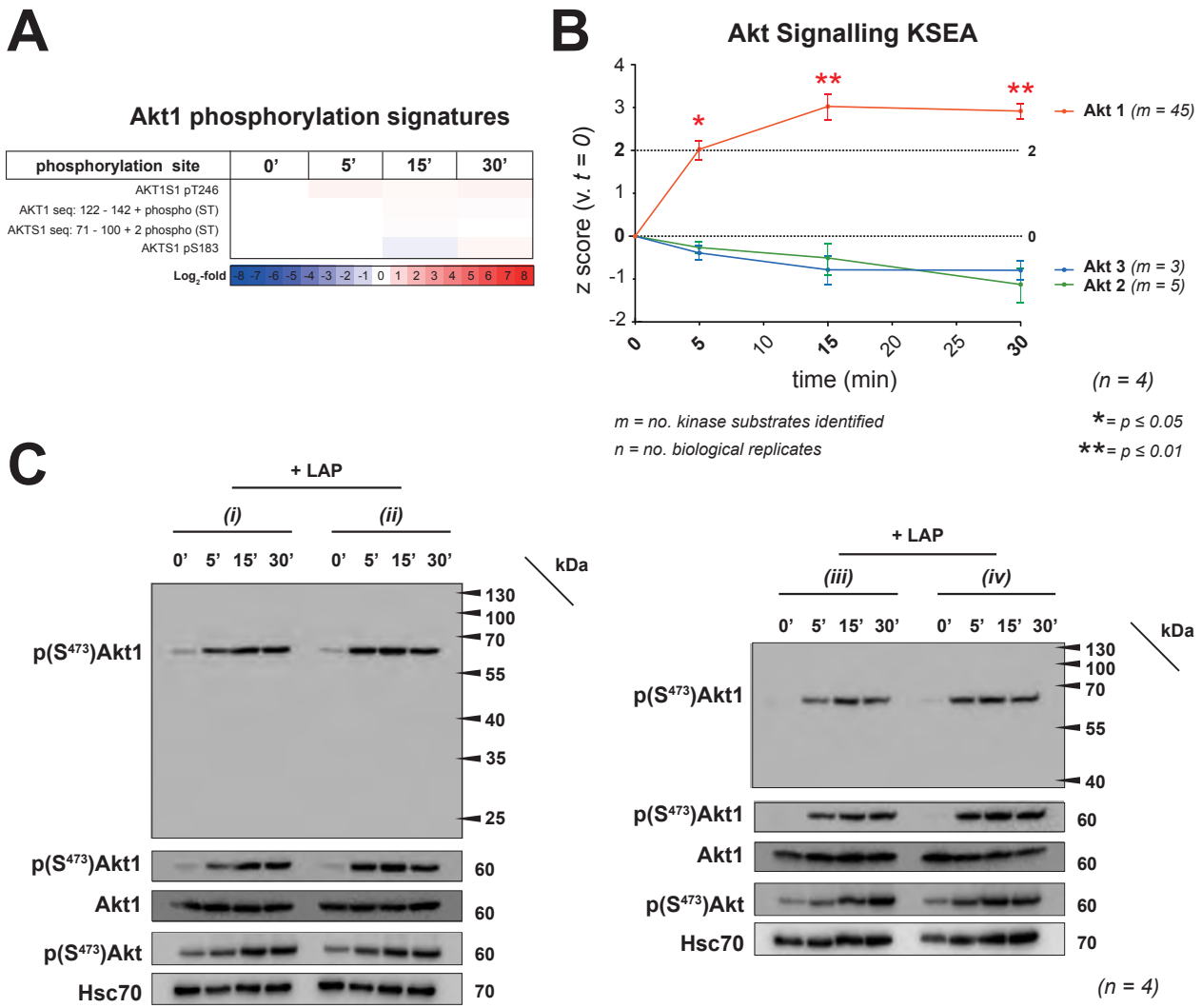

Figure 6.5.1

KSEA results suggests Akt isoform specific activation during signalling inducted upon integrin $\alpha_v\beta_6$ LAP ligand engagement and internalisation: Akt1 kinase activity is upregulated, but Akt2 and Akt3 activity decreases upon LAP ligand engagement and internalisation

Figure 6.5.1

KSEA results suggests Akt isoform specific activation during signalling inducted upon integrin $\alpha_v\beta_6$ LAP ligand engagement and internalisation: Akt1 kinase activity is upregulated, but Akt2 and Akt3 activity decreases upon LAP ligand engagement and internalisation

Results from KSEA analysis identified putative Akt isoform specific signalling downstream of integrin $\alpha_v\beta_6$ LAP ligand-engagement and internalisation in the BT-20 TNBC model. **(6.5.1 A)** Akt1 phosphorylation signatures directly identified from Akt1-derived phosphopeptide species detected by LC-MS/MS were not found to be significantly different in abundance compared to **0'** (t=0) baseline. **(6.5.1 B)** Akt1 kinase activity data generated from KSEA interrogation of 45 unique phosphopeptide species (m=45) directly detected that are known Akt1 substrates, indicate that Akt1 kinase activity increases significantly post integrin $\alpha_v\beta_6$ LAP-engagement and internalisation; reaching maximal activity at **15'** (t=15) compared to t=0 (baseline) ($p<0.05$*****, $p<0.01$******). However, KSEA suggested that Akt2 and Akt3 kinase activity decreases over the 30 min time-scale studied for integrin $\alpha_v\beta_6$ LAP ligand-engagement and internalisation. **(6.5.1 C)** To confirm KSEA-inferred Akt isoform-specific activity, the original lysates used for peptide preparation for LC-MS/MS were probed for: Akt1 phosphorylation at Ser473 (**pAkt1**^{S473}: 2 µg ml^{-1}, 9018S, CST), total Akt1 (**Akt1**: 2 µg ml^{-1}, 2938S, CST) and pan-pAkt (**pAkt**^{S473}: 2 µg ml^{-1}, 4060S, CST). A loading control was performed (**Hsc-70**: 0.2 µg ml^{-1}, sc-7298, Santa Cruz Biotech). Blots were revealed using Amersham ECL Detection Kit (RPN2106, GE Healthcare) and visualised using the Amersham™ Imager 600 (GE Healthcare Life Sciences Ltd) digital imaging system.

Concordant with KSEA, Akt1^{S473} phosphorylation was negligible (replicates i and ii) or absent (replicates iii and iv) at **0′** (t=0) but subsequently inducted from **5′** (t=5) post-internalisation; total Akt1 levels were constant across all timepoints (**0′ – 30′**). For all Akt isoforms evaluated using a pan-Akt antibody, phosphorylation at Ser473 was detected at **0′** (t=0), and subsequently upregulated from **5′** (t=5) onward.

To robustly validate the inferred, putative Akt1 dominance in signalling downstream of integrin $\alpha_v\beta_6$ LAP-ligand engagement and internalisation, parental lysates require probing for Akt2 and Akt3 isoforms alongside their Ser473 phosphorylation status to asses whether these Akt isoforms are indeed downregulated as indicated by KSEA.

Within the LC-MS/MS dataset, phosphopeptides mapping to ERK1 (**MAPK3**: **pT^{202}/pY^{204}** >6 log_2-fold; **pY^{204}** >3 log_2-fold) and ERK2 (**MAPK1**: **pT^{185}/pY^{187}** >5 log_2-fold; **pY^{187}** >6 log_2-fold) phosphorylation residues were directly identified (Figure 6.5.2A), exhibiting significant enrichment during integrin $\alpha_v\beta_6$ LAP-ligand internalisation **5′** (t=5) to **30′** (t=30) timepoints.

Based on identification of 40 known ERK1 (MAPK3) (m=40) and 35 known ERK2 (MAPK1) (m=35) substrates, KSEA evaluation of ERK activity (Figure 6.5.2B) inferred ERK1>ERK2 upregulation following integrin $\alpha_v\beta_6$–mediated LAP internalisation; ERK1 reaching maximal activity at **30′** (t=30; z-(score)=3.342; p<0.001***). Parental LC-MS/MS lysates were re-probed for phosphorylated and total ERK1/2 to validate these findings (Figure 6.5.2C). Induction of ERK1/2 phosphorylation from **5′** (t=5) onwards was confirmed, demonstrating integrin $\alpha_v\beta_6$–mediated LAP-ligand induced signalling in the BT-20 TNBC cell line is characterised by ERK1>ERK2 activity.

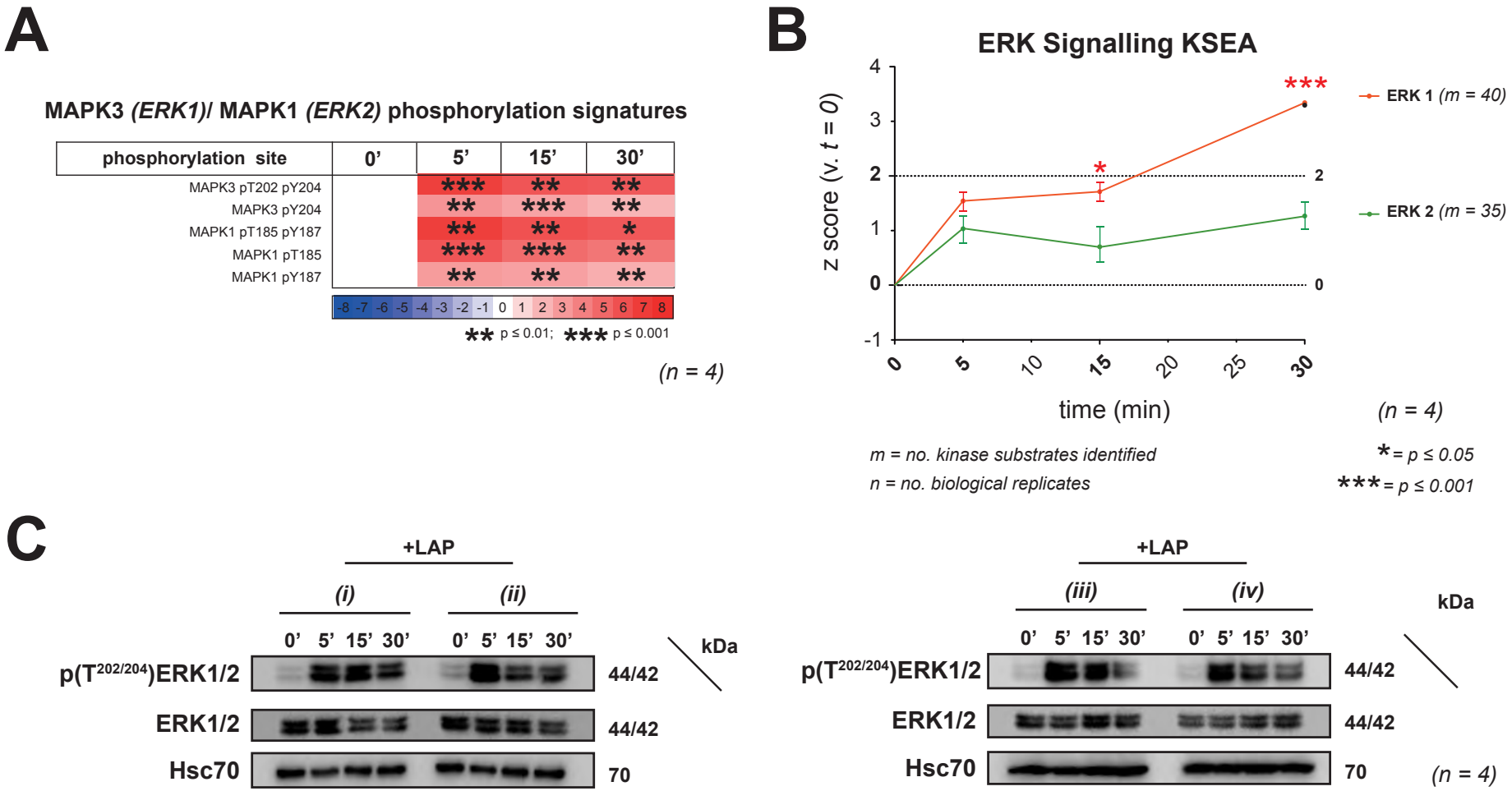

Figure 6.5.2
Phosphopeptide data and KSEA results suggest ERK1/2 phosphorylation occurs early (t=5) and its downstream kinase activity significantly mediates late (t=30) signalling events during integrin $\alpha_v\beta_6$ LAP ligand engagement and internalisation

Figure 6.5.2

Phosphopeptide data and KSEA results suggest ERK1/2 phosphorylation occurs early (t=5) and its downstream kinase activity significantly mediates late (t=30) signalling events during integrin $\alpha_v\beta_6$ LAP ligand engagement and internalisation

Directly detected phosphopeptide species and results from KSEA analysis indicate the significance of ERK1/2 phosphorylation and kinase activity downstream of integrin $\alpha_v\beta_6$ LAP ligand-engagement and internalisation in the BT-20 TNBC model. **(6.5.2 A)** ERK1/2 phosphorylation signatures directly identified from ERK1 (MAPK3) and ERK2 (MAPK1)-derived phosphopeptide species detected by LC-MS/MS were found to be significantly different in abundance compared to **0'** (t=0) baseline ($p<0.01$****** and $p<0.001$*******). ERK1/2 phosphorylation motifs were most significantly enriched at **5'** (t=5) at residues known to be associated with ERK1 (T202/Y204) and ERK2 (T185/Y187) activation. **(6.5.2 B)** ERK1 and ERK2 kinase activity exhibited markedly similar trends over time in terms of KSEA-modelled levels of kinase activity, based on the abundance of phosphopeptides detected that map to their known substrates (m=40 and m=35 respectively). ERK1/2 kinase activity increases significantly post integrin $\alpha_v\beta_6$ LAP-engagement and internalisation; reaching maximal activity at **30'** (t=30) compared to t=0 (baseline) ($p<0.05$***** and $p<0.001$*******). **(6.5.2 C)** To confirm ERK1/2 activity, the original lysates used for peptide preparation for LC-MS/MS were probed for pERK1/2 phosphorylation at Thr202/Tyr204 (**pERK1**$^{T202/Y204}$**/2**$^{T185/187}$: 2 µg ml^{-1}, 9101L, CST) and total ERK1/2 (**ERK1/2**: 1 µg ml^{-1}, 9102L, CST). A loading control was performed (**Hsc-70**: 0.2 µg ml^{-1}, sc-7298, Santa Cruz Biotech). Blots were revealed using Amersham ECL Detection Kit (RPN2106, GE Healthcare) and visualised using the Amersham™ Imager 600 (GE Healthcare Life Sciences Ltd) digital imaging system.

In addition to induction of Akt1^{S473} and ERK1$^{T202/Y204}$/ERK2$^{T185/Y187}$ phosphorylation, significant changes in site-specific EGFR phosphorylation motifs downstream of integrin $\alpha_v\beta_6$ LAP-ligand engagement and internalisation were directly detected and identified by LC-MS/MS (Figure 6.5.3A). National Cancer Institute (NCI) Pathway Analysis of phosphopeptides detected by LC-MS/MS indicated the involvement of EGFR (ErbB1) Signalling during integrin $\alpha_v\beta_6$ LAP-engagement and internalisation (Figure 6.5.3A i). Early EGFR phosphorylation events appear to be directed at Thr693 (**pEGFR**^{T693}: >3 log_2-fold enrichment; p<0.05*; p=0.012) and Ser1042 (**pEGFR**^{S1042}: >4 log_2-fold enrichment p<0.05*; p=0.022), which showed significant increases in abundance at **5′** (t=5) (Figure 6.5.3A ii).

Notably, EGFR underwent dephosphorylation at two motifs (Tyr1172 and Ser1104) which exhibited downregulation in abundance in comparison with **0′** (t=0) baseline; Tyr1172 showed significant downregulation at **15′** (**pEGFR**^{Y1172}: t=15; <−3 log_2-fold enrichment; p<0.05*; p=0.022) and **30′** (t=30; <−3 log_2-fold enrichment p<0.05*; p=0.028). Parental LC-MS/MS lysates were then probed by WB for EGFR phosphorylation at Tyr1086 (**pEGFR**^{Y1086}).

Curiously, **pEGFR**^{Y1086} appears to decrease across **5′** (t=5), **15′** (t=15) and **30′** (t=30) timepoints in comparison with baseline **0′** (t=0); suggesting EGFR undergoes dephosphorylation at Tyr1086 following integrin $\alpha_v\beta_6$ LAP-internalisation. Although the extent of the observed decrease in **pEGFR**^{Y1086} detected by WB was variable across the four biological replicates, a general trend was observed, being most marked in replicates (ii) and (iii).

To further investigate the putative EGFR regulation of signalling inducted downstream of integrin $\alpha_v\beta_6$ LAP-ligand engagement and internalisation, a kinase inhibition assay was combined with a ligand stimulation assay (Figure 6.5.3B). Using commercially available SMIs to target: EGFR (gefitinib/IRESSA® (**Gef**), AstraZeneca UK Ltd) and c-MET (PHA665752 (**PHA**), Tocris, R&D Systems) kinase activity either alone or in tandem, the BT-20 (Figure 6.5.3B), MDA-MB-468 and SUM159 (Figure 6.5.3C) TNBC cell lines were then challenged with LAP ligand to investigate the effects of RTK ablation on integrin $\alpha_v\beta_6$-mediated downstream signalling events.

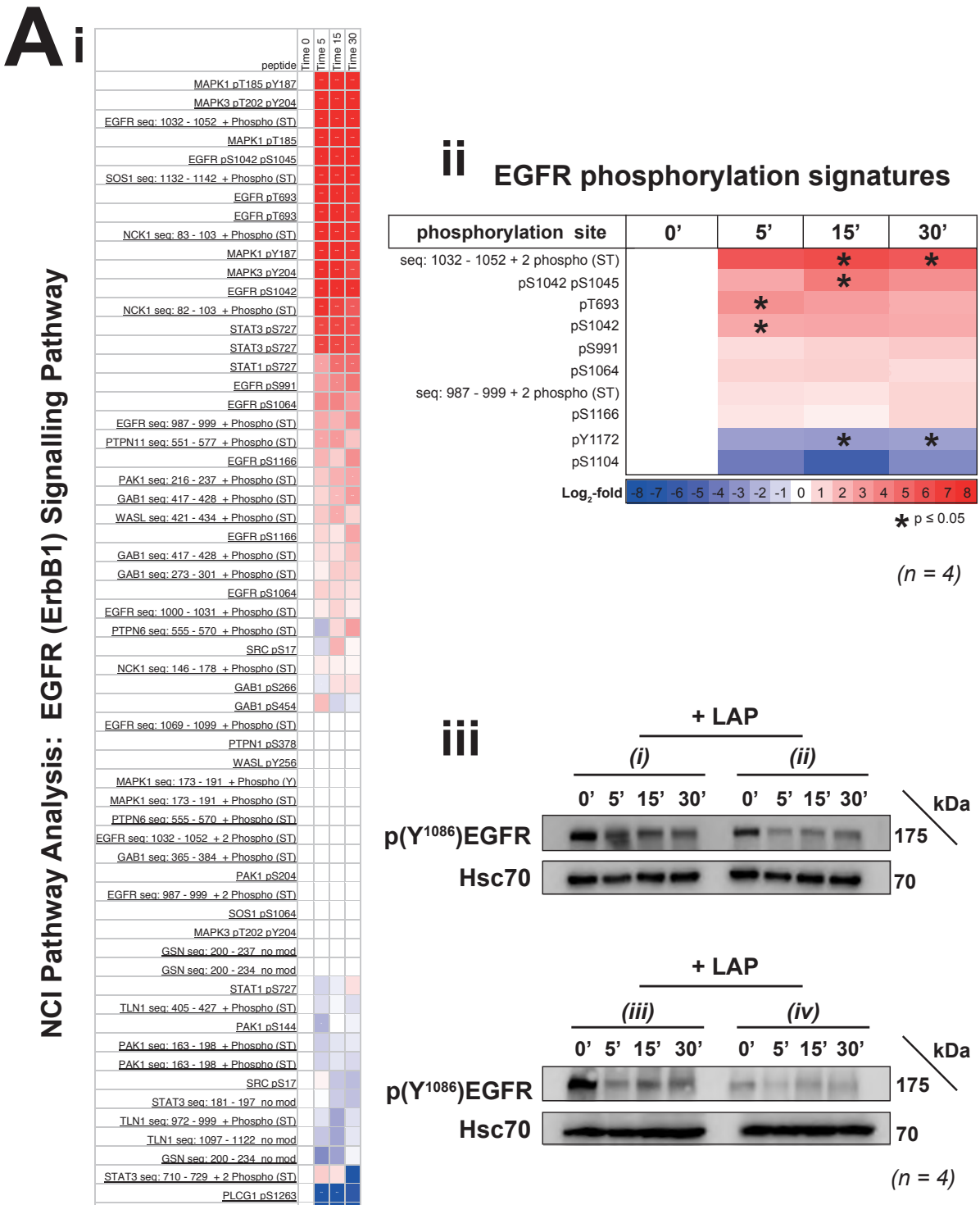

Figure 6.5.3 (A)
Duality of EGFR phosphorylation signatures characterise alteration in the BT-20 TNBC phosphoproteome during integrin $\alpha_v\beta_6$ LAP-ligand engagement and internalisation; significant upregulation of EGFR phosphorylation at Ser1042/1045 and Thr693 with concomitant significant downregulation of EGFR phosphorylation at Tyr1172 is observed during LAP internalisation

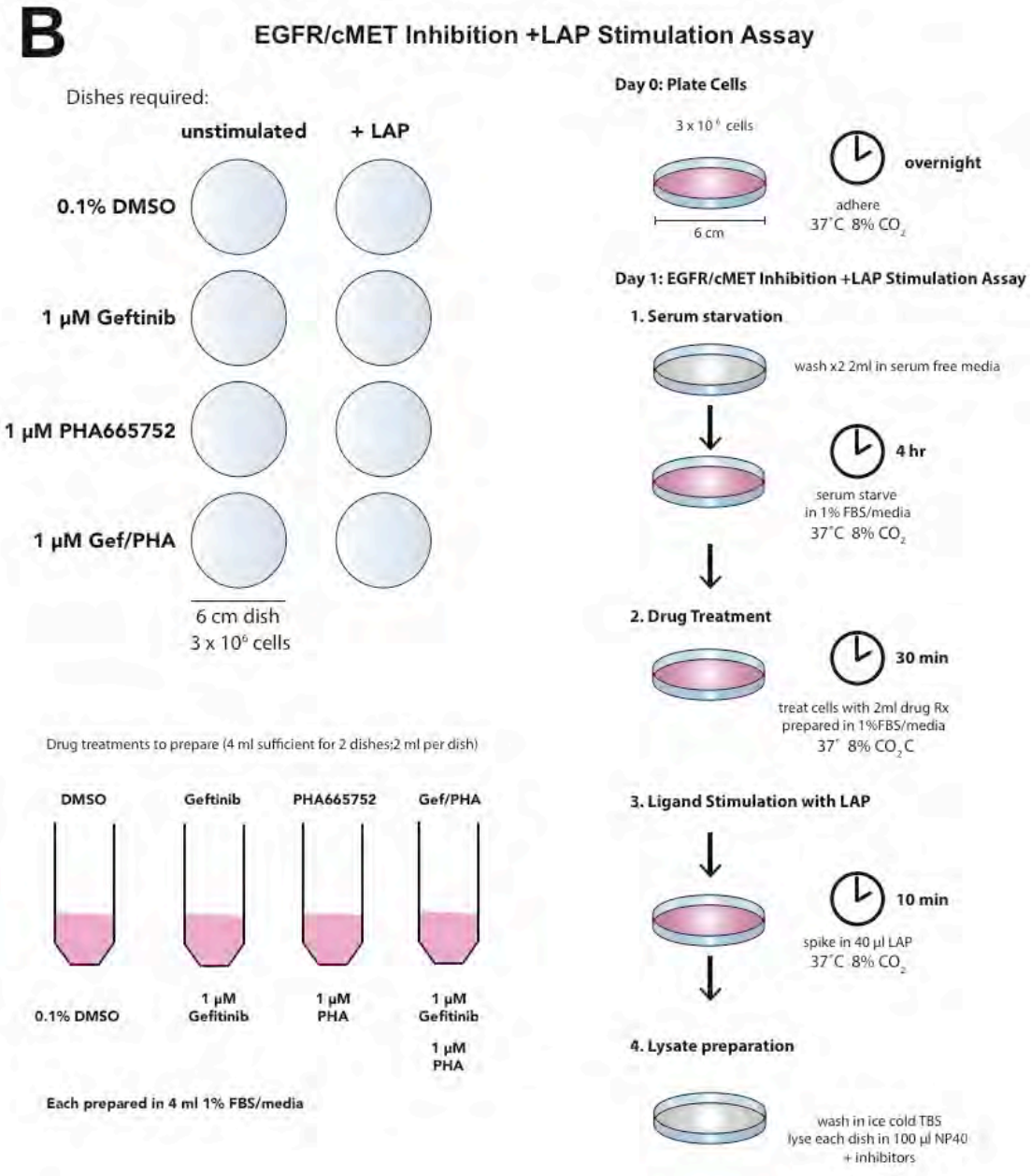

Figure 6.5.3 (B)
Schematic overview of a combined kinase-inhibition, LAP-ligand stimulation assay to investigate the regulatory effects of EGFR and c-MET RTKs during LAP-mediated integrin $\alpha_v\beta_6$ activation and downstream signalling events

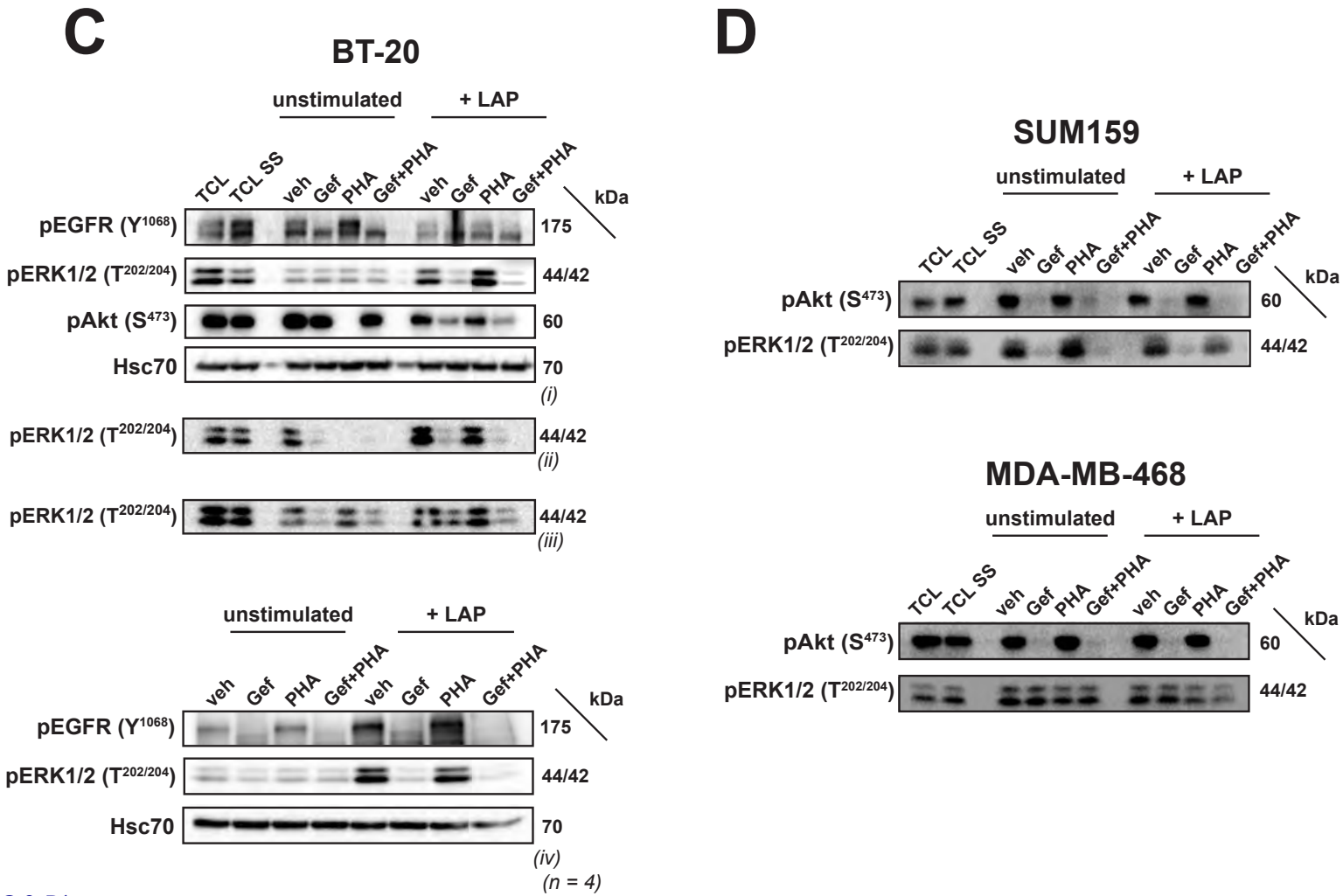

Figure 6.5.3 (C & D)
LAP-induced ERK1/2 activation is EGFR-dependent but independent of c-Met in the BT-20 and SUM159 TNBC cell line models and is unaffected in the MDA-MB-468 cell line bearing constitutively active ERK1/2

Figure 6.5.3
LAP-induced ERK1/2 activation is EGFR-dependent but independent of c-Met in the BT-20 and SUM159 TNBC cell line models and is unaffected in the MDA-MB-468 cell line bearing constitutively active ERK1/2

(6.5.3 A) NCI Pathway Analysis **(i)** highlighted EGFR (ErbB1) signalling pathway is active within the β_6-kinome during LAP internalisation. **(ii)** Phosphopeptide species mapping to EGFR phosphorylation sites were significantly enriched following LAP-ligand engagement and internalisation. Early (**5′**, t=5) EGFR phosphorylation events appear to be directed at Thr693 ($p<0.05$*; p=0.012) and Ser1042 ($p<0.05$*; p=0.022). Notably, two EGFR phosphopeptides (pY1172 and pS1104) were downregulated in comparison with **0′** baseline (t=0); pY1172 showing significant downregulation at **15′** (t=15; $p<0.05$*; p=0.022) and **30′** (t=30; $p<0.05$*; p=0.028). P-values are adjusted for multiple-testing correction using the Benjamini-Hochberg procedure. **(iii)** Lysates used for phosphoproteomics were probed for phosphorylation of the EGFR receptor at Tyr1086 (**pEGFR^{Y1086}**: 2 µg ml^{-1}, 2220S, CST) which demonstrated that following LAP ligand engagement and internalisation, phosphorylation at this residue appears to decay between 5′ and 30′ timepoints. A kinase inhibition/ligand stimulation assay **(6.5.3 B)** was used to investigate the role of RTK-integrin crosstalk in LAP-mediated signalling in the **(6.5.3 C)** BT-20 and **(6.5.3 D)** SUM159 and MDA-MB-468 cell lines, LAP-ligand stimulation assays were performed under EGFR and c-MET blockade conditions. Adherent cells were serum starved (1%FBS/α-MEM) for 4 hours prior to 30′ treatment under serum-free conditions with small molecule inhibitors to EGFR (**gefitinib** (**Gef**); 1 µM; AstraZeneca) or c-MET (**PHA665752** (**PHA**); 1 µM; R & D Systems), or with a 10% DMSO vehicle (**veh**) control. At the end of inhibitor treatments, human recombinant LAP (0.5 µg ml^{-1}, L3408, Sigma Aldrich) was spiked in to stimulate cells for 10′ in the presence of inhibitors. Upon completion, cell monolayers were washed and lysates harvested for Western blotting. Lysates were probed for EGFR phosphorylation at Tyr1068 (**pEGFR^{Y1068}**: 2 µg ml^{-1}, 2234S, CST); ERK1/2 phosphorylation at Thr202/204 (**pERK1/2$^{T202/204}$**: 2 µg ml^{-1}, 9101L, CST) and Akt phosphorylation at Ser473 (**pAkt1^{S473}**: 2 µg ml^{-1}, 9018S, CST). Loading controls are indicated (**Hsc-70**: 0.2 µg ml^{-1}, sc-7298, Santa Cruz Biotech). Blots were revealed using Amersham ECL Detection Kit (RPN2106, GE Healthcare) and visualised using the Amersham™ Imager 600 (GE Healthcare Life Sciences Ltd) digital imaging system. **Acknowledgements:** Replicate experiments (iii) and (iv) shown in **(6.5.3 C)** were performed by Mr Philip Adeniran (MSc student) and reproduced here with his kind permission.

Results from four biological replicate kinase inhibition/LAP-stimulation assays (n=4) consistently showed that LAP ligand induction of ERK1/2 phosphorylation (**pERK1**$^{T202/Y204}$/**pERK2**$^{T185/Y187}$) is EGFR dependent, but independent of c-MET, in the BT-20 cell line (Figure 6.5.3C). Treatment with 1 μM gefitinib (**Gef**) was sufficient to abrogate ERK1/2 phosphorylation downstream of LAP ligand stimulation in comparison with vehicle (**veh**) control; treatment with 1 μM PHA665752 (**PHA**) did not abolish nor reduce induction of ERK1/2 phosphorylation following LAP stimulation. Dual-targeting of EGFR/c-MET using a combination treatment (**Gef+PHA**) was also seen to ablate ERK1/2 phosphorylation downstream of LAP ligand stimulation.

A single experiment (n=1) was successfully probed for pan-Akt phosphorylation at Ser473 (**pAkt**^{S473}). This preliminary result showed that EGFR blockade (**Gef**) diminished but did not ablate **pAkt**^{S473} levels following LAP stimulation in comparison with LAP-stimulated vehicle (**veh**) control; c-MET blockade (**PHA**) appeared to mediate little or no effect on downstream **pAkt**^{S473} levels following LAP stimulation in comparison with LAP-stimulated vehicle (**veh**) control. As previously observed for ER1/2 phosphorylation, co-targeting of EGFR/c-MET using a combination treatment (**Gef+PHA**) was also seen to ablate Akt Ser473 phosphorylation downstream of LAP ligand stimulation.

To explore the broader, biological relevance of this putative integrin $\alpha_v\beta_6$/LAP-inducted/EGFR-dependent-ERK1/2-phosphorylation signalling axis in the BT-20 TNBC model, additional TNBC cell lines (SUM159 and MDA-MB-468) were briefly evaluated (n=1) (Figure 6.5.3D). As had been observed in the BT-20 cell line, EGFR functional blockade in the SUM159 cell line using 1 μM gefitinib (**Gef**) ablated downstream ERK1/2 phosphorylation (**pERK1**$^{T202/Y204}$/**pERK2**$^{T185/Y187}$) in comparison with LAP-stimulated vehicle (**veh**) control.

However, LAP-induced ERK1/2 phosphorylation was unaffected by EGFR inhibition in the MDA-MB-468 cell line. Levels of ERK1/2 phosphorylation in cells treated with 1 μM gefitinib (**Gef**) were comparable between ligand-naïve (unstimulated) and LAP-stimulated samples. The broadly consistent ERK1/2 phosphorylation levels across all ±kinase inhibition/±ligand stimulation conditions is concordant with the MDA-MB-468 constitutively active ERK status reported by Kovala and Poulin (2009).

In both the SUM159 and MDA-MB-468 cell lines, phosphorylation of Akt at Ser473 (**pAkt**^{S473}) downstream of LAP-stimulation was diminished by both EGFR blockade alone (**Gef**) and by EGFR/c-MET co-targeting treatment (**Gef+PHA**), in comparison with LAP-stimulated vehicle (**veh**) control. Inhibition of c-MET alone (**PHA**) elicited no effect on LAP-induced **pAkt**^{S473} levels in SUM159 and MDA-MB-468 cells. These results were concordant with **pAkt**^{S473} downregulation in the presence of 1 μM gefitinib (**Gef**) observed in the BT-20 cell line (Figure 6.5.3C).

Collectively, these preliminary investigations into the role of EGFR activity during integrin $\alpha_v\beta_6$–LAP engaged signalling (EGFR-integrin $\alpha_v\beta_6$ crosstalk) in TNBC, suggest that LAP-induced ERK1/2 phosphorylation (**pERK1**$^{T202/Y204}$/**pERK2**$^{T185/Y187}$) is EGFR-dependent, but independent of c-MET in TNBC cells (SUM159, BT-20); except in cells exhibiting constitutively active ERK1/2 (MDA-MB-468).

Furthermore, LAP-mediated Akt phosphorylation (**pAkt**^{S473}) is EGFR blockade sensitive but insenstive to c-MET blockade in TNBC cells (BT-20, MDA-MB-468, SUM159). These results implicate integrin $\alpha_v\beta_6$ dependency on replete EGFR activity to modulate signalling downstream of LAP-ligand engagement, supporting the concept of integrin $\alpha_v\beta_6$–EGFR crosstalk which warrants more extensive mechanistic dissection.

6.6 discussion

In light of the emerging clinical significance of integrin-derived signalling following cognate ligand-induced activation, internalisation and trafficking as determinants of patient outcome (in terms of disease progression, therapeutic sensitivity and acquisition of chemoresistance), a LAP ligand-based internalisation assay targeting the integrin $\alpha_v\beta_6$ was successfully developed (Figures 6.1.1 to 6.1.3) to permit novel phosphoproteomic dissection (Figure 6.2) of integrin $\alpha_v\beta_6$-mediated signalling events downstream of LAP-ligand engagement and internalisation in the BT-20 TNBC model.

The use of LAP ligand to interrogate integrin $\alpha_v\beta_6$–specific ligand-mediated processes in the BT-20 cell line was partly validated by abrogation of LAP engagement following cell surface integrin $\alpha_v\beta_6$ blockade with the inhibitory antibody clone 53A2 (Chapter V: Results Part III, Figure 5.2C). However, use of LAP to specifically bait the integrin $\alpha_v\beta_6$ to characterise receptor internalisation-associated kinetics and signalling events required more robust validation of a direct physical association between LAP and integrin $\alpha_v\beta_6$ that is demonstrably sustained during intracellular trafficking.

Attempts were made to demonstrate co-localisation of an Fc-tagged LAP ligand with the active integrin $\alpha_v\beta_6$ conformer (recognised by antibody clones 6.2E5 and 6.2G2) by IMF, but these proved unsuccessful (Supplemental Figure S6.4). It was hypothesised that steric hindrance may limit availability of epitopes when post-labelling adherent cells cultured in 2D in the presence of ligand; impeding successful antibody binding, especially if competing for epitopes proximal to the ligand-binding site. However, previous flow cytometry experiments (Chapter III: Results Part I, Figures 3.1.2 and 3.2.2) using antibodies 6.2E5 and 6.2G2 to label active, ligand-engaged integrin $\alpha_v\beta_6$ in the presence of ligands A20FMDV2-biotin and LAP-Fc were successful, negating the theory of steric hindrance impeding antibody binding for IMF analyses.

Furthermore, as antibodies 6.2E5 and 6.2G2 bound in the presence of ligand (Chapter III: Results Part I, Figures 3.1.2 and 3.2.2), it was concluded that these antibodies are not ligand-mimetic; precluding the possibility of epitope binding site competitive inhibition preventing successful IMF dual labelling of integrin

$\alpha_v\beta_6$/LAP-Fc. Therefore, further optimisation of the IMF protocol is required to permit successful demonstration of integrin $\alpha_v\beta_6$/LAP colocalisation to generate a sufficient evidence base to use LAP ligand as a means of specifically targeting the integrin $\alpha_v\beta_6$ adhesion receptor.

A set of co-IP experiments downstream of a LAP-Fc internalisation assay (originally designed to isolate integrin $\alpha_v\beta_6$/LAP complexes undergoing internalisation for proteomic interrogation), were revisited to address the question of integrin $\alpha_v\beta_6$/LAP specificity (Chapter II: Materials and Methods, Section 2.9). Results from three biological replicate IP experiments (n=3) demonstrated the integrin β_6–subunit was reproducibly immunoprecipitated using an Fc-tagged LAP ligand across all internalisation timepoints (Figure 6.1.2B and E; Supplementary Figure S6.1). This broadly confirmed the direct physical interaction between LAP and integrin $\alpha_v\beta_6$ is sustained during internalisation and intracellular trafficking.

Ideally, lysates would have been probed for LAP to robustly demonstrate co-IP of integrin $\alpha_v\beta_6$/LAP; alongside evaluation of other integrin receptors reported to engage LAP to further validate integrin $\alpha_v\beta_6$ specificity for LAP in the BT-20 TNBC model used. However, for the purposes of the LC-MS/MS dataset presented subsequently (Figure 6.2), these co-IP experiments provided additional evidence for the utility of LAP to study integrin $\alpha_v\beta_6$–mediated processes within the BT-20 cell line; but with caveats to prevent over- or misinterpretation of findings.

Inferential KSEA evaluation of known kinase substrates detected by LC-MS/MS (Figures 6.3.1 and 6.3.2) permitted identification of five putative kinase moieties implicated in early (**5'**, (t=5): **MAP3K8**; **MAPKAPK2**; **PDK1**; **TBK1**) and late (**30'**, (t=30): **Nuak1**) signal activation and temporal pathway modulation during integrin $\alpha_v\beta_6$ LAP-engagement and internalisation (target kinases tabulated in Supplementary Figure S6.2). These candidate kinases were selected for functional validation using commercially available SMIs and siRNA to interrogate their role in integrin $\alpha_v\beta_6$–dependent signalling and phenotypic outputs (ligand engagement, invasion, migration, proliferation).

Disappointingly, antibodies purchased to confirm siRNA silencing (Supplementary Figure S6.3) or phosphorylation status to determine SMI ablation of kinase activity (Supplementary Figure S6.4) were not successfully optimised nor validated within

the timescale of this project; limiting the robustness and reliability of subsequent experiments seeking to manipulate activity of the target kinases identified.

Despite an inability to robustly validate kinase inhibition, exploratory investigations were tentatively conducted using a MAP3K8/COT-targeting SMI (TC-S7006) to gain additional (if rudimentary) insight into the role of this kinase during LAP-induced integrin $\alpha_v\beta_6$-mediated activation and downstream signalling (Figure 6.4). In the absence of a working antibody to confirm inhibition of MAP3K8/COT activity and optimise treatment concentration, a concentration of 1 μM was chosen as a previous study had reported in vitro efficacy of a SMI targeting MAP3K8/COT at this concentration in human cytotoxic T lymphocytes (Chowdhury *et al* 2014).

Another study dissecting MAP3K8 pathway activity in human MM had targeted V-Raf Murine Sarcoma Viral Oncogene Homolog B (BRAF) and MAPK/ERK (MEK) kinases downstream of MAP3K8 using 1 μM BRAF and MEK SMIs to manipulate the MAP3K8 pathway (Johannessen *et al* 2010). It is acknowledged that cell line-specific titration of inhibitor concentrations to determine optimal efficacy would be preferable. However, allowing for the caveats associated with insufficient validation procedures that restrict interpretation of results, several interesting observations were made regarding the effects of MAP3K8/COT inhibitor treatment on integrin $\alpha_v\beta_6$–associated processes in the BT-20 TNBC model.

Notably, ERK1/2 phosphorylation downstream of LAP-ligand engagement was diminished in the presence of 1 μM TC-S7006 (**TC-S 7006**) in comparison with LAP-stimulated vehicle (**veh**) control (Figure 6.4C); one of the two biological repeats (ii) showed near ablation of ERK1/2 phosphorylation downstream of LAP stimulation in comparison with corresponding LAP-stimulated vehicle (**veh**) control. Phosphorylation of ERK1/2 downstream of EGFR and c-MET stimulation (with their respective cognate ligands EGF and HGF) was unaffected by the presence of a MAP3K8/COT inihibitor (1 μM TC-S7006), suggesting specific sensitivity of integrin $\alpha_v\beta_6$–mediated signalling following MAP3K8 targeting using 1 μM TC-S 7006.

Phosphorylation of Akt1 at Ser473 (**pAkt1**^{S473}) downstream of integrin $\alpha_v\beta_6$–directed LAP-stimulation is unaffected by the presence of a MAP3K8/COT inhibitor in comparison with corresponding LAP-stimulated vehicle (**veh**) control. Collectively, results from these preliminary signalling studies in the presence of the

MAP3K8/COT-targeting SMI TC-S 7006, implicate replete MAP3K8/COT kinase activity in LAP/integrin $\alpha_v\beta_6$-induced ERK1/2 phosphorylation; suggesting MAP3K8/COT may be a positive regulator of LAP ligand-induced, integrin $\alpha_v\beta_6$–derived outside-in signal transduction that warrants more robust characterisation.

Curiously, canonical integrin activation studies using divalent Mn^{2+} cations (n=4) (Figure 6.4D) or cognate ligand (n=2) (Figure 6.4E) in conjunction with 1 μM TC-S 7006 treatment suggested the presence of a MAP3K8/COT inhibitor potentiated the active integrin $\alpha_v\beta_6$ conformer (detected by the active conformer-sensitive antibody clone 6.2E5) following exposure to both Mn^{2+} ions and LAP ligand; but did not alter detection of surface integrin $\alpha_v\beta_6$ using a conformation-independent antibody (clone 53A2). Interestingly, potentiation of LAP-ligand-induced integrin $\alpha_v\beta_6$ activation in the presence of TC-S 7006 was also observed in the VB6 cell line (Figure 6.4F), suggesting possible broader biological relevance that warrants additional investigation.

Although inhibition or ablation of MAP3K8/COT could not be demonstrated to validate kinase abrogation by TC-S 7006 treatment, the consistency of results indicating that the presence of a MAP3K8/COT inhibitor did not affect cell surface levels of total integrin $\alpha_v\beta_6$ (demonstrated with antibody clone 53A2), but specifically promoted adoption of the active conformation (demonstrated with antibody clone 6.2E5) in response to canonical extracellular activators, suggest that functionally replete MAP3K8/COT may be implicated in the negative regulation of integrin $\alpha_v\beta_6$ receptor activation.

These intriguing and counterintuitive findings warrant further investigation to dissect the putative dichotomy of MAP3K8/COT activity during integrin $\alpha_v\beta_6$–mediated signalling and extracellular activation revealed in these exploratory studies. The existence of a moiety eliciting pleiotropic effects on the integrin $\alpha_v\beta_6$ receptor, acting as a positive regulator of signal transduction downstream of integrin $\alpha_v\beta_6$-activation (downstream signal agonist) but inhibitor of integrin $\alpha_v\beta_6$ activation (receptor activation antagonist), is not entirely illogical.

Ye *et al* (2017) described the pleiotropic effects of the polyphenol epigallocatechin gallate (EGCG) on integrin $\alpha_{IIb}\beta_3$ activation and EGFR signalling in

both a purified system and cell lines. The authors reported that EGCG inhibited talin-induced integrin $\alpha_{IIb}\beta_3$ activation but activates integrin in the absence of talin.

Ye and colleagues (2017) attributed the pleiotropic effects of EGCG on integrin $\alpha_{IIb}\beta_3$ activation to toplogical modulation of the integrin β_3-subunit transmembrane domain (TMD). EGCG decreased integrin β_3 TMD embedding, which opposed talin-mediated integrin $\alpha_{IIb}\beta_3$ activation. In the absence of talin, the EGCG-induced decrease in integrin β_3 TMD embedding disrupted the α–β subunit TMD interaction causing receptor activation. Furthermore, the authors described similar topological modulation of the EGFR TMD eliciting pleiotropic effects on receptor activation; EGCG was seen to activate EGFR in the absence of cognate EGF ligand, but inhibit EGF-induced activation. The authors concluded that EGCG exerted dichotomous transmembrane signalling effects through TMD topology modification.

In addition, the pleiotropic effects of several kinases on adhesion-mediated signalling have been reported. Rho kinase (ROCK) signalling has been shown to promote either pro-apoptotic or pro-survival outcomes in a cell type and microenvironment context-specific manner (Street and Bryan 2011). Therefore, the notion that MAP3K8/kinase may elicit pleiotropic effects in response to upstream integrin rececptor activation is plausible.

Indeed MAP3K8/COT has itself been ascribed the pleiotropic role of both tumour suppressor and oncogenic tumour promoter in a cancer-type specific manner; acting as tumour suppressor in intestinal and lung cancer (Gkirtzimanaki *et al* 2013) but exerting pro-tumourigenic effects as an oncogene in several cancers including ovarian (Gruosso *et al* 2015) and BrCa (Lee *et al* 2015). MAP3K8/COT mRNA overexpression in breast tumour tissue in comparison with adjacent normal breast tissue was reported in 35 cases of primary human BrCa reviewed by Sourvinos *et al* (1999), implicating MAP3K8 expression in breast tumourigenesis. The oncogenic role of MAP3K8 in ovarian high-grade serous carcinoma (HGSC) was dissected by Gruosso *et al* (2015). Immunohistochemical evaluation of MAP3K8 expression in 139 HGSC cases demonstrated a significant association between MAP3K8 protein levels and poorer patient outcome in terms of disease progression and treatment response, leading the authors to propose that MAP3K8 may prove a useful prognostic marker in HGSC.

Gruosso and colleagues (2015) also demonstrated that MAP3K8 activity imparted a pro-tumourigenic phenotype in SKOV3 and IGROV-1 human ovarian cancer cells in vitro, which was abrogated by treatment with a MAP3K8 SMI. Additional studies targeting activity of the MAP3K8 downstream effector MEK, indicated that MAP3K8 expression predicts efficacy of the MEK inhibitor selumetinib (AZD6244, AstraZeneca) in vivo using human HGSC patient-derived xenografts. The authors concluded that MAP3K8 is a key oncogenic mediator during ovarian tumourigenesis and is a predictive marker for efficacy of novel MEK-inhibitor based therapeutics, such as selumetinib (currently in phase II clinical trial for low grade ovarion or peritoneal cancer: ClinicalTrials.gov ID NCT00551070).

Disappointingly, since Sourvino et al's (1999) first report of MAP3K8 as an oncogenic factor in BrCa, little research regarding MAP3K8 in breast tumourigenesis and disease progression has been published. Therefore, in light of the preliminary data presented here that strongly implicate induction of MAP3K8 activity downstream of integrin $\alpha_v\beta_6$/LAP engagement and trafficking in the BT-20 TNBC model, additional research focussed on the pro-tumourigenic role of MAP3K8 in BrCa is duly warranted.

The use of an inferential computational model to interrogate the LC-MS/MS using KSEA was deemed appropriate to expedite analysis of relevant signal pathway modulation that would not be possible by manual data-mining of the >7 000 phosphopeptides identified. Indeed, testament to its relevance and utility, the KSEA approach first described by Casado *et al* (2013a) has subsequently been developed into a web-based bioinformatics app tool by Wiredja *et al* (2017) to expedite meaningful user interrogation of phosphoproteomic datasets.

Evaluation of the LC-MS/MS dataset by KSEA identified ERK1/2 and Akt phosphorylation as downstream mediators of LAP ligand/integrin $\alpha_v\beta_6$–derived signalling (Figure 6.5.1), concordant with established understanding of integrin-mediated signalling within a broader context. The association between integrin-mediated signalling and ERK1/2 phosphorylation has long been established for other integrin moieties (Moreno-Layseca and Streuli 2014) and logically, was identified by KSEA and validated by WB within this dataset.

Ahmed *et al* (2002a) described a direct association between the integrin β_6 subunit cytodomain and ERK2 in the HT-29 colorectal carcinoma cell line, successfully co-immunoprecipitating ERK2 with integrin β_6. The authors used 20mer peptide fragments to mapping to the integrin cytodomain (amino acids 737 – 788) to identify the putative ERK-binding sequence ^{749}RSKAKWQTGTNPLYR^{763}. Results presented here support the significance of ERK2, and more markedly ERK1, phosphorylation as key mediators of integrin $\alpha_v\beta_6$–derived downstream signalling events.

Hyperactivation of phosphoinositide 3-kinase (PI3K)/Akt kinase signalling cascade has long been implicated in a variety of human pathologies, including malignant disease. Within the context of BrCa, active (phosphorylated) Akt has been associated with tamoxifen resistance (Kirkegaard *et al* 2005), HER2 amplification (Tokunaga *et al* 2006) and doxorubicin resistance (Knuefermann *et al* 2003). Current research highlights the emerging significance of Akt-isoform specific signalling modulating divergent functional outputs in cancer, including BrCa (Clark and Toker 2014); with high cytoplasmic Akt 2 reportedly associated with improved overall survival (Kirkegaard *et al* 2005).

In their study revealing integrin $\alpha_v\beta_6$ inhibition with 264RAD potentiated trastuzumab efficacy in Her-2 driven BrCa, Moore *et al* (2014) reported downregulation of total Akt2 (active, phosphorylated Akt2 was not assessed) in trastuzumab/264RAD (HER-2/integrin inhibited) tumour samples in comparison with trastuzumab monotherapy. The authors implicated loss of Akt2 compensatory signals underlying integrin $\alpha_v\beta_6$/HER2 crosstalk that may drive the observed efficacy of dual-therapy in HER-2 positive BrCa.

Curiously, KSEA evaluation of Akt isoform-specific activity within the LC-MS/MS dataset revealed significant induction of Akt1 isoform activity associated with LAP-induced/integrin $\alpha_v\beta_6$–derived signalling during internalisation (Figure 6.5.2). The isoforms Akt2 and Akt3 were not significantly deactivated but showed a gradual declination in activity. Although this data does not fit with Moore et al's (2014) proposed mechanism for HER-2 BrCa, this apparent Akt1 specificity may be a TNBC, or indeed BT-20 cell line-specific phenomenon that warrants validation in other TNBC models. Previous studies have highlighted the significance Akt1 isoform specifically in BrCa.

Spears *et al* (2012) evaluated Akt isoform-specific phosphorylation at Thr308 (**pAkt^{T308}/Akt1/Akt2**) in FFPE samples obtained from the Edinburgh Breast Conservation cohort of 1812 BrCa samples using a proximity ligation assay (PLA) to discriminate Akt1 versus Akt2 phosphorylation status. The authors determined that high levels of pAkt1 were associated with reduced distant recurrence-free survival (DRFS) and overall survival (OS). Notably, patients with high expression of pAkt1 isoform only exhibited significantly reduced DRFS; pAkt2 levels were not associated with differences in patient outcome. Spears and colleagues (2012) concluded that Akt1 activation may lead to poorer survival in BrCa patients.

In light of the clinical signifiance of Akt1 phosphorylation demonstrated in Spear and colleagues' (2012) study, the finding that Akt1 activity being specifically upregulated during integrin $\alpha_v\beta_6$ LAP-engagement and internalisation warrants further mechanistic dissection in additional TNBC models to validate whether Akt1 is indeed a critical regulatory node in integrin $\alpha_v\beta_6$ –mediated signalling pathways. Evaluation of Akt1 activity within the broader context of BrCa tumourigenesis and disease progression would refine understanding of its temporal significance during BrCa natural history and relevance as a target for therapeutic intervention.

Interestingly, several phosphopeptides mapping to specific EGFR phosphorylation motifs were significantly enriched, and one motif was significantly downregulated within the LC-MS/MS dataset. Early EGFR phosphorylation events appear to be directed at Thr693 (**pEGFR^{T693}**) and Ser1042 (**pEGFR^{S1042}**), which showed significant increases in abundance at **5'** (t=5). Notably, EGFR phosphorylation at Tyr1172 significantly decreased abundance at **15'** and **30'** in comparison with phosphorylation status at baseline (**0'**; t=0). This provided direct (as opposed to inferential, computational KSEA) evidence for integrin $\alpha_v\beta_6$–EGFR crosstalk during LAP engagement and internalisation in the BT-20 TNBC cell line.

Based on pharmacokinetic data for gefitinib (IRESSA®, AstraZeneca) from Phase I clinical trials and U.S Food and Drug Administration (FDA) approved dosing of 250 mg/day, Mukohara *et al* (2005) determined that 1 μM was the maximum achievable plasma concentration. Therefore, single-dose 1 μM gefitinib was used to target EGFR activity for in vitro assays seeking to dissect EGFR-integrin $\alpha_v\beta_6$ crosstalk during LAP-engagement and internalisation that had been revealed by

the LC-MS/MS dataset. Integrin-EGFR crosstalk is not itself a novel concept. Moro *et al* (1998) first proposed a role for β_1 and α_v integrins during EGFR-derived mitogenic responses in human primary skin fibroblast and ECV304 endothelial cells adhering to immobilised fibronectin and collagen type I matrix proteins. Later, Moro *et al* (2002) demonstrated that β_1- and $\alpha_v\beta_3$-integrin-mediated EGFR-transactivation during mitosis was Src-kinase dependent.

Of particular interest, Moro and colleagues (2002) determined that these β_1- and $\alpha_v\beta_3$ integrin-mediated EGFR-transphosphorylation motifs were distinct from residues phosphorylated by classical EGFR activation inducted by EGF engagement. Integrins β_1 and $\alpha_v\beta_3$ were shown to induce phosphorylation of EGFR at tyrosine residues Tyr845 ($\mathbf{Y}^{845}$), Tyr1068 ($\mathbf{Y}^{1068}$), Tyr1086 ($\mathbf{Y}^{1086}$) and Tyr1173 ($\mathbf{Y}^{1173}$), but not Tyr1148 ($\mathbf{Y}^{1148}$) – a significant EGFR phosphorylation site in response to EGF. The authors proposed a novel mechamism for integrin-EGFR crosstalk driven by formation of a EGFR-Src-integrin-p130^{CAS} macromolecular complex that enabled EGFR transactivation. Finally, Moro and colleagues (2002) observed that integrin-mediated adhesion promoted increased cell surface EGFR expression, adding credence to the concept of co-operative reciprocity between integrin and EGFR receptors.

Concordant with Moro et al's (2002) description of integrin-mediated EGFR transactivation motifs, WB evaluation of single time-point LAP ligand stimulation assays demonstrated phosphorylation of EGFR at Tyr1068 ($\mathbf{Y}^{1068}$) in response to upstream LAP-ligand integrin $\alpha_v\beta_6$-stimulation that was diminished in the presence of gefitinib in the BT-20 TNBC cell line (Figure 6.5.3B). Curiously, evaluation of EGFR phosphorylation at Tyr1086 ($\mathbf{Y}^{1088}$) in the parental LC-MS/MS lysates revealed an apparent dephosphorylation of this residue during the LAP-internalisation time-course (**5'**; t=5 to (**30'**; t=30) in comparison with baseline (**0'**; t=5). The phosphorylation status of other specific residues relating to integrin-mediated EGFR transactivation described by Moro and colleagues (2002) was not evaluated by WB in parental LC-MS/MS lysates or LAP-stimulation assays owing to time and reagent constraints.

However, of particular interest are the Thr693 (**pEGFR**^{T693}) and Tyr1172 (**pEGFR**^{T1172}) EGFR phosphorylation motifs directly identified by LC-MS/MS, both of which are associated with altered EGFR-internalisation kinetics (PhosphoSite 2017). Interestingly, Winograd-Katz and Levitzki (2006) identified that EGFR

Thr669 (equivalent to human EGFR Thr693) undergoes p38 kinase-mediated phosphorylation in response to cisplatin treatment. The authors generated a mutant EGFR in which Thr669 was mutated to an alanine residue, which was less sensitive to p38-mediated phosphorylation. Furthermore, the authors characterised a cisplatin-induced regulatory axis governing EGFR internalisation. Winograd-Katz and Livitzki (2006) concluded that EGFR is a p38 substrate and that cisplatin treatment induces EGFR internalisation, which is regulated by p38-dependent EGFR phosphorylation at residue Thr669.

Presciently, within the LC-MS/MS dataset presented here, both EGFR phosphorylation at Thr693 and its upstream regulatory kinase p38 were found to be significantly enriched during integrin $\alpha_v\beta_6$ LAP-engagement and internalisation. Therefore, it may be possible that in agreement with Winograd-Katz and Livitzki (2006), and extending upon Moro et al's (2002) demonstration of α_v–integrin-induced EGFR transactivation, EGFR internalisation governed by p38-mediated Thr693 phosphorylation may be intrinsically linked with integrin $\alpha_v\beta_6$ ligand-induced activation and internalisation in the BT-20 TNBC model.

Furthermore, MAP3K8/COT (an upstream regulator of p38 kinase) was also found to be active within the LAP-induced integrin $\alpha_v\beta_6$-mediated kinome defined here by LC-MS/MS and KSEA. Therefore, a putative LAP-induced integrin $\alpha_v\beta_6$ derived signalling axis, involving MAP3K8/COT-p38-pEGFR^{T693} derailing receptor internalisation and associated signalling in a TNBC model assuredly warrants further spatiotemporal interrogation during breast tumourigenesis and disease progression.

Maiello *et al* (2015) reported that co-targeting of EGFR and MEK1/2 (using a combination therapy of the respective SMIs gefitinib and selumetinib) elicited a synergistic inhibitory growth effect in a panel of TNBC cell lines in vitro. Furthermore, this anti-proliferative effect using EGFR/MEK dual-targeting reduced Akt-phosphorylation and nearly abolished ERK1/2 activation. The authors concluded that potential utility of this treatment strategy in TNBC be evaluated in a broader context to determine in vivo and clinical relevance. However, as warned by Duncan *et al* (2012), kinome reprogramming in response to MEK inhibition has already been reported in TNBC, and may swiftly drive chemoresistance. Therefore, detailed mechanistic dissection of any putative signalling axes to be therapeutically targeted is critical.

Preliminary experiments were designed to explore the regulatory role of EGFR activity on integrin $\alpha_v\beta_6$ internalisation using IMF internalisation (Supplementary Figure S6.5A), time course stimulation (Supplementary Figure S6.5B) and 3D-physiomimetic mini-organotypic invasion assays (Supplementary Figure S6.5C) in the presence of inhibitory therapeutics gefitinib and/or 264RAD. These experiments were kindly performed by Mr Philip Adeniran (MSc student) and are included with his kind permission.

Although these preliminary datasets are incomplete, lacking the requisite complement of controls and deconvolution of single agent versus multi-agent therapeutic effects, some interesting results indicate ongoing mechanistic dissection of EGFR/integrin $\alpha_v\beta_6$ reciprocity in terms of receptor dynamics, downstream signal modulation and invasive phenotypic output is warranted. To define the pathological significance of integrin $\alpha_v\beta_6$/EGFR crosstalk inducting activity of downstream oncogenic factors already implicated in BrCa (MAP3K8/COT, p38, ERK1/2 and Akt1) would prove invaluable within the context of TNBC; a disease that disappointingly remains devoid of approved molecular targets and associated with poor outcome when conventional chemotherapy fails.

Interestingly, several other proteins of interest were directly detected within the LC-MS/MS dataset, with phosphopeptides mapping to key phosphorylation motifs showing significant enrichment in the β_6-kinome during integrin $\alpha_v\beta_6$ LAP-engagement and internalisation (Supplementary Figure S6.6). Nuclear Receptor Co-Repressor-1 (NCOR1) and -2 (NCOR2) showed enrichment within dataset, with NCOR1 phosphorylation at Ser70 showing significant enrichment (>2 $\log_2$-fold enrichment, $p<0.01$, $p=0.0029$ at maximal activity). Previous studies have shown that NCOR1 nonsense mutations and splice variants occur in BrCa (The Cancer Genome Atlas 2012); although an association was shown, a causal and/or functional link has not yet been established.

In addition, phosphopeptides mapping to the two highly homologous α and β isoforms of glycogen synthase kinase-3 (GSK3A/B) were also enriched in the LAP-induced β_6-kinome (**GSK3A**: >3 $\log_2$-fold enrichment, $p<0.01$, $p=0.0021$; **GSK3B**: >2 $\log_2$-fold enrichment, $p<0.05$, $p=0.017$ at maximal activity). Reviewing the Edinburgh Breast Conservation Series, Quintayo *et al* (2012) found that high expression of GSK3B has been associated with distant recurrence-free survival

(DRFS). Subsequently, demonstrated that GSK3 inhibition using novel SMIs overcame chemoresistance in both in vitro and in vivo BrCa models, further implicating an oncogenic and progressive role for this kinase in BrCa.

KEGG biological pathway analysis of the inferential KSEA dataset had revealed depletion of JAK/STAT signalling associated with the β_6-kinome during LAP internalisation. Interestingly, phosphopeptides mapping to the signal transducer and activator of transcription-3 (STAT3) phosphorylated at Ser727 were significantly enriched within the LC-MS/MS dataset (**STAT3**: >2 $\log_2$-fold enrichment, $p<0.001$, $p=0.0009$ at maximal activity). This infers that $pSTAT3^{S727}$ may be a key downstream regulatory event following integrin $\alpha_v\beta_6$ LAP-ligand engagement and internalisation.

In their comprehensive review of the role of STAT3 in human cancer, Xiong *et al* (2014) highlighted the significance of persistent STAT3 activation to drive multiple facets of incipient cancer biology including: immune evasion, proliferation and survival, malignant transformation and RTK cross-talk. Curiously, phosphorylation of STAT3 at Tyr705 ($pSTAT3^{Y705}$) is critical for STAT3 function, but $pSTAT3^{S727}$ has been shown to elicit both activation and inhibition of downstream transcription of STAT3 responsive genes. It has been shown that phosphorylation of STAT3 at Ser727 (as detected within this dataset) inhibits STAT3 phosphorylation at Tyr705 and thus suppresses functional activation, inhibits dimerization, nuclear translocation and DNA binding (Chung *et al* 1997).

Therefore, the significant upregulation of an inhibitory STAT3 phospho-motif ($pSTAT3^{S727}$) is concordant with KSEA-based biological pathway analysis that suggested JAK-STAT signalling-associated KEGG annotations were depleted in the β_6-kinome inducted during LAP internalisation. This putative STAT3 inhibition downstream of integrin $\alpha_v\beta_6$ ligand-engagement and activation warrants further investigation to ascertain the functional implications within the context of TNBC.

Finally, phosphopeptides mapping to protein kinase C delta (δ) isoform (PKCδ) phosphorylation of Ser or Thr at residues 301 – 318 were also enriched in this dataset. Rybin *et al* (2009) have described phosphorylation at Ser302 and Ser304 as novel sites of PKCδ autophosphorylation associated with activity. Therefore the PKCδ phosphophorylation motifs identified within the LC-MS/MS dataset may

implicate PKCδ activity within the β_6-kinome. Overexpression of PKCδ has been shown to promote tumour progression in human ductal pancreatic cancer in vitro and in vivo (Mauro *et al* 2010) and to support BrCa cell survival in vitro via ERK1/2 suppression (Lonne *et al* 2009). Therefore, further investigation into the role of activity downstream of integrin $\alpha_v\beta_6$ activity within the context of BrCa progression is justifiable.

Thus, further validation of mediators identified by LC-MS/MS data presented here as putative regulators of integrin $\alpha_v\beta_6$/LAP engagement and internalisation in TNBC is imperative to expedite the identification of novel molecular targets, be they receptors and/or signalling pathways, that can be validated for therapeutic intervention to improve TNBC patient outcomes and alleviate the personal and fiscal burdens of this malignant disease.

supplementary information S6

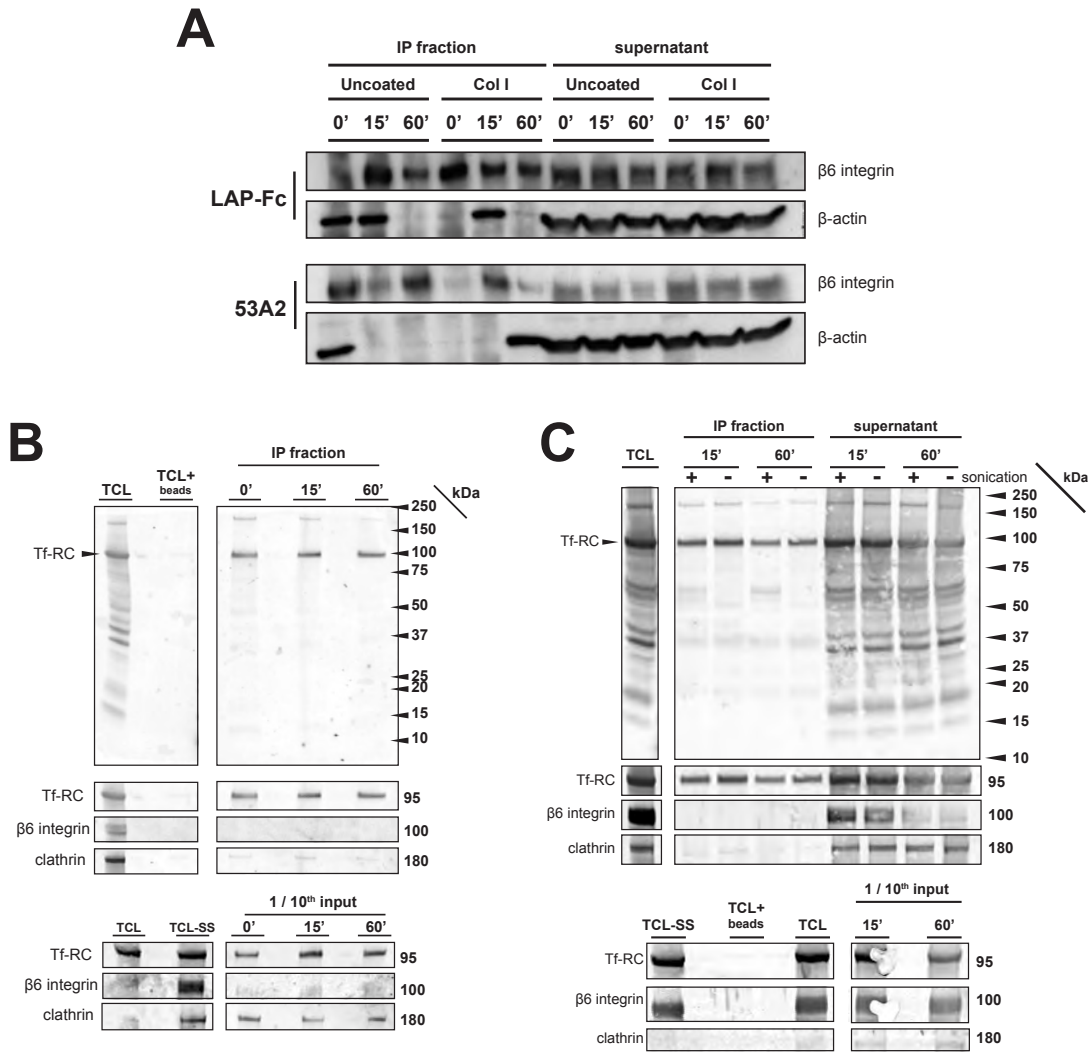

Supplementary Information (Figure) S6.1
Initial testing (**A & B**) and DTBP cross-link optimisation (**C**) of a LAP and transferrin Fc-tagged ligand-based internalisation assay to co-IP cognate receptors (integrin $\alpha_v\beta_6$ and Tf-RC) undergoing internalisation

Supplementary Information (Figure) S6.1

Initial testing (A & B) and DTBP cross-link optimisation (C) of a LAP and transferrin Fc-tagged ligand-based internalisation assay to co-IP cognate receptors (integrin $\alpha_v\beta_6$ and Tf-RC) undergoing internalisation

Preliminary co-IP experiments performed in the BT-20 cell line to **(A)** compare utility of an Fc-tagged LAP ligand or anti-integrin $\alpha_v\beta_6$ antibody clone 53A2 to isolate the integrin $\alpha_v\beta_6$ receptor undergoing internalisation to identify novel trafficking partners by proteomics, in comparison with an Fc-tagged transferrin control ligand **(B)**. Additional optimisation to stabilise internalised receptor complexes was performed **(C)** using the membrane permeant cross-linker DTBP. Experimental procedures for co-IP and WB are as previously described.

Candidate/ UniProt ID	Function	Maxima (min)	Maxima (z)	Maxima (p)	Relevance in cancer
COT (MAP3K8 / Tpl2) **P41279**	Oncogenic Ser/Thr protein kinase family. MAPK & JNK pathway agonist. Induces nuclear production of NF-κB (PhosphoSite 2015a).	**5**	**8.2**	***	Overexpression associated with resistance mechanisms to therapeutic BRAF inhibition [Vemurafenib] in metastatic melanoma (Johannessen *et al* 2010). RCC oncogene – siRNA silencing inhibited migration & proliferation of RCCs. miR-509-3p suppresses COT activity in RCC (Monsma *et al* 2015). COT phosphorylation of Pin1 (peptidyl-prolyl cis/trans isomerase) promotes tumourigenesis & aggressiveness in BrCa (Su *et al* 2015).
MAPK2 (MAPKAPK2) **P49137**	Stress activated Ser/Thr kinase involved in CK production, endocytosis, cytoskeletal remodelling, cell migration & cell cycle control (PhosphoSite 2015b).	**5**	**4.1**	***	MAPKAPK2 mediates resistance to H_2O_2 oxidative stress in human hepatobilliary cells. MAPKAPK2 inhibition induced caspase-3 & PARP cleavage, DNA breaks & cell death (Kim *et al* 2015). Mediates gemcitabine sensitivity/efficacy via MAPKAPK2/P38 signalling in PancCa cells (Ho-Bouldoires *et al* 2015).
Nuak1 **O60285**	Ser/Thr kinase involved in cell adhesion, proliferation, tumour progression, cell ploidy & senescence (PhosphoSite 2015c).	**30**	**2.5**	**	May act as tumorigenic factor promoting invasion & metastasis under regulation & phosphorylation by Akt1. Nuak1 expression correlates with NSCLC TNM staging. Inihibition impaired migration & invasion in A549 cells. Nuak1 silencing suppressed expression of MMP-2 & MMP-9, & reduced lung mets in xenograft mouse model of NSCLC (Kopper *et al* 2014). miR-96 functions as TS by targeting Nuak1 in Panc Ca (Chen *et al* 2013).
PDK1 (PDPK1) **O15530**	Ser/Thr "master kinase" phosphorylating a subgroup of the AGC kinases (PhosphoSite 2015d). Substrates include: Akt 1/2/3, PKC, PKN, RSK, S6K (p70S6K) & SGK (Huang *et al* 2014).	**5**	**8.1**	***	Constitutively active by transautophosphorylation? implicated in cancer. A novel & selective PDK1 inhibitor reduces BC cell invasion & tumour growth (C Raimondi AMUL poster session) PDK1 controls BC tumour growth in a kinase dependent but Akt-independent manner (Pearce *et al* 2010)
TBK1 **Q9UHD2**	Associates with TRAF3 & TANK to phosphorylate IFN regulatory factors. Attenuates retroviral budding by phosphorylating ESCRT-I complex VPS37C subunit (PhosphoSite 2015e).	**5**	**3.6**	***	TBK1 overexpression enhances tamoxifen resistance in BrCa (Armando Gagliardi *et al* 2012). Loss of TBK1 impairs mitotic phosphorylation of PLK1 in TBK1-sensitive lung Ca cells. TBK1 interacts with & inhibits mTOR in prostate Ca regulating dormancy in the bone marrow (mets) niche. TBK1 addiction in NSCLC promotes direct activation of pro-survival Akt signals.

Supplementary Information (Table) S6.2
Summary of five candidate kinases identified by KSEA for functional validation as putative regulators of LAP-engaged integrin $\alpha_v\beta_6$-mediated signalling during internalisation (**p<0.01; ***=p<0.001; z = KSEA z-score)

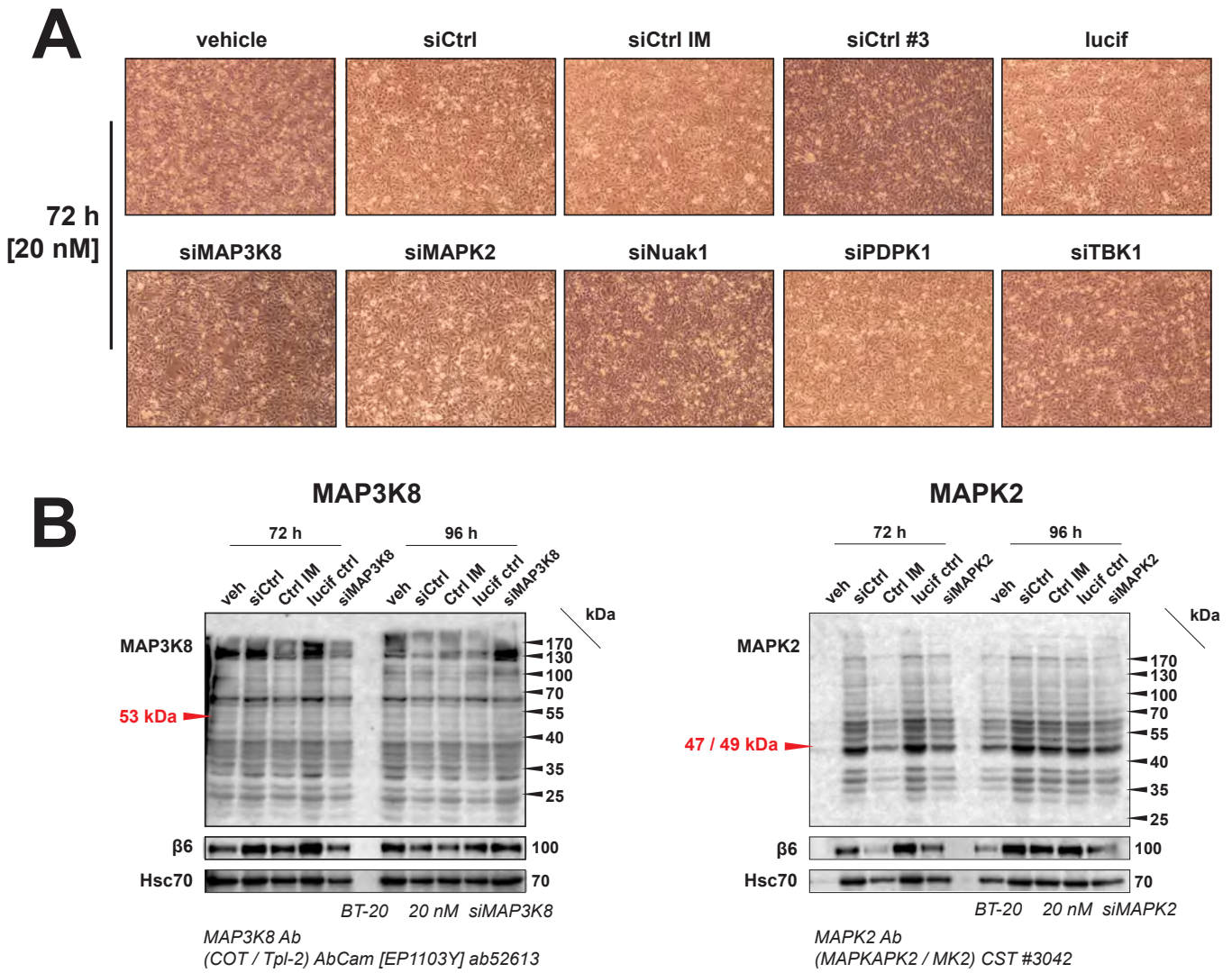

Supplementary Information (Figure) S6.3 (A & B)
Representative examples of antibody validation attempts using 20 nM siRNA to target kinases identified by KSEA

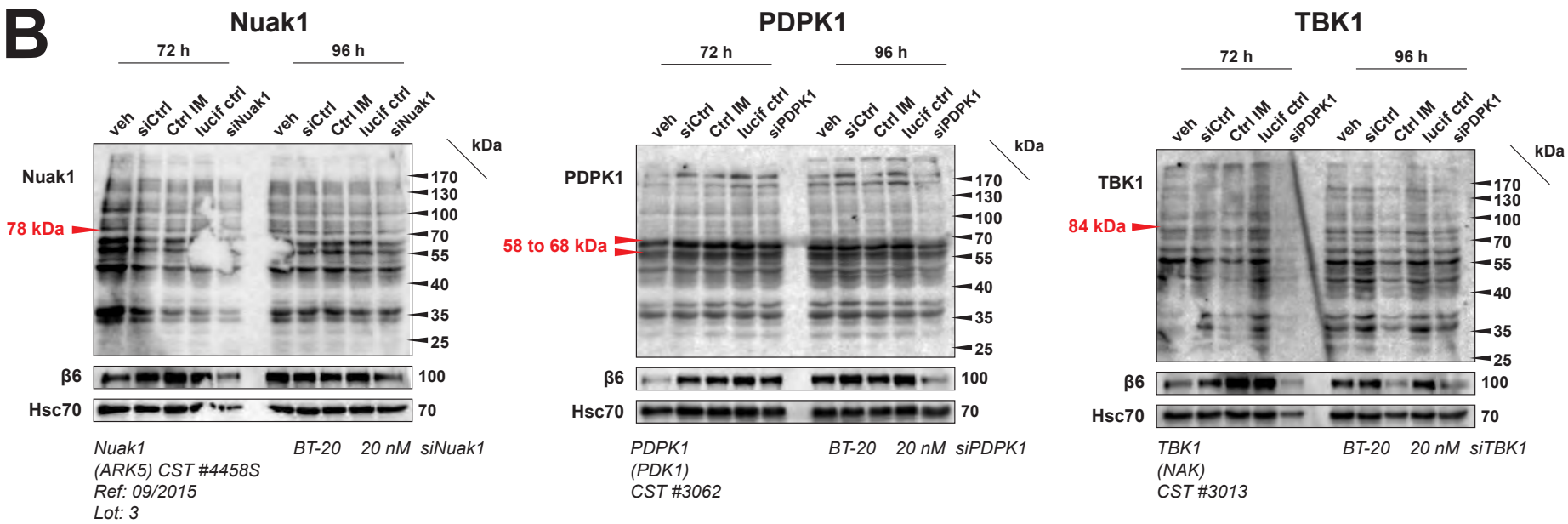

Supplementary Information (Figure) S6.3 (B)
Representative examples of antibody validation attempts using 20 nM siRNA to target kinases identified by KSEA

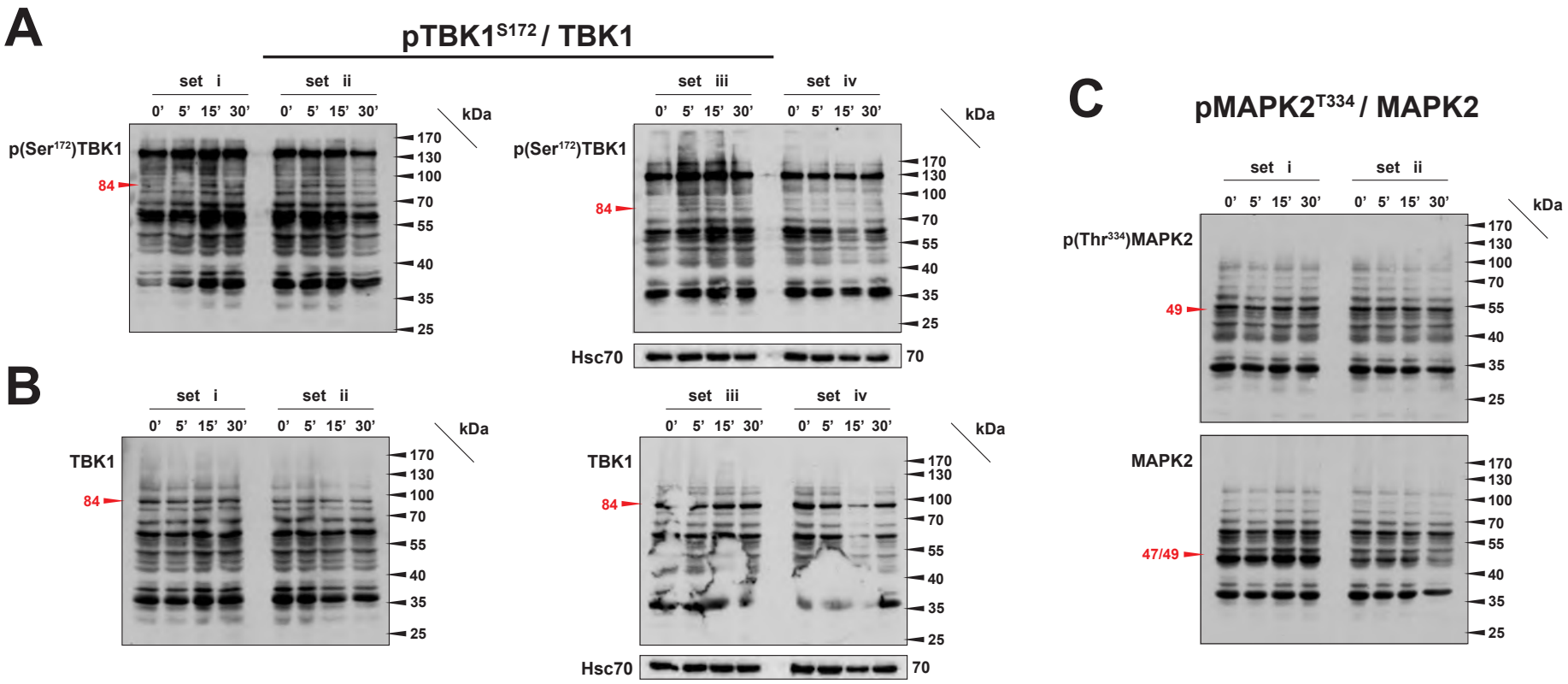

Supplementary Information (Figure) S6.4
Representative examples of antibody validation attempts to target kinases identified by KSEA : Probing the original LC-MS/MS lysates for pSer172TBK1 and pThr334MAPK2

Supplementary Information (Figures) S6.3 and S6.4
Representative examples of antibody validation attempts to target kinases identified by KSEA

To functionally interrogate the five target kinases identified by KSEA to define their putative regulatory role during integrin $\alpha_v\beta_6$ LAP-engagement and internalisation, siRNA (ON-TARGET®Plus siRNA, Dharmacon, GE Life Sciences) and antibodies were purchased against **(S6.3)** total kinase protein and **(S6.4)** antibodies mapping to a phosphorylation specific kinase residue. **(S6.3A)** Following transfection (INTERFER-in transfection reagent kit, PolyPlus) BT-20 cells were subject to 72 hour culture in the presence of 20 nM siRNA to target kinases (as indicated). **(S6.3B)** Representative examples of WB to confirm siRNA silencing are shown. Four non-targeting siRNA controls were evaluated to trouble-shoot ongoing issues with off-target siCtrl effects that had lead to an upregulation of target gene expression when evaluates by qPCR. **(S6.4)** Parental lysates for LC-MS/MS were probed using the phosphorylation site-specific antibodies to target kinases (best representative images shown). Experimental procedures and WB protocol are as previously described.

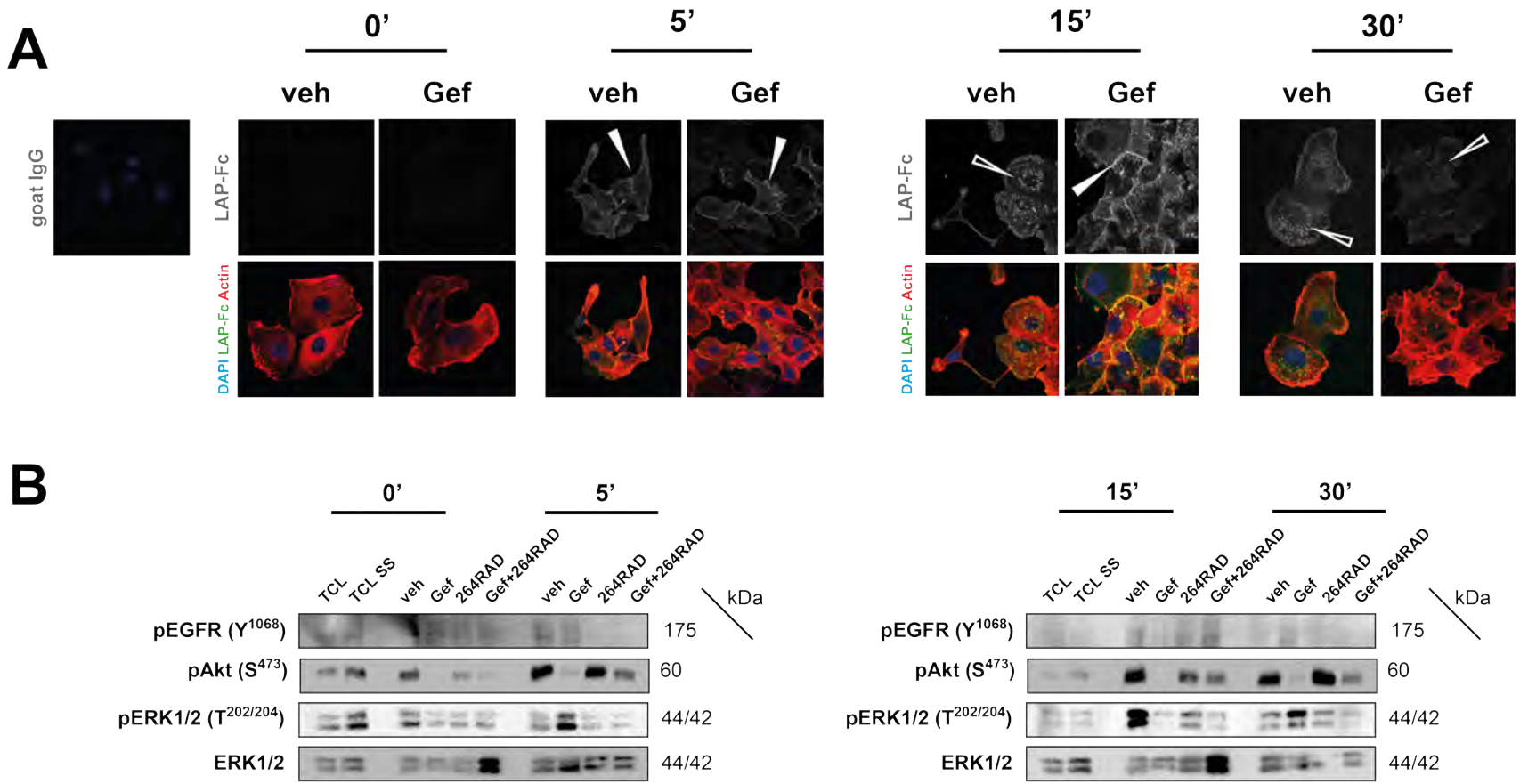

Supplementary Information (Figure) S6.5
Gefitinib inhibition of EGFR may modulate LAP-Fc internalisation and downstream LAP-ligand induced Akt phosphorylation at Ser473 in the BT-20 cell line whilst integrin β_6 blockade with 264RAD circumvents downstream effects EGFR blockade to promote Akt pSer473 phosphorylation even in the presence of gefitinib

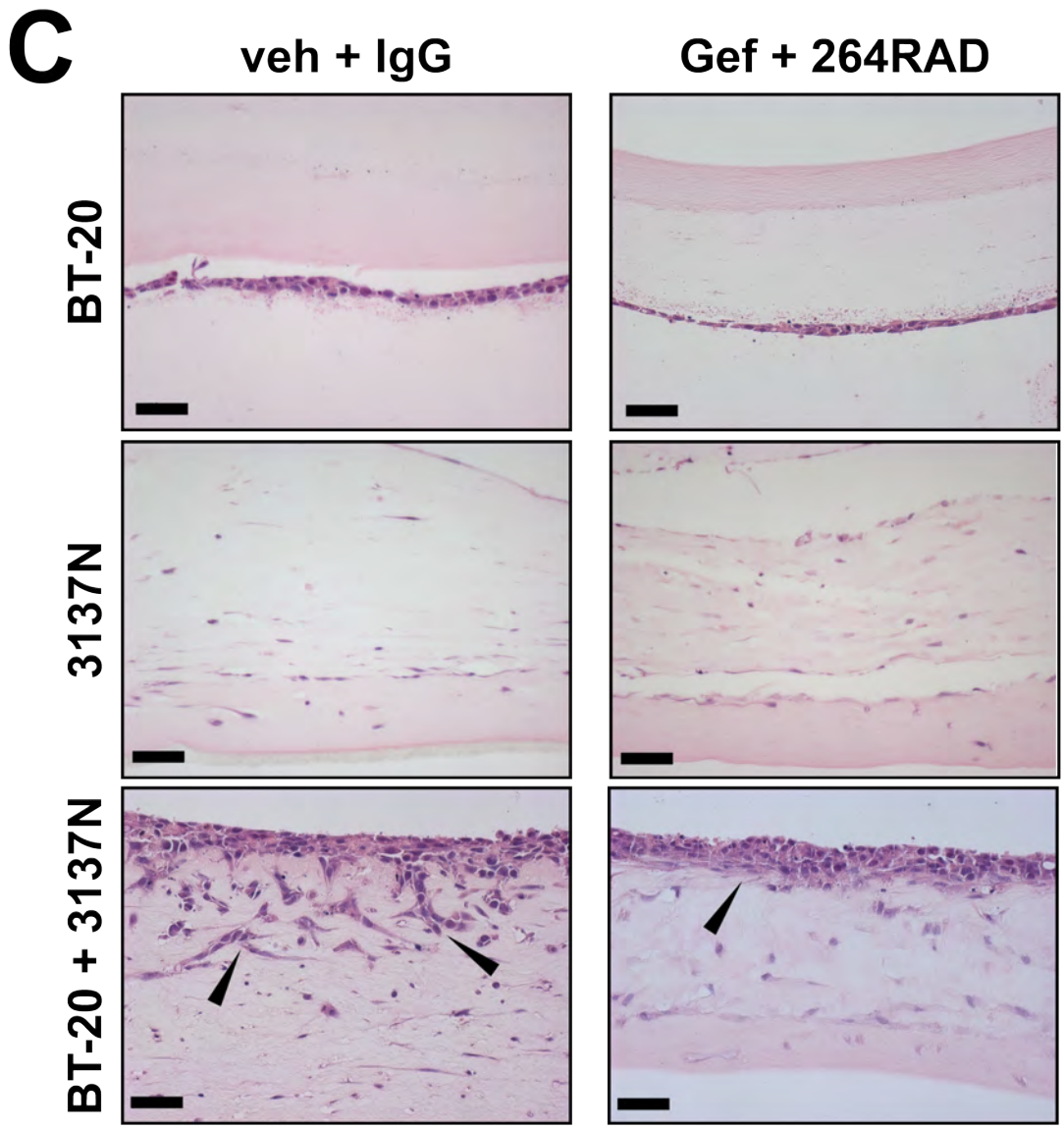

Supplementary Information (Figure) S6.5 (C)
Dual therapy simultaneously targeting both integrin $\alpha_v\beta_6$ and EGFR using the inhibitory therapeutics antibody 264RAD and Gefitinib may abrogate cellular invasion in a 3D-miniorganotypic physiomimetic model

Supplementary Information (Figure) S6.5

Gefitinib inhibition of EGFR may modulate LAP-Fc internalisation and downstream LAP-ligand induced Akt phosphorylation at Ser473 in the BT-20 cell line whilst integrin $\alpha_v\beta_6$ blockade with 264RAD circumvents downstream effects EGFR blockade to promote Akt pSer473 phosphorylation even in the presence of gefitinib; co-targeting of integrin $\alpha_v\beta_6$ and EGFR appeared to abrogate cellular invasion in a 3D-miniorganotypic physiomimetic model

To determine the effect of EGFR-integrin $\alpha_v\beta_6$ crosstalk during LAP-internalisation, a LAP-Fc internalisation assay was performed by confocal IMF in the presence of 1 μM gefitinib (**Gef**) **(A)**, in conjunction with **(B)** a serum-free signalling time-course assay following LAP-stimulation in the presence of 1 μM gefitinib (**Gef**), 10 μg ml^{-1} 264RAD (**264RAD**) or gefitinib+264RAD (**Gef+264RAD**) using the BT-20 cell line. **(C)** Preliminary experiments to evaluate integrin $\alpha_v\beta_6$ and EGFR on cellular invasion were performed using a 3D-miniorganotypic physiomimetic model. **(A)** Attempts to co-label LAP-Fc ligand and the active integrin (demonstrated by antibody 6.2E5) to determine whether LAP and integrin co-localise throughout internalisation and trafficking were unsuccessful as only LAP-Fc was successfully demonstrated. Owing to limited availability of antibody 6.2E5, extensive optimisation of staining could not be undertaken. **(B)** A signalling study met with limited success, but warrants repeating to interrogate whether EGFR phosphorylation at Tyr1068 and Tyr1086 is differential and if these residues play distinct roles in integrin $\alpha_v\beta_6$–mediated LAP internalisation. **(C)** Physiomimetic 3D-miniorganotypic models were prepared using BrCa cells alone (BT-20), normal breast fibroblasts alone (3137N) or an admixture of BrCa cells and normal breast fibroblasts (BT20+3137N). Cells were treated for 10 days with either **veh+IgG** control treatment (0.1% DMSO vehicle/human IgG(Fc') or **Gef+264RAD** (1 μM gefitinib and 10 μg ml^{-1} 264RAD) combination therapy. At the end of treatment, miniorganotypic gels were harvested, formalin fixed, paraffin embedded, sectioned at 4 μm and stained with haematoxylin and eosin (H&E). Treatment with gefitinib and 264RAD appeared to abrogate cellular invasion in comparison with combination control therapy. Images were acquired on the Axiophot. **Acknowledgements:** These experiments were designed and supervised by the author for Mr Philip Adeniran (MSc student), who kindly performed them during the tenure of his MSc project. The author prepared results figures for presentation; the data are reproduced here with Mr Adeniran's kind permission.

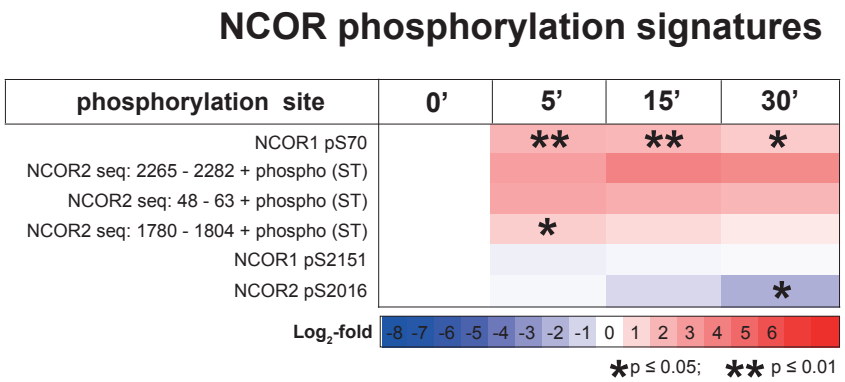

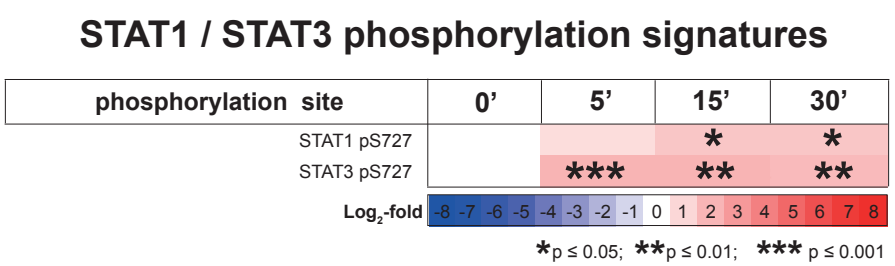

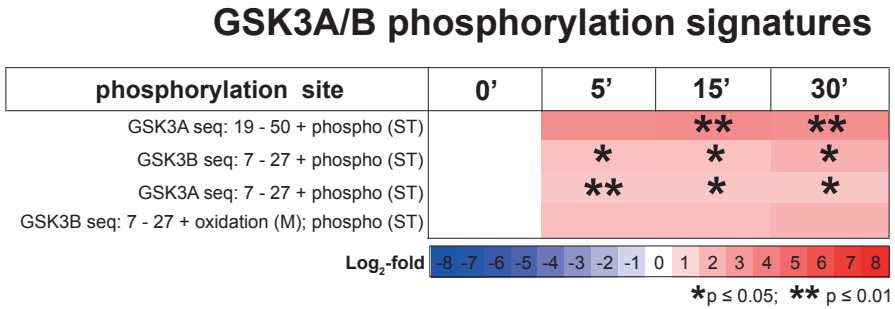

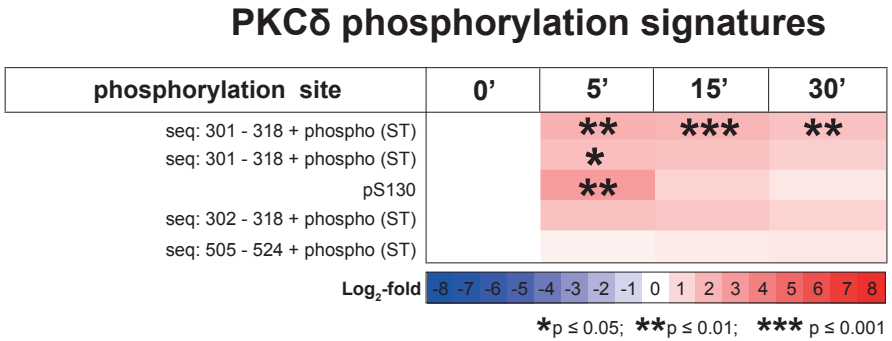

Supplementary Information (Figure) S6.6

Putative mediators of downstream signalling inducted upon LAP ligand-integrin $\alpha_v\beta_6$ engagement, activation and internalisation directly identified by phosphoproteomics

chapter VII

concluding remarks

7. future work and concluding remarks

7.1 future work

It is acknowledged that in order to exploit the full potential of this body of research, additional experimental work must be undertaken to more robustly validate and mechanistically dissect the exciting key findings presented here which attempt to determine the relevance of integrin $\alpha_v\beta_6$ activation status during breast tumourigenesis and disease progression.

It is essential to complete the validation datasets for antibody clones 6.2E5 and 6.2G2 to definitively establish their novel application as markers of integrin $\alpha_v\beta_6$ activation status. Although it has been demonstrated that these antibodies recognise conformers induced by extracellular ("outside-in") modes of activation, their ability to detect active integrin $\alpha_v\beta_6$ following intracellular ("inside-out") activation and to distinguish signalling-replete receptors specifically was not proven herein.

Genetic silencing or stable overexpression of known intracellular regulators of integrin activation and inhibition would permit validation of antibodies 6.2E5 and 6.2G2 as markers of bidirectional integrin $\alpha_v\beta_6$ activation. The ability of antibodies 6.2E5 and 6.2G2 to label the signalling replete, active integrin $\alpha_v\beta_6$ receptor subpopulation could be achieved by IMF co-localisation studies to demonstrate 6.2E5 and 6.2G2 immunopositivity in conjunction with canonical markers of

integrin activation, such as talin, vinculin, α-actinin and FAK, encompassing activation-specific phosphorylation residues such as $pFAK^{Y397}$.

The significant and novel finding in the MCF10 isogenic model that the active integrin $\alpha_v\beta_6$ undergoes subcellular redistribution upon neoplastic transformation and malignant progression in the presence of a (relatively) stable pool of cell surface active integrin $\alpha_v\beta_6$, pressingly requires further investigation. Ideally intracellular trafficking routes should be elucidated using antibody co-labelling IMF strategies, similar to those employed by Arjonen *et al* (2012) for their dissection of active versus inactive integrin β_1 trafficking in the MDA-MB-231 BrCa cell line.

Demonstration of active integrin $\alpha_v\beta_6$ using antibodies 6.2E5 and/or 6.2G2, in conjunction with known endosomal compartment-specific markers, would identify which intracellular trafficking routes the active integrin $\alpha_v\beta_6$ is directed along during its internalisation and determine whether the active conformer is differentially targeted for lysosomal and/or proteosomal degradation or recycling to the membrane. Application of these methods in alternative models seeking to recapitulate the process of neoplastic transformation and malignant progression, in breast or other tissue, would permit evaluation of the broader aetiopathological significance of integrin $\alpha_v\beta_6$ activation status and spatial restriction during the natural history of malignant disease.

It is acknowledged that extensive functional validation of candidates identified as novel, putative regulators of the integrin $\alpha_v\beta_6$–mediated adhesion environment (β_6-adhesome) and ligand engaged integrin $\alpha_v\beta_6$–mediated signalling networks (β_6-kinome) is requisite to establish a robust evidence base to reliably evaluate their role(s) in both the β_6-adhesome and β_6-kinome. Again, genetic manipulation strategies to silence or stably overexpress the candidate proteins of interest upstream of canonical functional and ligand-stimulation assays would permit extensive interrogation of the primacy of these putative regulators to elicit integrin $\alpha_v\beta_6$-mediated phenotypic outputs. The tumour suppressive, oncogenic or indeed pleiotropic roles of these regulators during tumourigenesis and disease progression could then be investigated.

7.2 concluding remarks

The global burden of morbidity and mortality associated with BrCa (WHO 2014), coupled with BrCa remaining the most prevalent cancer in the UK (CR-UK 2016), collectively justify the ongoing need for research seeking to identify novel biomarkers that may be used for screening and prevention, and/or patient stratification for responsiveness to novel molecular therapeutics to improve BrCa patient outcomes. The groundswell of evidence demonstrating both the clinical relevance of integrin $\alpha_v\beta_6$ expression as a prognostic marker in BrCa, and experimental evidence highlighting the potential therapeutic benefits of integrin $\alpha_v\beta_6$ functional abrogation to reduce breast tumour growth and metastasis in vivo, vindicate research efforts (such as those presented in this thesis) aiming to dissect the functional role of integrin $\alpha_v\beta_6$ during the natural history of BrCa from neoplastic transformation and tumourigenesis through progression to invasive disease.

Tumour cell expression of the epithelial-restricted integrin $\alpha_v\beta_6$ cellular adhesion receptor has long been associated with an invasive, pro-metastatic and more aggressive phenotype in both in vitro (Thomas *et al* 2001b, Nystrom *et al* 2006, Thomas *et al* 2006, Marsh *et al* 2008, Jones *et al* 2013) and in vivo (Van Aarsen *et al* 2008, Eberlein *et al* 2013, Moore *et al* 2014) experimental cancer models. Studies utilising patient-derived samples revealed the clinical significance of tumoural integrin $\alpha_v\beta_6$ expression, demonstrating its expression is a poor prognostic indicator in a variety of human cancers, including colorectal (Bates *et al* 2005, Yang *et al* 2012), ovarian (Ahmed *et al* 2002b), cervical (Hazelbag *et al* 2007) and breast cancer (BrCa) (Saha *et al* 2010, Moore *et al* 2014), and is predictive of risk of progression from in situ to invasive disease within the context of ductal carcinoma in situ (DCIS) (Allen *et al* 2014).

Thus, it is evident that the integrin $\alpha_v\beta_6$ receptor is functionally implicated in the process of breast tumourigenesis and disease progression, by mechanisms not yet exhaustively characterised nor unequivocally defined. Previous studies dissecting the protumourigenic effects of integrin adhesion receptors in human malignancy have revealed it is specifically the active integrin conformer that may drive integrin-mediated oncogenic functions.

Felding-Habermann *et al* (2001) first demonstrated that integrin $\alpha_v\beta_3$ in its active (bot not its inactive) conformation established an anchorage-independent, pro-

metastatic phenotype both in vitro and in vivo using the MDA-MB-231 BrCa model. Later, expression of the integrin β_1 specifically in its active state was found to correlate with prostate cancer metastatic potential in vivo (Lee *et al* 2013). Arjonen *et al* (2012) reported the differential endocytic trafficking kinetics of active versus inactive integrin β_1 in the MDA-MB-231 BrCa model, suggesting distinct conformer-specific fates for β_1 integrins. Indeed, derailed receptor internalisation and intracellular trafficking is an emerging cancer hallmark (Mosesson *et al* 2008). Therefore, perturbed endocytic regulation of integrin receptors and their consequent fate may ultimately be driven by receptor activation status and associated conformation.

Interestingly, it has been demonstrated that integrin activation and associated signalling is not restricted to the plasma lemma but also occurs within the intracellular environment to drive cancer cell-associated phenotypic traits such as circumvention of anoikis, anchorage-independence and metastasis. Specifically, active integrin β_1–derived signalling within endosomal compartments has been shown to suppress anoikis and promote metastasis in MDA-MB-231 BrCa cells (Alanko *et al* 2015). These findings further implicate an oncogenic role specifically attributable to active integrins, not only at the cell surface, but also during their intracellular trafficking. Mechanistic dissection of this concept warrants further investigation into other integrin receptor species implicated in breast tumourigenesis, such as the integrin $\alpha_v\beta_6$.

Therefore, based on existing literature (using both experimental BrCa models and clinical data) that established: i) a defined oncogenic role for the active integrin β_1 receptor using in vitro BrCa models, ii) integrin $\alpha_v\beta_6$ expression imparts a more aggressive, pro-invasive phenotype in human cancer cells in vitro and in vivo and iii) the clinical prognostic significance of tumoural integrin $\alpha_v\beta_6$ that is predictive of risk of progression to invasive disease, it was deemed pertinent to undertake a body of work seeking to investigate the role of integrin $\alpha_v\beta_6$ activation status during the natural history of human BrCa using established in vitro models.

Within the scope and purpose outlined at the beginning of this study, the research presented here has successfully addressed several of the original investigative aims seeking to characterise novel aspects of integrin $\alpha_v\beta_6$ activation status and associated signalling within the context of human BrCa. However, it is acknowledged that some of the initial research intentions were only partially

fulfilled, primarily owing to the financial and temporal constraints applicable to any programme of scientific enquiry and endeavour.

In summary, a monoclonal antibody-based approach to study the active integrin $\alpha_v\beta_6$ conformer was validated in vitro (Chapter III, Results Part I). These antibodies (6.2E5 and 6.2G2) were then used to interrogate facets of integrin $\alpha_v\beta_6$ receptor activation status during breast tumourigenesis and disease progression using an established in vitro model (MCF-10 isogenic cell line series) recapitulating the natural history of BrCa from neoplastic transformation through to malignant progression to poorly differentiated disease (Chapter IV, Results Part II).

Later, using the BT-20 model of triple negative BrCa (TNBC), investigations were designed, validated and executed to define a LAP-ligand engaged integrin $\alpha_v\beta_6$–mediated 2-dimensional (2-DE) adhesion environment (β_6–adhesome) (Chapter V, Results Part III) and characterise an integrin $\alpha_v\beta_6$-kinome (β_6–kinome) associated with LAP-ligand engagement and internalisation to dissect novel aspects of integrin $\alpha_v\beta_6$–mediated signalling that may later inform therapeutic targeting in TNBC.

Firstly, a means by which the conformationally distinct, signalling-replete, active subpopulation of integrin $\alpha_v\beta_6$ may be distinguished amongst the gross integrin $\alpha_v\beta_6$ receptor pool was successfully achieved through validation of two anti-integrin $\alpha_v\beta_6$ monoclonal antibodies (6.2E5 and 6.2G2, Biogen Idec), first described by Weinreb *et al* (2004) as novel, non-function blocking integrin $\alpha_v\beta_6$–specific antibodies. These antibodies had not been extensively evaluated previously for their ability to recognise a specific integrin $\alpha_v\beta_6$ conformer. Therefore, to robustly establish their ability to detect active integrin $\alpha_v\beta_6$ would permit salient interrogation of the aetiopathological role of integrin $\alpha_v\beta_6$ activation status in human disease, including BrCa.

Based on preliminary flow cytometry (FCM) and enzyme-linked immunosorbent assay (ELISA) results, Dr Danielle DiCara and Dr Antonio Saha demonstrated differential binding kinetics of antibodies 6.2E5 and 6.2G2 in comparison with the established ligand-mimetic antibody 10D5 (details provided in Chapter III, Results Part I; Introduction). Having excluded antibody affinity as the underlying cause, it was hypothesised that antibodies 6.2E5 and 6.2G2 may recognise an activation

epitope thus justifying the in-depth validation and characterisation reported in this body of work.

For the purposes of robust validation, the established integrin $\alpha_v\beta_6$ positive VB6 cell line engineered in-house was predominantly used for antibody characterisation studies. Experiments to evaluate the utility of antibodies 6.2E5 and 6.2G2 to recognise an active subpopulation of integrin $\alpha_v\beta_6$ (Chapter III, Results Part I) revealed that these antibodies each recognise conformation-sensitive (activation-associated) epitopes. Binding of 6.2E5 and 6.2G2 was seen to significantly increase in the presence of Mn^{2+} ions (Figures 3.1.1 and 3.1.2) and cognate ligand (LAP or A20FMDV2) engagement (Figure 3.2.1 and 3.2.2). This provided evidence for their ability to recognise an activation-associated epitope that is induced by canonical integrin activation methods.

Their ability to bind subsequent to integrin $\alpha_v\beta_6$ ligand-engagement suggested these antibodies are non-ligand mimetic and do not bind via the integrin α-β heterodimeric RGD cleft (as demonstrated by the established ligand-mimetic antibody 10D5, Figure 3.2.3.). These functional characterisations of cell surface binding kinetics lead to the conclusion that antibodies 6.2E5 and 6.2G2 each recognise an activation-associated epitope on the integrin $\alpha_v\beta_6$ that are also ligand-induced binding sites (LIBS); and thus may be classified as anti-LIBS antibodies.

Excitingly, their utility to label active integrin $\alpha_v\beta_6$ to discriminate subcellular distributions of distinct integrin $\alpha_v\beta_6$ conformers using immunofluorescence (IMF) methods as demonstrated in cells adhering to ligand (Figures 3.3.1 and 3.3.2) and live-labelled cells (Figures 3.3.3), showcased the novel utility of antibodies 6.2E5 and 6.2G2 to study the spatiotemporal distribution of active integrin $\alpha_v\beta_6$. Immunohistochemical (IHC) evaluation of antibodies 6.2E5 and 6.2G2 in matched formalin fixed paraffin-embedded (FFPE) and snap frozen primary patient-derived BrCa tissue samples (Figure 3.4.2) demonstrated their utility for detecting integrin $\alpha_v\beta_6$ in primary human tissue, but their ability to specifically discriminate the active integrin $\alpha_v\beta_6$ by IHC methods was not validated.

Therefore, in terms of the first research aim, a means by which the primed or active integrin $\alpha_v\beta_6$ conformer may be distinguished using the monoclonal antibodies

6.2E5 and 6.2G2 was successfully validated; permitting their use to further investigate integrin $\alpha_v\beta_6$ activation status in BrCa using conformer-specific antibodies to label active versus inactive/total integrin $\alpha_v\beta_6$ receptor populations in a manner previously outlined by Humphries (2004) and employed experimentally by Felding-Habermann *et al* (2001), Arjonen *et al* (2012), Lee *et al* (2013) and Alanko *et al* (2015) for $\alpha_v\beta_3$ and β_1 integrins.

It was acknowledged that recognition of the conformation-dependent activation-associated epitopes recognised respectively by antibodies 6.2E5 and 6.2G2 is sensitive to experimental procedures, thus conferring a critical caveat to their use. Therefore, any experimental procedures that may artificially reveal 6.2E5 and 6.2G2 cognate epitopes in a manner that does not reflect the in vivo conformational status of the integrin $\alpha_v\beta_6$ should be avoided and temper data interpretation.

Therefore, when using these newly validated tools to interrogate integrin $\alpha_v\beta_6$ activation status during breast tumourigenesis and disease progression using the MCF-10 in vitro model (Chapter IV, Results Part II), only FCM and IMF methods were employed as these had been validated for conservation of conformation-dependent 6.2E5 and 6.2G2 cognate epitopes. Integrin $\alpha_v\beta_6$ subpopulations were characterised across the MCF-10 model using a panel of anti-integrin $\alpha_v\beta_6$ antibodies comprising: conformer-specific (6.2E5, 6.2G2), non-conformer specific recognising all maturation states (620W7) and ligand mimetic (10D5) or non-ligand mimetic (53A2) antibodies.

Excitingly, FCM and IMF results (respectively evaluating cell surface integrin $\alpha_v\beta_6$ expression and subcellular distribution) revealed that although cell surface expression of active integrin $\alpha_v\beta_6$ recognised by antibodies 6.2E5 and 6.2G2 (relative to total integrin $\alpha_v\beta_6$ expression determined 10D5) was not significantly altered across the MCF-10 model (Figure 4.2), active integrin $\alpha_v\beta_6$ undergoes subcellular redistribution following neoplastic transformation (MCF10-AT and -KCl.2 variants) and malignant progression (MCF10-CA1h and –CA1a variants) in comparison with the MCF-10A benign parental cell line (Figure 4.3).

These results suggested derailed internalisation and trafficking kinetics of the active integrin $\alpha_v\beta_6$ conformer (as opposed to gross active integrin $\alpha_v\beta_6$

expression) may be a critical event during oncogenic transformation of the breast. Disappointingly, experiments to define active versus inactive integrin $\alpha_v\beta_6$ internalisation kinetics and trafficking routes within the MCF-10 model to characterise the nature of the observed, putative derailment associated with neoplastic transformation and malignant progression, could not be undertaken owing to restricted availability of antibodies 6.2E5 and 6.2G2.

The critical caveat to meaningful comparisons between active versus inactive integrin $\alpha_v\beta_6$ internalisation and trafficking kinetics is identification of a suitable antibody to robustly demonstrate cell surface and intracellular total integrin $\alpha_v\beta_6$ concomitantly. The function blocking antibodies 53A2 and 10D5 were used for surface labelling or static intracellular post-labelling of total integrin $\alpha_v\beta_6$ studies. However, using these antibodies to live-label cells for longitudinal studies of integrin $\alpha_v\beta_6$ receptor internalisation may not be suitable.

The antibody 10D5 is ligand-mimetic so may evoke a ligand-induced, "pseudo"-activated integrin $\alpha_v\beta_6$ response that may confound definition of strictly inactive integrin $\alpha_v\beta_6$ intracellular trafficking using this antibody. Furthermore, antibody 53A2 was used to label integrin $\alpha_v\beta_6$ in subsequent IMF internalisation assays (using both live-labelling and post-labelling methods) and was found to remain bounded predominantly at the plasma lemma (Chapter VI, Results Part IV; Figures 6.1 and 6.2). This may be due to low or absent internalisation of non-ligand engaged (inactive) integrin $\alpha_v\beta_6$, or may be a sequela of cell surface integrin $\alpha_v\beta_6$ functional abrogation using the non-ligand-mimetic inhibitory antibody 53A2; again, potentially confounding comparisons between active and inactive integrin subpopulations.

Therefore, an anti-integrin $\alpha_v\beta_6$ antibody to robustly label the inactive (or rather, non-activated) integrin $\alpha_v\beta_6$ conformer must first be identified and validated. A repository of anti-integrin antibodies generated in-house are fortuitously available (Desai 2011), so this is an achievable prospect. With validated antibodies to discriminate active and inactive integrin $\alpha_v\beta_6$ subpopulations in hand, IMF exploration of putative conformer-specific differential trafficking during breast tumourigenesis and disease progression (as implicated by findings using the MCF10 isogenic model) may be expedited.

Despite the utility of the MCF10 isogenic model to study the sequential neoplastic transformation of benign mammary epithelium, acquisition of invasive potential and progression to aggressive metastatic disease, several key limitations regarding the translatable clinical relevance of this model aiming to recapitulate the complexities of breast tumourigenesis in vitro. Firstly, the parental MCF-10A variant isolated from fibrocystic mammary epithelium and generated by spontaneous immortalisation in culture (Soule *et al* 1990, Dawson *et al* 1996) is not wholly representative of "normal" breast parenchyma; therefore, it has been astutely described as "non-malignant" for the purposes of this study. Secondly, the transformative event used to induce neoplastic transformation of the parental MCF-10A cell line was transfection with a plasmid vector (pHo6T1) containing the T24 bladder carninoma-derived Ha-ras oncogene (and aminoglycoside phosphotransferase gene to permit selection by geneticin antibiotic selection).

Reviewing data archived in the Sanger Catalogue of Somatic Mutations in Cancer, Fernández-Medarde and Santos (2011) reported distribution and frequency of ras mutations in human BrCa as follows: **H-ras**: 1% (542); **N-ras**: 2% (330) and **K-ras** 4% (544) (where values represent the percentage of clinical samples analysed and numbers in parentheses indicated total number of clinical samples analysed). Therefore, although H-ras mutations do occur in a small proportion of human BrCas, the generation of the neoplastic MCF-10AT variant using a urinary bladder-derived mutant H-ras may not be the best representative, most clinically relevant example of transformed breast epithelium.

Given the noted limitations of the MCF-10 isogenic cell line series, any interesting findings arising within this model would need robust interrogation within more clinically relevant models for broader biological validation; or ideally, within the context of human primary BrCa-tumour derived patient samples, to extrapolate the aetiopathological and therapeutic pertinence of preliminary discoveries unearthed using the MCF-10 model. Although the directly translatable clinical relevance of the MCF-10 model to recapitulate breast tumourigenesis and disease progression in vitro may be limited, its utility as a basic model of the natural history of BrCa to broadly interrogate the functional biology of mechanisms associated with a transformative oncogenic event may be justified. Therefore, use of the MCF-10 isogenic model (as utilised in this study) as a preliminary, exploratory tool is valid and revealed novel insights into the role of active integrin $\alpha_v\beta_6$ in BrCa that suggest altered intracellular trafficking may be associated with neoplastic

transformation and malignant progression; a finding that undoubtedly warrants further investigation.

Given that acquisition of an invasive phenotype is associated with altered cellular adhesion repertoires, it was deemed pertinent to characterise an as yet undefined integrin $\alpha_v\beta_6$–mediated adhesion environment (β_6 adhesome) during 2D-engagement to cognate ECM ligands latency-associated peptide of transforming growth factor β1 (LAP), fibronectin (Fn) and collagen type I (Col I). Given the prescient need for identification of novel molecular targets for therapeutic intervention in TNBC and poor patient outcome when first-line chemotherapies fail, it was deemed appropriate to commence this portion of research within the context of TNBC using the BT-20 and MDA-MB-468 TNBC cell lines.

The existence of an oncogenic integrin $\alpha_v\beta_5$/integrin $\alpha_v\beta_6$ switch conferring an anoikis-resistant survival advantage in oral squamous cell carcinoma (OSCC) cells that is mediated by integrin $\alpha_v\beta_6$ upregulation and downstream Akt activation, has been previously described (Janes and Watt 2004). These data suggest the acquisition of an integrin $\alpha_v\beta_6$–driven proteome may be a transformative event during carcinogenesis. Therefore, in kind collaboration with and under the supervision of Dr Mark R Morgan (Principal Investigator, Receptor Dynamics in Cancer Laboratory, Institute of Translational Medicine, University of Liverpool), experiments employing a 2D-enrichment (2D-E) strategy to isolate adhesion complexes for proteomic interrogation as described by Humphries *et al* (2009) and refined by Byron *et al* (2011), were undertaken to characterise global proteome changes inducted by specific ECM ligand engagement in TNBC cells (Chapter V, Results Part III).

Having demonstrated integrin $\alpha_v\beta_6$ is the predominant cell surface LAP receptor in the BT-20 cell line (Figure 5.2), LAP ligand was used to specifically "bait" integrin $\alpha_v\beta_6$-mediated adhesions in 2D-E experiments. Comparison of adhesion complexes formed on LAP with those formed on Fn or Col I permitted identification of putative molecular mediators of an integrin $\alpha_v\beta_6$–mediated adhesion environment (β_6 adhesome). Although integrin receptor switching was not observed as had been anticipated, four biological replicate experiments successfully and reproducibly yielded specific enrichment of integrin β_6 in LAP-induced adhesions (Figure 5.3).

Network mapping of proteins showing ≥2 log_2-fold enrichment in LAP-mediated adhesions in the BT-20 cell line (Figure 5.4) permitted identification of 7 putative regulators of the β_6 adhesome for functional validation based upon their unique enrichment to LAP in conjunction with a literature review: **DMBT-1**, **MARCKS**, **MXRA5**, **SEPT6**, **SEPT9**, **MYH9** and **MYH10**. Disappointingly, endeavours to functionally interrogate these target proteins using siRNA methods were thwarted by technical limitations relating to qPCR and gene silencing methods that could not be optimised within the time frame of this study (Supplementary Figure S6.2).

A single 2D-E experiment performed using MDA-MB-468 cells excitingly revealed unique and specific enrichment of EGFR in LAP-mediated adhesions in comparison with Fn-mediated adhesions. This finding tentatively suggests a relationship between the integrin $\alpha_v\beta_6$ and EGFR, concordant with previous studies that have reported integrin-EGFR crosstalk mediated by β_1 and α_v-integrins (Moro *et al* 1998, Moro *et al* 2002). Curiously, EGFR was not enriched in LAP-mediated adhesion complexes formed by BT-20 cells. Indeed, EGFR was not detected within the BT-20 2D-E/LC-MS/MS dataset. Therefore, further investigation into whether integrin $\alpha_v\beta_6$–EGFR crosstalk is a cell line specific phenomenon warrants further investigation.

Finally, in efforts to characterise active, ECM ligand-engaged integrin $\alpha_v\beta_6$–derived signalling (β_6–kinome) during internalisation, a LAP-ligand internalisation assay (Figure 6.1) coupled to downstream phosphoproteomics was employed using the BT-20 TNBC model to augment the 2D-E BT-20 dataset (Chapter VI, Results Part IV). Four biological replicate experiments were performed enabling LC-MS/MS identification of 88 533 tandem mass spectra corresponding to 8 874 unique peptide ions; of which 6 491 were phosphopeptides containing 7 129 phosphorylation sites mapping to 2 073 proteins identified (Figure 6.2).

Interrogation of the LC-MS/MS using inferential kinase substrate enrichment analysis (KSEA) permitted characterisation of changes in the BT-20 TNBC phosphoproteome during integrin $\alpha_v\beta_6$ LAP engagement and internalisation (Figure 6.3). This approach permitted identification of 5 putative kinase mediators of the β_6–kinome for functional validation using commercially available small molecule inhibitors (SMI): **MAP3K8/COT**, **MAPKAPK2**, **Nuak1**, **PDPK1** and **TBK1**.

The KSEA dataset was also probed using Gene Ontology (GO) Biological Pathway analysis which revealed that GO Pathway annotation terms relating to: i) inositol phosphate metabolism, ii) endocytosis and iii) MAPK signalling are upregulated in the β_6-kinome during integrin $\alpha_v\beta_6$ LAP-engagement and internalisation, whilst JAK/STAT signalling-related annotations are depleted. The phosphopeptide LC-MS/MS dataset was interrogated using National Cancer Institute (NCI) Ontological Pathway annotations which also revealed enrichment of (GO) terms relating to MAPK signalling (GO (Process): GO0000165P: MAPK Cascade and GO (Function): 0004707F: MAPK Activity), validating the primacy of MAPK signalling associated with integrin $\alpha_v\beta_6$ LAP engagement and internalisation inferred from KSEA.

Preliminary interrogation of the role of MAP3K8/COT kinase as mediator of the β_6-kinome during LAP internalisation curiously suggested a dichotomous role for MAP3K8/COT (Figure 6.4). Targeting MAP3K8 function using the commercial SMI TC-S7006 appeared to diminish ERK1/2 phosphorylation downstream of LAP stimulation, but potentiated cell surface integrin $\alpha_v\beta_6$ activation in response to canonical stimulus with divalent Mn^{2+}-ions and cognate LAP ligand.

Disappointingly, functional abrogation of MAP3K8/COT activity in these exploratory experiments could not be confirmed owing to antibody and siRNA validation issues (Supplementary Figure S6.3 and S6.4). The putative duality of MAP3K8/COT activity during integrin $\alpha_v\beta_6$ LAP-engagement undoubtedly warrants further investigation to dissect whether this kinase elicits pleiotropic effects within the context of TNBC, and more broadly, during breast tumourigenesis and disease progression.

Interrogation of the LAP-mediated β_6-kinome revealed interesting signalling motifs that also warrant further investigation and broader biological validation beyond the single cell line (BT-20) used to generate the phosphoproteomics dataset. Activation of Akt1 (Figure 6.5.1) and ERK1/2 (Figure 6.5.2) downstream of integrin $\alpha_v\beta_6$ LAP-ligand engagement were significantly implicated as downstream effectors of the β_6-kinome, concordant with previous findings (Kirk *et al* 2000, Ahmed *et al* 2002a, Janes and Watt 2004, Virtakoivu *et al* 2012), but novel with regard to the integrin $\alpha_v\beta_6$ receptor specifically within the context of TNBC.

Of marked, potential clinical significance was the finding of a putative functional relationship between integrin $\alpha_v\beta_6$ LAP-stimulation and downstream EGFR phosphorylation (Figure 6.5.3). NCI Pathway Analysis revealed enrichment for terms associated with EGFR (ErbB1) Signalling within the LC-MS/MS dataset. Notably, phosphorylation of EGFR at Thr693 (also referred to in literature as Thr669) was significantly enriched during integrin $\alpha_v\beta_6$ LAP-engagement and internalisation. This particular motif ($pEGFR^{T693}$) has been reported as critical for endocytic regulation of EGFR (Winograd-Katz and Levitzki 2006). Endocytic regulation of EGFR via Thr693 phosphorylation, together with previous reports of integrin-mediated EGFR transactivation (Moro *et al* 2002), undoubtedly warrant exhaustive functional interrogation to establish the possibility of co-regulatory cross-talk between integrin $\alpha_v\beta_6$ and EGFR during integrin $\alpha_v\beta_6$ ligand-induced activation and internalisation.

LAP-ligand stimulation assays in the presence of the EGFR targeting SMI gefitinib were performed to dissect the possibility of integrin $\alpha_v\beta_6$–EGFR crosstalk in TNBC using the BT-20 (Figure 6.5.3C), MDA-MB-468 and SUM159 (Figure 6.5.3D) cell lines. Results from these in vitro functional screens revealed that downstream ERK1/2 phosphorylation inducted by integrin $\alpha_v\beta_6$ LAP-engagement is EGFR-dependent in BT-20 and SUM159 TNBC cell lines, but not the MDA-MB-468 cell line harbouring constitutively active ERK1/2; whilst downstream Akt1 activation was diminished but not abolished following LAP stimulation in the presence of EGFR blockade. Collectively, these experiments provide further evidence for the exciting possibility of integrin $\alpha_v\beta_6$–EGFR crosstalk in TNBC that warrants additional interrogation.

In summary, this body of work has managed to:

i) validate a monoclonal antibody-based approach using antibody clones 6.2E5 and 6.2G2 to discriminate the active subpopulation of integrin $\alpha_v\beta_6$ for use in future research seeking to characterise the aetiopathological significance of integrin $\alpha_v\beta_6$ activation status in human disease, including BrCa

ii) demonstrate application of this newly validated antibody-based approach to characterise total cell surface expression and subcellular distribution of the active integrin $\alpha_v\beta_6$ subpopulation in the MCF-10 in vitro model of breast tumourigenesis and disease progression to reveal that although cell surface abundance remains

stable, the active integrin undergoes $\alpha_v\beta_6$ subcellular redistribution during neoplastic transformation and malignant progression implicating derailed internalisation and intracellular trafficking as oncogenic factors

iii) undertaken characterisation of an ECM-ligand engaged integrin $\alpha_v\beta_6$ –mediated adhesion environment to identify novel molecular mediators of the BT-20 TNBC β_6-adhesome including: DMBT-1, MARCKS, MXRA5, SEPT6, SEPT9, MYH9 and MYH10; and excitingly, unique enrichment of EGFR within the MDA-MB-468 TNBC β_6-adhesome

iv) harness the power of phosphoproteomics to define the β_6-kinome associated with integrin $\alpha_v\beta_6$ LAP-engagement and internalisation that is defined by induction of MAPK signalling, downstream ERK1/2 and Akt1 isoform activation which appears to be EGFR-dependent; inferential KSEA permitted identification of novel putative β_6-kinome mediators including: MAP3K8/COT, MAPKAPK2, Nuak1, PDPK1 and TBK1

Broadly, it is possible to hypothesise that it may not only be integrin $\alpha_v\beta_6$ activation status alone, but also its internalisation kinetics, intracellular trafficking routes and apparent EGFR-dependency that act in concert as oncogenic drivers during breast tumourigenesis and disease progression; a putative regulatory axis in BrCa that undoubtedly requires additional investigation. Indeed, each of the key findings presented here warrant further, more exhaustive functional interrogation and broader biological validation to establish their individual mechanistic and collective aetiopathological relevance within the context of breast tumourigenesis and disease progression. This would permit evaluation of the potential clinical significance of integrin $\alpha_v\beta_6$ activation status in BrCa that may be exploited to improve BrCa patient outcomes by refining treatment modalities that potentiate efficacy of existing regimens or prevent development of chemoresistance by co-targeting the active integrin $\alpha_v\beta_6$ in conjunction with conventional therapeutics to alleviate the fiscal, but more critically, the personal burden of this prevalent, malignant disease.

references

references

ADEREM, A. 1992. The MARCKS brothers: a family of protein kinase C substrates. *Cell,* 71**,** 713-6.

AHMED, N., NIU, J., DORAHY, D. J., GU, X., ANDREWS, S., MELDRUM, C. J., SCOTT, R. J., BAKER, M. S., MACREADIE, I. G. & AGREZ, M. V. 2002a. Direct integrin alphavbeta6-ERK binding: implications for tumour growth. *Oncogene,* 21**,** 1370-80.

AHMED, N., RILEY, C., OLIVA, K., BARKER, G., QUINN, M. A. & RICE, G. E. 2004. Expression and localization of alphavbeta6 integrin in extraplacental fetal membranes: possible role in human parturition. *Mol Hum Reprod,* 10**,** 173-9.

AHMED, N., RILEY, C., RICE, G. E., QUINN, M. A. & BAKER, M. S. 2002b. Alpha(v)beta(6) integrin-A marker for the malignant potential of epithelial ovarian cancer. *J Histochem Cytochem,* 50**,** 1371-80.

AJEIAN, J. N., HORTON, E. R., ASTUDILLO, P., BYRON, A., ASKARI, J. A., MILLON-FRÉMILLON, A., KNIGHT, D., KIMBER, S. J., HUMPHRIES, M. J. & HUMPHRIES, J. D. 2016. Proteomic analysis of integrin- associated complexes from mesenchymal stem cells. *Proteomics. Clinical Applications,* 10**,** 51-57.

AKAR, U., OZPOLAT, B., MEHTA, K., LOPEZ-BERESTEIN, G., ZHANG, D., UENO, N. T., HORTOBAGYI, G. N. & ARUN, B. 2010. Targeting p70S6K prevented lung metastasis in a breast cancer xenograft model. *Mol Cancer Ther,* 9**,** 1180-7.

AL-HAZMI, N., THOMAS, G. J., SPEIGHT, P. M. & WHAWELL, S. A. 2007. The 120 kDa cell-binding fragment of fibronectin up-regulates migration of alphavbeta6-expressing cells by increasing matrix metalloproteinase-2 and -9 secretion. *Eur J Oral Sci,* 115**,** 454-8.

ALANKO, J., MAI, A., JACQUEMET, G., SCHAUER, K., KAUKONEN, R., SAARI, M., GOUD, B. & IVASKA, J. 2015. Integrin endosomal signalling suppresses anoikis. *Nat Cell Biol,* 17**,** 1412-21.

ALLEN, J. L., COOKE, M. E. & ALLISTON, T. 2012. ECM stiffness primes the TGFbeta pathway to promote chondrocyte differentiation. *Mol Biol Cell,* 23**,** 3731-42.

ALLEN, M. D., THOMAS, G. J., CLARK, S., DAWOUD, M. M., VALLATH, S., PAYNE, S. J., GOMM, J. J., DREGER, S. A., DICKINSON, S., EDWARDS, D. R., PENNINGTON, C.

J., SESTAK, I., CUZICK, J., MARSHALL, J. F., HART, I. R. & JONES, J. L. 2014. Altered microenvironment promotes progression of preinvasive breast cancer: myoepithelial expression of alphavbeta6 integrin in DCIS identifies high-risk patients and predicts recurrence. *Clin Cancer Res,* 20**,** 344-57.

ALLEN, M. D., VAZIRI, R., GREEN, M., CHELALA, C., BRENTNALL, A. R., DREGER, S., VALLATH, S., NITCH-SMITH, H., HAYWARD, J., CARPENTER, R., HOLLIDAY, D. L., WALKER, R. A., HART, I. R. & JONES, J. L. 2011. Clinical and functional significance of alpha9beta1 integrin expression in breast cancer: a novel cell-surface marker of the basal phenotype that promotes tumour cell invasion. *J Pathol,* 223**,** 646-58.

ALMENDRO, V., KIM, H. J., CHENG, Y. K., GONEN, M., ITZKOVITZ, S., ARGANI, P., VAN OUDENAARDEN, A., SUKUMAR, S., MICHOR, F. & POLYAK, K. 2014. Genetic and phenotypic diversity in breast tumor metastases. *Cancer Res,* 74**,** 1338-48.

ANDRE, F. & ZIELINSKI, C. C. 2012. Optimal strategies for the treatment of metastatic triple-negative breast cancer with currently approved agents. *Ann Oncol,* 23 Suppl 6**,** vi46-51.

ANGELIS, D. & SPILIOTIS, E. T. 2016. Septin Mutations in Human Cancers. *Front Cell Dev Biol,* 4**,** 122.

ANGELUCCI, C., MAULUCCI, G., LAMA, G., PROIETTI, G., COLABIANCHI, A., PAPI, M., MAIORANA, A., DE SPIRITO, M., MICERA, A., BALZAMINO, O. B., DI LEONE, A., MASETTI, R. & SICA, G. 2012. Epithelial-stromal interactions in human breast cancer: effects on adhesion, plasma membrane fluidity and migration speed and directness. *PLoS One,* 7**,** e50804.

AOUDJIT, F. & VUORI, K. 2001. Integrin signaling inhibits paclitaxel-induced apoptosis in breast cancer cells. *Oncogene,* 20**,** 4995-5004.

AOUDJIT, F. & VUORI, K. 2012. Integrin signaling in cancer cell survival and chemoresistance. *Chemother Res Pract,* 2012**,** 283181.

ARJONEN, A., ALANKO, J., VELTEL, S. & IVASKA, J. 2012. Distinct recycling of active and inactive beta1 integrins. *Traffic,* 13**,** 610-25.

ARJONEN, A., KAUKONEN, R. & IVASKA, J. 2011. Filopodia and adhesion in cancer cell motility. *Cell Adhesion & Migration,* 5**,** 421-430.

ARJONEN, A., KAUKONEN, R., MATTILA, E., ROUHI, P., HOGNAS, G., SIHTO, H., MILLER, B. W., MORTON, J. P., BUCHER, E., TAIMEN, P., VIRTAKOIVU, R., CAO, Y., SANSOM, O. J., JOENSUU, H. & IVASKA, J. 2014. Mutant p53-associated myosin-X upregulation promotes breast cancer invasion and metastasis. *J Clin Invest,* 124**,** 1069-82.

ARMANDO GAGLIARDI, P., DI BLASIO, L., ORSO, F., SEANO, G., SESSA, R., TAVERNA, D., BUSSOLINO, F. & PRIMO, L. 2012. 3-Phosphoinositide-Dependent Kinase 1 Controls

Breast Tumor Growth in a Kinase-Dependent but Akt-Independent Manner. *Neoplasia,* 14**,** 719-IN19.

ARNAOUT, M. A., GOODMAN, S. L. & XIONG, J. P. 2007. Structure and mechanics of integrin-based cell adhesion. *Curr Opin Cell Biol,* 19**,** 495-507.

ARPINO, G., LAUCIRICA, R. & ELLEDGE, R. M. 2005. Premalignant and in situ breast disease: biology and clinical implications. *Ann Intern Med,* 143**,** 446-57.

ASKARI, J. A., BUCKLEY, P. A., MOULD, A. P. & HUMPHRIES, M. J. 2009. Linking integrin conformation to function. *J Cell Sci,* 122**,** 165-70.

ASPA. 1986. *Animals (Scientific Procedures) Act 1986* [Online]. The National Archives. Available: http://www.legislation.gov.uk/ukpga/1986/14/contents [Accessed 15th October 2014].

ATCC. 2012a. *Human skin cell lines; malignant melanoma: A375 (ATCC® CRL-1619™)* [Online]. Available: http://www.atcc.org/Products/All/CRL-1619.aspx [Accessed 19th October 2012].

ATCC. 2012b. *Human mammary gland; breast/epithelial cell lines: MCF-10A (ATCC® CRL-10317™)* [Online]. Available: http://www.atcc.org/Products/All/HTB-20.aspx [Accessed 25th May 2013].

ATCC. 2012c. *Human mammary gland; breast/epithelial cell lines: MDA-MB-231 (ATCC®HTB-26™)* [Online]. Available: http://www.atcc.org/Products/All/HTB-26.aspx [Accessed 25th May 2013].

ATCC. 2012d. *Mammary gland/breast; cell lines derived from metastatic site (pleural effusion): MDA-MB-468 (ATCC ® HTB-132™)* [Online]. American Type Culture Collection Available: http://www.atcc.org/Products/All/HTB-132.aspx [Accessed 25th November 2012].

ATCC. 2013a. *Human mammary gland/breast; epithelial cell lines: BT-20 (ATCC® HTB-19™)* [Online]. Available: http://www.atcc.org/Products/All/HTB-19.aspx [Accessed 13th January 2013].

ATCC. 2013b. *Human mammary gland; breast/duct cell lines: BT-474 (ATCC®HTB-20™)* [Online]. Available: http://www.atcc.org/Products/All/HTB-20.aspx [Accessed 25th May 2013].

ATHERTON, P., STUTCHBURY, B., JETHWA, D. & BALLESTREM, C. 2016. Mechanosensitive components of integrin adhesions: Role of vinculin. *Exp Cell Res,* 343**,** 21-7.

ATHERTON, P., STUTCHBURY, B., WANG, D. Y., JETHWA, D., TSANG, R., MEILER-RODRIGUEZ, E., WANG, P., BATE, N., ZENT, R., BARSUKOV, I. L., GOULT, B. T., CRITCHLEY, D. R. & BALLESTREM, C. 2015. Vinculin controls talin engagement with

the actomyosin machinery. *Nat Commun,* 6**,** 10038.

AZARE, J., LESLIE, K., AL-AHMADIE, H., GERALD, W., WEINREB, P. H., VIOLETTE, S. M. & BROMBERG, J. 2007. Constitutively activated Stat3 induces tumorigenesis and enhances cell motility of prostate epithelial cells through integrin beta 6. *Mol Cell Biol,* 27**,** 4444-53.

BAKER, B. M. & CHEN, C. S. 2012. Deconstructing the third dimension: how 3D culture microenvironments alter cellular cues. *J Cell Sci,* 125**,** 3015-24.

BANERJEE, S., BUHRLAGE, S. J., HUANG, H. T., DENG, X., ZHOU, W., WANG, J., TRAYNOR, R., PRESCOTT, A. R., ALESSI, D. R. & GRAY, N. S. 2014. Characterization of WZ4003 and HTH-01-015 as selective inhibitors of the LKB1-tumour-suppressor-activated NUAK kinases. *Biochem J,* 457**,** 215-25.

BARNABAS, N. & COHEN, D. 2013. Phenotypic and Molecular Characterization of MCF10DCIS and SUM Breast Cancer Cell Lines. *Int J Breast Cancer,* 2013**,** 872743.

BASOLO, F., ELLIOTT, J., TAIT, L., CHEN, X. Q., MALONEY, T., RUSSO, I. H., PAULEY, R., MOMIKI, S., CAAMANO, J., KLEIN-SZANTO, A. J. & ET AL. 1991. Transformation of human breast epithelial cells by c-Ha-ras oncogene. *Mol Carcinog,* 4**,** 25-35.

BASS, J. J., WILKINSON, D. J., RANKIN, D., PHILLIPS, B. E., SZEWCZYK, N. J., SMITH, K. & ATHERTON, P. J. 2017. An overview of technical considerations for Western blotting applications to physiological research. *Scand J Med Sci Sports,* 27**,** 4-25.

BATEMAN, A. C. & SHAW, E. C. 2013. Breast pathology. *Surgery (Oxford),* 31**,** 4-10.

BATES, R. C., BELLOVIN, D. I., BROWN, C., MAYNARD, E., WU, B., KAWAKATSU, H., SHEPPARD, D., OETTGEN, P. & MERCURIO, A. M. 2005. Transcriptional activation of integrin beta6 during the epithelial-mesenchymal transition defines a novel prognostic indicator of aggressive colon carcinoma. *J Clin Invest,* 115**,** 339-47.

BAZZONI, G., SHIH, D. T., BUCK, C. A. & HEMLER, M. E. 1995. Monoclonal antibody 9EG7 defines a novel beta 1 integrin epitope induced by soluble ligand and manganese, but inhibited by calcium. *J Biol Chem,* 270**,** 25570-7.

BEDNARCZYK, J. L., WYGANT, J. N., SZABO, M. C., MOLINARI-STOREY, L., RENZ, M., FONG, S. & MCINTYRE, B. W. 1993. Homotypic leukocyte aggregation triggered by a monoclonal antibody specific for a novel epitope expressed by the integrin beta 1 subunit: conversion of nonresponsive cells by transfecting human integrin alpha 4 subunit cDNA. *J Cell Biochem,* 51**,** 465-78.

BEHRENS, J. 1993. The role of cell adhesion molecules in cancer invasion and metastasis. *Breast Cancer Res Treat,* 24**,** 175-84.

BENDAS, G. & BORSIG, L. 2012. Cancer cell adhesion and metastasis: selectins, integrins,

and the inhibitory potential of heparins. *Int J Cell Biol,* 2012**,** 676731.

BERRYMAN, S., CLARK, S., MONAGHAN, P. & JACKSON, T. 2005. Early events in integrin alphavbeta6-mediated cell entry of foot-and-mouth disease virus. *J Virol,* 79**,** 8519-34.

BERTOS, N. R. & PARK, M. 2011. Breast cancer - one term, many entities? *J Clin Invest,* 121**,** 3789-96.

BEZDENEZHNYKH, N., SEMESIUK, N., LYKHOVA, O., ZHYLCHUK, V. & KUDRYAVETS, Y. 2014. Impact of stromal cell components of tumor microenvironment on epithelial-mesenchymal transition in breast cancer cells. *Exp Oncol,* 36**,** 72-8.

BHARADWAJ, M., STROHMEYER, N., COLO, G. P., HELENIUS, J., BEERENWINKEL, N., SCHILLER, H. B., FÄSSLER, R. & MÜLLER, D. J. 2017. αV-class integrins exert dual roles on α5β1 integrins to strengthen adhesion to fibronectin. *Nature Communications,* 8**,** 14348.

BINDEA, G., MLECNIK, B., HACKL, H., CHAROENTONG, P., TOSOLINI, M., KIRILOVSKY, A., FRIDMAN, W.-H., PAGÈS, F., TRAJANOSKI, Z. & GALON, J. 2009. ClueGO: a Cytoscape plug-in to decipher functionally grouped gene ontology and pathway annotation networks. *Bioinformatics,* 25**,** 1091-1093.

BLACKBURN, A. C., HILL, L. Z., ROBERTS, A. L., WANG, J., AUD, D., JUNG, J., NIKOLCHEVA, T., ALLARD, J., PELTZ, G., OTIS, C. N., CAO, Q. J., RICKETTS, R. S. J., NABER, S. P., MOLLENHAUER, J., POUSTKA, A., MALAMUD, D. & JERRY, D. J. 2007. Genetic Mapping in Mice Identifies DMBT1 as a Candidate Modifier of Mammary Tumors and Breast Cancer Risk. *The American Journal of Pathology,* 170**,** 2030-2041.

BONNANS, C., CHOU, J. & WERB, Z. 2014. Remodelling the extracellular matrix in development and disease. *Nat Rev Mol Cell Biol,* 15**,** 786-801.

BOUVARD, D., POUWELS, J., DE FRANCESCHI, N. & IVASKA, J. 2013. Integrin inactivators: balancing cellular functions in vitro and in vivo. *Nat Rev Mol Cell Biol.*

BOYER, A. P., COLLIER, T. S., VIDAVSKY, I. & BOSE, R. 2013. Quantitative proteomics with siRNA screening identifies novel mechanisms of trastuzumab resistance in HER2 amplified breast cancers. *Mol Cell Proteomics,* 12**,** 180-93.

BRAIDOTTI, P., NUCIFORO, P. G., MOLLENHAUER, J., POUSTKA, A., PELLEGRINI, C., MORO, A., BULFAMANTE, G., COGGI, G., BOSARI, S. & PIETRA, G. G. 2004. DMBT1 expression is down-regulated in breast cancer. *BMC Cancer,* 4**,** 46-46.

BRAKEBUSCH, C. & FASSLER, R. 2003. The integrin-actin connection, an eternal love affair. *Embo j,* 22**,** 2324-33.

BREITKREUTZ, D., BRAIMAN-WIKSMAN, L., DAUM, N., DENNING, M. F. & TENNENBAUM, T. 2007. Protein kinase C family: on the crossroads of cell signaling in skin and tumor

epithelium. *J Cancer Res Clin Oncol,* 133**,** 793-808.

BRETSCHER, M. S. 1989. Endocytosis and recycling of the fibronectin receptor in CHO cells. *Embo j,* 8**,** 1341-8.

BREUSS, J. M., GALLO, J., DELISSER, H. M., KLIMANSKAYA, I. V., FOLKESSON, H. G., PITTET, J. F., NISHIMURA, S. L., ALDAPE, K., LANDERS, D. V., CARPENTER, W. & ET AL. 1995. Expression of the beta 6 integrin subunit in development, neoplasia and tissue repair suggests a role in epithelial remodeling. *J Cell Sci,* 108 (Pt 6)**,** 2241-51.

BRITSCHGI, A., BILL, A., BRINKHAUS, H., ROTHWELL, C., CLAY, I., DUSS, S., REBHAN, M., RAMAN, P., GUY, C. T., WETZEL, K., GEORGE, E., POPA, M. O., LILLEY, S., CHOUDHURY, H., GOSLING, M., WANG, L., FITZGERALD, S., BORAWSKI, J., BAFFOE, J., LABOW, M., GAITHER, L. A. & BENTIRES-ALJ, M. 2013. Calcium-activated chloride channel ANO1 promotes breast cancer progression by activating EGFR and CAMK signaling. *Proc Natl Acad Sci U S A,* 110**,** E1026-34.

BROWN, M. C., CARY, L. A., JAMIESON, J. S., COOPER, J. A. & TURNER, C. E. 2005. Src and FAK kinases cooperate to phosphorylate paxillin kinase linker, stimulate its focal adhesion localization, and regulate cell spreading and protrusiveness. *Mol Biol Cell,* 16**,** 4316-28.

BROWNE, B. C., HOCHGRAFE, F., WU, J., MILLAR, E. K., BARRACLOUGH, J., STONE, A., MCCLOY, R. A., LEE, C. S., ROBERTS, C., ALI, N. A., BOULGHOURJIAN, A., SCHMICH, F., LINDING, R., FARROW, L., GEE, J. M., NICHOLSON, R. I., O'TOOLE, S. A., SUTHERLAND, R. L., MUSGROVE, E. A., BUTT, A. J. & DALY, R. J. 2013. Global characterization of signalling networks associated with tamoxifen resistance in breast cancer. *Febs j,* 280**,** 5237-57.

BUCHHEIT, C. L., RAYAVARAPU, R. R. & SCHAFER, Z. T. 2012. The regulation of cancer cell death and metabolism by extracellular matrix attachment. *Semin Cell Dev Biol,* 23**,** 402-11.

BURGESS, A. 2015. *Using ImageJ to Measure Cell Fluorescence* [Online]. Sydney, AUS: The Cell Division Lab, The Kinghorn Cancer Centre. Available: https://celldivisionlab.com/2015/08/12/using-imagej-to-measure-cell-fluorescence/ [Accessed 17th March 2017].

BUSK, M., PYTELA, R. & SHEPPARD, D. 1992. Characterization of the integrin alpha v beta 6 as a fibronectin-binding protein. *J Biol Chem,* 267**,** 5790-6.

BUSSARD, K. M., MUTKUS, L., STUMPF, K., GOMEZ-MANZANO, C. & MARINI, F. C. 2016. Tumor-associated stromal cells as key contributors to the tumor microenvironment. *Breast Cancer Res,* 18**,** 84.

BUTCHER, D. T., ALLISTON, T. & WEAVER, V. M. 2009. A tense situation: forcing tumour progression. *Nat Rev Cancer,* 9**,** 108-22.

BYRON, A. 2011. Analyzing the anatomy of integrin adhesions. *Sci Signal,* 4**,** jc3.

BYRON, A., ASKARI, J. A., HUMPHRIES, J. D., JACQUEMET, G., KOPER, E. J., WARWOOD, S., CHOI, C. K., STROUD, M. J., CHEN, C. S., KNIGHT, D. & HUMPHRIES, M. J. 2015. A proteomic approach reveals integrin activation state-dependent control of microtubule cortical targeting. *Nat Commun,* 6**,** 6135.

BYRON, A. & FRAME, M. C. 2016. Adhesion protein networks reveal functions proximal and distal to cell-matrix contacts. *Current Opinion in Cell Biology,* 39**,** 93-100.

BYRON, A., HUMPHRIES, J. D., ASKARI, J. A., CRAIG, S. E., MOULD, A. P. & HUMPHRIES, M. J. 2009. Anti-integrin monoclonal antibodies. *J Cell Sci,* 122**,** 4009-11.

BYRON, A., HUMPHRIES, J. D., BASS, M. D., KNIGHT, D. & HUMPHRIES, M. J. 2011. Proteomic analysis of integrin adhesion complexes. *Sci Signal,* 4**,** pt2.

BYRON, A., HUMPHRIES, J. D., CRAIG, S. E., KNIGHT, D. & HUMPHRIES, M. J. 2012. Proteomic analysis of alpha4beta1 integrin adhesion complexes reveals alpha-subunit-dependent protein recruitment. *Proteomics,* 12**,** 2107-14.

BYRON, A., HUMPHRIES, J. D. & HUMPHRIES, M. J. 2013. Defining the extracellular matrix using proteomics. *Int J Exp Pathol,* 94**,** 75-92.

BYRON, A., RANDLES, M. J., HUMPHRIES, J. D., MIRONOV, A., HAMIDI, H., HARRIS, S., MATHIESON, P. W., SALEEM, M. A., SATCHELL, S. C., ZENT, R., HUMPHRIES, M. J. & LENNON, R. 2014. Glomerular cell cross-talk influences composition and assembly of extracellular matrix. *J Am Soc Nephrol,* 25**,** 953-66.

CAL, S., FREIJE, J. M., LOPEZ, J. M., TAKADA, Y. & LOPEZ-OTIN, C. 2000. ADAM 23/MDC3, a human disintegrin that promotes cell adhesion via interaction with the alphavbeta3 integrin through an RGD-independent mechanism. *Mol Biol Cell,* 11**,** 1457-69.

CALDERWOOD, D. A., CAMPBELL, I. D. & CRITCHLEY, D. R. 2013. Talins and kindlins: partners in integrin-mediated adhesion. *Nat Rev Mol Cell Biol,* 14**,** 503-17.

CALDERWOOD, D. A., FUJIOKA, Y., DE PEREDA, J. M., GARCIA-ALVAREZ, B., NAKAMOTO, T., MARGOLIS, B., MCGLADE, C. J., LIDDINGTON, R. C. & GINSBERG, M. H. 2003. Integrin beta cytoplasmic domain interactions with phosphotyrosine-binding domains: a structural prototype for diversity in integrin signaling. *Proc Natl Acad Sci U S A,* 100**,** 2272-7.

CALVO, F. & SAHAI, E. 2011. Cell communication networks in cancer invasion. *Curr Opin Cell Biol,* 23**,** 621-9.

CAMPBELL, I. D. & HUMPHRIES, M. J. 2011. Integrin structure, activation, and interactions. *Cold Spring Harb Perspect Biol,* 3.

CANEL, M., SERRELS, A., FRAME, M. C. & BRUNTON, V. G. 2013. E-cadherin-integrin crosstalk in cancer invasion and metastasis. *J Cell Sci,* 126**,** 393-401.

CAO, R., CHEN, J., ZHANG, X., ZHAI, Y., QING, X., XING, W., ZHANG, L., MALIK, Y. S., YU, H. & ZHU, X. 2014. Breast cancer: Crucial role of myosin X in aggressiveness and metastasis. *Nat Rev Clin Oncol,* 11**,** 441-441.

CARAPUCA, E. F., GEMENETZIDIS, E., FEIG, C., BAPIRO, T. E., WILLIAMS, M. D., WILSON, A. S., DELVECCHIO, F. R., ARUMUGAM, P., GROSE, R. P., LEMOINE, N. R., RICHARDS, F. M. & KOCHER, H. M. 2016. Anti-stromal treatment together with chemotherapy targets multiple signalling pathways in pancreatic adenocarcinoma. *J Pathol,* 239**,** 286-96.

CARISEY, A., TSANG, R., GREINER, A. M., NIJENHUIS, N., HEATH, N., NAZGIEWICZ, A., KEMKEMER, R., DERBY, B., SPATZ, J. & BALLESTREM, C. 2013. Vinculin regulates the recruitment and release of core focal adhesion proteins in a force-dependent manner. *Curr Biol,* 23**,** 271-81.

CARMAN, C. V. 2012. Integrin and Cell Adhesion Molecules: Methods and Protocols. *In:* SHIMAOKA, M. (ed.) *Springer Protocols: Methods in Molecular Biology*. New York: Harvard Press.

CARPENTER, P. M., SIVADAS, P., HUA, S. S., XIAO, C., GUTIERREZ, A. B., NGO, T. & GERSHON, P. D. 2017. Migration of breast cancer cell lines in response to pulmonary laminin 332. *Cancer Med,* 6**,** 220-234.

CASADO, P., RODRIGUEZ-PRADOS, J. C., COSULICH, S. C., GUICHARD, S., VANHAESEBROECK, B., JOEL, S. & CUTILLAS, P. R. 2013a. Kinase-substrate enrichment analysis provides insights into the heterogeneity of signaling pathway activation in leukemia cells. *Sci Signal,* 6**,** rs6.

CASWELL, P. T., CHAN, M., LINDSAY, A. J., MCCAFFREY, M. W., BOETTIGER, D. & NORMAN, J. C. 2008. Rab-coupling protein coordinates recycling of alpha5beta1 integrin and EGFR1 to promote cell migration in 3D microenvironments. *J Cell Biol,* 183**,** 143-55.

CASWELL, P. T. & NORMAN, J. C. 2006. Integrin trafficking and the control of cell migration. *Traffic,* 7**,** 14-21.

CDC. 2016. *Global Cancer Statistics: Numer of Cases, Deaths and Survivors* [Online]. online: CDC. Available: http://www.cdc.gov/cancer/international/statistics.htm [Accessed 12th September 2016].

CHAFFER, C. L. & WEINBERG, R. A. 2011. A perspective on cancer cell metastasis. *Science,* 331**,** 1559-64.

CHANGEDE, R. & SHEETZ, M. 2017. Integrin and cadherin clusters: A robust way to organize

adhesions for cell mechanics. *Bioessays,* 39**,** 1-12.

CHANGEDE, R., XU, X., MARGADANT, F. & SHEETZ, M. P. 2015. Nascent Integrin Adhesions Form on All Matrix Rigidities after Integrin Activation. *Dev Cell,* 35**,** 614-21.

CHAVEZ, K. J., GARIMELLA, S. V. & LIPKOWITZ, S. 2010. Triple negative breast cancer cell lines: one tool in the search for better treatment of triple negative breast cancer. *Breast Dis,* 32**,** 35-48.

CHEN, C. H., CHENG, C. T., YUAN, Y., ZHAI, J., ARIF, M., FONG, L. W., WU, R. & ANN, D. K. 2015. Elevated MARCKS phosphorylation contributes to unresponsiveness of breast cancer to paclitaxel treatment. *Oncotarget,* 6**,** 15194-208.

CHEN, J., SALAS, A. & SPRINGER, T. A. 2003. Bistable regulation of integrin adhesiveness by a bipolar metal ion cluster. *Nat Struct Biol,* 10**,** 995-1001.

CHEN, P., LI, K., LIANG, Y., LI, L. & ZHU, X. 2013. High NUAK1 expression correlates with poor prognosis and involved in NSCLC cells migration and invasion. *Exp Lung Res,* 39**,** 9-17.

CHOWDHURY, F. Z., ESTRADA, L. D., MURRAY, S., FORMAN, J. & FARRAR, J. D. 2014. Pharmacological inhibition of TPL2/MAP3K8 blocks human cytotoxic T lymphocyte effector functions. *PLoS One,* 9**,** e92187.

CHUNG, J., UCHIDA, E., GRAMMER, T. C. & BLENIS, J. 1997. STAT3 serine phosphorylation by ERK-dependent and -independent pathways negatively modulates its tyrosine phosphorylation. *Mol Cell Biol,* 17**,** 6508-16.

CLARK, A. R. & TOKER, A. 2014. Signalling specificity in the Akt pathway in breast cancer. *Biochem Soc Trans,* 42**,** 1349-55.

CLINE, M. S., SMOOT, M., CERAMI, E., KUCHINSKY, A., LANDYS, N., WORKMAN, C., CHRISTMAS, R., AVILA-CAMPILO, I., CREECH, M., GROSS, B., HANSPERS, K., ISSERLIN, R., KELLEY, R., KILLCOYNE, S., LOTIA, S., MAERE, S., MORRIS, J., ONO, K., PAVLOVIC, V., PICO, A. R., VAILAYA, A., WANG, P. L., ADLER, A., CONKLIN, B. R., HOOD, L., KUIPER, M., SANDER, C., SCHMULEVICH, I., SCHWIKOWSKI, B., WARNER, G. J., IDEKER, T. & BADER, G. D. 2007. Integration of biological networks and gene expression data using Cytoscape. *Nat Protoc,* 2**,** 2366-82.

CLUZEL, C., SALTEL, F., LUSSI, J., PAULHE, F., IMHOF, B. A. & WEHRLE-HALLER, B. 2005. The mechanisms and dynamics of (alpha)v(beta)3 integrin clustering in living cells. *J Cell Biol,* 171**,** 383-92.

COLEMAN, S. J., CHIONI, A. M., GHALLAB, M., ANDERSON, R. K., LEMOINE, N. R., KOCHER, H. M. & GROSE, R. P. 2014a. Nuclear translocation of FGFR1 and FGF2 in pancreatic stellate cells facilitates pancreatic cancer cell invasion. *EMBO Mol Med,* 6**,** 467-81.

COLEMAN, S. J., WATT, J., ARUMUGAM, P., SOLAINI, L., CARAPUCA, E., GHALLAB, M., GROSE, R. P. & KOCHER, H. M. 2014b. Pancreatic cancer organotypics: High throughput, preclinical models for pharmacological agent evaluation. *World J Gastroenterol,* 20**,** 8471-81.

CONNOLLY, D., YANG, Z., CASTALDI, M., SIMMONS, N., OKTAY, M. H., CONIGLIO, S., FAZZARI, M. J., VERDIER-PINARD, P. & MONTAGNA, C. 2011. Septin 9 isoform expression, localization and epigenetic changes during human and mouse breast cancer progression. *Breast Cancer Res,* 13**,** R76.

CORGIAT, B. A., NORDMAN, J. C. & KABBANI, N. 2014. Chemical crosslinkers enhance detection of receptor interactomes. *Front Pharmacol,* 4**,** 171.

CORNING®INC. 2016. *Corning Matrigel®Matrix®: Overview* [Online]. Available: https://www.corning.com/emea/en/products/life-sciences/products/surfaces/matrigel-matrix.html [Accessed 30th March 2017].

COWLEY, M. J., PINESE, M., KASSAHN, K. S., WADDELL, N., PEARSON, J. V., GRIMMOND, S. M., BIANKIN, A. V., HAUTANIEMI, S. & WU, J. 2012. PINA v2.0: mining interactome modules. *Nucleic Acids Res,* 40**,** D862-5.

CR-UK. 2014. *Breast Cancer Risk Factors* [Online]. Available: http://www.cancerresearchuk.org/cancer-info/cancerstats/types/breast/riskfactors/breast-cancer-risk-factors [Accessed 11th November 2014].

CR-UK. 2016. *Breast Cancer Statistics* [Online]. online: CR-UK. Available: http://www.cancerresearchuk.org/health-professional/cancer-statistics/statistics-by-cancer-type/breast-cancer/ [Accessed 12th September 2016].

CRAIG, D., GAO, M., SCHULTEN, K. & VOGEL, V. 2004. Structural insights into how the MIDAS ion stabilizes integrin binding to an RGD peptide under force. *Structure,* 12**,** 2049-58.

CRISCITIELLO, C., ESPOSITO, A. & CURIGLIANO, G. 2014. Tumor-stroma crosstalk: targeting stroma in breast cancer. *Curr Opin Oncol,* 26**,** 551-5.

CRITCHLEY, D. R. 2009. Biochemical and structural properties of the integrin-associated cytoskeletal protein talin. *Annu Rev Biophys,* 38**,** 235-54.

CROWE, D. L. & OHANNESSIAN, A. 2004. Recruitment of focal adhesion kinase and paxillin to beta1 integrin promotes cancer cell migration via mitogen activated protein kinase activation. *BMC Cancer,* 4**,** 18.

CRT. 2013. *Cell Lines: DX3 Melanoma* [Online]. Available: http://www.cancertechnology.com/dx3-melanoma [Accessed 10th October 2014; 21:00 2014].

CRUM, C., LESTER, S. & COTRAN, R. 2003. The female genital system and breast. *Robbins Basic Pathology,* 7**,** 679-717.

CUMMINGS, M. C., SIMPSON, P. T., REID, L. E., JAYANTHAN, J., SKERMAN, J., SONG, S., MCCART REED, A. E., KUTASOVIC, J. R., MOREY, A. L., MARQUART, L., O'ROURKE, P. & LAKHANI, S. R. 2014. Metastatic progression of breast cancer: insights from 50 years of autopsies. *J Pathol,* 232**,** 23-31.

CUTILLAS, P. R. & VANHAESEBROECK, B. 2007. Quantitative profile of five murine core proteomes using label-free functional proteomics. *Mol Cell Proteomics,* 6**,** 1560-73.

CUTTS, R. J., GUERRA-ASSUNCAO, J. A., GADALETA, E., DAYEM ULLAH, A. Z. & CHELALA, C. 2015. BCCTBbp: the Breast Cancer Campaign Tissue Bank bioinformatics portal. *Nucleic Acids Res,* 43**,** D831-6.

CUZICK, J., SESTAK, I., PINDER, S. E., ELLIS, I. O., FORSYTH, S., BUNDRED, N. J., FORBES, J. F., BISHOP, H., FENTIMAN, I. S. & GEORGE, W. D. 2011. Effect of tamoxifen and radiotherapy in women with locally excised ductal carcinoma in situ: long-term results from the UK/ANZ DCIS trial. *Lancet Oncol,* 12**,** 21-9.

DABBS, D. J. 2008. Immunohistochemical protocols: back to the future. *Am J Clin Pathol,* 129**,** 355-6.

DAI, X., XIANG, L., LI, T. & BAI, Z. 2016. Cancer Hallmarks, Biomarkers and Breast Cancer Molecular Subtypes. *J Cancer,* 7**,** 1281-94.

DANEN, E. H. J. 2013. Integrins: An Overview of Structural and Functional Aspects. In: Madame Curie Bioscience Database [internet]. Austin (TX): Landes Bioscience.

DAVIDENKO, N., SCHUSTER, C. F., BAX, D. V., FARNDALE, R. W., HAMAIA, S., BEST, S. M. & CAMERON, R. E. 2016. Evaluation of cell binding to collagen and gelatin: a study of the effect of 2D and 3D architecture and surface chemistry. *Journal of Materials Science. Materials in Medicine,* 27**,** 148.

DAWSON, P. J., WOLMAN, S. R., TAIT, L., HEPPNER, G. H. & MILLER, F. R. 1996. MCF10AT: a model for the evolution of cancer from proliferative breast disease. *Am J Pathol,* 148**,** 313-9.

DAWSON, S. J., ROSENFELD, N. & CALDAS, C. 2013. Circulating tumor DNA to monitor metastatic breast cancer. *N Engl J Med,* 369**,** 93-4.

DAY, E. S., OSBORN, L. & WHITTY, A. 2002. Effect of divalent cations on the affinity and selectivity of alpha4 integrins towards the integrin ligands vascular cell adhesion molecule-1 and mucosal addressin cell adhesion molecule-1: Ca2+ activation of integrin alpha4beta1 confers a distinct ligand specificity. *Cell Commun Adhes,* 9**,** 205-19.

DE HOOG, C. L., FOSTER, L. J. & MANN, M. 2004. RNA and RNA binding proteins participate in early stages of cell spreading through spreading initiation centers. *Cell,* 117**,** 649-62.

DE SERVI, B., HERMANI, A., MEDUNJANIN, S. & MAYER, D. 2005. Impact of PKCdelta on estrogen receptor localization and activity in breast cancer cells. *Oncogene,* 24**,** 4946-55.

DERYCKE, L., STOVE, C., VERCOUTTER-EDOUART, A. S., DE WEVER, O., DOLLE, L., COLPAERT, N., DEPYPERE, H., MICHALSKI, J. C. & BRACKE, M. 2011. The role of non-muscle myosin IIA in aggregation and invasion of human MCF-7 breast cancer cells. *Int J Dev Biol,* 55**,** 835-40.

DESAI, A. 2011. *The Ability of Rat Monoclonal Antibodies to Recognise Different Subpopulations of αvβ6.* MSc Dissertation Queen Mary University of London.

DESGROSELLIER, J. S. & CHERESH, D. A. 2010. Integrins in cancer: biological implications and therapeutic opportunities. *Nat Rev Cancer,* 10**,** 9-22.

DIAZ, L. K., CRISTOFANILLI, M., ZHOU, X., WELCH, K. L., SMITH, T. L., YANG, Y., SNEIGE, N., SAHIN, A. A. & GILCREASE, M. Z. 2005. Beta4 integrin subunit gene expression correlates with tumor size and nuclear grade in early breast cancer. *Mod Pathol,* 18**,** 1165-75.

DICARA, D., RAPISARDA, C., SUTCLIFFE, J. L., VIOLETTE, S. M., WEINREB, P. H., HART, I. R., HOWARD, M. J. & MARSHALL, J. F. 2007. Structure-function analysis of Arg-Gly-Asp helix motifs in alpha v beta 6 integrin ligands. *J Biol Chem,* 282**,** 9657-65.

DICARA, D. & SAHA, A. 2006. Screening cytoplasmic tail deficient recombinant integrin αvβ6 variants derived from Weinacker et al (1994). Barts Cancer Institute.

DIECI, M. V., ORVIETO, E., DOMINICI, M., CONTE, P. & GUARNERI, V. 2014. Rare breast cancer subtypes: histological, molecular, and clinical peculiarities. *Oncologist,* 19**,** 805-13.

DOBROVOLNY, P. L. & BESS, D. 2011. Optimized PCR-based Detection of Mycoplasma. *Journal of Visualized Experiments : JoVE***,** 3057.

DOMON, B. & AEBERSOLD, R. 2010. Options and considerations when selecting a quantitative proteomics strategy. *Nat Biotechnol,* 28**,** 710-21.

DONG, X., HUDSON, N. E., LU, C. & SPRINGER, T. A. 2014. Structural determinants of integrin β-subunit specificity for latent TGF-β. *Nature structural & molecular biology,* 21**,** 1091-1096.

DOZYNKIEWICZ, M. A., JAMIESON, N. B., MACPHERSON, I., GRINDLAY, J., VAN DEN BERGHE, P. V., VON THUN, A., MORTON, J. P., GOURLEY, C., TIMPSON, P.,

NIXON, C., MCKAY, C. J., CARTER, R., STRACHAN, D., ANDERSON, K., SANSOM, O. J., CASWELL, P. T. & NORMAN, J. C. 2012. Rab25 and CLIC3 collaborate to promote integrin recycling from late endosomes/lysosomes and drive cancer progression. *Dev Cell,* 22**,** 131-45.

DRANSFIELD, I., CABANAS, C., CRAIG, A. & HOGG, N. 1992. Divalent cation regulation of the function of the leukocyte integrin LFA-1. *J Cell Biol,* 116**,** 219-26.

DRUGBANKV5.0. 2017. *Gefitinib* [Online]. Available: https://www.drugbank.ca/drugs/DB00317 [Accessed 22nd March 2017].

DU, J., ZU, Y., LI, J., DU, S., XU, Y., ZHANG, L., JIANG, L., WANG, Z., CHIEN, S. & YANG, C. 2016. Extracellular matrix stiffness dictates Wnt expression through integrin pathway. 6**,** 20395.

DUFFY, M. J., MCGOWAN, P. M. & GALLAGHER, W. M. 2008. Cancer invasion and metastasis: changing views. *J Pathol,* 214**,** 283-93.

DUNCAN, J. S., WHITTLE, M. C., NAKAMURA, K., ABELL, A. N., MIDLAND, A. A., ZAWISTOWSKI, J. S., JOHNSON, N. L., GRANGER, D. A., JORDAN, N. V., DARR, D. B., USARY, J., KUAN, P. F., SMALLEY, D. M., MAJOR, B., HE, X., HOADLEY, K. A., ZHOU, B., SHARPLESS, N. E., PEROU, C. M., KIM, W. Y., GOMEZ, S. M., CHEN, X., JIN, J., FRYE, S. V., EARP, H. S., GRAVES, L. M. & JOHNSON, G. L. 2012. Dynamic reprogramming of the kinome in response to targeted MEK inhibition in triple-negative breast cancer. *Cell,* 149**,** 307-21.

DUPERRET, E. K., DAHAL, A. & RIDKY, T. W. 2015. Focal-adhesion-independent integrin-αv regulation of FAK and c-Myc is necessary for 3D skin formation and tumor invasion. *Journal of Cell Science,* 128**,** 3997-4013.

EBERLEIN, C., KENDREW, J., MCDAID, K., ALFRED, A., KANG, J. S., JACOBS, V. N., ROSS, S. J., ROONEY, C., SMITH, N. R., RINKENBERGER, J., CAO, A., CHURCHMAN, A., MARSHALL, J. F., WEIR, H. M., BEDIAN, V., BLAKEY, D. C., FOLTZ, I. N. & BARRY, S. T. 2013. A human monoclonal antibody 264RAD targeting alphavbeta6 integrin reduces tumour growth and metastasis, and modulates key biomarkers in vivo. *Oncogene,* 32**,** 4406-16.

EBERLEIN, C., ROONEY, C., ROSS, S. J., FARREN, M., WEIR, H. M. & BARRY, S. T. 2015. E-Cadherin and EpCAM expression by NSCLC tumour cells associate with normal fibroblast activation through a pathway initiated by integrin alphavbeta6 and maintained through TGFbeta signalling. *Oncogene,* 34**,** 704-16.

EKE, I. & CORDES, N. 2015. Focal adhesion signaling and therapy resistance in cancer. *Semin Cancer Biol,* 31**,** 65-75.

EKE, I., SCHNEIDER, L., FORSTER, C., ZIPS, D., KUNZ-SCHUGHART, L. A. & CORDES, N. 2013a. EGFR/JIP-4/JNK2 signaling attenuates cetuximab-mediated radiosensitization

of squamous cell carcinoma cells. *Cancer Res,* 73**,** 297-306.

EKE, I., STORCH, K., KRAUSE, M. & CORDES, N. 2013b. Cetuximab attenuates its cytotoxic and radiosensitizing potential by inducing fibronectin biosynthesis. *Cancer Res,* 73**,** 5869-79.

ELAYADI, A. N., SAMLI, K. N., PRUDKIN, L., LIU, Y. H., BIAN, A., XIE, X. J., WISTUBA, II, ROTH, J. A., MCGUIRE, M. J. & BROWN, K. C. 2007. A peptide selected by biopanning identifies the integrin alphavbeta6 as a prognostic biomarker for nonsmall cell lung cancer. *Cancer Res,* 67**,** 5889-95.

ENGEBRAATEN, O., VOLLAN, H. K. & BORRESEN-DALE, A. L. 2013. Triple-negative breast cancer and the need for new therapeutic targets. *Am J Pathol,* 183**,** 1064-74.

ERNSTER, V. L., BALLARD-BARBASH, R., BARLOW, W. E., ZHENG, Y., WEAVER, D. L., CUTTER, G., YANKASKAS, B. C., ROSENBERG, R., CARNEY, P. A., KERLIKOWSKE, K., TAPLIN, S. H., URBAN, N. & GELLER, B. M. 2002. Detection of ductal carcinoma in situ in women undergoing screening mammography. *J Natl Cancer Inst,* 94**,** 1546-54.

EROLES, P., BOSCH, A., PEREZ-FIDALGO, J. A. & LLUCH, A. 2012. Molecular biology in breast cancer: intrinsic subtypes and signaling pathways. *Cancer Treat Rev,* 38**,** 698-707.

FAULL, R. J., WANG, J., LEAVESLEY, D. I., PUZON, W., RUSS, G. R., VESTWEBER, D. & TAKADA, Y. 1996. A novel activating anti-beta1 integrin monoclonal antibody binds to the cysteine-rich repeats in the beta1 chain. *J Biol Chem,* 271**,** 25099-106.

FAZEKAS, D., KOLTAI, M., TUREI, D., MODOS, D., PALFY, M., DUL, Z., ZSAKAI, L., SZALAY-BEKO, M., LENTI, K., FARKAS, I. J., VELLAI, T., CSERMELY, P. & KORCSMAROS, T. 2013. SignaLink 2 - a signaling pathway resource with multi-layered regulatory networks. *BMC Syst Biol,* 7**,** 7.

FELDING-HABERMANN, B. 2003. Integrin adhesion receptors in tumor metastasis. *Clin Exp Metastasis,* 20**,** 203-13.

FELDING-HABERMANN, B., O'TOOLE, T. E., SMITH, J. W., FRANSVEA, E., RUGGERI, Z. M., GINSBERG, M. H., HUGHES, P. E., PAMPORI, N., SHATTIL, S. J., SAVEN, A. & MUELLER, B. M. 2001. Integrin activation controls metastasis in human breast cancer. *Proc Natl Acad Sci U S A,* 98**,** 1853-8.

FIORE, M., FORLI, S. & MANETTI, F. 2015. Targeting Mitogen-Activated Protein Kinase-Activated Protein Kinase 2 (MAPKAPK2, MK2): Medicinal Chemistry Efforts To Lead Small Molecule Inhibitors to Clinical Trials. *Journal of Medicinal Chemistry*.

FOROZAN, F., VELDMAN, R., AMMERMAN, C. A., PARSA, N. Z., KALLIONIEMI, A., KALLIONIEMI, O. P. & ETHIER, S. P. 1999. Molecular cytogenetic analysis of 11 new breast cancer cell lines. *Br J Cancer,* 81**,** 1328-34.

FREED, E., GAILIT, J., VAN DER GEER, P., RUOSLAHTI, E. & HUNTER, T. 1989. A novel integrin beta subunit is associated with the vitronectin receptor alpha subunit (alpha v) in a human osteosarcoma cell line and is a substrate for protein kinase C. *Embo j,* 8**,** 2955-65.

FRELINGER, A. L., 3RD, COHEN, I., PLOW, E. F., SMITH, M. A., ROBERTS, J., LAM, S. C. & GINSBERG, M. H. 1990. Selective inhibition of integrin function by antibodies specific for ligand-occupied receptor conformers. *J Biol Chem,* 265**,** 6346-52.

FROELING, F. E., MIRZA, T. A., FEAKINS, R. M., SEEDHAR, A., ELIA, G., HART, I. R. & KOCHER, H. M. 2009. Organotypic culture model of pancreatic cancer demonstrates that stromal cells modulate E-cadherin, beta-catenin, and Ezrin expression in tumor cells. *Am J Pathol,* 175**,** 636-48.

GARCIA-ALVAREZ, B., DE PEREDA, J. M., CALDERWOOD, D. A., ULMER, T. S., CRITCHLEY, D., CAMPBELL, I. D., GINSBERG, M. H. & LIDDINGTON, R. C. 2003. Structural determinants of integrin recognition by talin. *Mol Cell,* 11**,** 49-58.

GILAD, R., MEIR, K., STEIN, I., GERMAN, L., PIKARSKY, E. & MABJEESH, N. J. 2015. High SEPT9_i1 protein expression is associated with high-grade prostate cancers. *PLoS One,* 10**,** e0124251.

GINSBERG, M. H., FRELINGER, A. L., LAM, S. C., FORSYTH, J., MCMILLAN, R., PLOW, E. F. & SHATTIL, S. J. 1990. Analysis of platelet aggregation disorders based on flow cytometric analysis of membrane glycoprotein IIb-IIIa with conformation-specific monoclonal antibodies. *Blood,* 76**,** 2017-23.

GKIRTZIMANAKI, K., GKOUSKOU, K. K., OLEKSIEWICZ, U., NIKOLAIDIS, G., VYRLA, D., LIONTOS, M., PELEKANOU, V., KANELLIS, D. C., EVANGELOU, K., STATHOPOULOS, E. N., FIELD, J. K., TSICHLIS, P. N., GORGOULIS, V., LILOGLOU, T. & ELIOPOULOS, A. G. 2013. TPL2 kinase is a suppressor of lung carcinogenesis. *Proc Natl Acad Sci U S A,* 110**,** E1470-9.

GOMM, J. J., BROWNE, P. J., COOPE, R. C., LIU, Q. Y., BULUWELA, L. & COOMBES, R. C. 1995. Isolation of pure populations of epithelial and myoepithelial cells from the normal human mammary gland using immunomagnetic separation with Dynabeads. *Anal Biochem,* 226**,** 91-9.

GONCALVES, R., WARNER, W. A., LUO, J. & ELLIS, M. J. 2014. New concepts in breast cancer genomics and genetics. *Breast Cancer Res,* 16**,** 460.

GRUOSSO, T., GARNIER, C., ABELANET, S., KIEFFER, Y., LEMESRE, V., BELLANGER, D., BIECHE, I., MARANGONI, E., SASTRE-GARAU, X., MIEULET, V. & MECHTA-GRIGORIOU, F. 2015. MAP3K8/TPL-2/COT is a potential predictive marker for MEK inhibitor treatment in high-grade serous ovarian carcinomas. *Nat Commun,* 6**,** 8583.

GUADAMILLAS, M. C., CEREZO, A. & DEL POZO, M. A. 2011. Overcoming anoikis--pathways

to anchorage-independent growth in cancer. *J Cell Sci,* 124**,** 3189-97.

GUDJONSSON, T., ADRIANCE, M. C., STERNLICHT, M. D., PETERSEN, O. W. & BISSELL, M. J. 2005. Myoepithelial cells: their origin and function in breast morphogenesis and neoplasia. *J Mammary Gland Biol Neoplasia,* 10**,** 261-72.

GUMBINER, B. M. 1996. Cell adhesion: the molecular basis of tissue architecture and morphogenesis. *Cell,* 84**,** 345-57.

GUO, W. & GIANCOTTI, F. G. 2004. Integrin signalling during tumour progression. *Nat Rev Mol Cell Biol,* 5**,** 816-26.

HAHM, K., LUKASHEV, M. E., LUO, Y., YANG, W. J., DOLINSKI, B. M., WEINREB, P. H., SIMON, K. J., CHUN WANG, L., LEONE, D. R., LOBB, R. R., MCCRANN, D. J., ALLAIRE, N. E., HORAN, G. S., FOGO, A., KALLURI, R., SHIELD, C. F., SHEPPARD, D., GARDNER, H. A. & VIOLETTE, S. M. 2007. αvβ6 Integrin Regulates Renal Fibrosis and Inflammation in Alport Mouse. *The American Journal of Pathology,* 170**,** 110-125.

HAHM, K., LUKASHEV, M. E., LUO, Y., YANG, W. J., DOLINSKI, B. M., WEINREB, P. H., SIMON, K. J., CHUN WANG, L., LEONE, D. R., LOBB, R. R., MCCRANN, D. J., ALLAIRE, N. E., HORAN, G. S., FOGO, A., KALLURI, R., SHIELD, C. F., 3RD, SHEPPARD, D., GARDNER, H. A. & VIOLETTE, S. M. 2007. Alphav beta6 integrin regulates renal fibrosis and inflammation in Alport mouse. *Am J Pathol,* 170**,** 110-25.

HALE, J. S., LI, M. & LATHIA, J. D. 2012. The malignant social network: cell-cell adhesion and communication in cancer stem cells. *Cell Adh Migr,* 6**,** 346-55.

HAMIDI, H., PIETILA, M. & IVASKA, J. 2016. The complexity of integrins in cancer and new scopes for therapeutic targeting. *Br J Cancer,* 115**,** 1017-1023.

HAMILL, K. J., KLIGYS, K., HOPKINSON, S. B. & JONES, J. C. R. 2009. Laminin deposition in the extracellular matrix: a complex picture emerges. *Journal of Cell Science,* 122**,** 4409-4417.

HAMMER, A., RIDER, L., OLADIMEJI, P., COOK, L., LI, Q., MATTINGLY, R. R. & DIAKONOVA, M. 2013. Tyrosyl phosphorylated PAK1 regulates breast cancer cell motility in response to prolactin through filamin A. *Mol Endocrinol,* 27**,** 455-65.

HANAHAN, D. & WEINBERG, R. A. 2000. The hallmarks of cancer. *Cell,* 100**,** 57-70.

HANAHAN, D. & WEINBERG, R. A. 2011. Hallmarks of cancer: the next generation. *Cell,* 144**,** 646-74.

HARBURGER, D. S. & CALDERWOOD, D. A. 2009. Integrin signalling at a glance. *J Cell Sci,* 122**,** 159-63.

HAUSNER, S. H., DICARA, D., MARIK, J., MARSHALL, J. F. & SUTCLIFFE, J. L. 2007. Use of a peptide derived from foot-and-mouth disease virus for the noninvasive imaging of human cancer: generation and evaluation of 4-[18F]fluorobenzoyl A20FMDV2 for in vivo imaging of integrin alphavbeta6 expression with positron emission tomography. *Cancer Res,* 67**,** 7833-40.

HAVAKI, S., KOULOUKOUSSA, M., AMAWI, K., DROSOS, Y., ARVANITIS, L. D., GOUTAS, N., VLACHODIMITROPOULOS, D., VASSILAROS, S. D., KATSANTONI, E. Z., VOLOUDAKIS-BALTATZIS, I., ALEPOROU-MARINOU, V., KITTAS, C. & MARINOS, E. 2007. Altered expression pattern of integrin alphavbeta3 correlates with actin cytoskeleton in primary cultures of human breast cancer. *Cancer Cell Int,* 7**,** 16.

HAZELBAG, S., KENTER, G. G., GORTER, A., DREEF, E. J., KOOPMAN, L. A., VIOLETTE, S. M., WEINREB, P. H. & FLEUREN, G. J. 2007. Overexpression of the alpha v beta 6 integrin in cervical squamous cell carcinoma is a prognostic factor for decreased survival. *J Pathol,* 212**,** 316-24.

HEINO, J. 2000. The collagen receptor integrins have distinct ligand recognition and signaling functions. *Matrix Biol,* 19**,** 319-23.

HEPPNER, G. H., MILLER, F. R. & SHEKHAR, P. M. 2000. Nontransgenic models of breast cancer. *Breast Cancer Res,* 2**,** 331-4.

HEROLD, C. I. & ANDERS, C. K. 2013. New targets for triple-negative breast cancer. *Oncology (Williston Park),* 27**,** 846-54.

HERZENBERG, L. A., PARKS, D., SAHAF, B., PEREZ, O., ROEDERER, M. & HERZENBERG, L. A. 2002. The history and future of the fluorescence activated cell sorter and flow cytometry: a view from Stanford. *Clin Chem,* 48**,** 1819-27.

HIRATA, H., TATSUMI, H., LIM, C. T. & SOKABE, M. 2014. Force-dependent vinculin binding to talin in live cells: a crucial step in anchoring the actin cytoskeleton to focal adhesions. *Am J Physiol Cell Physiol,* 306**,** C607-20.

HO-BOULDOIRES, T. H., CLAPERON, A., MERGEY, M., WENDUM, D., DESBOIS-MOUTHON, C., TAHRAOUI, S., FARTOUX, L., CHETTOUH, H., MERABTENE, F., SCATTON, O., GAESTEL, M., PRAZ, F., HOUSSET, C. & FOUASSIER, L. 2015. Mitogen-activated protein kinase-activated protein kinase 2 mediates resistance to hydrogen peroxide-induced oxidative stress in human hepatobiliary cancer cells. *Free Radic Biol Med.*

HOLLESTELLE, A., ELSTRODT, F., NAGEL, J. H., KALLEMEIJN, W. W. & SCHUTTE, M. 2007. Phosphatidylinositol-3-OH kinase or RAS pathway mutations in human breast cancer cell lines. *Mol Cancer Res,* 5**,** 195-201.

HONG, B., LI, H., ZHANG, M., XU, J., LU, Y., ZHENG, Y., QIAN, J., CHANG, J. T., YANG, J. & YI, Q. 2015. p38 MAPK inhibits breast cancer metastasis through regulation of stromal expansion. *Int J Cancer,* 136**,** 34-43.

HOOD, J. D. & CHERESH, D. A. 2002. Role of integrins in cell invasion and migration. *Nat Rev Cancer,* 2**,** 91-100.

HOOPMANN, M. R., MERRIHEW, G. E., VON HALLER, P. D. & MACCOSS, M. J. 2009. Post analysis data acquisition for the iterative MS/MS sampling of proteomics mixtures. *J Proteome Res,* 8**,** 1870-5.

HOPKINS, C. R. & TROWBRIDGE, I. S. 1983. Internalization and processing of transferrin and the transferrin receptor in human carcinoma A431 cells. *J Cell Biol,* 97**,** 508-21.

HSIAO, Y. H., CHOU, M. C., FOWLER, C., MASON, J. T. & MAN, Y. G. 2010. Breast cancer heterogeneity: mechanisms, proofs, and implications. *J Cancer,* 1**,** 6-13.

HTA. 2004. *Human Tissue Act* [Online]. Available: http://www.legislation.gov.uk/ukpga/2004/30/contents [Accessed 15th October 2014].

HU, M., YAO, J., CARROLL, D. K., WEREMOWICZ, S., CHEN, H., CARRASCO, D., RICHARDSON, A., VIOLETTE, S., NIKOLSKAYA, T., NIKOLSKY, Y., BAUERLEIN, E. L., HAHN, W. C., GELMAN, R. S., ALLRED, C., BISSELL, M. J., SCHNITT, S. & POLYAK, K. 2008. Regulation of in situ to invasive breast carcinoma transition. *Cancer Cell,* 13**,** 394-406.

HUANG, X., LV, W., ZHANG, J. H. & LU, D. L. 2014. miR96 functions as a tumor suppressor gene by targeting NUAK1 in pancreatic cancer. *Int J Mol Med,* 34**,** 1599-605.

HUGHES, P. E., DIAZ-GONZALEZ, F., LEONG, L., WU, C., MCDONALD, J. A., SHATTIL, S. J. & GINSBERG, M. H. 1996. Breaking the integrin hinge. A defined structural constraint regulates integrin signaling. *J Biol Chem,* 271**,** 6571-4.

HUMPHRIES, J. D., BYRON, A., BASS, M. D., CRAIG, S. E., PINNEY, J. W., KNIGHT, D. & HUMPHRIES, M. J. 2009. Proteomic analysis of integrin-associated complexes identifies RCC2 as a dual regulator of Rac1 and Arf6. *Sci Signal,* 2**,** ra51.

HUMPHRIES, J. D., WANG, P., STREULI, C., GEIGER, B., HUMPHRIES, M. J. & BALLESTREM, C. 2007. Vinculin controls focal adhesion formation by direct interactions with talin and actin. *The Journal of Cell Biology,* 179**,** 1043-1057.

HUMPHRIES, M. J. 1996. Integrin activation: the link between ligand binding and signal transduction. *Curr Opin Cell Biol,* 8**,** 632-40.

HUMPHRIES, M. J. 2002. Insights into integrin-ligand binding and activation from the first crystal structure. *Arthritis Res,* 4 Suppl 3**,** S69-78.

HUMPHRIES, M. J. 2004. Monoclonal antibodies as probes of integrin priming and activation. *Biochem Soc Trans,* 32**,** 407-11.

HUMPHRIES, M. J., MCEWAN, P. A., BARTON, S. J., BUCKLEY, P. A., BELLA, J. & MOULD, A. P. 2003. Integrin structure: heady advances in ligand binding, but activation still makes the knees wobble. *Trends Biochem Sci,* 28**,** 313-20.

HUMPHRIES, M. J., SYMONDS, E. J. & MOULD, A. P. 2003. Mapping functional residues onto integrin crystal structures. *Curr Opin Struct Biol,* 13**,** 236-43.

HURST, D. R. & WELCH, D. R. 2011. Metastasis suppressor genes at the interface between the environment and tumor cell growth. *Int Rev Cell Mol Biol,* 286**,** 107-80.

HUTTENLOCHER, A. & HORWITZ, A. R. 2011. Integrins in cell migration. *Cold Spring Harb Perspect Biol,* 3**,** a005074.

HYNES, R. O. 2002. Integrins: bidirectional, allosteric signaling machines. *Cell,* 110**,** 673-87.

HYNES, R. O. & NABA, A. 2012. Overview of the matrisome--an inventory of extracellular matrix constituents and functions. *Cold Spring Harb Perspect Biol,* 4**,** a004903.

IMPOLA, U., UITTO, V. J., HIETANEN, J., HAKKINEN, L., ZHANG, L., LARJAVA, H., ISAKA, K. & SAARIALHO-KERE, U. 2004. Differential expression of matrilysin-1 (MMP-7), 92 kD gelatinase (MMP-9), and metalloelastase (MMP-12) in oral verrucous and squamous cell cancer. *J Pathol,* 202**,** 14-22.

INGTHORSSON, S., SIGURDSSON, V., FRIDRIKSDOTTIR, A., JR., JONASSON, J. G., KJARTANSSON, J., MAGNUSSON, M. K. & GUDJONSSON, T. 2010. Endothelial cells stimulate growth of normal and cancerous breast epithelial cells in 3D culture. *BMC Res Notes,* 3**,** 184.

IORIO, V., TROUGHTON, L. D. & HAMILL, K. J. 2015. Laminins: Roles and Utility in Wound Repair. *Advances in Wound Care,* 4**,** 250-263.

ISKRATSCH, T., YU, C. H., MATHUR, A., LIU, S., STEVENIN, V., DWYER, J., HONE, J., EHLER, E. & SHEETZ, M. 2013. FHOD1 is needed for directed forces and adhesion maturation during cell spreading and migration. *Dev Cell,* 27**,** 545-59.

IVASKA, J. & HEINO, J. 2010. Interplay between cell adhesion and growth factor receptors: from the plasma membrane to the endosomes. *Cell Tissue Res,* 339**,** 111-20.

IVASKA, J. & HEINO, J. 2011. Cooperation between integrins and growth factor receptors in signaling and endocytosis. *Annu Rev Cell Dev Biol,* 27**,** 291-320.

JACKSON, T., SHEPPARD, D., DENYER, M., BLAKEMORE, W. & KING, A. M. 2000. The epithelial integrin alphavbeta6 is a receptor for foot-and-mouth disease virus. *J Virol,* 74**,** 4949-56.

JACQUEMET, G., MORGAN, M. R., BYRON, A., HUMPHRIES, J. D., CHOI, C. K., CHEN, C. S.,

CASWELL, P. T. & HUMPHRIES, M. J. 2013. Rac1 is deactivated at integrin activation sites through an IQGAP1-filamin-A-RacGAP1 pathway. *J Cell Sci,* 126**,** 4121-35.

JANES, S. M. & WATT, F. M. 2004. Switch from αvβ5 to αvβ6 integrin expression protects squamous cell carcinomas from anoikis. *The Journal of Cell Biology,* 166**,** 419-431.

JEMAL, A., BRAY, F., CENTER, M. M., FERLAY, J., WARD, E. & FORMAN, D. 2011. Global cancer statistics. *CA Cancer J Clin,* 61**,** 69-90.

JIANG, X., SHA, X., XIN, H., XU, X., GU, J., XIA, W., CHEN, S., XIE, Y., CHEN, L., CHEN, Y. & FANG, X. 2013. Integrin-facilitated transcytosis for enhanced penetration of advanced gliomas by poly(trimethylene carbonate)-based nanoparticles encapsulating paclitaxel. *Biomaterials,* 34**,** 2969-79.

JIN, H. & VARNER, J. 2004. Integrins: roles in cancer development and as treatment targets. *Br J Cancer,* 90**,** 561-5.

JOHANNESSEN, C. M., BOEHM, J. S., KIM, S. Y., THOMAS, S. R., WARDWELL, L., JOHNSON, L. A., EMERY, C. M., STRANSKY, N., COGDILL, A. P., BARRETINA, J., CAPONIGRO, G., HIERONYMUS, H., MURRAY, R. R., SALEHI-ASHTIANI, K., HILL, D. E., VIDAL, M., ZHAO, J. J., YANG, X., ALKAN, O., KIM, S., HARRIS, J. L., WILSON, C. J., MYER, V. E., FINAN, P. M., ROOT, D. E., ROBERTS, T. M., GOLUB, T., FLAHERTY, K. T., DUMMER, R., WEBER, B. L., SELLERS, W. R., SCHLEGEL, R., WARGO, J. A., HAHN, W. C. & GARRAWAY, L. A. 2010. COT drives resistance to RAF inhibition through MAP kinase pathway reactivation. *Nature,* 468**,** 968-72.

JOKINEN, J., DADU, E., NYKVIST, P., KAPYLA, J., WHITE, D. J., IVASKA, J., VEHVILAINEN, P., REUNANEN, H., LARJAVA, H., HAKKINEN, L. & HEINO, J. 2004. Integrin-mediated cell adhesion to type I collagen fibrils. *J Biol Chem,* 279**,** 31956-63.

JONES, A. V., LAMBERT, D. W., SPEIGHT, P. M. & WHAWELL, S. A. 2013. ADAM 10 is over expressed in oral squamous cell carcinoma and contributes to invasive behaviour through a functional association with alphavbeta6 integrin. *FEBS Lett,* 587**,** 3529-34.

KADABA, R., BIRKE, H., WANG, J., HOOPER, S., ANDL, C. D., DI MAGGIO, F., SOYLU, E., GHALLAB, M., BOR, D., FROELING, F. E., BHATTACHARYA, S., RUSTGI, A. K., SAHAI, E., CHELALA, C., SASIENI, P. & KOCHER, H. M. 2013. Imbalance of desmoplastic stromal cell numbers drives aggressive cancer processes. *J Pathol,* 230**,** 107-17.

KADOTA, M., YANG, H., GOMEZ, B., SATO, M. & CLIFFORD RJ, E. A. 2010. Delineating Genetic Alterations for Tumor Progression in the MCF10A Series of Breast Cancer Cell Lines. *PLOS ONE,* 5.

KAMATA, T., PUZON, W. & TAKADA, Y. 1994. Identification of putative ligand binding sites within I domain of integrin alpha 2 beta 1 (VLA-2, CD49b/CD29). *J Biol Chem,* 269**,** 9659-63.

KANCHANAWONG, P., SHTENGEL, G., PASAPERA, A. M., RAMKO, E. B., DAVIDSON, M. W., HESS, H. F. & WATERMAN, C. M. 2010. Nanoscale architecture of integrin-based cell adhesions. *Nature,* 468**,** 580-584.

KANE, L. P., MOLLENAUER, M. N., XU, Z., TURCK, C. W. & WEISS, A. 2002. Akt-dependent phosphorylation specifically regulates Cot induction of NF-kappa B-dependent transcription. *Mol Cell Biol,* 22**,** 5962-74.

KAO, J., SALARI, K., BOCANEGRA, M., CHOI, Y. L., GIRARD, L., GANDHI, J., KWEI, K. A., HERNANDEZ-BOUSSARD, T., WANG, P., GAZDAR, A. F., MINNA, J. D. & POLLACK, J. R. 2009. Molecular profiling of breast cancer cell lines defines relevant tumor models and provides a resource for cancer gene discovery. *PLoS One,* 4**,** e6146.

KAPP, T. G., RECHENMACHER, F., NEUBAUER, S., MALTSEV, O. V., CAVALCANTI-ADAM, E. A., ZARKA, R., REUNING, U., NOTNI, J., WESTER, H. J., MAS-MORUNO, C., SPATZ, J., GEIGER, B. & KESSLER, H. 2017. A Comprehensive Evaluation of the Activity and Selectivity Profile of Ligands for RGD-binding Integrins. *Sci Rep,* 7**,** 39805.

KATONO, K., SATO, Y., JIANG, S. X., KOBAYASHI, M., NAGASHIO, R., RYUGE, S., FUKUDA, E., GOSHIMA, N., SATOH, Y., SAEGUSA, M. & MASUDA, N. 2015. Prognostic significance of MYH9 expression in resected non-small cell lung cancer. *PLoS One,* 10**,** e0121460.

KENNY, P. A., LEE, G. Y., MYERS, C. A., NEVE, R. M., SEMEIKS, J. R., SPELLMAN, P. T., LORENZ, K., LEE, E. H., BARCELLOS-HOFF, M. H., PETERSEN, O. W., GRAY, J. W. & BISSELL, M. J. 2007. The morphologies of breast cancer cell lines in three-dimensional assays correlate with their profiles of gene expression. *Mol Oncol,* 1**,** 84-96.

KHAN, Z. & MARSHALL, J. F. 2016. The role of integrins in TGFbeta activation in the tumour stroma. *Cell Tissue Res,* 365**,** 657-73.

KIBBEY, M. C. 1994. Maintenance of the EHS sarcoma and Matrigel preparation. *Journal of tissue culture methods,* 16**,** 227-230.

KIM, B. G., GAO, M.-Q., CHOI, Y. P., KANG, S., PARK, H. R., KANG, K. S. & CHO, N. H. 2012. Invasive breast cancer induces laminin-332 upregulation and integrin β4 neoexpression in myofibroblasts to confer an anoikis-resistant phenotype during tissue remodeling. *Breast Cancer Research : BCR,* 14**,** R88-R88.

KIM, C., YE, F. & GINSBERG, M. H. 2011b. Regulation of integrin activation. *Annu Rev Cell Dev Biol,* 27**,** 321-45.

KIM, C., YE, F., HU, X. & GINSBERG, M. H. 2012. Talin activates integrins by altering the topology of the beta transmembrane domain. *J Cell Biol,* 197**,** 605-11.

KIM, G., KHANAL, P., KIM, J. Y., YUN, H. J., LIM, S. C., SHIM, J. H. & CHOI, H. S. 2015. COT

phosphorylates prolyl-isomerase Pin1 to promote tumorigenesis in breast cancer. *Mol Carcinog,* 54**,** 440-8.

KIM, S. H., TURNBULL, J. & GUIMOND, S. 2011a. Extracellular matrix and cell signalling: the dynamic cooperation of integrin, proteoglycan and growth factor receptor. *J Endocrinol,* 209**,** 139-51.

KIRK, R. I., SANDERSON, M. R. & LEREA, K. M. 2000. Threonine phosphorylation of the beta 3 integrin cytoplasmic tail, at a site recognized by PDK1 and Akt/PKB in vitro, regulates Shc binding. *J Biol Chem,* 275**,** 30901-6.

KIRKEGAARD, T., WITTON, C. J., MCGLYNN, L. M., TOVEY, S. M., DUNNE, B., LYON, A. & BARTLETT, J. M. 2005. AKT activation predicts outcome in breast cancer patients treated with tamoxifen. *J Pathol,* 207**,** 139-46.

KITO, K. & ITO, T. 2008. Mass spectrometry-based approaches toward absolute quantitative proteomics. *Curr Genomics,* 9**,** 263-74.

KNUEFERMANN, C., LU, Y., LIU, B., JIN, W., LIANG, K., WU, L., SCHMIDT, M., MILLS, G. B., MENDELSOHN, J. & FAN, Z. 2003. HER2/PI-3K/Akt activation leads to a multidrug resistance in human breast adenocarcinoma cells. *Oncogene,* 22**,** 3205-12.

KOGELBERG, H., TOLNER, B., THOMAS, G. J., DI CARA, D., MINOGUE, S., RAMESH, B., SODHA, S., MARSH, D., LOWDELL, M. W., MEYER, T., BEGENT, R. H. J., HART, I., MARSHALL, J. F. & CHESTER, K. 2008. Engineering a Single Chain Fv Antibody to αvβ6 Integrin using the Specificity-Determining Loop of a Foot-and-Mouth Disease Virus. *Journal of molecular biology,* 382**,** 385-401.

KOPPER, F., BINKOWSKI, A. M., BIERWIRTH, C. & DOBBELSTEIN, M. 2014. The MAPK-activated protein kinase 2 mediates gemcitabine sensitivity in pancreatic cancer cells. *Cell Cycle,* 13**,** 884-9.

KOVALA, T. & POULIN, J. 2009. ERK Inhibition by SU1498 Alters Expression of Bcl-2 Family Proteins in Breast Cancer Cells. *The FASEB Journal,* 23**,** 526.18.

KURIEN, B. T. & SCOFIELD, R. H. 2006. Western blotting. *Methods,* 38**,** 283-293.

LAKHANI, S. R., ELLIS, I. O., SCHNITT, S. J., TAN, P. H. & VAN DE VIJVER, M. J. 2012. *WHO Classification of Tumours of the Breast* USA, IACR / WHO.

LAKHTAKIA, R. & CHINOY, R. F. 2014. A Brief History of Breast Cancer: Part II - Evolution of surgical pathology. *Sultan Qaboos Univ Med J,* 14**,** e319-22.

LAMBERT, A. W., OZTURK, S. & THIAGALINGAM, S. 2012. Integrin Signaling in Mammary Epithelial Cells and Breast Cancer. *ISRN Oncology,* 2012**,** 493283.

LARJAVA, H., KOIVISTO, L., HEINO, J. & HAKKINEN, L. 2014. Integrins in periodontal disease. *Exp Cell Res,* 325**,** 104-10.

LARSEN, M. J., THOMASSEN, M., GERDES, A. M. & KRUSE, T. A. 2014. Hereditary breast cancer: clinical, pathological and molecular characteristics. *Breast Cancer (Auckl),* 8**,** 145-55.

LASFARGUES, E. Y., COUTINHO, W. G. & REDFIELD, E. S. 1978. Isolation of two human tumor epithelial cell lines from solid breast carcinomas. *J Natl Cancer Inst,* 61**,** 967-78.

LASFARGUES, E. Y. & OZZELLO, L. 1958. Cultivation of human breast carcinomas. *J Natl Cancer Inst,* 21**,** 1131-47.

LAUBY-SECRETAN, B., SCOCCIANTI, C., LOOMIS, D., GROSSE, Y., BIANCHINI, F. & STRAIF, K. 2016. Body Fatness and Cancer--Viewpoint of the IARC Working Group. *N Engl J Med,* 375**,** 794-8.

LAWRENCE, R. T., PEREZ, E. M., HERNANDEZ, D., MILLER, C. P., HAAS, K. M., IRIE, H. Y., LEE, S. I., BLAU, C. A. & VILLEN, J. 2015. The proteomic landscape of triple-negative breast cancer. *Cell Rep,* 11**,** 630-44.

LEE, H. W., CHOI, H. Y., JOO, K. M. & NAM, D. H. 2015. Tumor progression locus 2 (Tpl2) kinase as a novel therapeutic target for cancer: double-sided effects of Tpl2 on cancer. *Int J Mol Sci,* 16**,** 4471-91.

LEE, Y. C., JIN, J. K., CHENG, C. J., HUANG, C. F., SONG, J. H., HUANG, M., BROWN, W. S., ZHANG, S., YU-LEE, L. Y., YEH, E. T., MCINTYRE, B. W., LOGOTHETIS, C. J., GALLICK, G. E. & LIN, S. H. 2013. Targeting constitutively activated beta1 integrins inhibits prostate cancer metastasis. *Mol Cancer Res,* 11**,** 405-17.

LEGATE, K. R. & FASSLER, R. 2009. Mechanisms that regulate adaptor binding to beta-integrin cytoplasmic tails. *J Cell Sci,* 122**,** 187-98.

LEITINGER, B. 2011. Transmembrane collagen receptors. *Annu Rev Cell Dev Biol,* 27**,** 265-90.

LEITINGER, B., MCDOWALL, A., STANLEY, P. & HOGG, N. 2000. The regulation of integrin function by Ca2+. *Biochimica et Biophysica Acta (BBA) - Molecular Cell Research,* 1498**,** 91-98.

LENNON, R., BYRON, A., HUMPHRIES, J. D., RANDLES, M. J., CARISEY, A., MURPHY, S., KNIGHT, D., BRENCHLEY, P. E., ZENT, R. & HUMPHRIES, M. J. 2014. Global analysis reveals the complexity of the human glomerular extracellular matrix. *J Am Soc Nephrol,* 25**,** 939-51.

LEONOUDAKIS, D., HUANG, G., AKHAVAN, A., FATA, J. E., SINGH, M., GRAY, J. W. & MUSCHLER, J. L. 2014. Endocytic trafficking of laminin is controlled by dystroglycan and is disrupted in cancers. *J Cell Sci,* 127**,** 4894-903.

LEREA, K. M., CORDERO, K. P., SAKARIASSEN, K. S., KIRK, R. I. & FRIED, V. A. 1999. Phosphorylation sites in the integrin beta3 cytoplasmic domain in intact platelets. *J Biol Chem,* 274**,** 1914-9.

LESNIAK, D., XU, Y., DESCHENES, J., LAI, R., THOMS, J., MURRAY, D., GOSH, S., MACKEY, J. R., SABRI, S. & ABDULKARIM, B. 2009. Beta1-integrin circumvents the antiproliferative effects of trastuzumab in human epidermal growth factor receptor-2-positive breast cancer. *Cancer Res,* 69**,** 8620-8.

LESURF, R., AURE, M. R., MORK, H. H., VITELLI, V., LUNDGREN, S., BORRESEN-DALE, A. L., KRISTENSEN, V., WARNBERG, F., HALLETT, M. & SORLIE, T. 2016. Molecular Features of Subtype-Specific Progression from Ductal Carcinoma In Situ to Invasive Breast Cancer. *Cell Rep,* 16**,** 1166-79.

LEY, K., RIVERA-NIEVES, J., SANDBORN, W. J. & SHATTIL, S. 2016. Integrin-based therapeutics: biological basis, clinical use and new drugs. *Nat Rev Drug Discov,* 15**,** 173-83.

LGC©STANDARDS 2011. Cell Line Authentication Report (Ref: 710081047).

LI, N. F., GEMENETZIDIS, E., MARSHALL, F. J., DAVIES, D., YU, Y., FRESE, K., FROELING, F. E., WOOLF, A. K., FEAKINS, R. M., NAITO, Y., IACOBUZIO-DONAHUE, C., TUVESON, D. A., HART, I. R. & KOCHER, H. M. 2013. RhoC interacts with integrin alpha5beta1 and enhances its trafficking in migrating pancreatic carcinoma cells. *PLoS One,* 8**,** e81575.

LI, Y., MELNIKOV, A. A., LEVENSON, V., GUERRA, E., SIMEONE, P., ALBERTI, S. & DENG, Y. 2015. A seven-gene CpG-island methylation panel predicts breast cancer progression. *BMC Cancer,* 15**,** 417.

LI, Y.-R. & YANG, W.-X. 2016. Myosins as fundamental components during tumorigenesis: diverse and indispensable. *Oncotarget,* 7**,** 46785-46812.

LIDDINGTON, R. C. & GINSBERG, M. H. 2002. Integrin activation takes shape. *J Cell Biol,* 158**,** 833-9.

LIU, H., SADYGOV, R. G. & YATES, J. R., 3RD 2004. A model for random sampling and estimation of relative protein abundance in shotgun proteomics. *Anal Chem,* 76**,** 4193-201.

LIU, R., ZHANG, Z., LANG, Y., TANG, Z., PENG, Z., CAI, X., FU, X., FANG, W. & LI, L. 2017. High-level expression of MYH9 predicts poor prognosis in patients with colon cancer. *Int J Clin Exp Pathol,* 10**,** 5498-5505.

LONNE, G. K., MASOUMI, K. C., LENNARTSSON, J. & LARSSON, C. 2009. Protein kinase Cdelta supports survival of MDA-MB-231 breast cancer cells by suppressing the ERK1/2 pathway. *J Biol Chem,* 284**,** 33456-65.

LU, P., WEAVER, V. M. & WERB, Z. 2012. The extracellular matrix: a dynamic niche in cancer progression. *J Cell Biol,* 196**,** 395-406.

LU, S., SIMIN, K., KHAN, A. & MERCURIO, A. M. 2008. Analysis of integrin beta4 expression in human breast cancer: association with basal-like tumors and prognostic significance. *Clin Cancer Res,* 14**,** 1050-8.

LUCIANO, B. S., HSU, S., CHANNAVAJHALA, P. L., LIN, L. L. & CUOZZO, J. W. 2004. Phosphorylation of threonine 290 in the activation loop of Tpl2/Cot is necessary but not sufficient for kinase activity. *J Biol Chem,* 279**,** 52117-23.

LUO, B. H., CARMAN, C. V. & SPRINGER, T. A. 2007. Structural basis of integrin regulation and signaling. *Annu Rev Immunol,* 25**,** 619-47.

MADAMANCHI, A., ZIJLSTRA, A. & ZUTTER, M. M. 2014. Flipping the switch: integrin switching provides metastatic competence. *Sci Signal,* 7**,** pe9.

MAHMOOD, T. & YANG, P. C. 2012. Western blot: technique, theory, and trouble shooting. *N Am J Med Sci,* 4**,** 429-34.

MAIELLO, M. R., AMELIA, D., BEVILACQUA, S., GALLO, M., NORMANNO, N. & DE LUCA, A. 2015. EGFR and MEK Blockade in Triple Negative Breast Cancer Cells. *J Cell Biochem*.

MAKKI, J. 2015. Diversity of Breast Carcinoma: Histological Subtypes and Clinical Relevance. *Clinical Medicine Insights. Pathology,* 8**,** 23-31.

MALLER, O., MARTINSON, H. & SCHEDIN, P. 2010. Extracellular matrix composition reveals complex and dynamic stromal-epithelial interactions in the mammary gland. *J Mammary Gland Biol Neoplasia,* 15**,** 301-18.

MAN, Y. K., DICARA, D., CHAN, N., VESSILLIER, S., MATHER, S. J., ROWE, M. L., HOWARD, M. J., MARSHALL, J. F. & NISSIM, A. 2013. Structural guided scaffold phage display libraries as a source of bio-therapeutics. *PLoS One,* 8**,** e70452.

MANAI, M., THOMASSIN-PIANA, J., GAMOUDI, A., FINETTI, P., LOPEZ, M., EGHOZZI, R., AYADI, S., LAMINE, O. B., MANAI, M., RAHAL, K., CHARAFE-JAUFFRET, E., JACQUEMIER, J., VIENS, P., BIRNBAUM, D., BOUSSEN, H., CHAFFANET, M. & BERTUCCI, F. 2017. MARCKS protein overexpression in inflammatory breast cancer. *Oncotarget,* 8**,** 6246-6257.

MARGADANT, C., MONSUUR, H. N., NORMAN, J. C. & SONNENBERG, A. 2011. Mechanisms of integrin activation and trafficking. *Curr Opin Cell Biol,* 23**,** 607-14.

MARGADANT, C. & SONNENBERG, A. 2010. Integrin-TGF-beta crosstalk in fibrosis, cancer and wound healing. *EMBO Rep,* 11**,** 97-105.

MARSH, D., DICKINSON, S., NEILL, G. W., MARSHALL, J. F., HART, I. R. & THOMAS, G. J. 2008. alpha vbeta 6 Integrin promotes the invasion of morphoeic basal cell carcinoma through stromal modulation. *Cancer Res,* 68**,** 3295-303.

MAURO, L. V., GROSSONI, V. C., URTREGER, A. J., YANG, C., COLOMBO, L. L., MORANDI, A., PALLOTTA, M. G., KAZANIETZ, M. G., BAL DE KIER JOFFE, E. D. & PURICELLI, L. L. 2010. PKC Delta (PKCdelta) promotes tumoral progression of human ductal pancreatic cancer. *Pancreas,* 39**,** e31-41.

MCALISTER, D. 1879. The Law of the Geometric Mean. *Proc. R. Soc. Lond.,* 29**,** 367 - 376.

MCCLOY, R. A., ROGERS, S., CALDON, C. E., LORCA, T., CASTRO, A. & BURGESS, A. 2014. Partial inhibition of Cdk1 in G 2 phase overrides the SAC and decouples mitotic events. *Cell Cycle,* 13**,** 1400-12.

MELAN, M. A. 1995. Overview of Cell Fixation and Permeabilization. *In:* JAVOIS, L. C. (ed.) *Immunocytochemical Methods and Protocols.* Totowa, NJ: Humana Press.

MICHISHITA, M., VIDEM, V. & ARNAOUT, M. A. 1993. A novel divalent cation-binding site in the A domain of the beta 2 integrin CR3 (CD11b/CD18) is essential for ligand binding. *Cell,* 72**,** 857-67.

MILLARD, M., ODDE, S. & NEAMATI, N. 2011. Integrin targeted therapeutics. *Theranostics,* 1**,** 154-88.

MILLER, F. R., SANTNER, S. J., TAIT, L. & DAWSON, P. J. 2000. MCF10DCIS.com xenograft model of human comedo ductal carcinoma in situ. *J Natl Cancer Inst,* 92**,** 1185-6.

MILLER, L. 2010. *ImageJ Gel Analysis* [Online]. Available: http://www.lukemiller.org/ImageJ_gel_analysis.pdf [Accessed 17th March 2017 2017].

MOLITOR, T. P. & TRAKTMAN, P. 2013. Molecular genetic analysis of VRK1 in mammary epithelial cells: depletion slows proliferation in vitro and tumor growth and metastasis in vivo. *Oncogenesis,* 2**,** e48.

MOLLENHAUER, J., HELMKE, B., MULLER, H., KOLLENDER, G., KREBS, I., WIEMANN, S., HOLMSKOV, U., MADSEN, J., OTTO, H. F. & POUSTKA, A. 2002. An integrative model on the role of DMBT1 in epithelial cancer. *Cancer Detect Prev,* 26**,** 266-74.

MOLLENHAUER, J., HELMKE, B., MULLER, H., KOLLENDER, G., LYER, S., DIEDRICHS, L., HOLMSKOV, U., LIGTENBERG, T., HERBERTZ, S., KREBS, I., WIEMANN, S., MADSEN, J., BIKKER, F., SCHMITT, L., OTTO, H. F. & POUSTKA, A. 2002. Sequential changes of the DMBT1 expression and location in normal lung tissue and lung carcinomas. *Genes Chromosomes Cancer,* 35**,** 164-9.

MONAGHAN, P., GOLD, S., SIMPSON, J., ZHANG, Z., WEINREB, P. H., VIOLETTE, S. M., ALEXANDERSEN, S. & JACKSON, T. 2005. The alpha(v)beta6 integrin receptor for

Foot-and-mouth disease virus is expressed constitutively on the epithelial cells targeted in cattle. *J Gen Virol,* 86**,** 2769-80.

MONSMA, D. J., CHERBA, D. M., EUGSTER, E. E., DYLEWSKI, D. L., DAVIDSON, P. T., PETERSON, C. A., BORGMAN, A. S., WINN, M. E., DYKEMA, K. J., WEBB, C. P., MACKEIGAN, J. P., DUESBERY, N. S., NICKOLOFF, B. J. & MONKS, N. R. 2015. Melanoma patient derived xenografts acquire distinct Vemurafenib resistance mechanisms. *Am J Cancer Res,* 5**,** 1507-18.

MONTANEZ, E., USSAR, S., SCHIFFERER, M., BOSL, M., ZENT, R., MOSER, M. & FASSLER, R. 2008. Kindlin-2 controls bidirectional signaling of integrins. *Genes Dev,* 22**,** 1325-30.

MOORE, K. M., THOMAS, G. J., DUFFY, S. W., WARWICK, J., GABE, R., CHOU, P., ELLIS, I. O., GREEN, A. R., HAIDER, S., BROUILETTE, K., SAHA, A., VALLATH, S., BOWEN, R., CHELALA, C., ECCLES, D., TAPPER, W. J., THOMPSON, A. M., QUINLAN, P., JORDAN, L., GILLETT, C., BRENTNALL, A., VIOLETTE, S., WEINREB, P. H., KENDREW, J., BARRY, S. T., HART, I. R., JONES, J. L. & MARSHALL, J. F. 2014. Therapeutic targeting of integrin alphavbeta6 in breast cancer. *J Natl Cancer Inst,* 106.

MORENO-LAYSECA, P. & STREULI, C. H. 2014. Signalling pathways linking integrins with cell cycle progression. *Matrix Biol,* 34**,** 144-53.

MORGAN, M. R., HAMIDI, H., BASS, M. D., WARWOOD, S., BALLESTREM, C. & HUMPHRIES, M. J. 2013. Syndecan-4 phosphorylation is a control point for integrin recycling. *Dev Cell,* 24**,** 472-85.

MORGAN, M. R., JAZAYERI, M., RAMSAY, A. G., THOMAS, G. J., BOULANGER, M. J., HART, I. R. & MARSHALL, J. F. 2011. Psoriasin (S100A7) associates with integrin beta6 subunit and is required for alphavbeta6-dependent carcinoma cell invasion. *Oncogene,* 30**,** 1422-35.

MORGAN, M. R., THOMAS, G. J., RUSSELL, A., HART, I. R. & MARSHALL, J. F. 2004. The integrin cytoplasmic-tail motif EKQKVDLSTDC is sufficient to promote tumor cell invasion mediated by matrix metalloproteinase (MMP)-2 or MMP-9. *J Biol Chem,* 279**,** 26533-9.

MORO, L., DOLCE, L., CABODI, S., BERGATTO, E., BOERI ERBA, E., SMERIGLIO, M., TURCO, E., RETTA, S. F., GIUFFRIDA, M. G., VENTURINO, M., GODOVAC-ZIMMERMANN, J., CONTI, A., SCHAEFER, E., BEGUINOT, L., TACCHETTI, C., GAGGINI, P., SILENGO, L., TARONE, G. & DEFILIPPI, P. 2002. Integrin-induced epidermal growth factor (EGF) receptor activation requires c-Src and p130Cas and leads to phosphorylation of specific EGF receptor tyrosines. *J Biol Chem,* 277**,** 9405-14.

MORO, L., VENTURINO, M., BOZZO, C., SILENGO, L., ALTRUDA, F., BEGUINOT, L., TARONE, G. & DEFILIPPI, P. 1998. Integrins induce activation of EGF receptor: role in MAP kinase induction and adhesion-dependent cell survival. *Embo j,* 17**,** 6622-32.

MOSESSON, Y., MILLS, G. B. & YARDEN, Y. 2008. Derailed endocytosis: an emerging feature of cancer. *Nat Rev Cancer,* 8**,** 835-50.

MOULD, A. P., AKIYAMA, S. K. & HUMPHRIES, M. J. 1996. The inhibitory anti-beta1 integrin monoclonal antibody 13 recognizes an epitope that is attenuated by ligand occupancy. Evidence for allosteric inhibition of integrin function. *J Biol Chem,* 271**,** 20365-74.

MOULD, A. P., GARRATT, A. N., ASKARI, J. A., AKIYAMA, S. K. & HUMPHRIES, M. J. 1995a. Identification of a novel anti-integrin monoclonal antibody that recognises a ligand-induced binding site epitope on the beta 1 subunit. *FEBS Lett,* 363**,** 118-22.

MOULD, A. P., GARRATT, A. N., ASKARI, J. A., AKIYAMA, S. K. & HUMPHRIES, M. J. 1995b. Regulation of integrin alpha 5 beta 1 function by anti-integrin antibodies and divalent cations. *Biochem Soc Trans,* 23**,** 395S.

MU, Z., YANG, Z., YU, D., ZHAO, Z. & MUNGER, J. S. 2008. TGFbeta1 and TGFbeta3 are partially redundant effectors in brain vascular morphogenesis. *Mech Dev,* 125**,** 508-16.

MUKOHARA, T., ENGELMAN, J. A., HANNA, N. H., YEAP, B. Y., KOBAYASHI, S., LINDEMAN, N., HALMOS, B., PEARLBERG, J., TSUCHIHASHI, Z., CANTLEY, L. C., TENEN, D. G., JOHNSON, B. E. & JANNE, P. A. 2005. Differential effects of gefitinib and cetuximab on non-small-cell lung cancers bearing epidermal growth factor receptor mutations. *J Natl Cancer Inst,* 97**,** 1185-94.

MULLER, H., HU, J., POPP, R., SCHMIDT, M. H., MULLER-DECKER, K., MOLLENHAUER, J., FISSLTHALER, B., EBLE, J. A. & FLEMING, I. 2012. Deleted in malignant brain tumors 1 is present in the vascular extracellular matrix and promotes angiogenesis. *Arterioscler Thromb Vasc Biol,* 32**,** 442-8.

MULLER, P. A., CASWELL, P. T., DOYLE, B., IWANICKI, M. P., TAN, E. H., KARIM, S., LUKASHCHUK, N., GILLESPIE, D. A., LUDWIG, R. L., GOSSELIN, P., CROMER, A., BRUGGE, J. S., SANSOM, O. J., NORMAN, J. C. & VOUSDEN, K. H. 2009. Mutant p53 drives invasion by promoting integrin recycling. *Cell,* 139**,** 1327-41.

MUNGER, J. S., HUANG, X., KAWAKATSU, H., GRIFFITHS, M. J., DALTON, S. L., WU, J., PITTET, J. F., KAMINSKI, N., GARAT, C., MATTHAY, M. A., RIFKIN, D. B. & SHEPPARD, D. 1999. The integrin alpha v beta 6 binds and activates latent TGF beta 1: a mechanism for regulating pulmonary inflammation and fibrosis. *Cell,* 96**,** 319-28.

MUNGER, J. S. & SHEPPARD, D. 2011. Cross talk among TGF-beta signaling pathways, integrins, and the extracellular matrix. *Cold Spring Harb Perspect Biol,* 3**,** a005017.

NABA, A., CLAUSER, K. R., HOERSCH, S., LIU, H., CARR, S. A. & HYNES, R. O. 2012a. The matrisome: in silico definition and in vivo characterization by proteomics of normal and tumor extracellular matrices. *Mol Cell Proteomics,* 11**,** M111 014647.

NABA, A., HOERSCH, S. & HYNES, R. O. 2012b. Towards definition of an ECM parts list: an advance on GO categories. *Matrix Biol,* 31**,** 371-2.

NAGEL, W., ZEITLMANN, L., SCHILCHER, P., GEIGER, C., KOLANUS, J. & KOLANUS, W. 1998. Phosphoinositide 3-OH kinase activates the beta2 integrin adhesion pathway and induces membrane recruitment of cytohesin-1. *J Biol Chem,* 273**,** 14853-61.

NAKAGAWA, H., NUOVO, G. J., ZERVOS, E. E., MARTIN, E. W., JR., SALOVAARA, R., AALTONEN, L. A. & DE LA CHAPELLE, A. 2001. Age-related hypermethylation of the 5' region of MLH1 in normal colonic mucosa is associated with microsatellite-unstable colorectal cancer development. *Cancer Res,* 61**,** 6991-5.

NICE. 2009a. *Clinical Guideline [CG80]: Early and locally advanced breast cancer: diagnosis and treatment* [Online]. Available: https://www.nice.org.uk/guidance/cg80 [Accessed 21st July 2017].

NICE. 2009b. *Clinical Guideline [CG81] Advanced breast cancer: diagnosis and treatment* [Online]. [Accessed 21st July 2017].

NICE. 2011. *NICE Quality Standard 12: Breast Cancer Quality Standard* [Online]. Available: http://www.nice.org.uk/guidance/qs12/resources/guidance-breast-cancer-quality-standard-pdf [Accessed 11th November 2014].

NURDEN, A. T. 2006. Glanzmann thrombasthenia. *Orphanet Journal of Rare Diseases,* 1**,** 10-10.

NYSTROM, M. L., MCCULLOCH, D., WEINREB, P. H., VIOLETTE, S. M., SPEIGHT, P. M., MARSHALL, J. F., HART, I. R. & THOMAS, G. J. 2006. Cyclooxygenase-2 inhibition suppresses alphavbeta6 integrin-dependent oral squamous carcinoma invasion. *Cancer Res,* 66**,** 10833-42.

ORLOWSKI, A., KUKKURAINEN, S., POYRY, A., RISSANEN, S., VATTULAINEN, I., HYTONEN, V. P. & ROG, T. 2015. PIP2 and Talin Join Forces to Activate Integrin. *J Phys Chem B,* 119**,** 12381-9.

OSKARSSON, T. 2013. Extracellular matrix components in breast cancer progression and metastasis. *Breast,* 22 Suppl 2**,** S66-72.

OUDERKIRK, J. L. & KRENDEL, M. 2014. Non-muscle myosins in tumor progression, cancer cell invasion and metastasis. *Cytoskeleton (Hoboken, N.J.),* 71**,** 447-463.

OUDIN, M. J., JONAS, O., KOSCIUK, T., BROYE, L. C., GUIDO, B. C., WYCKOFF, J., RIQUELME, D., LAMAR, J. M., ASOKAN, S. B., WHITTAKER, C., MA, D., LANGER, R., CIMA, M. J., WISINSKI, K. B., HYNES, R. O., LAUFFENBURGER, D. A., KEELY, P. J., BEAR, J. E. & GERTLER, F. B. 2016. Tumor Cell-Driven Extracellular Matrix Remodeling Drives Haptotaxis during Metastatic Progression. *Cancer Discov,* 6**,** 516-31.

PARKIN, D. M. 2011. 9. Cancers attributable to inadequate physical exercise in the UK in 2010. *Br J Cancer,* 105 Suppl 2**,** S38-41.

PARKIN, D. M. & BOYD, L. 2011. 8. Cancers attributable to overweight and obesity in the UK in 2010. *Br J Cancer,* 105 Suppl 2**,** S34-7.

PARVANI, J. G., GALLIHER-BECKLEY, A. J., SCHIEMANN, B. J. & SCHIEMANN, W. P. 2013. Targeted inactivation of beta1 integrin induces beta3 integrin switching, which drives breast cancer metastasis by TGF-beta. *Mol Biol Cell,* 24**,** 3449-59.

PASZEK, M. J., DUFORT, C. C., ROSSIER, O., BAINER, R., MOUW, J. K., GODULA, K., HUDAK, J. E., LAKINS, J. N., WIJEKOON, A. C., CASSEREAU, L., RUBASHKIN, M. G., MAGBANUA, M. J., THORN, K. S., DAVIDSON, M. W., RUGO, H. S., PARK, J. W., HAMMER, D. A., GIANNONE, G., BERTOZZI, C. R. & WEAVER, V. M. 2014. The cancer glycocalyx mechanically primes integrin-mediated growth and survival. *Nature,* 511**,** 319-25.

PATEL, V. J., THALASSINOS, K., SLADE, S. E., CONNOLLY, J. B., CROMBIE, A., MURRELL, J. C. & SCRIVENS, J. H. 2009. A comparison of labeling and label-free mass spectrometry-based proteomics approaches. *J Proteome Res,* 8**,** 3752-9.

PAUL, N. R. 2014. *Proteomic and phosphoproteomic analysis of signalling by adhesion and growth factor receptors in mammary epithelial cells.* PhD Doctoral Thesis, University of Manchester.

PEARCE, L. R., KOMANDER, D. & ALESSI, D. R. 2010. The nuts and bolts of AGC protein kinases. *Nat Rev Mol Cell Biol,* 11**,** 9-22.

PEGORARO, S., ROS, G., CIANI, Y., SGARRA, R., PIAZZA, S. & MANFIOLETTI, G. 2015. A novel HMGA1-CCNE2-YAP axis regulates breast cancer aggressiveness. *Oncotarget,* 6**,** 19087-101.

PEROU, C. M., SORLIE, T., EISEN, M. B., VAN DE RIJN, M., JEFFREY, S. S., REES, C. A., POLLACK, J. R., ROSS, D. T., JOHNSEN, H., AKSLEN, L. A., FLUGE, O., PERGAMENSCHIKOV, A., WILLIAMS, C., ZHU, S. X., LONNING, P. E., BORRESEN-DALE, A. L., BROWN, P. O. & BOTSTEIN, D. 2000. Molecular portraits of human breast tumours. *Nature,* 406**,** 747-52.

PESHO, M. M., BLEDZKA, K., MICHALEC, L., CIERNIEWSKI, C. S. & PLOW, E. F. 2006. The specificity and function of the metal-binding sites in the integrin beta3 A-domain. *J Biol Chem,* 281**,** 23034-41.

PETITCLERC, E., STROMBLAD, S., VON SCHALSCHA, T. L., MITJANS, F., PIULATS, J., MONTGOMERY, A. M., CHERESH, D. A. & BROOKS, P. C. 1999. Integrin alpha(v)beta3 promotes M21 melanoma growth in human skin by regulating tumor cell survival. *Cancer Res,* 59**,** 2724-30.

PHOSPHOSITE. 2015a. *Cot (human)* [Online]. Available: http://www.phosphosite.org/proteinAction.do?id=711&showAllSites=true [Accessed 9th December 2015].

PHOSPHOSITE. 2015b. *MAPKAPK2 (human)* [Online]. Available: http://www.phosphosite.org/proteinAction.do?id=716 [Accessed 9th December 2015].

PHOSPHOSITE. 2015c. *Nuak1 (human)* [Online]. Available: http://www.phosphosite.org/proteinAction.do?id=802&showAllSites=true [Accessed 9th December 2015].

PHOSPHOSITE. 2015d. *PDK1 (human)* [Online]. Available: http://www.phosphosite.org/proteinAction.do?id=635&showAllSites=true [Accessed 9th December 2015].

PHOSPHOSITE. 2015e. *TBK1 (human)* [Online]. Available: http://www.phosphosite.org/proteinAction.do?id=825&showAllSites=true [Accessed 9th December 2015].

PHOSPHOSITE. 2017. *EGFR (human)* [Online]. [Accessed 30th August 2017 2017].

PICKUP, M. W., MOUW, J. K. & WEAVER, V. M. 2014. The extracellular matrix modulates the hallmarks of cancer. *EMBO Rep,* 15**,** 1243-53.

PLACE, A. E., JIN HUH, S. & POLYAK, K. 2011. The microenvironment in breast cancer progression: biology and implications for treatment. *Breast Cancer Res,* 13**,** 227.

POLYAK, K. 2011. Heterogeneity in breast cancer. *J Clin Invest,* 121**,** 3786-8.

POLYAK, K. 2014. Tumor heterogeneity confounds and illuminates: a case for Darwinian tumor evolution. *Nat Med,* 20**,** 344-6.

PONKA, P. & LOK, C. N. 1999. The transferrin receptor: role in health and disease. *Int J Biochem Cell Biol,* 31**,** 1111-37.

PORTE, J. & JENKINS, G. 2014. Assessment of the effect of potential antifibrotic compounds on total and alphaVbeta6 integrin-mediated TGF-beta activation. *Pharmacol Res Perspect,* 2**,** e00030.

POUS, C., KLIPFEL, L. & BAILLET, A. 2016. Cancer-Related Functions and Subcellular Localizations of Septins. *Front Cell Dev Biol,* 4**,** 126.

POUWELS, J., NEVO, J., PELLINEN, T., YLANNE, J. & IVASKA, J. 2012. Negative regulators of integrin activity. *J Cell Sci*. England.

POVEDA, J., SANZ, A. B., FERNANDEZ-FERNANDEZ, B., CARRASCO, S., RUIZ-ORTEGA, M., CANNATA-ORTIZ, P., ORTIZ, A. & SANCHEZ-NINO, M. D. 2017. MXRA5 is a TGF-beta1-regulated human protein with anti-inflammatory and anti-fibrotic properties. *J Cell Mol Med,* 21**,** 154-164.

PRAT, A., KARGINOVA, O., PARKER, J. S., FAN, C., HE, X., BIXBY, L., HARRELL, J. C., ROMAN, E., ADAMO, B., TROESTER, M. & PEROU, C. M. 2013. Characterization of cell lines derived from breast cancers and normal mammary tissues for the study of the intrinsic molecular subtypes. *Breast Cancer Res Treat,* 142**,** 237-55.

QU, Y., HAN, B., YU, Y., YAO, W., BOSE, S., KARLAN, B. Y., GIULIANO, A. E. & CUI, X. 2015. Evaluation of MCF10A as a Reliable Model for Normal Human Mammary Epithelial Cells. *PLoS One,* 10**,** e0131285.

QUAIL, D. F. & JOYCE, J. A. 2013. Microenvironmental regulation of tumor progression and metastasis. *Nat Med,* 19**,** 1423-37.

QUINTAYO, M. A., MUNRO, A. F., THOMAS, J., KUNKLER, I. H., JACK, W., KERR, G. R., DIXON, J. M., CHETTY, U. & BARTLETT, J. M. S. 2012. GSK3β and cyclin D1 expression predicts outcome in early breast cancer patients. *Breast Cancer Research and Treatment,* 136**,** 161-168.

RAAB-WESTPHAL, S., MARSHALL, J. F. & GOODMAN, S. L. 2017. Integrins as therapeutic targets: successes and cancers. *Cancers,* 9.

RAINERO, E., CASWELL, P. T., MULLER, P. A. J., GRINDLAY, J., MCCAFFREY, M. W., ZHANG, Q., WAKELAM, M. J. O., VOUSDEN, K. H., GRAZIANI, A. & NORMAN, J. C. 2012. Diacylglycerol kinase α controls RCP-dependent integrin trafficking to promote invasive migration. *The Journal of Cell Biology,* 196**,** 277-295.

RAINERO, E., VAN DEN BERGHE, P. V. E. & NORMAN, J. C. 2013. *In:* YARDEN, Y. & TARCIC, G. (eds.) *Vesicle Trafficking in Cancer*. Springer.

RAMSAY, A. G., KEPPLER, M. D., JAZAYERI, M., THOMAS, G. J., PARSONS, M., VIOLETTE, S., WEINREB, P., HART, I. R. & MARSHALL, J. F. 2007. HS1-associated protein X-1 regulates carcinoma cell migration and invasion via clathrin-mediated endocytosis of integrin alphavbeta6. *Cancer Res,* 67**,** 5275-84.

RANTALA, J. K., POUWELS, J., PELLINEN, T., VELTEL, S., LAASOLA, P., MATTILA, E., POTTER, C. S., DUFFY, T., SUNDBERG, J. P., KALLIONIEMI, O., ASKARI, J. A., HUMPHRIES, M. J., PARSONS, M., SALMI, M. & IVASKA, J. 2011. SHARPIN is an endogenous inhibitor of beta1-integrin activation. *Nat Cell Biol,* 13**,** 1315-24.

RAPISARDA, V., BORGHESAN, M., MIGUELA, V., ENCHEVA, V., SNIJDERS, A. P., LUJAMBIO, A. & O'LOGHLEN, A. 2017. Integrin Beta 3 Regulates Cellular Senescence by Activating the TGF-β Pathway. *Cell Reports,* 18**,** 2480-2493.

RASHID, S. T., HUMPHRIES, J. D., BYRON, A., DHAR, A., ASKARI, J. A., SELLEY, J. N., KNIGHT, D., GOLDIN, R. D., THURSZ, M. & HUMPHRIES, M. J. 2012. Proteomic analysis of extracellular matrix from the hepatic stellate cell line LX-2 identifies CYR61 and Wnt-5a as novel constituents of fibrotic liver. *J Proteome Res,* 11**,** 4052-64.

REDDY, K. B., GASCARD, P., PRICE, M. G., NEGRESCU, E. V. & FOX, J. E. 1998. Identification of an interaction between the m-band protein skelemin and beta-integrin subunits. Colocalization of a skelemin-like protein with beta1- and beta3-integrins in non-muscle cells. *J Biol Chem,* 273**,** 35039-47.

REDDY, K. B., SMITH, D. M. & PLOW, E. F. 2008. Analysis of Fyn function in hemostasis and alphaIIbbeta3-integrin signaling. *J Cell Sci,* 121**,** 1641-8.

REID, P. A. & WATTS, C. 1990. Cycling of cell-surface MHC glycoproteins through primaquine-sensitive intracellular compartments. *Nature,* 346**,** 655-7.

RESZKA, A. A., HAYASHI, Y. & HORWITZ, A. F. 1992. Identification of amino acid sequences in the integrin beta 1 cytoplasmic domain implicated in cytoskeletal association. *J Cell Biol,* 117**,** 1321-30.

REYES, C. D., PETRIE, T. A. & GARCIA, A. J. 2008. Mixed extracellular matrix ligands synergistically modulate integrin adhesion and signaling. *J Cell Physiol,* 217**,** 450-8.

REYNOLDS, A. R., HART, I. R., WATSON, A. R., WELTI, J. C., SILVA, R. G., ROBINSON, S. D., DA VIOLANTE, G., GOURLAOUEN, M., SALIH, M., JONES, M. C., JONES, D. T., SAUNDERS, G., KOSTOUROU, V., PERRON-SIERRA, F., NORMAN, J. C., TUCKER, G. C. & HODIVALA-DILKE, K. M. 2009. Stimulation of tumor growth and angiogenesis by low concentrations of RGD-mimetic integrin inhibitors. *Nat Med,* 15**,** 392-400.

RICH, T. A., WOODSON, A. H., LITTON, J. & ARUN, B. 2014. Hereditary breast cancer syndromes and genetic testing. *J Surg Oncol*.

RIVAS, G. A. & GONZALEZ-RODRIGUEZ, J. 1991. Calcium binding to human platelet integrin GPIIb/IIIa and to its constituent glycoproteins. Effects of lipids and temperature. *Biochem J,* 276 (Pt 1)**,** 35-40.

ROBERTS, M., BARRY, S., WOODS, A., VAN DER SLUIJS, P. & NORMAN, J. 2001. PDGF-regulated rab4-dependent recycling of alphavbeta3 integrin from early endosomes is necessary for cell adhesion and spreading. *Curr Biol,* 11**,** 1392-402.

ROBERTSON, J. 2014. *Phosphoproteomic analysis of adhesion of receptor signalling.* PhD Doctoral Thesis, University of Manchester.

ROBERTSON, J., JACQUEMET, G., BYRON, A., JONES, M. C., WARWOOD, S., SELLEY, J. N., KNIGHT, D., HUMPHRIES, J. D. & HUMPHRIES, M. J. 2015. Defining the phospho-adhesome through the phosphoproteomic analysis of integrin signalling. *Nat Commun,* 6**,** 6265.

ROCA-CUSACHS, P., DEL RIO, A., PUKLIN-FAUCHER, E., GAUTHIER, N. C., BIAIS, N. & SHEETZ, M. P. 2013. Integrin-dependent force transmission to the extracellular matrix by alpha-actinin triggers adhesion maturation. *Proc Natl Acad Sci U S A,* 110**,** E1361-70.

RODLER, E., KORDE, L. & GRALOW, J. 2010. Current treatment options in triple negative breast cancer. *Breast Dis,* 32**,** 99-122.

RYBIN, V. O., GUO, J., HARLETON, E., FEINMARK, S. J. & STEINBERG, S. F. 2009. Regulatory autophosphorylation sites on protein kinase C-delta at threonine-141 and threonine-295. *Biochemistry,* 48**,** 4642-51.

SAHA, A., ELLISON, D., THOMAS, G. J., VALLATH, S., MATHER, S. J., HART, I. R. & MARSHALL, J. F. 2010. High-resolution in vivo imaging of breast cancer by targeting the pro-invasive integrin alphavbeta6. *J Pathol,* 222**,** 52-63.

SAHAI, E. 2005. Mechanisms of cancer cell invasion. *Curr Opin Genet Dev,* 15**,** 87-96.

SAITO, R., SMOOT, M. E., ONO, K., RUSCHEINSKI, J., WANG, P. L., LOTIA, S., PICO, A. R., BADER, G. D. & IDEKER, T. 2012. A travel guide to Cytoscape plugins. *Nat Methods,* 9**,** 1069-76.

SAKAMOTO, H., BROEKELMANN, T., CHERESH, D. A., RAMIREZ, F., ROSENBLOOM, J. & MECHAM, R. P. 1996. Cell-type specific recognition of RGD- and non-RGD-containing cell binding domains in fibrillin-1. *J Biol Chem,* 271**,** 4916-22.

SALZANO, M., VAZQUEZ-CEDEIRA, M., SANZ-GARCIA, M., VALBUENA, A., BLANCO, S., FERNANDEZ, I. F. & LAZO, P. A. 2014. Vaccinia-related kinase 1 (VRK1) confers resistance to DNA-damaging agents in human breast cancer by affecting DNA damage response. *Oncotarget,* 5**,** 1770-8.

SAN SEBASTIAN, E., MERCERO, J. M., STOTE, R. H., DEJAEGERE, A., COSSIO, F. P. & LOPEZ, X. 2006. On the affinity regulation of the metal-ion-dependent adhesion sites in integrins. *J Am Chem Soc,* 128**,** 3554-63.

SANDIN, M., TELEMAN, J., MALMSTROM, J. & LEVANDER, F. 2014. Data processing methods and quality control strategies for label-free LC-MS protein quantification. *Biochim Biophys Acta,* 1844**,** 29-41.

SANEYASU, T., AKHTAR, R. & SAKAI, T. 2016. Molecular Cues Guiding Matrix Stiffness in Liver Fibrosis. *BioMed Research International,* 2016**,** 2646212.

SANTNER, S. J., DAWSON, P. J., TAIT, L., SOULE, H. D., ELIASON, J., MOHAMED, A. N., WOLMAN, S. R., HEPPNER, G. H. & MILLER, F. R. 2001. Malignant MCF10CA1 cell lines derived from premalignant human breast epithelial MCF10AT cells. *Breast Cancer Res Treat,* 65**,** 101-10.

SCHALLER, M. D., OTEY, C. A., HILDEBRAND, J. D. & PARSONS, J. T. 1995. Focal adhesion kinase and paxillin bind to peptides mimicking beta integrin cytoplasmic domains. *J Cell Biol,* 130**,** 1181-7.

SCHEDIN, P. & ELIAS, A. 2004. Multistep tumorigenesis and the microenvironment. *Breast Cancer Res,* 6**,** 93-101.

SCHEDIN, P. & KEELY, P. J. 2011. Mammary gland ECM remodeling, stiffness, and mechanosignaling in normal development and tumor progression. *Cold Spring Harb Perspect Biol,* 3**,** a003228.

SCHEID, M. P., PARSONS, M. & WOODGETT, J. R. 2005. Phosphoinositide-Dependent Phosphorylation of PDK1 Regulates Nuclear Translocation. *Molecular and Cellular Biology,* 25**,** 2347-2363.

SCHMIDT, E. V. 2002. Genes involved in breast cancer progression: analysis of global changes in gene expression or retroviral tagging? *Am J Pathol,* 161**,** 1973-7.

SCHNITT, S. J. 2010. Classification and prognosis of invasive breast cancer: from morphology to molecular taxonomy. *Mod Pathol,* 23 Suppl 2**,** S60-4.

SCOTT, M., MCCLUGGAGE, W. G., HILLAN, K. J., HALL, P. A. & RUSSELL, S. E. 2006. Altered patterns of transcription of the septin gene, SEPT9, in ovarian tumorigenesis. *Int J Cancer,* 118**,** 1325-9.

SERRELS, B., SANDILANDS, E., SERRELS, A., BAILLIE, G., HOUSLAY, M. D., BRUNTON, V. G., CANEL, M., MACHESKY, L. M., ANDERSON, K. I. & FRAME, M. C. 2010. A complex between FAK, RACK1, and PDE4D5 controls spreading initiation and cancer cell polarity. *Curr Biol,* 20**,** 1086-92.

SHANNON, P., MARKIEL, A., OZIER, O., BALIGA, N. S., WANG, J. T., RAMAGE, D., AMIN, N., SCHWIKOWSKI, B. & IDEKER, T. 2003. Cytoscape: a software environment for integrated models of biomolecular interaction networks. *Genome Res,* 13**,** 2498-504.

SHATTIL, S. J., KIM, C. & GINSBERG, M. H. 2010. The final steps of integrin activation: the end game. *Nat Rev Mol Cell Biol,* 11**,** 288-300.

SHEPPARD, D. 2015. Epithelial-mesenchymal interactions in fibrosis and repair. Transforming growth factor-beta activation by epithelial cells and fibroblasts. *Ann Am Thorac Soc,* 12 Suppl 1**,** S21-3.

SHEVCHENKO, A., WILM, M., VORM, O., JENSEN, O. N., PODTELEJNIKOV, A. V., NEUBAUER, G., SHEVCHENKO, A., MORTENSEN, P. & MANN, M. 1996. A strategy for identifying gel-separated proteins in sequence databases by MS alone. *Biochem Soc Trans,* 24**,** 893-6.

SHI, S. R., LIU, C., POOTRAKUL, L., TANG, L., YOUNG, A., CHEN, R., COTE, R. J. & TAYLOR,

C. R. 2008. Evaluation of the value of frozen tissue section used as "gold standard" for immunohistochemistry. *Am J Clin Pathol,* 129**,** 358-66.

SHI, S. R., SHI, Y. & TAYLOR, C. R. 2011. Antigen retrieval immunohistochemistry: review and future prospects in research and diagnosis over two decades. *J Histochem Cytochem,* 59**,** 13-32.

SHIMAOKA, M. & SPRINGER, T. A. 2003. Therapeutic antagonists and conformational regulation of integrin function. *Nat Rev Drug Discov,* 2**,** 703-16.

SHIMAOKA, M., TAKAGI, J. & SPRINGER, T. A. 2002. Conformational regulation of integrin structure and function. *Annu Rev Biophys Biomol Struct,* 31**,** 485-516.

SINN, H.-P. & KREIPE, H. 2013. A Brief Overview of the WHO Classification of Breast Tumors, 4th Edition, Focusing on Issues and Updates from the 3rd Edition. *Breast Care,* 8**,** 149-154.

SIPOS, B., HAHN, D., CARCELLER, A., PIULATS, J., HEDDERICH, J., KALTHOFF, H., GOODMAN, S. L., KOSMAHL, M. & KLOPPEL, G. 2004. Immunohistochemical screening for beta6-integrin subunit expression in adenocarcinomas using a novel monoclonal antibody reveals strong up-regulation in pancreatic ductal adenocarcinomas in vivo and in vitro. *Histopathology,* 45**,** 226-36.

SLOAN, E. K., POULIOT, N., STANLEY, K. L., CHIA, J., MOSELEY, J. M., HARDS, D. K. & ANDERSON, R. L. 2006. Tumor-specific expression of alphavbeta3 integrin promotes spontaneous metastasis of breast cancer to bone. *Breast Cancer Res,* 8**,** R20.

SMITH, J. W., PIOTROWICZ, R. S. & MATHIS, D. 1994. A mechanism for divalent cation regulation of beta 3-integrins. *J Biol Chem,* 269**,** 960-7.

SMOOT, M. E., ONO, K., RUSCHEINSKI, J., WANG, P. L. & IDEKER, T. 2011. Cytoscape 2.8: new features for data integration and network visualization. *Bioinformatics,* 27**,** 431-2.

SMYTH, G. K. 2004. Linear models and empirical bayes methods for assessing differential expression in microarray experiments. *Stat Appl Genet Mol Biol,* 3**,** Article3.

SORLIE, T. 2009. Introducing molecular subtyping of breast cancer into the clinic? *J Clin Oncol,* 27**,** 1153-4.

SORLIE, T., PEROU, C. M., TIBSHIRANI, R., AAS, T., GEISLER, S., JOHNSEN, H., HASTIE, T., EISEN, M. B., VAN DE RIJN, M., JEFFREY, S. S., THORSEN, T., QUIST, H., MATESE, J. C., BROWN, P. O., BOTSTEIN, D., LONNING, P. E. & BORRESEN-DALE, A. L. 2001. Gene expression patterns of breast carcinomas distinguish tumor subclasses with clinical implications. *Proc Natl Acad Sci U S A,* 98**,** 10869-74.

SOTERIOU, D., ISKENDER, B., BYRON, A., HUMPHRIES, J. D., BORG-BARTOLO, S., HADDOCK, M. C., BAXTER, M. A., KNIGHT, D., HUMPHRIES, M. J. & KIMBER, S. J.

2013. Comparative proteomic analysis of supportive and unsupportive extracellular matrix substrates for human embryonic stem cell maintenance. *J Biol Chem,* 288**,** 18716-31.

SOULE, H. D., MALONEY, T. M., WOLMAN, S. R., PETERSON, W. D., JR., BRENZ, R., MCGRATH, C. M., RUSSO, J., PAULEY, R. J., JONES, R. F. & BROOKS, S. C. 1990. Isolation and characterization of a spontaneously immortalized human breast epithelial cell line, MCF-10. *Cancer Res,* 50**,** 6075-86.

SOUNG, Y. H., CLIFFORD, J. L. & CHUNG, J. 2010. Crosstalk between integrin and receptor tyrosine kinase signaling in breast carcinoma progression. *BMB Rep,* 43**,** 311-8.

SOURVINOS, G., TSATSANIS, C. & SPANDIDOS, D. A. 1999. Overexpression of the Tpl-2/Cot oncogene in human breast cancer. *Oncogene,* 18**,** 4968-73.

SPANDIDOS, A., WANG, X., WANG, H. & SEED, B. 2010. PrimerBank: a resource of human and mouse PCR primer pairs for gene expression detection and quantification. *Nucleic Acids Res,* 38**,** D792-9.

SPEARS, M., CUNNINGHAM, C. A., TAYLOR, K. J., MALLON, E. A., THOMAS, J. S., KERR, G. R., JACK, W. J., KUNKLER, I. H., CAMERON, D. A., CHETTY, U. & BARTLETT, J. M. 2012. Proximity ligation assays for isoform-specific Akt activation in breast cancer identify activated Akt1 as a driver of progression. *J Pathol,* 227**,** 481-9.

SRICHAI, M. B. & ZENT, R. 2010. *In:* ZENT, R. & POZZI, A. (eds.) *Cell-Extracellular Matrix Interactions in Cancer.* Springer.

STAUNTON, D. E. 2006. Targeting Integrin Structure and Function in Disease. *Advances in Immunology,* 91**,** 111–157.

STAWOWY, P., MARGETA, C., BLASCHKE, F., LINDSCHAU, C., SPENCER-HANSCH, C., LEITGES, M., BIAGINI, G., FLECK, E. & GRAF, K. 2005. Protein kinase C epsilon mediates angiotensin II-induced activation of beta1-integrins in cardiac fibroblasts. *Cardiovasc Res,* 67**,** 50-9.

STEVENS, A. & LOWE, J. S. 2005. *Human histology,* Spain, Elsevier Mosby.

STEWART, R. L. & O'CONNOR, K. L. 2015. Clinical significance of the integrin alpha6beta4 in human malignancies. *Lab Invest,* 95**,** 976-86.

STRATFORD, A. L., REIPAS, K., HU, K., FOTOVATI, A., BROUGH, R., FRANKUM, J., TAKHAR, M., WATSON, P., ASHWORTH, A., LORD, C. J., LASHAM, A., PRINT, C. G. & DUNN, S. E. 2012. Targeting p90 ribosomal S6 kinase eliminates tumor-initiating cells by inactivating Y-box binding protein-1 in triple-negative breast cancers. *Stem Cells,* 30**,** 1338-48.

STREET, C. A. & BRYAN, B. A. 2011. Rho Kinase Proteins—Pleiotropic Modulators of Cell

Survival and Apoptosis. *Anticancer research,* 31**,** 3645-3657.

STRICKLAND, L. B., DAWSON, P. J., SANTNER, S. J. & MILLER, F. R. 2000. Progression of premalignant MCF10AT generates heterogeneous malignant variants with characteristic histologic types and immunohistochemical markers. *Breast Cancer Res Treat,* 64**,** 235-40.

SU, Z., CHEN, D., ZHANG, E., LI, Y., YU, Z., SHI, M., JIANG, Z., NI, L., YANG, S., GUI, Y., YE, J. & LAI, Y. 2015. MicroRNA-509-3p inhibits cancer cell proliferation and migration by targeting the mitogen-activated protein kinase kinase kinase 8 oncogene in renal cell carcinoma. *Mol Med Rep,* 12**,** 1535-43.

SUBBIAH, I. M. & GONZALEZ-ANGULO, A. M. 2014. Advances and future directions in the targeting of HER2-positive breast cancer: implications for the future. *Curr Treat Options Oncol,* 15**,** 41-54.

SUN, X., GAO, L., CHIEN, H. Y., LI, W. C. & ZHAO, J. 2013. The regulation and function of the NUAK family. *J Mol Endocrinol,* 51**,** R15-22.

SUN, Z., GUO, S. S. & FÄSSLER, R. 2016. Integrin-mediated mechanotransduction. *The Journal of Cell Biology*.

SUZUKI, A., LU, J., KUSAKAI, G., KISHIMOTO, A., OGURA, T. & ESUMI, H. 2004. ARK5 is a tumor invasion-associated factor downstream of Akt signaling. *Mol Cell Biol,* 24**,** 3526-35.

SUZUKI, A., OGURA, T. & ESUMI, H. 2006. NDR2 acts as the upstream kinase of ARK5 during insulin-like growth factor-1 signaling. *J Biol Chem,* 281**,** 13915-21.

TAHERIAN, A., LI, X., LIU, Y. & HAAS, T. A. 2011. Differences in integrin expression and signaling within human breast cancer cells. *BMC Cancer,* 11**,** 293.

TAKADA, Y. & PUZON, W. 1993. Identification of a regulatory region of integrin beta 1 subunit using activating and inhibiting antibodies. *J Biol Chem,* 268**,** 17597-601.

TAKAGI, J., KAMATA, T., MEREDITH, J., PUZON-MCLAUGHLIN, W. & TAKADA, Y. 1997. Changing ligand specificities of alphavbeta1 and alphavbeta3 integrins by swapping a short diverse sequence of the beta subunit. *J Biol Chem,* 272**,** 19794-800.

TAM, S. H., SASSOLI, P. M., JORDAN, R. E. & NAKADA, M. T. 1998. Abciximab (ReoPro, chimeric 7E3 Fab) demonstrates equivalent affinity and functional blockade of glycoprotein IIb/IIIa and alpha(v)beta3 integrins. *Circulation,* 98**,** 1085-91.

TAN, K. H., SIMONELLA, L., WEE, H. L., ROELLIN, A., LIM, Y. W., LIM, W. Y., CHIA, K. S., HARTMAN, M. & COOK, A. R. 2013. Quantifying the natural history of breast cancer. *Br J Cancer,* 109**,** 2035-43.

TANG, B., VU, M., BOOKER, T., SANTNER, S. J., MILLER, F. R., ANVER, M. R. & WAKEFIELD, L. M. 2003. TGF-beta switches from tumor suppressor to prometastatic factor in a model of breast cancer progression. *J Clin Invest,* 112**,** 1116-24.

TATLER, A. L. & JENKINS, G. 2012. TGF-beta activation and lung fibrosis. *Proc Am Thorac Soc,* 9**,** 130-6.

TAYLOR, M. A., PARVANI, J. G. & SCHIEMANN, W. P. 2010. The pathophysiology of epithelial-mesenchymal transition induced by transforming growth factor-beta in normal and malignant mammary epithelial cells. *J Mammary Gland Biol Neoplasia,* 15**,** 169-90.

TAYLOR, S. C., BERKELMAN, T., YADAV, G. & HAMMOND, M. 2013. A defined methodology for reliable quantification of Western blot data. *Mol Biotechnol,* 55**,** 217-26.

TCHATCHOU, S., RIEDEL, A., LYER, S., SCHMUTZHARD, J., STROBEL-FREIDEKIND, O., GRONERT-SUM, S., MIETAG, C., D'AMATO, M., SCHLEHE, B., HEMMINKI, K., SUTTER, C., DITSCH, N., BLACKBURN, A., HILL, L. Z., JERRY, D. J., BUGERT, P., WEBER, B. H., NIEDERACHER, D., ARNOLD, N., VARON-MATEEVA, R., WAPPENSCHMIDT, B., SCHMUTZLER, R. K., ENGEL, C., MEINDL, A., BARTRAM, C. R., MOLLENHAUER, J. & BURWINKEL, B. 2010. Identification of a DMBT1 polymorphism associated with increased breast cancer risk and decreased promoter activity. *Hum Mutat,* 31**,** 60-6.

TECKCHANDANI, A., MULKEARNS, E. E., RANDOLPH, T. W., TOIDA, N. & COOPER, J. A. 2012. The clathrin adaptor Dab2 recruits EH domain scaffold proteins to regulate integrin beta1 endocytosis. *Mol Biol Cell,* 23**,** 2905-16.

TERRANOVA, V. P., RAO, C. N., KALEBIC, T., MARGULIES, I. M. & LIOTTA, L. A. 1983. Laminin receptor on human breast carcinoma cells. *Proc Natl Acad Sci U S A,* 80**,** 444-8.

THE CANCER GENOME ATLAS, N. 2012. Comprehensive molecular portraits of human breast tumors. *Nature,* 490**,** 61-70.

THOMAS, G. J., HART, I. R., SPEIGHT, P. M. & MARSHALL, J. F. 2002. Binding of TGF-beta1 latency-associated peptide (LAP) to alpha(v)beta6 integrin modulates behaviour of squamous carcinoma cells. *Br J Cancer,* 87**,** 859-67.

THOMAS, G. J., LEWIS, M. P., HART, I. R., MARSHALL, J. F. & SPEIGHT, P. M. 2001a. AlphaVbeta6 integrin promotes invasion of squamous carcinoma cells through up-regulation of matrix metalloproteinase-9. *Int J Cancer,* 92**,** 641-50.

THOMAS, G. J., LEWIS, M. P., WHAWELL, S. A., RUSSELL, A., SHEPPARD, D., HART, I. R., SPEIGHT, P. M. & MARSHALL, J. F. 2001b. Expression of the alphavbeta6 integrin promotes migration and invasion in squamous carcinoma cells. *J Invest Dermatol,* 117**,** 67-73.

THOMAS, G. J., NYSTROM, M. L. & MARSHALL, J. F. 2006. Alphavbeta6 integrin in wound healing and cancer of the oral cavity. *J Oral Pathol Med,* 35**,** 1-10.

TIWARI, S., ASKARI, J. A., HUMPHRIES, M. J. & BULLEID, N. J. 2011. Divalent cations regulate the folding and activation status of integrins during their intracellular trafficking. *J Cell Sci,* 124**,** 1672-80.

TOKUNAGA, E., KIMURA, Y., OKI, E., UEDA, N., FUTATSUGI, M., MASHINO, K., YAMAMOTO, M., IKEBE, M., KAKEJI, Y., BABA, H. & MAEHARA, Y. 2006. Akt is frequently activated in HER2/neu-positive breast cancers and associated with poor prognosis among hormone-treated patients. *Int J Cancer,* 118**,** 284-9.

TOWBIN, H., STAEHELIN, T. & GORDON, J. 1979. Electrophoretic transfer of proteins from polyacrylamide gels to nitrocellulose sheets: procedure and some applications. *Proc Natl Acad Sci U S A,* 76**,** 4350-4.

TRUONG, H. H., XIONG, J., GHOTRA, V. P., NIRMALA, E., HAAZEN, L., LE DEVEDEC, S. E., BALCIOGLU, H. E., HE, S., SNAAR-JAGALSKA, B. E., VREUGDENHIL, E., MEERMAN, J. H., VAN DE WATER, B. & DANEN, E. H. 2014. beta1 integrin inhibition elicits a prometastatic switch through the TGFbeta-miR-200-ZEB network in E-cadherin-positive triple-negative breast cancer. *Sci Signal,* 7**,** ra15.

TSAI, H. C. & BAYLIN, S. B. 2011. Cancer epigenetics: linking basic biology to clinical medicine. *Cell Res,* 21**,** 502-17.

UNIPROTCONSORTIUM. 2017. *Homo sapiens (Human)* [Online]. Available: http://www.uniprot.org/taxonomy/9606.

VALDRAMIDOU, D., HUMPHRIES, M. J. & MOULD, A. P. 2008. Distinct roles of beta1 metal ion-dependent adhesion site (MIDAS), adjacent to MIDAS (ADMIDAS), and ligand-associated metal-binding site (LIMBS) cation-binding sites in ligand recognition by integrin alpha2beta1. *J Biol Chem,* 283**,** 32704-14.

VAN 'T VEER, L. J., DAI, H., VAN DE VIJVER, M. J., HE, Y. D., HART, A. A. M., MAO, M., PETERSE, H. L., VAN DER KOOY, K., MARTON, M. J., WITTEVEEN, A. T., SCHREIBER, G. J., KERKHOVEN, R. M., ROBERTS, C., LINSLEY, P. S., BERNARDS, R. & FRIEND, S. H. 2002. Gene expression profiling predicts clinical outcome of breast cancer. *Nature,* 415**,** 530-536.

VAN AARSEN, L. A., LEONE, D. R., HO, S., DOLINSKI, B. M., MCCOON, P. E., LEPAGE, D. J., KELLY, R., HEANEY, G., RAYHORN, P., REID, C., SIMON, K. J., HORAN, G. S., TAO, N., GARDNER, H. A., SKELLY, M. M., GOWN, A. M., THOMAS, G. J., WEINREB, P. H., FAWELL, S. E. & VIOLETTE, S. M. 2008. Antibody-mediated blockade of integrin alpha v beta 6 inhibits tumor progression in vivo by a transforming growth factor-beta-regulated mechanism. *Cancer Res,* 68**,** 561-70.

VAN WEERT AW, G. H., GROOTHUIS B, STOORVOGEL W. 2000. Primaquine interferes with

membrane recycling from endosomes to the plasma membrane through a direct interaction with endosomes which does not involve neutralisation of endosomal pH nor osmotic swelling of endosomes. *European Journal of Cell Biology,* 79**,** 394–399.

VAN'T VEER, L. J. & WEIGELT, B. 2003. Road map to metastasis. *Nat Med,* 9**,** 999-1000.

VARZAVAND, A., HACKER, W., MA, D., GIBSON-CORLEY, K., HAWAYEK, M., TAYH, O. J., BROWN, J. A., HENRY, M. D. & STIPP, C. S. 2016. α3β1 Integrin Suppresses Prostate Cancer Metastasis via Regulation of the Hippo Pathway. *Cancer Research,* 76**,** 6577-6587.

VAZQUEZ RODRIGUEZ, G., ABRAHAMSSON, A., JENSEN, L. D. & DABROSIN, C. 2017. Estradiol Promotes Breast Cancer Cell Migration via Recruitment and Activation of Neutrophils. *Cancer Immunol Res,* 5**,** 234-247.

VEISEH, O., KIEVIT, F. M., ELLENBOGEN, R. G. & ZHANG, M. 2011. Cancer cell invasion: treatment and monitoring opportunities in nanomedicine. *Adv Drug Deliv Rev,* 63**,** 582-96.

VERBISCK, N. V., COSTA, E. T., COSTA, F. F., CAVALHER, F. P., COSTA, M. D., MURAS, A., PAIXAO, V. A., MOURA, R., GRANATO, M. F., IERARDI, D. F., MACHADO, T., MELO, F., RIBEIRO, K. B., CUNHA, I. W., LIMA, V. C., MACIEL MDO, S., CARVALHO, A. L., SOARES, F. F., ZANATA, S., SOGAYAR, M. C., CHAMMAS, R. & CAMARGO, A. A. 2009. ADAM23 negatively modulates alpha(v)beta(3) integrin activation during metastasis. *Cancer Res,* 69**,** 5546-52.

VERCAUTEREN, D., VANDENBROUCKE, R. E., JONES, A. T., REJMAN, J., DEMEESTER, J., DE SMEDT, S. C., SANDERS, N. N. & BRAECKMANS, K. 2010. The use of inhibitors to study endocytic pathways of gene carriers: optimization and pitfalls. *Mol Ther,* 18**,** 561-9.

VIALE, G. 2012. The current state of breast cancer classification. *Ann Oncol,* 23 Suppl 10**,** x207-10.

VIEIRA, A. F., RIBEIRO, A. S., DIONÍSIO, M. R., SOUSA, B., NOBRE, A. R., ALBERGARIA, A., SANTIAGO-GÓMEZ, A., MENDES, N., GERHARD, R., SCHMITT, F., CLARKE, R. B. & PAREDES, J. 2014. P-cadherin signals through the laminin receptor α6β4 integrin to induce stem cell and invasive properties in basal-like breast cancer cells. *Oncotarget,* 5**,** 679-692.

VINAYAGAM, A., ZIRIN, J., ROESEL, C., HU, Y., YILMAZEL, B., SAMSONOVA, A. A., NEUMULLER, R. A., MOHR, S. E. & PERRIMON, N. 2014. Integrating protein-protein interaction networks with phenotypes reveals signs of interactions. *Nat Methods,* 11**,** 94-9.

VIRTAKOIVU, R., PELLINEN, T., RANTALA, J. K., PERALA, M. & IVASKA, J. 2012. Distinct roles of AKT isoforms in regulating beta1-integrin activity, migration, and invasion in

prostate cancer. *Mol Biol Cell,* 23**,** 3357-69.

VUONG, D., SIMPSON, P. T., GREEN, B., CUMMINGS, M. C. & LAKHANI, S. R. 2014. Molecular classification of breast cancer. *Virchows Arch,* 465**,** 1-14.

WANG, G. H., YAO, L., XU, H. W., TANG, W. T., FU, J. H., HU, X. F., CUI, L. & XU, X. M. 2013. Identification of MXRA5 as a novel biomarker in colorectal cancer. *Oncol Lett,* 5**,** 544-548.

WANG, T. N., ALBO, D. & TUSZYNSKI, G. P. 2002. Fibroblasts promote breast cancer cell invasion by upregulating tumor matrix metalloproteinase-9 production. *Surgery,* 132**,** 220-5.

WCRF. 2017. *Breast Cancer: Continuous Update Project Report* [Online]. Available: http://www.wcrf.org/int/research-we-fund/continuous-update-project-findings-reports/breast-cancer [Accessed 21st July 2017].

WEHRLE-HALLER, B. & IMHOF, B. A. 2003. Integrin-dependent pathologies. *J Pathol,* 200**,** 481-7.

WEI, C., CAO, Y., YANG, X., ZHENG, Z., GUAN, K., WANG, Q., TAI, Y., ZHANG, Y., MA, S., CAO, Y., GE, X., XU, C., LI, J., YAN, H., LING, Y., SONG, T., ZHU, L., ZHANG, B., XU, Q., HU, C., BIAN, X. W., HE, X. & ZHONG, H. 2014. Elevated expression of TANK-binding kinase 1 enhances tamoxifen resistance in breast cancer. *Proc Natl Acad Sci U S A,* 111**,** E601-10.

WEINACKER, A., CHEN, A., AGREZ, M., CONE, R. I., NISHIMURA, S., WAYNER, E., PYTELA, R. & SHEPPARD, D. 1994. Role of the integrin alpha v beta 6 in cell attachment to fibronectin. Heterologous expression of intact and secreted forms of the receptor. *J Biol Chem,* 269**,** 6940-8.

WEINREB, P. H., SIMON, K. J., RAYHORN, P., YANG, W. J., LEONE, D. R., DOLINSKI, B. M., PEARSE, B. R., YOKOTA, Y., KAWAKATSU, H., ATAKILIT, A., SHEPPARD, D. & VIOLETTE, S. M. 2004. Function-blocking integrin alphavbeta6 monoclonal antibodies: distinct ligand-mimetic and nonligand-mimetic classes. *J Biol Chem,* 279**,** 17875-87.

WELF, E. S., NAIK, U. P. & OGUNNAIKE, B. A. 2012. A spatial model for integrin clustering as a result of feedback between integrin activation and integrin binding. *Biophys J,* 103**,** 1379-89.

WHITE, D. E. & MULLER, W. J. 2007. Multifaceted roles of integrins in breast cancer metastasis. *J Mammary Gland Biol Neoplasia,* 12**,** 135-42.

WHITE, J. M. 2003. ADAMs: modulators of cell-cell and cell-matrix interactions. *Curr Opin Cell Biol,* 15**,** 598-606.

WHO. 2014. *Breast Cancer: prevention and control* [Online]. online. Available: http://www.who.int/cancer/detection/breastcancer/en/ [Accessed 7th November 2014].

WINOGRAD-KATZ, S. E. & LEVITZKI, A. 2006. Cisplatin induces PKB/Akt activation and p38(MAPK) phosphorylation of the EGF receptor. *Oncogene,* 25**,** 7381-90.

WIPFF, P. J., RIFKIN, D. B., MEISTER, J. J. & HINZ, B. 2007. Myofibroblast contraction activates latent TGF-beta1 from the extracellular matrix. *J Cell Biol,* 179**,** 1311-23.

WIREDJA, D. D., KOYUTURK, M. & CHANCE, M. R. 2017. The KSEA App: a web-based tool for kinase activity inference from quantitative phosphoproteomics. *Bioinformatics*.

WIXLER, V., GEERTS, D., LAPLANTINE, E., WESTHOFF, D., SMYTH, N., AUMAILLEY, M., SONNENBERG, A. & PAULSSON, M. 2000. The LIM-only protein DRAL/FHL2 binds to the cytoplasmic domain of several alpha and beta integrin chains and is recruited to adhesion complexes. *J Biol Chem,* 275**,** 33669-78.

WOLFENSON, H., LAVELIN, I. & GEIGER, B. 2013. Dynamic regulation of the structure and functions of integrin adhesions. *Dev Cell,* 24**,** 447-58.

WONG, J. W. & CAGNEY, G. 2010. An overview of label-free quantitation methods in proteomics by mass spectrometry. *Methods Mol Biol,* 604**,** 273-83.

WU, J., VALLENIUS, T., OVASKA, K., WESTERMARCK, J., MAKELA, T. P. & HAUTANIEMI, S. 2009. Integrated network analysis platform for protein-protein interactions. *Nat Methods,* 6**,** 75-7.

WU, Y., ZHANG, D. & KANG, S. 2013. Physical activity and risk of breast cancer: a meta-analysis of prospective studies. *Breast Cancer Res Treat,* 137**,** 869-82.

XIE, C., SHIMAOKA, M., XIAO, T., SCHWAB, P., KLICKSTEIN, L. B. & SPRINGER, T. A. 2004. The integrin alpha-subunit leg extends at a Ca2+-dependent epitope in the thigh/genu interface upon activation. *Proc Natl Acad Sci U S A,* 101**,** 15422-7.

XIONG, A., YANG, Z., SHEN, Y., ZHOU, J. & SHEN, Q. 2014. Transcription Factor STAT3 as a Novel Molecular Target for Cancer Prevention. *Cancers,* 6**,** 926-957.

XIONG, J., BALCIOGLU, H. E. & DANEN, E. H. 2013. Integrin signaling in control of tumor growth and progression. *Int J Biochem Cell Biol,* 45**,** 1012-1015.

YANG, S. B., DU, Y., WU, B. Y., XU, S. P., WEN, J. B., ZHU, M., CAI, C. H. & YANG, P. C. 2012. Integrin alphavbeta6 promotes tumor tolerance in colorectal cancer. *Cancer Immunol Immunother,* 61**,** 335-42.

YE, F., KIM, C. & GINSBERG, M. H. 2012. Reconstruction of integrin activation. *Blood,* 119**,** 26-

33.

YE, F., KIM, S.-J. & KIM, C. 2014. Intermolecular Transmembrane Domain Interactions Activate Integrin αIIbβ3. *The Journal of Biological Chemistry,* 289**,** 18507-18513.

YE, F., YANG, C., KIM, J., MACNEVIN, C. J., HAHN, K. M., PARK, D., GINSBERG, M. H. & KIM, C. 2017. Epigallocatechin gallate has pleiotropic effects on transmembrane signaling by altering the embedding of transmembrane domains. *J Biol Chem,* 292**,** 9858-9864.

YEH, Y. T., HUR, S. S., CHANG, J., WANG, K. C., CHIU, J. J., LI, Y. S. & CHIEN, S. 2012. Matrix stiffness regulates endothelial cell proliferation through septin 9. *PLoS One,* 7**,** e46889.

YOUNG, L., SUNG, J., STACEY, G. & MASTERS, J. R. 2010. Detection of Mycoplasma in cell cultures. *Nat Protoc,* 5**,** 929-34.

YU, C. H., LUO, W. & SHEETZ, M. P. 2012. Spatial-temporal reorganization of activated integrins. *Cell Adh Migr,* 6**,** 280-4.

ZAGORSKA, A., DEAK, M., CAMPBELL, D. G., BANERJEE, S., HIRANO, M., AIZAWA, S., PRESCOTT, A. R. & ALESSI, D. R. 2010. New roles for the LKB1-NUAK pathway in controlling myosin phosphatase complexes and cell adhesion. *Sci Signal,* 3**,** ra25.

ZAIDEL-BAR, R., ITZKOVITZ, S., MA'AYAN, A., IYENGAR, R. & GEIGER, B. 2007. Functional atlas of the integrin adhesome. *Nat Cell Biol,* 9**,** 858-67.

ZANTEK, N. D., WALKER-DANIELS, J., STEWART, J., HANSEN, R. K., ROBINSON, D., MIAO, H., WANG, B., KUNG, H. J., BISSELL, M. J. & KINCH, M. S. 2001. MCF-10A-NeoST: a new cell system for studying cell-ECM and cell-cell interactions in breast cancer. *Clin Cancer Res,* 7**,** 3640-8.

ZARZYNSKA, J. M. 2014. Two faces of TGF-beta1 in breast cancer. *Mediators Inflamm,* 2014**,** 141747.

ZHANG, J., TIAN, X. J., ZHANG, H., TENG, Y., LI, R., BAI, F., ELANKUMARAN, S. & XING, J. 2014. TGF-beta-induced epithelial-to-mesenchymal transition proceeds through stepwise activation of multiple feedback loops. *Sci Signal,* 7**,** ra91.

ZHANG, K. & CHEN, J. 2012. The regulation of integrin function by divalent cations. *Cell Adh Migr,* 6**,** 20-9.

ZHONG, X. & RESCORLA, F. J. 2012. Cell surface adhesion molecules and adhesion-initiated signaling: understanding of anoikis resistance mechanisms and therapeutic opportunities. *Cell Signal,* 24**,** 393-401.

ZHOU, B., GIBSON-CORLEY, K. N., HERNDON, M. E., SUN, Y., GUSTAFSON-WAGNER, E., TEOH-FITZGERALD, M., DOMANN, F. E., HENRY, M. D. & STIPP, C. S. 2014. Integrin α3β1 Can Function to Promote Spontaneous Metastasis and Lung Colonization of Invasive Breast Carcinoma. *Molecular cancer research : MCR,* 12**,** 143-154.

ZHOU, W., FAN, M. Y., WEI, Y. X., HUANG, S., CHEN, J. Y. & LIU, P. 2016. The expression of MYH9 in osteosarcoma and its effect on the migration and invasion abilities of tumor cell. *Asian Pac J Trop Med,* 9**,** 597-600.

ZHU, J., LUO, B. H., XIAO, T., ZHANG, C., NISHIDA, N. & SPRINGER, T. A. 2008. Structure of a complete integrin ectodomain in a physiologic resting state and activation and deactivation by applied forces. *Mol Cell,* 32**,** 849-61.

ZIEGLER, W. H., GINGRAS, A. R., CRITCHLEY, D. R. & EMSLEY, J. 2008. Integrin connections to the cytoskeleton through talin and vinculin. *Biochem Soc Trans,* 36**,** 235-9.

ZUTTER, M. M., SANTORO, S. A., STAATZ, W. D. & TSUNG, Y. L. 1995. Re-expression of the alpha 2 beta 1 integrin abrogates the malignant phenotype of breast carcinoma cells. *Proc Natl Acad Sci U S A,* 92**,** 7411-5.